



**Abnormal network oscillations in patients with  
Dementia with Lewy bodies and a mouse model  
of  $\alpha$ -synucleinopathy**

**Myrto Stylianou**

Thesis submitted for the degree of Doctor of Philosophy  
at Newcastle University

Supervisors:

*Dr Fiona LeBeau, Professor John-Paul Taylor*

Biosciences Institute

*January 2020*





## Abstract

Electrophysiology can reveal changes in neuronal oscillatory activity in the brain in relation to neurodegenerative disorders, including dementia with Lewy bodies (DLB). DLB, characterised by abnormal  $\alpha$ -synuclein ( $\alpha$ -syn) aggregation within neurons, is the second most common cause of dementia after Alzheimer's disease (AD). This thesis had two aims. Firstly, to identify resting-state EEG changes that reflect cognitive fluctuations, a DLB core symptom, and differentiate DLB from AD and Parkinson's disease dementia (PDD) patients and healthy controls. Secondly, to detect electrophysiological alterations in young mice over-expressing human mutant  $\alpha$ -syn while under urethane-induced anaesthesia, mimicking deep-sleep. The resulting slow-oscillation (SO) composed of Up-states (neuronal firing) and Down-states (neuronal "silence"), was recorded intra-cortically, from the hippocampus and medial prefrontal cortex (mPFC). The human EEG analysis replicated reports of a shift of power and dominant frequency (DF) from alpha to theta frequencies, in DLB/PDD patients compared to AD patients and controls. Contrary to previous work, the DF variability (DFV) over time was increased in AD and not in DLB/PDD patients, although a DLB-specific correlation between the DFV and cognitive fluctuations persisted. The DFV and power/DF distribution could differentiate between AD and DLB patients with high sensitivity (92.26%) and specificity (83.3%). Analysis of sleep patterns in  $\alpha$ -syn mice in both the mPFC and hippocampus revealed increased SO frequency, aberrant neuronal firing activity on Down-states, altered power distribution on Up-states and disturbed sleep spindle activity, compared to WT. A novel infra-slow modulation (ISM) was described in WT, presenting as bursts of power across frequencies every  $\sim 3.5$  min. In  $\alpha$ -syn mice, the ISM induced abnormally high levels of high frequency oscillatory power in the hippocampus. Our findings indicate altered neuronal oscillatory activity in DLB patients and  $\alpha$ -syn mice during rest and sleep respectively, suggesting that  $\alpha$ -syn affects the integrity of the networks underlying widespread, synchronous activity.



## Acknowledgements

Firstly, I want to thank my supervisor Dr Fiona LeBeau for believing in me from the beginning and giving me the opportunity to pursue this PhD. I am extremely grateful and consider myself very lucky to have been Fiona's student, as she has always been available, approachable, patient and willing to hear every idea, worry and problem. I want to thank her for giving me good advice when it comes to my work, such as knowing where the limits of an analysis are and always looking at the figure, and in life, teaching me that one must not be afraid to show who they are and what they have achieved. She has always been there for me and she never let me feel short of options, and for all that, I truly thank her.

I would also like to thank Professor John-Paul Taylor for his supervision, guidance and support, as well as the members of my review panel, Dr Peter Gallagher and Professor Adrian Rees, for their support and suggestions regarding my work's progress, as their comments have always proved tremendously useful.

A very big thank you to the Alzheimer's Society for funding this project and ultimately my PhD. I want to thank all the members of the doctoral training centre and especially the other participants, Ri, Lina, Julia and Alice, it was great working with you! I want to also thank the monitors of the Alzheimer's society for their support and for believing in us in such an overwhelming way. Meeting with them and other members of the Alzheimer's society gave me a true perspective of my work.

All of the work presented in this thesis is my own except for the collection of the human EEG data that was gathered as part of the CATFieLD study. Hence, I want to thank the researchers who collected this data as well as the participants who dedicated their time. Moreover, I would not be able to perform such an in-depth analysis of my data without expanding on a number of MATLAB scripts kindly offered by my colleagues. Therefore, I would like to thank Dr Nik Murphy for giving me the EEG data pre-processing MATLAB script and being a superb MATLAB tutor and Dr Luis Peraza Rodriguez for helping with any persistent glitches in the human EEG analysis code. The analysis of the animal electrophysiological data is largely based on the original MATLAB scripts provided by Dr Sabine Gretenkord, while Dr Boubker Zaiimi has helped me develop parts of the unit firing analysis.

Looking back at my time in Newcastle will always bring a smile to my face because of the amazing friends I made there these past few years. I want to thank Jean for sharing my awful sense of humour, for cooking delicious meals, for being a true friend in every way. I also want to thank Tamara for being the best post-doc, for her help and great advice, Beth and Clare for being amazing buddies, Anderson and Mo for always making me feel welcome, even part of their family, and Ashan, Felix and Mark for being irreplaceable members of the lunch club. Thank you all and I will miss you.

On the Cyprus front, I want to thank my parents Tassos and Marianna for always caring, always putting up with my mood swings, especially during the write up period, and for being the pillars of stability in my life. Thank you for all you have done for me, for your support and love. I would also like to thank my family, Artemis, Salome, Ioanna and Eftychia for always believing in me and being optimistic. The thesis write-up period would have not been the same without Michelle, Kalli, Eleni, Elena and Christina who made me laugh hard, helped get my mind off things and allowed me to vent when I needed it, and my second home Prozak kafeneio. Lastly, I want to thank Christos for always believing in me and reminding me that it is never the end of the world. Thank you for being there at all times, for understanding and making me smile.

## Conference presentations

### **North-East Postgraduate conference (NEPG)**

**Newcastle upon Tyne, UK (November 2016)**

Poster presentation: *Investigation for electrophysiological signatures of cognitive fluctuations in Dementia with Lewy bodies.*

### **Alzheimer's & Parkinson's disease (AD/PD) conference**

**Vienna, Austria (April 2017).**

Poster presentation: *Resting state EEG in dementia with Lewy bodies: Focus on fluctuations and comparison with Alzheimer's disease and Parkinson's disease dementia.*

### **Alzheimer's Society conference 2017**

**London, UK (May 2017)**

Poster presentation: *Investigation for electrophysiological signatures of cognitive fluctuations in Dementia with Lewy bodies.*

### **Alzheimer's Society conference 2018**

**London, UK (May 2018)**

Poster presentation: *Poster presentation: Quantitative electroencephalography as an aid for differential diagnosis in dementia with Lewy bodies.*

### **Forum for Neuroscience (FENS) conference**

**Berlin, Germany (July 2018)**

Poster presentation: *In vivo electrophysiological characterization of slow-wave sleep patterns in a mouse model of Lewy body dementia.*

**North-East Postgraduate conference (NEPG)**

**Newcastle upon Tyne, UK (November 2018)**

Poster presentation: *Altered slow-wave sleep patterns in a mouse model of Lewy body dementia.*

**Alzheimer's & Parkinson's diseases (AD/PD) conference**

**Lisbon, Portugal (April 2019)**

Poster presentation: *Changes in slow-wave sleep patterns in a mouse model of Lewy body dementia indicate disturbed network dynamics.*

**British Neuroscience Association Conference**

**Dublin, Ireland (May 2019)**

Poster presentation: *Disturbances in slow wave sleep-related oscillations in the medial prefrontal cortex of a mouse model of Lewy body dementia.*

**Annual conference of the Centre of Applied Neuroscience, University of Cyprus**

**Nicosia, Cyprus (September 2019)**

Oral presentation: *Electroencephalography as a marker of cognitive fluctuations in Lewy body dementia.*

## Publications

The work presented in Chapter 3 has been published with first authorship and the article can be found at the end of this thesis.

- Stylianos M, Murphy N, Luis P R, Graziadio S, Cromarty R, Killen A, O'Brien J T, Thomas A J, LeBeau F E N, Taylor J-P (2018) Quantitative electroencephalography as a marker of cognitive fluctuations in dementia with Lewy bodies and an aid to differential diagnosis. *Clinical Neurophysiology*, 129, 6,1209-1220. doi: 10.1016/j.clinph.2018.03.013.
- Gretenkord S, Olthof B M J, Stylianos M, Rees A, Gartside S E and LeBeau F E N. (2019) Electrical stimulation of the ventral tegmental area (VTA) evokes sleep-like state transitions in the rat medial prefrontal cortex (mPFC) via dopamine D<sub>1</sub>-like receptors. *European Journal of Neuroscience*. doi: 10.1111/ejn.14665.

## Table of contents

Abstract .....	iii
Acknowledgements.....	v
Conference presentations.....	vii
Publications .....	ix
Table of contents .....	x
List of figures .....	xvii
List of tables.....	xx
List of abbreviations.....	xxi
<b>1. Introduction.....</b>	<b>1</b>
1.1. Dementia with Lewy bodies: pathology and diagnosis.....	3
1.1.1. Lewy body dementia.....	3
1.1.2. Dementia pathology.....	4
1.1.2.1. Lewy body dementia .....	4
1.1.2.2. Alzheimer’s disease .....	5
1.1.2.3. Mixed pathology .....	6
1.1.3. DLB Diagnosis.....	7
1.2. The electrophysiological rhythms of the brain during wakefulness .....	9
1.2.1. Origin of the EEG.....	9
1.2.2. The hippocampus .....	10
1.2.3. The medial prefrontal cortex (mPFC).....	11
1.2.4. Brain oscillations.....	13
1.2.5. EEG frequency rhythms during the awake state.....	14
1.2.5.1. Alpha rhythm.....	14
1.2.5.2. Theta rhythm.....	14
1.2.5.3. Beta rhythm.....	15
1.2.5.4. Gamma and high-gamma rhythms.....	16
1.3. Electroencephalography as a diagnostic and research tool in DLB.....	18
1.3.1. EEG changes in DLB.....	18
1.3.2. EEG signatures of cognitive fluctuations in DLB.....	18
1.3.3. Polysomnography .....	20
1.3.4. Hyperexcitability in dementia .....	21
1.4. Sleep .....	24
1.4.1. Sleep architecture and microstructure .....	24
1.4.2. Neuronal mechanisms of SWS in the cortex .....	24
1.4.3. Neuronal mechanisms of SWS in hippocampus.....	27

1.4.4.	Oscillatory patterns accompanying SWS and their mechanisms of generation .....	28
1.4.4.1.	Sleep spindles .....	28
1.4.4.2.	Sharp wave ripples .....	29
1.4.4.3.	Higher frequency oscillations nested on the Up-state.....	29
1.4.5.	REM sleep and waking.....	30
1.4.6.	Sleep microstructure .....	33
1.5.	Sleep and memory consolidation .....	35
1.5.1.	Slow wave sleep as a framework for synaptic plasticity .....	35
1.5.2.	High frequency rhythms are involved in memory consolidation.....	35
1.5.2.1.	Spindles.....	35
1.5.2.2.	Sharp-wave ripples (SWRs).....	36
1.5.2.3.	High frequency oscillations on the Up-state.....	36
1.5.2.4.	Interactions between spindles, SWRs and high frequency oscillations .....	37
1.5.3.	REM sleep and memory.....	38
1.6.	Sleep and dementia .....	39
1.6.1.	Sleep-related EEG alterations in dementia patients .....	39
1.6.2.	Sleep and cognition in dementia .....	40
1.6.3.	Sleep and epilepsy in dementia .....	41
1.7.	Modelling dementia and sleep.....	42
1.7.1.	Animal models of dementia .....	42
1.7.1.1.	The A30P mouse model .....	43
1.7.2.	EEG changes in mouse models of $\alpha$ -synucleinopathy .....	44
1.7.3.	The mechanisms underlying sleep changes in dementia .....	47
1.7.3.1.	Dementia pathology interfering with sleep .....	47
1.7.3.2.	Sleep interfering with dementia pathology .....	48
1.8.	Thesis objectives.....	50
1.8.1.	EEG changes in DLB patients.....	50
1.8.2.	Sleep study in the A30P mouse model of dementia.....	50
1.8.3.	Aims .....	53
<b>2.</b>	<b>Methods.....</b>	<b>54</b>
2.1.	Human EEG analysis .....	56
2.1.1.	Diagnostic groups.....	56
2.1.2.	EEG recordings.....	56
2.1.3.	Pre-processing .....	57
2.1.4.	Variable extraction .....	58

2.1.5.	Statistical analysis .....	59
2.2.	Animal electrophysiological recordings.....	61
2.2.1.	Animals.....	61
2.2.2.	Anaesthesia and Surgery .....	61
2.2.3.	Data recording and acquisition .....	62
2.2.4.	Histological verification of recording site position.....	63
2.2.5.	Data Analysis.....	63
2.2.6.	Spindle detection .....	69
2.2.7.	Sharp wave ripple detection .....	69
2.2.8.	Statistical analysis .....	72
<b>3.</b>	<b>Human EEG analysis.....</b>	<b>73</b>
3.1.	Introduction.....	75
3.2.	Methods.....	77
3.3.	Results.....	79
3.3.1.	Data and Demographics .....	79
3.3.2.	Changes in percentage power in patients with dementia.....	80
3.3.3.	Changes in the dominant frequency (DF) in dementia patients .....	82
3.3.4.	Changes in the DF prevalence (DFP) in dementia patients.....	84
3.3.5.	The DF variability (DFV) in dementia patients .....	86
3.3.6.	Correlation between the CAF score and the DFV.....	88
3.3.7.	Exploratory GEE and ROC curve analysis .....	88
3.4.	Discussion .....	90
3.4.1.	Summary of the main findings .....	90
3.4.2.	DLB/PDD patients have a slower resting EEG rhythm than healthy controls and AD patients.....	90
3.4.3.	The DFV and cognitive fluctuations correlate only in DLB patients .....	91
3.4.4.	The DFV is greater in AD patients compared to all other diagnostic groups.....	93
3.4.5.	Our study contradicts previous reports in literature.....	95
3.4.6.	QEEG measures can differentiate between AD and DLB patients with high sensitivity and specificity.....	96
3.5.	Conclusion.....	97
<b>4.</b>	<b>Analysis of the SO in A30P animals.....</b>	<b>98</b>
4.1.	Introduction.....	100

4.2.	Methods .....	103
4.3.	Results .....	106
4.3.1.	Characterisation of the SO cycle in the mPFC of A30P mice.....	106
4.3.1.1.	A30P mice have altered SO cycle patterns in the mPFC .....	106
4.3.1.2.	A30P mice have an altered distribution of high frequency activity in the SO cycle in the mPFC.....	109
4.3.2.	Characterisation of the SO cycle in hippocampus of A30P mice.....	113
4.3.2.1.	A30P mice have altered SO cycle patterns in the hippocampus .....	113
4.3.2.2.	A30P mice have an altered distribution of high frequency activity in the SO cycle in the hippocampus .....	113
4.3.3.	A30P mice have altered neuronal firing patterns in relation to the SO.....	116
4.3.4.	No changes in mPFC/CA1 SO coherence in A30P mice .....	119
4.3.5.	Sleep spindles are altered in the mPFC of A30P mice.....	120
4.3.6.	Hippocampal SWRs are normal in A30P mice .....	124
4.4.	Discussion.....	125
4.4.1.	Summary of the main findings.....	125
4.4.2.	A30P mice have aberrant neuronal firing in the mPFC .....	125
4.4.3.	The SO frequency is faster and the Up- and Down-states are shorter in A30P animals .....	126
4.4.4.	Altered network dynamics and hyperexcitability underlie SO disturbances in A30P animals .....	127
4.4.5.	Compensation mechanisms may control $\alpha$ -syn-related network hyperexcitability.....	129
4.4.6.	Possible cholinergic/thalamic implications in the altered SO in A30P animals.....	131
4.4.7.	Changes in high frequency oscillations on the Up-state in A30P mice.....	133
4.4.8.	A30P animals have a spindle dysfunction .....	135
4.4.9.	SWS disturbances can have detrimental effects .....	138
4.4.10.	The subregional profile of the SO in the mPFC.....	139
4.5.	Conclusion .....	140
<b>5.</b>	<b>The infra-slow modulation (ISM).....</b>	<b>141</b>
5.1.	Introduction .....	143
5.2.	Methods .....	145

5.3.	Results.....	152
5.3.1.	General characterisation of the ISM .....	152
5.3.2.	The ISM is characterised by increases in high frequency activity .....	155
5.3.2.1.	Changes in high frequency activity in the SO cycle in the mPFC during the ISM.....	158
5.3.2.2.	Changes in high frequency activity in the SO cycle in the hippocampus during the ISM .....	161
5.3.3.	Changes in SO cycle patterns during the ISM .....	164
5.3.3.1.	SO cycle characterisation in the mPFC during the ISM .....	164
5.3.3.2.	SO cycle characterisation in the hippocampus during the ISM .....	168
5.3.4.	The SO / theta band power ratio increases during the ISM .....	170
5.3.5.	Changes in neuronal firing during the ISM.....	171
5.3.6.	The relative spindle density decreases during the ISM.....	175
5.4.	Discussion .....	176
5.4.1.	Summary of the main findings .....	176
5.4.2.	The ISM is characterised by a shift of power to higher frequency bands.....	176
5.4.3.	The ISM does not reflect the activated state.....	177
5.4.4.	The ISM is an infra slow oscillation (ISO) .....	179
5.4.5.	Neurons change their firing in different ways in relation to the ISM ...	181
5.4.6.	The pre-ISM and post-ISM periods are functionally important.....	182
5.4.7.	The ISM could be initiated by the thalamus or the cholinergic system.....	183
5.4.8.	The ISM influences the SO .....	185
5.5.	Conclusion.....	187
<b>6.</b>	<b>The ISM in A30P animals .....</b>	<b>188</b>
6.1.	Introduction.....	190
6.2.	Methods.....	191
6.3.	Results.....	193
6.3.1.	The ISM core characteristics in A30P mice .....	193
6.3.2.	High frequency oscillatory activity in A30P mice during the ISM .....	195
6.3.2.1.	A30P mice show no changes in high frequency oscillatory power in the mPFC during the ISM.....	195
6.3.2.2.	A30P mice have increased high frequency oscillatory power in the hippocampus during the ISM .....	195
6.3.3.	The properties of the SO in A30P mice during the ISM .....	198

6.3.3.1.	A-syn related changes in the SO cycle in the mPFC during the ISM .....	198
6.3.3.2.	A-syn related changes in the SO cycle in the hippocampus during the ISM .....	201
6.3.4.	The relative spindle density does not change in A30P mice during the ISM.....	203
6.3.5.	Changes in neuronal firing patterns in A30P mice during the ISM .....	203
6.4.	Discussion .....	207
6.4.1.	Summary of the main findings.....	207
6.4.2.	A30P mice show an increase of high frequency oscillatory activity in the hippocampus during the ISM.....	207
6.4.3.	A30P animals have hyperexcitable networks generating high frequency oscillations.....	208
6.4.4.	A30P mice have normal levels of high frequency activity in the mPFC during the ISM.....	209
6.4.5.	The pre-ISM and post-ISM segments are also altered in the CA1 in A30P mice.....	210
6.4.6.	Possible thalamic alterations in A30P mice can influence the ISM ....	211
6.4.7.	A30P animals have altered sleep microstructure .....	211
6.4.8.	The ISM decreases the SO amplitude in the CA1 of A30P mice.....	212
6.4.9.	A30P animals have a less efficient SWS.....	213
6.5.	Conclusion .....	215
<b>7.</b>	<b>Discussion .....</b>	<b>216</b>
7.1.	Overview of the main findings .....	218
7.2.	Early DLB is characterised by an excitation/inhibition imbalance.....	220
7.2.1.	EEG disturbances in DLB patients .....	220
7.2.2.	Hyperexcitability in the A30P mouse model .....	221
7.2.3.	Possible mechanisms underlying hyperexcitability.....	223
7.2.3.1.	Hyperexcitability and altered neuronal membrane dynamics.....	223
7.2.3.2.	A compensation mechanism may control the hyperexcitability .....	225
7.3.	The ISM and the resting state are governed by ISOs .....	227
7.4.	Cholinergic and thalamic implications .....	229
7.5.	SWS disturbances can have detrimental effects .....	231
7.6.	The clinical significance of our findings in A30P mice .....	232
7.7.	Limitations and future work .....	234

7.7.1. Human EEG analysis.....	234
7.7.2. Investigation of the SO and ISM in A30P and WT mice.....	234
<b>Appendix .....</b>	<b>238</b>
Appendix A .....	238
Appendix B .....	239
Appendix C .....	240
Appendix D: .....	244
Appendix E .....	246
Appendix F.....	249
Appendix G.....	250
Appendix H.....	252
<b>References.....</b>	<b>255</b>

## List of figures

<b>Figure 1.1:</b> The spread of pathology in the brain of patients with Lewy body dementia (LDB) according to the Newcastle-McKeith criteria (2017).....	5
<b>Figure 1.2:</b> Architecture of the hippocampus.....	11
<b>Figure 1.3:</b> The dominant frequency variability in patients with AD and DLB and healthy controls. ....	20
<b>Figure 1.4:</b> The dorsal and ventral pathways of the ascending reticular activating system (ARAS) in the rodent brain. ....	32
<b>Figure 1.5:</b> REM/NREM sleep alternations rely upon the interaction between REM-on and REM-off neurons in the dorsal ARAS pathway.....	32
<b>Figure 1.6:</b> Example of the cyclic alternating pattern (CAP) in a human subject during slow wave sleep. ....	34
<b>Figure 2.1:</b> Placement of the 128 electrodes according to the 10-20 placement system. ....	57
<b>Figure 2.2:</b> Schematic diagram illustrating the process of extracting each of the four main quantitative EEG variables used in this study, for one participant in the posterior region. ....	60
<b>Figure 2.3:</b> Methods of acute, <i>in vivo</i> electrophysiological recordings in mice under urethane-induced anaesthesia .....	68
<b>Figure 2.4:</b> Analysis of unit firing in relation to the SO cycle.....	68
<b>Figure 2.5:</b> Spindle detection method in the ACC subregion of the mPFC, during urethane-induced SWS. ....	70
<b>Figure 2.6:</b> Sharp-wave ripple (SWRs) detection method in the CA1 of the hippocampus during urethane-induced SWS. ....	71
<b>Figure 3.1:</b> Analysis of percentage power of the resting state EEG in the dementia sub-groups. ....	81
<b>Figure 3.2:</b> Analysis of the dominant frequency (DF) in the dementia sub-groups. ...	83
<b>Figure 3.3:</b> Analysis of the dominant frequency prevalence (DFP) in the dementia sub-groups. ....	85

<b>Figure 3.4:</b> Analysis of the dominant frequency variability (DFV) in the dementia sub-groups.....	87
<b>Figure 3.5:</b> The capacity of quantitative EEG measures to enable differential DLB/AD diagnosis.....	89
<b>Figure 4.1:</b> Changes in the SO cycle in the mPFC of A30P animals. ....	108
<b>Figure 4.2:</b> Changes in the distribution of the high frequency oscillatory power on the normalised SO cycle in the mPFC of A30P animals. ....	112
<b>Figure 4.3:</b> Changes in the SO cycle in the hippocampus of A30P mice. ....	115
<b>Figure 4.4:</b> Changes in the unit firing patterns in relation to the SO in the mPFC of A30P mice. ....	118
<b>Figure 4.5:</b> The maximum hippocampal/mPFC SO coherence and its frequency in A30P and WT mice.....	119
<b>Figure 4.6:</b> Changes in the sleep spindle characteristics in the mPFC of A30P mice. ....	123
<b>Figure 4.7:</b> Normalised firing rate of narrow-spike cells (red; putative interneurons) and wide-spike cells (blue; putative pyramidal cells) during Up-states. ....	135
<b>Figure 5.1:</b> The PSD across frequency bands during the slow-wave sleep in WT mice. ....	147
<b>Figure 5.2:</b> The ISM identification technique.....	148
<b>Figure 5.3:</b> An example of the LFP and spectrogram of a recording from the mPFC subregions of a WT animal, illustrating the ISM events. ....	153
<b>Figure 5.4:</b> An example of the LFP and spectrogram of an electrophysiological recording from the hippocampus of a WT animal, illustrating the ISM events.....	154
<b>Figure 5.5:</b> Examples of an LFP trace, the high frequency oscillatory power in the SO cycle and the spectrogram from one PrL electrode of the mPFC during the ISM. ..	156
<b>Figure 5.6:</b> Examples of an LFP trace, the high frequency oscillatory power in the SO cycle and the spectrogram from the CA1 region of the hippocampus during the ISM. ....	157
<b>Figure 5.7:</b> Changes in high frequency oscillatory power in the SO cycle in relation to the ISM, in the mPFC of WT animals.....	160

<b>Figure 5.8:</b> Changes in high frequency oscillatory power in the SO cycle in relation to the ISM in the hippocampus of WT animals. ....	163
<b>Figure 5.9:</b> Example traces demonstrating the evolution of the ISM in the LFP and its expression as increased beta band power. ....	166
<b>Figure 5.10:</b> Changes in the SO frequency and amplitude in relation to the ISM in the PrL subregion of the mPFC of WT mice. ....	167
<b>Figure 5.11:</b> Changes in the SO frequency and amplitude in relation to the ISM in the hippocampus of WT mice. ....	169
<b>Figure 5.12:</b> The SO/theta band power ratio in the PrL subregion of the mPFC and the hippocampus of WT animals. ....	170
<b>Figure 5.13:</b> Changes in unit firing patterns in WT animals in relation to the ISM. .	174
<b>Figure 6.1:</b> Changes in ISM frequency in the mPFC of A30P mice. ....	194
<b>Figure 6.2:</b> Changes in high frequency oscillatory power in the SO cycle in relation to the ISM in the hippocampus of A30P mice. ....	197
<b>Figure 6.3:</b> Changes in the SO cycle in relation to the ISM in the PrL subregion of the mPFC of A30P mice. ....	200
<b>Figure 6.4:</b> Changes in the SO cycle in relation to the ISM in the hippocampus of A30P mice. ....	202
<b>Figure 6.5:</b> Changes in neuronal firing patterns in relation to the ISM in the mPFC of A30P mice. ....	206
<b>Figure 7.1:</b> Alterations in the dynamics that govern the Up- and Down-states in local neuronal circuits, in A30P compared to WT mice. ....	227

## List of tables

<b>Table 3.1:</b> Demographics table for the healthy controls and dementia patients who participated in our study.....	79
<b>Table 4.1:</b> Characterisation of the SO cycle in the mPFC of WT and A30P mice. .	107
<b>Table 4.2:</b> Characterisation of the high frequency oscillatory activity in the SO cycle, in the mPFC of WT and A30P mice. ....	111
<b>Table 4.3:</b> Characterisation of the high frequency oscillatory power in the SO cycle in the hippocampus of WT and A30P animals.....	114
<b>Table 4.4:</b> The number of units and the mPFC subregion they were recorded from .....	117
<b>Table 4.5:</b> Characterisation of the unit firing patterns in the mPFC of WT and A30P mice. ....	117
<b>Table 4.6:</b> Sleep spindle characterisation in the mPFC region of A30P and WT animals. ....	122
<b>Table 4.7:</b> Characterisation of sharp wave ripples (SWR) in the CA1 of the hippocampus in WT and A30P animals. ....	124
<b>Table 5.1:</b> The SO/theta band power ratio in relation to the ISM in the mPFC of WT animals. ....	171
<b>Table 5.2:</b> Changes in neuronal firing patterns in relation to the ISM in the mPFC of WT mice.....	173
<b>Table 5.3:</b> The relative spindle density in relation to the ISM in the mPFC of WT mice. ....	175
<b>Table 6.1:</b> The relative spindle density in relation to the ISM in the mPFC of WT and A30P animals.....	203
<b>Table 6.2:</b> Unit firing patterns in relation to the ISM in the mPFC of WT and A30P mice. ....	205

## List of abbreviations

5-HT	5-Hydroxytryptophan
A30P	Alanine to proline exchange in position 30
A $\beta$	Amyloid-beta
ACC	Anterior cingulate cortex
ACh	Acetylcholine
AChI	Acetylcholinesterase inhibitors
AD	Alzheimer's disease
AHP	After-hyperpolarisation
AMPA	$\alpha$ -amino-3-hydroxy-5-methyl-4-isoxazolepropionic acid receptor
ANOVA	Analysis of variance
APP	Amyloid precursor protein
ARAS	Ascending reticular arousal system
ATP	Adenosine triphosphate
A-SYN	Alpha-synuclein
AUC	Area under the curve
BF	Basal forebrain
BOLD	Blood-oxygen-level-dependent
Ca <sup>+</sup>	Calcium ion
CA3-1	Cornus ammonis region 1-3
CAF	Clinician assessment of fluctuations scale
CAMCOG	Cambridge Cognitive Examination
CAP	Cyclic alternating pattern
CF	Cognitive fluctuation
CNS	Central nervous system
CSA	Compressed spectral array
CT	Computed tomography
DAN	Dorsal attention network
DG	Dentate gyrus
DLB	Dementia with Lewy bodies
DF	Dominant frequency
DFP	Dominant frequency prevalence
DFV	Dominant frequency variability
DMN	Default mode network
DNA	Deoxyribonucleic acid
DP	Dorsal peduncular region
E/I	Excitatory/Inhibitory
EC	Entorhinal cortex
EEG	Electroencephalogram
EPSP	Excitatory postsynaptic potential

ER	Entoplasmic reticulum
FFT	Fast Fourier transform
fMRI	Functional MRI
GABA	$\gamma$ -aminobutyric acid
GABA <sub>A</sub> R	GABA <sub>A</sub> receptor
GABA <sub>B</sub> R	GABA <sub>B</sub> receptor
GEE	Generalised estimating equations
ICA	Independent component analysis
IL	Infralimbic cortex
ING	Interneuron gamma
ISI	Inter-spike interval
ISM	Infra-slow modulation
ISO	Infra-slow oscillation
IPSP	Inhibitory postsynaptic potential
IQR	Interquartile range
K <sup>+</sup>	Potassium ion
L-DOPA	Levodopa
LBD	Lewy body dementia
LC	Locus coeruleus
LDT	Laterodorsal tegmentum
LED	Levodopa equivalent dose
LFP	Local field potential
MACHR	Muscarinic acetylcholine receptor
mGluR	Metabotropic glutamate receptor
MMSE	Mini-Mental Scale Exam
MPFC	Medial prefrontal cortex
MPTP	1-methyl-4-phenyl-1,2,3,6-tetrahydropyridine
MRI	Magnetic resonance imaging
MSA	Multiple system atrophy
N1-N4	Sleep stage 1-4
Na <sup>+</sup>	Sodium ion
NACHR	Nicotinic acetylcholine receptor
NMDAR	N-Methyl-D-aspartic acid receptor
NREM	Non rapid eye movement sleep
PCC	Posterior cingulate cortex
PD	Parkinson's disease
PDD	Parkinson's disease dementia
PET	Positron emission tomography
PFA	Paraformaldehyde
PING	Pyramidal-interneuron gamma
PPT	Pedunculopontine tegmentum
PrL	Prelimbic cortex

PSD	Power spectral density
PV+	Parvalbumin positive
QEEG	Quantitative electroencephalography
RBD	Rapid eye movement sleep behaviour disorder
REM	Rapid eye movement
RmANOVA	Repeated measures analysis of variance
RN	Raphe nuclei
ROC	Receiver operating characteristic
RSN	Resting state network
SCN	Suprachiasmatic nucleus
SD	Standard deviation
SEM	Standard error of the mean
SNc	Substantia nigra pars compacta
SO	Slow oscillation
SOM+	Somatostatin positive
SPECT	Single photon emission computed tomography
SWA	Slow wave activity
SWS	Slow wave sleep
TRN	Thalamic reticular nucleus
UPr	Unfolded protein response
UPDRS	Unified Parkinson's Disease Rating Scale
VAN	Ventral attention network
VTA	Ventral tegmental area
WT	Wild type

## **Chapter 1. Introduction**



## **1.1. Dementia with Lewy bodies: pathology and diagnosis**

### **1.1.1. *Lewy body dementia***

According to the World Health Organization, dementia is “an umbrella term for several diseases affecting memory, other cognitive abilities and behaviour that interfere significantly with the ability to maintain daily living activities”. Although age is its strongest risk factor, dementia is not a normal part of ageing (WHO, 2017). The most common subtypes of dementia are progressive neurodegenerative types, including Alzheimer’s disease (AD) accounting for > 80% of all cases, Lewy body dementia (LBD) and frontotemporal dementia (FTD) (Ponjoan et al., 2019). There has been a steep increase in the number of worldwide dementia cases from 35.6 million in 2010 to 50 million in 2017, with the numbers expected to reach 152 million by 2050 (Fymat, 2018). In view of the increasing age of the population in the western world and the enormous economic burden dementia poses for the individual and the state, identifying better and more permanent ways of treating the different dementia subtypes is essential (MacLin et al., 2019).

Lewy body dementia (LBD) is a term encompassing dementia with Lewy bodies (DLB) and Parkinson’s disease dementia (PDD). Both conditions share a common symptom profile, pathology and treatment (McKeith et al., 1996; Walker et al., 2015; McKeith et al., 2004). DLB is the second most common cause of dementia, with Lewy body pathology discovered in approximately 15 - 20% of dementia cases to reach post-mortem examination (Jellinger & Attems, 2011). A recent meta-analysis of epidemiological studies estimated DLB prevalence to reach 7.5% of all dementia cases (Vann Jones & O’Brien, 2014). However, only 5% of dementia patients receive a DLB diagnosis suggesting that DLB is currently underdiagnosed (Kane et al., 2018). The main DLB symptoms are dementia, cognitive fluctuations, rapid eye movement (REM) sleep behaviour disorder (RBD), parkinsonism and visual hallucinations, with all or some symptoms occurring at the same time (McKeith et al., 2017). DLB and PDD are managed in similar ways, but DLB is considered a primary dementia diagnosis and PDD a primary motor diagnosis (Aldridge et al., 2018).

## 1.1.2. ***Dementia pathology***

### 1.1.2.1. *Lewy body dementia*

LBDs are characterised by the presence of abnormal intracellular aggregated  $\alpha$ -synuclein ( $\alpha$ -syn) inclusions, the Lewy bodies, in the somata of neuronal and non-neuronal cells in the brain (Spillantini et al., 1998). Similar inclusions in the neuronal processes are known as Lewy neurites. Lewy body and Lewy neurite pathology is also characteristic of Parkinson's disease (PD), while another  $\alpha$ -synucleinopathy called multiple system atrophy (MSA) is characterised by  $\alpha$ -syn accumulation in oligodendrocytes, but not Lewy body pathology (Jellinger & Lantos, 2010).  $\alpha$ -Synuclein ( $\alpha$ -syn) is a 140 amino-acid protein encoded by the SNCA gene, and it is normally predominantly localized in the pre-synaptic terminal where it is involved in synaptic vesicle trafficking in a neuronal activity-dependent manner (Fortin et al., 2005). Specifically,  $\alpha$ -syn complements the function of cysteine-string protein  $\alpha$  (CSP $\alpha$ ), which is a molecular chaperone that facilitates conformational changes in the synaptic proteins necessary for neurotransmitter release, vesicle recycling and synaptic integrity (Bonini & Giasson, 2005). Pre-synaptic  $\alpha$ -syn also interacts with microtubules, promoting their assembly (Cartelli et al., 2016).

In LBDs,  $\alpha$ -syn becomes misfolded and aggregates to form of oligomers and/or Lewy bodies (Ghosh et al., 2017), hence resulting in a loss of  $\alpha$ -syn function as well as in the formation of toxic protein species that contribute to the neurodegeneration that is evident in LBDs (Kim et al., 2014). Autosomal recessive mutations have been described in the SNCA gene in rare cases of familial of PD, which increase the intrinsic propensity of  $\alpha$ -syn to aggregate (Siddiqui et al., 2016). Although the majority of DLB and PD cases were initially classified as sporadic (Chai & Lim, 2014), today we know that there are a number of genetic factors that can increase the risk of developing these diseases (review by Del Tredici & Braak, 2016). The most interesting findings come from whole genome-association studies (GWAS), which have identified genetic variants in a number of protein-encoding genes that in combination could explain 31% of cases (Guerreiro et al., 2018). Finally, the risk of developing dementia has also been correlated with phenotypic traits such as education, which together with genetic variation factors can explain 60% of DLB cases (Guerreiro et al., 2019).

DLB and PDD cases show a similar spread of pathology, although DLB cases have been proposed to show more pathology in the neocortex, and the PDD cases in

the substantia nigra (SN) (Figure 1.1; Outeiro et al., 2019). Lewy bodies have also been detected in the peripheral nervous system and in several organs including the gastro-intestinal, respiratory and cardiovascular systems of LBD patients (Beach et al., 2010). Interestingly, the Lewy body distribution does not correlate with disease duration, age of onset or the presence or absence of cognitive and motor symptoms (Weisman et al., 2007). Therefore, new theories support the idea that neurotoxicity is in fact mediated by heterogeneously folded oligomeric  $\alpha$ -syn and not Lewy bodies (Ghiglieri et al., 2018). The detrimental effects of  $\alpha$ -syn oligomers have been characterised and include membrane permeabilisation, altered synaptic transmission and plasticity, reduced protein degradation and impairment of mitochondrial and endoplasmic reticular function (Feng et al., 2010; Rockenstein et al., 2014; Tsigelny et al., 2012). Moreover, it has been proposed that the clustering of  $\alpha$ -syn in Lewy bodies may in fact be a neuroprotective mechanism aimed at removing toxic oligomers (Tanaka et al., 2004).

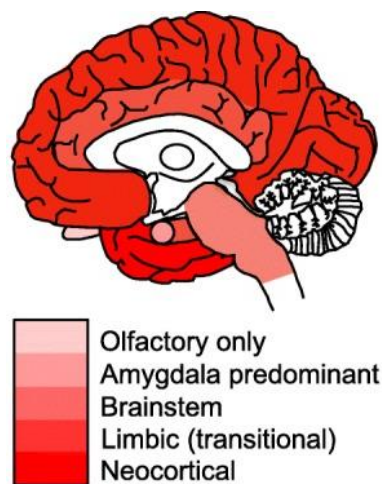


**Figure 1.1:** The spread of pathology in the brain of patients with Lewy body dementia (LBD) according to the Newcastle-McKeith criteria (2017). The main Lewy body staging subtypes in LBD are: the brainstem-dominant (IX/X motor nucleus, locus coeruleus, and substantia nigra), limbic (amygdala, transentorhinal cortex, cingulate cortex), diffuse neocortical (frontal, temporal, parietal, lobes) and the olfactory only, and amygdala predominant stages. Adapted from Outeiro et al., (2019).

#### 1.1.2.2. Alzheimer's disease

The main pathological hallmark of Alzheimer's disease (AD) is the misfolding and aggregation of amyloid- $\beta$  ( $A\beta$ ) and hyper-phosphorylated tau, which cluster to form extracellular amyloid plaques and intracellular neurofibrillary tangles respectively

(Ashford, 2019; Perl, 2010). The most popular hypothesis for the development and spread AD pathology is the amyloid cascade hypothesis, which states that the amyloid precursor protein (APP) is aberrantly processed resulting in greater production than clearance of the A $\beta$  peptide, especially of the “sticky” A $\beta$ 42 isoform (Hardy & Higgins, 1992). A $\beta$ 42 monomers cluster into soluble oligomers, and then into insoluble fibrils of the beta-sheet conformation, before finally forming plaques (Barage & Sonawane, 2015). A $\beta$  oligomers are the main neurotoxic form as they induce oxidative damage and promote tau hyperphosphorylation and hence oligomerisation (Sakono & Zako, 2010; Sengupta et al., 2016). Tau accumulation also has deleterious effects on synapses and mitochondria and correlates better than A $\beta$  with neuronal and synaptic loss (Kumar et al., 2015). Like  $\alpha$ -syn, both A $\beta$ 42 and tau act in a seed-like manner, spreading pathology from subcortical structures, or the entorhinal cortex (EC), to the rest of the brain (DeVos et al., 2018). Late stage amyloid plaques also have a defined toxic effect as they attract microglia, that in turn release proinflammatory cytokines, promoting further A $\beta$ 42 production (Dal Prà et al., 2015)

#### 1.1.2.3. Mixed pathology

LBD and AD pathology often occur concomitantly (Hansen et al., 1989). Post-mortem studies have shown that about a third to half of AD patients have some level of Lewy body pathology (Murray et al., 2010) and vice versa, 50% of DLB patients have amyloid plaques and tau tangles. The cases that were deemed as “mixed” also showed a faster disease evolution, with greater cognitive dysfunction compared to AD and DLB, and greater cortical atrophy compared to DLB (Toledo et al., 2016). Analysis of the cerebrospinal fluid (CSF) can provide valuable insight into early biochemical changes in the brain in relation to dementia, as it comes into direct contact with the extracellular space of the brain (Maji et al., 2010). CSF studies have shown that 40% of DLB patients tested had high levels A $\beta$  that correlated with lower cognition (van Steenoven et al., 2019), and high tau levels that correlated with greater disease severity and mortality (Lemstra et al., 2017). Moreover, tau exists in 50% of LBD pathology and is particularly toxic, as it correlates with greater Lewy body load and faster disease progression (Bohnen & Hu, 2019). Finally, mixed AD/Lewy body pathology is believed to influence the topographic distribution of  $\alpha$ -syn pathology, rendering the areas of their location more susceptible to  $\alpha$ -syn aggregation and neurodegeneration (Outeiro et al., 2019).

### **1.1.3. DLB Diagnosis**

Clinical DLB diagnosis requires the presence of dementia, the central symptom of this disease, which is defined as a progressive cognitive decline (McKeith *et al.*, 2017). In the 2005 consensus DLB criteria, dementia needs to occur in conjunction with two out of three core clinical features of DLB as specified at the time, these are: cognitive fluctuations (CF), recurrent visual hallucinations and parkinsonism, for a probable DLB diagnosis (McKeith *et al.*, 2005). At the updated 2017 criteria, RBD was added as a fourth core feature (McKeith *et al.*, 2017). RBD is a condition where the mechanisms causing muscle atonia during REM sleep are lost and is the best known predictor of synucleinopathies, occurring in 80 – 90% of patients (Peever & Fuller, 2017). In the 2017 DLB criteria (McKeith *et al.*, 2017), the importance of biomarkers was also acknowledged. A biomarker, or “biological marker”, is an objective indication of the medical state of a patient that can be measured accurately and reproducibly (Strimbu & Tavel, 2010). Hence, with the 2017 DLB criteria a probable DLB diagnosis can alternatively be supported by one core clinical feature and one or more biomarker(s), even with the absence of other core clinical features (McKeith *et al.*, 2017).

The suggested indicative biomarkers according to the 2017 DLB criteria include a loss in nigrostriatal dopaminergic neurons that is assessed by single photon emission computed tomography (SPECT) and positron emission tomography (PET) imaging, and changes in the sleep profile assessed by polysomnography (McKeith *et al.*, 2017). Polysomnography measuring brain activity during sleep with concomitant assessment of eye and muscle movement to ensure REM sleep and identify changes in muscle tone respectively, identify RBD with a sensitivity of 98% for synucleinopathies (Boeve *et al.*, 2013). There are also supportive biomarkers, including a relative preservation of medial lobe grey matter assessed by magnetic resonance imaging (MRI) / computed tomography (CT), and changes in the electroencephalogram (EEG; Cromarty *et al.*, 2016), which are the focus of this thesis and are extensively discussed below (section 1.3.1).

Although it is currently too early for a rigorous assessment of the specificity and sensitivity of the 2017 criteria, the specificity and sensitivity of the 2005 criteria has been improving over time (Rizzo *et al.*, 2018). A 2013 meta-analysis has estimated high specificity for DLB diagnosis at 79-100% (Huang *et al.*, 2013), suggesting that this

high percentage of patients diagnosed with DLB had indeed received the right diagnosis. However, the same study found a low sensitivity in DLB diagnosis ranging from a low of 12% to 88% (Huang et al., 2013), suggesting that several DLB patients did not receive a DLB diagnosis. The low sensitivity in diagnosing DLB can at least partly be attributed to the misdiagnosis of DLB as AD, especially at early disease stages, as DLB can have a similar diagnostic profile to AD characterised by progressive cognitive decline (Metzler-Baddeley, 2007). Since LBD patients are sensitive to neuroleptics (McKeith et al., 1992) and demonstrate a faster disease progression (Olichney et al., 1998), an early, accurate diagnosis is important.

In order to distinguish between PDD and DLB an arbitrary 1-year rule was introduced, where the occurrence of dementia before, or within 1 year after motor features appear, leads to a primary DLB diagnosis (McKeith et al., 2005). However, distinguishing between PDD and DLB is not as critical as distinguishing between DLB and AD, as the patients usually have similar disease management and treatments. However, when it comes to routine patient care, differentiating a primary movement disorder or dementia diagnosis can be important (Lippa et al., 2007). As previously mentioned, the Lewy pathology in PDD and DLB is identical in terms of the molecular profile of  $\alpha$ -syn aggregation and may only have subtle differences in the progression of pathology (section 1.1.2.1; Outeiro et al., 2019).

## **1.2. The electrophysiological rhythms of the brain during wakefulness**

### **1.2.1. *Origin of the EEG***

Ionic transmembrane currents in the brain produced by the synchronised activity of large neuronal populations (Henry, 2006). Excitatory postsynaptic potentials (EPSPs) arise due to the inflow of positive ions (e.g. Na<sup>+</sup>) while inhibitory post-synaptic potentials (IPSP), arise either by the inflow of negative ions (e.g. Cl<sup>-</sup>) or the outflow of positive ions (e.g. K<sup>+</sup>) (Amzica & da Silva, 2017). This ion movement results in the formation of active sinks and sources in the extracellular space around the active excitatory and inhibitory synapse that are compensated by currents of the opposite direction along the soma-dendritic membrane, resulting in a sink-source configuration (dipole) (Henry, 2006). The dendrites of cortical pyramidal neurons are aligned perpendicularly to the cortical surface and when these cells are activated in a synchronous way, they form electrical dipoles between the soma and apical dendrites (da Silva, 2009). These dipoles are detectable by electrodes on the surface of the scalp during electroencephalography (EEG), or through surface or intra-cortical electrode probes most commonly used in animal models (Hooper & Schmidt, 2017).

In the next paragraphs we will examine the neuronal circuits of the hippocampus and the medial prefrontal cortex (mPFC), two regions that are involved in cognitive function with a pivotal role in memory consolidation (Colgin, 2011). These circuits are particularly rich in pyramidal neurons that release the neurotransmitter glutamate, the most abundant excitatory neurotransmitter in the brain (Spruston, 2008). The hippocampal and cortical circuits are also rich in different subtypes of interneurons, which release the neurotransmitter  $\gamma$ -amino-butyric acid (GABA) and have an inhibitory function (Massi et al., 2012). Neurotransmitters are chemical agents that bind to specific receptors and induce EPSPs or IPSPs on target cells, depending on whether they have an excitatory or an inhibitory function (Snyder, 2017). Glutamate binds to the ionotropic N-methyl-D-aspartate receptors (NMDAR), 2  $\alpha$ -amino-3-hydroxy-5-methyl-4-isoxazolepropionic acid receptors (AMPA) and kainate receptors, directly eliciting the opening of an ion channel in the cell membrane, allowing the inflow of ions into the target neuron (Meldrum, 2000). Glutamate also binds to metabotropic receptors (mGluR1-8), initiating an intracellular signalling cascade that can lead to a change in membrane potential (Meldrum, 2000). GABA can bind to the ionotropic

GABA<sub>A</sub> receptor (GABA<sub>A</sub>R) and the metabotropic GABA<sub>B</sub> receptor (GABA<sub>B</sub>R), inducing inhibition in the target neuron.

Another type of neurotransmitter that will be discussed in this thesis is acetylcholine (ACh) which acts as a neuromodulator in the brain, as it can be either excitatory or inhibitory, ultimately changing the state of a group of neurons in response to a change in the environmental conditions (Picciotto et al., 2012). ACh acts through two types of receptors that can be pre- and post-synaptic: metabotropic muscarinic receptors (mAChRs) that can have an inhibitory or excitatory effect, and ionotropic nicotinic receptors (nAChRs) that always have an excitatory effect (Changeux et al., 1998). Other neurotransmitters that act as neuromodulators in the brain are dopamine, serotonin and norepinephrine (Avery & Krichmar, 2017). Dopamine originates from the ventral tegmental area (VTA) or the substantia nigra pars compacta (SNc) and acts through the dopaminergic receptors D1-D5 found in the striatum, thalamus, amygdala, hippocampus, and PFC. Serotonin originates from the raphe nuclei (RN) and acts on 5-HT receptors in the cortex, ventral striatum, hippocampus, and amygdala, while norepinephrine originates from the locus coeruleus (LC) and acts on adrenergic receptors in numerous cortical and sub-cortical regions (review by Avery & Krichmar, 2017).

### **1.2.2. The hippocampus**

The hippocampus is a structure that lies deep in the medial temporal cortex and consists of the dentate gyrus (DG), the subiculum and the pyramidal *cornu ammonis* (CA) and its subfields (CA1 - 4; Figure 1.2; review by Somogyi et al., 2010). As mentioned above, the hippocampus is composed of pyramidal neurons, and inhibitory GABAergic interneurons that make up about 10% of the total neuronal population (Buzsáki et al., 1983). The pyramidal cell somata are in the pyramidal layer and their basal dendrites arborise in the *stratum oriens* and the apical dendrites in the *stratum radiatum* and *lacunosum moleculare* (Freund & Buzsáki, 1998). In the hippocampus there is a large population of parvalbumin expressing (PV+) interneurons, reaching 20 - 25% of all interneurons. PV+ interneurons are fast spiking and can be classified as basket cells or axo-axonic/chandelier cells. Each PV+ basket cell contacts the cell soma and proximal dendrites of > 1500 - 2500 pyramidal cells, while axo-axonic interneurons contact the axons of > 1000 pyramidal cells (Klausberger & Somogyi, 2008). Interneurons contact both pyramidal cells and other interneurons, while both

interneurons and pyramidal cells are regulated by cholinergic, dopaminergic, serotonergic and noradrenergic neurons (Avery & Krichmar, 2017).

The hippocampus has a pivotal role in memory as was evident early in patients with hippocampal damage, who were impaired in forming and recalling declarative episodic memories, especially ones recently formed (Clark et al., 2005; Savage et al., 2004; Bird & Burgess, 2008). The hippocampus may influence long-established episodic memory but is not involved in declarative semantic memory (Kropotov & Kropotov, 2009a). Rodent studies have revealed that the hippocampus is also pivotal for spatial memory formation through the activity of place cells, which fire when the animal is located at specific locations during exploration (O'Keefe et al., 1998; Booth & Poe, 2006). These neuronal representations of space are stable for a long time and have "replay" activation patterns during sleep, that are believed to underlie memory transfer to the cortex (Bird & Burgess, 2008).

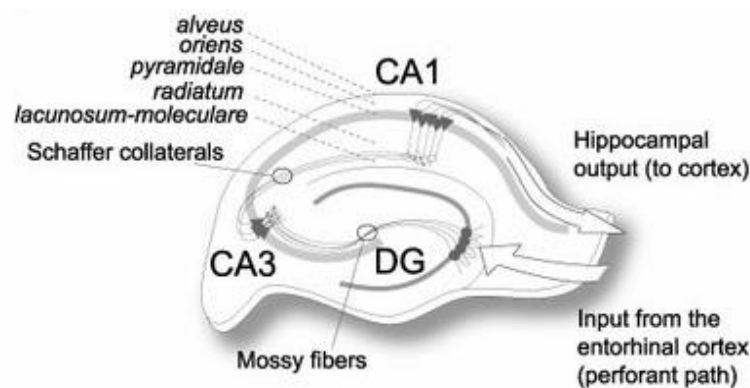


**Figure 1.2:** Architecture of the hippocampus. The laminae of the hippocampus and the main neuronal circuits of the hippocampus are shown. Information enters the hippocampus through the entorhinal cortex (EC) and then projects into the dentate gyrus (DG) via the perforant pathway, and then from the DG to the CA3 via the mossy fibre pathway. The CA3 projects to the CA1 via the Schaffer collaterals and eventually the CA1 projects back to the EC. CA3 axons also contact CA3 somata in a recurrent feedback loop, while the EC contacts directly the CA3 and CA1 regions (not shown). Adapted from Uusisaari (2003).

### 1.2.3. *The medial prefrontal cortex (mPFC)*

The neocortex is the largest region of the cortex and is responsible for the more complex brain functions characterising mammals. The neocortex has a stratified pattern of six layers, each with different neuronal populations, connectivity and function, while it is also divided into different areas, characterised by a different

cytoarchitecture, connectivity, function and gene expression (O'Leary et al., 2007). The prefrontal cortex (PFC) is one of the most recently evolved neocortical areas in the history of mammals, and is highly interconnected with the thalamus, brainstem, basal ganglia, and limbic system (Fuster, 2001). In humans, the PFC is disproportionately large compared to other species including rodents and primates (Donahue et al., 2018). Moreover, the human and non-human primate PFC can be divided into the ventromedial region (orbitofrontal and medial areas) that is associated with emotional processing, memory and higher-order processing, and the dorsolateral (posterior area) region that is associated with motor control, sensory processing and performance monitoring (Wood & Grafman, 2003).

In the rodent brain, the medial PFC (mPFC) is functionally subdivided in a manner that was deemed anatomically and functionally similar to the ventromedial PFC in non-human primates, and to a lesser extent to the dorsolateral region (Uylings et al., 2003). Specifically, the rodent mPFC is important for higher order cognitive functioning including working memory, executive functioning such as decision-making, goal orientated behaviours and attentional selection (Euston et al., 2012). The rodent mPFC is divided on an architectural and functional basis into the anterior cingulate cortex (ACC), prelimbic (PrL), infralimbic (IL) and dorsal peduncular (DP) regions (Van De Werd et al., 2010). Moreover, there is a ventral-dorsal gradient of specialisation across the mPFC, with the ventral mPFC (DP, IL, ventral PrL) being involved in autonomic/emotional control, and the dorsal mPFC (dorsal PrL and ACC) in the control of actions (Riga et al., 2014). This specialisation can be attributed to the interconnectivity of these regions with other structures, as the ventral mPFC communicates with areas involved in pain perception, homeostatic drive, stress and anxiety (Riga et al., 2014), while the dorsal mPFC communicates with sensory/motor areas and projects directly to the spinal cord (Euston et al., 2012).

The mPFC network consists of pyramidal neurons (80 – 90%) and GABAergic interneurons including fast-spiking PV+ interneurons and somatostatin positive (SOM+) interneurons (Riga et al., 2014). PV+ interneurons exert powerful and widespread inhibition on pyramidal cell firing that generates fast local rhythms, while the effect of SOM+ interneurons on the pyramidal firing is weaker and more variable, as they are believed to control long-range inputs in the region (Kvitsiani et al., 2013). In terms of laminar organisation, pyramidal cells are located in both superficial (layers

2-3) and deep (layers 5-6) layers of the mPFC. The mPFC layers and regions are highly interconnected with one another, integrating the different inputs to the mPFC (see below), before projecting to numerous cortical and subcortical regions, exerting control over autonomic, limbic and cognitive function (Riga et al., 2014).

Both deep and superficial mPFC layers receive long-range inputs from cortical and subcortical structures, including the thalamus (Riga et al., 2014). The thalamus is a complex of diencephalic nuclei that relays information to the cortex, mediating the processes of sensation, perception and consciousness (Rikhye et al., 2018). There is a strong thalamic input to the mPFC, with terminals on both pyramidal cells and interneurons (Cruikshank *et al.*, 2012). The mPFC also receives dense afferents from the hippocampus but interestingly, the mPFC has no direct link back to the hippocampus in rodents and other species. The influence of the mPFC over the hippocampus is mediated via projections to the EC and to the nucleus reuniens, where mPFC terminals contact the dendrites of cells that directly excite hippocampal neurons, particularly in the CA1 (Vertes et al., 2007; Bertram & Zhang, 1999). The mPFC also receives noradrenergic and dopaminergic inputs, which play a role in working memory, attention, wakefulness and arousal (Riga et al., 2014).

#### **1.2.4. Brain oscillations**

The EEG signal is a composite of different sinusoidal waves that have been categorised according to their frequency into distinct bands named after Greek letter nomenclature. The main frequency bands that can be seen in the awake state in humans are theta (4 Hz – 8 Hz), alpha (8 Hz – 15 Hz), beta (15 Hz – 30 Hz) gamma (30 – 80 Hz) and high-gamma (> 80 Hz), and they are also characterised by distinct regional distribution and function (Teplan, 2002; Kropotov 2009). Faster rhythms are associated with more cognitively active states and are generally generated locally, while slow rhythms are more widespread and predominate during rest and sleep (Wang, 2010). Often, these rhythms are competing but they can also coexist within the same structures or networks, interacting with one another (Buzsaki & Draguhn, 2004). Therefore, analysis of oscillation patterns can provide rich information that can be traced to alterations in communication between and within neuronal networks in relation to behaviour in the different types of dementia (Babiloni et al., 2006; Barber et al., 2000; Jackson et al., 2008). Quantitative EEG (qEEG) is a computational approach of analysis that decomposes and recomposes the EEG signal ( $\mu\text{V}$  in time) as power

over frequency ( $\mu\text{V}^2/\text{Hz}$ ), allowing for the extraction of information about the patterns characterising the different rhythms (da Silva, 2009).

## **1.2.5. EEG frequency rhythms during the awake state**

### **1.2.5.1. Alpha rhythm**

Alpha activity occurring at 8 – 15 Hz in humans is the resting rhythm of the brain. Spontaneous alpha activity in humans is upregulated during internal mental states, and downregulated with attentional shifts to the external world and during various cognitive tasks (Knyazev et al., 2011). Alpha activity is comprised of different components of thalamo-cortical and cortico-cortical origin (Moretti, 2015). Loss of long-range synchrony in lower frequency alpha activity (8 – 10 Hz) occurs during attentional demands; while upper frequency alpha activity (10 – 14 Hz) is local and occurs during active cognitive processing (Klimesch et al., 2007). Functional MRI (fMRI) and EEG studies in humans have shown that increases in long-range alpha power occur during rest, and are thought to reflect a widespread, top-down inhibition of non-essential activity, allowing a state of internal reflection. Decreases in alpha power reflect a loss of the aforementioned inhibition, as local, fast oscillatory activity emerges upon a shift of attention to the external world (Klimesch et al., 2007; Bazanova & Vernon, 2014).

Resting state networks (RSNs) are widespread networks in the brain that show high levels of synchronous activity during rest (Knyazev et al., 2011). Hence, the widespread alpha oscillation is ideal for modulating faster oscillatory activity in the nodes of these networks, in a tightly regulated manner (Klimesch et al., 2007). The most extensively studied RSN is the default mode network (DMN). Spontaneous DMN activity is upregulated during internal states, self-referential thoughts, episodic and autobiographic memory retrieval and integration of cognitive and emotional processing, and downregulated upon attention-demanding states (Binnewijzend et al., 2012). Key regions in the DMN are the precuneus/posterior cingulate cortex (PCC), the mPFC and the medial and lateral inferior parietal cortices (Knyazev et al., 2011).

### **1.2.5.2. Theta rhythm**

Theta activity is recorded at 4 – 8 Hz in humans, and at 4 – 7 Hz in rodents. There are two main types of theta, frontal-medial (FM-theta) and hippocampal theta (Scheeringa et al., 2008; Wulff et al., 2009). FM-theta in humans is a task-related rhythm that appears during mental tasks that demand attention and working memory

(Mitchell et al., 2008). Functional MRI studies in humans have shown that theta power decreases during rest in the areas that are associated with DMN. Upon engagement in working memory related tasks, FM-theta increases in the hippocampus and the temporal, cingulate and frontal cortices (Scheeringa et al., 2008), suggesting that it is actively involved in cognition. FM-theta originates from the mid-cingulate cortex, an area that receives and integrates cortical and sub-cortical information and the pre-supplementary motor area. This topology suggests a role for the theta rhythm in synchronising goal-orientated information in order to make a decision (Cavanagh & Frank, 2014). Recently, similar synchronisation of FM-theta was shown between motor areas and the mPFC in rodents, suggesting that theta activity underlies behavioural adaptation in these animals, similar to humans (Narayanan et al., 2006).

Hippocampal theta activity has been most extensively studied in rodents (Gottesmann, 1992) and arises during movement, while it is also involved in active perceiving of stimuli, as it is present while whisking and sniffing (Molter et al., 2012). Thus, it has been suggested that hippocampal theta contains ongoing sensory information linking it with information from other modalities or related to motivational or emotional states (Colgin, 2013). In rodents, this rhythm is generated in the medial septum (MS) through pacemaker GABAergic cells that fire rhythmically at theta frequencies and are phase-locked to theta rhythms in the hippocampus (Stewart & Fox, 1989). Although theta oscillations have been recorded in the human hippocampus (Cantero et al., 2003), rodent hippocampal theta activity is believed to be analogous to a slower, 1.5 – 3 Hz rhythm in humans (Ferrara et al., 2012). Hippocampal and cortical theta oscillations are separate rhythms. Nonetheless, rodent studies have shown that the two theta rhythms become synchronous during exploratory activity in the context of decision-making (Scheeringa et al., 2008; Remondes & Wilson, 2013).

#### 1.2.5.3. Beta rhythm

Beta frequency activity (15 – 30 Hz) was originally thought to reflect an idling rhythm of the human motor system, as it maintains the status quo and resists new movement (Kropotov & Kropotov, 2009b). However, beta activity is now known to be associated with cognitive functions, specifically in normal awake states, when a person is attentive or engaged in problem solving and decision-making (Engel & Fries, 2010). Similar to its function in the motor system, the beta rhythm is also associated with maintaining the current cognitive state, as beta activity increases with top-down

control, and decreases with the input of external information (Engel & Fries, 2010). Consistent with this, beta activity decreases during attention demanding tasks and increases upon self-referential thinking, a profile that is similar to the activation in DMN regions such as the parietal cortices, precuneus and mPFC (Mantini et al., 2007). Thus, beta frequency activity seems to maintain the status-quo of the DMN (Neuner et al., 2014).

In the somatosensory cortex beta frequency oscillations are generated by layer 5 pyramidal cells influenced by low-threshold spiking SOM+ interneurons in layer 1, that fire at 5 – 30 Hz (Li et al., 2013). SOM+ interneurons are interlinked through assemblies of intercellular channels called the gap-junctions that allow direct cell–cell transfer of ions and small molecules (Roopun et al., 2006). Moreover, PV+ interneurons are modulated by pyramidal cells in a feedforward manner (Roopun et al., 2006), and receive corticothalamic input (Nigro et al., 2018). Interestingly, it was recently shown that the local silencing of PV+ interneurons induced an increase in beta power in the cortex, especially in deep cortical layers. Thus, PV+ interneurons might control the emergence of the beta rhythm by inhibiting the SOM+ interneurons that drive beta oscillations (Kuki et al., 2015). Hence, the interaction between PV+ and SOM+ interneurons drives the balance between gamma and beta rhythms (see below about the gamma rhythm).

#### 1.2.5.4. *Gamma and high-gamma rhythms*

Gamma frequency oscillations (30 – 80 Hz) have been identified in several cortical and sub-cortical regions, especially the hippocampus (Buzsáki & Silva, 2012). Gamma activity can be viewed as a “signature of engaged networks”, as it is modulated by sensory input and internal processes like attention, working memory and learning (Jia & Kohn, 2011). The gamma rhythm therefore, provides a means of linking distributed cell assemblies processing relevant information together to carry out higher cognitive tasks (Colgin et al., 2009). In the rodent hippocampus, gamma frequency oscillations have been shown to interact closely with theta oscillations in the context of learning. During spatial learning paradigms, the “place cells” encoding different spatial information fire at gamma frequencies on a progressively earlier phase of the theta cycle across successive theta cycles. Hence, early gamma activity on the theta cycles may represent compressed representations of space and/or future locations (Colgin, 2013). Hippocampal theta phase also influences the amplitude of gamma waves and

the phase of high-gamma frequency waves during active exploration REM sleep (Belluscio et al., 2012).

Gamma frequency oscillations have been particularly well studied in the hippocampus, although this rhythm can also be recorded in the neocortex (Bartos et al., 2007; Whittington & Traub, 2003). The generation of gamma oscillations depends upon the activity of fast-spiking, PV+ interneurons, as their firing is phase-locked to gamma oscillations, in both the hippocampus and cortex (Klausberger & Somogyi, 2008; Colgin & Moser, 2010; Tukker et al., 2007; Sohal et al., 2009). Two main models of gamma-generation have been proposed for the hippocampal gamma generator, the interneuron network gamma (ING) model and the pyramidal-ING (PING) model. According to ING, gamma generation depends on interneurons and is maintained and propagated by gap-junctions (Jia & Kohn, 2011; Craig & McBain, 2015). However, this model applies to more local neuronal assemblies, and cannot explain the wide spread of the gamma rhythm seen in the neocortex (Neske & Connors, 2016). The PING model suggests that pyramidal cells fire EPSPs on PV+ interneurons that in turn evoke IPSPs that inhibit the pyramidal cells. This recurrent cycle gives rise to gamma oscillations and is a favourable model of gamma generation in both the CA3 region of the hippocampus and the cortex (review by Whittington et al., 2000).

The hippocampus generates both low frequency gamma (30 – 80 Hz) and high frequency gamma activity (> 80 Hz). These two rhythms have different functional roles and are generated by partly distinct, and partly overlapping, classes of GABAergic interneurons (Colgin & Moser, 2010). Fast-gamma in the hippocampus and the EC is thought to promote the transition and encoding of sensory information to the hippocampus and dominates during exploration (Colgin et al., 2009). On the other hand, slower gamma activity is important for memory retrieval as it increases with exploration in familiar environments and with correct performance in associative memory tasks (Colgin et al., 2009). These two gamma rhythms are also of different origins, with slower gamma activity generated in the CA3 region and propagated to the CA1, and faster gamma activity generated in the EC and then relayed to the DG (Colgin & Moser, 2010). Both low gamma and high-gamma are relayed to the CA1 region from the CA3, and modulate its activity, although the CA1 can also generate its own, faster gamma rhythm *in vitro* (62 – 100 Hz) (Butler et al., 2016; Wulff et al., 2009).

### **1.3. Electroencephalography as a diagnostic and research tool in DLB**

#### **1.3.1. *EEG changes in DLB***

Numerous studies have shown alterations in the EEG of patients with different dementia subtypes. A well-established EEG finding is a shift of the dominant alpha rhythm towards the lower theta range that is evident throughout the cortex, especially in posterior regions (Briel et al., 1999; Neufeld et al., 1994; Stylianou et al., 2018). This dominant frequency (DF) slowing has been included as a supportive biomarker with the new diagnostic criteria for DLB (McKeith et al., 2017). A similar “EEG slowing” can also be seen in AD patients but only in the more advanced stages of the disease (Jackson et al., 2008). A number of studies have shown that a variety of qEEG measures, including measures of reactivity and paroxysmal activity (Roks et al., 2008), coherence (Snaedal et al., 2012), temporal variability in frequency (Andersson et al., 2008), even combinations < 25 different qEEG variables, could differentiate DLB patients, AD patients and controls with high sensitivity and specificity (Garn et al., 2017).

#### **1.3.2. *EEG signatures of cognitive fluctuations in DLB***

Specific qEEG patterns have also been shown to relate to cognitive fluctuations (CF), one of the core symptoms for DLB diagnosis. CFs are defined as spontaneous alterations in cognition, attention and arousal (McKeith et al., 2004). Although CF-like events are seen in all major dementia diseases, they have been established as a target for differential DLB diagnosis due to their higher prevalence in DLB, reaching 90% of cases compared to 20% of AD, 35 - 50% of vascular dementia and 29% of PDD cases. CFs are also qualitatively different between DLB and AD as in DLB they relate more to executive and perceptual performance, and in AD they are primarily linked to forgetfulness and confusion (Zupancic et al., 2011). Recent studies have identified CFs at the prodromal stage of DLB, where the presence of CFs predict the conversion from non-amnesic mild cognitive decline to full DLB (Sadiq et al., 2017). Clinical scales have been devised for the psychometric assessment of fluctuations, including the Clinician Assessment of Fluctuation (CAF) scale (Walker et al., 2000). One systematic review has demonstrated that the clinical scales of CFs are of moderate quality in differentiating between the commonalities of AD and DLB (Lee et al. 2012). The authors of this review suggested that the restricted capacity of these clinical scales to

identify CFs, may be attributed to the high variability in severity and in the time window in which CFs occur (Lee et al. 2012).

The nature of CFs, and the fact that they appear and disappear irrespective of external stimuli, suggest that they are the product of internally driven processes (Bradshaw et al., 2004). Thus, qEEG was considered a suitable means of detecting underlying network changes related to CFs that could possibly be developed into a DLB biomarker. Early qEEG work showed a correlation between epoch-by-epoch variability in the dominant frequency (DF) and CFs, as measured by the CAF score, in DLB patients compared to healthy controls (Walker et al., 2000). Another study also showed that DLB patients had greater DF variability (DFV) compared to AD patients in posterior derivations, and used the DFV (together with other qEEG measures) to group the patients into diagnostic groups with high accuracy (Bonanni et al. 2008; Figure 1.3). The Bonanni group later applied the same method on the data from different cohorts of patients from different institutions, and obtained similar results (Bonanni et al., 2016). The increase in DFV found in DLB patients was interpreted as an increase in dynamic brain function, resulting in abnormal shifts of the DMN from the resting state to attentional states and vice versa, giving rise to CFs.

Recent evidence contradicts the aforementioned theory of increased dynamic brain function in DLB, and suggest that DLB is characterised by a lack of dynamic brain function instead. fMRI studies have shown prolonged cognitive processing in the DMN of DLB patients (Firbank et al., 2018), and a more temporally rigid global network in DLB patients compared to healthy controls (Schumacher et al., 2018). Moreover, Schumacher et al. (2019) showed a reduction in shifts between the EEG-microstates, ~100 ms long periods that represent the EEG correlates of fMRI resting-state networks, in DLB compared to AD patients and healthy controls. Interestingly, the magnitude of the reduction in the EEG-microstate shifts was correlated with CFs in the DLB patients. These findings led the authors to suggest that CFs in DLB patients are related to a reduction in resting state variability (Schumacher et al., 2019).

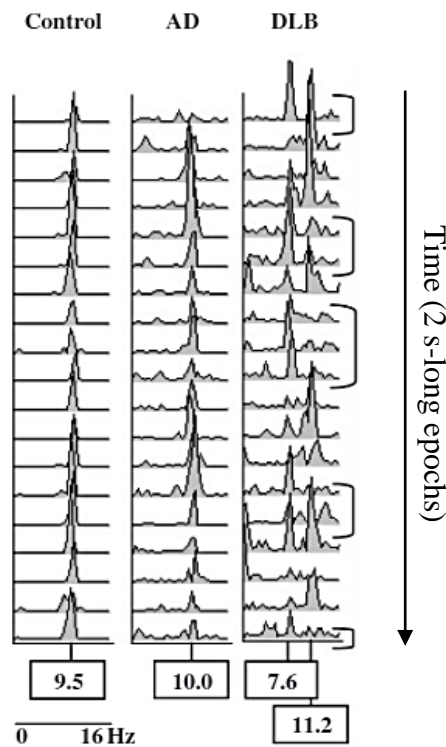


**Figure 1.3:** The dominant frequency variability in patients with AD and DLB and healthy controls. The compressed spectral array (CSA) of EEG recordings from occipital derivations in one control, one AD patients and one DLB patient. The CSA shows the dominant frequency (DF) which is the frequency with the highest power, as recorded in 2 s-long epochs. The occurrence of more than one peaks and the shift in the DF over time in the DLB group represents the DF variability (DFV). Adapted from Bonanni et al. (2008).

### 1.3.3. Polysomnography

Another EEG-related biomarker of DLB is polysomnography. As mentioned earlier, RBD is one of the core symptoms of DLB and polysomnography, which is a sleep EEG, can help identify these events (Donaghy & McKeith, 2014). Polysomnography can help detect REM sleep that is characterised by theta frequency activity in the brain, while simultaneous electro-oculography records the accompanying increase in eye movement. The concurrent loss of muscle atonia that characterises RBD can be measured by chin movements recorded through the electromyogram (Boeve et al., 2003). This biomarker has a very high specificity of 98% for synucleinopathies (Boeve et al., 2003), and 84% for DLB cases confirmed post-mortem (Ferman et al., 2011).

#### **1.3.4. *Hyperexcitability in dementia***

Seizures manifest in the EEG as uncontrolled activity in the brain and an epilepsy diagnosis is given to a patient following two or more seizures (Stafstrom & Carmant, 2015). The clinical picture of seizures can differ according to their site(s) of onset and extend of spread in the brain (Stafstrom & Carmant, 2015). Seizures of focal onset can be accompanied by impairment of awareness or not, and can have a motor or non-motor manifestation. Generalised onset seizures are characterised by impaired awareness and can have non-motor (absence seizures) or a motor manifestation (Stafstrom & Carmant, 2015). The most common type of seizures are tonic-clonic seizures, which last about a minute and involve a mix of sudden muscle stiffness and rhythmic jerking in a set pattern, as well as other symptoms (Guerrini & Takahashi, 2013).

There is increasing evidence for a relationship between epilepsy and dementia, with most studies focusing on AD. AD patients have a 10-fold increased risk of developing seizures and epilepsy compared to age-matched controls, while the incidence of seizures amongst AD patients reaches 8 – 20% (Friedman et al., 2012). Moreover, patients with early onset AD are even more likely to develop seizures, suggesting a connection between AD-pathology and epilepsy (Sánchez et al., 2018). The most common type of seizures seen in AD are complex partial seizures that are characterised by déjà vu or jamais vu, speech arrest, staring spells, unexplained emotions or sensory phenomena (Vossel et al., 2014). These seizures are highly associated with AD-related hippocampal sclerosis. Models of temporal lobe epilepsy have shown that the cell loss and/or changes in the hippocampal circuits result in excitability within the network that cannot be contained, so-called hyperexcitability (Vossel et al., 2014). Changes in hippocampal circuits, such as cell-loss and gliosis in the CA1 region, are one of the pathological hallmarks of AD and are associated with A $\beta$  accumulation (Serrano-Pozo et al., 2011).

Early demographic studies led to the assumption that epilepsy was a late result of AD pathology. However, recent evidence suggests that epileptiform activity can in fact contribute to dementia-related cognitive decline as epilepsy emerges soon after (within 6 years) or even before any cognitive symptoms (Sarkis et al., 2016). In line with these findings a study by Vossel et al. (2017) investigated for epileptiform activity in 33 AD patients without seizure history using overnight video-EEG and

magnetoencephalography (MEG) with simultaneous EEG. The study found that 41% of AD patients had some form of epileptiform activity compared to 11% in healthy controls, mostly recorded from the temporal cortex. Importantly, AD patients with epileptiform activity had a steeper cognitive decline compared to AD patients without evidence of seizure activity (Vossel et al., 2017). In addition, another study that introduced implants in 2 AD patients without epilepsy found prominent epileptiform spikes in the medial temporal lobe of both patients (Lam et al., 2017).

There is less evidence from LBD patients regarding epilepsy prevalence, although there are clear indications of a relationship between the two diagnoses. One of the best established qEEG findings in LBDs is the presence of transient sharp-waves, predominantly in posterior derivations (Briel et al., 1999), that are also used as a supportive feature for diagnosis (McKeith et al., 2017). Interestingly, there are also reports in the literature of epilepsy cases mimicking DLB (Park et al., 2014; Ukai et al., 2017). Furthermore, a recent study investigated the incidences of epilepsy-related manifestations in AD, DLB and FTD, and found that DLB patients had an 11.5% cumulative probability of developing seizures compared to 13.4% in AD and 5% in FTD, while in patients with mixed AD/DLB pathology the probability reached 20.7% (Beagle et al., 2017). Moreover, the DLB patients were more likely to develop myoclonus with a probability of 58.1% (Beagle et al., 2017). Myoclonus describes the involuntary jerking of a muscle, or group of muscles, that is due to aberrant neuronal activity in the motor cortex (Guerrini & Takahashi, 2013). Morris and colleagues (2015) showed that DLB patients had changes in molecular markers indicative of hyperexcitability in the hippocampus, while a mouse model overexpressing  $\alpha$ -syn had epileptiform and seizure activity in the parietal cortex (Morris et al., 2015).

One of the core symptoms of DLB are visual hallucinations (McKeith et al., 2017). According to the deafferentation hypothesis, visual hallucinations are the result of impaired processing from the eye to the primary visual cortex, resulting in a compensatory cortical hyperexcitability that manifests as visual hallucinations (Elder et al., 2019). Transcranial magnetic stimulation (TMS) studies have shown that visual cortical excitability correlated with visual hallucinations in DLB, although it was not a characteristic of DLB per se (Taylor et al., 2011). This correlation may be the result of inherently more hyperexcitability and/or a loss of inhibition. MRI studies have shown a loss of regional visual cortical inhibition in PDD, while neuropathological studies have

shown a similar finding in DLB (Erskine et al., 2017). These studies indicate a potential importance for hyperexcitability in the generation of DLB symptoms. However, we need to keep in mind that there are other theories for the generation of visual hallucinations in LBD that do not involve hyperexcitability (Taylor et al., 2011).

## **1.4. Sleep**

### **1.4.1. *Sleep architecture and microstructure***

Although we have all experienced sleep and the effects of its deprivation, we rarely hear the textbook definition: Sleep is a natural and reversible state of reduced responsiveness to external stimuli that involves loss of consciousness (Rasch & Born, 2013). Sleep is regulated by sleep-wake homeostasis mechanisms as the accumulation of waking by-products inhibits the systems that promote wakefulness, resulting in sleep induction (Watson et al., 2016). These systems interact with the circadian rhythm (Zhang et al., 2019), an internal clock of the 24-hour sleep/wake cycle (Videnovic & Golombek, 2013).

All mammals experience sleep that consists of two main states that can be recorded via the EEG all over the cortex: REM and non-REM sleep (NREM). NREM sleep can be further subdivided into NREM sleep stages N1, N2 and N3/4 in humans (Wolpert, 1969). These stages comprise sleep architecture / macrostructure. The EEG faster rhythms characterising the awake state shift to the slower theta rhythm with the emergence of N1 sleep. N2 sleep is characterised by slow wave activity (SWA) which describes oscillatory power at 0.1 – 4 Hz, bursts of 8 – 15 Hz activity known as sleep spindles, and K-complexes that describe a slow wave followed by a spindle (Brown et al., 2012). N2 sleep is followed by N3/4 or slow-wave sleep (SWS; < 1 Hz), and greater SWA (< 20%). Spindles persist during N3 while hippocampus-derived events of high frequency known as sharp-wave ripples also appear (Brown et al., 2012). Then, we enter REM sleep, which is characterised by faster, low-amplitude activity that resembles awake-like oscillations, and is characterised by muscle atonia (Peever & Fuller, 2017). In humans, each NREM/REM cycle lasts about 90 minutes (Rasch & Born, 2013). In rodents, sleep is much more fragmented, and the N2 sleep stage and SWS are not distinct. However, REM and NREM sleep stages are clearly distinct (Lacroix et al., 2018).

### **1.4.2. *Neuronal mechanisms of SWS in the cortex***

In humans, SWS originates in different prefrontal-orbitofrontal regions, with some regions like the insula and cingulate gyrus being particularly involved. The SWS then propagates from anterior to posterior cortical regions through the cingulate gyrus (Murphy et al., 2009; Riedner et al., 2011). Rodent studies have helped elucidate the

cellular mechanisms that underlie SWS. Intracellular recordings in rodents have shown that SWS consists of periods of neuronal firing known as the Up-state, and neuronally silent periods known as the Down-state (Steriade et al., 1993a). Up-state induction requires an initial activation that “kick-starts” the system and is derived from local activity in cortical layer 5 (Silva et al., 1991). Proposed mechanisms for this include the summation of EPSPs in a number of pyramidal neurons and/or the persistent firing of some of the pyramidal cells in this layer during the Down-state (Neske, 2015). The intrinsic properties of the pyramidal cells in this region are crucial for the initiation of the Up-state, as some of them exhibit intrinsic rhythmicity while others produce bursts of action potentials (Lőrincz et al., 2015). The excitatory input that generates an Up-state in the local cortical network then spreads, recruiting pyramidal cells in other areas to enter an Up-state. This spread of SWS has been shown in rodents both during natural sleep and under ketamine/xylazine and urethane anaesthesia (Luczak et al., 2007).

During the Up-state, both excitatory and inhibitory synaptic inputs are present, as shown in numerous studies in animal models (Neske, 2015). Glutamate, acting via NMDAR activity is particularly important, as following NMDAR blockade the Up-state duration is reduced *in vivo* and abolished completely *in vitro* (Steriade et al., 1993a; Major et al., 2013). GABAergic inhibition is also important for Up-state maintenance, as the application of a GABA<sub>A</sub>R antagonist *in vitro* leads to shorter and less frequent Up-states (Haider et al., 2006). PV+ basket cells contact the pyramidal cell soma and vice versa, giving rise to a feedback loop where excitation is followed by equal amounts of inhibition. This balanced system maintains the pyramidal neurons at a near-firing threshold membrane potential (Haider et al., 2006; Shu et al., 2003). The inhibition arises mostly from the recruitment of local interneurons including PV+ basket cells, which are contacted by long-distance excitatory axons (Sanchez-Vives et al., 2010).

The Up-states of the slow oscillation (SO) are terminated in a highly synchronised manner across neurons (Volgushev et al., 2006). The main proposed mechanism for termination of the Up-state is the activation of K<sup>+</sup> conductances, which reduce the excitation in the neurons maintaining the Up-state, resulting in network disfacilitation. Network disfacilitation describes a form of inhibition where cortical networks become hyperpolarised and hence inactive due to lack of excitatory input (Timofeev et al., 2001). Recent data in naturally moving mice also suggest that a small

proportion of interneurons might fire towards the end of the Up-state (Funk et al., 2017). These interneurons are SOM+ Martinotti cells in layer 1, which are activated by pyramidal cells through synaptic facilitation (a form of short-term plasticity that enhances synaptic transmission for  $< 1$ s; Silberberg and Markram, 2007), and are interlinked through gap-junctions (Roopun et al., 2006). Thus, the output of the SOM+ Martinotti cells is widespread and strong enough to inhibit pyramidal cells by synaptic spill-over of GABA, which then binds to pre-synaptic GABA<sub>B</sub>Rs on pyramidal cells inducing hyperpolarisation (Funk et al., 2017; Zucca et al., 2017). A role for PV+ interneurons is also supported by evidence that GABA depletion, specifically in these cells, results in a shortening of the Up-state and increased firing of pyramidal neurons in naturally sleeping and anaesthetised mice (Kuki et al., 2015). PV+ cells exert their action by inhibiting pyramidal cells but if this inhibition is impaired, it results in a higher level of depolarisation of the pyramidal cells that can then easily shift to another Up-state (Kuki et al., 2015).

The thalamus and brainstem structures also influence the SO, in all mammalian species. With the end of the Down-state, T-type Ca<sup>2+</sup> channels in the thalamus become activated, resulting in low-threshold Ca<sup>2+</sup> spikes, which elicit an influx of Ca<sup>2+</sup> across the thalamocortical neurons, bursts of action potentials and an Up-state in the cortex (Crunelli & Hughes, 2010). In turn, corticothalamic input activates GABAergic neurons in the thalamic reticular nucleus (TRN), an almost exclusively GABAergic nucleus that responds with a high frequency discharge onto thalamocortical neurons. The TRN spiking inhibits the thalamocortical projections, thus terminating the cycle (Destexhe et al., 1998). Although the cortex can generate an SO independently of the thalamus (Timofeev, 2000), thalamic inactivation has been shown to affect the cortical SO in anaesthetised cats, and specifically to reduce the SO amplitude and the Up-state density (Lemieux et al., 2014). Thus, although the thalamocortical input is not necessary for Up-state initiation, it is important for maintaining a stable oscillation across the cortex (Steriade et al., 1993a).

The cortical SO is also influenced by cholinergic modulations. The basal forebrain (BF) is the main source of cholinergic input to the neocortex and also projects to the limbic regions including the cingulate cortex, EC, hippocampus and amygdala (Ballinger et al., 2016). A second major source of cholinergic input to the cortex is the brainstem cholinergic system that contacts sub-cortical structures such as the basal

forebrain, the hippocampus and the thalamus that in turn projects to the cortex (Newman et al., 2012). Pharmacological reactivation of the severed cholinergic input in naturally sleeping rats resulted in rhythmic Up- and Down-states (David et al., 2013). The SO generation relied on a population of intrinsically bursting pyramidal neurons at cortical layer 5, which fire at 0.2 – 2 Hz and are activated via cholinergic input on mAChRs (Lőrincz *et al.*, 2015). These neurons may correspond to the population mentioned earlier that initiates the Down-state to Up-state transition. Other deep brain structures that may influence the SO are cholinergic inputs from the pedunculo-pontine tegmentum (PPT), noradrenergic input from locus coeruleus (LC) and serotonergic input from the dorsal raphe nucleus, as they all contain neurons that preferably fire on the Up- or Down-state, although their effect is less prominent (see review by Neske, 2015).

#### **1.4.3. *Neuronal mechanisms of SWS in hippocampus***

SOs have also been characterised in the rodent hippocampus, including the DG, subiculum, CA1 and CA3 subregions (Penttonen et al., 1999). On the Up-state, the majority of CA1 pyramidal neurons fire action potentials both during natural sleep (Isomura et al., 2006) and under urethane anaesthesia (Sharma et al., 2010). The CA1 has a local SO rhythm that is independent of the cortical SO rhythm in terms of initiation, coordination and coherence and is sensitive to cholinergic modulation (Wolansky et al., 2006; Lockmann et al., 2016; Sharma et al., 2010). However, the hippocampal SO activity still correlates with SO activity in the EC and the neocortex, and it is never present in the absence of cortical SOs, while the opposite is observed regularly (Wolansky et al., 2006). Moreover, an anterior-posterior direction of information flow from the prefrontal cortex to the hippocampus has been extensively shown in rats, with the SO starting in the prefrontal cortex and progressing to the DG and then the CA1 and CA3 regions (Isomura et al., 2006; Vyazovskiy et al., 2009). Furthermore, deep recordings in the human brain have confirmed that the SO propagates from the prefrontal cortex to the hippocampus (Nir et al., 2011). The aforementioned studies clearly suggest that the cortex has control over the local hippocampal SO, although it is possible that both regions are also modulated by ascending activating systems and/or the thalamus (Wolansky et al., 2006).

#### **1.4.4. *Oscillatory patterns accompanying SWS and their mechanisms of generation***

The organisation of the SO into Up- and Down-states provides the framework for higher frequency oscillations to emerge, which interact with the SO and are involved in memory consolidation and plasticity (Sirota et al., 2003). The oscillations that will be discussed in detail are the sleep spindles, the sharp wave ripple (SWRs) and the beta (15 – 30 Hz), gamma (30 – 80 Hz) and high gamma rhythms (80 – 130 Hz) nested on the Up-state (Valderrama et al., 2012; review by Neske, 2015).

##### **1.4.4.1. Sleep spindles**

Sleep spindles describe spontaneous waxing and waning oscillations between 8 and 15 Hz that occur during N2 and N3/4 stages of sleep (Destexhe et al., 1998). Sleep spindles appear mostly at the Down- to Up-state transition, although some higher frequency spindles (> 13 Hz) occur at the Up- to Down-state transition in more central and posterior regions of the brain (Cox et al., 2017). These two types of spindles do not seem to have a distinct functional role, as they both interact with the SO and are involved in the processes of plasticity and memory consolidation (Cox et al., 2017).

Spindles are generated in the thalamus during SWS through an interplay with the TRN, and are relayed to the cortex where they are sustained and synchronised, in both humans and animal models (Steriade et al., 1987; Andrillon et al., 2011). This interaction between the thalamus and TRN results in thalamocortical oscillations composed of cycles of excitatory (spike) and inhibitory (wave) phases. Thalamocortical neurons send excitatory outputs from the thalamus to cortical pyramidal neurons in layers 3 – 6. In turn, corticothalamic pyramidal neurons mainly from layer 6, project back to the thalamus. Although GABAergic cells are found in both the thalamus and cortex, the main inhibitory input that drives the spindle comes from the TRN (Bonjean et al., 2011; Luczak & Barthó, 2012).

At the start of the cycle, thalamocortical neurons generate highly synchronised EPSPs in the TRN that elicit a burst of action potentials in TRN GABAergic interneurons (Brown et al., 2012). This inhibitory activity induces large and prolonged IPSPs in thalamocortical neurons, at a spindle frequency (4 – 7 Hz). The resulting hyperpolarisation removes the inactivation of low-threshold (T-type) Ca<sup>2+</sup> channels in thalamocortical neurons, which allow the influx of Ca<sup>2+</sup> in thalamocortical dendrites (Fuentelba et al., 2004). This Ca<sup>2+</sup> pool can be immediately utilised by thalamocortical

neurons upon their recovery from the IPSP, in order to produce a low-threshold  $\text{Ca}^{2+}$  spike at a low depolarisation level (Coulon et al., 2012). The resulting burst of firing activity in thalamocortical neurons leads to EPSPs in cortical neurons, giving rise to a spindle (Blumenfeld, 2005). Spindles do not occur during high frequency activity, i.e. during wakefulness and REM sleep (Brown et al., 2012).

#### 1.4.4.2. Sharp wave ripples

The sharp –wave ripple (SWR) complex is composed of sharp-waves which are large negative potentials (40 – 100 Hz) recorded in the CA1 *stratum radiatum*, and high frequency ripples (100 – 300 Hz) which occur in the *stratum pyramidale* (Buzsáki and Silva, 2012). In rodents, SWRs are most frequent during SWS but they can also occur during immobility at wakefulness (Wang & Ikemoto, 2016). SPWs are generated by the synchronous bursting of pyramidal neurons in the CA3 that induce the depolarisation of the apical dendrites in the CA1 through Schaffer collaterals. SWRs are considered the default state of the hippocampus but during REM sleep and active wakefulness, CA3 projections are inhibited, preventing SWR activity. During NREM sleep the CA2 projections become disinhibited, allowing SWRs to occur (Chenkov et al., 2017). Fast-spiking PV+ are also crucial for SWR generation as their stimulation is sufficient for SWRs to emerge (Buzsáki, 2015). By eliciting fast spiking perisomatic inhibition on the pyramidal neuronal soma, PV+ interneurons create a temporal window for rebound activation that increases the probability of a SWR to occur. SWRs are terminated by hyperpolarisation and a refractory period mediated by  $\text{K}^+$  channel conductance (Buzsáki, 2015). SWRs are crucial for memory consolidation (see section 1.5.2.2).

#### 1.4.4.3. Higher frequency oscillations nested on the Up-state

The SO modulates the high frequency rhythms that are nested within the Up-state, including beta (15 – 30 Hz) and gamma (30 – 80 Hz) frequency oscillations in the cortex (Jing et al., 2016), and gamma and high-gamma frequency (80 – 130 Hz) oscillations in the hippocampus (Valderrama et al., 2012; Steriade et al., 1996). In rodents, neurons in the mPFC fire more action potentials per Up-state compared to motor and sensory regions, with a discharge of 3 – 6 spikes per Up-state, while they also have greater power in the beta (15 – 30 Hz) and gamma (50 – 80 Hz) oscillations on the Up-state (Ruiz-Mejias et al., 2011). In the rodent hippocampus, gamma oscillation power is recorded during the Up-state in most layers and regions, including the CA1 and CA3, and is accompanied by greater neuronal firing (Colgin, 2011).

Beta and gamma band oscillations are governed by similar mechanisms in the awake and asleep brain (Destexhe et al., 2007). NMDAR blockade in ferret PFC slices not only resulted in decreased Up-state duration and Up-state frequency in the spontaneously generated SO, but also in increased power of the nested beta/gamma oscillations (Rebollo et al., 2018). PV+ interneurons also modulate both the Up-state length and the high frequency oscillations on the Up-state (Brown et al., 2012). In a mouse model of GABA depletion in PV+ interneurons, the authors found decreased gamma and high-gamma power in superficial cortical layers and increased beta power in deeper layers (Kuki et al., 2015). The authors concluded that PV+ cells maintain the Up-state and gamma and high-gamma frequency oscillations in superficial layers, while suppressing beta in deeper layers through inhibiting SOM+ interneurons. SOM+ are disinhibited with decreasing PV+ function, giving rise to beta activity, as previously described (Kuki et al., 2015). Finally, thalamocortical cells contact PV+ cells in upper cortical levels, as well as pyramidal cells in the mammalian prefrontal cortex (Cruikshank et al., 2012). Thalamic inactivation results in an immediate decrease in beta/gamma oscillations on the Up-state, suggesting that the thalamic input is also important in driving high frequency oscillations on the Up-state (Lemieux et al., 2014).

#### **1.4.5. REM sleep and waking**

REM sleep describes periods of active sleep accompanied by rapid eye movements, loss of muscle tone, muscle twitches, elevated arousal level and autonomic and respiratory activation. The EEG also changes, with emerging low amplitude, high frequency oscillatory activity in the cortex that is similar to the activity seen during waking (see review by Peever and Fuller, 2017). REM sleep is seen in all vertebrate species, but there are some differences in REM sleep between humans and rodents (Peever & Fuller, 2017). In humans REM periods appear every 90 - 120 min and last for about 10 min (Carskadon & Dement, 1980), while in rodents REM periods appear every 10-15 min and last about 1 min (Yasenkov & Deboer, 2012). Most importantly, in rodents, REM sleep is mostly defined by hippocampal theta activity. Specifically, there is a long-lasting burst of low-theta (4 – 7 Hz) activity and intermittent bursts of high-theta (7 – 12 Hz) activity during normal sleep and under urethane-induced anaesthesia, that can also be recorded in the cortex (review by Brown et al., 2012). In contrast, chronic electrode implant studies in humans have shown that REM sleep is characterised by intermittent theta activity limited to 1 s-long epochs and a

rhythmic delta (1.5 – 3 Hz) that might represent high and low theta respectively (Bódizs et al., 2001).

Waking and REM sleep are controlled by the ascending reticular activating system (ARAS) composed of nerve fibres ascending from the brain stem and branching off on their way to the forebrain (Pal & Mallick, 2007). The ARAS is composed of the dorsal and ventral pathways (Figure 4.1; Brown et al., 2012b). Acetylcholine (ACh) is a major neurotransmitter in the ARAS (Hentschke et al., 2007) and it generally promotes oscillations that are associated with wakefulness and REM sleep, particularly theta activity and theta/gamma coupling in the hippocampus and beta/gamma oscillations in the hippocampus and cortex, in rodents (Whittington et al., 2000; Cantero et al., 2003). The cholinergic drive of ARAS is derived from cholinergic neurons originating from brain stem cholinergic system projecting to the thalamus, and from the basal forebrain (BF) projecting directly to the cortex and the hippocampus (review by Brown et al., 2012; Figure 1.4). In contrast, serotonin functions in an opposing manner to ACh, inhibiting both the BF and brain stem cholinergic neurons, hence blocking theta and gamma activity (Cape & Jones, 1998). REM/NREM sleep alternations rely upon the interaction between REM-on and REM-off neurons in the dorsal ARAS pathway (Figure 1.5).

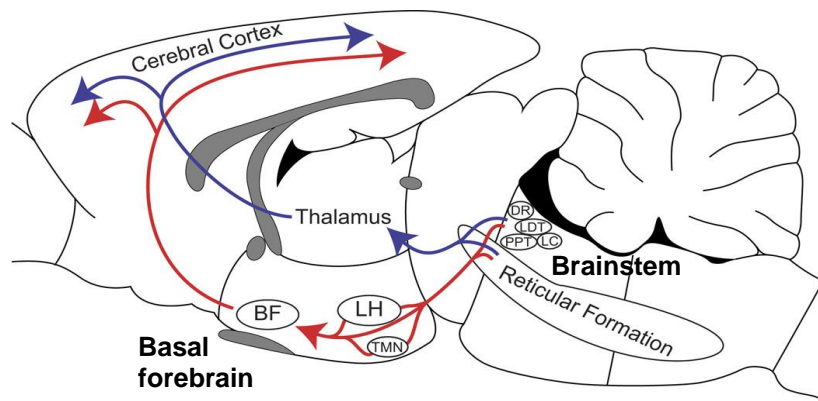


**Figure 1.4:** The dorsal and ventral pathways of the ascending reticular activating system (ARAS) in the rodent brain. The dorsal pathway (blue) originates in pontine and midbrain reticular formation, with cholinergic neurons from the pedunculo pontine and laterodorsal tegmental nuclei (LDT/PPT) and glutamatergic neurons, which project to thalamic nuclei that in turn innervate several regions of the cerebral cortex. The ventral pathway (red) also originates in pontine/midbrain regions and projects to the lateral hypothalamic (LH) and tuberomammillary (TMN) nuclei of the hypothalamus, and the basal forebrain (BF). LH and TMN outputs also contact the BF, which in turn projects to the cortex. Noradrenergic neurons of the locus coeruleus (LC), serotonergic neurons in the dorsal raphe (DR), histamine neurons of the TMN and orexinergic neurons in the LH contribute to both pathways and send direct projections to the cortex. Adapted from Brown et al. (2012), originally adapted from Paxinos and Watson (1998).

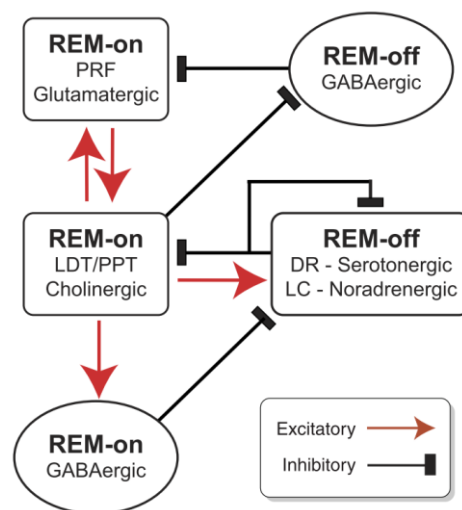


**Figure 1.5:** REM/NREM sleep alternations rely upon the interaction between REM-on and REM-off neurons in the dorsal ARAS pathway. REM-on neurons, which are cholinergic neurons in the LDT/PPT, increase their firing before and during REM and excite pontine reticular formation (PRF) glutamatergic REM-on cells, and activate GABAergic interneurons that inhibit their adjacent REM-off neurons. REM-on output also acts in a self-inhibiting manner by inhibiting GABAergic REM-off interneurons, releasing REM-on neurons in the PRF from their inhibition. REM-on cells increasingly excite REM-off cells in the dorsal raphe (DR) and LC, which inhibit LDT/PPT REM-on neurons, during waking and NREM sleep. For REM sleep to emerge, these REM-off neurons become self-inhibited, leading to disinhibition of REM-on neurons. Figure adapted from Brown et al. (2012).

#### **1.4.6. Sleep microstructure**

Sleep macrostructure is composed of dynamically alternating microstates (Halász, 2004). The cyclic alternating pattern (CAP; 0.002 – 0.02 Hz) is a rhythm that is well characterised in humans, and is composed of microactivation periods that reflect cortical arousal (phase A) and their intermediate SWS periods (phase B) (Terzano et al., 1985). The A phase can be categorised into subtypes (A1, A2, A3) according to the percentage of SWA activity occurring in each phase (Figure 1.6). Hence, it appears that the CAP cycle offers a homeostatic mechanisms that buffers the levels of SWA (Parrino & Vaudano, 2018). The A phase subtypes have a variety of manifestations depending on the depth of sleep in which they occur, the age of the individual and homeostatic sleep pressure (Parrino et al., 2012). The A1 subtype consists of slow modulations (delta, K-complexes) and occurs mostly during sleep-stage transitions. Moreover, A1 events act as a gating mechanism, filtering external stimuli during SWS without inducing sleep discontinuation and thus, benefiting sleep-related cognitive processing (Combi et al., 2009; Ferri et al., 2008). The A3 subtype has faster oscillatory components (e.g. theta, alpha, beta activity). Phase A3 events occur at the NREM-REM transition and reflect sleep discontinuity in the cortex, providing a window for monitoring sleep and driving arousal if necessary (Parrino & Vaudano, 2018). Finally, the A2 subtype combines a mixture of A1 and A3 characteristics.

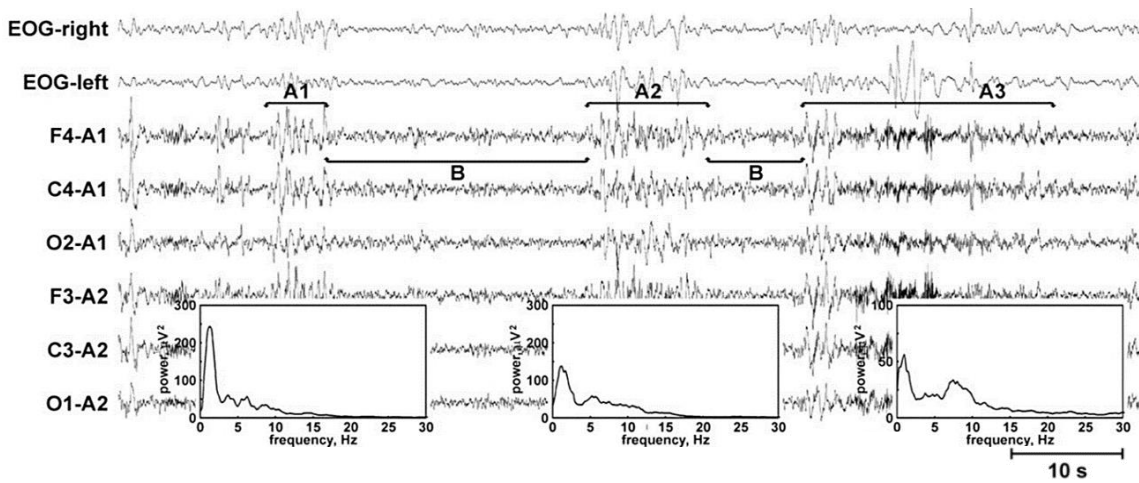


**Figure 1.6:** Example of the cyclic alternating pattern (CAP) in a human subject during slow wave sleep. Short CAP sequence composed by three A phases (A1, A2, and A3) and the intermediate B phase. As shown in the power spectra, the A phase subtypes are characterised by different levels of percentage of SWA activity: subtype A1 is composed mostly of SWA (> 80%), subtype A2 contains about 50% - 80% of SWA and the rest is low voltage fast activity, while subtype A3 is predominated by faster activity (> 50%). Adapted from Parrino et al. (2012).

## **1.5. Sleep and memory consolidation**

### **1.5.1. *Slow wave sleep as a framework for synaptic plasticity***

SWS plays an essential role in the strengthening of synapses in relation to learning and memory, as SWA is believed to reflect synaptic density and/or strength in the cortex (Marshall et al., 2006; Van Someren et al., 2011). A number of behavioural studies, have shown that sleep deprivation, and the selective deprivation of SWS, impairs episodic memory in humans (review by Walker, 2009). For example, Yoo et al (2007) showed that sleep deprivation affected the participants' performance in a memory-encoding task, while comcomidant MRI revealed a decrease in activity in the hippocampus and prefrontal cortex during the memory acquisition phase (Yoo et al., 2007). The communication between the hippocampus and cortex is facilitated by the Up-state, as it provides a widespread temporal framework for distant neurons in the two regions to communicate, and bind into the functional assemblies that underlie memory consolidation (Mölle et al., 2006). This communication allows the declarative memories acquired when awake, to become increasingly cortically-dependent and hippocampally-independent, thus protecting them from interference and forgetting (Mander et al., 2016). On the other hand, Down-states are crucial for synaptic strength homeostasis (Watson et al., 2016). According to the synaptic homeostasis hypothesis, synaptic plasticity-mediated changes in the cortex during wakefulness result in a widespread increase in synaptic strength, which if not limited, will not be energetically sustainable over time (Tononi & Cirelli, 2006). Thus, the Down-state offers the opportunity to downscale, allowing only "relevant" synapses to remain and promoting the efficient use of grey matter (Vyazovskiy et al., 2009; Vyazovskiy and Harris, 2013).

### **1.5.2. *High frequency rhythms are involved in memory consolidation***

#### **1.5.2.1. Spindles**

Sleep spindles are very important for memory consolidation as they facilitate the communication between the hippocampus and the cortex (Sirota et al., 2003). There is evidence from healthy humans that inducing SO-like stimulation through TMS increased the SWA and sleep spindles, and improved the subjects' performance on a memory task the following day (Marshall et al., 2006). Moreover, the spindle density and amplitude increased in normal subjects after performing tasks that require learning, while these changes in spindle amplitude and density predicted performance

in a memory task (Cox et al., 2012). In contrast, spindle dysfunction in patients with schizophrenia is associated with reduced memory consolidation (Manoach & Stickgold, 2019). Deficits in spindles are also seen in patients with dementia (Westerberg *et al.*, 2012).

#### 1.5.2.2. Sharp-wave ripples (SWRs)

During SWRs, the pattern of activation in the hippocampus is a temporally compressed version of neuronal firing patterns in waking animals, termed hippocampal replay. This led to the hypothesis that with novel information, there is a transient synaptic reorganisation of hippocampal circuits (Buzsáki, 2015). Moreover, the memory replay is thought to strengthen synapses and transfer memories to the cortex. The ACC is particularly relevant in this process, as it is involved in the storage and expression of long-term episodic memory (Meltzer et al., 2007). One study found that most ACC neurons showed increased activity before a SWR, while a small portion of neurons also showed increased activation after the SWR (Wang & Ikemoto, 2016). Thus, the cortically-generated SO triggers the SWR in the hippocampus which in return transfers information from the hippocampus to the cortex for long-term storage (Buzsáki, 2015).

#### 1.5.2.3. High frequency oscillations on the Up-state

As outlined above, high frequency activity occurring on the Up-state of the SO is very similar to activity seen in the awake brain activity. Thus, gamma oscillations on the Up-state may resemble “microwake”- like activity patterns of “relevant” events that are transferred from the hippocampus to the cortex for permanent storage/consolidation (Destexhe et al., 2007). In support to this theory, gamma frequency activity patterns during SWS in humans resemble the activity of the DMN during the awake state, including activation of the mPFC (Valderrama et al., 2012). Gamma activity enhances the coordinated firing between cell populations in a manner that can then induce Hebbian like synaptic plasticity in their targets, strengthening synapses and imprinting memories (Le Van Quyen et al., 2010). Hence, gamma activity power in the regions normally engaged in the DMN during sleep, may partly enforce the large-scale dynamics of wakefulness, promoting memory consolidation (Dang-Vu et al., 2008).

Fast oscillations in the hippocampus have been shown to also eliminate memories within the rodent hippocampal network. Isomura et al. (2006) suggested that

during the Up-state, the output of the DG to the CA3 can strengthen the connection between mossy terminals and new “relevant” pyramidal neurons, while suppressing the rest of the CA3 neurons through widespread inhibition. On the Down-state, this suppression is absent allowing for a local gamma/ripple activity to reorganise the CA1-CA3 circuits locally (Isomura et al., 2006). Thus, fast oscillations in the hippocampus can function as a medium of communicating with the cortex via activity on the Up-state while allowing self-organisation of the hippocampus on the Down-state (Hahn et al., 2007; Isomura et al., 2006).

#### 1.5.2.4. Interactions between spindles, SWRs and high frequency oscillations

Gamma oscillations and hippocampal SWRs are distinct phenomena but they have multiple physiological mechanisms and anatomical substrates in common, in both humans and animal models (Colgin & Moser, 2010). In the absence of theta activity (wakefulness or REM sleep), the CA3 input to the CA1 can either result in the generation of SWR or of gamma activity (Colgin & Moser, 2010). The two rhythms also interact, as the frequency and amplitude of the gamma oscillations in the hippocampus was shown to correlate with the magnitude of the preceding SWR, in naturally sleeping rats (Sullivan et al., 2011). Moreover, both the hippocampal gamma activity and SWRs were modulated by gamma activity in the DG and EC, showing a cortical control over the hippocampal rhythm (Sullivan et al., 2011). There is also flow of information from the hippocampus to the cortex that is elicited by gamma and SWR activity on the Up-state, as shown in both humans and anaesthetised rats (Clemens et al., 2011; Le Van Quyen et al., 2010).

Spindles in the humans and animal cortex are also coherent with gamma and beta oscillations and SWRs in the hippocampus during SWS, serving as a substrate for memory consolidation (Rasch & Born, 2013). The spindle phase modulates spike activity as well as gamma and ripple activity, with hippocampal SWRs occurring on the troughs of the spindle cycle. This relationship was also demonstrated in the rodent mPFC and hippocampus. The mPFC is a region highly involved in memory and cognitive function (Varela & Wilson, 2019). The mPFC/hippocampus interaction is bidirectional as the spindle can reach the EC-hippocampal networks and induce a SWR, while the hippocampal SWR can prolong the duration and enhance the expression of the spindle in the cortex (Varela & Wilson, 2019). Moreover, mPFC neurons fire almost immediately after hippocampal neurons (100 ms) and preferentially

around the time of SWRs, and this mPFC neuronal firing is accompanied by the generation of a spindle (Wierzynski et al., 2009). This interaction between the mPFC and hippocampus is anatomically supported in rodents by inputs from the ventral CA1 and subiculum of the hippocampus to the mPFC (Riga et al., 2014). Finally, computational modelling studies have supported that there is increased local and interregional coupling between spindles and beta oscillations in the cortex on the Up-state of the SO (Kopell et al., 2000).

### **1.5.3. *REM sleep and memory***

REM sleep is important for preparing the brain for waking up and has a role in memory consolidation (Peever and Fuller, 2017). Recent optogenetic studies in rodents silenced the MS GABAergic neurons responsible for generating hippocampal theta during REM sleep (Salib et al., 2019; Yoder & Pang, 2005). Silencing the MS interneurons reduced the animals' capacity to consolidate previously learned novel object recognition and fear-conditioned memories. REM sleep is thought to provide a period of functional disconnection between the hippocampus and the cortex that is necessary for the reorganisation of memory traces (Wierzynski et al., 2009), as REM-related  $\text{Ca}^{2+}$  spikes within dendrites can maintain or prune synapses (Li et al., 2017). Moreover, there is evidence of neuronal replay in the rodent hippocampus during REM sleep, with neuronal firing being more likely to occur on the trough of the theta cycle than the peaks, as seen in wakefulness. Since spike induced plasticity depends on the theta phase, the firing of these neurons on the trough may suggest that their activity helps erase episodic memory from the hippocampus upon becoming encoded in the cortex (Booth & Poe, 2006).

## 1.6. Sleep and dementia

### 1.6.1. *Sleep-related EEG alterations in dementia patients*

A reduction in sleep quality and quantity, accompanied by changes in sleep architecture, are a characteristic of ageing in humans (Vaz Fragoso et al., 2015). Age-related changes in sleep include a shorter sleep duration, night-time awakenings, and daytime somnolence. EEG studies have shown a reduction in SWS, a higher percentage of stage 2 sleep, lower SWS amplitude and longer Up- and Down-states (Carrier et al., 2011). However, age-related sleep disturbances are distinct from sleep disturbances associated with different dementia subtypes and PD, and they often appear long before any cognitive or motor symptoms (Bohnen & Hu, 2019). In AD, night-time sleep fragmentation is the most common sleep-associated symptom along with early awakenings and increased daytime somnolence (Rothman & Mattson, 2012). DLB patients are more affected by sleep disturbances than AD patients, with 90% of patients reporting sleep fragmentation as well as other symptoms like poor sleep quality, insomnia, RBD, increased sleep latency and vivid dreams (Fernández-Arcos et al., 2019). Moreover, sleep problems in DLB are associated with a greater degree of clinical impairment compared to patients with AD (Chwiszczuk et al., 2016).

Polysomnographic studies in patients with dementia have shown alterations in sleep architecture. AD is associated with decreased SWS and REM sleep, increased time spent in stages N1 and N2 of NREM sleep, prolonged REM latency and increased sleep fragmentation, resulting in an overall decrease in sleep duration (Lim et al., 2014). Recently, AD patients at an early stage of the disease demonstrated a correlation between a reduction in SWA levels and greater Tau pathology, and to a lesser extent greater A $\beta$  pathology (Mander et al., 2015; Lucey et al., 2019). Polysomnographic studies in DLB patients and PDD patients have also found poor sleep continuity, longer sleep latency and REM sleep latency, RBD and reduced REM sleep while DLB patients specifically, had less N1 and more N2 sleep (Terzaghi et al., 2013). In addition, a recent video-polysomnographic analysis in DLB patients showed additional features including persistence of wake-like activity (alpha/theta rhythms) occipitally, intermittent rhythmic delta activity frontally and rapid-eye movement and sustained EMG activity at sleep onset (Fernández-Arcos et al., 2019). The authors also found transient sharp waves in NREM sleep, low-frequency sleep spindles in stage

N2, an absence of sleep spindles and K complexes in NREM sleep and a delta slowing during REM sleep (Fernández-Arcos et al., 2019).

### **1.6.2. *Sleep and cognition in dementia***

Considering the pivotal role of sleep, especially SWS, in memory consolidation, one would expect that the sleep disturbances seen in patients with dementia should affect memory processing (Mander et al., 2016). This has been extensively described in AD, as memory impairment appears years before any hippocampal A $\beta$  deposits or atrophy, but concomitantly to pathology in cortical regions (Westerberg et al., 2012). Interestingly, the levels of A $\beta$  burden in the mPFC of AD patients has been associated with lower levels of SWA and a decrease in hippocampus-mediated memory retention assessed by a memory task (Mander et al., 2015). A reduction in SWA has also been correlated with increased tau levels in patients with early stage AD (Lucey & Holtzman, 2015).

As outlined above (sections 1.4.4.1, 1.4.4.2), cortical spindles and their synchrony with the SWRs on the SO are important in for memory consolidation. Lower spindle density and amplitude in posterior cortical areas has been observed in DLB (Fernández-Arcos et al., 2019; Ozaki et al., 2012) while in PD, these EEG characteristics predict dementia development (Latreille et al., 2015). Spindles are dependent on thalamocortical reciprocal connectivity while MRI studies have shown functional and structural alterations in these regions (Kotagal et al., 2012), as well as early decrease in cholinergic neurotransmission that progresses with dementia in DLB patients (Schmeichel et al., 2008). Thus, reduced/altered sleep spindles could have cognitive implications in DLB patients, supporting a possible relationship between sleep and cognitive dysfunction in relation to  $\alpha$ -syn pathology. In addition, Lewy body pathology is evident in the hippocampus of DLB patients , which is directly implicated in declarative memory consolidation and recall (Marshall et al., 2006). DLB patients most prominently exhibit Lewy neurites in axon terminal in the CA2 region and Lewy bodies in the EC (Adamowicz et al., 2017), while lower levels of Lewy pathology are seen in the CA1, CA3 and subiculum. Lastly, Lewy pathology in the CA1 region, which is the main output of the CA2, correlated with memory testing results in these patients (Adamowicz et al., 2017).

Memory impairment is not a main characteristic of early stage DLB. In fact, relative memory preservation is one of the main differences between DLB and AD, with memory impairments only appearing at more advanced stages of DLB (McKeith et al., 2017). Other clinical features of dementia such as impairments in attention and in visuospatial and frontal-executive functions are more prominent at the early stages of the disease (Donaghy & McKeith, 2014). Interestingly, these cognitive functions are also affected by sleep deprivation, with highlighted deficits in selective attention and working memory tasks (Alhola & Polo-Kantola, 2007). Vigilance that describes sustained attention and requires robust working memory (Lim & Dinges, 2008) is highly impaired in sleep deprived individuals (Naghavi & Nyberg, 2005) and in DLB patients (Ferman & Boeve, 2007). Moreover, sleep deprivation as well as DLB have been linked with lower accuracy and speed in performing tasks of divided attention (Calderon et al., 2001). Hence, the cognitive impairment seen in DLB may at least partly be facilitated by sleep deprivation (Guarnieri & Sorbi, 2015).

### **1.6.3. *Sleep and epilepsy in dementia***

Aberrant neuronal activity is tightly linked to disruptions in sleep-related mechanisms (Beenhakker & Huguenard, 2009). In patients with epilepsy, epileptic seizures, interictal spiking and high frequency oscillations (> 80 Hz), which are thought to be the best EEG indicators of epilepsy, are more likely to occur during SWS compared to waking (Frauscher et al., 2015). There is also evidence to support a relationship between dementia-related hyperexcitability and sleep. An EEG study in five AD patients with epilepsy found a high correlation between the amount of epileptiform discharges detected during NREM sleep, compared to REM sleep and wakefulness (Horváth et al., 2017). Moreover, chronic electrode implant recordings in two AD patients (without clinical epilepsy) showed that epileptiform spikes were most prominent and frequent during sleep compared to awake states (Lam et al., 2017). In both these studies, the epileptiform activity was most prominent in the medial temporal lobe that is located directly above the hippocampus (Beenhakker & Huguenard, 2009). Therefore, dementia-related perturbations in hippocampal circuits underlying SWR generation could have a devastating impact on the hippocampus and the surrounding cortical regions. An overnight polysomnographic study identified sharp-wave activity during NREM SWS in 2/31 DLB patients (Fernández-Arcos et al., 2019). However, there are no reports of chronic electrode implant recordings in DLB patients.

## 1.7. Modelling dementia and sleep

### 1.7.1. *Animal models of dementia*

Experimental models are essential to improve our understanding of neurodegenerative disorders. Over the last few decades animal models have been increasingly used in dementia research (Koprach et al., 2017). Models used so far include rodents, monkeys, worms and fruit-flies, which express/overexpress human mutant forms of the proteins that aggregate in the different dementia subtypes to form insoluble protein clusters. Such proteins are a human mutant form of tau, the amyloid precursor protein (APP) and the proteins that cleave APP to A $\beta$  (presenilin 1 and 2) to model AD, and mutant  $\alpha$ -syn to model PD/LBD. These mutations are often isolated in familial cases of the disease (Drummond & Wisniewski, 2017). Developing such models is a challenging task and there is no single animal model that encompass all aspects of the human disease, including cognitive, behavioural and histopathological abnormalities, in any dementia subtype. However, the variety of models that exist today allow us to study different aspects dementia (Fifel et al., 2016).

A number of  $\alpha$ -syn transgenic mice have been created to model LBD and PD (review by Koprach 2017). Models of  $\alpha$ -synucleinopathy are created through inducing the over-expression of wild-type (WT) human  $\alpha$ -syn, or the expression of human mutant  $\alpha$ -syn. The mutations in the human  $\alpha$ -syn encoding gene (SNCA) introduced in animal models are usually missense mutations identified in families with inherited Lewy body disease, including the A53T and A30P mutations (Polymeropoulos et al., 1997). Custom SNCA mutations have also been created that increase the “stickiness” and toxicity of  $\alpha$ -syn, such as the Y39C mutation (Tofaris et al., 2006). In addition, more than one mutation can be introduced in the same model (Lelan et al., 2011). For example, the A30P\*A53T mutant line, expresses the double mutant form of  $\alpha$ -syn in dopaminergic neurons, thus modelling the cell loss and motor deficits seen in PD (Kilpeläinen et al., 2019). Most  $\alpha$ -syn models are not capable of forming Lewy bodies, but they express the mutated protein at high levels, which is also phosphorylated at serine-129, ubiquitinated (post-translation modification that targets proteins for degradation), proteinase K resistant and detergent insoluble, and induces neuroinflammation, as seen in humans (Koprach et al., 2017). Lewy body-like structures can be seen in the E46K expressing mice (Emmer et al., 2011), and in  $\alpha$ -

synucleinopathy models that also express amyloid- $\beta$  and tau mutations (Clinton et al., 2010; Badiola et al., 2011).

SNCA mutations are usually introduced in mice under the influence of a promoter (Koprach et al., 2017), and most promoters induce a widespread expression of the transgene (Hatami & Chesselet, 2014). For example, expression of the A53T mutation under the prion promoter leads to extensive pathology and motor deficits from 2 months of age, but not to cognitive impairment (Giasson et al., 2002). In contrast, A53T expressed under the  $Ca^{2+}$ /calmodulin-dependent protein kinase II (CaMKII) promoter induces  $\alpha$ -syn expression in the forebrain, hippocampus and substantia nigra, as well as progressive cell loss, gliosis and cognitive impairment, combining both the motor and cognitive deficits of LBD (Nuber et al., 2008). The thymus cell antigen 1 (Thy-1) promoter induces expression of the transgene mostly in the cortex and limbic system, but the levels and pattern of expression in other structures can often vary between models (Hatami & Chesselet, 2014). A53T-Thy-1 mice have severe motor impairments that lead to paralysis and death at 12 months and thus resemble PD (Martin et al., 2014), while A30P-Thy-1 mice are more similar to DLB in terms of protein expression, pathology and phenotype (see Section 1.7.1.1). The E57K mutation under the Thy-1 promoter also leads to expression in the neocortex, limbic system, thalamus, basal ganglia and substantia nigra, and to the development of cognitive deficits from 2 - 4 months of age (Rockenstein et al., 2014).

Other promoters used to drive  $\alpha$ -syn expression are specific to an neuronal subtype such as tyrosine hydroxylase (TH) -expressing neurons in the A30P\*A53T mice (Kilpeläinen et al., 2019), or regions such as dopaminergic neurons in the substantia nigra and ventral tegmental area (Lin et al., 2012). More elaborate animal models of  $\alpha$ -synucleinopathy involve tetracycline-controlled transcriptional activation of the mutant SNCA after birth (Lim et al., 2011), or utilise viral vectors. Rat models have been developed that express either the A53T or A30P mutations, or overexpress WT  $\alpha$ -syn in the substantia nigra and reticular formation, to model PD (Kirik et al., 2002). However, although viral injection studies may induce  $\alpha$ -syn like cell loss, they do not result in cognitive impairment (Klein et al., 2002).

#### 1.7.1.1. *The A30P mouse model*

The A30P is a mouse model of  $\alpha$ -synucleinopathy that overexpresses human mutant  $\alpha$ -syn (with the A30P missense mutation) under the Thy-1 promoter (Kahle et

al., 2001), which promotes expression mostly in neuronal cells, in particularly high levels in the hippocampus and striatum (Kemshead et al., 1982) and in lower levels in the substantia nigra (Neumann et al., 2002). Hence, due to the topology of mutant  $\alpha$ -syn expression, A30P mouse models has cognitive symptoms of  $\alpha$ -synucleinopathy in addition to motor symptoms, similarly to DLB. Specifically, A30P mice have motor deficits at 14 months of age as well as DLB-related cognitive deficits from 12 months, such as impaired spatial learning, memory and fear conditioning behaviour (Freichel et al., 2007; Newman et al., 2012).

These cognitive and motor symptoms seen in A30P mice are accompanied by fibrilisation of  $\alpha$ -syn in the brain stem, midbrain and spinal cord (Freichel et al., 2007; Newman et al., 2012). A30P mice also show evidence of serine-129 phosphorylated (PSer129)  $\alpha$ -syn in the lateral hypothalamus, amygdala, hippocampus and cortical regions, at 16 – 19 months of age. PSer129 is one of the main pathological modifications in  $\alpha$ -synucleinopathies and it was accompanied by dystrophic neurites and axon terminals in A30P mice (Schell et al., 2009). Moreover, A30P mice have an age-dependent reduction in gamma oscillatory power in the hippocampus shown *in vitro*, and an age-dependent mitochondrial dysfunction (Robson et al., 2018). More subtle  $\alpha$ -syn-induced changes have been shown at earlier ages, such as evidence for a very fine motor impairment at 2 months (Ekmark-Lewén et al., 2018), and altered electrophysiological activity and behaviour defects in a locomotor test from 2 months of age (Tweedy et al., 2018). Thus, the A30P model was chosen because it is a well characterised model of DLB in terms of  $\alpha$ -syn expression, pathology and phenotype, and we can relate our findings to previous studies that investigated different aspects of this model.

### **1.7.2. EEG changes in mouse models of $\alpha$ -synucleinopathy**

Changes in EEG activity are common in animal models of dementia. One study in a mouse model of  $\alpha$ -syn overexpression (Thy1-aSyn) has shown a shift of power from higher (alpha) to lower (delta, theta) frequencies during NREM and REM sleep, and a decrease in gamma activity at resting state, at 9 - 10 months of age (McDowell et al., 2014). A shift of the dominant frequency from alpha to theta frequencies was also identified at rest in mice expressing human WT  $\alpha$ -syn (SYN mice) at 4 - 8 months of age (Morris et al., 2015). These findings can be directly related to the slowing of the EEG that is observed in LBD patients (Briel et al., 1999). *In vitro* data has also shown

an age dependent decrease in gamma power in the A30P mouse model at > 9 months of age (Robson et al., 2018). This EEG slowing was reversed in the SYN mouse model (Morris et al., 2015) with the administration of cholinesterase inhibitors, as seen in the patient groups (McKeith et al., 2004; Brassen & Adler, 2003), suggesting that the EEG slowing is the result of a cholinergic dysfunction. Finally, animal models of AD also show similar shifts of power towards lower frequencies during sleep (Wisor et al., 2005; Zhang et al., 2005) and wakefulness (Kent et al., 2018; Platt et al., 2011).

As seen in patients with dementia, animal models of dementia also show changes in sleep architecture. The previously mentioned study in the Thy1-aSyn mice also looked at sleep architecture and found that otherwise healthy mice (9 - 10 months old) had increased NREM sleep (not of the SWS type) and an overall decreased in REM sleep (McDowell et al., 2014). In a mouse model of PD induced by MPTP (1-methyl-4-phenyl-1,2,3,6-tetrahydropyridine) administration, a neurotoxin that causes PD symptoms by destroying dopaminergic neurons in the SN, decreased SWA during natural sleep (Zavalko et al., 2013). These studies replicate the evidence of poor sleep continuity, altered NREM sleep patterns, longer REM sleep latency and reduced REM sleep seen in LBD patients (Fernández-Arcos et al., 2019). However, the number of sleep studies in rodent models of LBD are limited, while rodent models of PD use neurotoxins such as MPTP that selectively ablate dopaminergic neurons and are thus more restricted (review by Fifel et al., 2016). Hence, most evidence of how the dementia-related pathology affects sleep comes from rodent models of AD, as the mechanisms between AD and DLB as well as other proteinopathies often overlap.

Numerous sleep abnormalities have been identified in mouse models of AD (Sethi et al., 2015; Van Erum et al., 2019). Interestingly, the TgCRND8 mouse model of AD (double mutant form of the human APP protein) had increased wakefulness and reduced NREM sleep at all ages, even before the occurrence of cognitive dysfunction (Colby-Milley et al., 2015). It is therefore possible that the changes seen in sleep architecture in relation to AD pathology precede the dementia symptoms, reflecting early changes in the underlying circuits. Moreover, electrophysiological recordings from the prefrontal cortex of the triple transgenic model of AD (3xTg-AD; 20 months of age) expressing both progressive A $\beta$  and Tau pathology during natural sleep, showed a decrease in SO frequency compared to WT mice due to longer Down-states (Castano-Prat et al., 2019). In addition, the authors found a greater SO cycle length

variability, a shift of EEG power towards lower frequencies and a reduced relative Up/Down neuronal firing rate in these animals (Castano-Prat et al., 2019). The earliest change observed at 7 months was a reduction in Up-state length. The authors interpreted these findings as difficulties into transitioning between Up- and Down-states, due to alterations in cortical GABA<sub>A</sub>R and NMDAR function (Castano-Prat et al., 2019). A different study recording brain activity from a mouse model of tauopathy (rTg4510; 7 month old) under ketamine/xylazine anaesthesia, also found a slower SO frequency due to longer Down-states, reduced neuronal firing rates, and a longer latency to the first spike and inter-spike intervals (ISI) on the Up-state (Menkes-Caspi et al., 2015). In contrast, another sleep study in a mouse model of AD (APP<sup>swe</sup>/PS1 $\Delta$ E9; 6 – 8 month old) found an increase in the SO frequency and a loss of SO synchrony across the cortex, the hippocampus and thalamus (Busche et al., 2015). These discrepancies might indicate differences between the animal models used and thus, more studies are necessary to delineate these inconsistencies.

Over the last decade, numerous publications have reported evidence of early neuronal or network hyperexcitability in the cortex and hippocampus in animal models of neurodegeneration, most notable of AD, during sleep (Hall et al., 2015; Jin et al., 2018; Palop et al., 2011; Hazra et al., 2013; Davis et al., 2014). In a Tau mouse model of AD (rTg4510; 7-8 month old), a decrease in the number and amplitude of SWRs was accompanied by greater pyramidal cell firing in the CA1 and decreased inhibition, suggesting a disruption in the control of neuronal recruitment and firing during SWRs (Witton et al., 2016). In the 3xTg-AD mouse model at 3 weeks of age, there was clear hippocampal and EC epileptogenicity before the occurrence of any cognitive symptoms, that could be reversed by immunisation for the mutant A $\beta$  protein (Kazim et al., 2017). In a drosophila model of AD, it was shown that A $\beta$  accumulation induced neuronal excitability and sleep loss (Tabuchi et al., 2015).

Less research has been conducted in DLB in relation to hyperexcitability and sleep, with one study showing that the SYN mouse model at 4 - 8 months of age had interictal spikes in the parietal cortex and molecular changes indicative of hyperexcitability in the hippocampus (Morris et al., 2015). The Thy1-aSyn mouse model of  $\alpha$ -syn overexpression progressively showed a hyperactive genotype that was accompanied by a reduction in REM sleep (McDowell et al., 2014). These studies provide crucial insight about the role of hyperexcitability in dementia as it is difficult to

identify such early, subtle changes in patients, particularly in deep structures like the hippocampus (Palop et al., 2011).

### **1.7.3. *The mechanisms underlying sleep changes in dementia***

Animal studies have been pivotal in improving our understanding of the mechanisms that underlie sleep-disturbances in relation to dementia. Hence, in the next paragraphs we will examine how the dementia-related pathology and sleep disturbances interact, in both patients and animal models.

#### **1.7.3.1. *Dementia pathology interfering with sleep***

Sleep induction, maintenance and termination, as well as alternations between REM and NREM states, require tight control between and within several systems in the basal brain, midbrain and forebrain (Brown et al., 2012). Therefore, it is to be expected that the abnormal clustering and accumulation of proteins like A $\beta$  and  $\alpha$ -syn and the associated neurodegeneration, would affect sleep architecture (Porter et al., 2015). In fact, AD, DLB/PDD and PD patients show early signs of pathology in the brainstem cholinergic system, with DLB/PDD and PD patients showing a particular loss of neurons in PPT/LDT nuclei, resulting in a substantial loss of cholinergic tone in the cortex (Tiraboschi et al., 2002; Contestabile, 2011; Kotagal et al., 2012). In view of the involvement of these nuclei in REM/NREM sleep control (Peever & Fuller, 2017) as outlined above (section 1.4.5), cholinergic cell loss is thought to be related to the sleep architecture alterations seen in DLB/PDD and PD patients (Carnicelli et al., 2019; Latreille et al., 2015; Pao et al., 2013; Rothman & Mattson, 2012). Moreover, DLB/PDD and PD are characterised by a decrease in the response of the thalamus to cholinergic inputs due to a loss of nAChRs (Pimlott et al., 2006). Lastly, a clear correlation was identified between cholinergic dysfunction and sleep disruption in animal models of AD (Wisor et al., 2005; Zhang et al., 2005).

Circadian dysregulation is another common finding in dementia patients and animal models (Videnovic & Golombek, 2013). Neurons in the suprachiasmatic nucleus (SCN), which is the main “switch” of the circadian rhythm, are susceptible to abnormal protein deposition and cytotoxicity, with detrimental effects in the control of the SCN over sleep-wake patterns (Bohnen & Hu, 2019). In AD patients, the SCN and its output are disrupted (Goudsmit et al., 1990), while disruption of the SCN in a transgenic animal model of AD altered the circadian rhythms of wheel running, which

increased to > 24 hours (Wisor et al., 2005). Moreover, in patients with PD and AD, there are signs of pathology and neurodegeneration in the LC, the noradrenergic nucleus whose function is light dependent and is involved in the sleep/waking transition (Zarow et al., 2003). Furthermore, PD patients are less responsive to dopaminergic medications (levodopa) administered later in the day, suggesting a circadian rhythm-related dopamine deficiency (Gehrman et al., 2005). A role of dopamine in circadian regulation is also evident in rodent and monkey models of dopaminergic neuronal loss, as they show altered sleep patterns including REM sleep reduction and RBD-like signs (Barraud et al., 2009). Thus, a number of neuronal cell types control the circadian rhythm and these are sensitive to protein misfolding-induced cytotoxicity, resulting in altered sleep/wake patterns (Rothman & Mattson, 2012).

#### 1.7.3.2. Sleep interfering with dementia pathology

The mechanisms discussed so far concern changes in sleep architecture and involve pathology in sub-cortical structures. However, as previously described, animal models of dementia show disturbances in the SO which is a locally generated rhythm (Neske, 2015). It is possible that changes in the cholinergic nuclei, or the thalamus for example, affect the cortical SO (Lemieux et al., 2014; Steriade et al., 1993a), although abnormal protein accumulation within the frontal lobe can directly affect local receptor function and hence SWS (Colom-Cadena et al., 2017; Nikolaus et al., 2009).

Although there is clear evidence for the impact of abnormal protein accumulation in sleep, there is increasing evidence to support that this relationship is not unidirectional and that sleep alterations exacerbate pathological protein accumulation (Mander et al., 2016). One of the main mechanisms linking sleep fragmentation and dementia is altered protein clearance. The metabolic and oxidative by-products which accumulate during waking are cleared via the glymphatic system (Bohnen & Hu, 2019), a waste clearance system in the brain that utilises a system of perivascular tunnels formed by astroglial cells, to remove soluble proteins and metabolites, including soluble A $\beta$  (Jessen et al., 2015). During natural SWS and under anaesthesia, the levels of clearance in the glymphatic system increase due to a decrease in brain activity and increased interstitial fluid (ISF) flow (Jessen et al., 2015). While greater SWA and hence better SWS quality correlates with accelerated A $\beta$  clearance in healthy humans, acute SWS-disruption increases overnight A $\beta$  levels by 25 - 30% (Lucey & Holtzman, 2015). In mice, acute sleep deprivation correlates with

increased soluble A $\beta$  levels in the brain while chronic deprivation increases amyloid plaques. Long-term, low-quality sleep is also associated with increased Tau levels, as Tau is cleared in a slower fashion than amyloid- $\beta$  (Ju et al., 2017).

Although  $\alpha$ -syn clearance through the glymphatic system has not been determined yet (Valdinocci et al., 2017), blocking  $\alpha$ -syn clearance in a mouse model of PD was shown to aggravate the phenotype (Zou et al., 2019). However, more studies need to be conducted to determine the role of  $\alpha$ -syn clearance and production in relation to SWS. Finally, in addition to the clearance deficit seen in AD, A $\beta$  and tau production are also increased as a result of sleep fragmentation and the related disruption of SWS (Lucey et al., 2018). In time, this dysregulation increases the risk for plaque and tangle formation (Ju et al., 2017). A similar mechanisms might be in place in relation to  $\alpha$ -syn production during SWS disruption but again, this theory needs to be investigated experimentally.

Sleep is also a state that allows restorative cellular processes to occur, which counteract the negative impact of the accumulated oxidative stress of wakefulness by the replenishment of ATP, the repair of DNA damage etc. (Xie et al., 2013). The restorative function of SWS can be compared to that of anti-oxidative agents, as they have been shown to prevent the accumulation of oxidative stress markers in the hippocampus and improve A $\beta$ -related memory deficits in animal models of AD (review by Cedernaes et al., 2017). Sleep fragmentation on the other hand has been shown to increase oxidative stress in the rodent brain, including the LC and hippocampus, both of which are inherently sensitive to cellular damage (Mathangi et al., 2012; Zhang et al., 2014; Silva et al., 2004). Furthermore, abnormal protein accumulation in healthy cells affects the endoplasmic-reticulum (ER) induced unfolded protein response (UPR). Studies in young, healthy mice have shown that the UPR limits the protein load, even under sleep deprivation. However with ageing and the emergence of fragmented sleep patterns the UPR system malfunctions, leading to protein accumulation (Naidoo et al., 2008). Consequently, the UPR may be even more affected by fragmented sleep patterns in dementia, obstructing toxic protein clearance within cells. It is therefore clear that sleep and the dementia-related pathology function in a vicious feedback loop, with one aggravating the other (Bohnen & Hu, 2019).

## **1.8. Thesis objectives**

The overall aim of this thesis was to investigate changes in network oscillations due to  $\alpha$ -syn pathology, in both the sleep and awake states using rodents and humans respectively.

### **1.8.1. *EEG changes in DLB patients***

In the third Chapter of this thesis, we present our analysis of resting-state EEG data from patients with DLB, PDD, AD and healthy controls. Our first aim was to identify DLB-specific changes in the EEG. Earlier studies focused on investigating the capacity of qEEG measures in aiding DLB differential diagnosis in clinical settings. Hence, they utilized methods such as assessment of DLB-related EEG changes by visual observation (Bonanni et al., 2010, 2008), or attempted to develop an online method that analyses several qEEG measures during EEG data acquisition (Garn et al., 2017). However, we took a less clinically-orientated approach as we were also interested in untangling the mechanisms underlying qEEG changes in DLB patients. Thus, we performed extensive pre-processing analysis of the EEG signal and proceeded with a thorough analysis of a number of qEEG measures within different frequency ranges and brain regions, between DLB, PDD and AD patients and healthy controls. We focused on variables described in previous studies such as the EEG slowing, the dominant frequency (DF) and DF variability (DFV). Our second aim was to investigate whether these qEEG variables correlated with CFs measured by the CAF score. Lastly, our third aim was to test whether these qEEG variables could differentiate between DLB and AD patients and thus, be potentially useful for the development of an EEG-based DLB biomarker.

### **1.8.2. *Sleep study in the A30P mouse model of dementia***

Changes in sleep oscillations occur in patients with DLB, but EEG sleep studies are difficult to conduct in patients with dementia. Therefore, we aimed to make a detailed assessment of changes in network oscillations during sleep using a rodent model of DLB. Data from my experiments would hopefully help direct future research to determine if any changes observed in rodents could translate to humans.

In the fourth Chapter of this thesis, we present our analysis of electrophysiological recordings in young A30P mice (2.5 – 4 months) under urethane

induced anaesthesia, and contrast our findings with similar recordings from wild-type (WT) mice of the same age. Anaesthesia is a widely used model of sleep that mimics several of its elements: the loss of consciousness, the reduced sensory awareness and behavioural responsiveness, and the SO (Suzuki & Smith, 1988). Urethane is a particularly good model of sleep, as at moderate concentrations it exerts its effect by hyperpolarising cortical neurons through modulating potassium conductance, and not through GABAergic antagonism like other anaesthetics (Hara & Harris, 2002). Therefore, it does not disturb the balance between excitation and inhibition in the brain, nor does it inhibit neuronal firing, similar to isoflurane for example, which is an allosteric GABA<sub>A</sub>R agonist (Adragna & Klein, 2003; Ferron et al., 2009). The anaesthetic ketamine in combination with an  $\alpha$ 2-adrenergic agonist (xylazine or medetomidine) was also considered, as it induces spontaneous, natural-sleep like SO through the non-competitive inhibition of NMDA receptors. However, ketamine can only induce deep anaesthesia for approximately 50 minutes in rodents (Swindle et al., 2002), while urethane has a more long-standing effect (> 2 hours), and was thus considered more appropriate for a sleep study (Lee & Jones, 2018).

Urethane was traditionally used as a model of NREM and REM sleep by manipulating the levels of anaesthesia, with NREM sleep modelled with deeper levels of urethane anaesthesia and REM sleep with more superficial levels (Détári et al., 1997). However, more recent studies have shown the presence of REM-like activity under deep urethane anaesthesia in rats and mice (Zhurakovskaya et al., 2016; Clement et al., 2008; Yanovsky et al., 2014; Pagliardini et al., 2013). These REM-like states or, as also called “activated states”, manifest abruptly as periods of increased theta activity in the rodent hippocampus, similarly to what we can observe under natural REM sleep (Katsageorgiou et al., 2018) and are accompanied by increased low-voltage fast activity (gamma; 25 – 40 Hz) in the cortex (Clement et al., 2008; Pagliardini et al., 2013). Moreover, each activated/deactivated state cycle lasts about 9 minutes in rats (Clement et al., 2018), and 14 minutes in mice, with each activated state lasting about 4 minutes (Pagliardini et al., 2013). Thus, the NREM-REM cycle duration replicates findings in rodents under natural sleep (Trachsel et al., 1991; McShane et al., 2012). Thus, urethane anaesthesia also allows the investigation of REM-like activity, although caution is required before coming to any conclusions (Zhurakovskaya et al., 2019).

Our study utilises A30P mice at a young age of 2.5 – 4 months (Freichel et al., 2007; Kahle et al., 2000). A30P mice at this age do not express gross cognitive and motor symptoms, proteinase-K resistance  $\alpha$ -syn aggregates or neurodegeneration (Schell et al., 2009), although there is evidence of an early widespread expression of soluble mutant  $\alpha$ -syn (Newman et al., 2012). Thus, it is possible that these young A30P animals have more subtle  $\alpha$ -syn related changes. In fact, there is evidence for a very fine motor impairment (Ekmark-Lewén et al., 2018), altered behaviour in a locomotor test and abnormal electrophysiological activity at 2 months of age (Tweedy et al., 2018). Moreover, these animals might have oligomeric  $\alpha$ -syn forms that are less easily detected immunohistochemically, as A30P  $\alpha$ -syn aggregates rapidly to form oligomers upon *in vitro* incubation (Li et al., 2019). Therefore, young A30P mice constitute a good model for studying the early stages of pre-symptomatic  $\alpha$ -synucleinopathy, particularly DLB, as proposed by Kahle *et al.* (2001) due to the topographic expression of the mutant  $\alpha$ -syn in the brain.

We obtained acute electrophysiological recordings from the subregions of the mPFC: anterior cingulate cortex (ACC), prelimbic (PrL), infralimbic (IL), dorsal peduncular region (DP), and/or the CA1 of the hippocampus, in age-matched WT and A30P animals. These areas have Lewy-related pathology in both DLB patients (Mak et al., 2014) and A30P animals at later age stages of disease (Kahle et al., 2001), and are involved in memory consolidation (Euston et al., 2012) and the function of the DMN (Raichle, 2015). Moreover, the mPFC and hippocampus show synchronous SWS activity as well in sleep state alternations (Durán et al., 2018). The CA1 pyramidal layer was chosen in particular as it is the location where SWRs are best recorded (Buzsáki & Silva, 2012), and because it receives neocortical input through the nucleus reuniens, and EC input through the CA3 region of the hippocampus (Vertes et al., 2007).

We then proceeded to analyse our recordings for an array of EEG characteristics including the frequency and amplitude of the SO, the length of the Up- and Down-states and the power in high frequency bands: beta (15 – 30 Hz), gamma (30 – 80 Hz) and high gamma (80 – 130 Hz), in the SO cycle. Moreover, several characteristics of sleep spindles were investigated in the mPFC, and of SWRs in the CA1 of the hippocampus. We also looked at unit data from the mPFC region, in order to identify possible changes in neuronal firing in relation to the SO cycle. Finally, we investigated

for changes in the SO synchrony between the mPFC and CA1 and hence, in the widespread synchronicity of the SO in the brain of these mice.

During our recordings in both WT and A30P animals under deep-urethane anaesthesia, we noticed the occurrence of a cyclic event characterised by bursts of oscillatory power, which we named the infra-slow modulation (ISM). The same event was previously observed in our lab in the urethane-anaesthetised rat (Gretenkord, 2015). Hence, in the fifth Chapter we proceeded to characterise this event in the WT animals, in the mPFC and hippocampus in terms of its rhythmicity, SO cycle state lengths, high frequency oscillatory power content on the SO cycle and neuronal-firing patterns. Finally, in the sixth Chapter, we compared the aforementioned characteristics of the ISM between WT and A30P animals, in order to identify any alterations that may be related to the  $\alpha$ -syn pathology.

### **1.8.3. Aims**

#### Human EEG analysis

- To investigate for the “EEG slowing” in DLB patients and compare the power, DF and DFV distribution patterns in DLB patients to AD and PDD patients and aged-matched controls.
- To investigate for correlations between qEEG measures with CFs measured by the CAF score.
- To assess the capacity these qEEG measures to differentiate between AD and DLB patients.

#### Electrophysiological investigation in the A30P mouse models

- To identify electrophysiological changes in the mPFC and CA1 region of the hippocampus in young A30P animals compared to age-matched WT, during urethane-induced anaesthesia mimicking SWS.
- To characterise a cyclic phenomenon (ISM) observed under urethane anaesthesia in WT mice.
- To identify differences in the electrophysiological characteristics of the ISM between young A30P and WT animals, in the mPFC and CA1 region of the hippocampus.

## **Chapter 2. Methods**



## **2.1. Human EEG analysis**

### **2.1.1. *Diagnostic groups***

EEG recordings were obtained before the start of this project as part of the Cognitive and Attentional Function in Lewy Body Diseases (CATFieLD) study. The patients included in this study were individuals who were referred to local old age psychiatry and neurology services and diagnosis was determined by two independent experienced clinicians (Alan J. Thomas and John-Paul Taylor). Controls were healthy age-matched volunteers. Patients with DLB fulfilled the 2005 and 2017 revised criteria for probable DLB (McKeith et al., 2005, 2017) and patients with PDD fulfilled the criteria for probable PDD (Emre et al., 2007). Individuals with AD met the revised criteria of the National Institute of Neurological and Communicative Diseases and Stroke/AD and Related Disorders Association for probable AD (McKhann et al., 2011). The clinical assessment of fluctuation (CAF) score was assessed by the clinicians and CFs were defined on the basis that they were typical of those seen in DLB and internally driven rather than a response to external environmental factors. Healthy participants demonstrated no evidence of dementia as determined by the Cambridge Cognitive Examination (CAMCOG) score ( $> 80$ ) and from clinical history. Exclusion criteria for all participants included significant history of neurological or psychiatric conditions. Prescriptions of acetylcholinesterase inhibitors (AChEIs), memantine and dopaminergic medications were allowed. Ethical approval was provided by the Northumberland Tyne and Wear NHS Trust and Newcastle University ethics committee.

### **2.1.2. *EEG recordings***

As mentioned above, the EEG recordings were obtained as part of the CATFieLD study. These high-density, eyes-closed resting-state EEG recordings were obtained using 128 channel ANT Waveguard caps (ANT Neuro, Netherlands) with an Ag/AgCl electrode montage set according to the 10-20 placement system (Oostenveld & Praamstra 2001; Figure 2.1). Electrode impedance with kept below 5 k $\Omega$ . A reference electrode (Fz) was used, no filters were applied during acquisition and the sampling frequency was set at 1024 Hz per channel. The patients that received medication had normally taken AChEIs at least 4 hours before recordings were performed, while the time of the last Levodopa dose was 1-3 hours prior to the EEG session.

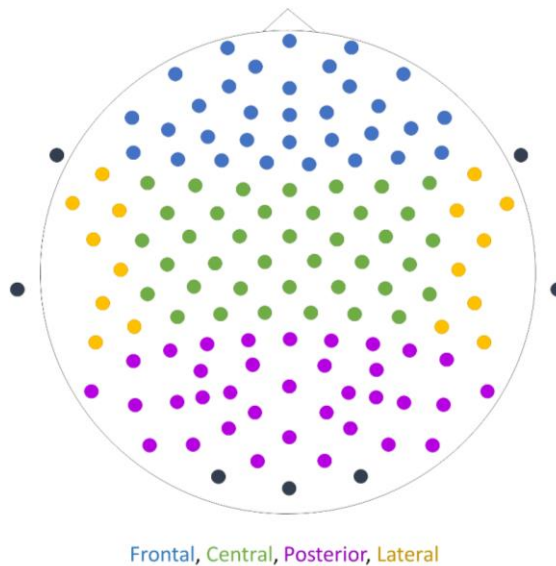


**Figure 2.1:** Placement of the 128 electrodes according to the 10-20 placement system. The signal recorded from the electrodes indicated with black colour was selected out as it was deemed too noisy. The colours indicate the grouping of the electrodes into four regions: blue = frontal, green = central, purple = posterior, yellow = lateral. Adapted from Stylianou et al. (2018).

### 2.1.3. *Pre-processing*

Pre-processing of the EEG recordings was performed off-line after acquisition on the MATLAB environment (MATLAB R2016b, The MathWorks Inc., Natick, MA, 2016), using the EEGLAB toolbox version 13 (Delorme & Makeig, 2004) and scripts kindly offered by Dr Nik Murphy. The EEG signal was filtered with a 4 Hz high-pass and a 46 Hz low-pass filter. Lower frequencies were filtered out as they imposed noise on the higher frequencies that were of more interest, and because the EEG generally has a limited accuracy in estimating very low and very high frequencies (Niedermeyer & Lopes da Silva, 2004). A notch filter was applied at 50 Hz. Recordings from all electrodes were visually inspected in the power-time domain and rejected if they had a kurtosis value over 3, or if they contained clear and consistent artefacts such as electrooculogram (EOG) and electromyogram (EMG) artefacts. The number of EEG channels / electrodes removed was kept to the minimum possible (mean =  $17.7 \pm 6.7$ , min.= 0, max.= 33).

Independent component analysis (ICA) was used to accurately estimate and remove the presence of additional ocular, muscular, and other non-neuronal activity (Kropotov & Kropotov, 2009c). Individual recordings were reduced to 30 principal

components and then decomposed using the extended RUNICA algorithm (Bell & Sejnowski, 1995; Delorme & Makeig, 2004). Components representing existing templates for muscular, ocular, and electrical (50 Hz line noise) artefacts (Jung et al., 2000) were rejected (mean =  $5.2 \pm 1.6$ , min. = 0, max.= 9) and the remaining independent components remixed. The recordings were then segmented into 2 s-long epochs and were inspected for any remaining artefacts. Epochs containing large artefacts were removed across channels, in a conservative manner. Finally, the removed channels were replaced using spherical spline interpolation (Ferree, 2006). As a final step, the EEG montage was changed to average reference.

#### **2.1.4. Variable extraction**

The power spectral density (PSD) for each 2-s epoch was estimated using Bartlett's method (Bartlett, 1950) with a 0.25 Hz frequency resolution using a 4 s FFT (fast Fourier transform) size and a Hamming window. To compensate for the between subject variability in factors such as brain neurophysiology, anatomy and physical tissue properties, the data were transformed to relative power (Rodriguez et al., 1999). Seven subjects were rejected from further analysis due to an insufficient number of clean data (< 48 epochs). For the remaining 73 subjects (21 healthy controls, 18 AD, 17 DLB and 17 PDD), the recordings were truncated to the first 47 epochs (total length of 94 s) and electrodes were grouped into four regions: frontal, central, posterior and lateral (Figure 2.1).

The mean relative power distributed in each of three frequency bands: theta (4 – 7.75 Hz), alpha (8 – 13.75 Hz), beta (14 – 20.75 Hz), was extracted as a percentage of the total power in that range. Higher frequencies were excluded as they are prone to contamination by electromyogram rhythms (Whitham et al., 2007). The DF - the frequency with the highest power - was extracted for each epoch to calculate the mean dominant frequency (DF) and DF variability (DFV; SD from the mean) across epochs, for the slow-theta (4 – 5.5 Hz), fast-theta (5.5 – 7.75 Hz), theta, alpha and theta/alpha (4 – 13.75 Hz) frequency ranges. Since the DF was limited within the theta-alpha range, beta band activity was excluded. The theta-alpha DF was used to calculate the Frequency Prevalence (FP) distribution, which is the percentage of epochs having a DF falling within the slow-theta, fast-theta and alpha frequency ranges. These measures were calculated for each patient, for each diagnostic group and for each

band and region combination. See Figure 2.2 for a full description of the methods of variable extraction.

### **2.1.5. Statistical analysis**

All statistical analysis was performed on IBM SPSS Statistics 25. First, we tested our data for normal distribution using the Shapiro-Wilk test and logarithmically transformed the data if necessary to achieve it. We also tested the data for heteroscedasticity using Levene's test for equal variances. The normally distributed data was then statistically compared using mixed repeated measures ANOVA (rmANOVA) analysis, with region as the within-subjects factor and diagnosis as the between-subjects factor. When a significant interaction was found we followed up by univariate ANOVA and post-hoc analysis with a Bonferonni correction.

When the issues of heteroscedasticity could not be solved, we performed Welch's ANOVA followed by the Games-Howell test. For non-normally distributed data we performed Kruskal-Wallis H test followed by post-hoc analysis. Pearson's product-moment correlation and Spearman's rank correlation were used to investigate for correlations between these variables and the CAF score and the MMSE score for each diagnostic group. Manual correction for multiple comparisons by appropriating the level of  $\alpha$  significance ( $\alpha/N$ ) was performed for the non-parametric statistical analyses and for the correlation analyses, where Bonferonni correction was not available with the statistical software (IBM SPSS Statistics 25).

In order to assess the capacity of the qEEG variables that were significantly different between the AD and DLB, and the DLB and PDD groups to predict diagnosis, the generalised estimating equations (GEE) procedure were used. This method allows the analysis of repeated measurements without the assumption for normal distribution (Carr & Chi, 1992). The qEEG variables that introduce multi-collinearity to the model (variance inflation factor  $> 5$ ) were excluded from this analysis. Region was defined as the within-subjects variable, diagnosis as the between-subjects variable and the qEEG variables and the CAF score as the co-factor. The variables that significantly predicted diagnosis were then used to calculate the receiver operating characteristic (ROC) curve, and obtain the area under the curve (AUC), sensitivity and specificity with asymptotic confidence intervals. The sensitivity/specificity cut-off was determined using Youden's index.

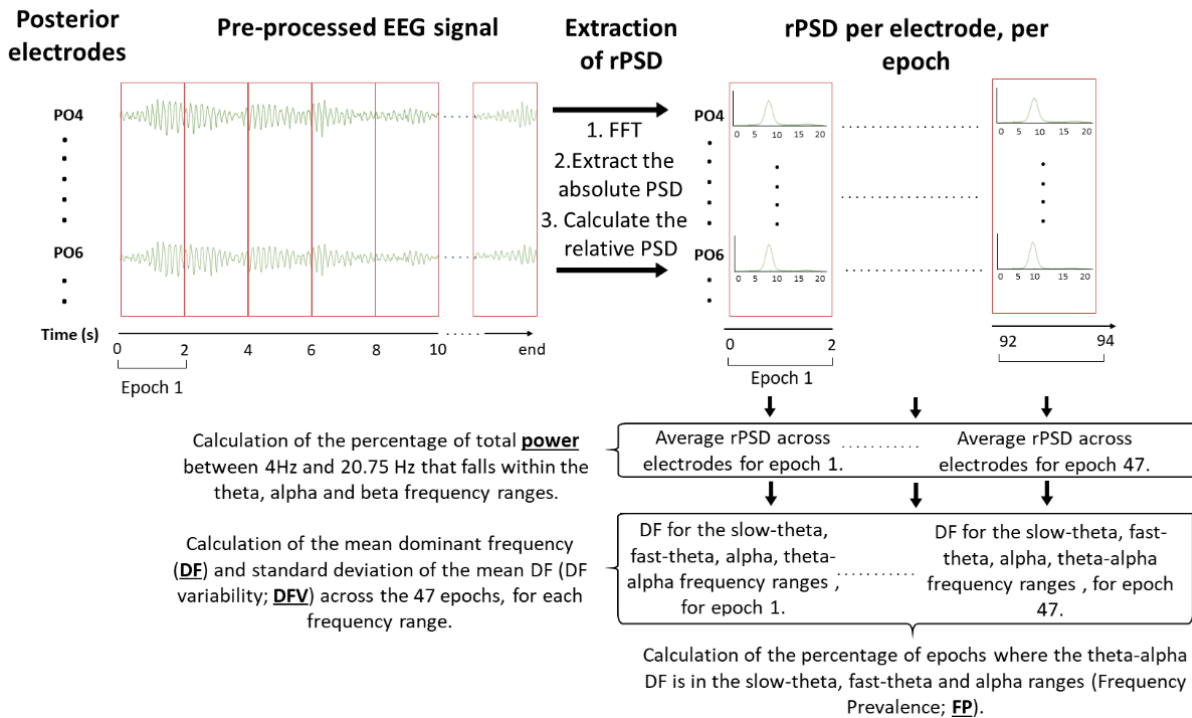


**Figure 2.2:** Schematic diagram illustrating the process of extracting each of the four main quantitative EEG variables used in this study, for one participant in the posterior region. The filtered, pre-processed EEG signal on each of the electrodes in posterior derivations ( $N = 35$ ) is windowed in 2 sec long epochs. The signal undergoes fast-Fourier transform (FFT) and using Bartlett's method the absolute power spectral density (PSD) is calculated for each epoch, for each electrode. The relative PSD (rPSD) is then calculated to normalize the signal. The mean rPSD is obtained across posterior electrodes, for each epoch (up to 47 epochs) of the recording, and the percentage of the total power in the 3 Hz – 20.75 Hz range allocated to the theta (4 – 7.75 Hz), alpha (8 – 13.75 Hz) and beta (14 – 20.75 Hz) frequency ranges is calculated. The frequency with the highest power within the slow-theta (4 – 5.5 Hz), fast-theta (5.5 – 7.75 Hz), alpha and theta-alpha (4 – 13.75 Hz) frequency ranges was identified within each epoch, and that value corresponded to the dominant frequency (DF). The mean DF and the standard deviation of the mean DF (DF variability; DFV) across epochs were then calculated. Finally, the DF within each epoch was assessed and was characterised to be in the slow-theta, fast-theta or alpha range. The epochs that were characterised by a DF within each of these ranges are shown as a percentage of the total number of epochs. These percentages were the slow-theta, fast-theta and alpha frequency prevalence (FP). The same procedure was followed for the other three cortical regions. Adapted from Stylianou et al. (2018).

## **2.2. Animal electrophysiological recordings**

### **2.2.1. Animals**

A30P mice, which are mice of C57BL/6 background expressing human mutant A30P  $\alpha$ -syn under the control of the CNS specific promoter Thy-1 (Kahle et al., 2000, Neumann et al., 2002), were used. The line was generated from frozen sperm supplied by Dr. P. Kahle, University of Tübingen and used to inseminate a WT female to generate a heterozygous line. The pups were genotyped to obtain a homozygous A30P pair and a wild-type (WT) pair that founded the two lines of animals used for these experiments. These lines were bred in house and were stopped in a timely manner to avoid excessive inbreeding.

All procedures described below were in accordance with the UK Animals (Scientific Procedures) Act 1986 and the European Union Directive 2010/63/EU. WT and A30P mice were bred in house at Newcastle University's animal facility in a temperature- and humidity-controlled environment consistent with the ARRIVE (Animal Research: Reporting of *In Vivo* Experiments) guidelines. Mice were kept in an enriched environment (cage toys) under a 12 hour light:dark cycle (lights on 7 am - 7 pm) with access to food and water *ad libitum*. Mice were group housed and experiments were commenced ~2 hours into the light (sleep) phase of the circadian cycle. Our previous *in vitro* studies using the A30P mouse line have suggested greater network cortical hyperexcitability in young male mice compared to female mice (Tweedy et al 2018). Therefore, in this study only male mice aged 2.5 – 4 months were used.

### **2.2.2. Anaesthesia and Surgery**

The animals were initially anaesthetised with 4 % isoflurane in order to administer the first urethane dose (0.6 ml of 20 g/kg in water for injection; Sigma-Aldrich) by intraperitoneal (i.p.) injection. After injection, the mice were immediately fixed in a stereotaxic frame (Kopf, Tujunga, CA, USA). A heating pad with feedback temperature control via a rectal probe (Harvard Apparatus, Holliston, MA, USA) maintained the core temperature of the mouse at 36.8°C. The animal breathed spontaneously but to maintain an oxygen saturation of > 90%, medical oxygen (BOC Industrial Gases, UK) was supplied through a tube mounted to the nose bar of the stereotaxic frame. Right after the initial urethane injection and for the duration of the surgery (20 - 30 min), 1% isoflurane was also provided through the mask. The isoflurane concentration was gradually lowered to

0%, when deep urethane anaesthesia was achieved. The level of anaesthesia was confirmed by absence of the pedal withdrawal reflex. The reflex was checked regularly and additional doses of urethane (0.1 ml) were given i.p. at later stages of the experiments, usually > 4 h after the first dose, if REM sleep or the pedal reflex emerged. After a urethane top-up, recordings would re-commence about 30 min later, when stable SOs had re-emerged.

A skin incision was made in the scalp and infused with lidocaine, before the periosteum was retracted to expose bregma. A craniotomy was drilled above the left mPFC and/or the right hippocampus. Electrodes (see below) were implanted into the left mPFC (AP = +2, ML = - 0.4, DV = 2.5 mm) and/or right hippocampus passing through the CA1 region of the hippocampus (AP = -2, ML = +2, DV = 2 mm, at 7.8° angle). The electrode was lowered ventrally, through the dura, using a one-axis oil-filled hydraulic micromanipulator (Narishige, Japan).

### **2.2.3. Data recording and acquisition**

Multi-channel recordings were made in all subregions of the mPFC in the left hemispheres and/or the contralateral hippocampus passing through the CA1 with single shank 16-channel silicon probes (150 µm inter-site spacing; 25 µm diameter, Atlas Neuroengineering, Leuven, Belgium). Before insertion, the silicon probe was coated with a fluorescent dye (Dil,) (1,1'-dioctadecyl-3,3,3',3'-tetramethylindocarbocyanine; Molecular probes, Eugene, Oregon, USA), dissolved in DMSO (1.5 - 2.5 mg/ml). Local field potential (LFP) and single unit recordings were carried out in each subregion of the mPFC: ACC, PrL, IL and DP. Post-hoc histology confirmed the correct positioning of the electrode probes (see below). Each of the signal channels was passed through a unity-gain headstage (Plexon, Texas, USA), and was then amplified (×1000) and filtered (0.07 – 300 Hz for LFP) by a Plexon preamplifier (Plexon, Texas, USA). Unit data was amplified at x40000 and filtered at > 200 Hz. The LFP was digitised at 1 kHz while unit data was digitised at 40 kHz and recorded on a PC (DELL Intel 4-core) running Plexon software (Sort Client).

#### **2.2.4. *Histological verification of recording site position***

After the experiment the mouse was sacrificed by injection with Euthatal (0.2 ml i.p.). The brain was removed from the skull and post-fixed in 4% paraformaldehyde (PFA) 0.1 M phosphate buffer solution (PBS) at 4°C, for approximately 48 hrs. The brain was then transferred for cryoprotection in a 30% sucrose solution for 48 - 72 hours. Coronal sections (60 µm) were cut on a cooled vibratome (Zeiss Hyrax V50, Zeiss, Oberkochen, Germany) and collected in 0.1 M PBS. DAPI (4',6-diamidino-2-phenylindole; Sigma-Aldrich) staining and Dil (D282, Thermo Fisher Scientific) was used to verify the position of the silicon probes (Figure 2.3A). After staining, sections were mounted and cover-slipped using mounting medium (Sigma-Aldrich). The location of the electrodes was verified using the Fiji plugin on ImageJ (Schindelin et al., 2012; Schneider, Rasband and Eliceiri, 2012).

#### **2.2.5. *Data Analysis***

##### **2.2.5.1. *Data pre-processing***

The raw local field potential (LFP) signal contained 50 Hz noise as well as higher frequency harmonics and was therefore notch filtered around 50 Hz, 100 Hz, 150 Hz, 200 Hz, 250 Hz, and 300 Hz, using a linear-phase finite impulse response filter (FIR) created using 'fdatool.m' in combination with the MATLAB (Mathworks, Nantick, MA, USA) 'filtfilt.m' function. Recordings from electrode contacts that were noisy or broken were not used in the analysis. The LFP recordings used were concatenated sections from the original 30 min-long recordings. Parts of the recording were automatically removed via a custom written code in MATLAB, to avoid including non-SO segments. The same segments were also removed from the unit data. The resulting LFP recordings were approximately 20 min long. For the mPFC we used all 16 channels, while for the hippocampus we only used the channel that was located at the CA1 pyramidal layer, as verified through the histological analysis.

All data analysis was performed offline using custom MATLAB (Mathworks, Nantick, MA, USA) scripts. The Up- and Down-state detection and wavelet power extraction scripts were expansions of the original script written by Sabine Gretenkord. The unit spiking analysis and the spindle, SWR and non-SO segment identification and analysis scripts were custom made for this project.

#### 2.2.5.2. Up- and Down-state detection

During slow oscillations (SO), high frequency oscillations occur transiently during the Up-state, and are absent during the Down-state (Steriade et al., 1993a). Thus to investigate these nested oscillations in more detail it was first necessary to detect Up- and Down-states (UDS). UDS detection (Figure 2.3B) was performed using the phase of the SO, as described previously (Massi et al., 2012), except that the Hilbert transform (rather than the wavelet transform) was used to calculate the phase of the SO. The LFP was first band-pass filtered for the SO (0.1 – 0.9 Hz) and the instantaneous phase  $\phi(t)$  was calculated using the Hilbert transform. The threshold to discriminate between Up- and Down-states was  $\cos(\phi(t) = 0)$  (Gretenkord et al., 2017). To qualify as an Up-state, the duration of the event had to exceed 300 ms and the average amplitude of the Up-state of the SO band-passed signal had to be larger than 0.05 mV. The mean Up- and Down- state lengths were calculated for each channel, for each recording. The SO cycle length was calculated as the length of the Down-state + the length of the following Up-state. The variability over time in the Up- and Down-state lengths and the SO cycle length were calculated as the SD of the mean for each variable, across SO cycles. The number of SO cycles was used to calculate the frequency of the SO.

#### 2.2.5.3. Calculation of slow oscillation amplitude

The amplitude of the SO was calculated using the SO-filtered LFP (0.1 – 0.9 Hz). The SO amplitude was calculated as the peak-to-trough amplitude (maximum during Up state – minimum during Down state) for each cycle.

#### 2.2.5.4. Calculation of the UDS phase vector

Time points of Up- and Down-state transitions were calculated from the UDS detection logical vector. A cycle always consisted of a Down-state and an Up-state and contained three transitions: transition 1: Up-to-Down transition (i.e. end of the Up-state to beginning of the Down-state) 2: Down-to-Up transition (i.e. end of the Down-state to beginning of the Up-state) 3: Up-to-Down transition (i.e. end of the Up-state to beginning of the Down-state). A phase vector was calculated where 0 was the time point of transition 1, 50 was the time point of transition 2, and 100 was the time point of transition 3. The time points in between were filled with linearly spaced intermediate values, so that a phase vector was achieved with linear phase progression during the Down-state, and linear phase progression during the Up-state. All UDS were then divided into 40 bins per state (Gretenkord et al., 2017; Figure 2.3B).

#### 2.2.5.5. Calculation of power at higher frequencies

Before calculating high frequency oscillatory power, the LFP data for each electrode channel was normalised with the zscore Matlab function, hence eliminating the unit of measurement. The normalised signal was then transformed using a continuous wavelet transform and specifically a complex Morlet wavelet, for the theta (4 – 7.9 Hz), beta (15 – 29.9 Hz), gamma (30 – 79.9 Hz) and high-gamma (80 – 130 Hz) frequency bands (Gretenkord et al., 2017; Massi et al., 2012; Figure 2.3C). The instantaneous area power was then calculated using trapezoidal numerical integration over all frequencies in the given band. The mean power per bin of the UDS phase vector was calculated for each UDS cycle, leading to the alignment of the power to a normalised cycle. This compensated for the variable lengths of UDS cycles within a particular data segment, and thus allowed a mean power over the normalised UDS cycle to be calculated for each electrode channel, for each animal (Gretenkord et al., 2017; Figure 2.3D)

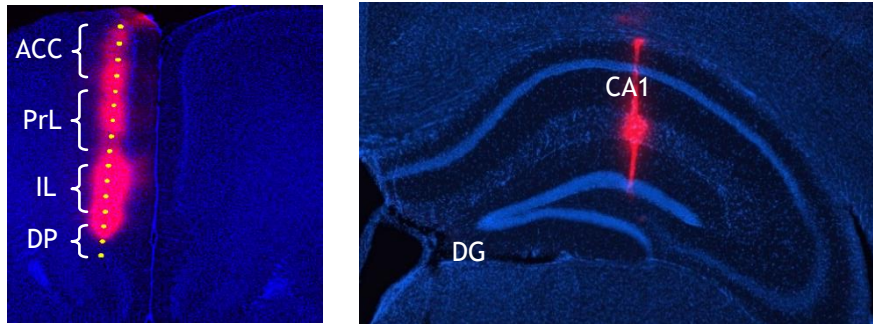
#### 2.2.5.6. Single unit analysis

Single units in the mPFC were sorted online first using the Plexon Sort Client and then offline using the Plexon Offline sorter. During offline sorting, all waveforms were aligned to the global minimum and inter-spike intervals (ISIs) that were shorter than the absolute refractory period ( $< 1$  ms) were automatically removed. Only units which could be well distinguished were included in the analysis. In most cases one unit per channel was recorded although occasionally, two units could be isolated. No units were obtained from the hippocampus. The unit firing time point data was down-sampled to 1 kHz, accounting for the number of spikes at each of the down-sampled points. Measures of coherence between the SO-band passed LFP and the unit firing were obtained using the mscohere function in MATLAB with a  $2^{14}$  window and no-overlap. The threshold for analysing a unit was set at 10 spikes/min (0.17 Hz) while for coherence analysis it was set at 30 spikes/min (0.5 Hz).

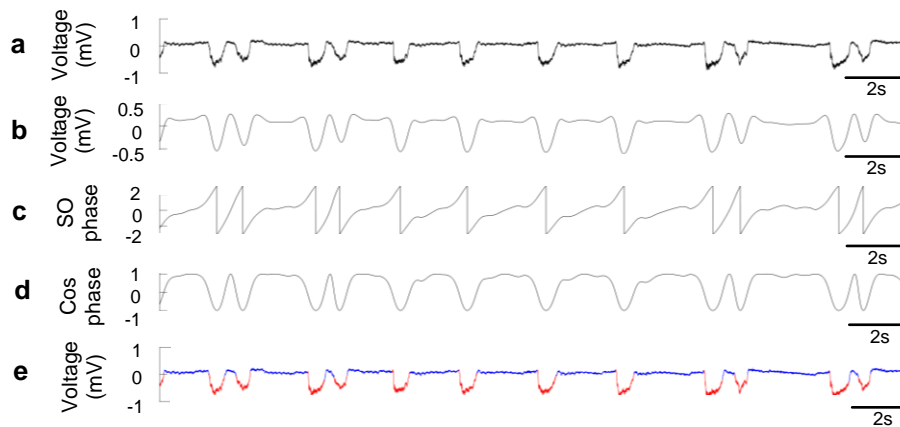
The time points of unit firing were compared to the normalised Up-Down cycle to identify whether they occurred during an Up- or a Down-state (Figure 2.4). The percentage of firing on the Up- and Down-states was calculated as a percentage of the total firing. The unit firing frequency on Up-state was calculated as a fraction of the total number of spikes occurring on the Up-states by the length of all the Up-states combined. We also calculated the unit firing frequency for the duration of the recording, by dividing the total number of spikes recorded irrespective of state, divided by the

duration of the recording. In a similar way, we also calculated the inter-spike interval (ISI) on the Up-state and for the duration of the recording. We also estimated the latency to the first unit on the Up-state. Finally, we found the maximum coherence between the SO and unit firing on the Up-state and identified the frequency it occurred at (0.1 – 0.9 Hz; Figure 2.4).

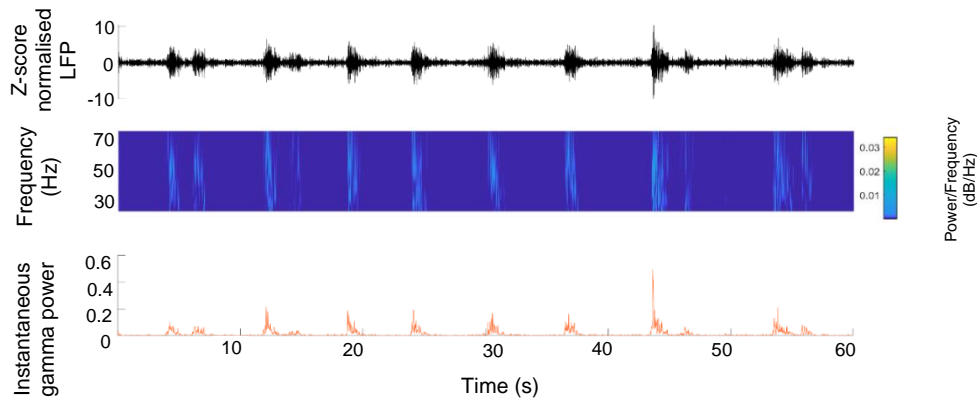
### A) Electrode positioning



### B) Up-Down state detection



### C) High frequency oscillatory power extraction in the SO cycle



### D) High frequency power distribution on the normalised SO cycle

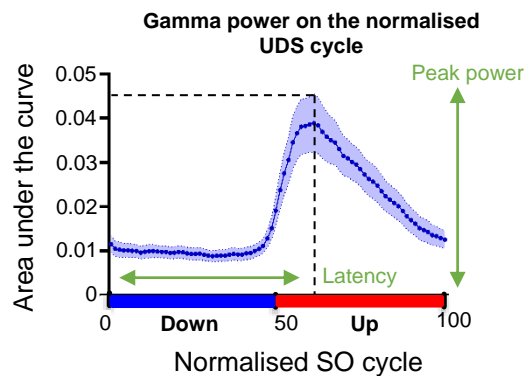


**Figure 2.3:** Methods of acute, *in vivo* electrophysiological recordings in mice under urethane-induced anaesthesia **A)** Example of the electrode tract in the medial prefrontal cortex (mPFC) and its 4 subregions: anterior cingulate cortex (ACC), prelimbic cortex (PrL), infralimbic cortex (IL) and dorsal peduncular (DP), and in the hippocampus passing through the CA1, stained with Dil and DAPI. **B)** Up- and Down-state detection method. The **a)** LFP was **b)** band-passed for the SO (0.1 – 0.9 Hz) and **c)** a Hilbert transform) was used to calculate the phase of the SO. **d)** The threshold to discriminate between Up- and Down-states was  $\cos(\phi(t) = 0)$ . **e)** The mean Up- and Down state-lengths were calculated for each channel, for each recording. **C)** Example of power extraction in the gamma band in the mPFC. The LFP data for each electrode channel was normalised using the z-score and was then transformed using a Morlet wavelet, for that frequency band (here gamma: 30 – 79.9 Hz). The instantaneous area power was calculated using trapezoidal numerical integration over all frequencies in the given band. **D)** The average gamma band power distribution in the SO cycle across one recording. Each SO cycle (Down-state + Up-state) was normalised (0 = start of Down-state, 50 = Down to Up-state transition, 100 = end of Up-state) and the area under the curve (power) was calculated for each point in this cycle, for each frequency range. The high frequency power at each point was averaged across SO cycle (blue curve), allowing the extraction the average power on the Up- and Down-state and of the peak power and its latency in the SO cycle, for each frequency band.

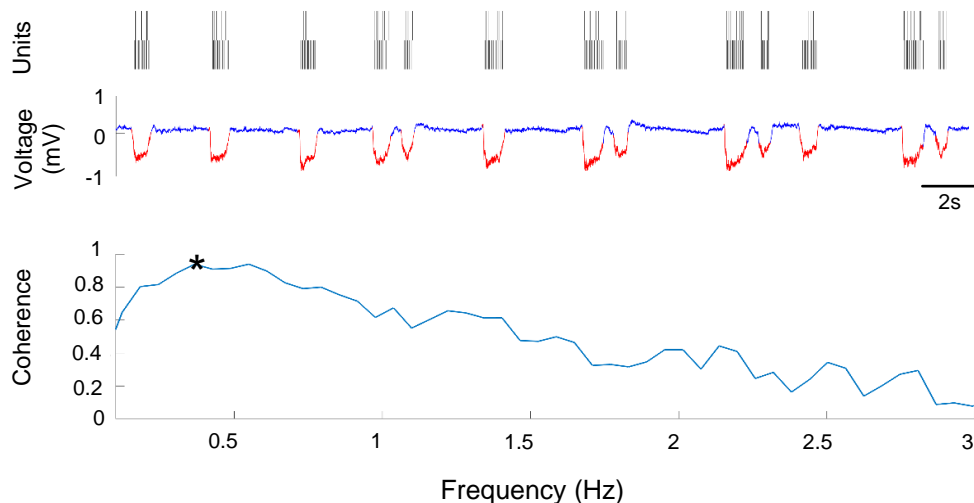


**Figure 2.4:** Analysis of unit firing in relation to the SO cycle. The SO cycle composed of a Down-state (blue) and the following Up-state (red), in the ACC subregion of the mPFC. The peak coherence between unit firing and the SO band-passed signal is shown at the bottom. The asterisk indicated the maximum coherence.

### **2.2.6. Spindle detection**

Our methods for spindle detection were adapted from Kim et al. (2015) (Figure 2.5). Firstly, the instantaneous amplitude of the spindle band-passed LFP (8 – 15 Hz) was computed using the Hilbert transform. Secondly, the instantaneous amplitude was smoothed with a 40 ms kernel. The points of the smoothed signal that crossed the upper threshold (2.5 x the mean amplitude of the smoothed signal) were identified as potential spindles. Peaks in the spindle that were less than 200 ms apart were considered part of the same spindle. The crossing points of the lower threshold (1.5 x the mean amplitude of the smoothed signal) determined the length of each spindle event. Finally, spindles that were shorter than 200 ms and longer than 2 s were rejected (Kim et al., 2015). The instantaneous frequency was calculated as the number of cycles of the spindle band-passed LFP that crossed the upper threshold encapsulated by the smoothed signal for each identified spindle, divided by the spindle duration.

### **2.2.7. Sharp wave ripple detection**

We also adapted the methods described by Kim et al. (2015) for sharp-wave ripple (SWR) detection (Figure 2.6). We used only recordings where the CA1 pyramidal layer could be confirmed histologically. Firstly, the instantaneous amplitude of the SWR band-passed LFP (80 – 130 Hz) was computed using the Hilbert transform. The instantaneous amplitude was smoothed with a 15 ms kernel. The points of the smoothed signal that crossed the upper threshold (mean amplitude of the analytical signal + 2\*SD) were identified as potential ripples. Ripples with peaks less than 100 ms apart were considered one SWR. The length of the ripples was determined by the crossing points of the lower threshold (mean amplitude of the analytical signal + 4\*SD). Finally, ripples that were shorter than 20 ms and longer than 400 ms were rejected. The instantaneous frequency was calculated as the number of cycles of the ripple band-passed LFP that crossed the upper threshold encapsulated by the smoothed signal for each identified ripple, divided by the duration of the ripples.

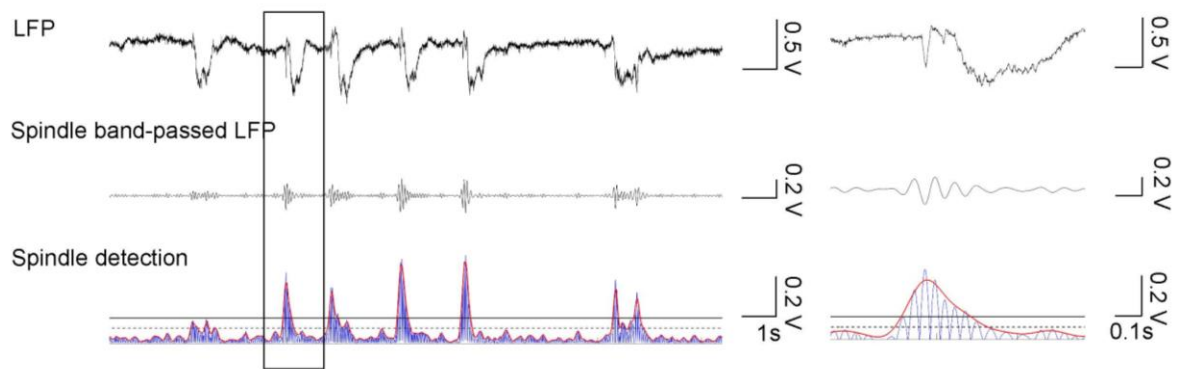


**Figure 2.5:** Spindle detection method in the ACC subregion of the mPFC, during urethane-induced SWS. The local field potential (LFP) from the ACC channel, the band-passed LFP for the spindle frequency range (8 – 15 Hz) and the spindle detection technique for a 30 s-long segment of recording. An enlarged, 1 s-long segment of the spindle is also shown (on the right). The blue line indicates the spindle band-passed LFP normalised to the baseline. The red line indicates the smoothed instantaneous amplitude of the analytical signal (Hilbert transform on the band-passed signal). A 40 ms kernel was applied (red line) and the points of the kernelled signal that crossed the upper threshold (2.5x the mean amplitude of the smoothed signal) were identified as potential spindles. The length of the spindles was determined by the crossing points of the lower threshold (1.5x the mean amplitude of the smoothed signal; dotted line). The spindle detection method was adapted from Kim *et al.* (2015).

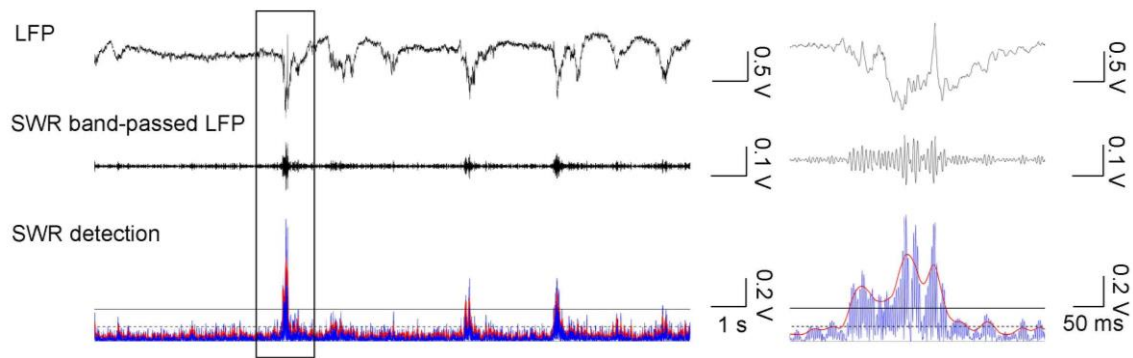


**Figure 2.6:** Sharp-wave ripple (SWRs) detection method in the CA1 of the hippocampus during urethane-induced SWS. The local field potential (LFP), the SWR band-passed LFP (80 – 130 Hz) and the SWRs detection method for a 30 s-long segment of recording. The blue line indicates the SWRs band-passed LFP normalised to the baseline (80 – 130 Hz). An enlarged, 1 s-long segment of the SWR is also shown (on the right). The red line indicates the smoothed instantaneous amplitude of the analytical signal (Hilbert transform on the ripple band-passed signal). A 15 ms kernel was used for smoothing (red line). The points of the smoothed signal that crossed the upper threshold (mean amplitude of the analytical signal + 4\*SD; continuous line) were identified as potential SWRs. The length of the SWRs was determined by the crossing points of the lower threshold (mean amplitude of the analytical signal + 4\*SD; interrupted line). The SWR detection method was adapted from Kim *et al.* (2015).

### **2.2.8. Statistical analysis**

Firstly, we ensured a Gaussian distribution of data and homogeneity of variance using the Kolmogorov-Smirnov and Levene's Test respectively. If these could not be established we performed a logarithmic or a square root transformation of the data. Normally distributed data was analysed using one-way, two-way or mixed rmANOVA analysis, with different between- and within-subjects variables depending on the analysis (specified in each Chapter's methods section). Identifying differences between mPFC subregions was out of the scope of our analysis, but subregion was included as a repeated measure due to the variability it can induce, particularly in high frequency power-related variables (Gretenkord et al., 2017). Thus, we do report findings of a significant effect of subregion when found, but we did not proceed with separate analyses between regions in the WT and A30P animals. Upon identifying a significant effect of genotypic group or an interaction between the group and a repeated variable, we proceeded with univariate ANOVA analysis with a Bonferonni correction. We also performed univariate ANOVA analyses in cases where there were no repeated measures. In cases where we had to proceed with non-parametric analyses, the exact test used is described in the Methods sub-section of that Results Chapter. Normally distributed data is presented as the mean  $\pm$  standard error of the mean (SEM), and non-normally distributed data is presented as the median  $\pm$  interquartile range (IQR).

## **Chapter 3. Human EEG analysis**



### 3.1. Introduction

Quantitative electroencephalography (qEEG) is emerging as a technique for early, and differential dementia diagnosis, as it can provide insight into changes in rhythmic brain activity and consequently, reveal local or widespread network dysfunction (Micanovic & Pal, 2014). The most prominent qEEG finding in DLB and PDD is a shift of power and dominant frequency (DF) from the alpha towards the high-theta frequency range, described as “EEG slowing” (Briel et al., 1999). This EEG slowing is most prevalent posteriorly (Briel et al., 1999) and although it is also observed in AD patients (Jackson et al., 2008), it is not as prominent as in the Lewy body diseases – DLB and PDD (Roks et al., 2008). In studies quantifying differences between DLB or DLB/PDD, or AD and healthy controls, qEEG variables such as coherence (Snaedal et al., 2012), temporal dominant frequency variability (DFV; Andersson et al., 2008), the power ratio between frequency bands and combinations of ~25 qEEG measures (Garn et al., 2017), have achieved high diagnostic sensitivity and specificity, reaching 100% in the latter study.

Previous investigations have found electrophysiological correlations of cognitive fluctuations (CFs) in DLB patients, one of the core symptoms of DLB, which refer to spontaneous alterations in cognition, attention and arousal (McKeith et al., 2017). As discussed in the Introduction (section 1.1.3), CFs are an important diagnostic feature for DLB (Ballard et al., 2002; Zupancic et al., 2011) and thus, their identification through a biomarker such as the EEG would be a valuable diagnostic tool. Early work using qEEG has shown a correlation between epoch-by-epoch DFV and CFs measured by the CAF score, in DLB patients compared with healthy controls (Walker et al., 2000). Later work also showed that DLB patients with CFs had greater DFV compared to AD patients in posterior brain regions, and used the DFV together with other qEEG measures to classify AD, PDD-CFs, PDD-without CFs and DLB patients and controls (Bonanni et al., 2008). More recently, a multi-center cohort analysis has verified these results (Bonanni et al., 2016).

The ability of the qEEG to identify EEG patterns in DLB patients and signatures of CFs, a DLB-specific symptom, suggest that qEEG could be utilised to investigate for a neurophysiological divergence between DLB and other dementias. However, the qEEG investigations performed so far have not yet managed to identify differences (Garn et al., 2017; Engedal et al., 2015) between DLB and PDD. Generally, these LBD

subtypes are similar with respect neuropathological processes, symptoms and treatment, but they differ in the order of symptom manifestation (Metzler-Baddeley, 2007). According to the 1-year rule, a PDD diagnosis is given if motor symptoms appear before or within a year of dementia onset, otherwise a DLB diagnosis is given (McKeith et al., 2004). This discrepancy between DLB and PDD suggests differences in the brain-regions involved and the evolution of the pathology (Outeiro et al., 2019). Thus, potential qEEG differences between PDD and DLB are of research interest, as they could provide insight for better understanding these LBD subtypes.

Earlier qEEG studies focused on investigating the capacity of EEG measures in aiding DLB differential diagnosis in clinical settings. Hence, they utilized methods such as assessment by visual observation (Bonanni et al., 2008), or attempted to develop an online method that performs analysis during and right-after EEG acquisition (Garn et al., 2017). Here we took a less clinically-orientated approach, as our primary goal was to characterize and compare the resting EEG rhythm in AD, DLB and PDD patients in relation to healthy controls, and to investigate for DLB specific signatures of CFs. Thus, we performed extensive pre-processing analysis of the EEG signal and a thorough analysis for differences in qEEG measures within different frequency ranges and brain regions, between diagnostic groups.

Based on the literature, we hypothesized that dementia patients will exhibit a differential pattern in the distribution of qEEG measures of power and DF within different frequency ranges compared to healthy controls. Moreover, we expected that these qEEG measures in addition to DF variability (DFV) in time will differ between the dementia groups. We also hypothesized that greater DFV will only characterize patients with LBD and possibly only DLB, and that greater DFV will correlate with more CFs within these groups. Finally, to assess the possible utility of these qEEG measures in the development of biomarkers, the qEEG measures that were found to be significantly different between groups were used to predict dementia diagnosis.

The data presented in this chapter has been published with first authorship.

## **3.2. Methods**

### **3.2.1. *Data extraction***

For our analysis we analysed eyes-closed, resting-state EEG recordings with a 128-electrode resolution, from age matched DLB, PDD, AD and healthy control patients. A number of patients and recordings were excluded, and the remaining recordings were pre-processed, as described in Methods (section 2.1.1).

The mean relative percentage power spectral density (rPSD) was extracted in 3 frequency bands of interest: theta (4 – 7.75 Hz), alpha (8 – 13.75 Hz), beta (14 – 30.75 Hz), in each of 4 cortical regions (frontal, central, posterior, lateral). Next, we extracted the dominant frequency (DF) which is the frequency with the highest rPSD, and the DF variability (DFV) indicating the standard deviation (SD) of the mean DF over time, in the theta, alpha and theta-alpha (4 – 13.75 Hz) frequency bands, in the 4 cortical regions. We also looked in the DF prevalence (DFP) that was extracted for the theta, slow-theta (4 – 5.5 Hz), fast-theta (5.75 – 7 Hz), alpha and theta-alpha frequency bands. See the Methods section 2.1.4 for the detailed data analysis and data extraction method.

We also investigated whether the aforementioned variables correlated with cognitive fluctuations measured by the CAF score, and with cognitive decline measured by the Mini-Mental State Examination (MMSE) scale. Lastly, we investigated whether the qEEG variables that were significantly different between AD and DLB patients could be used to differentiate between the two diagnostic groups, and the levels of sensitivity, specificity and accuracy of this differentiation.

### **3.2.2. *Statistical analysis***

First, we tested our data for normal distribution using the Shapiro-Wilk test, and logarithmically transformed the data if necessary. We also tested the data for heteroscedasticity using Levene's test for equal variances. The mean power, theta-alpha DF and theta, alpha and theta-alpha DFV were normally distributed while the DFV (for all frequency ranges) and the theta-alpha DF values were logarithmically transformed to achieve homogeneity of variance/homoscedasticity.

The normally distributed data was then statistically compared using mixed rmANOVA analysis, with region as the within-subjects factor and diagnosis as the between-subjects factor. Our analysis did not aim to compare the aforementioned data between cortical regions, nor to investigate how this distribution could interact with diagnosis. Thus, we do not report significant changes in the repeated measures, as it is beyond the scope of this analysis. However, we still performed mixed rmANOVA analysis with the region as the within-subjects variable, to identify any interactions between variables. Upon identifying a significant effect of diagnosis in the mixed rmANOVA analysis, we followed up by univariate ANOVA and post-hoc analysis with a Bonferonni correction. Non-parametric analysis was performed for the theta and alpha DF as we could not solve the issue of heteroscedasticity. Hence we performed Welch's ANOVA followed by the Games-Howell test. For the DFP data we could not solve the issue of normality and thus, we performed Kruskal-Wallis H test followed by post-hoc analysis. Manual correction for multiple comparisons by appropriating the level of  $\alpha$  significance ( $\alpha/N$ ) was performed for the non-parametric statistical analyses, as Bonferonni correction was not available for these tests by the statistical software.

Pearson's product-moment correlation (parametric data) and Spearman's rank correlation (non-parametric data) were used to investigate for correlations between these variables and the CAF score and the MMSE score, for each diagnostic group. Manual correction for multiple comparisons by appropriating the level of  $\alpha$  significance ( $\alpha/N$ ) was also performed for the correlation analyses. Lastly, in order to assess the capacity of the qEEG variables that were significantly different between the AD and DLB, and the DLB and PDD groups to predict diagnosis, the generalised estimating equations (GEE) procedure were used. The variables that significantly predicted diagnosis were then used to calculate the receiver operating characteristic (ROC) curve, and obtain the area under the curve (AUC), sensitivity and specificity with asymptotic confidence intervals. Our method for this analysis is described in detail in the Methods section 2.1.4.

### 3.3. Results

#### 3.3.1. Data and Demographics

Data from a total of 73 individuals (21 healthy controls, 18 AD, 17 DLB, 17 PDD; **Table 3.1**) were further analyzed after data extraction. Participants were well matched for age at diagnosis and age at the time of the recording ( $p > 0.05$ ), as well as MMSE score ( $p > 0.05$ ). The PDD and DLB groups had significantly higher CAF scores than AD patients ( $p < 0.01$ ;  $p < 0.05$  respectively), with the PDD group also showing a higher CAF score than the DLB group ( $p < 0.01$ ). Lastly, the neuropsychiatric inventory (NPI) total and Unified Parkinson's disease rating scale (UPDRS) scores were higher in the DLB/PDD subjects compared to the other groups, and in the PDD compared to the DLB group ( $p < 0.01$ ).

**Table 3.1:** Demographics table for the healthy controls and dementia patients who participated in our study: controls (N = 21), AD (N = 18), DLB (N = 17) and PDD (N = 17). L-DOPA = levodopa, LED = L-DOPA equivalent dose, AChEIs = acetylcholinesterase inhibitors, MMSE=Mini mental state examination, CAF = Clinician's assessment of fluctuations scale, UPDRS = Unified Parkinson's disease rating scale, NPI = Neuropsychiatric inventory total score. 1 PDD patient (5.9%) was on memantine (not shown).

Variable	Controls (N = 21)	AD (N = 18)	DLB (N = 17)	PDD (N = 17)
Age in yrs $\pm$ SD	76.19 $\pm$ 5.32	76.06 $\pm$ 7.81	75.71 $\pm$ 5.34	75.44 $\pm$ 4.66
Males (%)	66.7 %	88.9%	88.2%	100%
L-DOPA	-	0%	52.9%	100%
LED	-	0%	348.94	423.42
AChEIs	-	94.4%	88.2%	76.5%
Age at diagnosis (yrs $\pm$ SD)	-	74.64 $\pm$ 7.63	73 $\pm$ 5.11	74.07 $\pm$ 6.29
Diagnosis duration (yrs $\pm$ SD)	-	1.5 $\pm$ 0.9	1.08 $\pm$ 0.70	0.94 $\pm$ 0.73
MMSE	29.19 $\pm$ 0.87	23.67 $\pm$ 1.68	25 $\pm$ 2.89	23.94 $\pm$ 2.59
CAF	-	0.47 $\pm$ 0.87	2.76 $\pm$ 3.78	6.59 $\pm$ 4.29
NPI total	-	7.29 $\pm$ 7.61	8 $\pm$ 5.27	20.35 $\pm$ 12.9
UPDRS	1.14 $\pm$ 1.42	1.67 $\pm$ 1.61	13.82 $\pm$ 5.32	27.06 $\pm$ 11.44

### **3.3.2. Changes in percentage power in patients with dementia**

The first variable we analysed was the rPSD/power distribution in the theta (4 – 7.75 Hz), alpha (8 – 13.75 Hz) and beta (14 – 30.75 Hz) frequency bands, as a percentage of the total power (4 – 48 Hz). Statistical analysis showed a significant effect of diagnosis on the mean power in all bands: theta:  $F(3, 69) = 39.48, p < 0.01$ , alpha:  $F(3, 69) = 14.49, p < 0.01$  and beta:  $F(3, 69) = 12.825, p < 0.01$  (Figure 3.1). In all regions, PDD and DLB groups had higher theta power than AD patients and healthy controls. The opposite pattern was observed in the alpha and beta ranges. Specifically, in the alpha band, controls had significantly higher power than PDD patients in all regions, and compared to DLB patients frontally, posteriorly and laterally. Moreover, AD patients had greater alpha power than PDD patients posteriorly and laterally and also to DLB patients frontally, posteriorly and laterally. In the beta range, DLB patients had lower power than AD patients and controls in all regions. PDD patients had lower power than healthy controls in all regions and than AD patients frontally, centrally and posteriorly.

Our analysis revealed a shift of spectral power from higher to lower frequency bands in DLB and PDD patients, as they had significantly increased theta and alpha power and decreased beta power compared to AD patients and controls. AD patients have a similar percentage power content in each band as healthy controls. These results were most significant posteriorly, but were evident in all regions.

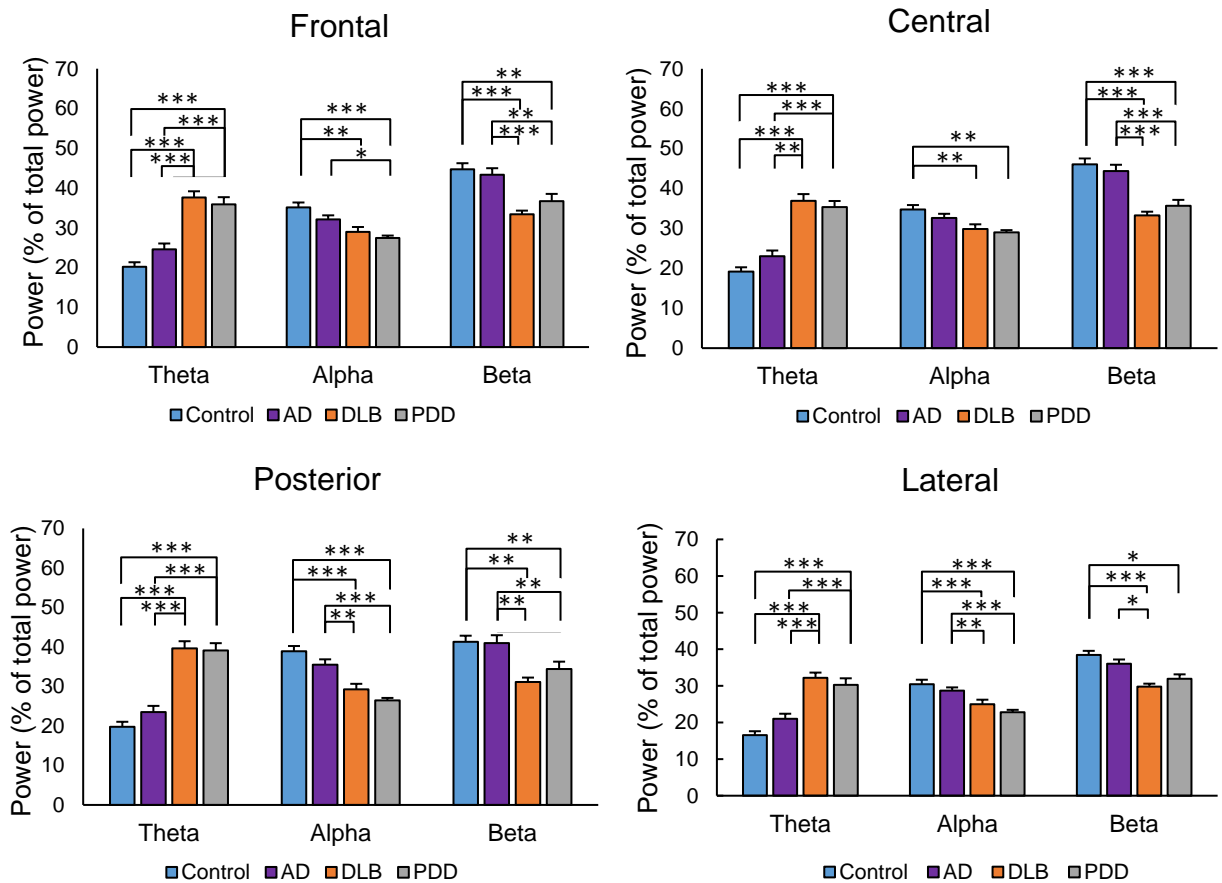


**Figure 3.1:** Analysis of percentage power of the resting state EEG in the dementia sub-groups. The mean percentage distribution of the total relative power in three frequency bands (Hz): theta (4 - 7.75), alpha (8 - 13.5) and beta (14 - 30.75), for each of four diagnostic groups: healthy controls (N = 21), AD (N = 18), DLB (N = 17) and PDD (N = 17) patients, for the anterior, central, posterior and lateral regions. Error bars indicate the SEM. Asterisks indicate statistical significance: \*\* =  $p < 0.05$ , \*\*\* =  $p < 0.001$ . Adapted from Stylianou et al. (2018).

### 3.3.3. **Changes in the dominant frequency (DF) in dementia patients**

Next, we looked at the mean dominant frequency (DF), which describes the frequency with the highest power in the theta (4 - 7.75 Hz), alpha (8 - 13.75 Hz) and theta-alpha (4 - 13.75 Hz) frequency bands. This analysis aimed to clarify our findings of a shift of power towards lower frequencies in DLB and PDD groups compared to healthy controls and AD patients (Table 3.3). Mixed rmANOVA analysis showed a significant effect of diagnosis in the mean theta-alpha DF ( $F(3, 69) = 36.78, p < 0.001$ ), which was significantly higher in all cortical regions in controls and AD patients compared to the other patient groups (Figure 3.2A).

The theta and alpha DF were analysed using Welch's ANOVA. The mean theta DF was significant in all regions (frontal:  $F(3, 69) = 6.92, p < 0.001$ ; central:  $F(3, 69) = 6.35, p < 0.01$ , posterior:  $F(3, 69) = 10.38, p < 0.001$ , lateral:  $F(3, 69) = 7.93, p < 0.001$ ; Figure 3.2B). Specifically, the theta DF was significantly higher in controls compared to the PDD group frontally, to the AD, DLB and PDD groups centrally and posteriorly, and to the DLB and PDD groups laterally. Significant differences between groups were also found in the alpha DF, in all regions: frontal:  $F(3, 69) = 5.06, p < 0.01$ ; central:  $F(3, 69) = 8.55, p < 0.001$ , posterior:  $F(3, 69) = 9.6, p < 0.001$ , lateral:  $F(3, 69) = 5.98, p < 0.01$  (Figure 3.2C). The DLB group had significantly lower alpha DF than the control and AD group in all regions. The PDD group had higher alpha DF than the DLB group frontally, the AD group centrally and posteriorly and the control group laterally. A trend for a greater alpha DF in the AD compared to the control group was observed, but was not statistically verified.

The DF analysis verified the previous observation of a shift of power from higher to lower frequencies, in DLB and PDD patients compared to healthy controls and AD patients (Bonanni et al., 2008; Walker et al., 2000). This analysis also revealed that the DF in the DLB and PDD patient groups now lies in the theta range (4 – 7.75 Hz) instead of the alpha range (8 – 13.75 Hz; Table 3.3).

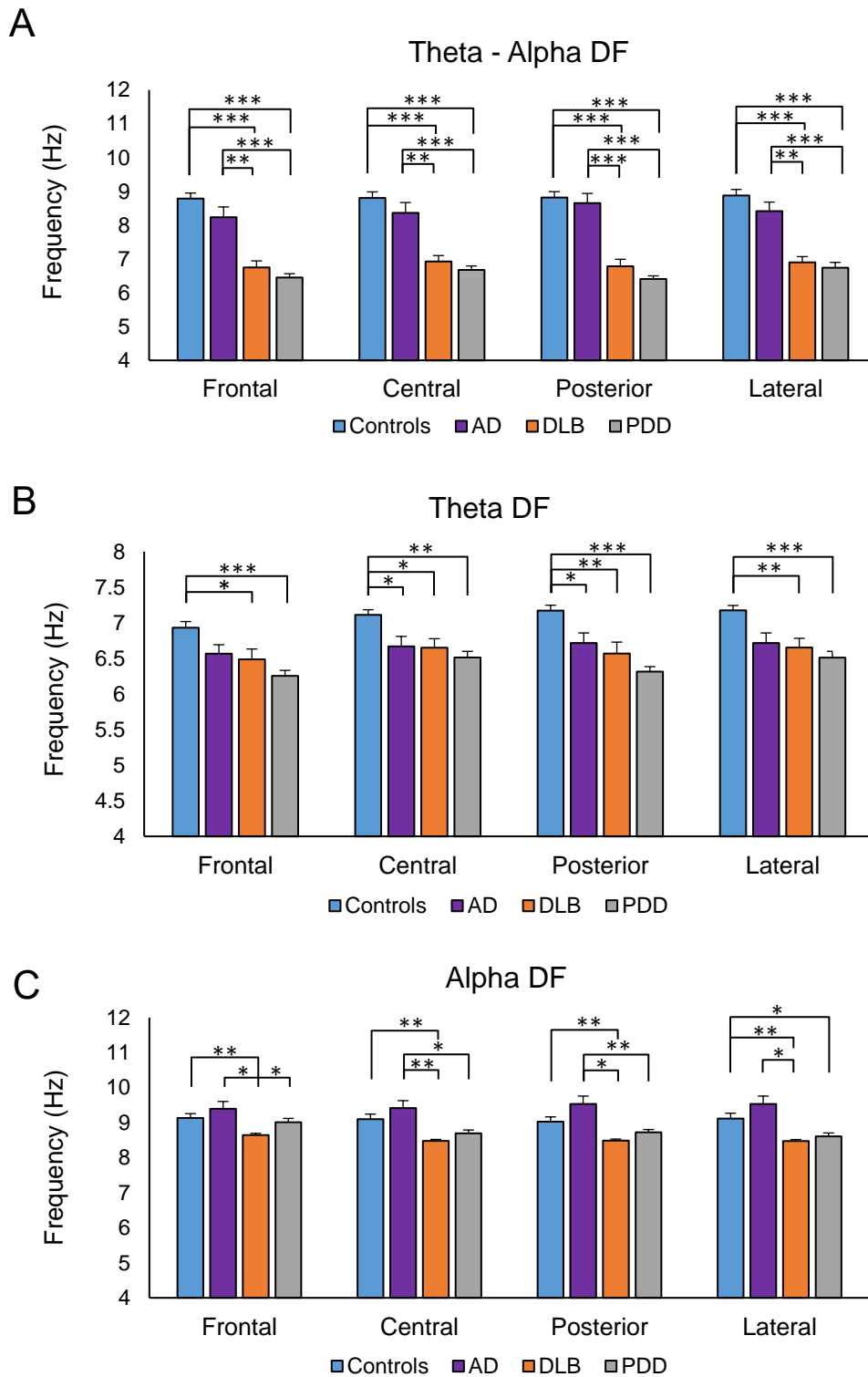


**Figure 3.2:** Analysis of the dominant frequency (DF) in the dementia sub-groups. The mean DF is shown for the A) theta-alpha (4 – 13.75 Hz), B) theta (4 – 7.75 Hz) and C) alpha (8 – 13.75 Hz) frequency ranges, for each of four diagnostic groups: healthy controls (N = 21), AD (N = 18), DLB (N = 17) and PDD (N = 17) patients, in the frontal, central, posterior and lateral regions. Error bars indicate the SEM. Asterisks indicate statistical significance: \*\* =  $p < 0.05$ , \*\*\* =  $p < 0.001$ . Adapted from Stylianou et al. (2018).

### 3.3.4. **Changes in the DF prevalence (DFP) in dementia patients**

The next variable of interest was the dominant frequency prevalence (DFP) in slow-theta (4 – 5.5Hz) fast-theta (5.75 – 7.75 Hz) and alpha (8 – 13.75 Hz) frequency bands. The DFP describes the percentage of epochs (from the total number of epochs) in which each DF was measured. The average DFP was calculated for each recording. The theta range was sub-divided into slow-theta and fast-theta, to better comprehend the DFP distribution.

The mean alpha DFP (Figure 3.3) was significantly higher in controls compared to all disease groups (DLB/PPD:  $p < 0.001$ ; AC:  $p < 0.01$ ), and in AD patients compared to DLB and PDD patients ( $p < 0.001$ ), in all regions. In the fast-theta range the opposite pattern was observed, with controls exhibiting lower DFP compared to AD patients in all regions ( $p < 0.05$ ), and to DLB and PDD patients in all regions ( $p < 0.001$ ). Finally, in the slow-theta range controls had significantly lower DFP than AD patients in all regions (frontal, central:  $p < 0.01$ ; posterior, lateral:  $p < 0.05$ ), and to DLB ( $p < 0.01$ ) and PDD patients ( $p < 0.001$ ) in all regions. AD patients also have significantly lower slow-theta DFP than PDD patients frontally, posteriorly and laterally ( $p < 0.05$ ).

The DFP analysis has strengthened our findings of an EEG “slowing” in DLB and PDD patients compared to AD patients and controls. Interestingly, this analysis has also revealed a small EEG slowing in AD patients compared to controls, as they demonstrate greater fast-theta DFP, while controls have predominantly alpha DFP.

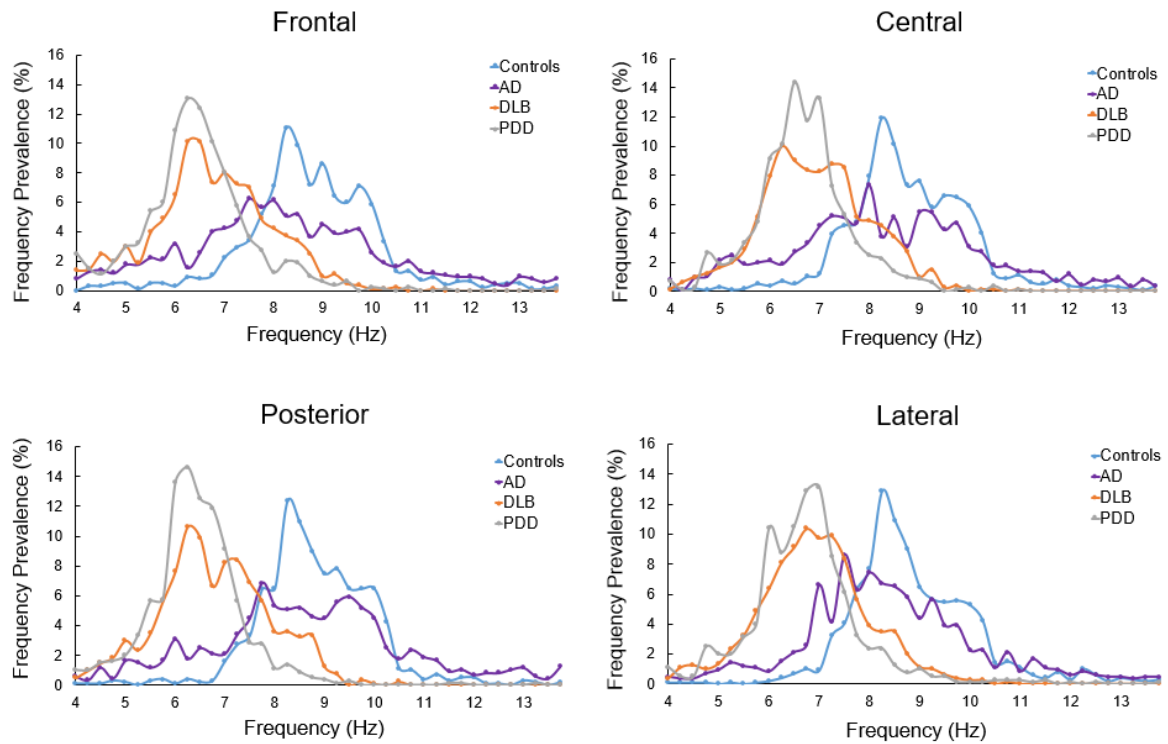


**Figure 3.3:** Analysis of the dominant frequency prevalence (DFP) in the dementia subgroups. The mean DFP (the percentage distribution of the mean DF in each frequency point in the theta-alpha frequency range with 0.25 Hz resolution) for each of four diagnostic groups: healthy controls (N = 21), AD (N = 18), DLB (N = 17) and PDD (N = 17) patients, in the frontal, central, posterior and lateral regions. Adapted from Stylianou et al. (2018).

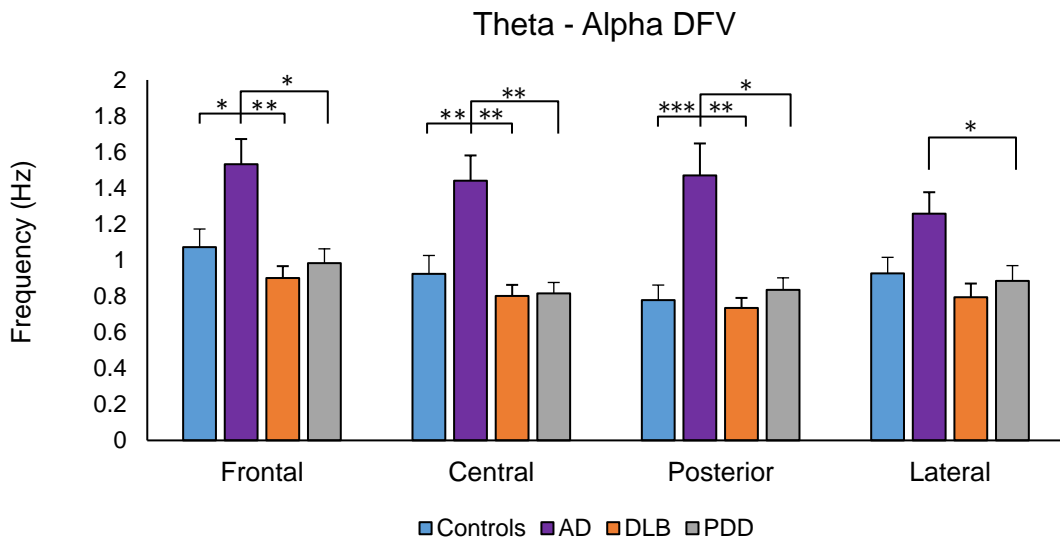
### 3.3.5. *The DF variability (DFV) in dementia patients*

The DF variability (DFV) describes the variability of the DF over time in the theta, alpha, theta-alpha frequency bands. The DFV is the SD of the DF over epochs and averaged across recordings and, therefore, shows how stable or variable the DF is over time.

Our analysis revealed a significant effect of diagnosis in the theta/alpha ( $F(3, 69) = 8.91, p < 0.001$ ) and alpha ( $F(3, 69) = 6.29, p < 0.01$ ) ranges, but not in the theta range (Figure 3.4). In the theta-alpha range, the AD group had a significantly higher DFV compared to the control, DLB and PDD groups in the frontal, central and posterior regions, and only to the DLB group laterally (Figure 3.4A). In the alpha band, AD patients had significantly higher DFV compared to the DLB group centrally and posteriorly, and to healthy controls posteriorly (Figure 3.4B).

In contrast to previous studies (Bonanni et al., 2008; 2010) our study found greater DFV in AD patients compared to healthy controls and to DLB and PDD patients. The latter DLB/PDD did not show significantly different DFV compared to healthy controls. Thus, this AD-specific increase in DFV is a novel finding.

A



B

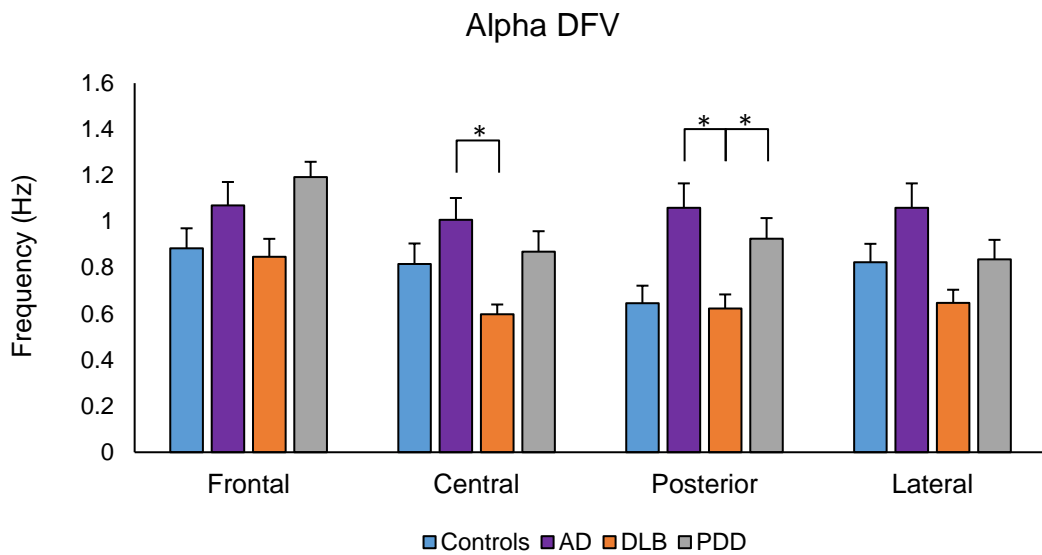


**Figure 3.4:** Analysis of the dominant frequency variability (DFV) in the dementia sub-groups. The mean DFV in the **A**) theta-alpha (4 – 13.75 Hz) and **B**) alpha (8 – 13.75 Hz) frequency ranges, for each of four diagnostic groups: healthy controls (N = 21), AD (N = 18), DLB (N = 17) and PDD (N = 17) patients, in the frontal, central, posterior and lateral regions. Error bars indicate the SEM. Asterisks indicate statistical significance: \* =  $p < 0.05$ , \*\* =  $p < 0.01$ , \*\*\* =  $p < 0.01$ . Adapted from Stylianou et al. (2018).

### **3.3.6. Correlation between the CAF score and the DFV**

We assessed correlations between CFs as measured by CAF and the qEEG measures of DFV and EEG “slowing”, for all the different diagnostic groups, in each frequency band and cortical region. This analysis revealed that, only within the DLB group, was there a strong correlation between the CAF score and the theta DFV in the central ( $r = 0.789, p < 0.000$ ), posterior ( $r = 0.652, p < 0.005$ ) and lateral regions ( $r = 0.805, p < 0.001$ ). A positive, DLB specific correlation with CAF was also found with slow-theta DFP in the frontal ( $r = 0.679, p = 0.003$ ), central ( $r = 0.747, p = 0.001$ ), posterior ( $r = 0.792, p < 0.001$ ) and lateral ( $r = 0.794, p = 0.001$ ) regions. A correlation between the CAF and MMSE score was only found in the PDD group ( $r = -0.671, p < 0.05$ ), while no significant correlation was found for any variable and the LED, for any group and region. Thus, although DLB patients do not have greater DFV compared to controls, they show a disease specific correlation between increased theta DFV (as the DF is now in the theta range) and CFs. The DF slowing in DLB patients also correlates with CFs. The correlations between the DF slowing and increased DFV with the CAF score are DLB specific.

### **3.3.7. Exploratory GEE and ROC curve analysis**

Lastly, we decided to investigate the ability of our EEG variables to differentiate between DLB and AD, as these dementia subtypes often manifest in similar ways at disease onset (Ballard et al., 2002). Thus, we performed GEE analysis for the variables that were significantly different between the AD and DLB diagnostic groups (theta power, alpha power, theta-alpha DFV, alpha DFV, alpha DF and fast-theta DFP). The alpha-theta DF and alpha DFP were rejected from this analysis as they introduced marked multicollinearity. The qEEG variables that best predicted diagnosis were the theta power (%) ( $Wald\ chi-square = 15.74, df = 1, p < 0.01$ ), the fast-theta DFP ( $Wald\ chi-square = 8.1, df = 1, p < 0.01$ ) and the theta-alpha SD ( $Wald\ chi-square = 7.549, df = 1, p < 0.01$ ). ROC analysis (Figure 3.5) yielded AUC = 94% (90.4% - 97.9%), sensitivity = 92.26% (CI = 80.4% – 100%) and specificity = 83.3% (CI = 73.6% - 93%). Thus, the extent of the DF slowing and DF over time can differentiate AD and DLB patients with high specificity, sensitivity and accuracy.

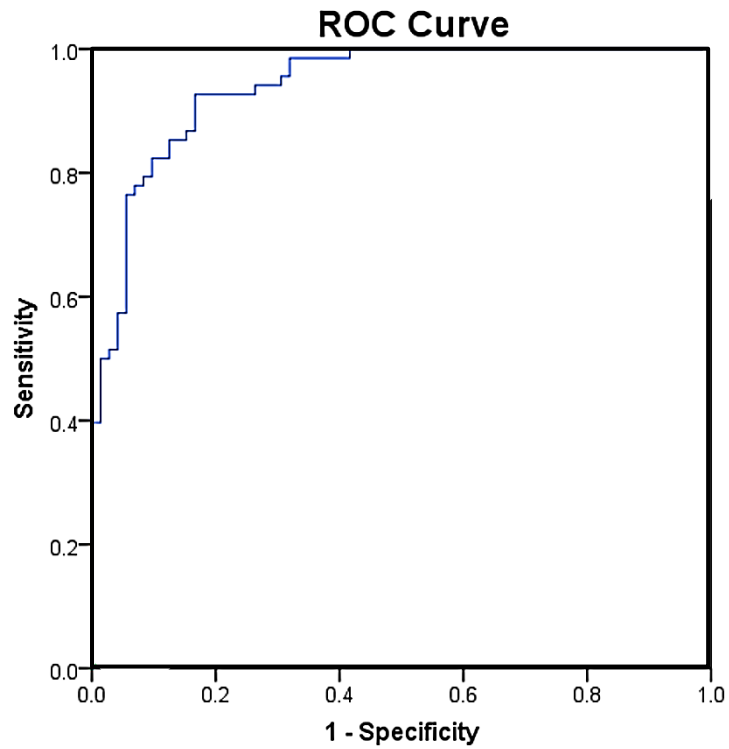


**Figure 3.5:** The capacity of quantitative EEG measures to enable differential DLB/AD diagnosis. Receiver operating curves (ROC) for a model composed of fast-theta dominant frequency prevalence (DFP), theta power and theta-alpha dominant frequency variability (DFV), for differentiating between Alzheimer’s disease (AD; N = 18) and dementia with Lewy bodies (DLB; N = 17) with mild dementia. Adapted from Stylianou et al. (2018).

### 3.4. Discussion

#### 3.4.1. *Summary of the main findings*

A summary of the key findings from Chapter 3 is presented below:

- Greater theta-alpha DFV in AD patients compared to controls, DLB and PDD patients. No differences in the DFV between the DLB group and healthy controls.
- A significant, DLB specific positive correlation found between the CAF score and the theta DFV and the slow-theta DFP.
- Increased theta and decreased alpha and beta power in DLB and PDD patients compared to AD patients and healthy controls.
- A shift of the DF and DFP from the alpha to the theta frequency range in DLB and PDD patients, compared to AD patients and healthy controls.
- A subtle shift of the DFP towards the fast-theta frequency range in AD patients compared to healthy controls.
- A model composed of the theta power, fast-theta DFP and theta-alpha DFV could predict a DLB versus an AD diagnosis with high sensitivity (92.26%), specificity (83.3%) and accuracy (94%).

#### 3.4.2. *DLB/PDD patients have a slower resting EEG rhythm than healthy controls and AD patients*

One of the best described qEEG features in DLB and PDD patients is a shift of power from higher to lower frequency bands compared to healthy controls and in some studies compared to AD patients, mostly in posterior cortical regions (Briel et al., 1999; Barber et al., 2000; Bonanni et al., 2008; Roks et al., 2008). In our analysis we looked within four different cortical regions (frontal, central, posterior, lateral) compared to a maximum of three regions previously reported (frontal, posterior, lateral; Bonanni et al., 2008), and analysed three measures of EEG spectral distribution, the percentage power, DF and DFP, all of which confirmed an “EEG slowing” in our DLB/PDD patients compared to AD patients and controls.

In AD patients, a small EEG slowing was also evident by a shift of the DFP from the alpha to the fast-theta and slow-theta ranges, compared to healthy controls. This finding indicates that a higher percentage of the DF measurements occurred within the

theta-band, than in the alpha-band, in the AD patients compared to control subjects. This altered DF distribution towards lower frequencies in AD was “masked” with the calculation of the mean theta-alpha DF, as this measure does not account for variability. The DF in AD patients is highly variable over time and can take values towards the higher edge of the alpha band, thus influencing the mean DF. This is evident by the significantly greater theta-alpha DFV in the AD compared to the other diagnostic groups, and the trends for greater alpha DFV and alpha DF that characterise AD patients.

A cholinergic deficit may partly account for the EEG slowing in DLB/PDD and AD, as it has been shown that the administration of AChEIs can reverse the EEG slowing observed in both diseases (Bosboom et al., 2009; Babiloni et al., 2013; Adler et al., 2004). However, the loss of cholinergic neurons projecting to the cortex is greater and has a faster progression in DLB and PDD compared to AD (Lippa et al., 1999) where the cholinergic deficit is not yet severe at early stages of the disease (Bohnen & Albin, 2011). Pathological protein-related synaptic dysfunction that occurs before neuronal degeneration has also been associated with cognitive decline in AD and is thought to be even greater in DLB (Selkoe, 2002; Schulz-Schaeffer, 2010). Thus, a more advanced cholinergic deficit and synaptic dysfunction in the LBD groups could account for the greater extent of EEG slowing observed compared to the AD group, particularly given the relatively early disease stage and mild cognitive impairment of our participant populations.

### **3.4.3. *The DFV and cognitive fluctuations correlate only in DLB patients***

Previous studies have shown a significant DFV increase in DLB patients compared to healthy controls, that correlated with CFs measured by the CAF score (Walker et al., 2000; Bonanni et al., 2008). Although we did not find an increase in the DFV of DLB patients compared to healthy controls, we did find a positive correlation between the DFV in the theta band and the CAF score within the DLB group (Bonanni et al., 2015). This correlation was only significant in the theta frequency range, likely due to the shift of the DF from the alpha towards the theta frequencies in DLB patients. A positive correlation was also found between slow-theta DFP and the CAF score in DLB patients. Both these correlations were only seen in the DLB group and not in the PDD or AD groups.

One of the main theories regarding CF generation is that they arise due to disturbances in large-scale networks that govern attention (O'Dowd et al., 2019). The aforementioned qEEG studies showing a correlation between DFV and CFs in DLB patients (Walker et al., 2000; Bonanni et al., 2008), led to the belief that DLB (and not AD) is associated with an increase in dynamic brain function and in the activity of the networks that govern the resting state, specifically the DMN (Franciotti et al., 2013). However, more recent studies have shown that the DMN might not be affected in DLB patients (Schumacher et al., 2018; Peraza et al., 2014; Firbank et al., 2016). Moreover, an fMRI study has shown prolonged DMN deactivation during a cognitive processing task in DLB patients, suggesting an inability of the DMN to shift back to the activated state rather than an increase in its function (Firbank et al., 2018). Another fMRI study showed a reduction in shifts between the EEG-microstates (~100 ms long periods that represent the EEG correlates of fMRI resting-state networks) in DLB compared to AD and healthy controls, with the magnitude of the reduction correlating with the extent of CFs (Schumacher et al., 2019). These findings suggest that DLB is characterised by a loss of dynamic brain function that is related to CFs.

There is also evidence of an aberrant interaction between the fronto-parietal attention networks and the DMN in DLB patients. The fronto-parietal attention networks include the ventral and dorsal attention networks (VAN; DAN), where DAN mediates a top-down voluntary allocation of attention, while VAN is important for detecting unanticipated stimuli and shifting attention (Vossel et al., 2014). Moreover, the DAN and VAN networks have an anti-correlated activation pattern to the DMN. DAN and VAN have been previously shown to have altered activity in DLB patients during attentional tasks, including a DAN/VAN disconnectivity that obstructs the DAN regulation over VAN (Peraza et al., 2014; Kobeleva et al., 2017; Franciotti et al., 2013; Firbank et al., 2016; Chabran et al., 2018). One study also showed a correlation between CF severity and decreased fronto-parietal connectivity in DLB patients who showed increased DFV (Franciotti et al., 2013). Thus, we postulated that the DFV/CF correlation seen within the DLB group could indicate changes in the functional connectivity changes between attentional and the DMN networks.

Given the neuropathological similarities between PDD and DLB and the absence of other qEEG differences between these groups (Jellinger & Korczyn, 2018), the lack of a correlation between CAF and our qEEG measures in PDD was unexpected.

Previous studies have reported that PDD patients with high CF scores show an EEG-slowness (Bonanni et al., 2008) and have more DLB-like symptoms such as visual hallucinations, while patients with fewer CFs resemble PD (Varanese et al., 2010). This heterogeneity in our PDD patients may have affected our capacity to identify a correlation between the EEG measures and CAF score in this group. Moreover, DLB patients with parkinsonism have more impaired reaction times and vigilance measures that relate to CFs, compared to patients without motor symptoms, implying a connection between CFs and dopaminergic impairment (Ballard et al., 2002). Furthermore, there is evidence of a negative correlation between dopaminergic neuron numbers indicated by dopamine transporter scan (DaT) and CFs (Iizuka & Kameyama, 2016) in DLB. Finally, a few studies have suggested that CFs can be slightly less common in PDD than in DLB, which can also account for the lack of qEEG/CF correlations in the PDD group (Ballard et al., 2002; Savica et al., 2013)

Since PDD is characterised by greater dopaminergic impairment than DLB, this additional pathology could have a more dominant aetiological role in the CFs seen in PDD as compared to DLB. CFs are likely to have at least two dimensions - attention as discussed above and arousal (Bliwise et al. 2012). These dimensions are not discriminated by the CAF score but may be differentially expressed in our DLB and PDD groups given arousal/sleepiness is strongly influenced by dopaminergic medications (Piggott et al., 2007). Another factor may be the amyloid burden as this is significantly greater in DLB compared to PDD patients (Donaghy et al., 2015), while the cortical A $\beta$  deposition relates more to dementia severity, visual hallucinations and delusion in DLB than PDD (McKeith et al., 2004). DLB is also characterised by a greater amyloid load in the putamen (Hepp et al., 2016), which is involved in attentional networks and in DLB has altered functional connectivity that correlates with CAF (Peraza et al., 2014). Ultimately, improved quantification scales of CFs may help to unpick these challenges.

#### **3.4.4. *The DFV is greater in AD patients compared to all other diagnostic groups.***

Previous studies have also shown that DLB patients had a significantly higher DFV compared to AD patients, which did not differ significantly from controls, and that a higher DFV was an accurate indicator of DLB versus AD diagnosis (Bonanni et al., 2008). Here, we found that AD patients had a significantly higher theta-alpha DFV

compared to all other diagnostic groups, in most cortical regions. A later study on the same initial cohort of patients as the one used in this study verified our finding of greater theta-alpha DFV in the AD group but only in posterior derivations due to the use of a lower EEG spatial resolution (Peraza et al., 2018). We also looked at the DFV in the theta and alpha bands independently and we identified a greater alpha DFV in AD patients compared to controls and DLB patients posteriorly, and to DLB patients alone centrally.

These findings of an increase in DFV in AD patients could be part of the pathology or alternatively, the result of a compensation mechanism that may occur at early stages of AD. At rest, early stage AD patients may have increased activity, and functional connectivity, in resting state networks which correlate with a lower MMSE score (Peraza et al., 2015). However, at more advanced stages of the disease, activity and connectivity decrease to levels lower than those seen in controls (Agosta et al. 2012). Therefore, increases in DFV may be associated with a compensation mechanism in early stage AD.

A finding we have not discussed so far is the decrease in beta band power seen in DLB and PDD patients compared to controls and AD patients. This finding replicates previous reports in the literature (Andersson et al., 2008), although there is little research focused on the beta rhythm in relation to DLB. Beta frequency activity is the idling rhythm of the motor cortex while it is also involved in cognitive function and specifically in maintaining the current cognitive state (Neuner et al., 2014). Beta activity increases with top-down control and periods of self-referential thinking and decreases with attention demanding tasks and the input of external information (Engel & Fries, 2010). It is, therefore, not surprising that beta activity overlaps with activation in DMN regions, the parietal cortices, precuneus and mPFC (Engel & Fries, 2010; Mantini et al., 2007). However, in DLB patients, beta power functional connectivity is reduced over long-distance, in fronto-parietal and fronto-temporal areas spatially overlapping with the DMN and the aforementioned attention networks (Pievani et al., 2011; Andersson et al., 2008; Peraza et al., 2018). Thus, changes in the underlying network dynamics could also affect beta band activity, in addition to theta/alpha band activity. However, we did not investigate for further changes in the beta rhythm in terms of the DF and DFV, nor for a relationship between these measures and CFs in DLB patients, as this analysis was outside of our scope. A study designed to investigate the power

content of higher-frequency oscillations such as beta and gamma would be of great interest.

### **3.4.5. *Our study contradicts previous reports in literature***

A number of other factors may account for the discrepancies between our findings and those of previous studies. The lack of a greater DFV in DLB patients compared to controls may be attributed to the fact that the majority of our DLB patients were on acetylcholinesterase inhibitors (AChEIs), although we would argue that this adds to the clinical relevance of our findings, particularly from a diagnostic perspective; it is likely that any use of the EEG will be when patients are beginning or have already been initiated on treatment. In DLB patients, CFs have been shown to correlate with cholinergic imbalances in networks involved in the resting state (Delli Pizzi et al., 2015). AChEIs restore this imbalance and improve both the cognitive symptoms of DLB and the electrophysiological markers, including the EEG spectrum and connectivity (Onofrij et al., 2003). That said, it is important to acknowledge that more AD (94.4%) than DLB (88.2%) patients were on AChEIs in our study groups and the former group showed greater DFV. However, as outlined above, cholinergic deficits are greater and occur earlier in DLB compared to AD (Tiraboschi et al., 2002), while the brainstem cholinergic innervations of the thalamus are relatively spared in AD (Mesulam, 2004), but not in DLB (Taylor et al., 2017). Hence, at the stage of mild dementia AChEIs could have a differential effect in DLB and AD.

Although AChEIs may have normalized the DFV in DLB patients in relation to healthy individuals, the CAF/DFV correlation was still maintained within our DLB group. In previous studies, none (Walker et al., 2000), or only a small proportion (Bonanni et al., 2008) of the patients were on AChEIs. Differences in the participant cohorts, as well as methodological differences in the analysis of the recordings must also be considered. Specifically, we used a different pre-processing and spatial analysis approach, as well as a different way to estimate DFV; here DFV was defined as the standard deviation from the mean DF across epochs, in an epoch-by-epoch basis, while in Bonanni et al. (2008; 2016), DFV was defined using a visual rating of DF range on sequential EEG segments.

#### **3.4.6. *QEEG measures can differentiate between AD and DLB patients with high sensitivity and specificity***

We also proceeded with a preliminary analysis to investigate the capacity of the qEEG variables to correctly differentiate between AD and DLB patients with mild cognitive decline indicated by the MMSE score and hence, early dementia. The theta power, fast-theta DFP and theta-alpha DFV yielded accuracy of 94% (CI = 90.4% - 97.9%), sensitivity of 92.26% (CI = 80.4% - 100%) and specificity of 83.3% (73.6% - 93%). The high predictive accuracy of this model is in-line with previous classifications using qEEG variables, although different EEG pre-processing and analysis methods were used (Andersson et al., 2008; Garn et al., 2017). Hence, these qEEG measures of the DFV and EEG slowing could potentially be of clinical importance and become implemented in an EEG-based diagnostic tool for DLB. However, they would have to be tested in a separated patient cohort first, and be assessed for feasibility and cost-effectiveness in a clinical setting.

### **3.5. Conclusion**

Our findings confirm the well-established slowing of the EEG in the Lewy body dementia groups compared to healthy controls and AD patients. Although we did not find higher DFV in DLB patients compared to controls as expected, theta DFV and slow-theta DFP were positively correlated with CFs as measured by CAF. This DLB specific correlation suggests that a slower and more temporally variable DF specifically relates to the CFs seen in DLB, and could reveal differential mechanisms underlying CFs in dementia subtypes. Another novel finding was a significantly higher DFV in AD patients compared to the other diagnostic groups. Exploratory analysis showed that qEEG measures could predict a DLB versus an AD diagnosis with high accuracy, sensitivity and specificity. In conclusion, this study supports the hypothesis that qEEG analysis can be a valuable tool for identifying CFs in DLB and for differential diagnosis between dementia subtypes, once replicated with low density EEG currently used in standard clinical practice after the feasibility and cost-effectiveness of these methodologies has been investigated.

## **Chapter 4. Analysis of the SO in A30P animals**



## 4.1. Introduction

Slow wave sleep (SWS) defined by the slow oscillation (SO; < 0.1 Hz), is the hallmark of NREM sleep in all vertebrate species including humans. SWS in rodents is often modelled by urethane anaesthesia, which induces the SO that can be recorded throughout the cortex (Clement et al., 2008; Pagliardini et al., 2013) and the hippocampus (Yanovsky et al., 2014; Wolansky et al., 2006). The SO is an oscillation between the so-called Up- and Down-states (Steriade et al., 1993a), and is governed by a balance between excitation and inhibition (see review by Neske, 2015). Intracellular recordings show that Up-states are periods of depolarisation and action potential firing, while Down-states are characterized by hyperpolarization and the lack of neuronal firing (Steriade et al., 1993a; Luczak et al., 2007). A high level of synchrony within, and across, cortical and subcortical regions suggests a regulatory input from the thalamus, driving local cortical circuits (Fernandez et al., 2018; Lemieux et al., 2014).

The mPFC is a cortical region that is involved in higher-cognitive function and that generates a strong SO (Varela & Wilson, 2019; Colgin, 2011; Gretenkord et al., 2017). A recent study in the rat mPFC under urethane anaesthesia showed a highly synchronous SO of similar amplitude across its four subregions (ACC, PrL, IL and DP), and across hemispheres (Gretenkord et al., 2017). The mPFC SO rhythm, is synchronous to the hippocampal SO (Sharma et al., 2010; Wolansky et al., 2006; Colgin, 2011). Highly synchronous communication between the two regions during SWS is essential for memory consolidation (Wierzynski et al., 2009; Mölle & Born, 2009; Riga et al., 2014; Varela & Wilson, 2019). This communication takes the form of higher-frequency rhythms that are nested on the Up-state of the SO under natural sleep and anaesthesia (Colgin, 2011). Beta and gamma rhythms can be recorded on the Up-state in the cortex (Steriade et al., 1996; Valencia et al., 2013; Gretenkord et al., 2017), while gamma and high-gamma rhythms are most prominent in the hippocampus (Colgin et al., 2009), during natural sleep and under anaesthesia.

Both natural sleep and urethane-induced SWS are also characterised by two transient, high frequency electrophysiological events, the sleep spindles (Barthó et al., 2014; Puig et al., 2008; Steriade et al., 1993a) and sharp-wave ripples (SWRs) (Buzsáki & Silva, 2012; Mölle et al., 2006; Buzsáki et al., 1983). Sleep spindles are a sleep-related phenomenon of great importance in memory consolidation (Astori et al.,

2013), and sleep maintenance (Parrino & Vaudano, 2018). Sleep spindles are generated in the thalamus via the activity of excitatory thalamocortical neurons and inhibitory neurons in the TRN (Destexhe et al., 1998). Sleep spindles occur usually at the Down- to Up- state transition, although higher frequency spindles have also been characterised to occur at the Up- to Down-state transition (Kim et al., 2015).

SWRs are highly synchronous hippocampal events reflecting the firing of CA1 pyramidal cells and the accompanied high frequency oscillation in the CA1 (Buzsáki & Silva, 2012). SWRs occur on the Up-state of the SO during natural sleep and under anaesthesia (Mölle et al., 2006), but they are of a slower frequency (100 – 120 Hz) in the urethane-anaesthetized rat than during natural sleep (200 Hz; Ylinen et al., 1995). Cortical sleep spindles and hippocampal SWRs are synchronous with one another and their interaction facilitates the transfer of memories for consolidation from the hippocampus to the cortex (Eschenko et al., 2008; Sullivan et al., 2011; Valero et al., 2017), particularly between the CA1 region of the hippocampus and the mPFC (Wang & Ikemoto, 2016; Kiss et al., 2013).

DLB patients have early  $\alpha$ -syn pathology in the mPFC, hippocampus and thalamus (Adamowicz et al., 2017; Taylor et al., 2017). Impairments in these regions could affect the generation of sleep-related oscillations and their function (Latreille et al., 2015). Aged A30P animals exhibit a range of cognitive deficits including impaired hippocampal spatial memory that as mentioned, also involves the mPFC (Kahle et al., 2001; Freichel et al., 2007). After 12 months of age, A30P mice show non-soluble  $\alpha$ -syn pathology in the hippocampus and cortex (Freichel et al., 2007; Schell et al., 2009). However, it is possible that oligomeric, mutant  $\alpha$ -syn species are present earlier in these regions, obstructing neuronal function (Diógenes et al., 2012). In our lab, we have found a number of subtle changes in young mice, including changes in the balance between excitation and inhibition that could potentially affect the SO cycle (Robson et al., 2018; Tweedy et al., 2018)

In this study we aimed to identify changes in the SO in young A30P animals in the subregions of the mPFC and in the CA1 of the hippocampus. Therefore, we looked at the SO amplitude, frequency and the length of the components of the SO cycle; i.e. the Up- and Down-state, and how these vary over time. We also looked at higher-frequency oscillations nested on the Up-state, the levels of high frequency activity and unit firing in the SO cycle and the unit firing / SO coherence. To investigate for changes

in long-range synchrony we looked at the coherence of the SO between the mPFC subregions and the CA1. Finally, we looked at the density and characteristics of spindles and SWRs in the mPFC and CA1 respectively, in WT and A30P mice.

## **4.2. Methods**

### **4.2.1. Animals**

For the WT cohort, we initially carried out mPFC recordings in 14 animals but 2 animals without evidence of the infra-slow modulation (ISM; see Chapter 5 for detailed analysis) were excluded. Four more animals were excluded due to urethane-induced breathing artefacts that contaminated the data. In total therefore, we had mPFC recordings from 8 mice. We also had hippocampal CA1 region data for 6 / 8 mPFC recordings, but 1 was rejected due to an incorrect placement of the electrode probe, as verified by *ex vivo* immunohistochemistry. We also used CA1-only recordings for 2 animals, giving a total of 7 CA1 recordings for analysis. Simultaneous recordings between the mPFC and CA1 were performed in 5/7 animals and could be analysed for preliminary SO coherence analysis between the two regions.

The A30P cohort originally consisted of 19 animals for the mPFC and one without ISM was excluded. Two of the animals were excluded due to broken electrode contacts for at least one mPFC subregion and another 3 were rejected due to urethane-induced breathing artefacts. We also obtained recordings from the CA1 from 6 of these animals. Three additional hippocampal-only recordings were obtained but one was rejected due to incorrect placement of the electrode, again revealed by *ex-vivo* immunohistochemistry. One of these recordings was excluded from power-related analyses as it had minor urethane artefacts, but it was included in the SO state length analysis and mPFC/CA1 coherence analysis. Thus, we overall analysed 6 simultaneous mPFC/CA1 recordings for SO coherence between the two regions.

Out of 8 mPFC recordings in WT animals one did not have unit data, resulting in N = 7 WT animals for mPFC unit analysis. In the A30P cohort, we also used the 2 animals that were missing electrodes in one mPFC subregion, as subregion was not considered in this analysis. Thus, we analysed unit data from the mPFC of 15 A30P animals. We did not record unit data from the CA1.

### **4.2.2. Recordings**

The data used for this analysis was recorded approximately 1 – 1.5 hours after the initial dose of urethane, when regular SWS had been established. Data was analysed from only the first 30 min of recording as, although SWS lasted about 3 hours after the first urethane dose before a top-up was necessary, we wanted to analyse

data obtained from a consistent, deep plane of anaesthesia. We observed that within the SO there were brief bursts of high oscillatory power, which reflect the ISM (described in detail in Chapter 5). For the recordings and analysis of SWA presented in this Chapter, segments containing the ISM were automatically removed and the remaining SWS segments were concatenated, resulting in ~ 15-min long segments of data. Regular SO could be recorded simultaneously in all subregions of the mPFC (ACC, PrL, IL, DP) and the CA1 of the hippocampus in both A30P and WT mice aged 2.5 - 4 months.

#### **4.2.3. *Analysis of the SO cycle and wavelet power***

Several characteristics of the SO were analysed including the mean Up- and Down-state lengths and their variability over time (SD), the mean cycle length and its variability over time, the SO frequency and the mean SO amplitude. In addition, the high frequency oscillatory power in the SO was determined in 3 frequency bands: beta (15 – 29.9 Hz), gamma (30 – 79.9 Hz) and high-gamma (80 – 130 Hz), for the Up- and Down-states. All the aforementioned variables were extracted as described in Methods sections 2.2.5.1 - 2.2.5.5. High frequency gamma is within the SWR range in the CA1 but in this study, SWRs were detected separately (Methods section 2.2.7) as high-gamma oscillations and SWRs are separate rhythms (Sullivan et al., 2011).

#### **4.2.4. *Analysis of neuronal firing in relation to the SO***

The unit data was extracted and analysed as described in Methods section 2.2.5.6. We calculated the unit firing frequency and ISI on the Up-state and for the duration of the recording, and the latency to the first unit on the Up-state. We also looked at the percentage of the total firing occurring on the Up- and Down-states as well as the maximum unit firing / SO coherence.

#### **4.2.5. *SO coherence between the mPFC and CA1***

For animals where simultaneous recordings were performed in the contralateral mPFC (4 subregions) and CA1, the SO coherence was calculated for the SO frequency range. The “mscohere” function in MATLAB was used with a 2<sup>12</sup> window and no-overlap, to obtain the maximum coherence between the two signals and the frequency at which it occurred (Methods section 2.2.5.6) .

#### **4.2.6. *Sleep spindles and SWRs***

We also investigated for changes in the patterns of sleep spindles in the mPFC and of SWRs in the CA1 of WT and A30P animals, detected as described in section 2.2.6. For both spindles and SWRs we looked at the event duration and variability in duration, the event amplitude and variability in amplitude, the event latency in the normalized SO cycle, the absolute (spindle no/ recording duration) and relative spindle density (spindle no / Up-state number), the instantaneous frequency and the percentage of large amplitude events.

#### **4.2.7. *Statistical analysis***

As described in methods section 2.2.8, the data was first checked for a normal distribution and homoscedasticity and if necessary transformed to achieved these criteria. Specifically, we performed a logarithmic transformation for power on the Up- and Down-states and the mean peak power for all frequency bands in the mPFC and CA1, to achieve a normal distribution. Non-parametric Mann-Whitney U-test with a Welch exact-correction analysis was performed for the SWR data and the SO coherence between the CA1 and mPFC subregions. The later analysis was considered preliminary due to the small sample size: WT (N=5) and A30P (N = 6). Hence, we did not account for the relationship between mPFC subregions. The non-parametric data are presented as median and interquartile range (IQR).

For the rest of the data that was normally distributed, we performed mixed rmANOVA analyses where mPFC subregion (4 levels) was set as the within-subjects variable and the animal genotype as the between-subjects variable. Differences between mPFC subregions were out of the scope of this study, however proceeded with mPFC subregions as a repeated measure to identify any mixed effects / interactions with the genotype (Gretenkord et al., 2017). The outcome of the rmANOVA analysis for the mPFC subregion is reported and if the assumption of sphericity was violated a Huyhn-Feldt correction was applied. If a significant difference was found for genotype or a subregion/genotype interaction, follow-up univariate ANOVA analysis with a Bonferroni correction was performed for each mPFC subregion. Univariate ANOVA analysis was also performed for unit data, as we combined units from all subregions of the mPFC. Parametric data is presented as mean  $\pm$  standard error of the mean (SEM).

### 4.3. Results

#### 4.3.1. *Characterisation of the SO cycle in the mPFC of A30P mice*

In order to assess the impact of  $\alpha$ -syn on the generation of SWS we used urethane anaesthesia which, as described previously, induces a regular SO in both the mPFC and CA1 of the hippocampus in WT animals (Clement et al., 2008; Pagliardini et al., 2013; Destexhe et al., 1998; Gretenkord et al., 2017). Under urethane anaesthesia in both genotypes in addition to regular SO, we also observed regular periods where the fast oscillations associated with the SO showed a marked increase in power (ISM) but as outlined in section 2.2.5.1, these are excluded in this analysis.

##### 4.3.1.1. *A30P mice have altered SO cycle patterns in the mPFC*

Recordings in the mPFC showed robust SO in both WT and A30P mice (Figure 4.1A). Thus, we proceeded to characterise and compare the SO amplitude, frequency and the lengths of the Up- and Down-states that compose it, in the mPFC subregions, in the two animal genotypes (Figure 4.1B).

RmANOVA analysis revealed that the frequency of the SO in the mPFC was significantly faster in A30P mice compared to WTs ( $F(1, 19) = 9.64, p < 0.01$ ) in all subregions of the mPFC. As expected, the SO cycle length was significantly shorter in A30P mice ( $F(1, 19) = 9.41, p = 0.01$ ), in all subregions of the mPFC. This change in SO frequency could be due to shorter Up- and/or Down-states in A30P mice compared to WTs. Therefore, we analysed the Up- and Down-states separately and found that the Up-state was significantly shorter ( $F(1, 19) = 5.93, p < 0.05$ ) and less variable over time ( $F(1, 19) = 10.14, p < 0.01$ ) in the IL and PrL regions in A30P mice. In addition, the Down-state was also significantly shorter ( $F(1, 19) = 9.63, p < 0.01$ ) and less variable ( $F(1, 19) = 14, p < 0.001$ ) in all mPFC subregions in A30P mice. Consequently, the SO cycle length variability ( $F(1, 19) = 15.96, p < 0.01$ ) was also significantly lower in A30P compared to WT animals. The amplitude of the SO was not significantly different between the WT and A30P mice (Table 4.1).

A significant overall effect of region was found for Down-state length ( $F(3, 57) = 7.64, p < 0.01$ ) and SO cycle length ( $F(2.115, 48.65) = 7.65, p < 0.01$ ), with lower values found in the ACC compared to the IL and DP ( $p < 0.05$ ). Cycle length variability over time was also affected by region ( $F(3, 57) = 6.48, p < 0.01$ ), with the ACC showing

greater variability than the IL ( $p < 0.01$ ) and DP regions ( $p < 0.05$ ). Regarding the SO amplitude ( $F(3, 57) = 11, p < 0.01$ ), the ACC had a significantly smaller SO amplitude than the DP ( $p < 0.001$ ), PrL ( $p < 0.01$ ) and IL regions ( $p < 0.05$ ). No interactions were found between the genotype and region.

Our findings indicate that A30P mice have a faster SO oscillation than WT animals that can be attributed mostly to shorter Down-states as well as shorter Up-states and hence SO cycles. We also observed lower state length variability over time in A30P animals, suggesting a shortage of longer states.

**Table 4.1:** Characterisation of the SO cycle in the mPFC of WT and A30P mice. The average of each variable  $\pm$  SEM is shown for each of the four subregions of the mPFC (ACC, PrL, IL, DP), in WT (N = 13) and A30P (N = 8) mice. Variables also shown in Figure 4.1 are in Italics.

Variable	Genotype	Region			
		ACC	PL	IL	DP
SO amplitude (mV)	WT	0.43 $\pm$ 0.04	0.49 $\pm$ 0.06	0.55 $\pm$ 0.05	0.52 $\pm$ 0.04
	A30P	0.34 $\pm$ 0.03	0.42 $\pm$ 0.04	0.47 $\pm$ 0.03	0.47 $\pm$ 0.03
<i>SO frequency (Hz)</i>	WT	0.26 $\pm$ 0.02	0.28 $\pm$ 0.02	0.3 $\pm$ 0.02	0.29 $\pm$ 0.02
	A30P	0.36 $\pm$ 0.02	0.37 $\pm$ 0.02	0.37 $\pm$ 0.02	0.37 $\pm$ 0.02
SO cycle length (s)	WT	3.78 $\pm$ 0.32	3.47 $\pm$ 0.2	3.28 $\pm$ 0.17	3.32 $\pm$ 0.15
	A30P	2.89 $\pm$ 0.16	2.79 $\pm$ 0.13	2.77 $\pm$ 0.11	2.72 $\pm$ 0.12
<i>Up-state length (s)</i>	WT	1.47 $\pm$ 0.16	1.33 $\pm$ 0.08	1.33 $\pm$ 0.07	1.28 $\pm$ 0.05
	A30P	1.21 $\pm$ 0.04	1.16 $\pm$ 0.02	1.2 $\pm$ 0.03	1.16 $\pm$ 0.03
<i>Down-state length (s)</i>	WT	2.32 $\pm$ 0.17	2.14 $\pm$ 0.13	1.97 $\pm$ 0.14	2.05 $\pm$ 0.12
	A30P	1.75 $\pm$ 0.12	1.66 $\pm$ 0.1	1.65 $\pm$ 0.1	1.59 $\pm$ 0.1
<i>SO cycle length SD (s)</i>	WT	2.43 $\pm$ 0.28	2.22 $\pm$ 0.19	2.06 $\pm$ 0.21	2.15 $\pm$ 0.21
	A30P	1.45 $\pm$ 0.14	1.37 $\pm$ 0.12	1.3 $\pm$ 0.11	1.25 $\pm$ 0.13
<i>Up-state length SD (s)</i>	WT	0.69 $\pm$ 0.09	0.65 $\pm$ 0.08	0.64 $\pm$ 0.07	0.59 $\pm$ 0.04
	A30P	0.52 $\pm$ 0.04	0.46 $\pm$ 0.01	0.49 $\pm$ 0.02	0.45 $\pm$ 0.02
<i>Down-state length SD (s)</i>	WT	2.07 $\pm$ 0.27	1.91 $\pm$ 0.18	1.72 $\pm$ 0.22	1.86 $\pm$ 0.21
	A30P	1.21 $\pm$ 0.13	1.14 $\pm$ 0.13	1.05 $\pm$ 0.1	1.02 $\pm$ 0.12

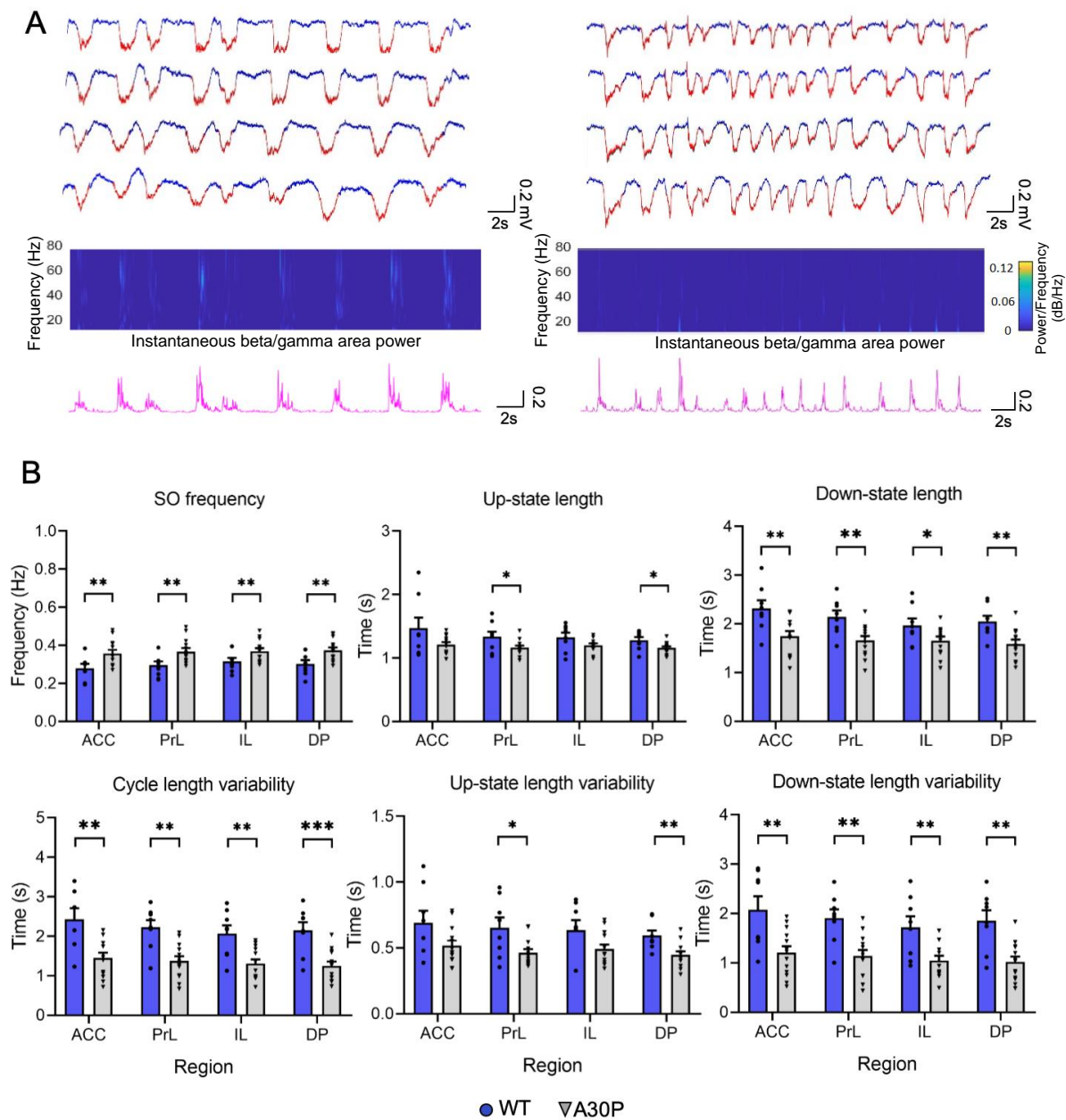


**Figure 4.1:** Changes in the SO cycle in the mPFC of A30P animals. **A)** An example of Up- and Down-state detection in the ACC of a WT and an A30P mouse, and a spectrogram showing power in the beta/gamma frequency range. **B)** The Up-Down cycle characteristics examined are: the SO frequency (0.1 – 0.9 Hz), the mean length of the Up-state and Down-state and the mean Up-state, Down-state and SO cycle (Down-state + Up-state) length variability over time. Each variable is investigated in the 4 subregions of the mPFC (ACC, PrL, IL, DP), in WT (N = 13; blue) and A30P (N = 8; grey) mice. Measures of variability reflect the SD of the mean for each variable, over time. Error bars indicate the SEM and asterisks indicate significance: \* =  $p < 0.05$ , \*\* =  $p < 0.01$ , \*\*\* =  $p < 0.001$ .

#### 4.3.1.2. A30P mice have an altered distribution of high frequency activity in the SO cycle in the mPFC

Next, we looked at the power content of the SO (Figure 4.1A; Figure 4.2). Normally, neuronal firing and hence higher-frequency activity is restrained on the Up-state of the SO, while the Down-state is neuronally “silent” (Steriade et al., 1993a). Hence, we examined the average power content of the Up-state and Down-state, and the peak power and its latency in the SO cycle in 3 frequency bands: beta (15 – 29.9 Hz), gamma (30 – 79.9 Hz) and high-gamma (80 – 129.9 Hz), in the mPFC subregions of 8 WT and 13 A30P animals (Figure 4.2; Table 4.2).

Our rmANOVA analysis revealed significant differences between A30P and WT animals only in the latency to the beta ( $F(1,19) = 6.36, p < 0.05$ ; Figure 4.2A) and gamma ( $F(1,19) = 6.81, p < 0.05$ ; Figure 4.2B) peak power in the IL and PrL regions. The normalized SO cycle consists of the Down- followed by the Up-state, where 0 is the beginning of the Down-state, 50 is the Down-to-Up-transition and 100 the Up-state termination. Hence, in the case of the PrL region for example, the beta peak latency of  $61.48 \% \pm 0.8 \%$  in A30P animals is greater than the beta peak latency of  $58.53 \% \pm 0.84 \%$  in WT animals. Thus, the beta peak power is “delayed” on the Up-state in A30P animals as it comes at a later point in the SO cycle, although it still occurs on the Up-state as the latency is greater than 50. The high frequency power-related variables that were not significantly different between genotypes are shown in Appendix A.

We also found a significant effect of region in a number of power-related variables, but not an effect of genotype or a genotype/region interaction and hence, we characterised this regional difference in A30P and WT animals combined. The mean power on the Up-state in the beta ( $F(1.83, 30.59) = 5.81, p < 0.01$ ) and gamma bands ( $F(1.94, 36.89) = 10.06, p < 0.001$ ) was greater in the PrL region compared to the DP ( $p < 0.01$ ) and IL ( $p < 0.05$ ) regions. Regarding the peak power, we found a significant effect of region in the beta peak power ( $F(1.84, 34.99) = 7.27, p < 0.001$ ), with a greater peak power in the PrL compared to the DP ( $p < 0.01$ ) and IL ( $p < 0.05$ ) subregions and in the DP compared to the IL subregion ( $p < 0.05$ ). The gamma peak power ( $F(2.01, 38.09) = 11.58, p < 0.001$ ) was lowest in the DP compared to the IL ( $p < 0.05$ ), PrL ( $p < 0.001$ ) and ACC ( $p < 0.01$ ), and the second lowest in the IL subregion as it was shorter than the PrL ( $p < 0.01$ ). Finally the high-gamma peak ( $F(2.381, 45.18) = 5.16, p < 0.01$ ) had a greater peak in the PrL compared to the DP ( $p < 0.05$ ) region. Thus, power and the peak-power on the Up-state are greater in the dorsal mPFC,

mostly the PrL subregion, compared to the ventral mPFC (Table 4.2). In summary, no significant differences were found between WT and A30P animals in the average power on the Up- and Down-state, or in the peak power, in any frequency band. However, we found that the distribution of power on the Up-state is altered in A30P animals, as is evident from a greater latency to peak power in both the beta and gamma frequency bands. The beta band peak power also appears to have a bimodal peak distribution in A30P animals, but we only investigated the location and peak of the first maximum point and hence have no statistical evidence regarding this observation. The average power on the Up-state and the peak power in all frequency bands had a dorsal to ventral decay between mPFC subregions.

**Table 4.2:** Characterisation of the high frequency oscillatory activity in the SO cycle, in the mPFC of WT and A30P mice. The average of each variable  $\pm$  SEM are shown for 3 frequency bands (Beta, Gamma, High-Gamma), in the mPFC subregions (ACC, PrL, IL, DP), in WT (N = 8) and A30P (N = 13) mice. Variables also shown in Figure 4.2 are in *Italics*.

	Band	Genotype	Region			
			ACC	PL	IL	DP
<b>Power on the Up-state</b> ( $\times 10^3$ )	Beta	WT	9.28 $\pm$ 1.7	10.34 $\pm$ 1.39	7.64 $\pm$ 1.37	6.77 $\pm$ 1.19
		A30P	16.62 $\pm$ 3.51	12 $\pm$ 1.76	8.5 $\pm$ 1.22	6.98 $\pm$ 1.04
	Gamma	WT	21.50 $\pm$ 4.75	19.78 $\pm$ 2.72	15.76 $\pm$ 3.27	11.95 $\pm$ 2.29
		A30P	29.93 $\pm$ 5.95	23.52 $\pm$ 3.49	15.99 $\pm$ 3.09	12.49 $\pm$ 2.33
	High-Gamma	WT	10.11 $\pm$ 1.94	9.26 $\pm$ 1.17	7.41 $\pm$ 1.2	6.78 $\pm$ 1.24
		A30P	15.06 $\pm$ 3.33	11.19 $\pm$ 2.13	8.82 $\pm$ 2.2	7.9 $\pm$ 1.76
<b>Power on the Down-state</b> ( $\times 10^3$ )	Beta	WT	4.41 $\pm$ 0.9	4.03 $\pm$ 0.7	3.16 $\pm$ 0.36	2.71 $\pm$ 0.53
		A30P	7.46 $\pm$ 1.61	87.92 $\pm$ 23.37	61.27 $\pm$ 11.04	39.57 $\pm$ 4.6
	Gamma	WT	8.29 $\pm$ 1.9	8.01 $\pm$ 1.9	6.41 $\pm$ 0.93	5.91 $\pm$ 1.41
		A30P	12.7 $\pm$ 2.55	8.56 $\pm$ 1.54	7.37 $\pm$ 1.68	7.02 $\pm$ 1.53
	High-Gamma	WT	6.53 $\pm$ 1.46	6.29 $\pm$ 1.26	5.71 $\pm$ 0.94	5.51 $\pm$ 1.14
		A30P	10.79 $\pm$ 2.62	8.1 $\pm$ 1.87	7.25 $\pm$ 1.99	6.92 $\pm$ 1.62
<b>Peak power</b> ( $\times 10^3$ )	<i>Beta</i>	<i>WT</i>	<i>55.78 <math>\pm</math> 9.55</i>	<i>64.75 <math>\pm</math> 9.39</i>	<i>47.21 <math>\pm</math> 8.56</i>	<i>38.28 <math>\pm</math> 6.89</i>
		<i>A30P</i>	<i>76.82 <math>\pm</math> 18.93</i>	<i>58.24 <math>\pm</math> 12.47</i>	<i>49.16 <math>\pm</math> 13.56</i>	<i>42.38 <math>\pm</math> 11.18</i>
	<i>Gamma</i>	<i>WT</i>	<i>93.12 <math>\pm</math> 17.26</i>	<i>86.59 <math>\pm</math> 11.89</i>	<i>65.00 <math>\pm</math> 12.8</i>	<i>54.14 <math>\pm</math> 9.29</i>
		<i>A30P</i>	<i>135.12 <math>\pm</math> 28.76</i>	<i>102.92 <math>\pm</math> 14.8</i>	<i>69.15 <math>\pm</math> 11.42</i>	<i>53.48 <math>\pm</math> 8.68</i>
	High-Gamma	WT	58.5 $\pm$ 1.31	58.76 $\pm$ 0.93	57.35 $\pm$ 1.08	58.16 $\pm$ 0.98
		A30P	76.82 $\pm$ 18.93	58.24 $\pm$ 12.47	49.16 $\pm$ 13.56	42.38 $\pm$ 11.18
<b>Latency to peak power</b>	<i>Beta</i>	<i>WT</i>	<i>57.38 <math>\pm</math> 2.43</i>	<i>58.53 <math>\pm</math> 0.84</i>	<i>58.77 <math>\pm</math> 1.13</i>	<i>60.72 <math>\pm</math> 1.33</i>
		<i>A30P</i>	<i>60.35 <math>\pm</math> 1.28</i>	<i>61.48 <math>\pm</math> 0.8</i>	<i>63.22 <math>\pm</math> 0.94</i>	<i>64.28 <math>\pm</math> 1.43</i>
	<i>Gamma</i>	<i>WT</i>	<i>67.17 <math>\pm</math> 1.07</i>	<i>61.94 <math>\pm</math> 1.02</i>	<i>60.41 <math>\pm</math> 1.83</i>	<i>62.73 <math>\pm</math> 0.86</i>
		<i>A30P</i>	<i>62.49 <math>\pm</math> 1.41</i>	<i>65.2 <math>\pm</math> 0.92</i>	<i>65.46 <math>\pm</math> 0.68</i>	<i>65.39 <math>\pm</math> 1.02</i>
	High-Gamma	WT	51.63 $\pm$ 11.56	48.9 $\pm$ 8.66	40.01 $\pm$ 8.6	36.85 $\pm$ 8.42
		A30P	58.25 $\pm$ 0.76	58.88 $\pm$ 0.94	57.21 $\pm$ 0.99	56.37 $\pm$ 1.16

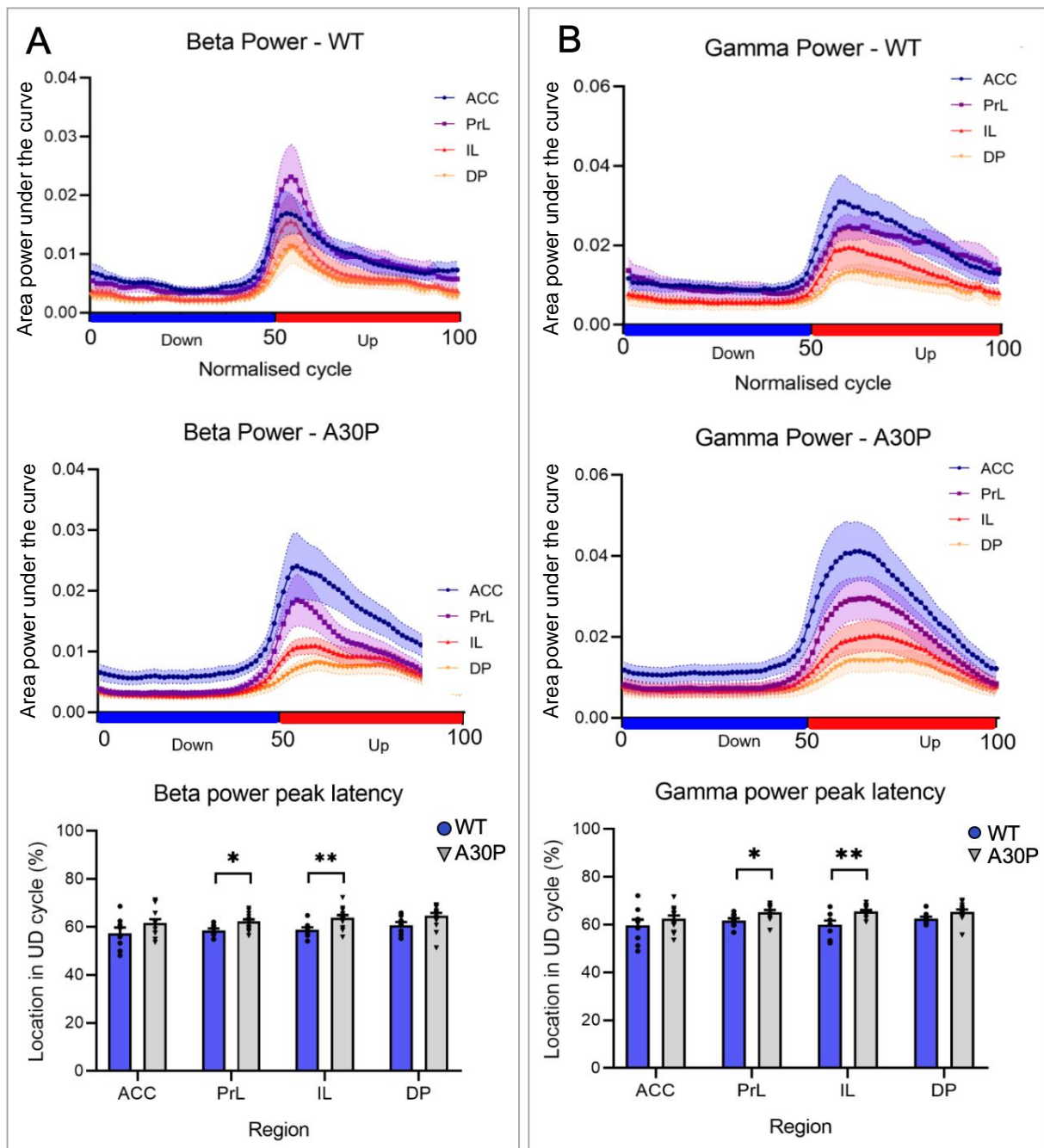


**Figure 4.2:** Changes in the distribution of the high frequency oscillatory power on the normalised SO cycle in the mPFC of A30P animals. The latency of the peak power in the **A)** beta (15 – 29.9 Hz) and **B)** gamma (30 – 79.9 Hz) frequency bands is shown for in the SO cycle (0 = start of Down-state, 50 = Down to Up-state transition, 100 = end of Up-state), in the mPFC subregions (ACC, PrL, IL, DP), in A30P (N = 13) and WT (N = 8) animals. Error bars indicate the SEM and asterisks indicate significance: \* =  $p < 0.05$ , \*\* =  $p < 0.01$ .

### 4.3.2. **Characterisation of the SO cycle in hippocampus of A30P mice**

As shown by Wolansky *et al.*, (2006), SOs are readily observed in the CA1 region of the hippocampus under urethane anaesthesia. Recordings in the CA1 of the hippocampus showed robust SO in both WT (N = 7) and A30P (N = 8) mice (Figure 4.3A). Hence, we proceeded with similar analyses of the SO characteristics and its power content for this region (Figure 4.3).

#### 4.3.2.1. A30P mice have altered SO cycle patterns in the hippocampus

Consistent with the changes outlined above for the mPFC, our analysis revealed that the hippocampal SO was also significantly faster in A30P mice compared to WTs ( $F(1, 13) = 17.57, p < 0.01$ ). The increased SO frequency in A30P animals can be attributed to a shorter SO cycle length ( $F(1, 13) = 14.54, p < 0.01$ ), composed of both shorter Up- ( $F(1, 13) = 6.49, p < 0.05$ ) and Down-states ( $F(1, 13) = 10.19, p < 0.01$ ). Moreover, the state-length variability over time was lower in both Up- and Down-states: SO cycle ( $F(1, 13) = 18.07, p < 0.01$ ), Up-state ( $F(1, 13) = 8.27, p < 0.05$ ) and Down-state ( $F(1, 13) = 13.65, p < 0.01$ ). Again, as observed in the mPFC, the SO amplitude did not differ between WT ( $0.56 \pm 0.06$  mV) and A30P mice ( $0.45 \pm 0.05$  mV). Thus, the SO is clearly faster in the CA1 of A30P animals as well as the mPFC, due to shorter Up- and Down-state and lower state-length variability that could indicate a reduction in the number of longer states (Figure 4.3B).

#### 4.3.2.2. A30P mice have an altered distribution of high frequency activity in the SO cycle in the hippocampus

Higher-frequency oscillations are also nested on the Up-state of the hippocampal SO (Sharma *et al.*, 2010; Figure 4.3A). Univariate ANOVA analysis for the power content of the SO, revealed increased latency to peak power in the normalised SO cycle in the gamma frequency band in A30P mice ( $F(1, 13) = 5.48, p < 0.05$ ). We did not see a shift of the beta peak power but this is expected as beta activity has only been described as a functional rhythm in the hippocampus during exploration (Berke *et al.*, 2008; Leung, 1992). Thus, similar to the mPFC we found a delay in the occurrence of the gamma peak power on the Up-state, but we did not find any differences in the average power of fast-oscillatory activity on the Up- or Down-states (Figure 4.3C; Table 4.3). The data that was not significantly different between genotypes is shown in Appendix B.

**Table 4.3:** Characterisation of the high frequency oscillatory power in the SO cycle in the hippocampus of WT and A30P animals. The average of each variable  $\pm$  SEM is shown for 3 frequency bands (beta, gamma, high-gamma), for the WT (N = 7) and A30P (N = 8) animal groups. Variables also shown in Figure 4.3 are in *Italics*.

<b>Variable</b>	<b>Band</b>	<b>WT</b>	<b>A30P</b>
Power on the Up-state ( $\times 10^3$ )	Beta	40.86 $\pm$ 12.5	68.21 $\pm$ 8.42
	Gamma	76.8 $\pm$ 25.55	95.21 $\pm$ 14.95
	High-gamma	18.26 $\pm$ 5.28	24.49 $\pm$ 4.64
Power on the Down-state ( $\times 10^3$ )	Beta	17.45 $\pm$ 4.07	31.8 $\pm$ 6.03
	Gamma	27.5 $\pm$ 6.21	49.69 $\pm$ 12.03
	High-gamma	7.2 $\pm$ 1.78	16.47 $\pm$ 3.31
<i>Peak power (<math>\times 10^3</math>)</i>	Beta	60.36 $\pm$ 3.26	66.34 $\pm$ 1.68
	<i>Gamma</i>	<i>59.47 <math>\pm</math> 2.77</i>	<i>66.71 <math>\pm</math> 1.38</i>
	High-gamma	59.12 $\pm$ 1.79	63.9 $\pm$ 1.52
<i>Latency to peak power</i>	Beta	269.56 $\pm$ 115.57	292.02 $\pm$ 34.24
	<i>Gamma</i>	<i>494.7 <math>\pm</math> 211.99</i>	<i>445.33 <math>\pm</math> 68.38</i>
	High-gamma	129.26 $\pm$ 31.43	150.1 $\pm$ 17.87

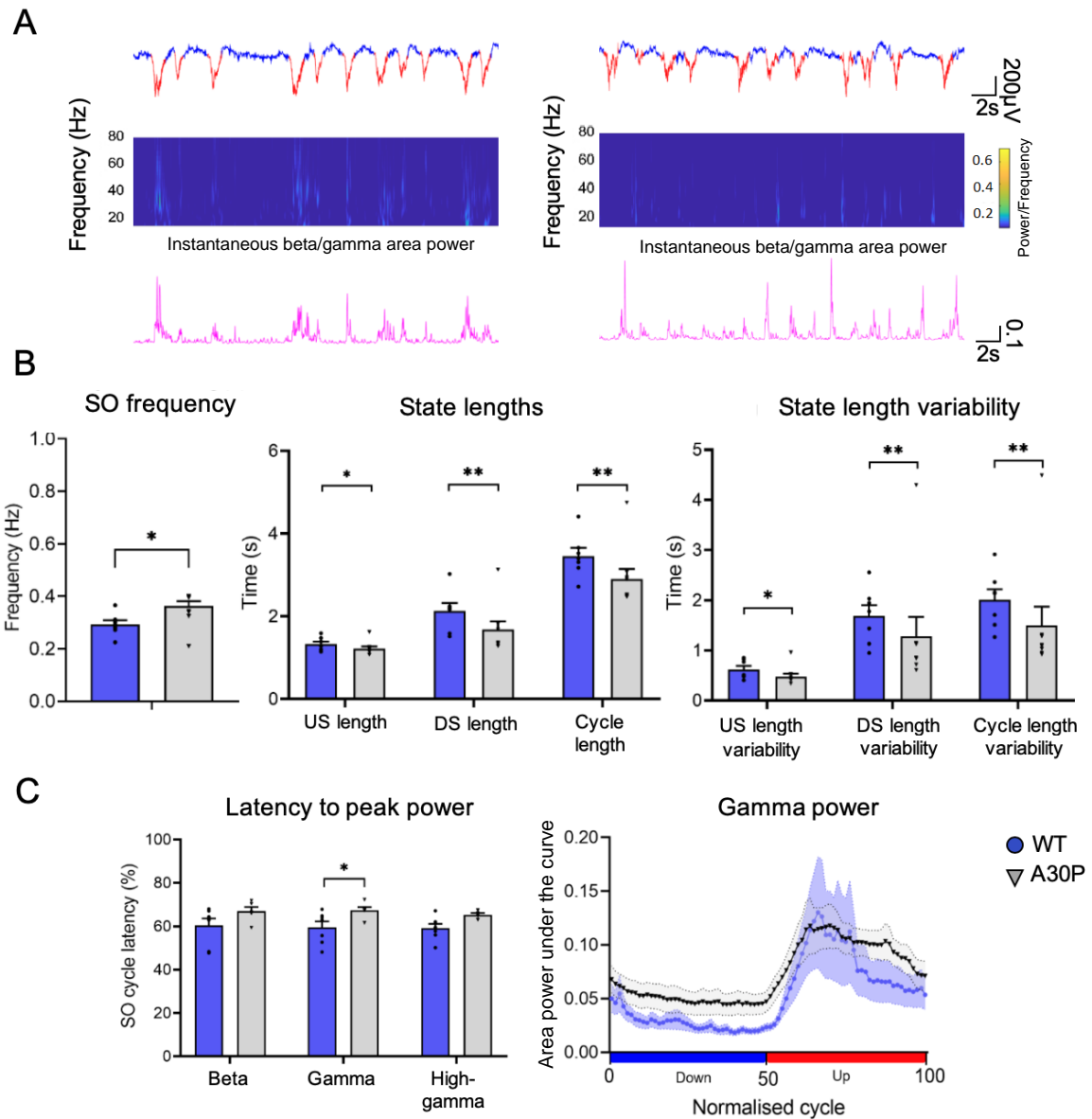


**Figure 4.3:** Changes in the SO cycle in the hippocampus of A30P mice. **A)** Example of Up- and Down-state detection in relation to beta/gamma frequency power. **B)** The SO frequency, the mean length of the Up-state (UD), Down-state (DS) and SO cycle and the mean Up-state, Down-state and Up-Down cycle length variability over time (SD), in WT (N = 7; blue) and A30P (N = 8; grey) mice. **C)** Changes in the distribution of beta (15 – 30 Hz), gamma (30 – 80 Hz) and high-gamma (80 – 130 Hz) power in the SO cycle, in the CA1 of WT (N = 7; blue) and A30P (N=7; grey) mice. The bar chart shows the latency of the peak of power in the normalised SO cycle for the different frequency bands. The distribution of gamma power is shown in the normalised SO cycle (0 = start of Down-state, 50 = Down' to Up-state transition, 100 = end of Up-state), in A30P (N = 7) and WT animals (N = 7). Measures of variability reflect the SD of the mean for each variable, over time. Error bars indicate the SEM and asterisks indicate statistical significance: \* =  $p < 0.05$ , \*\* =  $p < 0.01$ .

### 4.3.3. ***A30P mice have altered neuronal firing patterns in relation to the SO***

During the SO, neurons fire predominantly on the Up-state of the field potential, which corresponds to depolarization of the cortical pyramidal cells (Figure 4.4A; Steriade et al., 1996; Dang-Vu *et al.*, 2008). It is possible that abnormal  $\alpha$ -syn expression in A30P mice could lead to changes in the neuronal firing. Therefore, we looked for differences in spike frequency and ISI on the Up-state and for the recording duration, the latency to the first spike on the normalized SO cycle, and the percentage of firing occurring on the Down-state. Measurements were made for neurons in the 4 subregions of the mPFC combined in both A30P (N = 15 mice; N = 56 units) and WT animals (N = 7 mice; N = 28 units) (Figure 4.4; Table 4.4; Table 4.5). The maximum unit firing / SO coherence was also investigated in 12 A30P and 7 WT animals, with 50 and 23 units respectively.

The unit firing frequency and ISI on the Up-state and for the recording duration were not significantly different between WT and A30P animals, neither was the latency to the first unit on the Up-state (Table 4.5). However, in A30P mice the percentage of total neuronal firing occurring on the Up-state was significantly lower compared to WT animals ( $F(1, 20) = 4.75, p < 0.05$ ; Table 4.5; Figure 4.4B,C), suggesting altered neuronal firing in relation to the SO cycle. Indeed when we analysed the unit firing / SO coherence we found that it was significantly lower in A30P compared to WT animals ( $F(1, 17) = 4.95, p < 0.05$ ). Our findings suggest that while there is no increase in neuronal firing in A30P animals, there is an increase in the percentage of “abnormal” firing on the Down-state. This shift of firing to the Down-state explains the decreased synchrony observed between the SO and unit firing in A30P animals (Figure 4.4D).

**Table 4.4:** The number of units and the mPFC subregion they were recorded from: ACC, IL, PrL, DP, in WT (N = 7; units = 23) and A30P animals (N = 15; units = 56).

		<b>A30P animals</b>														
<b>Units / Region</b>	<b>1</b>	<b>2</b>	<b>3</b>	<b>4</b>	<b>5</b>	<b>6</b>	<b>7</b>	<b>8</b>	<b>9</b>	<b>10</b>	<b>11</b>	<b>12</b>	<b>13</b>	<b>14</b>	<b>15</b>	
ACC	-	-	-	-	1	1	-	-	1	-	1	-	2	1	-	
PrL	2	2	-	-	1	-	-	-	2	2	-	1	-	1	-	
IL	3	4	1	-	5	-	1	1	1	1	1	-	-	-	1	
DP	3	1	-	1	2	-	1	1	-	3	1	-	-	-	1	
		<b>WT animals</b>														
<b>Units / Region</b>	<b>1</b>	<b>2</b>	<b>3</b>	<b>4</b>	<b>5</b>	<b>6</b>	<b>7</b>									
ACC	-	-	2	1	2	1	-									
PrL	-	2	-	-	2	-	2									
IL	1	1	-	-	2	-	2									
DP	-	1	-	1	1	-	2									

**Table 4.5:** Characterisation of the unit firing patterns in the mPFC of WT and A30P mice. The average of each variable  $\pm$  SEM are shown for the WT (N = 7) and A30P (N = 15) mice, with 23 and 56 units respectively, except the unit firing / SO coherence: WT (N = 7; 23 units) and A30P (N = 12; 50 units). Variables also shown in Figure 4.4 are in *Italics*.

<b>Variable</b>	<b>WT</b>	<b>A30P</b>
Spike frequency / recording duration (Hz)	1.28 $\pm$ 0.19	1.58 $\pm$ 0.28
Spike frequency on the Up-state (Hz)	2.76 $\pm$ 1.47	3.39 $\pm$ 2.71
ISI / recording duration (s)	1.04 $\pm$ 0.23	1.83 $\pm$ 0.65
ISI on the Up-state (s)	0.29 $\pm$ 0.06	0.38 $\pm$ 0.05
Percentage of firing on Up-state (%)	89.87 $\pm$ 2.18	80.33 $\pm$ 3.38
<i>Percentage of firing on Down-state (%)</i>	<i>10.13 <math>\pm</math> 2.18</i>	<i>19.67 <math>\pm</math> 3.38</i>
Latency to the first unit on Up-state	61.85 $\pm$ 1.47	65.04 $\pm$ 1.33
<i>Unit firing / SO coherence</i>	<i>0.68 <math>\pm</math> 0.06</i>	<i>0.57 <math>\pm</math> 0.05</i>
Unit firing / SO coherence frequency (Hz)	0.4 $\pm$ 0.05	0.45 $\pm$ 0.03

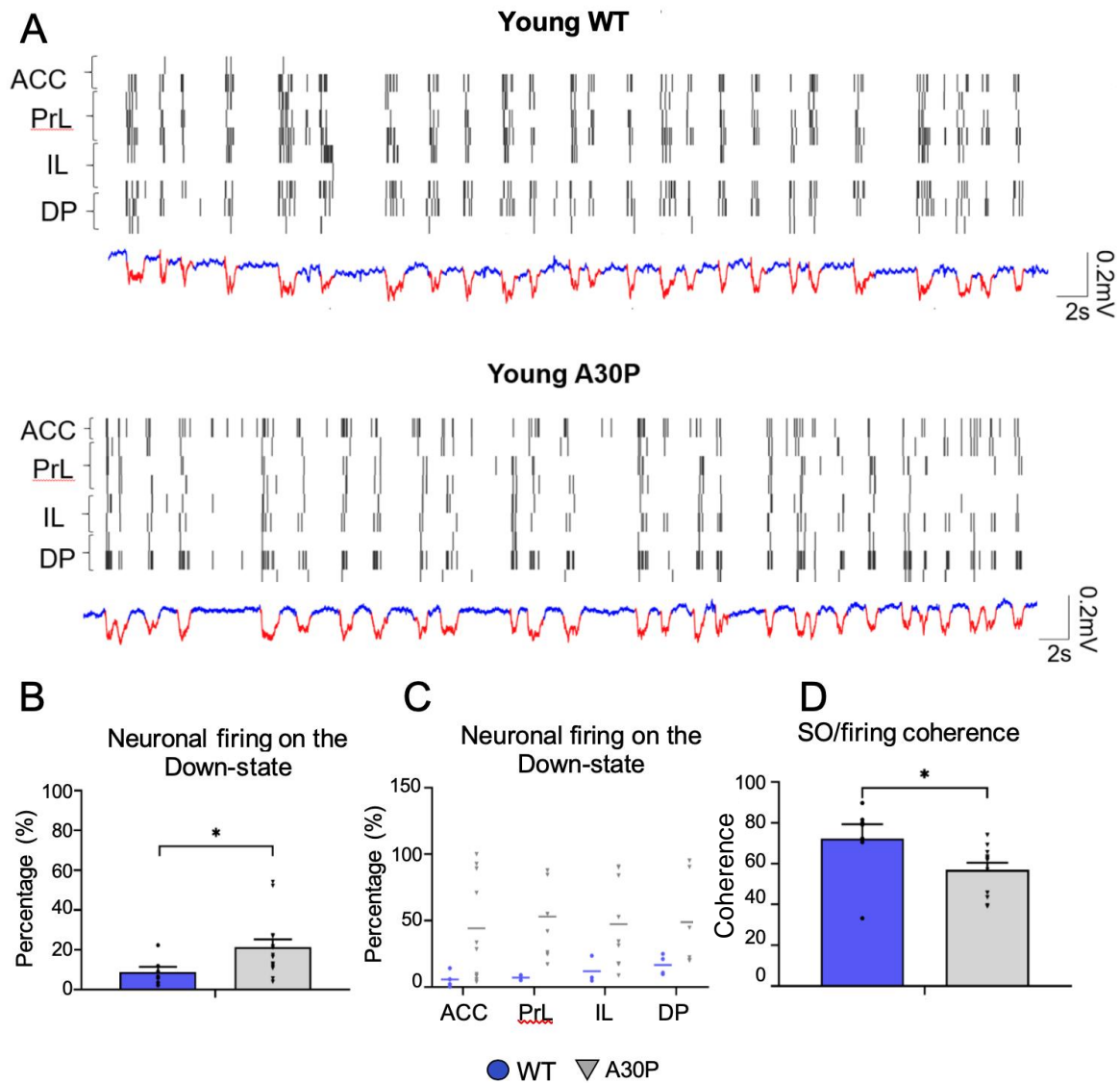


**Figure 4.4:** Changes in the unit firing patterns in relation to the SO in the mPFC of A30P mice. **A)** Example raster plots showing unit firing in relation to an ACC channel in a WT and an A30P mouse. **B)** The percentage of the total firing occurring on the Down-state, for all the units recorded from WT (N = 8, black) and A30P (N = 15, red) animals, across all mPFC subregions: ACC (WT = 5/7 , A30P = 9/13 ), PrL ( WT = 3/6, A30P = 8/16), IL (WT = 4/5, A30P = 7/13) and DP (WT = 4/5, A30P = 7/9). **C)** The percentage of firing on the Down-state for each mPFC subregion is shown but it was not statistically investigated. **D)** The average unit firing / SO coherence across all units recorded from each animal (WT = 8, A30P = 12), for all mPFC regions combined: ACC (WT = 5/7 , A30P = 10/15 ), PrL (WT = 3/6, A30P = 9/19), IL (WT = 4/6, A30P = 9/19) and DP (WT = 5/7, A30P = 6/12). Numbers indicate the N of animals / N of units. Error bars indicate the SEM. Asterisks indicate statistical significance: \* =  $p < 0.05$ .

#### 4.3.4. No changes in mPFC/CA1 SO coherence in A30P mice

Due to the small size of the mouse brain we could only record simultaneously from the mPFC and hippocampus from contralateral hemispheres. However, these contralateral recordings have been previously shown to be synchronous with one another (Gordon et al., 2011). Mann-Whitney U-test with a Welch exact-correction for the dual recordings from WT (N = 5) and A30P (N = 6) animals showed no changes in coherence between the CA1 of the hippocampus and any of the mPFC subregions (Figure 4.5). As mentioned above, we did not investigate for an effect of mPFC subregion as this analysis is considered preliminary due to the small sample size.

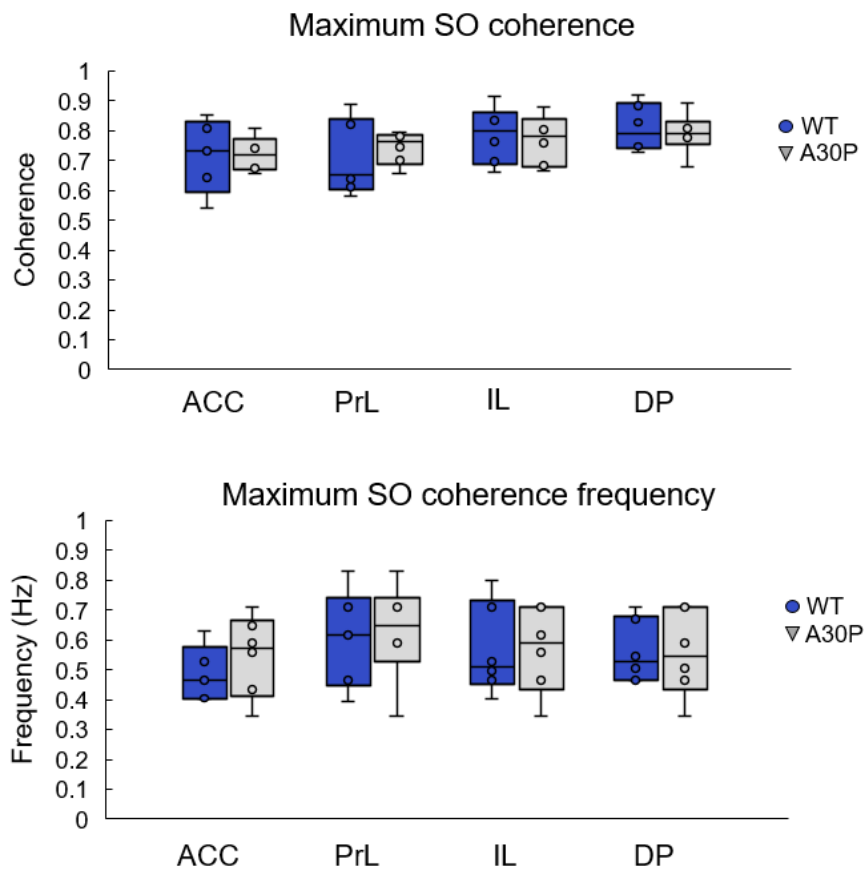


**Figure 4.5:** The maximum hippocampal/mPFC SO coherence and its frequency in A30P and WT mice. The median SO coherence  $\pm$  IQR and the median frequency at maximum coherence  $\pm$  IQR are shown for the four subregions of the mPFC (ACC, PrL, IL, DP), in WT (N = 5) and A30P (N = 6) animals.

#### 4.3.5. ***Sleep spindles are altered in the mPFC of A30P mice***

Sleep spindles play a critical role in memory consolidation (Siapas & Wilson, 1998) and are altered in DLB patients (Fernández-Arcos et al., 2019). Therefore, we compared the spindle properties between WT and A30P animals. Sleep spindles (8 - 15 Hz) with a duration > 0.3 s, were observed in the LFP (Figure 4.6A), in all subregions of the mPFC in both WT (N = 8) and A30P mice (N = 13). Instantaneous spindle frequency was not significantly different across the mPFC subregions, nor between WT and A30P mice. The average instantaneous spindle frequency in the mPFC (averaged across regions) was 10.65 Hz  $\pm$  0.039 Hz in WT and 10.7 Hz  $\pm$  0.06 Hz in A30P mice, values that are consistent with spindle frequencies recorded in the mPFC in other studies under urethane anaesthesia (Barthó et al., 2014). Moreover, as reported previously (Jobert et al., 1992), spindles were found to occur at the beginning of the Up-state in both A30P (62.3  $\pm$  1.26) and WT (56.2  $\pm$  1.14) animals in the normalized cycle (1 = Down-state beginning, 50 = Up-Down transition, 100 = Up-state termination) (Figure 4.6; Table 4.6).

Although there was no difference in spindle frequency between WT and A30P animals, the spindle duration was significantly shorter in A30P mice compared to WT ( $F(1, 19) = 14.21, p < 0.01$ ), in all mPFC subregions ( $p < 0.01$ ). Spindle length was also less variable over time in A30P animals ( $F(1, 19) = 6.6, p < 0.05$ ) in the DP, IL and PrL regions. Spindle amplitude was not significantly different between A30P and WT animals. Interestingly, spindle amplitude variability was significantly lower in A30P compared to WT animals ( $F(1, 19) = 8.27, p < 0.01$ ) in the PrL and DP subregions, with a trend for the other subregions as well. These findings could suggest that A30P mice have fewer spindles of high amplitude compared to WT mice. See Figure 4.6B for the full comparison and Table 4.6 for all the values.

To determine whether A30P mice have fewer high amplitude spindles, we looked at the percentage of spindles exceeding a threshold of mean amplitude + 5\*SD. As expected, A30P animals had a significantly lower percentage of high-amplitude spindles ( $F(1, 19) = 6.17, p < 0.05$ ) in all subregions. Finally, we compared the total number of spindles occurring on the Up-states in A30P compared to WT animals. When looking at the number of spindles occurring in relation to the total recording duration (absolute spindle density) we found no significant difference between the two groups. However, when looking at the number of spindles in relation to the number of

Up-states (relative spindle density) we found a significant decrease in A30P mice ( $F(1,19) = 4.71, p < 0.05$ ), in the ACC and PrL regions, with a similar trend in the other subregions (Figure 4.6B; Table 4.6).

We also found a significant effect of region in a number of variables but not a region/genotype interaction. Hence, we proceeded to characterise regional differences in the WT and A30P mice combined. A significant effect of region was identified ( $F(1.74, 33.05) = 14.76, p < 0.001$ ) in spindle length, with longer spindles occurring in the DP and IL compared to the PrL ( $p < 0.001$ ) and ACC ( $p < 0.05$ ) subregions. Moreover, there was lower spindle length variability ( $F(2.04, 38.75) = 12.31, p < 0.001$ ) in the PrL and ACC compared to the DP and IL subregions ( $p < 0.05$ ). Spindles were also of shorter amplitude ( $F(2.29, 43.53) = 7.14, p < 0.01$ ) in the DP compared to all the other subregions ( $p < 0.05$ ), and had a lower spindle amplitude variability ( $F(2.16, 41.01) = 4.77, p < 0.05$ ) in the DP compared to the PrL ( $p < 0.01$ ) subregion. Moreover, the number of high-amplitude spindles ( $F(2.17, 41.22) = 7.99, p < 0.001$ ) was lower in the DP compared to the ACC, IL ( $p < 0.01$ ) and PrL ( $p < 0.05$ ) subregions, and in the IL compared to the PL ( $p < 0.05$ ) subregion. Finally, the number of spindles/Up-state ( $F(2.05, 39.03) = 13.21, p < 0.001$ ) was highest in the ACC compared to the other regions ( $p < 0.01$ ).

In conclusion, we found that the instantaneous spindle frequency was not significantly different between A30P and WT animals, but the length of the spindle was shorter in A30P animals. Moreover, although the average spindle amplitude did not differ between A30Ps and WT animals, A30P mice had lower spindle amplitude variability over time and fewer high-amplitude spindles. In addition, A30P mice had a lower relative spindle density (spindle no / Up-state) but not absolute spindle density (spindle no / recording duration), suggesting that the increased SO frequency in these animals (section 4.3.1) compensates for the total spindle number. However, A30P have fewer spindles per Up-state. This decrease in relative spindle density in A30P mice might be the result of an incapacity to produce longer and larger amplitude spindles. Finally, the regional differences we found suggest that more dorsal areas of the mPFC produce spindles of greater amplitude and duration.

**Table 4.6:** Sleep spindle characterisation in the mPFC region of A30P and WT animals. The average of each variable  $\pm$  SEM is shown for the each mPFC.subregion (ACC, PrL, IL, DP), in A30P (N = 13) and WT (N = 8) animals. Variables also shown in Figure 4.6 are in *Italics*.

Variable	Genotype	Region			
		ACC	PL	IL	DP
Instantaneous frequency (Hz)	WT	55.28 $\pm$ 3.72	54.65 $\pm$ 5.7	54.01 $\pm$ 5.96	49.04 $\pm$ 3.55
	A30P	49.01 $\pm$ 2.82	44.9 $\pm$ 2.68	45.61 $\pm$ 2.56	45.96 $\pm$ 2.75
Spindle latency in the normalised SO cycle	WT	58.46 $\pm$ 2.82	63.03 $\pm$ 1.77	63.95 $\pm$ 1.36	66.23 $\pm$ 1.28
	A30P	58.07 $\pm$ 2.13	59.91 $\pm$ 2.1	63.45 $\pm$ 1.57	65.3 $\pm$ 1.78
Absolute spindle density	WT	0.33 $\pm$ 0.01	0.31 $\pm$ 0.01	0.31 $\pm$ 0.02	0.31 $\pm$ 0.02
	A30P	0.3 $\pm$ 0.01	0.28 $\pm$ 0.01	0.29 $\pm$ 0.02	0.29 $\pm$ 0.02
<i>Relative spindle density</i>	WT	1.25 $\pm$ 0.14	1.08 $\pm$ 0.1	1.02 $\pm$ 0.1	1.01 $\pm$ 0.09
	A30P	0.86 $\pm$ 0.06	0.79 $\pm$ 0.06	0.8 $\pm$ 0.07	0.79 $\pm$ 0.07
Spindle length (s)	WT	0.39 $\pm$ 0.01	0.39 $\pm$ 0.01	0.41 $\pm$ 0.01	0.41 $\pm$ 0.02
	A30P	0.36 $\pm$ 0.01	0.35 $\pm$ 0.01	0.37 $\pm$ 0.01	0.38 $\pm$ 0.02
Spindle length variability (s)	WT	0.16 $\pm$ 0.02	0.16 $\pm$ 0.01	0.19 $\pm$ 0.02	0.2 $\pm$ 0.03
	A30P	0.16 $\pm$ 0.02	0.14 $\pm$ 0.01	0.16 $\pm$ 0.02	0.17 $\pm$ 0.03
Spindle amplitude ( $\mu$ V)	WT	48.2 $\pm$ 3.36	44.38 $\pm$ 2.65	41.96 $\pm$ 2.64	40.99 $\pm$ 2.96
	A30P	56.55 $\pm$ 3.06	53.31 $\pm$ 3.37	50.12 $\pm$ 2.76	45.17 $\pm$ 2.42
Spindle amplitude variability ( $\mu$ V)	WT	22.28 $\pm$ 2.33	21.8 $\pm$ 1.97	19.5 $\pm$ 2.58	19.61 $\pm$ 2.43
	A30P	17.98 $\pm$ 1.22	18.89 $\pm$ 1.46	16.8 $\pm$ 1.06	13.7 $\pm$ 0.56
High-amplitude spindles (> 5*mean amplitude; %)	WT	26.21 $\pm$ 4.14	23.74 $\pm$ 3.37	20.43 $\pm$ 2.34	20.5 $\pm$ 2.36
	A30P	19.16 $\pm$ 2.44	19.98 $\pm$ 2.59	16.67 $\pm$ 1.95	12.35 $\pm$ 1.72

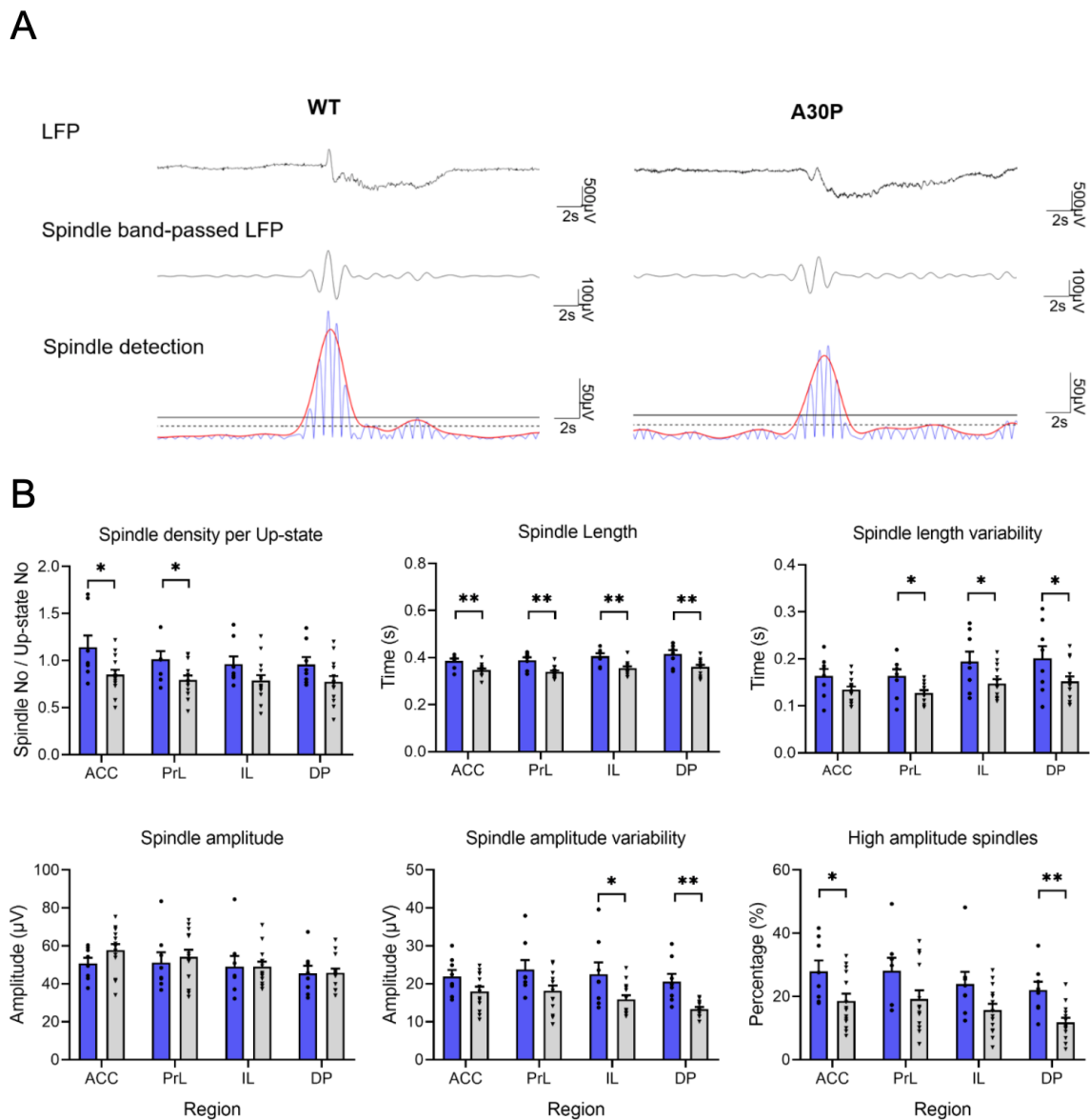


**Figure 4.6:** Changes in the sleep spindle characteristics in the mPFC of A30P mice. **A)** Examples of spindles including the LFP, the spindle-band passed LFP and detection of the spindle, in the ACC of a WT and an A30P animal. **B)** The characteristics of the spindles that were analysed including the spindle density per Up-state number, the spindle length and length variability over time, the spindle amplitude and amplitude variability over time and the percentage of “high amplitude” spindles. Measures of variability reflect the SD of the mean for each variable, over time. These variables were extracted for the four subregions of the mPFC (ACC, PrL, IL, DP) in WT (N = 8, grey) and A30P (N = 13, blue) mice. Error bars indicate the SEM and asterisks indicate significance: \* =  $p < 0.05$ , \*\* =  $p < 0.01$ .

#### 4.3.6. *Hippocampal SWRs are normal in A30P mice*

As cortical spindles are temporally correlated with hippocampal SWRs (Siapas & Wilson, 1998; Clemens et al., 2011), which also play a critical role in memory consolidation (Witton et al., 2016). We therefore also looked at hippocampal SWRs recorded in the CA1 pyramidal cell layer in A30P (N = 6) and WT (N = 7) mice (Table 4.7). SWRs had an instantaneous frequency of  $87.48 \pm 6.46$  Hz in WTs and  $83.43 \pm 1.73$  Hz in A30P animals. Moreover, they were located at the beginning of the SO cycle, with a latency of  $59.58 \pm 8.3\%$  Hz in WTs and  $61.84 \pm 6.45\%$  in A30P animals. Somewhat surprisingly we found no significant differences between ripples in any of the variables tested including the instantaneous ripple frequency, ripple duration, ripple amplitude and in the variability over time of these measures. Furthermore, the total number SWRs and the number of SWRs per Up-state were also not significantly different between genotypes.

**Table 4.7:** Characterisation of sharp wave ripples (SWR) in the CA1 of the hippocampus in WT and A30P animals. The median of each variable  $\pm$  IQR is shown for WT (N = 7) and A30P (N = 6) mice.

Variable	WT	A30P
Length (ms)	$194.8 \pm 74.37$	$160.64 \pm 32.47$
Length variability ( $\mu$ s)	$90.7 \pm 28.3$	$88.02 \pm 14.5$
Amplitude ( $\mu$ V)	$34.63 \pm 16.13$	$28.34 \pm 12.45$
Amplitude variability ( $\mu$ V)	$11.51 \pm 7.79$	$9.77 \pm 11.06$
Ripple no. / recording duration (s)	$0.16 \pm 0.06$	$0.13 \pm 0.05$
Ripple no. / cycle no.(x1000)	$1.13 \pm 0.91$	$1.24 \pm 5.48$
Latency in the SO cycle (%)	$59.58 \pm 8.3$	$61.84 \pm 6.45$
Peak in the SO cycle	$24.6 \pm 15.27$	$24.04 \pm 4.79$
Instantaneous frequency (Hz)	$87.48 \pm 6.46$	$83.43 \pm 1.73$
Instantaneous frequency variability (Hz)	$18.26 \pm 4.79$	$17.12 \pm 3.69$

## 4.4. Discussion

### 4.4.1. *Summary of the main findings*

The key findings of our analysis of the SO in A30P compared to WT animals are presented below:

- In the mPFC and CA1 region of the hippocampus, A30P mice had an increased SO frequency due to a decrease in Down- and Up-state length and a decrease in state-length variability over time.
- A30P animals had an increased latency to the peak power in the beta and gamma bands on the Up-state in the mPFC region, and in the gamma band in the hippocampus. No other changes were found in relation to the high frequency oscillatory power in the SO cycle.
- In the mPFC region, A30P animal had aberrant neuronal firing, indicated by a greater percentage of the total neuronal firing occurring on the Down-state and a lower coherence between unit firing and the SO.
- A30P animals had fewer spindles per Up-state, a shorter spindle duration, lower spindle amplitude variability over time and fewer high-amplitude spindles.
- No differences we found in SWR characteristics and in SO coherence between the CA1 and mPFC regions, between A30P and WT's mice.

### 4.4.2. *A30P mice have aberrant neuronal firing in the mPFC*

Two of the most interesting findings of this study are the increase in percentage firing occurring on the Down-state and the decrease in SO/unit firing coherence, in A30P animals compared to WT animals. These findings indicate aberrant neuronal firing as a consequence of early  $\alpha$ -syn pathology, which might reflect an early cortical network hyperexcitability. We did not find any differences in unit frequency on the Up-state (spike no / total time on Up-state), suggesting that the unit firing is untimely, but not excessive. Moreover, although we have not analysed unit data from the hippocampus, we have previously shown in our lab that CA3 slices from young A30P animals have a more depolarised resting membrane potential and show epileptiform activity *in vitro* (Tweedy et al., 2018). The CA1 region of the hippocampus receives projections from the CA3 through the Schaffer collaterals and thus, is allso likely to be hyperexcitable in A30P mice.

Our findings of aberrant neuronal activity in A30P mice are consistent with an increasing number of studies in support of hyperexcitability in relation to dementia and DLB, in humans and animals models (Vossel et al., 2017; Jin et al., 2018; Morris et al., 2015; Beagle et al., 2017). Hyperexcitability was shown molecularly through the use of molecular markers in pyramidal neurons (Palop et al., 2011; Palop & Mucke, 2009; Drexel et al., 2012), and electrophysiologically *in vitro* and *in vivo*, in animal models of A $\beta$  and Tau aggregation (Palop et al., 2007; Noebels, 2011; Busche et al., 2012; Vucic et al., 2008). In relation to DLB, one study has provided molecular evidence of network hyperexcitability in the hippocampus of both DLB patients and a mouse model overexpressing  $\alpha$ -syn (Morris et al., 2015). Moreover, DLB patients had a high-prevalence of myoclonus while the  $\alpha$ -syn mice had clear epileptic/epileptiform activity in the parietal cortex, over the hippocampus (Morris et al., 2015). Although the mechanism by which pathological  $\alpha$ -syn can induce hyperexcitability is currently unknown, in the next paragraphs I will examine how our findings in A30P animals may be related to neuronal hyperexcitability and other  $\alpha$ -syn related mechanisms.

#### **4.4.3. *The SO frequency is faster and the Up- and Down-states are shorter in A30P animals***

Another main finding of this study was an increase in the SO frequency recorded under urethane anaesthesia, in both the mPFC and CA1 of A30P animals. The consequent decrease in the SO cycle period was mostly attributed to a decrease in Down-state length and to a lesser extent, a decrease in Up-state length. We also saw a decrease in Down-state length variability over time that may have contributed to the decreased SO frequency through the loss of longer Down-states. Considering that the SO cycle relies on a balance between the mechanisms that initiate, maintain and terminate the Up-state and Down-states (Introduction section 1.4.2; Neske, 2015), we believe that this balance has been altered in young A30P animals. In fact, previous studies have shown a relationship between an increase in SO frequency and hyperexcitability (Busche et al., 2015). In a mouse model of A $\beta$ , a net decrease in Down-state duration was observed that was accompanied by disturbances in long-range synchrony. Both defects were reversed after enhancing GABA<sub>A</sub>R function (Busche et al., 2015). In another study, the optogenetically-induced increase in SO frequency induced hyperexcitability in the hippocampus of an A $\beta$  model of AD (Kastanenka et al., 2019). Thus, it is highly possible that the network hyperexcitability can influence the SO in A30P animals, and vice versa.

Although the hippocampus has a local SO generator (Lockmann et al., 2016; Wolansky et al., 2006; Sharma et al., 2010), the SO in the CA1 is heavily influenced by the cortex (Vertes et al., 2007; Beckstead, 1979; Sesack et al., 1989). Hence, it is possible that the changes in the SO in the CA1 region of the hippocampus can be attributed to changes in the cortical SO. Our analysis has shown that the two regions oscillate coherently in the SO frequency range as previously reported (Sirota et al., 2003), in both A30P and WT animals, suggesting that even if there is a local dysfunction in the hippocampus, the influence of the cortex over the CA1 persists.

#### **4.4.4. *Altered network dynamics and hyperexcitability underlie SO disturbances in A30P animals***

One of our main findings is a decrease in Down-state length and less Down-state length variability over time in A30P animals, in both the mPFC and CA1. The main mechanism that controls the Down-state are K<sup>+</sup> conductances, which are activated as a result of the intense pyramidal firing during the Up-state. K<sup>+</sup> conductance activation results in a decrease in synaptic currents and to widespread disfacilitation in the network (Timofeev et al., 2001) that prevents intrinsically firing layer 5 pyramidal cells from inducing another Up-state until the resting membrane potential has been restored (Sanchez-Vives et al., 2010). Our findings of decreased Down-state lengths and of increased neuronal firing on the Down-state could, therefore, relate to a failure of long-lasting disfacilitation.

This hyperpolarisation/disfacilitation mechanism can be the result of disturbed membrane dynamics relevant to K<sup>+</sup> and/or Ca<sup>2+</sup> channel dysfunction or altered neurotransmitter receptor function (see Discussion section 7.2.3.1). In fact, previous work in our lab has demonstrated that CA3 pyramidal cells from young A30P animals have a more depolarized resting membrane potential than WT animals (Tweedy et al., 2018), while altered membrane dynamics have been extensively reported in mouse models of dementia (Hall et al., 2015; Moulard et al., 2001; Hazra et al., 2013). Hence, if the pyramidal cells in A30P animals are capable of recovering faster from the refractory period, they would also more easily transition to an Up-state. Thus, Up-states would emerge more frequently and the Down-states would be shorter, as seen in the A30P mice in our study. At the same time, some neurons could also fire on the normally “silent” Down-state state, resulting in the greater firing on the Down-state, again as we have observed in A30P mice.

The Up-state is highly dependent on NMDAR-mediated glutamatergic activity (see below section 4.4.5) and GABAergic inhibition (Haider et al., 2006). GABAergic PV+ basket cells contact the pyramidal cell soma while pyramidal axons contact PV+ interneurons, giving rise to a feedback loop where excitation is followed by equal amounts of inhibition. This balanced system maintains the pyramidal neurons close to firing threshold, thus, if the excitation/inhibition (E/I) balance is disturbed, the duration of the Up-state will be altered too (Haider et al., 2006). In fact, reduced GABA<sub>A</sub>R function can shorten Up-state duration in the ferret neocortex *in vitro* (Sanchez-Vives & McCormick, 2000). Recent data showed a decrease in PV+ interneuron numbers in young A30P mice (Tweedy et al., 2020, unpublished). Such a loss in inhibition on pyramidal neurons would result in an uncontrolled increase in the membrane potential of these neurons and consequently in the activation K<sup>+</sup> conductances, the hyperpolarisation of the pyramidal neurons and the premature termination of the Up-state, as seen in our experiments.

Inhibitory activity is also actively involved in the termination of the Up-state (Funk et al., 2017; Zucca et al., 2017). SOM+ interneurons are particularly important, as GABA depletion in SOM+ interneurons induced an increase in Up-state duration in naturally sleeping mice (Kuki et al., 2015). This effect relied on a small population of SOM+ GABA<sub>A</sub> neurons in cortical layer 1, which can inhibit pyramidal cells by synaptic spill-over to pre-synaptic GABA<sub>B</sub>Rs, and distal dendrites of pyramidal cells through GABA<sub>A</sub>Rs and possibly GABA<sub>B</sub>Rs (Silberberg & Markram, 2007). In fact, the application of GABA<sub>B</sub>Rs antagonists in the rat EC *in vitro* was also shown to increase the Up-state duration (Mann et al., 2009). However, we must keep in mind that although SOM+ mediated inhibition can facilitate the synchronous termination of the Up-state, it is not capable of solely driving the Up-state termination (Mann et al., 2009).

GABA<sub>B</sub>Rs can also be found on the presynaptic terminals of GABAergic interneurons in the mouse hippocampus, including PV+ and SOM+ interneurons (Liu et al., 2019). Presynaptic GABA<sub>B</sub>Rs are less efficient in influencing GABA release in PV+ interneurons compared to other subtypes, such as SOM+ interneurons (Sloviter et al., 1999). Thus,  $\alpha$ -syn related changes in the release of GABA or its binding to GABA<sub>B</sub>Rs could affect the release of GABA in the hippocampus in an interneuron-specific manner. If SOM+ interneurons are involved in the generation of the hippocampal SO, we would expect that an alteration in the release of GABA or the

efficiency of GABA<sub>B</sub>Rs could also affect the local SO, but we cannot know the extent and nature of the effect.

In conclusion, both a decrease in GABA<sub>A</sub> PV+ interneuron-mediated inhibition, and an increase in GABA<sub>B</sub> and/or SOM+ interneuron-mediated inhibition, could result in a decrease in Up-state length, as seen in our A30P mice. Although we have some evidence that young A30P mice have a decrease in PV+ interneuron numbers (unpublished data), we currently have no indications about changes in SOM+ neurons or in the function or composition of GABA<sub>B</sub>Rs. We also postulate that SOM+ interneurons could also be hyperexcitable, exerting their inhibitory effect under lower depolarization levels as seen in other neurodegenerative disorders (Zhang et al., 2016). As SOM+ interneurons are activated by pyramidal cells, if both these cell types are hyperexcitable, the effect of SOM+ interneurons over GABA<sub>B</sub>Rs on pyramidal neurons would be greater, terminating the Up-state earlier (Niethard et al., 2018). In another scenario, the function of GABA<sub>B</sub>Rs could be altered, resulting in earlier hyperpolarization of the pyramidal neurons (Gerrard et al., 2018). These ideas would be interesting to explore in the future.

#### **4.4.5. Compensation mechanisms may control $\alpha$ -syn-related network hyperexcitability**

Although we have evidence of altered network dynamics in A30P mice that shift the E/I balance towards a more excitable state, we do not see increased neuronal firing or high frequency power, or a decrease in SO synchrony between the mPFC and hippocampus. This discrepancy might indicate the occurrence of a compensation mechanism in the young A30P animals used in this study (Palop et al., 2011). *In vitro* and *in vivo* electrophysiological studies have shown evidence of compensatory mechanisms taking place in relation to hyperexcitability in rodent models of epilepsy and AD (Palop et al., 2007; Busche et al., 2012; Noebels, 2011).

In animal models of AD, the hyperexcitability observed in the hippocampus of these animals was associated with impairment in NMDARs, such as changes in the phosphorylation of the subunit NR2B, or loss of pyramidal spines (Palop et al., 2007). The Up-state is highly dependent on NMDAR-mediated glutamatergic activity, as NMDAR antagonists reduce Up-state duration and can even abolish them (Major et al., 2013; Rebollo et al., 2018; Sanchez-Vives & McCormick, 2000; Steriade et al.,

1993b). Our findings of  $\alpha$ -syn-related network hyperexcitability imply a more excited, rather than inhibited network, but it is still possible that this hyperexcitability could co-exist with a compensation mechanism that downregulates NMDAR function. Such compensatory mechanisms that limit excitation would also explain our findings of aberrant but not increased neuronal firing in relation to the SO cycle, and could contribute to the decrease in Up-state length observed in A30P animals.

Another potential compensatory mechanism in response to hyperexcitability is an increase in inhibitory activity. In fact, *in vitro* research in our lab has shown greater PV+ interneuron-mediated IPSP frequency and amplitude recorded in the pyramidal cells in the CA3 of the hippocampus in young A30P animals (Tweedy et al., 2018). A scenario of a compensatory mechanism driven by increased PV+ interneuron function is supported by findings that these neurons express mutant  $\alpha$ -syn in the A53T model of DLB (Martin et al., 2014). However, a possible PV+ interneuron-mediated compensation mechanism does not imply a net increase in excitation in the SO generating network. In fact, such a net increase in GABA<sub>A</sub>R-mediated inhibition would result in longer Up-states as seen in a mouse model with PV-interneuron dysfunction (Kuki et al., 2015), and possibly a decrease in Down-state number as seen in a mouse model of AD (Busche et al., 2015). Thus, PV+ interneuron upregulation might be in place to control the hyperexcitability and the E/I balance.

The hyperexcitability/compensation hypothesis proposed here corresponds to an early stage of  $\alpha$ -syn pathology in A30P animals, as the mice are young (2.5 - 4 months) and have minimal evidence of insoluble  $\alpha$ -syn inclusion formation at this stage (Kahle et al., 2001; Freichel et al., 2007). It is possible that with age and increased pathology the compensatory mechanisms will fail, which would lead to a different SO profile in older A30P mice. We have actually shown in our lab that the early hippocampal network hyperexcitability observed in young A30P mice *in vitro*, is reduced by 10 months of age (Tweedy et al., 2018). Moreover, most studies in aged animal models of dementia during natural sleep have reported a lower SO frequency compared to the age matched control mice (Castano-Prat et al., 2019; Menkes-Caspi et al., 2015). These studies have also reported reduced high frequency oscillatory activity and unit firing on the Up-state, and lower intra-cortical and interregional synchrony. Hence, it is possible that A30P animals could age to show a similar slowing of the SO

concomitantly to cell damage and ageing, but this hypothesis needs to be verified experimentally.

#### **4.4.6. Possible cholinergic/thalamic implications in the altered SO in A30P animals**

Another candidate mechanism for the SO alterations observed in A30P mice are changes in the cholinergic inputs to the cortex, which can originate from the basal forebrain cholinergic system. Another source of cholinergic modulation is the brainstem cholinergic system (PPT/LDT) projection to the thalamus that in turn contacts numerous cortical regions (McCormick, 1989; Wester & Contreras, 2013), including the mPFC (Riga et al., 2014) and the nucleus reuniens that directly contacts the CA1 region of the hippocampus in rodents (Bertram & Zhang, 1999; Brown et al., 2012). Moreover, the thalamic drive is important (but not necessary) for initiating the SO in these animals, as it acts to synchronise the SO across the cortex and hippocampus (Wang & Ikemoto, 2016). Therefore, a change in the cholinergic drive could directly influence cortical activity directly or indirectly through influencing the thalamus (Lemieux et al., 2014). For example, the addition of a cholinergic drive (mACh) in *in vitro* mouse thalamocortical slices initiates the SO, while in incremental doses it increases the Up-state duration and frequency of spontaneous SOs (Lőrincz et al., 2015). In the same preparation, cholinergic signalling blockade during SWA reduces Up- and Down-state duration (Lőrincz et al., 2015), similarly to what we see in our study. Hence, it is possible that a loss of cholinergic drive would also alter the thalamic influence over the SO in A30P animals.

A30P animals have indications of early  $\alpha$ -syn pathology in the PFC and hippocampus at 4 months that increase with age (Schell et al., 2009). However, there is little evidence for  $\alpha$ -syn pathology in thalamic or cholinergic nuclei (Kahle et al., 2001; Freichel et al., 2007). However, it is possible that the cholinergic changes in young A30P mice are subtle and have not been detected using the current immunohistochemical approaches. The aforementioned studies have focused on insoluble polymers of  $\alpha$ -syn and not in soluble monomers and oligomers that can also influence neuronal function (Killinger et al., 2019). Hence, we cannot derive definitive conclusions without the appropriate immunohistochemical analysis for insoluble

forms of  $\alpha$ -syn. Such an analysis would be particularly interesting as DLB patients exhibit excessive thalamic pathology, including the reticulo-thalamo-cortical (dorsal) activating system in which the PPT/LDT belong (O'Dowd et al., 2019; Schmeichel et al., 2008).

The function of the cholinergic system in relation to sleep is to monitor and pace the locally generated SO throughout the cortex. While a strong cholinergic tone has been shown to increase the signal-to-noise ratio of the ACh input to the cortex in *in vivo* rat slices, a low cholinergic tone favours the faster, locally generated SO (Wester & Contreras, 2013). In a human, overnight EEG study, the cholinergic system-modulated SO has been characterised as a "Type I" SO, which is more prominent during sleep induction, and is synchronous across the cortex and of large amplitude (Bernardi et al., 2018). At deeper levels of sleep, smaller Type II SOs appear that have different cortical origins, and are less synchronous with one another (Bernardi et al., 2018). These two types of SO persist during SWS and interact with each other, with type I synchronising Type II oscillations. Upon dysfunction of the thalamic input to the cortex, the local Type II SO could take over, resulting in a faster and less controlled SO, as seen in A30P animals (Bernardi et al., 2018). However, although we observed an increase in SO frequency we did not see a decrease in SO amplitude or high frequency power on the Up-state.

This discrepancy can be attributed to the capacity of the cortex to compensate for the loss of cholinergic input. Although the acute loss of the cholinergic input to the cat cortex was shown to have a detrimental impact to the SO in terms of high frequency activity, SO amplitude and SO frequency (Steriade et al., 1996), local circuits recover quickly through up-regulating intra-cortical synapses (Lemieux *et al.*, 2014). Thus, under the assumption of altered thalamocortical connectivity in A30P mice, a type II SO prevalence could explain our findings of a faster, less flexible SO rhythm. At the same time, the amplitude of the SO and the power of fast-frequency oscillations are not affected. The oscillation amplitude is proportional to the number of cells firing simultaneously as shown (Reichinnek et al., 2010), and to the the number of active synapses (Tononi & Cirelli, 2006), as shown in cat and rodent models respectively. Hence, a compensatory upregulation of synapses may account for our findings of a normal SO amplitude and high frequency oscillatory power.

#### **4.4.7. Changes in high frequency oscillations on the Up-state in A30P mice**

The only significant finding in A30P mice in terms of the fast oscillations associated with the Up-state was an increase in latency to peak power in the beta and gamma frequency bands, in the mPFC (IL, PrL). There was also an increase in latency to peak power in the gamma frequency range, in the CA1 region of the hippocampus. We did not find any changes in terms of average high frequency power on the Up- and Down-states or peak power in any frequency band, in any mPFC subregion. These findings suggest that the amount of power on the Up-state is similar in A30P and WT animals, but the distribution of power on the Up-state is altered in A30P animals. This conclusion is consistent with the fact that we did not see any increase in firing rate on the Up-state either.

The fact that the latency to peak power was altered in the beta frequency range in the mPFC, and in the gamma frequency range in the CA1, are clearly related to the rhythms these regions inherently generate (Colgin, 2011; Buzsáki & Silva, 2012). Beta band power is particularly high on the Up-state in the ACC compared to other cortical regions, including the somatosensory and motor cortices (Ruiz-Mejias et al., 2011), while gamma oscillations are well documented on the Up-state in both the mPFC and the CA1 region of the hippocampus (Sullivan et al., 2011; Colgin, 2011). Although we did see a greater percentage firing occurring on the Down-state, such small changes in firing rate might not translate to significant changes in oscillatory power. Indeed, we did not see any significant changes in power in any frequency band on the Down- state.

Luczak and Barthó (2012) described two types of Up-states in rats under ketamine/xylazine anaesthesia. The first called simultaneous onset (so-) Up-states were short in duration, and characterised by strong interneuron firing that was phase-locked to the spindle activity at the start of the state (Luczak & Barthó, 2012). Interneurons fired at the start of so-Up-states while pyramidal cells had a more variable timing profile between and within Up-states. On the other hand, traveling wave- (tw-) Up-states were of longer duration and were generated locally in the cortex and progressively spread across the cortical regions (Figure 4.7A,C). Tw-Up-states were characterised by a brief, variable increase in interneuron activity after tw-Up-state onset and a stronger, long-lasting activity of pyramidal cells (Figure 4.7B,D; Luczak and Barthó, (2012). A close inspection of the so-SO shape (Figure 4.7A,C) reveals that it resembles the beta power distribution on the Up-state observed in the mPFC of A30P

animals (Figure 4.2A). In both figures we can see that the power distribution occurs in a bimodal way, a finding that was not described statistically in our study as we only investigated for location of the greatest peak power in the normalised SO cycle.

The close resemblance between the high frequency power distribution on the Up-state in A30P animals in our study, and the so-Up-states, may indicate that more so-Up-states occur in these animals than in WTs. Moreover, this theory is compatible with our findings of a decrease in Up-state duration in A30P animals, as so-Up-states are shorter. However, under the assumption of an increase in so-Up-states we would also expect an increase in the number of spindles, as they are coherent with the so-Up-state start (Luczak & Barthó, 2012). As will be discussed in the next paragraphs though, we observed a decrease in spindle density/Up-state number instead. Thus, it is unlikely that A30P mice have more so-Up-states, although this discrepancy could be associated with a spindle deficit (see the next section).

Another possibility that we consider more likely is that changes in E/I balance in the local cortical networks of A30P mice result in altered neuronal dynamics that resemble the so-Up-state in terms of high frequency oscillatory power distribution on the Up-state. We have proposed that A30P animals have neuronal network hyperexcitability, and possibly an interneuron-mediated compensation mechanism, supported by *in vitro* findings of greater IPSPs in the CA3 of these animals (Tweedy et al., 2018). This mechanism implies synchronous interneuron activity and less synchronous pyramidal activity, similar to so-Up-states (Luczak & Barthó, 2012). Thus, the high frequency oscillations on the Up-state may be initiated with relatively high synchronicity due to the over-compensating activity of interneurons, but the engagement of pyramidal neurons during the Up-state is more variable due to their hyperexcitability.

The cortex can also drive the Up-state initiation in the hippocampus and in turn, induce higher-frequency oscillation synchrony between the two regions that is necessary for memory consolidation (Vertes et al., 2007; Beckstead, 1979; Sesack et al., 1989). Thus, if the neuronal engagement to the SO is altered in the cortex, the timing of neuronal firing would also be affected in the hippocampus. Consequently, we would expect a similar increase in latency in local fast-frequency rhythms, as seen in the gamma frequency range in A30P mice. Alternatively, the increased gamma peak latency in the CA1 observed in A30P mice could reflect a local dysfunction, as high

frequency oscillations are also generated by a pyramidal neuron/PV+ interneuron interplay in this region (Colgin, 2011).

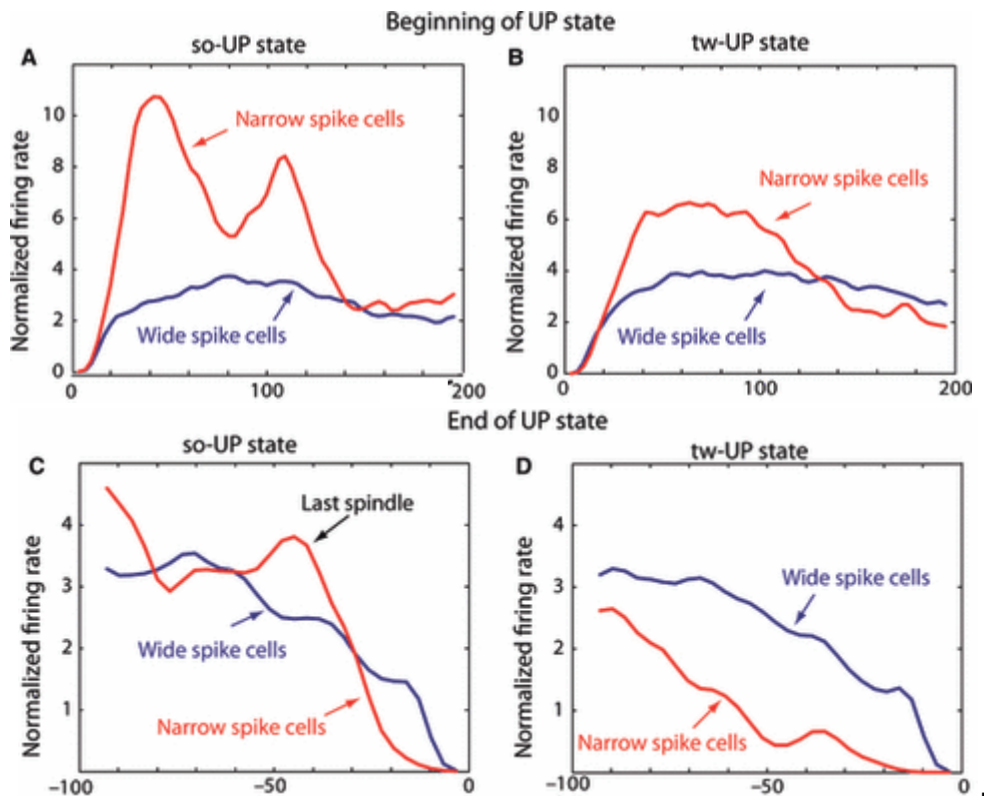


**Figure 4.7:** Normalised firing rate of narrow-spike cells (red; putative interneurons) and wide-spike cells (blue; putative pyramidal cells) during Up-states. **A)** Normalised activity during the beginning of so-UP-states and **B)** tw-UP-states. So-Up-states show a bimodal distribution of narrow-spike cell activity. **C)** Normalized activity triggered at the end of so-Up-states and **D)** tw-UP-states. At the end, the activity of narrow-spike cells returned to baseline before wide-spike cells, especially in the tw-UP-state case. Adapted by Luczak and Barthó (2012).

#### 4.4.8. *A30P animals have a spindle dysfunction*

One of our most interesting findings was the spindle dysfunction observed in A30P animals, characterised by a lower spindle number per Up-state (relative density), and fewer high-amplitude spindles, accompanied by decreased variability in spindle amplitude. We also found a shorter spindle duration in A30P animals but the instantaneous spindle frequency was not affected, suggesting that spindle cycles had the same frequency but were composed of fewer events. These changes can be traced back to alterations in the dynamics of the spindle-generating network (Destexhe et al., 1998). Sleep spindles are generated in the thalamus but their duration is determined by a feedback loop between excitatory thalamocortical cells and the inhibitory TRN

cells (see Introduction for details; Brown *et al.*, 2012). This system is also influenced by a corticothalamic input (Blumenfeld, 2005).

The decrease in spindle duration we observed in A30P mice can be related to the mechanisms that drive spindle termination. According to a study by Barthó *et al.*, (2014) in rats during sleep and under urethane-induced anaesthesia, inhibitory activity from the TRN gradually declines during the spindle, allowing thalamocortical neurons to respond with a rebound burst that terminates the spindle cycle. Thus, the decrease in TRN activity towards the end of the spindle drives spindle termination. They also suggest that the oscillation is predetermined by the TRN network's state at the beginning of the oscillation (Barthó *et al.*, 2014). The network's state is influenced by local neuromodulators and most importantly by cortical inputs that can desynchronize the network with spindle progression (Timofeev *et al.*, 2001; Bonjean *et al.*, 2011). Therefore, our observation of shorter spindles could be attributed to either altered engagement of TRN neurons in the spindle event, or due to an altered cortical input. Under our proposed model of network hyperexcitability in the cortex, this desynchronization between the thalamus and cortex could occur earlier in the spindle cycle resulting in shorter spindles.

Spindle amplitude correlates with the level of cortical neuronal involvement in the spindle (Andrillon *et al.*, 2011). Other factors including the type of spindle (fast or slow frequency), or the stage of sleep (kept consistent in our study) do not influence spindle amplitude (Cox *et al.*, 2012). Hence, the lack of higher amplitude spindles we observe in A30P mice might reflect a lack of capacity for regional recruitment in the cortex (Martin *et al.*, 2013). Moreover, we also found that the relative spindle density was decreased in A30P mice. Corticothalamic neurons are able to trigger bursts of spikes in the TRN, but if the cortical network is weakened and the corticothalamic input to the TRN is reduced, fewer spindles would be evoked (Barthó *et al.*, 2014). Thus, the cortical networks in A30P animals may be incapable of producing and eliciting strong synchronous activity to the hippocampus. Finally, *in vivo* intracellular recordings from thalamic and cortical neurons in experimental models have shown that the spindle density inversely correlates with the thalamic hyperpolarisation levels (Steriade & Timofeev, 2003; Andrillon *et al.*, 2011). Overall, our findings of spindle dysfunction in the young A30P animals reflect a loss of function in the thalamocortical system.

The TRN has different anatomical subregions with distinct connectivity (review by Vantomme et al., 2019). The prefrontal cortex, including the mPFC, is mostly interconnected with the rostral TRN, while sensory regions including visual, auditory and somatosensory modalities are interconnected with the medial and frontal TRN. All TRN regions receive input from thalamic nuclei. Thus, these various thalamic-TRN-cortical networks can differentially control local SOs and spindle activity in the cortex (Vantomme et al., 2019). For example, manipulation of TRN GABAergic activity in mice by genetic inactivation of the T-type  $\text{Ca}^{2+}$  channels that facilitate TRN spiking, resulted in spindle depletion in the sensory cortex (Lewis et al., 2015). However, spindle activity in the prefrontal cortex was not altered. Moreover, rodent studies of optogenetic activation of hypothalamic GABAergic input to the TRN led to a shift from NREM to wake state in the sensory cortex, while variations in the membrane potential of TRN neurons result in a shift from delta to spindle-rich activity (Herrera et al., 2016). In our study we did see some changes in spindle activity in the mPFC of A30P mice, which if specific to the prefrontal cortex, might indicate disturbances in the thalamic-TRN-prefrontal circuit that involves this region. Alternatively, if the spindle deficit is also seen in sensory regions, we could speculate of more widespread  $\alpha$ -syn related changes in the TRN, or in its thalamic and/or hypothalamic input. Thus, it would be interesting to proceed with recordings from sensory cortices to see how extensive this spindle deficit is in A30P animals.

Interestingly, spindle deficiencies have been observed in patients with LBD and PD as well as AD (Reynolds et al., 1988). A polysomnographic study found that several patients with DLB had no sleep spindles while others had lower-frequency sleep spindles and K-complexes in N2 and SWS (Fernández-Arcos et al., 2019). A similar decrease in spindle density was found in PD patients (Christensen et al., 2014). Furthermore, another study showed that the PD patients who went on to develop dementia had significantly decreased spindle and fast spindle density (13 – 15 Hz) and lower spindle amplitude in posterior cortical areas at an earlier stage (Latreille et al., 2015). These reports from patients resemble our results of a lower spindle density and fewer high-amplitude spindles in A30P mouse model, although we did not distinguish between spindle subtypes.

The above-mentioned electrophysiological spindle changes in LBD patients have been suggested to relate to the early cholinergic dysfunction characterising Lewy

body disease (Latreille et al., 2015). Cholinergic deficiency can also impact the spindle-generating system. The brainstem sends cholinergic projections to the TRN via the pontine cholinergic projection system (Brown et al., 2012). However, PD, PDD and DLB patients show a reduction in thalamic cholinergic innervation from this system, particularly from the PPT/LDT nuclei, which are extremely susceptible to Lewy body pathology (Kotagal et al., 2012). If this cholinergic system is ablated spindle generation is decreased (Brown et al., 2012), while inhibiting acetylcholine breakdown increased spindle density (Ozaki et al., 2012). Furthermore, young A30P animals have insoluble  $\alpha$ -syn aggregates in the pontine reticular formation (Freichel et al., 2007), which is involved in spindle formation through the dorsal ARAS pathway (Brown et al., 2012). Dysfunction of the pontine reticular formation could possibly contribute to the changes in spindles in A30P mice. There is evidence of  $\alpha$ -syn pathology in the cortex, but not in the thalamus, of young A30P animals (Schell et al., 2009), although as discussed earlier we lack studies looking for soluble  $\alpha$ -syn monomers and oligomers, which can also have detrimental effects in synaptic function (Kaufmann et al., 2016).

#### **4.4.9. SWS disturbances can have detrimental effects**

The loss of sleep spindles can have numerous implications for a patient. Firstly, spindles and SWRs in the hippocampus are highly coordinated with each other in the context of the SO, with SWRs clustering in the trough of spindles (Staresina et al., 2015). This synchrony mediates the transfer of information from the hippocampus to the cortex facilitating memory consolidation (Colgin, 2011; Witton et al., 2016). In view of the high degree of synchrony between these events, we had expected SWRs to also be altered in A30 mice. However, we found no significant differences in SWRs between WT and A30P animals. Due to the low number of concomitant CA1/mPFC recordings in both WT and A30P mice we did not look at the spindle/SWR coherence. Thus, a next step would be to carry out more dual recordings to investigate the synchrony between spindles and SWRs occurring in each region respectively, and their synchrony with the SO.

In addition to the importance of sleep spindles in memory consolidation, spindles are also considered pivotal in “protecting” sleep from internal or external perturbations. Thus, a disruption in spindle activity could allow these perturbations to induce awakenings (Terzano & Parrino, 2000). According to the glymphatic hypothesis of dementia, sleep interruptions and the resulting wake cortical activity prevent  $\alpha$ -syn

clearance while promoting excess  $\alpha$ -syn production (section 1.7.3.1; Bohnen & Hu, 2019). Hence, a spindle dysfunction could set off a cycle of increasing levels of  $\alpha$ -syn and SWS interruption (Mander et al., 2016). In addition, a recent study has shown that an increase in SO frequency can initiate a vicious cycle of increased A $\beta$  production and cytotoxicity in a mouse model of AD (Kastanenka et al., 2019). We would not be surprised if a similar cycle underlies abnormal  $\alpha$ -syn production and neurodegeneration in A30P mice.

#### **4.4.10. *The subregional profile of the SO in the mPFC***

Comparing the electrophysiological SO patterns between mPFC subregions in relation to the WT and A30P genotypes was not one of the main aims of our study. However, although the mPFC subregions tend to have a synchronous SO, they are characterised by different levels of high frequency activity on the Up-states (Gretenkord et al., 2017). Thus, we did consider the mPFC subregion in our rmANOVA analysis and reported its effects, but we did not proceed with separate rmANOVA analyses in A30P and WT animals. In terms of wavelet power, the highest peak power and average power on the Up-state were seen in the dorsal (mostly PrL, ACC) compared to the ventral (IL, DP) mPFC. These findings are consistent with a previous study in the rat mPFC, of a dorsal to ventral gradient of power in the mPFC (Gretenkord et al., 2017). The same study also found a shorter latency to peak power in the ventral mPFC but we did not see that in our mice in this study. Regarding SO cycle lengths we found small differences between the ACC and the other subregions, including a slightly longer SO cycle length. This finding was unexpected as the mPFC subregions have a synchronous SO (Gretenkord et al., 2017) and it might relate to a rat versus mouse difference. However, as already discussed this regional comparison was out of the scope of our analysis.

More dorsal areas of the mPFC produced spindles of greater amplitude and relative density and of shorter duration. Previous work has also reported greater spindle power on the Up-state in the ACC and PrL (dorsal) subregions in the rat under urethane anaesthesia, suggesting that our findings are compatible with the existing literature (Gretenkord et al., 2017). Our findings could also relate to the different types of spindles, as there are two types occurring preferentially at the start and end of the Up-state respectively. The spindle subtypes may have a differential pattern of expression across the mPFC subregions (Clemens et al., 2011).

## 4.5. Conclusion

The A30P mouse model shows a number of alterations in SWS patterns such as aberrant neuronal firing in the SO cycle in the mPFC, a higher SO frequency and shorter Up- and Down-states in the mPFC and CA1 of the hippocampus. We also found that A30P animals have an altered distribution of power in the beta and gamma, and in the gamma frequency bands on the Up-state, in the mPFC and CA1 regions respectively. Finally, we found that A30P animals have altered spindle patterns, including a lower spindle density, shorter spindle-duration and fewer high-amplitude spindles. Again, spindle alterations may relate to  $\alpha$ -syn-related changes in the cortical networks or a thalamic or cholinergic dysfunction. A30P mice had no differences in SO synchrony between the cortex and hippocampus, in SWR patterns or in higher frequency power levels in the SO cycle, compared to WT animals. We suggest that our findings can be attributed to mutant  $\alpha$ -syn-induced hyperexcitability in the neuronal networks of young A30P animals. A compensatory mechanism and/or alterations in thalamic networks may also co-exist.

Considering the importance of SWS, high frequency nested rhythms and spindles in higher cognitive function, we would expect these changes in their patterns to lead to cognitive impairments. Moreover, the reduced sleep spindles could allow for more sleep fragmentation, thus promoting more  $\alpha$ -syn pathology via a glymphatic hypothesis-mediated mechanism. However, the fact that these changes appear early in A30P animals and are associated with low levels of  $\alpha$ -syn pathology, highlights that sleep and hyperexcitability could constitute potential targets for early intervention, in order to delay the development of subsequent pathology.

## **Chapter 5. The infra-slow modulation (ISM)**



## 5.1. Introduction

Urethane induced-anaesthesia has been used as a model of NREM and REM sleep by manipulating the levels of anaesthesia (Hara and Harris, 2002). More recent studies have shown the presence of faster-activity states under deep urethane anaesthesia in rodents that resemble the REM state (Clement *et al.*, 2008; Pagliardini, Gosgnach and Dickson, 2013). The aforementioned REM-like states seen under urethane anaesthesia or, as also called “activated states”, manifest abruptly as periods of increased low-voltage fast activity (25 – 40 Hz) in the cortex and greater theta activity in the hippocampus in rodents (Clement *et al.*, 2008; Pagliardini *et al.*, 2013). These states can be detected by a decrease in the SO/theta band power ratio, similarly to REM sleep (Clement *et al.*, 2008). Each activated/deactivated state cycle lasts about 9 minutes in rats (Clement *et al.*, 2018), and 14 minutes in mice, with each activated state lasting about 4 minutes (Pagliardini *et al.*, 2013). During the activated state, the breathing rate and its variability increased in comparison to SWS periods, similarly to what is seen in humans during REM sleep (Pagliardini 2013). Therefore, urethane anaesthesia offers the opportunity to detect and analyse patterns of sleep macrostructure.

Further cyclic alterations on a slower time scale have also been observed, called the infra-slow oscillations (ISO), which occur at a frequency  $< 0.1$  Hz (Hughes *et al.*, 2011). ISOs in humans can be detected through the functional MRI (fMRI), where they appear as fluctuations in the local blood oxygenation level dependent (BOLD) imaging signal, indicating changes in local neuronal activity (Palva & Palva, 2012). Concurrent EEG recordings have shown that the ISOs identified in cortical and sub-cortical regions modulate higher frequency oscillation (Watson *et al.*, 2016; Hughes *et al.*, 2011). The resting human brain exhibits fluctuations  $< 0.1$  Hz in the fMRI BOLD (blood oxygen level dependent) signal in resting state networks (RSNs) that correlate with activity in the alpha range (Hughes *et al.*, 2011). A simultaneous fMRI/EEG analysis in rats has shown that ISOs during rest can modulate activity in the gamma frequency range (Pan *et al.*, 2013), while *in vivo* intracranial recordings have revealed the occurrence of an ISO in the cortex during natural sleep in mice (Lecci *et al.*, 2017). In *in vitro* preparations, induced ISOs in cholinergic nuclei were accompanied by alpha activity (8 – 13Hz) (Hughes *et al.*, 2011) while computational models of cortical activity have also demonstrated that ISOs can modulate the power of 1 – 40 Hz oscillations

(Lundqvist et al., 2013). Hence, these widespread, infra-slow rhythms are able to control faster, local oscillations.

One of the best studied ISOs in humans, in the context of sleep, is the cyclic alternating pattern (CAP) that occurs at 0.002 – 0.02 Hz (Terzano & Parrino, 1993; Parrino et al., 2006). CAP is composed of different electrophysiological events of higher frequency that occur in a cyclic manner in the form of an ISO, and compose the microstructure of sleep. CAP states regulate the balance between awake and sleep-promoting systems, state shifts and the NREM/REM transition in humans (Parrino & Vaudano, 2018). Although CAP has not been reported under urethane-anaesthesia, CAP-like rhythms have been characterised during natural sleep in rodents (Lecci et al., 2017). Hence, it would be particularly interesting if sleep microstructure could also be characterised under urethane anaesthesia.

During our recordings under deep urethane anaesthesia, we noticed the emergence of periods characterised by a burst of power across frequency bands, which manifested as a sharp increase in power on the spectrogram, in both the mPFC and hippocampus. A similar event was previously described in our lab in the urethane anaesthetised rat (Gretenkord et al., 2015). Due to its stereotypic fashion we named this phenomenon the “infra-slow modulation” (ISM) and we proceeded to investigate it further to better understand its nature.

## **5.2. Methods**

### **5.2.1. *Animals and recordings***

To better understand the ISM, we proceeded to analyse 30 minute-long mPFC recordings from WT animals. From a total of 16 WT animals used in our study, 2 did not have ISM. We recorded SWS activity from the mPFC and/or CA1 regions of these animals, and after rejecting some of recordings as described in detail in section 4.2.1 of the previous Chapter, we used 8 mPFC and 7 CA1 recordings for our analysis.

To study ISM data, we analysed the same 30 min long-LFP recordings used for SO analysis, from both the mPFC and CA1 probes. In fact, the non-ISM data used for this analysis is the same data used in Chapter 4. Therefore, the anaesthesia regime, frame mounting and electrode techniques are the same. It is important to highlight that during these recording the animals were under deep anaesthesia characterised by SWS (< 1Hz) and the absence of a pedal withdrawal reflex. We also utilised the same unit data for the mPFC as in section 4.3.3.

### **5.2.2. *ISM identification technique***

The notch-filtered LFP recordings were visually inspected for epochs of incomplete ISM events at the start or end of the recording, which were then were rejected. The power spectral (PSD) density was estimated using 2 s-long FFT and Bartlett's method (Bartlett, 1950) and a Hamming window with double the size (4 s), giving a 0.25 Hz frequency resolution (discrete fast Fourier transform). We then used the PSD/power to calculate power within different frequency bands: SO (0.25 – 0.75 Hz); delta (1.5 – 3.75 Hz), theta (4 - 7.75 Hz), alpha/spindle (8 – 14.75 Hz), beta (15 – 29.75 Hz) and gamma (30 - 79.75 Hz), for each electrode. The power for each band was averaged across each of the electrodes for each of the 4 subregions of the mPFC (Figure 5.1).

The power in the beta frequency band was used to detect the ISM events, as the start of the ISM was visually most clear in the beta band-filtered EEG signal (Figure 5.1). The power in the beta band was first smoothed using the “smooth” function in Matlab (level 6) and then the minimum point of the smoothed beta power was deducted to normalise it to the baseline (Figure 5.2A). An ISM-like template was automatically created for each recording using a fixed maximum point of 3 for the mPFC and 4 for

the CA1 of the hippocampus, the mean amplitude of the smoothed beta power and a minimum of 0. This template had a duration of 60 s that is approximately the duration of each ISM event, while different fixed maxima were chosen for the CA1 and mPFC regions to optimise detection. The template was used in a sliding window manner to identify the ISM, where each window had the size of the template (60 s), while the beginning of each window was 2 s away (1 epoch) from the beginning of the previous window and thus, the windows were overlapping. For each x-value of each window, we calculated the absolute difference between the y-value at the template and the smoothed beta power signal. These values were then summed up for each window, giving the total deviation of the beta power signal from the template. We then transformed the value for each window (total deviation from the template) into a percentage of the greatest deviation, thus creating a “disimilarity index” between the beta power signal and the template. All disimilarity values were subtracted from a 100, to get a “similarity index” instead. By setting a threshold of > 25% we could identify the windows that were so similar to the template they could be considered an ISM event. Consecutive windows that exceeded the threshold or were disrupted for up to 4 s (2 epochs) were considered the same ISM event.

For each of the identified ISM events we found the maximum point and proceeded to refine the ISM identification (Figure 5.2B). We found the first crossing point of the average line before and after the ISM peak, and if there was not another crossing within 2 epochs before the start of ISM or 2 epochs after the ISM, that crossing was identified as the edge of the ISM. If there was another crossing within 2 epochs, the previous/next epoch was examined and so on. After detection of the ISM, we identified the 30 s (15 epochs), before and after the ISM as pre-ISM, and post-ISM segments, respectively, as these periods appeared to be distinct both from the ISM and non-ISM periods.

## Medial prefrontal cortex (mPFC)

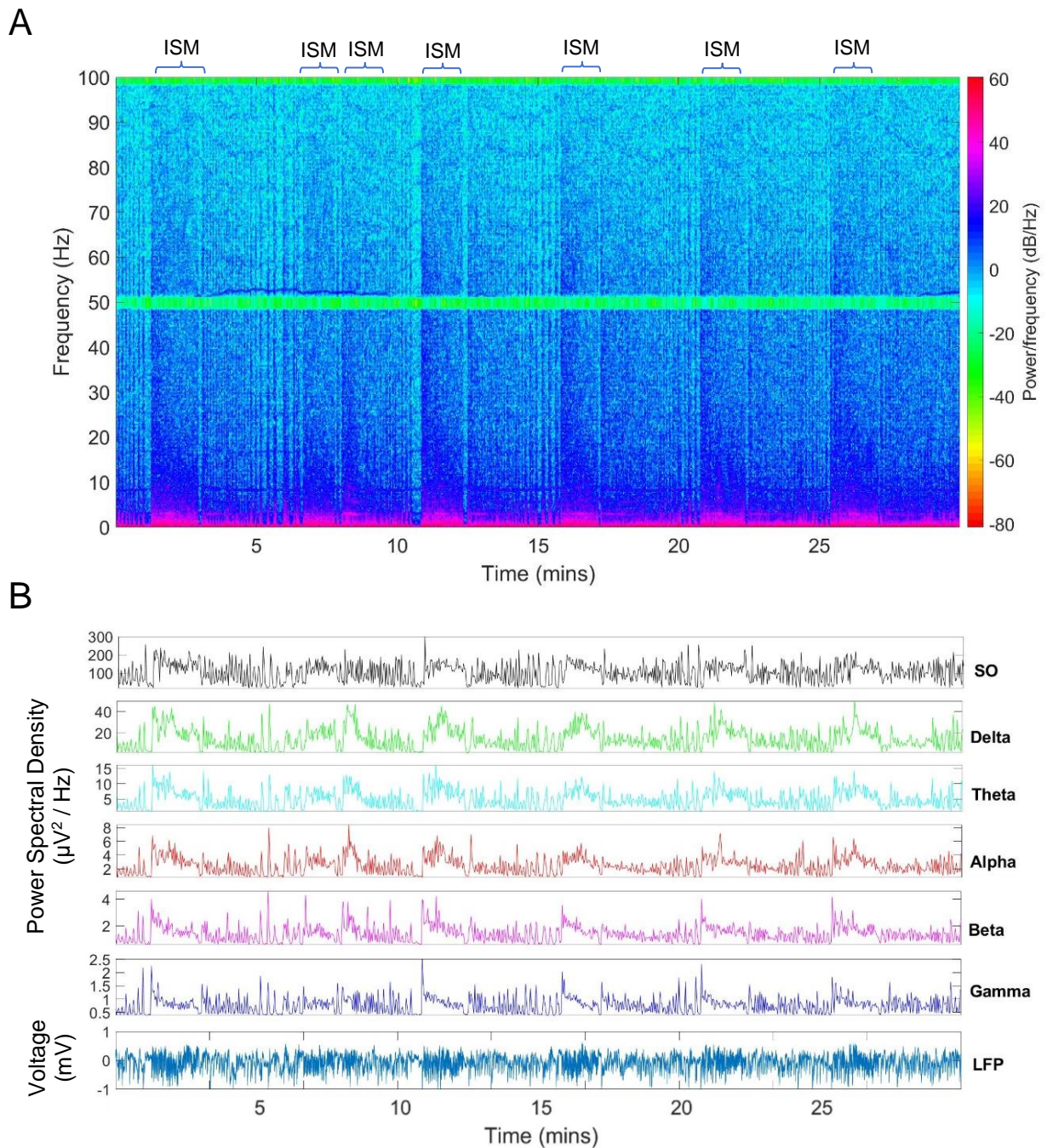


**Figure 5.1:** The PSD across frequency bands during the slow-wave sleep in WT mice. **A)** 30 min-long recording from the mPFC, showing the occurrences of the ISM as seen in the spectrogram (PrL; electrode 12) and **B)** in the power spectral density (PSD) of the LFP signal. The average PSD is shown across all 16 channels of the mPFC, for each of 6 power bands: SO (0.25 – 0.75 Hz); delta (1.5 – 3.75 Hz), theta (4 – 7.75 Hz), alpha/spindle (8 – 14.75 Hz), beta (15 – 29.75 Hz) and gamma (30 – 79.75 Hz). The lower trace shows the LFP signal.

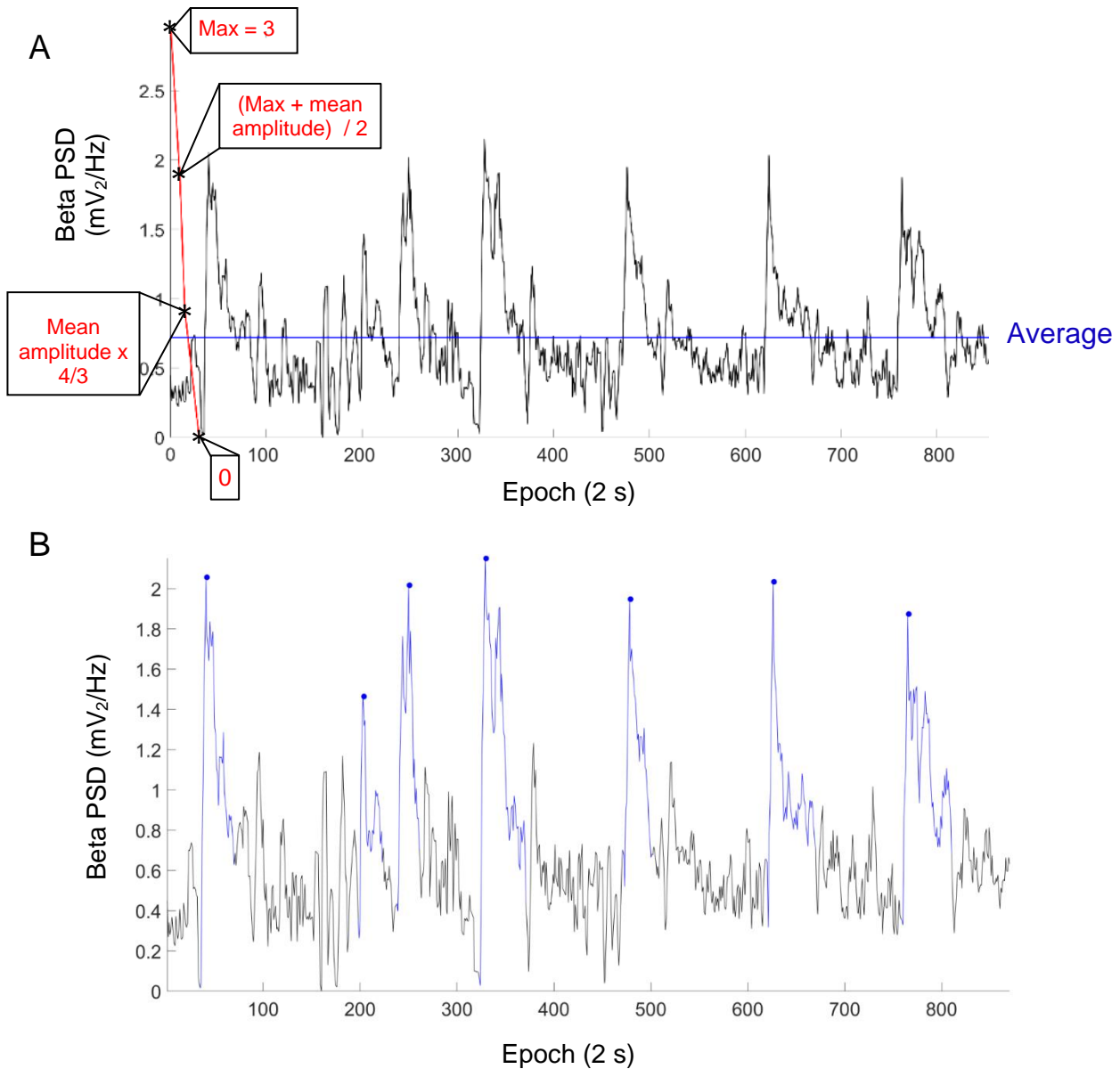


**Figure 5.2:** The ISM identification technique. **A)** Basic ISM identification. The power in the beta frequency band averaged across mPFC sub-regions, after being smoothed and normalised to the baseline, which was used to identify the ISM. The 60 s-long running template (red line) and its constituent parts are also shown (asterisks), including the average amplitude of the normalised beta power. This smoothed, normalised to the baseline, beta frequency power evolved over 2 s-long epochs. **B)** Refinement of the ISM periods (blue segments) and the ISM peak (blue dots) that was used to determine the beginning and end of the ISM.

### **5.2.3. ISM variable extraction**

All ISM data was extracted into MATLAB and plotted on Excel. To characterise the ISM we extracted the mean interval length between ISM events and used it to calculate the ISM frequency. We also calculated the ISM duration and its variability between ISM events within the same recording. To analyse the ISM in depth we extracted a number of variables for each of four segments: A) non-ISM: the concatenated non-ISM data used in Chapter 4, B) the 30 s-long pre-ISM segment, 3) ISM and 4) the 30 s-long post-ISM segment. The pre-ISM, ISM and post-ISM segments were treated as part of the same ISM event. All the variables were extracted for the four subregions of the mPFC (ACC, PrL, IL, DP) and for the CA1 region, except the unit and spindle data which were only extracted for the mPFC. Our findings are expressed as the mean  $\pm$  SEM.

#### **5.2.3.1. PSD power**

In order to calculate the SO / theta band power ratio, we extracted the PSD for these two frequency bands for the non-ISM, pre-ISM, ISM and post-ISM segments. The PSD shows the absolute power in each frequency range. We used a 4 s-long FFT (fast Fourier transform) size and an 8 sec Hamming window, resulting in a sampling frequency of 0.125 Hz that is close to the minimum Up-Down cycle length of interest (0.1 Hz). The frequency ranges of interest were 0.125 – 0.875 Hz for the SO frequency range and 4 – 7.875 Hz for the theta frequency range.

#### **5.2.3.2. Up-Down cycle length and power content**

To characterise the Up-Down cycle we extracted the same Up-Down cycle characteristics investigated in the non-ISM analysis and looked for differences between the non-ISM, pre-ISM, ISM and post-ISM segments. The variables investigated were the mean Up-state, Down-state and SO cycle (Down-state +Up-state) length and their mean length variability over time (SD), the SO frequency and the amplitude of the SO. The distribution of power in the SO cycle was also analysed as described in Methods (section 2.2.5.5). For this analysis, we only used the frequency bands that are known to have functional activity on the Up-state: beta (15 – 29.9 Hz), gamma (30 – 79.9 Hz) and high-gamma (80 – 129.9 Hz), as well as the theta band that is involved in the activated/REM sleep (4 - 7.9 Hz).

#### 5.2.3.3. Unit analysis

To analyse unit data we performed two types of unit analysis. Firstly, we investigated 6 unit-related variables which were averaged for each animal: the number of spikes and the ISI for the duration of the recording and for the Up-state only, the percentage of units firing on the Up-state and the coherence between the SO and unit firing. However, we were concerned that this method that involves averaging across units for each animal and then for each segment, could mask changes in our variables between segments. To address this issue and better understand how unit activity evolves during the ISM, we proceeded with a second analysis where we treated all units as individual samples, without averaging across animals.

Moreover, upon inspection of the raster plots we noticed that units changed their firing in different ways in relation to the ISM. To investigate the individual neurons behaviour, we calculated the percentage change in firing on the ISM compared to the non-ISM segment, for each unit. Units were then grouped into those that increased their firing rate ( $> 115\%$ ), did not change their firing rate ( $85\% - 115\%$ ) or decreased their firing rate ( $< 85\%$ ) on the Up-state. However, we did not perform statistical analysis for these variables.

#### 5.2.3.4. Spindle density

Spindles were identified as described in Methods section 2.2.6 and their density was calculated by dividing the number of spindles by the number of Up-states/cycles for that segment. This variable was only calculated for the mPFC.

#### 5.2.3.5. Statistical analysis

To characterise the frequency and duration of the ISM in the WT animals in the mPFC, we performed one-way rmANOVA analysis. To analyse variables associated with the amplitude, frequency and Up-state, Down-state and SO cycle lengths, as well as variables related to oscillatory power in the normalised SO cycle, we performed two-way rmANOVA analysis with 2 repeated measures, the ISM segment (non-ISM, pre-ISM, ISM, post-ISM) and subregion (ACC, PrL, IL, DP). We only proceeded with further, one-way rmANOVA analyses for each subregion if a significant interaction was found between band and region. If not, only the data from the PrL region is presented and plotted. The PrL region was chosen, as together with the ACC these regions are of the greatest functional importance in relation to cognition (Euston et al., 2012). A similar analysis was also performed for characterisation of the SO cycle, the spindle

density and the SO/theta band power ratio in the mPFC. For unit related variables from the mPFC and all our variables from the hippocampus where we had no sub-regions, we performed one-way rmANOVA with segment as the between subjects variable.

## 5.3. Results

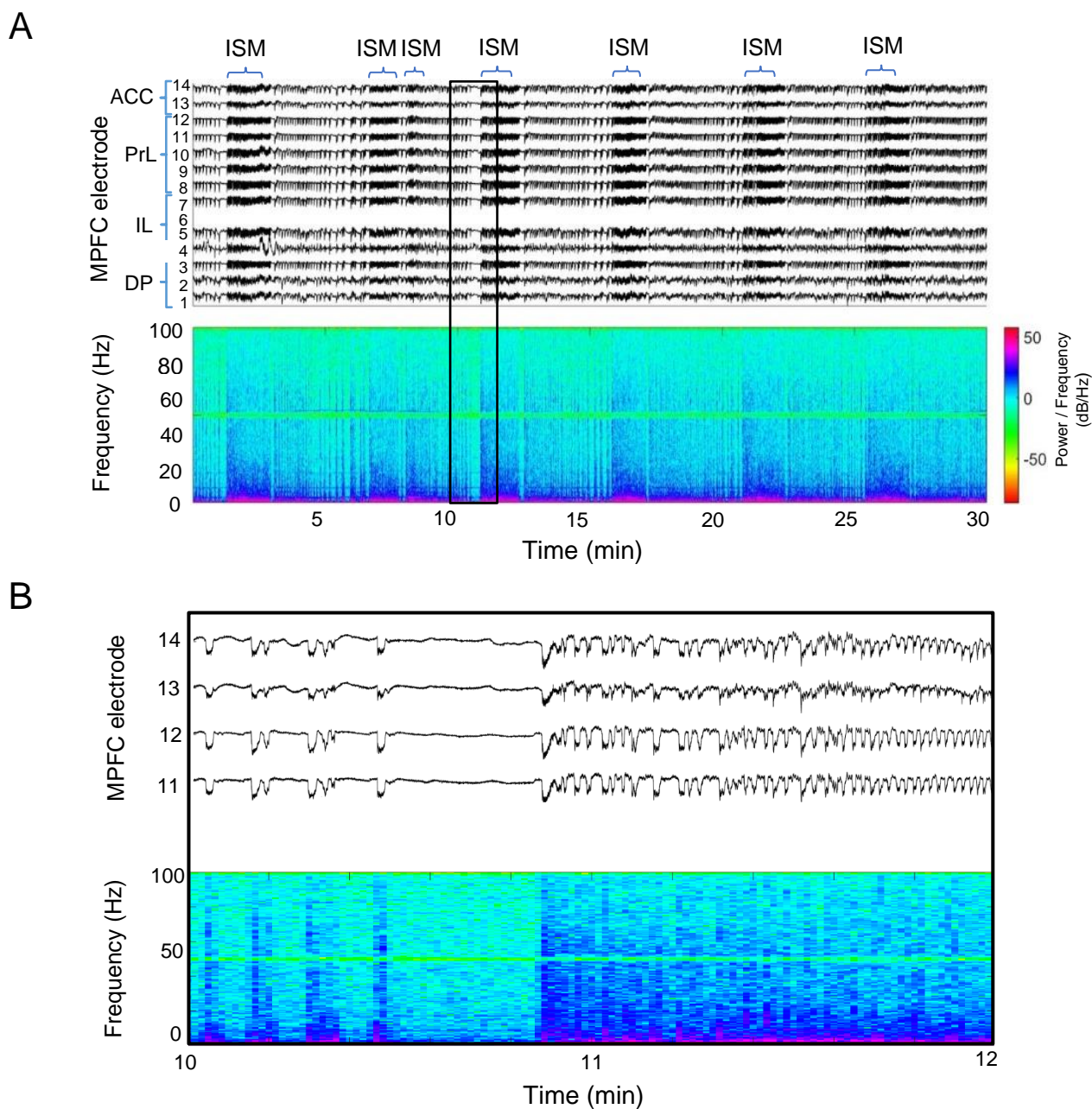
### 5.3.1. *General characterisation of the ISM*

We termed the name infra-slow modulation (ISM) to describe the rhythmic occurrence of increased oscillatory power first seen in all mPFC subregions (Figure 5.1). The ISM is characterised by a sharp-onset increase in power across all frequency ranges, clearly evident in the spectrogram. In some cases, the sharp onset of ISM is preceded by a longer Down-state. After the onset of the ISM, the increase in fast oscillatory activity generally decays slowly, before reaching baseline levels. Moreover, looking at the LFP we can observe that the SO rhythm persists during the ISM but is of higher frequency, before slowly returning to the baseline SO frequency (Figure 5.3). The ISM was also observed in the CA1 of hippocampus (Figure 5.4), synchronous with the ISM in the mPFC. These events were detected under urethane-anaesthesia induced SWS, characterised by the SO (< 1 Hz) and no response of the pedal withdrawal reflex. Overall, the ISM was present in 2/16 recordings in WT animals (section 5.2.1).

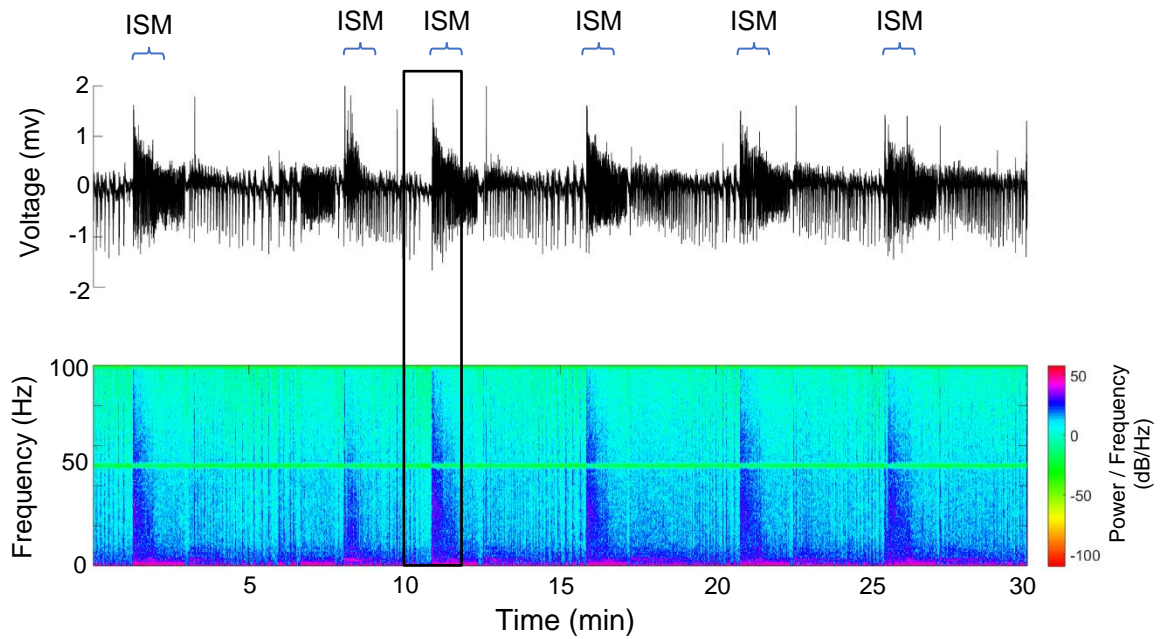
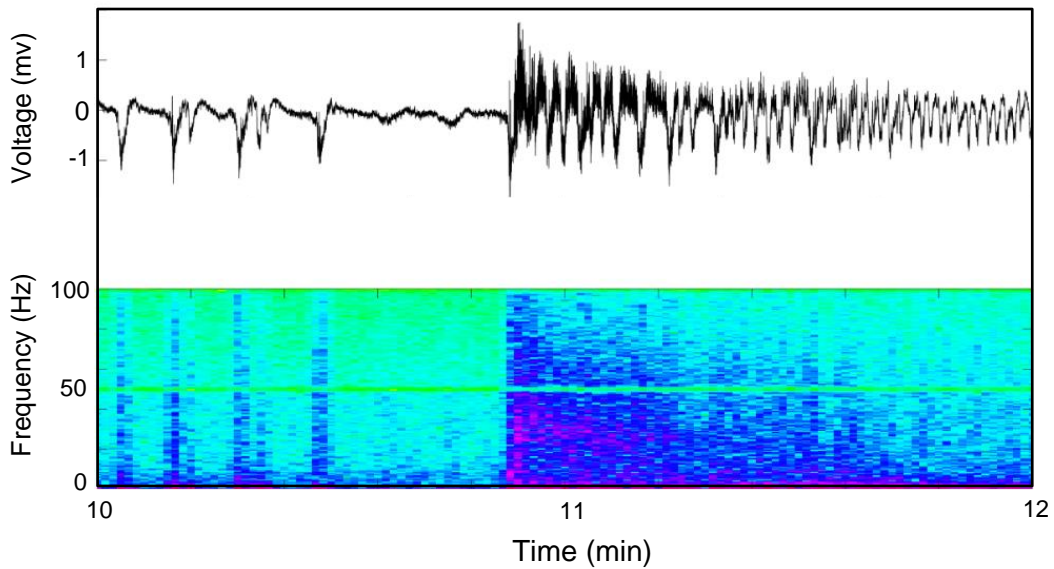
To investigate the changes in oscillatory power during the ISM, we extracted the PSD (showing the absolute power) in a continuous range of frequency bands: SO (0.25 – 0.75 Hz); delta (1.5 – 3.75 Hz), theta (4 - 7.75 Hz), alpha/spindle (8 – 14.75 Hz), beta (15 – 29.75 Hz) and gamma (30 - 79.75 Hz), over 2 s-long epochs. Visual inspection showed that the ISM was accompanied by an increase in absolute power across all frequency bands (Figure 5.1).

The power in the beta frequency range was used to identify the ISM, as described in Method's section 5.2.2. ISM detection revealed that in the mPFC, the mean ISM interval was  $3.7 \pm 0.2$  min that translates to an ISM frequency of  $0.0045 \text{ Hz} \pm 0.0003 \text{ Hz}$  (Figure 5.3). The mean ISM duration was  $1 \pm 0.11$  min, while the mean variability of ISM duration was  $0.38 \pm 0.05$ s. In the CA1 region of the hippocampus, the average interval between ISM events was  $3.89 \pm 0.35$  min that corresponds to an ISM frequency of  $0.0043 \text{ Hz} \pm 0.0006 \text{ Hz}$  (Figure 5.4). The duration of these events was  $0.95 \pm 0.02$  min while the variability in the duration of ISM events within the same recording was  $0.29 \pm 0.09$  min. Therefore, the ISM in both the mPFC and CA1 of the hippocampus can be characterised as rhythmic and although we did not look at ISM-

coherence between the two regions, it appears and evolves in a similar way in the two regions.



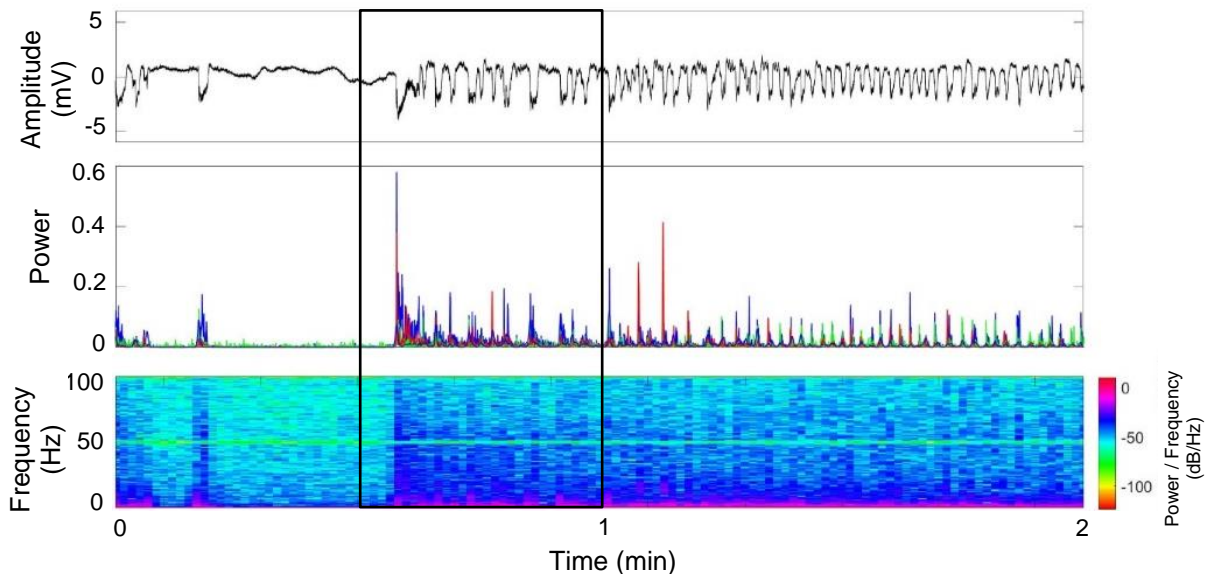
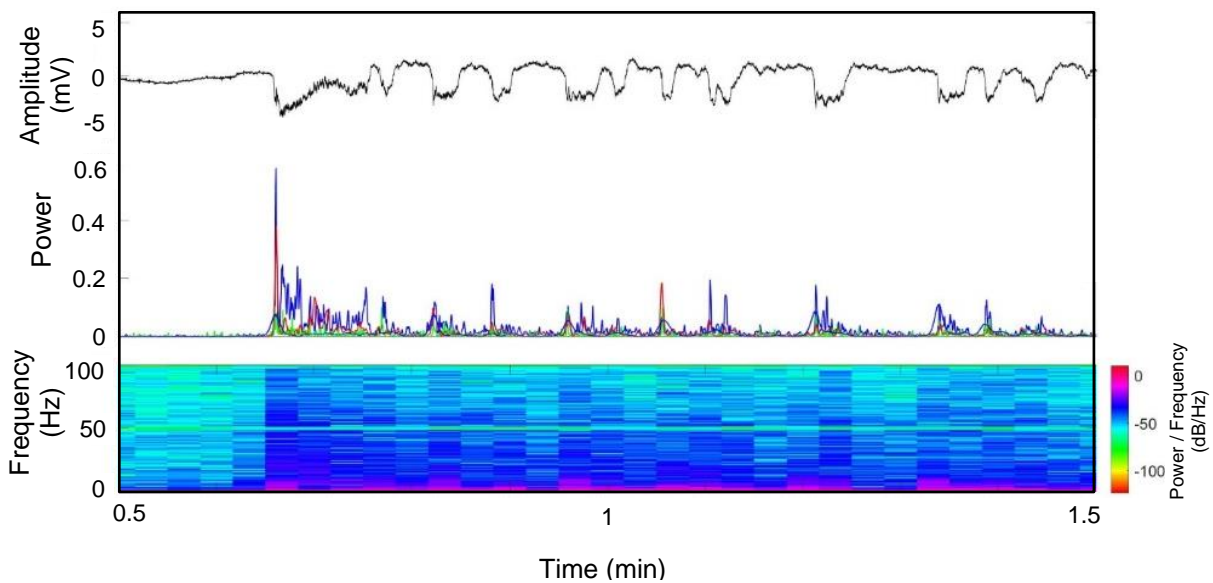
**Figure 5.3:** An example of the LFP and spectrogram of a recording from the mPFC subregions of a WT animal, illustrating the ISM events. The recordings from electrodes 6, 15, 16 have been rejected and the remaining electrodes are grouped in the mPFC subregions (ACC, IL, PrL, DP). **A**) The LFP and spectrogram for a 30 min-long recording in the mPFC. The spectrogram for channel 12 is also shown. **B**) An expanded 2 min-long segment from 2 PrL and 2 ACC electrodes (electrodes 11, 12, 13, 14; bottom to top).

**A****B**

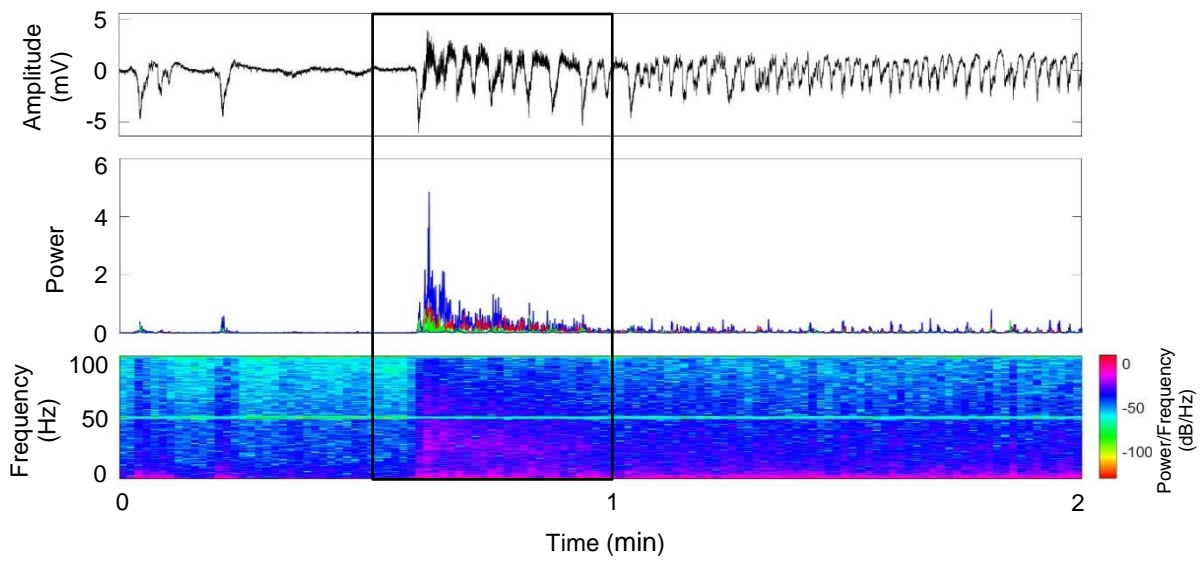
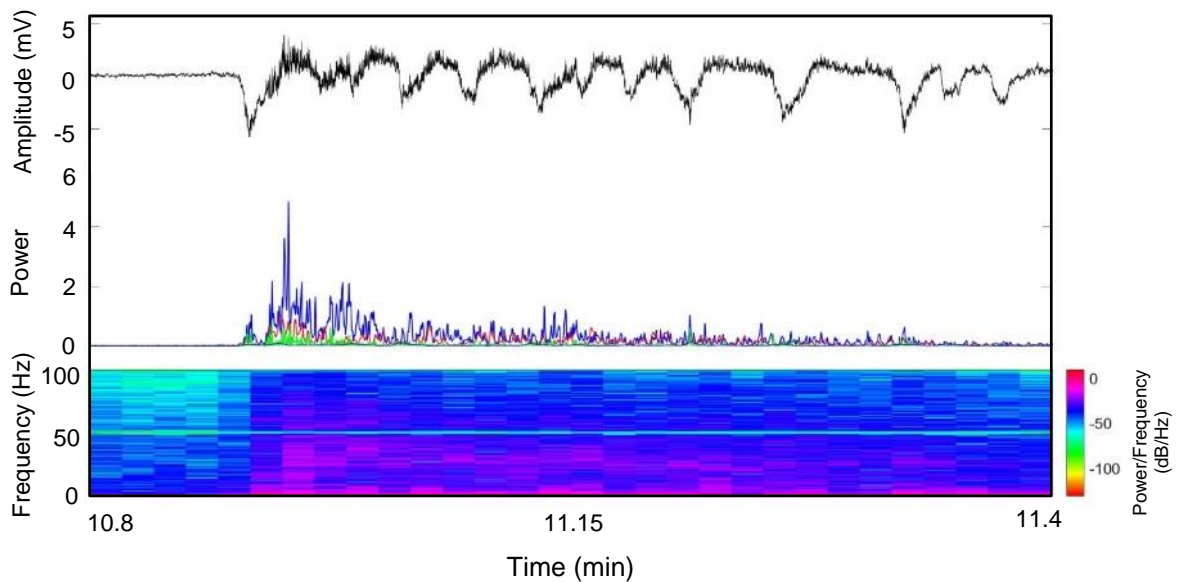
**Figure 5.4:** An example of the LFP and spectrogram of an electrophysiological recording from the hippocampus of a WT animal, illustrating the ISM events. This recording from the CA1 of the hippocampus was simultaneous with the mPFC recording from the contralateral hemisphere shown in Figure 5.3. **A)** The LFP and spectrogram for a 30 min-long recording in the CA1. **B)** An expanded 2 min-long segment of the recording.

### **5.3.2. *The ISM is characterised by increases in high frequency activity***

As discussed earlier, we observed that the ISM is characterised by an increase in power across frequency bands visible in the spectrogram, both in the mPFC (Figure 5.1; Figure 5.3) and in the CA1 (Figure 5.4). In order to verify our observations and to determine whether the observed increase in power was on the Up-state, Down-state or both and how it was distributed in the SO cycle, we proceeded with analysis of the normalised power in the SO cycle. We extracted the average power on the Up-and Down-states, identified the peak power and calculated the latency to the peak power for the 4 frequency bands that were deemed most physiologically significant: theta, beta, gamma and high-gamma, in the mPFC (Figure 5.5) and CA1 (Figure 5.6). The high frequency power was extracted through wavelet analysis on the normalised LFP (z-score function) and it is therefore comparable between animal recordings.

**A****B**

**Figure 5.5:** Examples of an LFP trace, the high frequency oscillatory power in the SO cycle and the spectrogram from one PrL electrode of the mPFC during the ISM. **A)** A 2 min-long-segment of recording is shown and **B)** an expanded 30 s-long segment. The wavelet power is extracted for 4 frequency bands: theta (4 – 7.75 Hz; black), beta (15 – 29.75 Hz; red), gamma (30 – 79.75 Hz, blue), and high-gamma (80 – 130 Hz; green).

**A****B**

**Figure 5.6:** Examples of an LFP trace, the high frequency oscillatory power in the SO cycle and the spectrogram from the CA1 region of the hippocampus during the ISM. This recording is simultaneous with the mPFC recording in Figure 5.5, from the contralateral hemisphere. **A)** A 2 min-long segment of recording is shown and **B)** an expanded 30 s-long segment. The wavelet power is extracted for 4 frequency bands: theta (4 – 7.9 Hz; black), beta (15 – 29.9 Hz; red), gamma (30 – 79.9 Hz, blue), and high-gamma (80 – 130 Hz; green).

### 5.3.2.1. Changes in high frequency activity in the SO cycle in the mPFC during the ISM

Firstly, we looked for changes in (average) power in each frequency range, on the Up-state (Figure 5.7A; Appendix C, “WT” columns). We found a significant increase in power in the beta frequency range during the ISM ( $F(3, 21) = 23.66, p < 0.001$ ) compared to the pre-ISM, ISM and post-ISM segments. The segments also differed in power on the Up-state in the theta ( $F(2.04, 15.1) = 7.58, p < 0.01$ ), gamma ( $F(2.16, 15.1) = 7.25, p < 0.01$ ) and high-gamma frequency ranges ( $F(1.16, 8.1) = 5.46, p < 0.05$ ), with greater levels of power found in the ISM compared to the pre-ISM and post-ISM segments. However, power in the theta, gamma and high-gamma frequency bands during the ISM was not actually significantly different to the non-ISM period.

Interestingly, we also found changes in high frequency oscillatory power on the Down-state where fast oscillations do not normally occur (Figure 5.7B). Specifically, we found a small but significant increase in theta ( $F(3, 21) = 9.8, p < 0.01$ ), beta ( $F(3, 21) = 16.48, p < 0.01$ ) and gamma ( $F(3,21) = 11.74, p < 0.01$ ) power on the Down-state during the ISM compared to all other segments. There was no change in the high-gamma power on the Down-state between the segments.

Another characteristic that describes power on the Up-state is the peak power in the normalised cycle and the latency to peak power in relation to the beginning of the cycle (Figure 5.7C). We found no effect of segment regarding the latency to peak power between segments (Appendix C; “WT” column). This demonstrates that the time of occurrence of the maximum power on the Up-state is the same during the ISM and non-ISM segments. However, we did find a difference in peak power amplitude in all frequency bands: theta ( $F(1.57, 11.01) = 19.53, p < 0.001$ ), beta ( $F(3,21) = 49.48, p < 0.001$ ), gamma, ( $F(3, 21) = 117.3, p < 0.001$ ), high-gamma ( $F(1.01, 7.1) = 42.58, p < 0.01$ ). Interestingly, the peak power amplitude in the beta, gamma and high-gamma ranges was significantly greater in the non-ISM compared to the pre-ISM, ISM and post-ISM segments. In the theta frequency range, the peak power amplitude during the ISM was greater than the pre-ISM and post-ISM segments. In the beta and theta frequency bands, the post-ISM peak power amplitude was smaller than the ISM peak.

We also found a small effect of region in the gamma peak power ( $F(1.47, 10.29) = 6.01, p < 0.05$ ) as well as a band/region interaction ( $F(5.28, 36.96) = 3.95, p < 0.01$ ). The effect of region was identified as a greater peak power in the PrL region compared

to the DP region ( $p < 0.01$ ). One-way rmANOVA analysis for each region showed a very high effect of segment in all regions: DP ( $F(3, 21) = 90.52, p < 0.001$ ), IL ( $F(3, 21) = 126.68, p < 0.001$ ), PrL ( $F(3, 21) = 91.45, p < 0.001$ ) and ACC ( $F(3, 21) = 46.92, p < 0.001$ ), that was attributed to a greater gamma peak power in the non-ISM compared to all other segments ( $p < 0.001$ ). The high-gamma peak power ( $F(1.56, 12.27) = 5.28, p < 0.05$ ) was greater in the PrL compared to the DP region ( $p < 0.01$ ). We did not identify a significant effect of region or region/segment interaction power on the Up-state and Down-state, or in the latency to the peak power in any frequency range (Figure 5.7).

Our findings reveal that the ISM period is characterised by an increase in power in the beta frequency band on the Up-state during the ISM, compared to the non-ISM periods. Furthermore, we also found an increase in theta, beta and gamma frequency power on the Down-state, in comparison to the non-ISM period. Interestingly, the ISM had significantly greater power in relation to the periods immediately preceding or following the ISM on the Up and Down-state, suggesting there are periods of reduced activity just before and after the large burst of power that defines the ISM. Finally, we found that the peak power for all frequency bands was smaller in the ISM-related segments compared to the non-ISM segment. In the ISM, this decrease in peak power could be attributed to more aberrant activity related to the increased high frequency power on the Down-state, while in the pre-ISM and post-ISM states it could be related to less activity on the Up-state.

## Medial prefrontal cortex (mPFC)

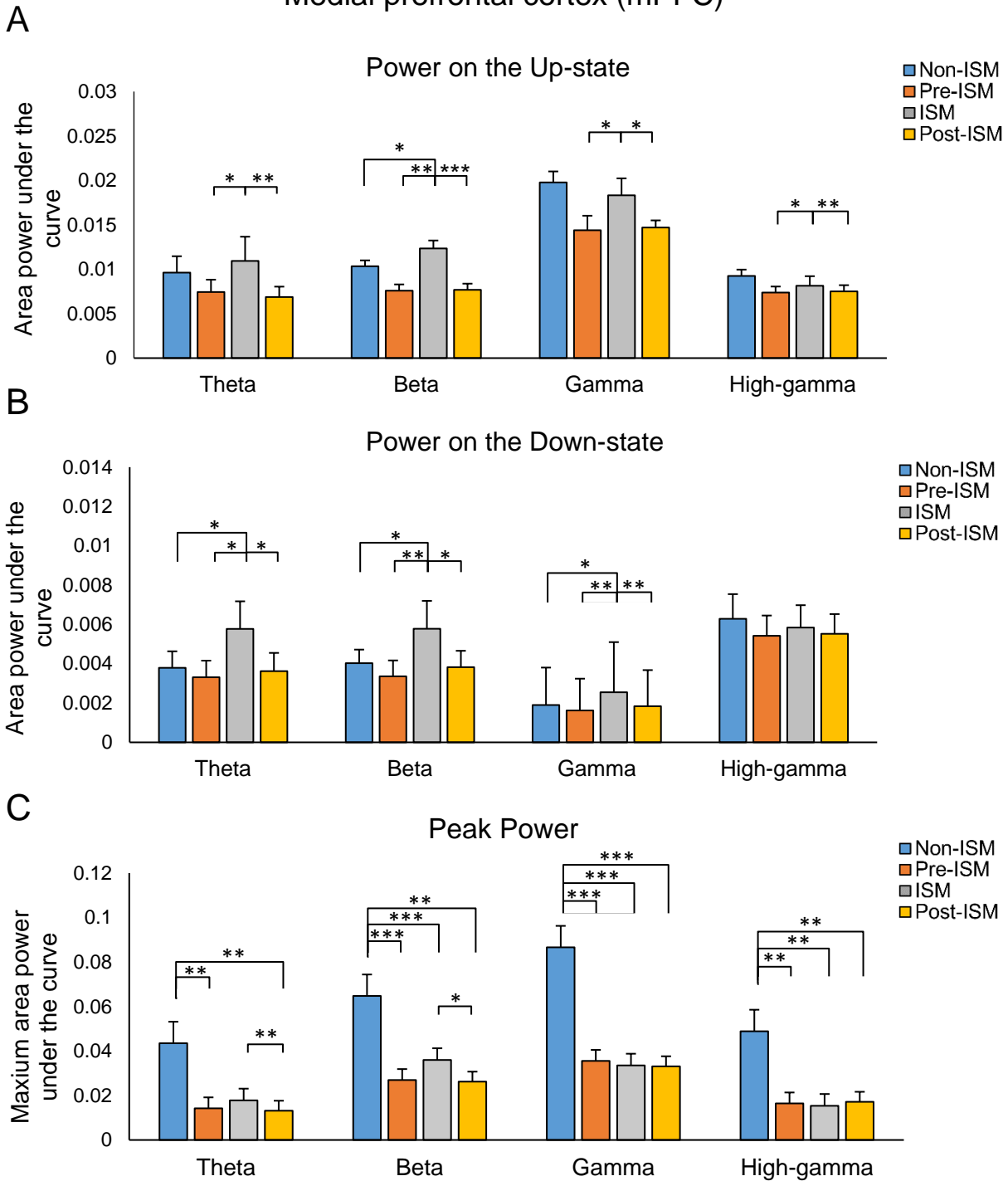


**Figure 5.7:** Changes in high frequency oscillatory power in the SO cycle in relation to the ISM, in the mPFC of WT animals. The power in the SO cycle is characterised in 4 frequency bands: theta (4 – 7.9 Hz), beta (15 – 29.9 Hz), gamma (30 – 79.9 Hz) and high-gamma (80 – 130 Hz), in 4 segments: non-ISM, pre-ISM, ISM and post-ISM in WT (N = 8) mice. **A)** Mean power on the Up-state. **B)** Mean power on the Down-state. **C)** Peak power in the normalised SO cycle (Down-state + Up-state). Error bars indicate the SEM. Asterisks indicate statistical significance: \* =  $p < 0.05$ , \*\* =  $p < 0.01$ , \*\*\* =  $p < 0.001$ .

### 5.3.2.2. Changes in high frequency activity in the SO cycle in the hippocampus during the ISM

In view of the findings of greater high frequency oscillatory power on both the Up- and the Down-state in the mPFC during the ISM, we proceeded to analyse the power content of the Up-Down cycle in the CA1 of the hippocampus, across the ISM segments in a similar manner (Figure 5.8; Appendix D - “WT” column). On the Up-state (Figure 5.8A), we found a significant increase in power in the beta ( $F(2.23, 13.35) = 5.97, p < 0.05$ ) and gamma ( $F(1.63, 9.76) = 5.39, p < 0.05$ ) frequency bands, during the ISM compared to the pre-ISM and post-ISM segments, but not the non-ISM segment. This finding demonstrates that the slight reduction in power occurring just before and after the ISM that we saw in the mPFC, is more evident in the hippocampus.

On the Down-state (Figure 5.8B), we found significantly greater gamma frequency power ( $F(3, 18) = 9.12, p < 0.05$ ) during the ISM compared to the pre-ISM segment, while it is worth mentioning a similar trend for the post-ISM ( $p = 0.054$ ) and non-ISM segments ( $p = 0.67$ ), but these did not quite reach statistical significance. This lack of significance might relate to the wide confidence intervals (95%), that are -0.757 – 0.007 for the pre-ISM Vs ISM segments, and -0.019 – 0.549 for the post-ISM Vs ISM segment. We also found significantly greater theta ( $F(3, 18) = 11.18, p < 0.001$ ), beta ( $F(3, 18) = 8.41, p < 0.05$ ) and high-gamma ( $F(1.43, 8.6) = 6.89, p < 0.05$ ) band power on the Down-state during the ISM compared to the pre- and post-ISM segments. Thus, the ISM has greater high frequency oscillatory power compared to the pre-ISM and post-ISM segments, and possibly compared to the non-ISM segment, although it did not reach statistical significance as in the mPFC.

We then looked at the peak power and the latency to peak power across the normalised SO cycle (Figure 5.8C), within each frequency band. The only significant difference found was in peak power in the gamma ( $F(3, 18) = 3.7, p < 0.05$ ) and theta ( $F(1.48, 8.89) = 17.01, p < 0.01$ ) frequency ranges, as the non-ISM segment had a significantly greater peak power compared to the other segments similar to the changes seen in the mPFC. The pre-ISM segment also had significantly lower theta peak power than the ISM segment. The latency to the peak power did not differ between genotypes in any frequency band.

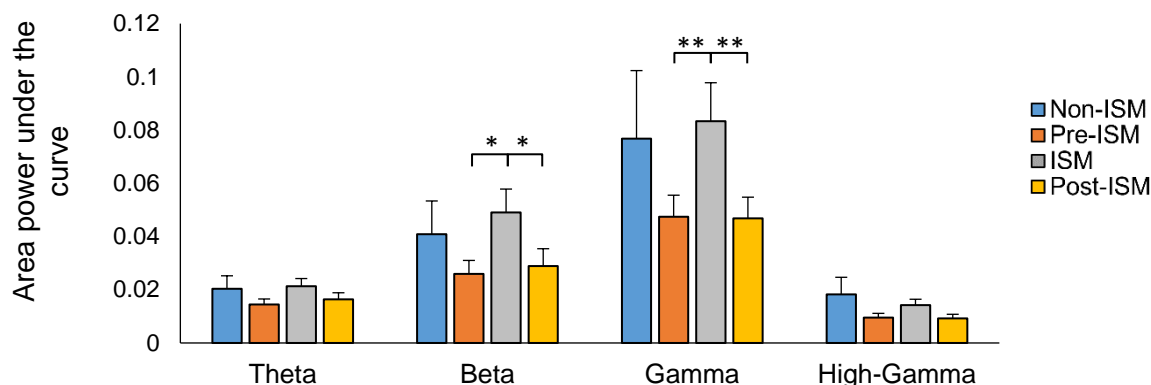
Analysis of power in the normalised SO cycle during the ISM revealed an increase in power in the beta and gamma frequency bands on the Up-state, and in all

frequency bands on the Down-state, in comparison to the pre-ISM and post-ISM segments. Hence, the finding of lower high frequency activity preceding and following the ISM is replicated in the CA1 as well. However, no differences were found between power on the Up- and Down-states during the ISM compared to the non-ISM segment. Analysis of the peak power on the Up-state showed a reduced peak power in the theta and gamma frequency bands during the ISM compared to the other segments. Hence, a change in power distribution during the SO is also evident in the CA1, but to a lesser extent compared to the mPFC.

A

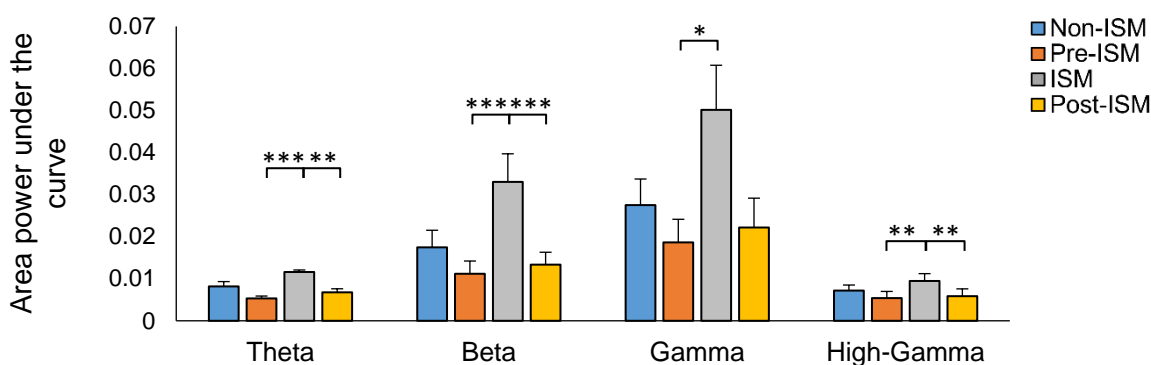
CA1 region of the hippocampus

Power on the Up-state



B

Power on the Down-state



C

Peak power

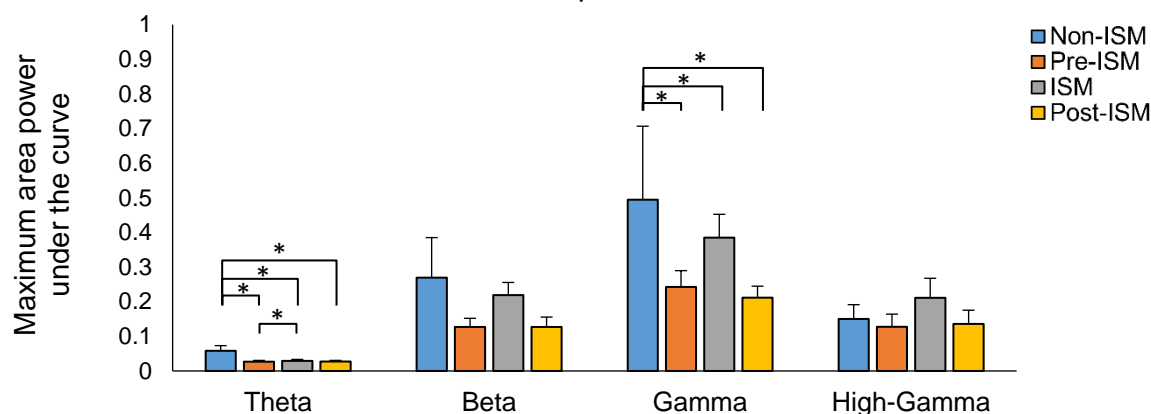


**Figure 5.8:** Changes in high frequency oscillatory power in the SO cycle in relation to the ISM in the hippocampus of WT animals. The power in the SO cycle was investigated in 4 frequency bands: theta (4 – 7.9 Hz), beta (15 – 29.9 Hz), gamma (30 – 79.9 Hz) and high-gamma (80 – 130 Hz), in 4 segments: non-ISM, pre-ISM, VMS and post-ISM, in WT (N = 8) mice. **A)** The mean power on the Up-state. **B)** mean power on the Down-state. **C)** The peak power in the normalised SO cycle (Down-state + Up-state). Error bars indicate the SEM. Asterisks indicate statistical significance: \* =  $p < 0.05$ , \*\* =  $p < 0.01$ , \*\*\* =  $p < 0.001$ .

### 5.3.3. *Changes in SO cycle patterns during the ISM*

As can be seen in Figure 5.9, the ISM is also characterised by an increase in SO frequency and amplitude in the mPFC and CA1 of the hippocampus. We also observed that occasionally the ISM is preceded by a longer Down-state (Figure 5.3 & 5.4). Hence, we proceeded to analyse the SO cycle components, the Up- and Down-states which were automatically detected, and to extract SO amplitude and frequency. To verify our observations, we performed two-way rmANOVA analyses with two repeated measures, the segment and mPFC region, for each relevant variable in the mPFC. A similar analysis of the characteristics of the SO was also performed for the CA1, with the ISM segment as the only repeated measure.

#### 5.3.3.1. SO cycle characterisation in the mPFC during the ISM

Firstly, we analysed the SO cycle in the mPFC and its subregions (Figure 5.10, Appendix E) in relation to the ISM. Analysis of the SO amplitude revealed a significant effect of segment ( $F(1.17, 8.13) = 13.94, p < 0.01$ ), with greater SO amplitude found in the ISM compared to all other segments (Figure 5.10A). We also found an effect of region ( $F(3, 21) = 13.94, p < 0.01$ ), with lower SO amplitude in the ACC compared to the PrL region ( $p < 0.05$ ).

We then looked at the SO frequency and found a significant effect of segment ( $F(3, 21) = 11.25, p < 0.001$ ), due to higher SO frequency in the ISM compared to the non-ISM and post-ISM segment (Figure 5.10B). As expected, we also found an effect of segment in SO cycle (Down-state + Up-state) length ( $F(3, 21) = 25.15, p < 0.001$ ), with shorter SO cycles during the ISM compared to the non-ISM, pre-ISM and post-ISM segments (Figure 5.10C). The post-ISM segment also had shorter cycles compared to the non-ISM segment. The decrease in cycle length during the ISM can be attributed to both shorter Up- ( $F(3, 21) = 25.37, p < 0.001$ ) and Down-states ( $F(1.77, 12.37) = 19.84, p < 0.001$ ; Figure 5.10C). Specifically, the Up-state was shorter during the ISM compared to the non-ISM and pre-ISM segments. The pre-ISM and post-ISM segments also had shorter Up-states compared to the non-ISM segment. The Down-state was also shorter on the ISM segment compared to all other segments.

We also found an effect of segment in state-length variability over time in the SO cycle ( $F(3, 21) = 11.29, p < 0.001$ ), and in both the Up-state ( $F(3, 21) = 7.88, p < 0.01$ ) and Down-state ( $F(3, 21) = 9.32, p < 0.001$ ; Figure 5.10D). The cycle length

variability was lower during the ISM compared to the non-ISM and post-ISM segments ( $p < 0.05$ ). The Up-state length variability was shorter only during the ISM compared to the pre-ISM segment ( $p < 0.05$ ). The Down-state length variability was shorter during the ISM compared to all other segments ( $p < 0.05$ ; Figure 5.10).

Our results verify our observations that the ISM is a period characterised by a greater SO amplitude and frequency, The higher SO frequency and hence the shorter SO cycle of the ISM, can be attributed to both shorter Up- and Down-states. The pre-ISM segment was most similar to non-ISM periods, although we had observed that the ISM is often preceded by a longer Down-state. The fact that our observation was not verified through statistical analysis may be attributed to averaging the state lengths for the 30 s-long pre-ISM segments. A single long Down-state just prior to the ISM was insufficient to change the overall SO frequency for the pre-ISM period. The post-ISM period on the other hand, appears to be a transition between the ISM and non-ISM periods. We also found decreased variability in state length over time during the ISM, which may be interpreted as an absence of longer states. In conclusion, our findings are consistent with our observations of an abrupt start to the ISM characterised by an increase in SO frequency, followed by a period of gradual decline before the baseline SO frequency is restored. Moreover, it is important to note that our findings show a clear SO during the ISM and thus, this event does not reflect a transition to a different sleep-like state.

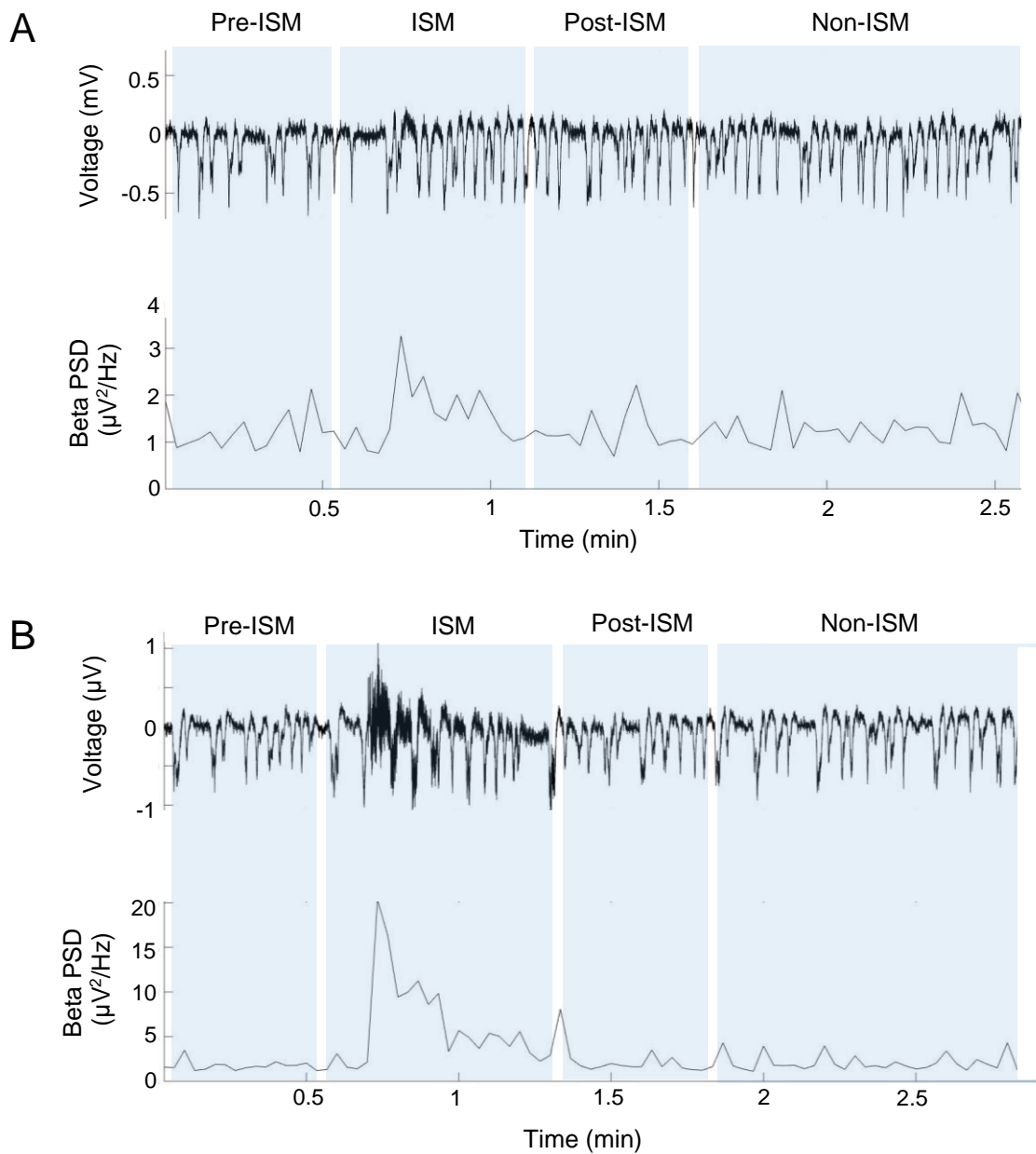


**Figure 5.9:** Example traces demonstrating the evolution of the ISM in the LFP and its expression as increased beta band power. The LFP and power (PSD) in the beta band for the same segment **A**) in the PrL subregion of the mPFC and **B**) the CA1 region of the hippocampus.

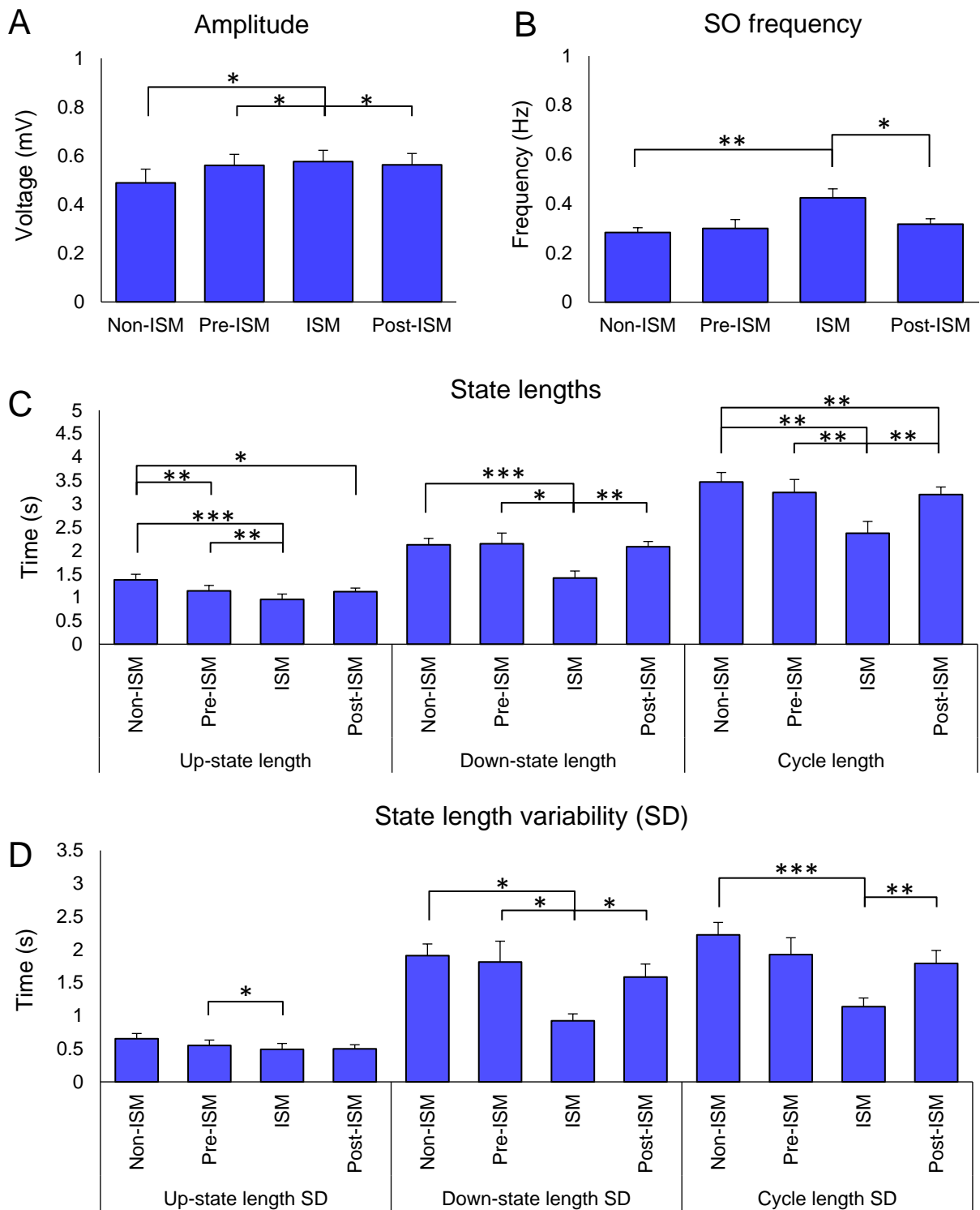


**Figure 5.10:** Changes in the SO frequency and amplitude in relation to the ISM in the PrL subregion of the mPFC of WT mice. **A)** The SO frequency, **B)** SO amplitude, **C)** the mean Up-state, Down-state and cycle lengths and **D)** the variability of these variables in time (SD), in the non-ISM, pre-ISM, ISM and post-ISM segments in WT ( $N = 7$ ) animals. Error bars indicate the SEM. Asterisks indicate statistical significance:  $* = p < 0.05$ ,  $** = p < 0.01$ ,  $*** = p < 0.001$ .

### 5.3.3.2. SO cycle characterisation in the hippocampus during the ISM

As can be seen in Figure 5.7B there also were marked changes in the SO during the ISM in the CA1 region of the hippocampus. Therefore, we performed one-way rmANOVA analyses to quantify the characteristics of the SO in the CA1 of the hippocampus as well (Figure 5.11; Appendix F, “WT” column).

Firstly, we looked at the SO amplitude, which was significantly higher in the non-ISM, pre-ISM and post-ISM periods compared to the ISM period ( $F(1.51, 9.03) = 12.15, p < 0.05$ ; Figure 5.11A). There was also an increase in SO frequency during the pre-ISM and ISM segments compared to the non-ISM ones ( $F(3, 18) = 8.08, p < 0.05$ ; Figure 5.11B). SO cycle length in the ISM was decreased compared to non-ISM periods ( $F(3, 18) = 4.58, p < 0.05$ ). As observed in the mPFC, our findings of a shorter SO cycle can be attributed to both shorter Up- ( $F(3, 18) = 14.65, p < 0.001$ ) and Down-states ( $F(3, 18) = 3.54, p < 0.05$ ) during the ISM (Figure 5.11C). The Up-state was shorter during the ISM compared to all other segments, while the Down-state was shorter during the ISM compared to the non-ISM segment. Finally, we looked at cycle length variability, which was significantly decreased during the pre-ISM, ISM and post-ISM segments compared to non-ISM ones ( $F(3, 18) = 4.55, p < 0.05$ ). This finding can be attributed to lower Down-state length variability in the same segments ( $F(3, 18) = 4.5, p < 0.05$ ; Figure 5.11D).

Our analysis verified that the SO in the CA1 regions during the ISM is also characterised by a greater amplitude and frequency compared to non-ISM segments. Moreover, the SO cycle was significantly shorter in the ISM only compared to non-ISM segments. The Up-states were shorter during the ISM compared to all other segments, while the Down-state length did not differ between segments. It, therefore, appears that the changes in the SO and the evolution of the ISM are not as clear in the CA1 as in the mPFC, with respect to the pre-ISM and post-ISM segments. Moreover, we found more restricted changes in state length variability compared to the mPFC. Thus, the SO is also altered during the ISM in the CA1 of the hippocampus, but to a lesser extent than the mPFC.

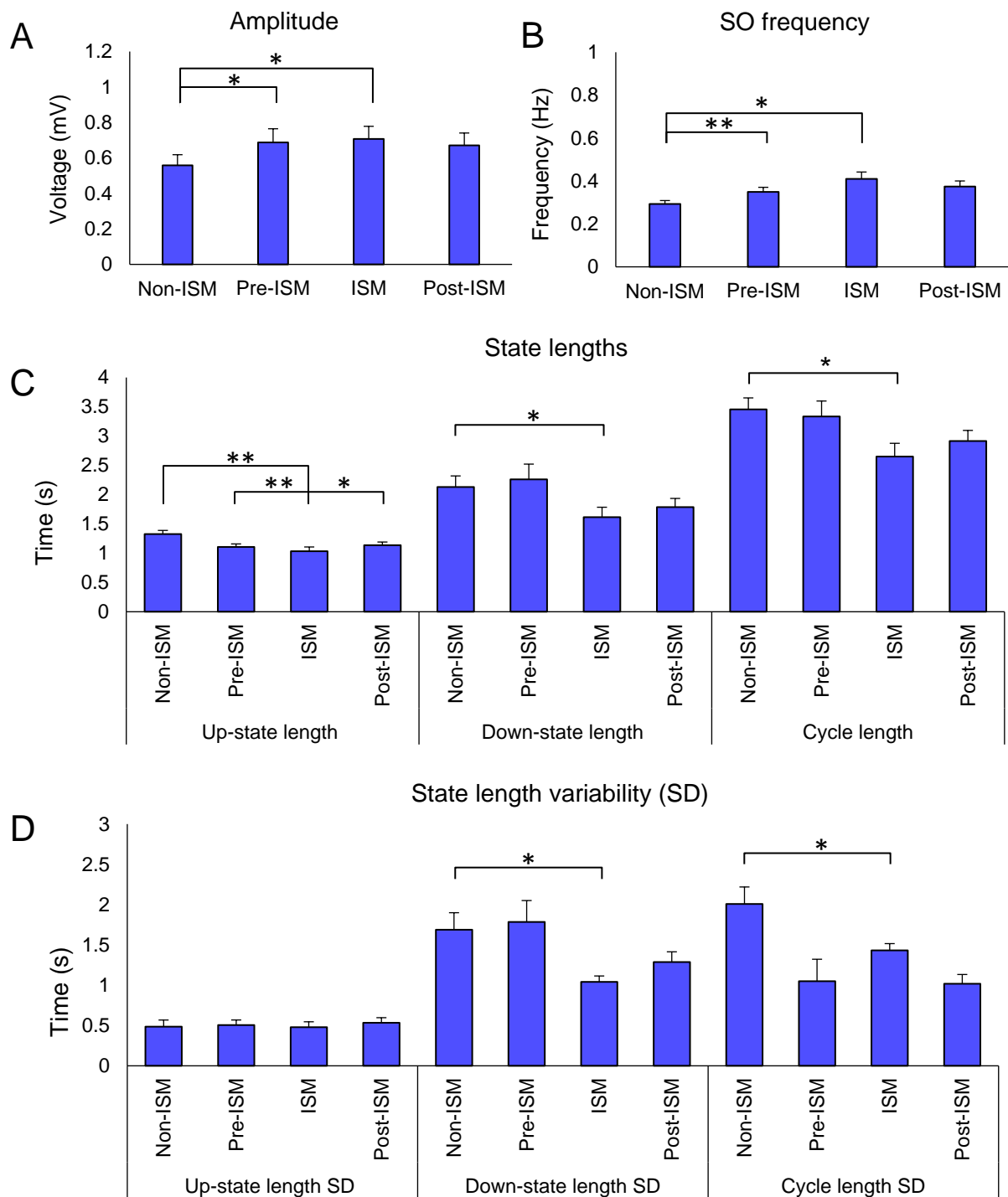


**Figure 5.11:** Changes in the SO frequency and amplitude in relation to the ISM in the hippocampus of WT mice. The **A**) SO frequency, **B**) SO amplitude, **C**) the Up-state, Down-state and cycle lengths and **D**) the variability of these variables in time (SD) during the non-ISM, pre-ISM, ISM and post-ISM segments in WT mice (N = 7). Error bars indicate the SEM. Asterisks indicate statistical significance: \* =  $p < 0.05$ , \*\* =  $p < 0.01$ .

### 5.3.4. The SO / theta band power ratio increases during the ISM

The SO / theta power ratio has been used as a method to detect activated states under urethane-induced anaesthesia and REM states under natural sleep (Clement et al., 2008). Hence, we also looked at the SO/theta power ratio using the power (PSD) extracted for the SO and theta frequency ranges, in the mPFC and CA1 of the hippocampus (Table 5.1; Figure 5.12).

In the mPFC, the SO/theta power ratio ( $F(3, 21) = 18.87, p < 0.05$ ) was significantly lower during the ISM compared to the non-ISM and post-ISM segments (Figure 5.12A), while a similar pattern can be observed for the pre-ISM segment. In the CA1 of the hippocampus, the SO/theta band power ratio ( $F(3, 21) = 9.29, p < 0.05$ ) was also lower during the ISM compared to non-ISM and pre-ISM segments ( $p < 0.05$ ), while a similar pattern can be observed for the post-ISM segment (Figure 5.12B). Finally, we also found a significant effect of mPFC region in the SO/theta power ratio ( $F(3, 21) = 4.18, p < 0.05$ ), with a lower SO/theta power ratio in the ACC compared to the DP and IL regions.

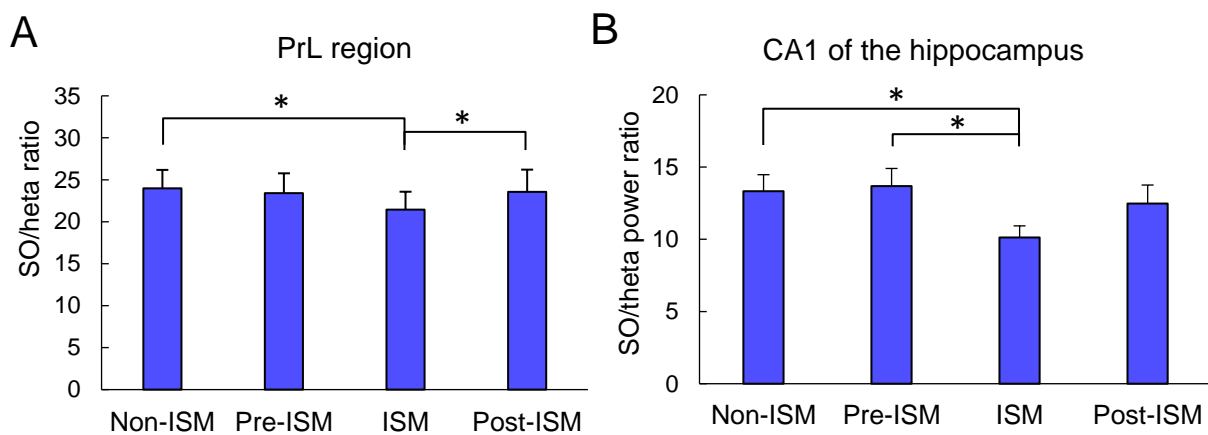


**Figure 5.12:** The SO/theta band power ratio in the PrL subregion of the mPFC and the hippocampus of WT animals. These variables were assessed in 8 WT animals in the mPFC and 7 WT animals in the CA1 of the hippocampus. Error bars indicate the SEM. Asterisks indicate statistical significance:  $* = p < 0.05$ .

**Table 5.1:** The SO/theta band power ratio in relation to the ISM in the mPFC of WT animals. The average SO/theta band power ratio  $\pm$  SEM is shown for each mPFC subregion (ACC, PrL, IL, DP), for a each segment (non-ISM, pre-ISM, ISM, post-ISM), in WT mice (N = 8).

SO/theta band power ratio				
	Non-ISM	Pre-ISM	ISM	Post-ISM
<b>ACC</b>	17.53 $\pm$ 1.61	17.82 $\pm$ 1.75	15.83 $\pm$ 1.7	17.3 $\pm$ 1.86
<b>PrL</b>	23.97 $\pm$ 2.2	23.41 $\pm$ 2.36	21.44 $\pm$ 2.13	23.55 $\pm$ 2.66
<b>IL</b>	23.39 $\pm$ 2.01	23.05 $\pm$ 1.76	21.01 $\pm$ 1.87	23.37 $\pm$ 2.1
<b>DP</b>	22.02 $\pm$ 1.2	22.08 $\pm$ 1.04	20.22 $\pm$ 1.22	21.79 $\pm$ 1.28

### 5.3.5. *Changes in neuronal firing during the ISM*

Finally, we looked at neuronal/unit firing in relation to the SO cycle during the ISM (Figure 5.13A; Normally, in WT animals neurons only fire on the Up-state, while during the Down-state neurons are “silent”. Hence, we were interested to see whether the increase in high frequency activity seen on the Up- and Down-state during the ISM would also translate to increased neuronal firing.

As previously described (section 5.2.3.3) we performed two types of unit-related analysis. Firstly, we looked at the 6 variables of interest after averaging them across units for each animal: the ISI for the recording duration and on the Up-state, the spike frequency for the recording duration and on the Up-state, the percentage of units firing on the Up-state and the unit firing / SO coherence (Table 4.5, “WT” column). Our analysis in 7 WT animals with 23 units revealed a small effect of ISM segment on the ISI of neuronal firing for the recording duration ( $F(3, 18) = 3.72, p < 0.05$ ), and in the spike frequency for the recording duration ( $F(3, 18) = 3.27, p < 0.05$ ). Although all the assumptions of the test were met, post-hoc analysis did not identify significant differences between specific segments for these two variables. The failure of the post-hoc analysis confirmed our concerns that this analysis would obscure the changes between ISM segments for each unit. Hence, we proceeded with the second analysis where we treated all units as individual samples.

One-way rmANOVA analysis for 23 WT units for each of the same 6 variables (See above; Table 5.2) revealed a significant effect of segment in the ISI for the recording duration (irrespective of state;  $F(1.53, 33.68) = 6.03, p < 0.01$ ), as the ISI was significantly shorter in the ISM compared to the non-ISM segment ( $p < 0.05$ ). A trend for shorter ISIs for the recording duration was also seen in the ISM ( $p = 0.053$ ;  $CI = -0.194 - 0.001$ ) and post-ISM segments ( $p = 0.05$ ;  $CI = -0.181 - 0.001$ ) in relation to the pre-ISM segment. However when we looked at the ISIs on the Up-state alone there was no significant difference between groups, suggesting that the shorter ISI for the recording duration may be attributed to higher SO frequency and thus, more frequent Up-states. There were no significant differences in the firing rate on the Up-state nor in the percentage of units firing on the Up-state. However, the unit firing / SO coherence ( $F(3, 57) = 5.89, p < 0.01$ ;  $N = 20$ ) was significantly lower in the ISM compared to the pre-ISM and post-ISM periods ( $p < 0.01$ ; Figure 5.13B,C).

Upon inspection of the raster plots for individual neuronal firing patterns (5.13A) we noticed that units changed their firing in different ways in relation to the ISM. Thus, we decided to look into each unit's firing behaviour ( $N = 23$ ) and calculated the percentage change in firing rate during the ISM compared to the non-ISM segment. Units were grouped into those that increased their firing rate ( $> 115\%$ ), did not change their firing rate ( $85\% - 115\%$ ) or decreased their firing rate ( $< 85\%$ ) on the Up-state. Overall, about half of neurons increased their firing during the ISM ( $N = 9$ ), with an average percentage increase of  $72.55\% \pm 20.28\%$ . The remaining units either showed no change in firing rate ( $N = 10$ ;  $106.2\% \pm 4.58\%$ ) or a decrease in firing rate ( $N = 4$ ;  $62.19\% \pm 6.59\%$ ) during the ISM compared to the non-ISM segment (Figure 5.13D,E). Although no statistical analysis was performed, these data clearly demonstrate that neuronal firing rate is differentially affected by the ISM.

In summary, neurons change their firing in different ways in response to the ISM, with  $\sim 40\%$  of neurons in the mPFC increasing their firing rate while the rest either have unaltered ( $\sim 40\%$ ) or reduced firing rates ( $\sim 20\%$ ). This variability in neuronal firing in relation to the ISM has obscured the results of our statistical analysis. We only found a shorter ISI for the recording duration during the ISM compared to non-ISM segments which could relate to an increased firing rate, or the shorter SO cycle that occurred during the ISM. The ISM also appears to have less synchronised firing in relation to the SO, compared to its preceding and following periods. A more in-depth analysis of

single unit behaviour in relation to the ISM, including the pre-ISM and post-ISM segments, could provide valuable insight regarding the nature of the ISM, especially considering the increases in high frequency power during this event.

**Table 5.2:** Changes in neuronal firing patterns in relation to the ISM in the mPFC of WT mice. These variables reflect the activity of 23 units recorded in WT animals (N = 7), and were either averaged across all units/animal ( $\pm$  SEM), or treated as single units ( $\pm$  SEM). Each variable was calculated for the pre-ISM, ISM and post-ISM segments, for all mPFC regions combined. Variables also shown in Figure 5.13 are in *Italics*.

<b>Characterisation of averaged units/animal</b>				
<b>Variable</b>	<b>Non-ISM</b>	<b>Pre-ISM</b>	<b>ISM</b>	<b>Post-ISM</b>
Spike frequency / recording duration (Hz)	1.28 $\pm$ 0.19	1.26 $\pm$ 0.2	1.37 $\pm$ 0.21	1.47 $\pm$ 0.22
Spike frequency on the Up-state (Hz)	3.18 $\pm$ 0.56	2.72 $\pm$ 0.42	2.84 $\pm$ 0.44	3.04 $\pm$ 0.45
ISI / recording duration (s)	1.04 $\pm$ 0.23	1.17 $\pm$ 0.17	0.98 $\pm$ 0.18	0.93 $\pm$ 0.15
ISI on the Up-state (s)	0.29 $\pm$ 0.06	0.34 $\pm$ 0.08	0.33 $\pm$ 0.07	0.29 $\pm$ 0.06
Firing on Up-state (%)	91.59 $\pm$ 2.3	93.04 $\pm$ 3.2	92.88 $\pm$ 2.11	90.62 $\pm$ 2.76
Unit firing / SO coherence	0.71 $\pm$ 0.07	0.74 $\pm$ 0.05	0.65 $\pm$ 0.06	0.71 $\pm$ 0.04
<b>Single unit characterisation</b>				
<b>Variable</b>	<b>Non-ISM</b>	<b>Pre-ISM</b>	<b>ISM</b>	<b>Post-ISM</b>
Spike frequency / recording duration (Hz)	1.22 $\pm$ 0.14	1.24 $\pm$ 0.14	1.34 $\pm$ 0.15	1.44 $\pm$ 0.16
Spike frequency on the Up-state (Hz)	2.94 $\pm$ 0.37	2.63 $\pm$ 0.3	2.79 $\pm$ 0.33	2.93 $\pm$ 0.34
<i>ISI / recording duration (s)</i>	<i>1.25 <math>\pm</math> 0.22</i>	<i>1.28 <math>\pm</math> 0.14</i>	<i>1.09 <math>\pm</math> 0.15</i>	<i>1.06 <math>\pm</math> 0.13</i>
ISI on the Up-state (s)	0.33 $\pm$ 0.04	0.33 $\pm$ 0.05	0.33 $\pm$ 0.04	0.32 $\pm$ 0.04
Firing on Up-state (%)	89.55 $\pm$ 1.61	91.98 $\pm$ 2.42	90.88 $\pm$ 1.35	88.07 $\pm$ 1.74
<i>Unit firing / SO coherence</i>	<i>0.72 <math>\pm</math> 0.04</i>	<i>0.77 <math>\pm</math> 0.02</i>	<i>0.68 <math>\pm</math> 0.03</i>	<i>0.75 <math>\pm</math> 0.03</i>

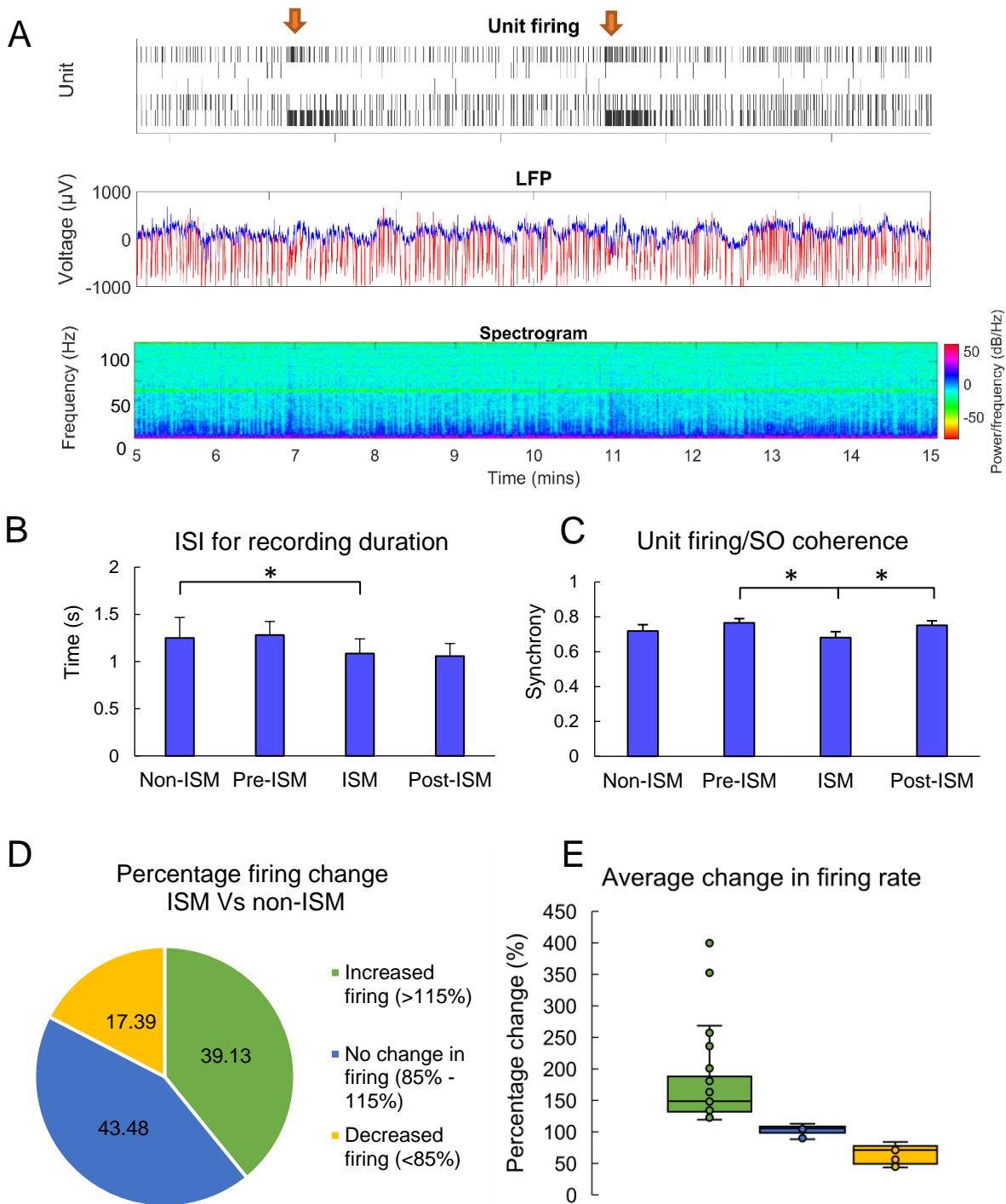


**Figure 5.13:** Changes in unit firing patterns in WT animals in relation to the ISM. **A)** An example of unit firing in the mPFC in relation to the spectrogram and LFP (red = Up-state, blue = Down-state). **B-C)** The variables that were significantly different across frequency bands: the ISI for the duration of the recording and the unit firing / SO coherence. **D-E)** The behaviour of units in the ISM in relation to non-ISM periods. **D)** The percentage of cells to decrease (< 85%), increase (> 115%) or not change its firing rate (85% - 115%) and **E)** the percentage change in each category. These variables were calculated using 23 units from WT (N = 8) animals. Error bars indicate the SEM. Asterisks indicate statistical significance: \* =  $p < 0.05$ .

### 5.3.6. *The relative spindle density decreases during the ISM*

We also looked at the spindles in the mPFC during the ISM and characterised the relative spindle density, corresponding to the number of spindles per Up-state. We calculated the relative spindle density for the non-ISM, pre-ISM, ISM and post-ISM periods, in the 4 mPFC subregions. Two-way rmANOVA analysis showed a significant effect of segment ( $F(3, 21) = 6.41, p < 0.01$ ), with post-hoc analysis showing significantly fewer spindles / Up-state during the ISM compared to the non-ISM period ( $p < 0.05$ ). We also found a significant region/segment interaction ( $F(9, 63) = 3.06, p < 0.01$ ) which we investigated further with one-way rmANOVA analyses for each region. In the DP and PrL, although there was a significant effect of segment (DP:  $F(9, 63) = 4.34, p < 0.05$ ; PrL:  $F(9, 63) = 6.28, p < 0.05$ ), post-hoc analysis only revealed a pattern for fewer spindles/Up-state in the ISM compared to the non-ISM period (DP:  $p = 0.054, CI = -0.003 - 0.394$ ; PrL:  $p = 0.052, CI = -0.002 - 0.5$ ). This lack of significance again might relate to the low sample size, as indicated by the wide CI. In the IL ( $F(9, 63) = 5.88, p < 0.01$ ) and ACC ( $F(9, 63) = 7.38, p < 0.05$ ) significantly fewer spindles / Up-state were found in the ISM compared to ISM segments ( $p < 0.05$ ).

**Table 5.3:** The relative spindle density in relation to the ISM in the mPFC of WT mice. The average spindle density  $\pm$  SEM is shown for each mPFC subregion (ACC, IL, PrL, DP) and ISM segment (non-ISM, pre-ISM, ISM, post-ISM), in WT mice (N = 8).

	<b>Non-ISM</b>	<b>Pre-ISM</b>	<b>ISM</b>	<b>Post-ISM</b>
<b>ACC</b>	0.86 $\pm$ 0.06	0.77 $\pm$ 0.06	0.65 $\pm$ 0.05	0.67 $\pm$ 0.05
<b>PL</b>	0.79 $\pm$ 0.05	0.77 $\pm$ 0.07	0.65 $\pm$ 0.06	0.65 $\pm$ 0.05
<b>IL</b>	0.78 $\pm$ 0.06	0.79 $\pm$ 0.07	0.68 $\pm$ 0.07	0.68 $\pm$ 0.06
<b>DP</b>	0.77 $\pm$ 0.07	0.77 $\pm$ 0.08	0.65 $\pm$ 0.07	0.64 $\pm$ 0.07

## 5.4. Discussion

### 5.4.1. *Summary of the main findings*

The main findings of our characterisation of the ISM in WT mice in the mPFC and CA1 regions of the hippocampus are presented below:

- The ISM had a periodicity of ~3.5 min (0.0047 Hz) in the mPFC, and of ~3.9 min (0.0042 Hz) in the CA1 region of the hippocampus, and lasts ~1 min.
- In the mPFC during the ISM there was an increase in beta band power on the Up-state and an increase in theta, beta and gamma band power on the normally “silent” Down-state, compared to non-ISM segments.
- The peak power on the Up-state was lower during the ISM, pre-ISM and post-ISM segments compared to non-ISM periods, in all frequency bands in the mPFC, and in the beta and gamma frequency bands in the CA1 region.
- In both the mPFC and hippocampus, the ISM had greater power across all frequency bands on the Up- and Down-states during the ISM compared to pre-ISM and post-ISM segments.
- The SO / theta band power ratio was lower during the ISM compared to the non-ISM period.
- In both the mPFC and hippocampus, the ISM segments had a greater SO amplitude and frequency, and shorter and less variable Up- and Down-states over time, compared to the non-ISM segment.
- Neurons in the mPFC changed their firing rate in different ways during the ISM, with ~40% of neurons increasing their firing rate compared to non-ISM periods.
- In the mPFC, the ISM had a lower relative spindle density during the ISM compared to the non-ISM segment.

### 5.4.2. *The ISM is characterised by a shift of power to higher frequency bands*

The most important feature of the ISM was a marked change in the power of the high frequency oscillations occurring during the SO. First, we looked at the average power on the Up-state, which is the part of the SO where higher frequency oscillations are expected to occur (Steriade et al., 1993b), and found that in the mPFC the ISM was characterised by an increase in beta band power. Interestingly, the ISM was also characterised by an increase in theta, beta and gamma band power on the normally

neuronally “silent” Down-state. In the CA1 region of the hippocampus, there was also a significant increase in power in these frequency bands on the Up- and Down-states during the ISM, but only in relation to the pre-ISM and post-ISM segments (discussed later at section 5.4.6). However, there was a clear trend for a general increase in high frequency power on the Down-state in the CA1 as well, especially in the gamma frequency range. Thus, our analysis confirmed our observation that the ISM is an event characterised by an increase in oscillatory power across a range of frequency bands, partly due to an increase in beta power on the Up-state but mostly due to “abnormal” high frequency activity on the Down-state.

We also looked at the peak power and the latency to the peak power on the normalised SO cycle (Down-state + Up-state). We found that, as expected, the peak power occurred on the Up-state in all frequency bands: theta, beta, gamma, high-gamma. However, in the mPFC the peak power was lower during the ISM compared to the non-ISM segment, in all frequency bands. This is an interesting finding as we also found that during the ISM, higher frequency oscillatory power on the Up-state was mostly unaltered or, in the case of beta band power, it was increased. Similarly, in the CA1 region, the peak power on the Up-state was lower during the ISM than the non-ISM segment, in the theta and gamma frequency ranges. Therefore, our findings suggest that the peak power of high frequency activity occurs in a more distributed manner on the Up-state.

### **5.4.3. *The ISM does not reflect the activated state***

Although the ISM shares some similarities with the spontaneous alternations observed in natural sleep states described previously by Clement and colleagues (2006) and later by others in rodents under urethane-induced anaesthesia (Pagliardini et al., 2013; Zhurakovskaya et al., 2016), there are also key differences. In terms of the similarities, the activated states are characterised by a shift of power from the SO to the theta band (Clement et al., 2008), with the resulting increase in SO/theta power ratio being used to identify the activated state in relation to the deactivated state (Pagliardini et al., 2013). Similarly, we found an increase in ratio of SO and theta absolute power (PSD) during the ISM. The activated state is also characterised by an increase in gamma band power (Pagliardini et al., 2013) and indeed, we found greater gamma band power on the Down-state in both the mPFC and CA1 region of the hippocampus during the ISM. Finally, the ISM similar to activated states had an abrupt

onset (Clement et al., 2008) with a sudden increase in fast oscillatory activity that could be seen visually in the spectrogram.

However, there are numerous differences between activated states and the ISM, which lead us to believe they are not exactly the same phenomena. One of the main differences is that we do not see a loss of the SO and a clear emergence of theta during the ISM, as would be expected with the activated states (Clement et al., 2008). In fact, the SO increases in both frequency and amplitude, clearly demonstrating that the ISM is not a REM-like transition. Moreover, the ISM had a much shorter periodicity (approx. 3.5 min) than the activated/deactivated state cycles (approx. 9 min; Clement et al., 2008; Pagliardini, Gosgnach and Dickson, 2013). One could argue that this discrepancy can be attributed to different levels of anaesthesia. In the previously mentioned studies, anaesthesia was achieved and maintained via intravenous urethane administration (Pagliardini et al., 2013; Clement et al., 2008), while we induced anaesthesia via intraperitoneal injections. Hence, the plane of anaesthesia could have been less constant in our study. However, we had no eye blink or pedal withdrawal reflexes suggesting that the animals were indeed under deep anaesthesia. Furthermore, Clement et al. (2008) did not find changes in the periodicity of activated/inactivated states with deeper levels of anaesthesia and although they did not investigate more superficial levels of anaesthesia, they concluded that the activated state had a consistent periodicity irrespective of anaesthesia level. Thus, we believe that this discrepancy in periodicity between the ISM and activated/deactivated states cannot be fully attributed to the plane of anaesthesia.

Another key difference between the ISM and the activated states is that in addition to the increase in REM-like activity in the theta and gamma band power (on the Down-state) that is expected in the activated-state, we also see an increase in beta band power during the ISM. Specifically, we found a significant increase of beta band power on both the Up- and Down-state in the mPFC during the ISM compared to non-periods. A similar trend for an increase in beta band power on the Down-state during the ISM is seen in the CA1 as well. These findings indicate a particular role for beta frequency activity during the ISM in the mPFC. The frequency range used here for the beta band overlaps with the gamma frequency range as described by Pagliardini and colleagues (25 – 40 Hz). Thus, the increase in power that we observe in the beta band could correspond to an increase in gamma activity as described by Pagliardini et al.

(2013). On the other hand, the increase in beta band power during the ISM could be distinct and functionally significant, as will be discussed below. Finally, we found a decrease in spindle density during the ISM compared to non-ISM periods in the mPFC. In contrast, both the activated states under urethane anaesthesia and REM during natural sleep are preceded by intense spindle activity in the rodent cortex instead (Clement et al., 2008).

#### **5.4.4. *The ISM is an infra slow oscillation (ISO)***

An alternative family of rhythms that have been reported to occur during NREM sleep and which more closely resemble the ISM, are the infra-slow oscillations (ISO). ISOs have been observed under urethane anaesthesia in the rodent hippocampus (Penttonen et al., 1999), auditory cortex and thalamic and brain-stem nuclei (Filippov et al., 2008), and in a number of brain regions during natural sleep (see review by Palva & Palva, 2012). Several studies have also described ISOs in both the human (Ko et al., 2011; Vanhatalo et al., 2004), and monkey cortex (Leopold et al., 2003), where they regulate activity in the theta, alpha and beta/gamma frequency bands during sleep or awake states (review by Watson, 2018).

One of the best studied ISOs during sleep seen in humans is the cyclic alternating pattern (CAP), composed of microactivation periods that reflect cortical arousal (phase A) and their intermediate SWS periods (phase B) (Introduction section 1.4.6, Terzano and Parrino, 1993; Parrino et al., 2006). The A phase can be further categorised into subtypes according to the percentage of SWA activity present: subtype A1 is composed mostly of SWA (> 80%), with 20% of activity being low-voltage fast activity. Subtype A2 contains about 50% - 80% of SWA, and the rest is low-voltage fast activity, while subtype A3 is predominantly consists of faster activity (> 50%) (Parrino et al., 2006). Although the cyclic nature of CAP and the ISM are comparable, CAP has a frequency of 0.002 – 0.02 Hz, while the ISM has a lower frequency of 0.005 Hz. However, considering that our experiments are in a mouse model of sleep under urethane anaesthesia, it is not impossible that the two rhythms are related.

One possibility is that the ISM is related to A1 subtype CAP modulations. A1 events, which drive the staging of NREM sleep, are characterised by slow, high-amplitude activity such as delta bursts or K-complexes, while a train of A1 events can be seen to coalesce within the SO (Mendez et al., 2016; Parrino et al., 2006). Hence,

the A1 modulation contains higher frequency activity that is integrated in the SO, similarly to the ISM. In rodents, a CAP A1-like rhythm was described by Lecci and colleagues (2017) in naturally sleeping mice, in four cortical regions including the mPFC (Lecci et al., 2017; Manconi et al., 2017). The rodent rhythm had a frequency of 0.02 Hz and has also been identified in the human supplementary somatosensory cortex during sleep, with a similar duration and interval (Lecci et al., 2017; Lázár et al., 2019). This 0.02 Hz rhythm was deemed important for memory consolidation in humans, as it was preceded by SWRs in the CA1, and crucial for “sleep protection” against perturbations (Lázár et al., 2019). Hence, if the ISM we have observed is similar to the ISO described by Lecci and Lazar, then this suggests the ISM may also have a key role in in sleep protection and memory consolidation as well.

One of the key similarities of the 0.02 Hz rhythm and the ISM is that the 0.02 Hz rhythm is also accompanied by increased theta and beta band power (16 – 20 Hz), although this result was not discussed further by the authors (Lecci et al., 2017). However, the 0.02 Hz rhythm was also characterised by increased sigma (10 – 15 Hz) power during NREM sleep and the occurrence of spindles. Although we did not investigate power in the sigma frequency range, we found a decrease in spindle density during the ISM compared to non-ISM periods in the mPFC. Moreover, the 0.02 Hz rhythm has the highest frequency in the CAP frequency spectrum (0.02 – 0.05 Hz) which is much faster than the ISM frequency in the mPFC (0.005 Hz). The 0.02 Hz rhythm also has double the duration of the ISM (110 s). Again, these discrepancies might relate to the effect of urethane anaesthesia on sleep patterns, although this assumption needs to be verified. In conclusion, although the ISM and 0.02 Hz rhythms have a similar power content, the different time-frames and the decrease in spindle activity suggest that the two rhythms are distinct.

Alternatively, the ISM could reflect an A3 subtype CAP modulation. A3 events can manifest as alpha activity, polyphasic bursts and arousals as described by the American Academy of Sleep Medicine (AASM), which involve a shift of SO frequency power to theta, alpha and beta rhythms (Parrino et al., 2012). Although the A3 CAP subtype has only been characterised in humans so far, it appears to contain higher frequency oscillations, similarly to the ISM. In addition, A3 events are characterised by < 50% SWA, suggesting a shift of power from the SO to higher frequencies (Parrino et al., 2006). In our study, we found a decrease SO/theta power ratio during the ISM,

although we did not investigate the actual percentage power content of the ISM for each frequency band. Finally, A3 events are believed to offer a window for assessing the current levels of sleep and, under the right circumstances, they can induce a transition from NREM to REM sleep. In our study, we do not see REM/activated states but we believe that the level of anaesthesia could have influenced the capacity of the A3/ISM events to shift NREM sleep to a REM state, although the A3 modulation may still be evident.

Bearing in mind that the main characteristic of the A1 subtype CAP modulation is an increase in spindles (Lecci et al., 2017) and we did not see that during the ISM, together with the spectral content of the ISM, we can propose that the ISM is most likely an A3-like and not an A1-like event. During natural sleep or lower urethane anaesthesia levels it is possible that if the ISM corresponds to an A3-like event it could shift the NREM state to REM sleep. The A1 modulation might not be as evident under anaesthesia in the mPFC, as it is not prominent in this region anyway (Lecci et al., 2017). A study in mice during natural sleep would help elucidate this theory.

#### **5.4.5. *Neurons change their firing in different ways in relation to the ISM***

The analysis of single neuron firing in the mPFC during the ISM was inconclusive. In view of our findings of increased high frequency oscillatory activity on the Down-state during the ISM compared to the other segments, we also expected to see an increase in neuronal firing on Down-state. However, we only found a significant decrease in unit firing / SO coherence during the ISM compared to the non-ISM segment, which suggests a trend to more aberrant firing. In order to delineate this inconsistency, we closely inspected the raster plots showing neuronal firing for each unit, and noticed that different neurons changed their firing in different ways during the ISM. About 40% of neurons increased their firing during the ISM, while the remainder showed either no change or a decreased firing rate.

Our findings of different neuronal firing responses in relation to the ISM, can be explained by the observation that that NREM sleep homogenises neuronal activity (Watson et al., 2016). Specifically, sleep appears to upscale slow-firing pyramidal neurons, and to decrease the activity of fast-firing pyramidal neurons in the cortex, which correspond to strong and weak synapses respectively (Vyazovskiy et al., 2009). During “arousals” such as A3-like events, or during activated states, it is proposed that

these neurons would revert to their normal firing patterns (Watson et al., 2016). Most pyramidal neurons are considered to be of the “fast-spiking” compared to the “slow-spiking” type (Watson et al., 2016), and hence, they would decrease their firing rate during the SO. However, these suppressed “fast-spiking” cells could revert back to their high frequency spiking activity during the ISM, explaining our findings of an increase in neuronal firing rate during these events in about 40% of the recorded units.

#### **5.4.6. *The pre-ISM and post-ISM periods are functionally important***

Sleep-related ISOs have also been quantified as periods of reduced high frequency activity instead of periods of greater high frequency activity (Miyawaki et al., 2017). The small-amplitude irregular activity observed in the mPFC, hippocampus and thalamus of naturally sleeping rats, is characterised by long-lasting periods of suppressed activity during NREM sleep that lasts longer (~ 4.5 s) than a Down-state (Bergmann et al., 1987; Jarosiewicz, McNaughton and Skaggs, 2002). These so-called LOW states are characterised by decreased neuronal firing along with a reduction in spindles and in oscillatory activity in the hippocampus, PFC and thalamus (Miyawaki et al., 2017). Although the LOW state does not describe an ISM-related event, LOW periods have been described to occur before and after periods of high-neuronal activity (Miyawaki et al., 2017). Pre-ISM segments were also characterised by a decrease in oscillatory activity in relation to the ISM, in both the mPFC and CA1 of the hippocampus. Thus the pre-ISM segments resemble LOW states.

The pre-ISM segment in our study had longer Up- and Down-states and a lower SO frequency compared to the ISM, but it was not significantly different compared to the non-ISM segment. This finding was surprising, as we had noticed that the ISM was often preceded by an abnormally long Down-state. However, statistical analysis did not verify our observation in terms of average SO frequency, Down-state length or Down-state length variability, likely due to averaging our variables across each 30 s pre-ISM segment and then across recordings and animals. In a later analysis we could analyse a shorter pre-ISM segment, to assess the apparent prolonged Down-state in more detail. Moreover, the unit firing analysis did not provide reliable insight about the pre-ISM and post-ISM segments, except that they have a higher unit firing / SO coherence compared to the ISM period. This finding shows that the pre-ISM and post-ISM segments are characterised by well-timed firing during the SO cycle. We would also expect to see a decrease in unit firing on the Up-state during the pre-ISM and

post-ISM segments compared to the ISM, that would correspond to the decrease seen in high frequency power in the SO cycle. However, probably due to the variable behaviour of single units in relation to the ISM we did not see such effects.

Whether or not the pre-ISM period reflects the LOW states described by Miyawaki et al. (2017), the notion that high activity states are preceded by periods of low activity levels could still be relevant to the ISM. Periods of reduced activity just before energy-demanding events are considered necessary for cellular repair and restoration of organelles (Miyawaki et al., 2017). A homeostatic hypothesis may also apply to the post-ISM period, which also had lower oscillatory power on the Up- and Down-states, compared to the ISM periods. The post-ISM period appears as an intermediate period between ISM and non-ISM periods in terms of state lengths and their variability. Thus, the post-ISM period likely constitutes a period of adaptation back to the baseline SO and possibly, serves as a period of restoration. Overall, we believe that the ISM is an ISO, possibly initiated by a period of reduced activity (long Down-state) followed by a period intense activity (the ISM) and then a gradual return to baseline levels (post-ISM).

#### **5.4.7. *The ISM could be initiated by the thalamus or the cholinergic system***

The thalamus is the most prominent ISO generator, as it produces a widely described ISO characterised by cyclic paroxysms of action potentials with a 0.02 – 0.2 Hz frequency (Destexhe et al., 1998). This rhythm is believed to be the result of astrocytic releases of ATP, occurring with a frequency of 0.003 - 0.1 Hz (Parri & Crunelli, 2001). During NREM sleep, the phase of the thalamic 0.02 - 0.2 Hz rhythm controls oscillations at 2 – 4 Hz and the amplitude of alpha oscillations nested in their troughs of the slower oscillation (Vanhatalo et al., 2004; Lőrincz et al., 2015). In turn, alpha oscillations control the occurrence of theta, beta and gamma oscillations in different brain regions (Hughes et al., 2011; Palva & Palva, 2012). Thus, the 0.02 – 0.2 Hz rhythm, although much faster than the ISM (0.005 Hz in the mPFC, 0.004 Hz in the CA1), appears to control higher frequency oscillatory activity in a similar manner.

The thalamus is a heavily interconnected region and, therefore, influences numerous cortical regions such as the mPFC, and sub-cortical structures such as the hippocampus. The deep layers of the mPFC are heavily connected to the thalamus, with inter-laminar connections driving feedforward inhibition between corticothalamic

circuits, mediating processes of sensation, perception and consciousness (Cruikshank et al., 2012; Riga et al., 2014). The thalamocortical projections also synapse directly with PV+ interneurons in the superficial cortical layers, promoting the generation of beta/gamma rhythms (Lemieux et al., 2015). Moreover, the thalamus can influence the cortical SO, as an Up-state is elicited immediately after a burst of firing in thalamic cells (Destexhe et al., 1998), as well as hippocampal pyramidal cells (Bertram & Zhang, 1999). Hence, the thalamus could alter the SO frequency and faster oscillations nested on the Up-state in both the mPFC and CA1, in a synchronous and prominent way as the ISM does.

As discussed earlier, our hypothesis is that the ISM may reflect the CAP, A-type event seen in humans during natural sleep (Terzano and Parrino, 1993; Parrino et al., 2006). The exact origin of CAP is still unknown, but it is believed to result from a thalamo-cortical interplay (Parrino & Vaudano, 2018). In human subjects, it has been proposed that A1 activity is driven by thalamocortical inputs to the cortex, a theory that also fits the spindle-manifestation of A1 events (Ferri et al., 2008). On the other hand, A3 activity may be the result of the resting state networks (RSNs) which can be influenced by sub-cortical structures such as the thalamus (Mendez et al., 2016). The thalamus is the main pacemaker of alpha activity (Bazanov & Vernon, 2014) and has been shown to participate in RSNs (De Luca et al., 2006). Hence, it is reasonable that A3 induces increases in power in the theta and beta/gamma frequency bands that are regulated by alpha frequency activity, similarly to our study.

The generation of the A3 event in the thalamus is believed to rely on the influence of the dorsal ascending reticular activating system (ARAS) pathway (Terzano & Parrino, 2000), which is pivotal for controlling the alternations between NREM sleep, REM sleep and waking. In fact, cholinergic neurons in the PPT/LDT nuclei in the brainstem cholinergic system directly modulate the thalamus (Brown et al., 2012). Thus, since these cholinergic nuclei control the REM to NREM sleep transitions, they likely modulate the A3 event, which occurs right before REM sleep starts (Parrino et al., 2006). If the ISM is indeed similar to the A3 CAP event then it might also be controlled by cholinergic inputs (Terzano and Parrino, 2000). However, to confirm the hypothesis that the ISM and A3 events are the same, we should investigate whether the ISM is followed by REM states under lighter urethane anaesthesia (Clement et al., 2008).

The cholinergic system could also influence the cortex and hippocampus directly via projections from the basal forebrain (BF) cholinergic system. The BF cholinergic system is part of the ventral ARAS pathway that is also involved in the homeostasis of NREM sleep, REM sleep and waking (Brown et al., 2012). Moreover, the BF cholinergic system participates in the regulation of RSNs including the DMN, and could, therefore, also be involved in the modulation of higher-frequency oscillations through RSN function (Nair et al., 2018).

Whether the ISM is related to the A3 CAP modulation or not, we firmly believe that it most likely reflects a thalamic and/or a cholinergic phenomenon. Nevertheless, to confirm our hypothesis we would have to conduct the appropriate pharmacological and/or electrophysiological manipulation of the thalamic and BF cholinergic nuclei to see how these alter the ISM.

#### **5.4.8. *The ISM influences the SO***

Another important finding that we have not discussed so far is an increase in SO frequency during the ISM that can be attributed to a decrease in both Up- and Down-state lengths. As extensively argued in the Chapter 4, the SO cycle is governed by the local balance of inhibition and excitation (Neske, 2015). Therefore, it is not surprising that under a state of altered excitation/inhibition (E/I) such as during the ISM, the SO is also influenced. The E/I balance that drives the SO can also be influenced by thalamocortical inputs. As discussed in the above section, the thalamus can induce the generation of Up-states in the cortex, resulting in an increase in Up-state number and shorter Down-states as seen during the ISM (Lemieux et al., 2014). Thus, changes in local mPFC neuronal circuits and/or in the thalamocortical inputs that possibly drive the ISM, could lead to a shift in the E/I balance that governs the SO in the cortex and in shorter Up- and Down-states. As discussed earlier, the cortical SO also influences the hippocampal SO rhythm (Sharma et al., 2010).

Another important observation is an increase in SO amplitude during the ISM. Although we do not know how the ISM affects the SO amplitude, we can postulate that an increase in neuronal activity contributing to the SO may be the reason. Oscillation amplitude is proportional to the number of cells firing simultaneously (Reichinnek et al., 2010). Furthermore, both the SO frequency and amplitude have been positively correlated with the number of activate synapses during learning (Molle et al. 2011,

Tononi and Cirelli, 2006). Thus, it is possible that ultimately the ISM induces the participation of more neurons in the SO, giving rise to a greater SO amplitude and frequency. In fact, thalamocortical neurons contact the dendrites of pyramidal cells in cortical layer 5 of the rodent prefrontal cortex (Rah et al., 2015) where the Up-state is generated (Lőrincz et al., 2015), and PV+ interneurons in cortical layer 1 (Cruikshank et al., 2012). In the ISM, the increased activity of both neurotransmitter systems would promote not only the aforementioned changes in the SO but would also influence higher-frequency oscillations and neuronal firing.

## **5.5. Conclusion**

The ISM is a period characterised by an increase in power in high frequency oscillatory power during the Up-state, but especially during the normally neuronally “silent” Down-state. Moreover, the SO persists during the ISM, but is characterised by an increase in frequency and amplitude. In addition, the ISM is characterised by a decrease in spindle density while different neurons change their firing patterns in different ways, with 50% increasing their firing. Although we cannot be sure of the exact nature of the ISM, we believe that it is a thalamically and/or cholinergically driven ISO that modulates higher frequency activity in a number of regions, including the mPFC and CA1 of the hippocampus. It is possible that the ISM reflects an A3 subtype CAP modulation and/or that is related to the activity of resting state networks. Finally, we believe that the ISM is of functional importance and should be investigated further to understand its generation and functional significance.

## **Chapter 6. The ISM in A30P animals**



## 6.1. Introduction

Sleep architecture and quality is affected early in the disease course in LBD patients (Pao et al., 2013). Polysomnographic studies in DLB patients and PDD patients have shown poor sleep continuity, longer sleep onset and REM sleep latency, RBD and reduced REM sleep (Terzaghi et al., 2013; Pao et al., 2013). A recent video-polysomnographic analysis in DLB patients showed additional features including persistence of wake-like activity (alpha/theta) occipitally, intermittent rhythmic delta frontally and rapid-eye movement and sustained EMG activity at sleep onset (Fernández-Arcos et al., 2019). DLB patients also had transient sharp waves in NREM sleep, low-frequency sleep spindles in stage N2, an absence of sleep spindles and K complexes in NREM sleep, and a delta slowing during REM sleep (Fernández-Arcos et al., 2019). Overall, such a broad range of sleep-related activity dysfunction would be expected to affect the normal generation and function of slow-wave sleep (SWS). Abnormalities in SWS in DLB patients could then impact cognition and memory consolidation (Guarnieri & Sorbi, 2015), and the clearance of the toxic by-products of cellular activity (Bohnen & Hu, 2019).

Changes in sleep architecture (sleep staging) are also expected to coincide with changes in sleep microstructure, the smaller building components of the different sleep stages (Carnicelli et al., 2019). In the previous chapter, we postulated that the ISM constitutes an ISO, possibly related to the CAP A-subtype modulation seen in humans during sleep (Parrino et al., 2012). Alternatively, the ISM may mirror a different type of ISO, as several ISOs have been described in rodents during sleep or anaesthesia (Lőrincz et al., 2015; Lecci et al., 2017; Hughes et al., 2011). Whatever the mechanism that underlies the ISM we have observed in WT mice, it reflects the state of the underlying network and could be informative about possible perturbations due to disease.

In view of the changes in both the SO and the fast oscillations associated with the Up-state that we have observed in A30P mice (Chapter 4), we wanted to determine whether there were also any changes in the ISM that could arise from the  $\alpha$ -syn pathology.

## **6.2. Methods**

### **6.2.1. *Animals and recordings***

In order to compare the pre-ISM, ISM, post-ISM and non-ISM segments between WT and A30P animals, we used the same WT recordings used in Chapter 5 to characterise the ISM (section 5.2.1). Hence, we had 8 mPFC and 7 CA1 recordings from WT animals. The A30P cohort originally consisted of 22 animals, out of which 1 did not have ISM. We obtained recordings from the mPFC and/or the CA1 regions from these animals and after rejecting a few recordings on the grounds of excessive noise or due to broken electrode contacts (section 4.2.1), we analysed 13 mPFC and 8 CA1 recordings from A30P mice. One of the CA1 recordings was excluded from power-related analyses due to small urethane-anaesthesia breathing artefacts, but it was included in the SO state length analysis.

The non-ISM data used for this analysis are the same data used in Chapter 4, for both WT and A30P animals, while all of the WT animal ISM data are that presented in Chapter 5. Hence, the data used in this analysis are derived from the initial 30 min-long recordings described in the Methods section 2.2.1. The anaesthesia regime, frame mounting and electrode insertion techniques are also as described previously in sections 2.2.2 – 2.2.3. It is important to highlight that during these recordings the animals were under deep anaesthesia characterised by the SO ( $< 1$  Hz), and the absence of a pedal withdrawal reflex. We also utilised the same unit data for the mPFC as in section 4.3.3.

### **6.2.2. *ISM variable extraction***

Firstly, we compared the mean ISM duration and periodicity between genotypic groups (WT, A30P). Moreover, we looked at the characteristics of the SO cycle and specifically at the average amplitude and frequency of the SO, the length of the Up- and Down-segments and SO cycle, as well as the length variability of these segments over time. We also analysed the average high frequency oscillatory power on the Up- and Down-states, as well as the peak power and the latency to the peak on the normalised SO cycle. All the above-mentioned variables were extracted for the ISM segments (non-ISM, pre-ISM, ISM, post-ISM), in the mPFC subregions (ACC, PrL, IL, DP) and in the CA1. For each segment we also calculated the relative spindle density (spindle number / Up-state number) and the unit firing properties for the mPFC region.

### **6.2.3. Statistical analysis**

To compare the ISM characteristics (frequency and duration) in A30P and WT animals in the mPFC, we performed mixed rmANOVA analysis with the mPFC subregion (ACC, PrL, IL, DP) as the repeated variable and the genotype as the between subjects variable. To analyse the SO cycle, amplitude, frequency and state lengths and oscillatory power in the SO cycle, we performed mixed rmANOVA analyses with the ISM segment (non-ISM, pre-ISM, ISM and post-ISM) and mPFC subregion as the repeated measures, and the genotype as the between-subjects variable. Upon finding a significant effect of genotypic group or a genotype/segment interaction, we performed univariate ANOVA analysis with a Bonferroni correction for that segment for the PrL region, unless a genotype/region effect was found when we performed univariate ANOVA analysis for each segment/region combination.

Regarding our analysis for the CA1 region of the hippocampus, we performed univariate ANOVA analysis for the core characteristics of the ISM. For the rest of the hippocampal data, i.e. SO cycle, amplitude, frequency and state lengths and oscillatory power in the SO cycle, we performed mixed rmANOVA analysis with the ISM segment as the repeated measure and the genotypic group as the between-subjects variable. Follow-up univariate ANOVA analysis with a Bonferroni correction was performed upon identifying a significant effect of genotype, for each ISM segment. The effects of segment and/or region for the mPFC and CA1 can be found in the Appendix section specified.

## 6.3. Results

### 6.3.1. *The ISM core characteristics in A30P mice*

In order to determine whether over-expression of human mutant  $\alpha$ -syn had an impact on the occurrence of the ISM, we compared the frequency and duration of ISM events between A30P and WT mice. As performed in the analysis of WT mice (Chapter 5), we looked at 30 min-long recordings from the period immediately after a stable SO was obtained following induction of anaesthesia (Figure 6.1A).

In the mPFC, data from 13 A30P animals showed that the average ISM interval was  $4.5 \pm 0.21$  min, which translates to an ISM frequency of  $0.0037 \pm 0.0004$  Hz, compared to an ISM interval of  $3.7 \pm 0.2$  min and an ISM frequency of  $0.0045 \text{ Hz} \pm 0.0003$  Hz in the mPFC of WT animals ( $N = 8$ ; Figure 6.1B). The mean ISM duration in A30P animals was  $0.95 \pm 0.05$  min while the mean variability of ISM duration was  $0.38 \pm 0.05$ s. In WT animals, the mean ISM duration was  $1 \pm 0.11$  min, while the mean variability of ISM duration was  $0.38 \pm 0.05$  min (Figure 6.1C).

In the CA1 of the hippocampus of A30P animals ( $N = 8$ ), the mean ISM interval was  $3.8 \pm 0.31$  min that corresponds to an ISM frequency of  $0.0044 \pm 0.0005$  Hz, compared an average  $3.89 \pm 0.35$  min-long ISM intervals and an ISM frequency of  $0.0043 \text{ Hz} \pm 0.0006$  Hz in WT animals ( $N = 7$ ). The mean ISM duration  $1.11 \pm 0.11$  min and the variability between ISM events in the same animal was  $0.5 \pm 0.1$  min. In WT animals, the ISM duration was  $0.95 \pm 0.02$  min while the variability in the duration of ISM events within the same recording was  $0.29 \pm 0.09$  min.

Statistical analysis between WT and A30P animals for the mPFC region showed a significant difference in interval length, which were longer ( $F(1, 19) = 6.48, p < 0.05$ ) in A30P compared to WT animals (Figure 6.1C). Ultimately, this translates to a lower ISM frequency in A30P compared to WT animals in the mPFC. No group differences were found in ISM duration, or duration variability in the mPFC (Figure 6.1D), or in any ISM characteristic for the CA1 region of the hippocampus.

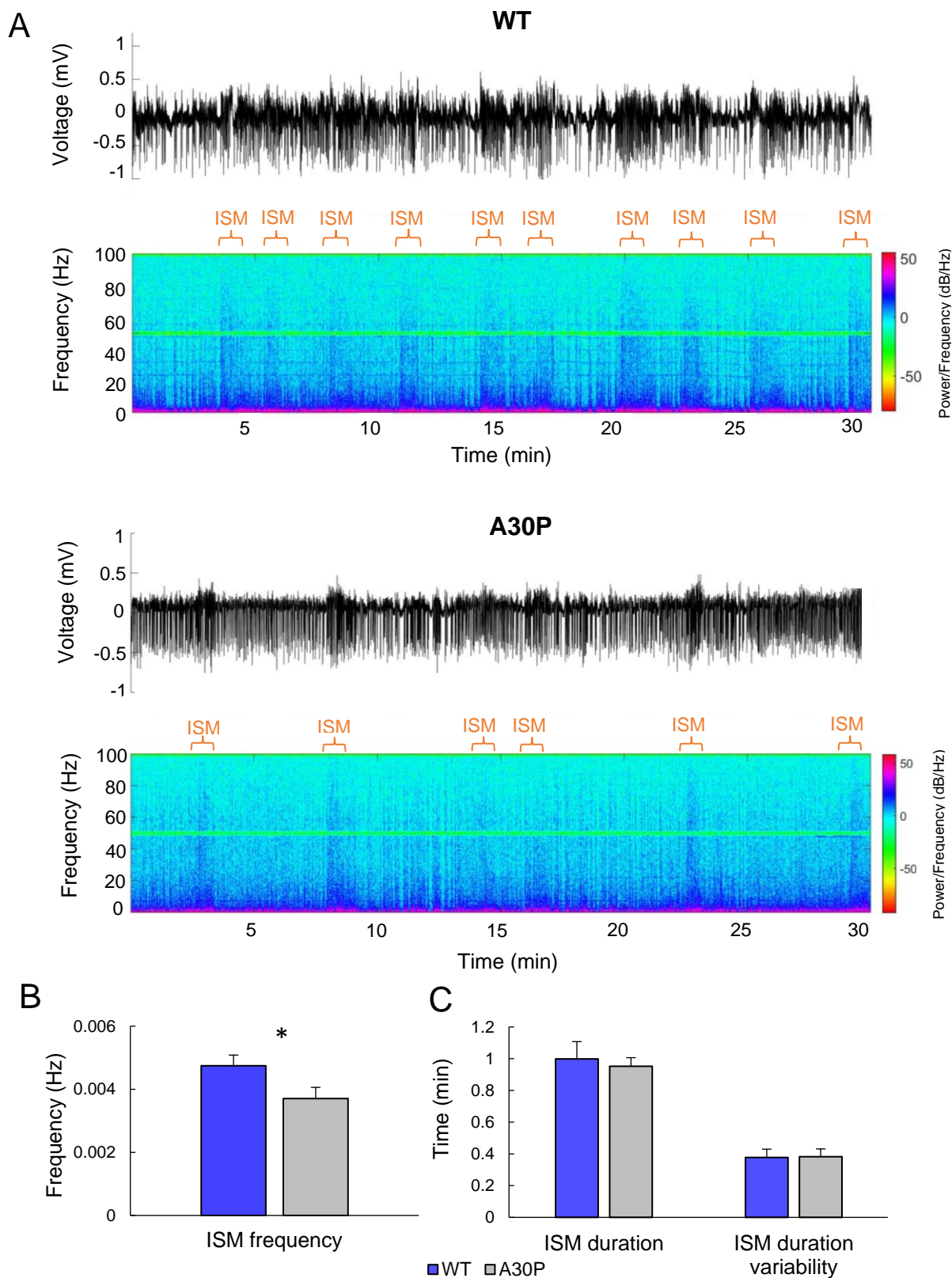


**Figure 6.1:** Changes in ISM frequency in the mPFC of A30P mice. **A)** Examples of the LFP and spectrogram in the PrL subregion of the mPFC. 30 min long extracellular field recordings are shown from a WT and A30P animal. **B)** The ISM frequency and **C)** the average ISM duration and duration variability over time, for the mPFC of 8 WT (blue) and 13 A30P (grey) animals. Error bars indicate the SEM. Asterisks indicate statistical significance:  $* = p < 0.05$ .

### 6.3.2. ***High frequency oscillatory activity in A30P mice during the ISM***

In Chapter 4, we reported that there were no major differences in the high frequency oscillatory power in the SO cycle between A30P and WT animals, during non-ISM periods. We did however identify an increase in latency to the peak power in the beta and gamma frequency bands in the mPFC, and an increase in latency to the peak power in the gamma frequency band in the CA1, in A30P mice. Furthermore, in Chapter 5, we found that in WT animals the ISM was characterised by increases of power in high frequency oscillatory activity, especially during the normally “silent” Down-state. Hence, we were interested to examine whether A30P animals exhibited changes in the ISM in terms of high frequency oscillatory activity in the SO cycle. Thus, we examined the power content of the SO for the different ISM segments, for four frequency bands that were deemed of physiological importance: theta (4 – 7.9 Hz), beta (8 – 14.9 Hz) and gamma (30 – 79.9 Hz) and high-gamma (80 – 130 Hz). In our analysis we included 8 WT and 13 A30P animals for the mPFC region analysis, and 7 WT and 7 A30P animals for the CA1 region analysis. The variables of interest were the average power on the Up-state and the Down-state, and the peak power and the latency to the peak power in the normalised SO cycle, for each frequency band.

#### 6.3.2.1. *A30P mice show no changes in high frequency oscillatory power in the mPFC during the ISM*

Our analysis in the mPFC revealed an effect of segment and/or region in a number of variables. All the values can be found in Appendix C and the statistical analysis in Appendix G. However, we found no differences between genotypes or any interactions between the segment and region with the genotype.

#### 6.3.2.2. *A30P mice have increased high frequency oscillatory power in the hippocampus during the ISM*

In contrast to the mPFC, our analysis in the hippocampus revealed extensive differences in high frequency oscillatory activity in the SO cycle between A30P and WT animals (Figure 6.2). Regarding the mean high frequency oscillatory power on the Up-state (Figure 6.2A) we found that it was significantly greater in A30P animals in all frequency bands investigated: theta ( $F(1, 12) = 11.89, p < 0.01$ ), beta ( $F(1, 12) = 9.69, p < 0.01$ ), gamma ( $F(1, 12) = 5.71, p < 0.05$ ) and high-gamma ( $F(1, 12) = 4.9, p < 0.05$ ). Post-hoc univariate analysis showed that this difference between groups occurred in the pre-ISM, ISM and post-ISM segments but not in the non-ISM periods,

consistent with our data shown in Chapter 5 (section 5.3.2.2). High frequency oscillatory power on the Down-state (Figure 6.2B) was also greater in A30P compared to WT mice in all frequency bands: theta ( $F(1, 12) = 16.27, p < 0.01$ ), beta ( $F(1, 12) = 24.04, p < 0.001$ ), gamma ( $F(1, 12) = 15.2, p < 0.01$ ) and high-gamma ( $F(1, 12) = 6.87, p < 0.05$ ), in the pre-ISM, ISM and post-ISM segments but not in the non-ISM segment.

The peak power on the Up-state also differed between groups in the beta ( $F(1, 12) = 8.13, p < 0.05$ ) and theta ( $F(1, 12) = 6.76, p < 0.05$ ) frequency ranges (Figure 6.2C). Although there was no significant effect of genotype or a genotype/segment interaction regarding the gamma peak power, the p-value for an effect of genotype was quite low ( $p = 0.053$ ). Although the partial Eta squared value was large (0.713) indicating a large effect size (Ferguson, 2009), we decided to proceed with post-hoc analysis for this variable as well. Univariate ANOVA analysis for the peak power showed a significant increase in theta, beta and gamma peak power in A30P mice during the ISM segment, compared to WT animals. Moreover, A30P mice had a higher beta and gamma peak power in the post-ISM segment, and a higher beta peak power in the pre-ISM segment, compared to WT mice. The latency to peak power did not differ between genotypic groups for any frequency band. Analysis of the non-ISM data in Chapter 4 showed a significant increase in latency to peak gamma power in A30P mice, but was not statistically significant in this analysis where the ISM segments were also considered. All the values can be found in Appendix D.

To summarise, the mean high frequency oscillatory power on the Up- and Down-states was greater in A30P animals during the ISM and the periods preceding and following these events, compared to WT animals. However, there were not differences in high frequency oscillatory power in the SO cycle during non-ISM periods, between the two genotypes. The theta, beta and gamma peak power was also higher during the ISM in A30P compared to WT mice, while an increase in high frequency peak power was also observed in the pre-ISM and post-ISM segments in these animals. Analysis of the ISM properties revealed interesting differences between WT and A30P animals that were not be observed during the non-ISM segments.

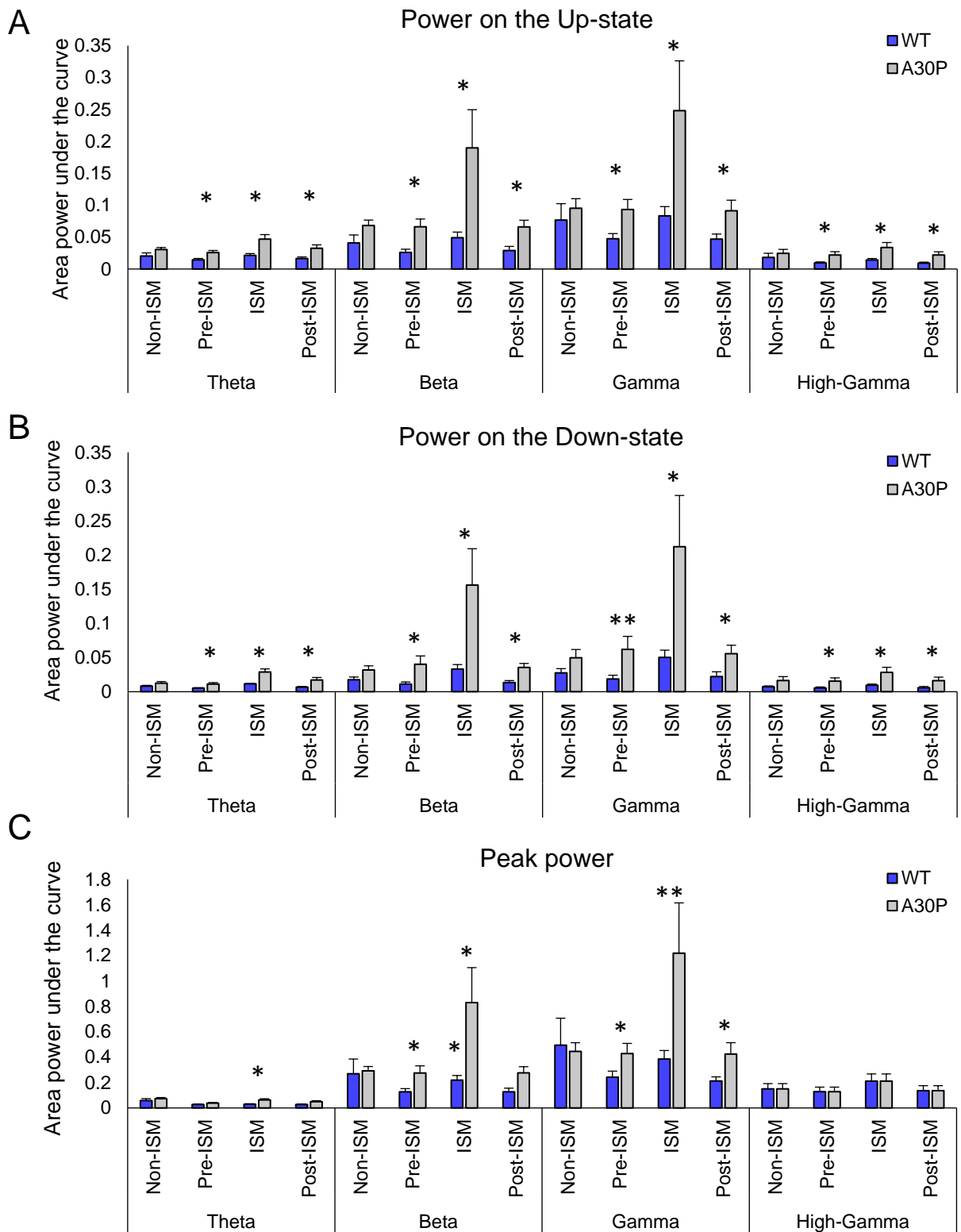


**Figure 6.2:** Changes in high frequency oscillatory power in the SO cycle in relation to the ISM in the hippocampus of A30P mice. **A)** The mean power on the Up-state, **B)** the mean power on the Down-state and **C)** the latency to peak power on the normalised SO cycle (Down-state + Up-state), in the theta (8 – 14.9 Hz), beta (15 – 29.9 Hz), gamma (30 – 79.9 Hz) and high-gamma (80 – 130 Hz) frequency bands, during the non-ISM, pre-ISM, ISM and post-ISM segments, in WT (N = 7) and A30P (N = 7) animals. Error bars indicate the SEM. Asterisks indicate significance: \* =  $p < 0.05$ , \*\* =  $p < 0.01$ .

### 6.3.3. *The properties of the SO in A30P mice during the ISM*

In Chapter 4, we showed that A30P animals had a higher SO frequency, shorter Up- and Down-states, and less state-length variability over time compared to WT animals in both the mPFC and CA1 regions. Moreover, in Chapter 5, where we characterised the ISM in WT animals we found a number of changes in the SO during these events including an increase in amplitude and frequency and shorter Up- and Down-states. We therefore wondered whether additional changes would be observed in the SO in A30P mice during the ISM. Thus, we proceeded to compare the SO characteristics in the ISM segments (non-ISM, pre-ISM, ISM, post-ISM), in the mPFC subregions and in the CA1 region of the hippocampus, in WT and A30P animals. The variables of interest were the SO frequency and amplitude, the mean SO cycle, Down-state and Up-state lengths and the mean variability of these variables over time. We analysed 8 WT and 13 A30P recordings from the mPFC, and 7 WT and 8 A30P recordings from the CA1.

#### 6.3.3.1. *A-syn related changes in the SO cycle in the mPFC during the ISM*

Our rmANOVA analysis revealed no differences in SO amplitude between A30P animals and WT animals, and no interactions between the genotype and the segment or region regarding this variable (Figure 6.3A). However, we did find a significant effect of genotype in the SO cycle length ( $F(1, 19) = 4.43, p < 0.05$ ) and Up-state length ( $F(1, 19) = 5.25, p < 0.05$ ). We also found a genotype/segment interaction in the SO frequency ( $F(3, 57) = 4.07, p < 0.05$ ) and the Up-state ( $F(3, 57) = 4.16, p < 0.05$ ), Down-state ( $F(3, 57) = 6.6, p < 0.01$ ) and SO cycle length ( $F(3, 57) = 7.7, p < 0.001$ ). Thus, we proceeded with univariate ANOVA analysis for these variables, for each segment/region combination, to compare between genotypic groups (Figure 6.3B,C).

The follow-up analysis revealed that A30P animals had a significantly higher SO frequency compared to WT animals during the non-ISM segments in all mPFC subregions (ACC, PrL, DP:  $p < 0.01$ ; IL:  $p < 0.05$ ; Figure 6.3B). A similar difference between the two groups was also shown in the pre-ISM segment in the DP subregion ( $p < 0.05$ ). A30P animals also had a shorter SO cycle compared to WT animals during the non-ISM segment in all mPFC subregions (ACC, PrL, DP:  $p < 0.01$ ; IL:  $p < 0.05$ ), and during the pre-ISM segment, in the DP and ACC subregions ( $p < 0.05$ ; Figure 6.3C). Moreover, A30P mice had shorter Down-states compared to WT mice during the non-ISM (ACC, PrL:  $p < 0.01$ ; DP:  $p < 0.01$ ), pre-ISM (ACC, DP:  $p < 0.05$ ) and

post-ISM segments (DP:  $p < 0.05$ ). Finally, the Up-state was shorter in A30P animals compared to WT animals in the non-ISM, pre-ISM and post-ISM segments in the PrL subregion ( $p < 0.05$ ), while the post-ISM segment was also shorter in the DP subregion ( $p < 0.05$ ; Figure 6.3C).

The initial rmANOVA analysis also revealed a significant effect of genotype over the length variability of the SO cycle ( $F(3, 57) = 18.27, p < 0.001$ ), the Up-state ( $F(3, 57) = 19.36, p < 0.001$ ) and Down-state ( $F(2.76, 52.57) = 14.64, p < 0.001$ ; Figure 6.3D), over time. Furthermore, we found significant genotype/segment interactions in the SO cycle length variability ( $F(8.15, 53.6) = 9.23, p < 0.001$ ) and Down-state length variability over time ( $F(2.77, 52.57) = 8.82, p < 0.001$ ). Thus, we proceeded with univariate ANOVA analysis for the Up-state, Down-state and SO cycle length variability, for each segment / mPFC subregion combination. We found that A30P mice had significantly lower SO cycle length variability compared to WT animals during the non-ISM and pre-ISM segments in all mPFC subregions ( $p < 0.01$ ), and during the post-ISM segment in the PrL ( $p < 0.05$ ) and DP ( $p < 0.01$ ) subregions. A30P mice also had a lower Down-state length variability compared to WT mice during the non-ISM and pre-ISM segments in all mPFC regions ( $p < 0.01$ ), and during the post-ISM region in the DP ( $p < 0.01$ ) and PrL subregions ( $p < 0.05$ ). Finally, A30P animals had shorter Up-state length variability compared to WT animals during the non-ISM and pre-ISM segments, in the DP ( $p < 0.01$ ;  $p < 0.05$ ) and PrL ( $p < 0.05$ ) subregions. An influence of segment and/or region was also found for these variables (Appendix E; Appendix H.i)

In this analysis we replicated our previous findings outlined in Chapter 4 of an increase in SO frequency, shorter SO cycle and Down-state lengths, as well as lower SO cycle, Up-state and Down-state length variability over time, in non-ISM segments, in A30P animals compared to WTs. The findings of a decrease in SO cycle, Up-state, Down-state length variability over time in A30P mice also persist in the pre-ISM and post-ISM segments. However, the only difference between genotypic groups during the ISM is a decrease in Up-state length in A30P animals that is also seen in the pre-ISM and post-ISM segments.

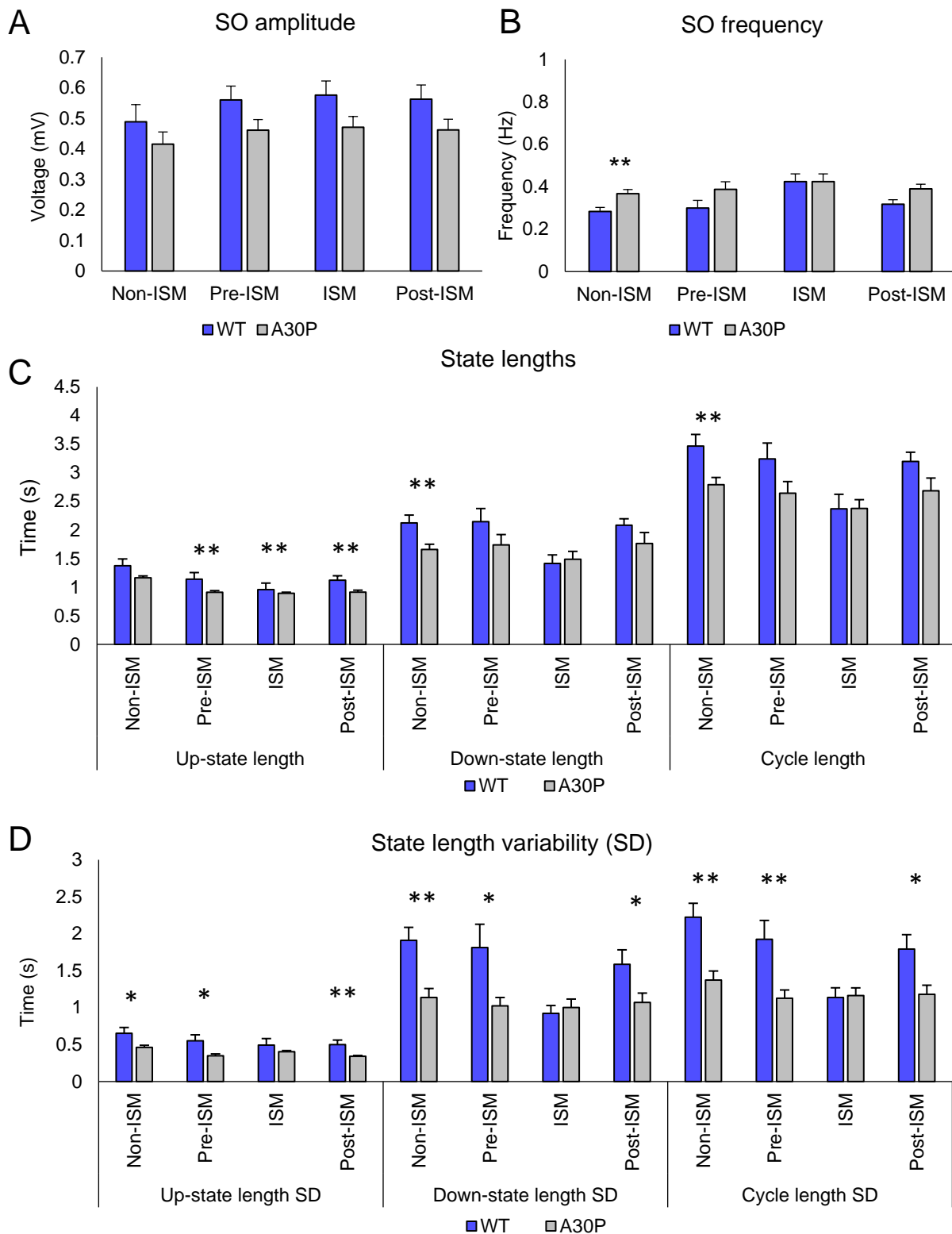


**Figure 6.3:** Changes in the SO cycle in relation to the ISM in the PrL subregion of the mPFC of A30P mice. **A)** The SO amplitude, **B)** SO frequency, **C)** the mean Up-state, Down-state and cycle lengths and **D)** the variability of state-length variables in time (SD), during the non-ISM, pre-ISM, ISM and post-ISM segments, in WT (N = 8) and A30P (N = 13) animals. Error bars indicate the SEM. Asterisks indicate significance: \* =  $p < 0.05$ , \*\* =  $p < 0.01$ , \*\*\* =  $p < 0.001$ .

### 6.3.3.2. A-syn related changes in the SO cycle in the hippocampus during the ISM

Analysis of the SO amplitude in the CA1 region of the hippocampus did not reveal a significant difference between genotypic groups. However, our analysis did show a significant interaction between the genotype and segment. Follow-up univariate ANOVA analysis showed that A30P animals had a lower SO amplitude during the ISM and post-ISM segments, compared to WT animals (Figure 6.4A). We also found a clear effect of genotype in SO frequency ( $F(1, 13) = 8.4, p < 0.05$ ), cycle length ( $F(1, 13) = 10.45, p < 0.01$ ) and Up-state length ( $F(1, 13) = 10.44, p < 0.01$ ). Follow-up univariate ANOVA analysis showed that A30P mice had a higher SO frequency (Figure 6.4B), and a shorter SO cycle length and Up-state length (Figure 6.4C) compared to WT mice, in the non-ISM, pre-ISM and post-ISM segments. Regarding Down-state length, we did not find a significant effect of group but there was a segment/group interaction ( $F(1.79, 23.32) = 12.26, p < 0.001$ ). Univariate analysis for each segment showed that A30P mice had significantly longer Down-states in the non-ISM segment compared to WT mice (Figure 6.4C). Finally, we found that A30P animals showed less variability over time in Down-state length ( $F(1, 13) = 21.31, p < 0.001$ ) and SO cycle length ( $F(1, 13) = 36.03, p < 0.001$ ), in all segments (Figure 6.4D). A significant effect of segment was evident in most variables (Appendix F, Appendix H.ii).

Our findings from the CA1 of the hippocampus regarding the SO generally replicate our findings from the mPFC region. We found that A30P mice had a higher SO frequency and shorter SO cycles, Up-states and Down-states as well as lower variability over time in the lengths of these variables, in the non-ISM, pre-ISM and post-ISM segments, compared to WT mice. We also replicated the finding of shorter Up-states during the ISM in A30P mice. The most interesting finding from the CA1 region was a decrease in SO amplitude in A30P animals that is significant in the ISM and post-ISM segments, while it appears to extend to the other segments of the ISM as well.

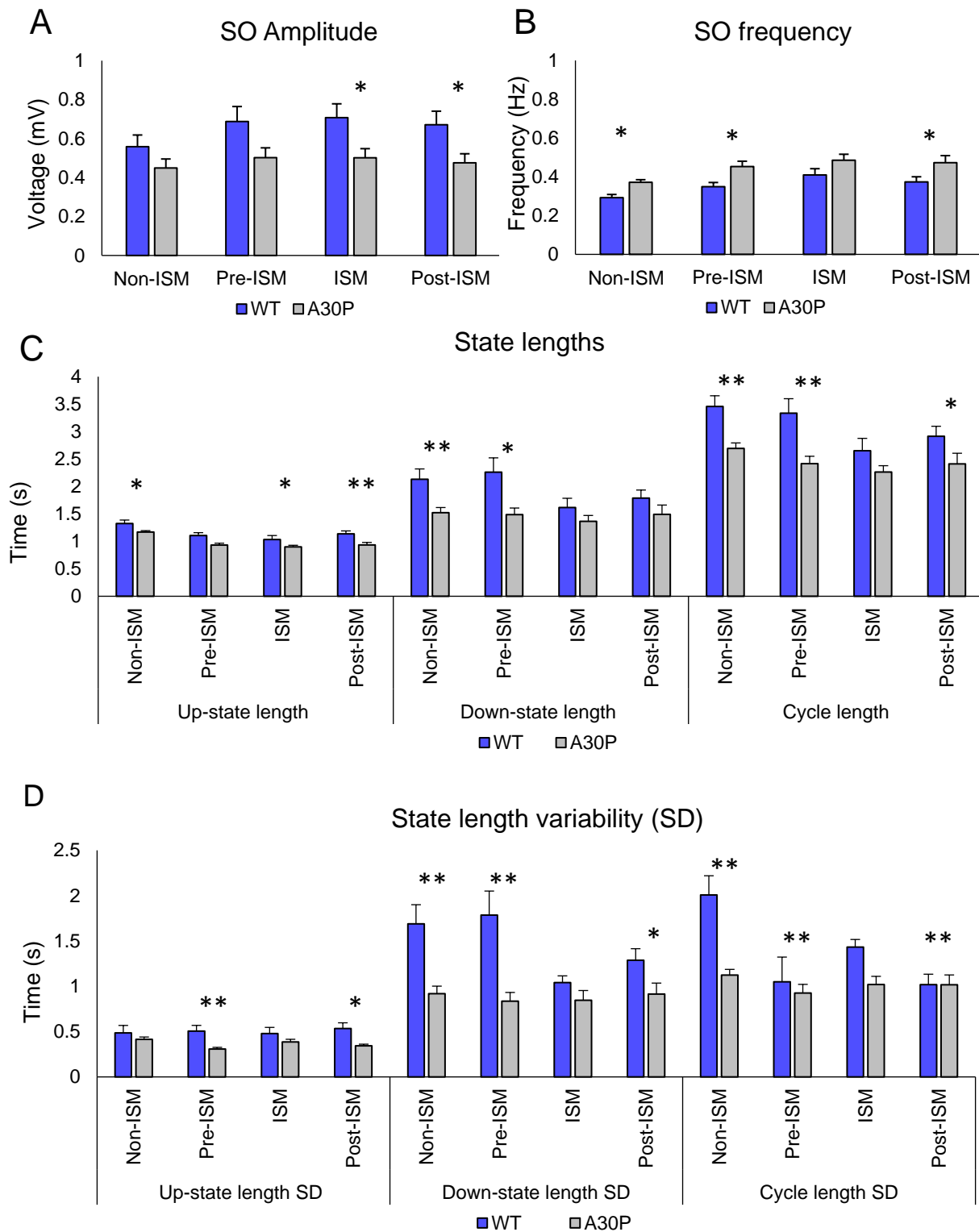


**Figure 6.4:** Changes in the SO cycle in relation to the ISM in the hippocampus of A30P mice. **A)** The SO amplitude, **B)** SO frequency, **C)** the mean Up-state, Down-state and cycle lengths and **D)** the variability of these variables in time (SD), during the non-ISM, pre-ISM, ISM and post-ISM segments, in WT (N = 7) and A30P (N = 8) animals. Error bars indicate the SEM. Asterisks indicate statistical significance: \* =  $p < 0.05$ , \*\* =  $p < 0.01$ , \*\*\* =  $p < 0.001$ .

### 6.3.4. *The relative spindle density does not change in A30P mice during the ISM*

We found no differences in the relative spindle density measured by the number of spindles / Up-state number, in any segment of the ISM in A30P compared to WT mice ( $F(1, 19) = 2.81, p = 0.11$ ; Table 6.1).

**Table 6.1:** The relative spindle density in relation to the ISM in the mPFC of WT and A30P animals. The average relative spindle density (spindle number / Up-state number)  $\pm$  SEM is shown for the mPFC subregions (ACC, PrL, IL and DP), for the non-ISM, pre-ISM, ISM and post-ISM segments, in WT (N = 8) animals and A30P (N = 13) mice.

	WT				A30P			
	Non-ISM	Pre-ISM	ISM	Post-ISM	Non-ISM	Pre-ISM	ISM	Post-ISM
ACC	1.14 $\pm$ 0.13	0.99 $\pm$ 0.123	0.8 $\pm$ 0.13	0.86 $\pm$ 0.1	0.86 $\pm$ 0.06	0.77 $\pm$ 0.06	0.65 $\pm$ 0.05	0.67 $\pm$ 0.05
PrL	1.01 $\pm$ 0.08	0.94 $\pm$ 0.09	0.77 $\pm$ 0.1	0.80 $\pm$ 0.07	0.79 $\pm$ 0.05	0.77 $\pm$ 0.07	0.65 $\pm$ 0.06	0.65 $\pm$ 0.05
IL	0.96 $\pm$ 0.08	0.93 $\pm$ 0.09	0.74 $\pm$ 0.08	0.78 $\pm$ 0.01	0.78 $\pm$ 0.06	0.79 $\pm$ 0.07	0.68 $\pm$ 0.07	0.68 $\pm$ 0.06
DP	1 $\pm$ 0.08	0.94 $\pm$ 0.09	0.76 $\pm$ 0.09	0.79 $\pm$ 0.08	0.77 $\pm$ 0.07	0.77 $\pm$ 0.08	0.65 $\pm$ 0.07	0.64 $\pm$ 0.07

### 6.3.5. *Changes in neuronal firing patterns in A30P mice during the ISM*

As outlined above in Chapter 4 (section 4.3.3) we know that during the non-ISM segment A30P mice had increased firing on the Down-state, and a lower SO/unit firing coherence in the mPFC, compared to WT animals. In Chapter 5 (section 5.3.5) we showed that putative pyramidal neurons in the mPFC of the WT group changed their firing rate during the ISM in variable ways, with approximately 40% of the cells increasing their firing rate during the ISM, while the rest of the neurons either decreased or had no change in firing rate. Moreover, in section 6.3.2.1 we showed that A30P mice did not have any changes in high frequency oscillatory activity in the SO cycle compared to WT animals during the ISM in the mPFC region, that could indicate a similar neuronal firing activity in the two genotypic groups. However, we proceeded to specifically investigate for any alterations in unit firing activity in A30P mice during the ISM in the mPFC region.

We therefore assessed five properties of neuronal firing in WT and A30P animals during the ISM including: the spike frequency and ISI for the recording duration (Up- and Down-states) and only on the Up-state, and the percentage of unit firing on the Up-state, in 15 A30P and 7 WT animals with 56 and 24 units respectively (Table 6.2). The maximum unit firing / SO coherence was also investigated in 12 A30P and 7 WT animals, with 50 and 23 units respectively.

We only found a significant effect of genotype in the percentage of the total unit firing occurring on the Up-state ( $F(1, 20) = 10.07, p < 0.001$ ). Follow-up Univariate ANOVA analysis revealed that A30P mice had a lower percentage of neuronal firing occurring on the Up-state during the non-ISM ( $p < 0.05$ ), ISM ( $p < 0.01$ ) and post-ISM ( $p < 0.05$ ) segments, compared to WT mice. This finding therefore implies that a greater percentage of unit firing occurs on the normally neuronally “silent” Down-state in A30P mice. It is also worth reporting that we found a trend for an effect of genotypic groups in the unit firing / SO coherence ( $F(1, 17) = 3.88, p = 0.066$ ), and specifically a decrease in the unit firing / SO coherence in A30P compared to WT animals, although we did not proceed with a follow-up analysis for each segment.

We also performed rmANOVA analysis for each unit separately. No differences were found for the ISI and spike frequency on the Up-state, or for the total recording duration (Figure 6.5A,B). This analysis also revealed a significantly lower percentage of the total neuronal firing occurring on the Up-state ( $F(1, 77) = 6.07, p < 0.05$ ), and a lower unit firing / SO coherence in A30P compared to WT animals ( $F(1, 66) = 7.16, p < 0.01$ ; Figure 6.5C). Post-hoc analysis showed that A30P animals had a significantly lower percentage of unit firing occurring on the Up-state compared to WT animals, in the non-ISM and ISM segments. The unit firing / SO coherence was significantly lower in A30P animals in all segments of the ISM (Figure 6.5D).

The differences we identified between A30P and WT animals are consistent with differences that we showed in the SO analysis in Chapter 4. Interestingly, we found that the increased aberrant firing, reflected by a lower percentage of firing on the Up-state and decreased unit firing / SO coherence, also persists in the ISM and the pre-ISM and post-ISM segments in A30P animals.

**Table 6.2:** Unit firing patterns in relation to the ISM in the mPFC of WT and A30P mice. The average of each variable  $\pm$  SEM was calculated both across animals (WT: N = 7; A30P N = 15), and units (WT: N = 23, A30P: N = 56), in each genotypic group. Variables also shown in Figure 6.5 are in *Italics*.

<b>Characterisation of averaged units</b>								
	<b>WT</b>				<b>A30P</b>			
<b>Variable</b>	<b>Non-ISM</b>	<b>Pre-ISM</b>	<b>ISM</b>	<b>Post-ISM</b>	<b>Non-ISM</b>	<b>Pre-ISM</b>	<b>ISM</b>	<b>Post-ISM</b>
Spike frequency / recording duration (Hz)	1.28 $\pm$ 0.19	1.26 $\pm$ 0.2	1.37 $\pm$ 0.21	1.47 $\pm$ 0.22	1.58 $\pm$ 0.28	1.69 $\pm$ 0.22	1.75 $\pm$ 0.23	1.76 $\pm$ 0.25
Spike frequency on the Up-state (Hz)	3.18 $\pm$ 0.56	2.72 $\pm$ 0.42	2.84 $\pm$ 0.44	3.04 $\pm$ 0.45	3.01 $\pm$ 0.5	3.28 $\pm$ 0.43	3.17 $\pm$ 0.41	3.18 $\pm$ 0.43
ISI for the recording duration (s)	1.04 $\pm$ 0.23	1.17 $\pm$ 0.17	0.98 $\pm$ 0.18	0.93 $\pm$ 0.15	1.83 $\pm$ 0.65	1.45 $\pm$ 0.24	1.24 $\pm$ 0.18	1.32 $\pm$ 0.25
ISI on the Up-state (s)	0.29 $\pm$ 0.06	0.34 $\pm$ 0.08	0.33 $\pm$ 0.07	0.29 $\pm$ 0.06	0.38 $\pm$ 0.05	0.31 $\pm$ 0.04	0.32 $\pm$ 0.03	0.35 $\pm$ 0.04
Firing on the Up-state (%)	91.59 $\pm$ 2.3	93.04 $\pm$ 3.2	92.88 $\pm$ 2.11	90.62 $\pm$ 2.76	79.71 $\pm$ 3.39	81.31 $\pm$ 4.41	78.71 $\pm$ 3.04	77.66 $\pm$ 3.75
Unit firing / SO coherence	0.71 $\pm$ 0.07	0.74 $\pm$ 0.05	0.65 $\pm$ 0.06	0.71 $\pm$ 0.04	0.54 $\pm$ 0.06	0.6 $\pm$ 0.04	0.52 $\pm$ 0.05	0.58 $\pm$ 0.05
<b>Single unit characterisation</b>								
	<b>WT</b>				<b>A30P</b>			
<b>Variable</b>	<b>Non-ISM</b>	<b>Pre-ISM</b>	<b>ISM</b>	<b>Post-ISM</b>	<b>Non-ISM</b>	<b>Pre-ISM</b>	<b>ISM</b>	<b>Post-ISM</b>
Spike frequency / recording duration (Hz)	1.22 $\pm$ 0.14	1.24 $\pm$ 0.14	1.34 $\pm$ 0.15	1.44 $\pm$ 0.16	1.89 $\pm$ 0.23	1.88 $\pm$ 0.2	2.02 $\pm$ 0.21	2.04 $\pm$ 0.21
Spike frequency on the Up-state (Hz)	2.94 $\pm$ 0.37	2.63 $\pm$ 0.3	2.79 $\pm$ 0.33	2.93 $\pm$ 0.34	3.66 $\pm$ 0.44	3.76 $\pm$ 0.41	3.7 $\pm$ 0.39	3.74 $\pm$ 0.4
<i>ISI for the recording duration (s)</i>	1.25 $\pm$ 0.22	1.28 $\pm$ 0.14	1.09 $\pm$ 0.15	1.06 $\pm$ 0.13	1.1 $\pm$ 0.13	1.29 $\pm$ 0.17	1.06 $\pm$ 0.11	1.13 $\pm$ 0.15
<i>ISI on the Up-state (s)</i>	0.33 $\pm$ 0.04	0.33 $\pm$ 0.05	0.33 $\pm$ 0.04	0.32 $\pm$ 0.04	0.31 $\pm$ 0.03	0.27 $\pm$ 0.02	0.29 $\pm$ 0.03	0.3 $\pm$ 0.03
<i>Firing on the Up-state (%)</i>	89.55 $\pm$ 1.61	91.98 $\pm$ 2.42	90.88 $\pm$ 1.35	88.07 $\pm$ 1.74	83.49 $\pm$ 1.59	86.45 $\pm$ 1.8	81.11 $\pm$ 1.9	82.02 $\pm$ 1.99
<i>Unit firing / SO coherence</i>	0.72 $\pm$ 0.04	0.77 $\pm$ 0.02	0.68 $\pm$ 0.03	0.75 $\pm$ 0.03	0.57 $\pm$ 0.04	0.65 $\pm$ 0.02	0.58 $\pm$ 0.03	0.64 $\pm$ 0.02

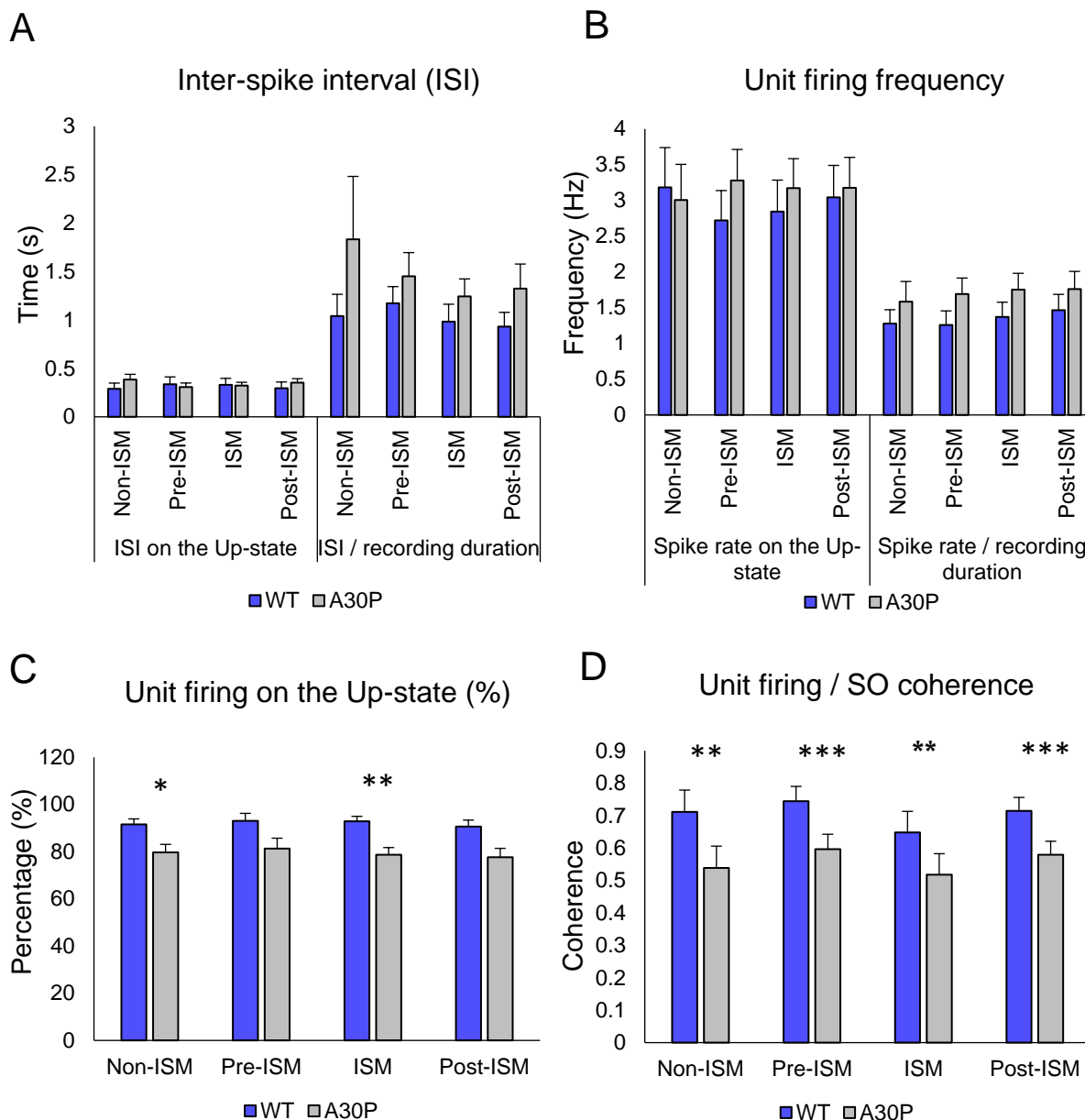


**Figure 6.5:** Changes in neuronal firing patterns in relation to the ISM in the mPFC of A30P mice. **A)** The average inter-spike interval (ISI) on the Up-state and for the recording duration (Up-state + Down-state). **B)** The spike rate on the Up-state and for the recording duration (Up-state + Down-state). **C)** The percentage of unit firing that occurs on the Up-state. **D)** The unit firing / SO coherence. These variables were investigated in the non-ISM, pre-ISM, ISM and post-ISM segments in WT mice (N = 7) with 23 units and in A30P mice (N = 15) with 56 units. Each variable was averaged across all units, irrespective of animal. Error bars show the SEM. Asterisks indicate significance: \* =  $p < 0.05$ , \*\* =  $p < 0.01$ , \*\*\* =  $p < 0.001$ .

## 6.4. Discussion

### 6.4.1. *Summary of the main findings*

Here we summarise the most important differences in SO patterns found between WT and A30P animals during the ISM.

- A30P animals had a lower ISM frequency (0.0037 Hz) compared to WT animals (0.0045 Hz), only in the mPFC region.
- In the CA1 region of the hippocampus, A30P animals had increased power in all frequency bands on the Up- and Down-states during the pre-ISM, ISM and post-ISM segments, and a greater theta, beta and gamma peak power during the ISM, compared to WT mice. No changes were seen in Up-state associated high frequency oscillations in the mPFC of A30P mice.
- In the mPFC and CA1 regions, A30P mice had shorter Up-states during the ISM, pre-ISM and post-ISM segments compared to WT mice.
- In the CA1 region of the hippocampus, A30P animals had lower SO amplitude in the ISM and post-ISM segments compared to WT animals.
- In the mPFC, A30P animals had a greater percentage of the total firing occurring on the Down-state and a decreased unit firing / SO synchrony during the pre-ISM, ISM and post-ISM segments, compared to WT animals.

### 6.4.2. *A30P mice show an increase of high frequency oscillatory activity in the hippocampus during the ISM*

We have shown in Chapter 5 that in WT mice, the ISM is accompanied by an increase in beta frequency power on the Up-state in the mPFC region. Moreover, we found that WT mice had an increase in power in the theta, beta and gamma frequency bands on the normally neuronally “silent” Down-state during the ISM, in both the mPFC and CA1 regions. In this chapter where we compared the ISM between A30P and WT animals, we found that A30P animals showed an even larger increase in high frequency oscillatory power on both the Up- and Down-states during the ISM. However, this increase in high frequency oscillatory power was specific for the CA1 region of the hippocampus, adding to our hypothesis from Chapter 4 that the CA1 region of the hippocampus of A30P mice is hyperexcitable. In the mPFC region in A30P mice, we did not see changes in high frequency oscillatory power during the ISM. However, in the mPFC there was more aberrant neuronal firing in relation to the SO

cycle, specifically, an increase in the percentage of the total firing occurring on the Down-state and a decrease in unit firing / SO coherence. These findings replicate the changes in the non-ISM segments as outlined in Chapter 4 and suggest that the local mPFC circuit is also hyperexcitable in A30P mice. Ideally, these observations of changes in unit firing patterns would also be tested in the hippocampus of A30P mice, but we did not have sufficient unit data from that region.

#### **6.4.3. A30P animals have hyperexcitable networks generating high frequency oscillations**

As described above, A30P animals showed a greater increase in high frequency oscillatory power in the SO during the ISM in the CA1 region of the hippocampus, compared to WT animals. Such an increase in oscillatory power suggests that the excitation/inhibition (E/I) balance that governs the local neuronal circuit has shifted towards excitability in A30P mice. A change in fast oscillation power can be related back to the neurons generating the high frequency rhythms in the hippocampus (Ferguson & Gao, 2018). We know that gamma/high-gamma frequency activity relies on feedback loops between pyramidal cells and PV+ interneurons in the CA3 region of the hippocampus, and are then relayed to the CA1 region via the Schaffer collaterals (Buzsáki & Silva, 2012), both during the awake state and the Up-state of the SO (Destexhe et al., 2007). High-gamma frequency activity is generated mostly in the EC and is also relayed to the CA1 region (Colgin et al., 2009). Although the CA1 is also capable of generating its own gamma/high-gamma activity *in vitro*, the *in vivo* recorded gamma/high-gamma activity in the CA1 reflects the influence of the CA3 and EC rhythms over this region (Craig & McBain, 2015). Hence, hyperexcitability in pyramidal neurons and/or in PV+ interneurons in the above mentioned hippocampal circuits could result in an increase in gamma/high-gamma frequency power in the CA1 of the hippocampus during the ISM (Rebollo et al., 2018), as seen in A30P animals.

The CA3 region of the hippocampus can also produce theta and beta frequency oscillations that influence the CA1 region, both *in vitro* through carbachol application and *in vivo*, during REM sleep, through the activation of mAChRs (Cantero et al., 2003). As argued in the previous chapter (section 5.4.3), we do not believe that the ISM reflects REM sleep but similar mechanisms of generating theta frequency oscillations could be implicated in REM sleep and the ISM, especially if the ISM is an ACh-mediated rhythm as considered in section 5.4.7. Beta and gamma frequency

oscillations can also be induced by carbachol *in vitro*, and rely on GABA<sub>A</sub>R and AMPAR/kainate receptor activity as the blockade of these receptors' function reduces beta/gamma oscillatory activity (Whittington et al., 2000). Thus, the ISM could boost theta, beta and gamma frequency activity, generated by the hyperexcitable pyramidal neurons in the hippocampus of A30P mice.

The increase in high frequency oscillatory power during the SO in the CA1 of the hippocampus might also relate to the known properties of the hippocampus. The hippocampus is capable of producing highly synchronous activity and is prone to epileptogenicity as it constitutes the source of hypersynchronous activity in a number of epileptic and neurodegenerative conditions (Beenhakker & Huguenard, 2009; Buzsáki, 2015; Beagle et al., 2017; Vossel et al., 2017). Recent studies have shown that DLB patients also exhibit epileptiform activity (Beagle et al., 2017) and molecular signs of hyperexcitability in their hippocampus (Morris et al., 2015). The hippocampus has also been shown to be hyperexcitable and to exhibit epileptic-like activity in  $\alpha$ -syn animal models, both *in vitro* (Tweedy et al., 2018) and *in vivo* (Morris et al., 2015). The SO offers a window of highly coherent activity, both spatially and temporally, while the hippocampal SO specifically (Wolansky et al., 2006) has been shown to lower the “epilepsy” threshold in a medio-temporal lobe epilepsy model (Nazer & Dickson, 2009). Thus, the local hippocampal SO rhythm may facilitate the large increase in high frequency seen in A30P animals.

#### **6.4.4. *A30P mice have normal levels of high frequency activity in the mPFC during the ISM***

In the mPFC of A30P mice we also observed increases in high frequency oscillatory power on the Up- or the Down-state during the ISM, but these increases were comparable to our findings in WT mice (Chapter 5). The generation of gamma/high-gamma frequency oscillations in the mPFC also relies on feedback loops between pyramidal cells and PV+ interneurons, similarly to the hippocampus (Colgin et al., 2009; Wulff et al., 2009; Mann et al., 2009; Buzsáki & Silva, 2012; Sullivan et al., 2011). Theta and beta oscillations in the cortex are generated by layer 5 pyramidal cells influenced by low-threshold spiking SOM+ interneurons in layer 1 (Li et al., 2013; Kuki et al., 2015). SOM+ and PV+ interneurons as well as pyramidal cells receive corticothalamic inputs that drive the increase in beta/gamma power on the Up-state by enhancing the aforementioned loops (Nigro et al., 2018; Lemieux et al., 2014). Hence,

in view of our hypothesis that the ISM is a thalamically-derived rhythm, as suggested in Chapter 5 (section 5.4.7), we expected to see abnormal increases in high frequency oscillatory activity during the ISM in the hyperexcitable mPFC network in A30P animals, compared to WT animals.

The fact that we did not see a significant difference in high frequency activity in the SO cycle in the mPFC of A30P mice perhaps suggests that a compensation mechanism might better preserve the E/I balance in this region at the early stage of pathology. In Chapter 4 (section 4.4.5) we suggested that PV+ interneurons may up-regulate their function in response to the hyperexcitability. This hypothesis is supported by previous findings in our lab of an increase in IPSP amplitude and frequency *in vitro* in the young A30P mice (Tweedy et al., 2018). We also proposed that pyramidal cells might down-regulate their firing activity in relation to hyperexcitability, as seen in other animal models of dementia (Palop et al., 2007). It is therefore possible that such compensation mechanisms are present in both the hippocampus and mPFC of A30P mice, successfully containing the hyperexcitability during non-ISM periods. However, the ISM causes a large increase in excitatory drive that may override the compensation mechanisms, as it is evident through the aberrant increases in high frequency oscillatory power seen in the hippocampus of A30P mice during this event. In the mPFC the compensation mechanism may be more robust, maintaining the normal levels of high frequency activity during the ISM. Alternatively, the mPFC could have a lower level of  $\alpha$ -syn pathology compared to the CA1 and thus, be less affected in terms of network activity. Further immunohistochemical studies are needed to resolve this issue, although current evidence suggest that both the mPFC and hippocampus regions exhibit early, subtle evidence of  $\alpha$ -syn pathology in A30P mice (Schell et al., 2009).

#### **6.4.5. *The pre-ISM and post-ISM segments are also altered in the CA1 in A30P mice***

In the previous chapter, we proposed that the pre-ISM and post-ISM periods are epochs of reduced activity that may be important for cellular restoration (Miyawaki et al., 2017). However, in A30P mice we found that the pre-ISM and post-ISM segments, as well as the ISM segment, had significantly greater levels of power in the theta, beta and gamma frequency bands on both the Up- and Down-states, compared to WT animals. We also saw that the pre-ISM and post-ISM segments were characterised by

an increase in peak power on the Up-state in the beta and gamma frequency bands, in A30P compared to WT mice. Again these findings were specific for the hippocampus and not replicated in the mPFC region and suggest that the pre-ISM and post-ISM might be less efficient in restoring the “neuronal fatigue” induced by high cellular activity during the ISM.

#### **6.4.6. *Possible thalamic alterations in A30P mice can influence the ISM***

So far, we have suggested that the abnormal increase in high frequency power occurring in the hippocampus during the ISM are due to  $\alpha$ -syn-induced changes in the local circuit. However, it is also possible that the external drive that generates the ISM is altered by the pathology, in addition to local circuit changes. As discussed in Chapter 5 (section 5.4.7), the ISM may be related to the thalamic ISO characterised by cyclic paroxysmal bursts of action potentials and alpha oscillations (Lorincz et al., 2009). The thalamic activity is facilitated by the activation of mGluRs and mAChRs in addition to glial waves of  $\text{Ca}^{2+}$  release. The excessive, pathology-induced activation of these receptors, and an elevated  $\text{Ca}^{2+}$  influx driven by glial cell waves, could turn these paroxysmal events into epileptiform activity (review by Watson, 2018). In fact, young A30P mice have evidence of  $\alpha$ -syn induced changes in glial cells (Tweedy et al., 2018), while  $\text{A}\beta_{1-42}$  has been shown to alter the properties of different receptors in animal models of AD (Texidó et al., 2011). Thus, while the thalamic ISO could lead to a moderate increase in high frequency oscillation power in WT mice (Lemieux et al., 2014), in A30P animals it could result in excessive increases in high frequency power that cannot be contained on the Up-state (Hughes et al., 2011; English et al., 2014), as seen in our study. This theory of hyperexcitability in the thalamus of A30P mice needs to be investigated further through local electrophysiological recordings.

#### **6.4.7. *A30P animals have altered sleep microstructure***

A key difference we observed between genotypes was that A30P animals had a lower ISM frequency (0.0037 Hz) compared to WT (0.0047 Hz) animals in the mPFC. Assuming that the ISM and A3 subtype CAP modulations are the same, or similar events (Chapter 5, section 5.4.4), a lower ISM frequency in A30P mice would be consistent with the decrease in CAP rate seen in patients with RBD. Moreover, the RBD patients who converted to DLB had fewer A1 and A3 events than those who did not convert (Melpignano et al., 2019). Similarly, MCI patients that also represent an

early dementia stage, had decreased A1 events and increased A3 events during SWS. However, in 2 years the MCI patients who developed amnesic dementia had decreased A3 and A1 events, disrupted SWS and less REM sleep (Carnicelli et al., 2019). Thus, it appears that A1 events decrease and A3 events increase at the early/prodromal dementia stage, while A3 events eventually decrease with the development of dementia. Although we would expect that young A30P animals represent a prodromal DLB stage, our results of a lower ISM event frequency match the data from the dementia converters (Carnicelli et al., 2019; Melpignano et al., 2019). Finally, a decrease in A3 events is expected in dementia because a decrease in REM sleep episodes is seen in most dementia subtypes (Hita-Yañez et al., 2013; Fernández-Arcos et al., 2019). Thus, it is possible that if the ISM and A3 modulation are indeed the same event, fewer REM events could occur during natural sleep or lighter urethane anaesthesia in A30P animals.

The fact that the reduced frequency of ISM events is seen in the mPFC of A30P animals and not the CA1, which is the region mostly affected in terms of high frequency oscillatory power, appears contradictory. A possible explanation is that the hippocampus and mPFC respond in different ways to a common thalamic or cholinergic ISM source, as previously argued. This assumption may relate back to the fact that the hippocampus has its own SO rhythm (Wolansky et al., 2006). Although the hippocampal SO is modulated by the cortex to a large extent (Vertes et al., 2007), it can also have a separate response to stimuli (Sharma et al., 2010). On the other hand, the cortex is capable of developing compensation mechanisms to counteract changes in its input from the thalamus during SWS (Lemieux et al., 2014). It is therefore possible that the compensation mechanism that better restores the E/I balance during the ISM in the mPFC also suppresses ISM frequency and/or its effects in this region.

#### **6.4.8. *The ISM decreases the SO amplitude in the CA1 of A30P mice***

During non-ISM periods, and in most cases during the pre-ISM and post-ISM segments, we found extensive differences between A30P and WT animals in the duration of the SO and its constituent Up- and Down-states (as seen in Chapter 4). However, we did not find notable changes in the SO in A30P mice during the ISM, except for a decrease in Up-state length during the ISM in both the mPFC and CA1 of these animals compared to WT mice. Interestingly though, we found a decrease in SO amplitude in the CA1 of A30P animals, which could indicate a decrease in the number

of engaged pyramidal neurons, or a loss in synchrony of the synaptic activity (Eschenko et al., 2008; Marshall et al., 2006). This idea of a decrease in neuronal participation in the SO is consistent with the rest of our work, that supports that early  $\alpha$ -syn pathology in A30P mice has influenced neuronal function, particularly in the CA1 region of the hippocampus.

#### **6.4.9. A30P animals have a less efficient SWS**

It would be surprising if the increases in high frequency power in the SO during the ISM in A30P animals did not affect some of the essential functions of sleep, including waste clearance and memory consolidation (Porter et al., 2015). According to the glymphatic hypothesis, excess brain activation during SWS can result in lower levels of A $\beta$ , tau and likely  $\alpha$ -syn clearance (Mander et al., 2016). Inefficient clearing of these by-products of cellular function can induce cytotoxicity in local circuits, especially in regions that have fast-spiking, high energy demanding neurons like the CA1 of the hippocampus (Bohnen & Hu, 2019). Moreover, increased sleep fragmentation can induce greater production of A $\beta$ , tau and  $\alpha$ -syn (Lucey et al., 2018), that in turn further disrupts SWS, leading to a vicious cycle that drives further pathology (Ju et al., 2017). Therefore, the early changes in sleep microstructure in A30P mice could be related to early  $\alpha$ -syn pathology and contribute to disease progression.

If the ISM is an A3-like event, our result of reduced ISM frequency in the mPFC might suggest a decrease in REM sleep, as A3 events immediately precede REM transitions during natural sleep (Terzano & Parrino, 2000). Although we do not know the extent to which A3 events modulate REM sleep and vice versa, a decrease in A3 under pathological conditions may reflect the incapacity of the cortical networks to achieve > 80% SWA or to transition to a REM state (Carnicelli et al., 2019). REM sleep is essential for the dissociation of the cortex and the hippocampus during SWS, allowing for the re-arrangement of local circuits that is pivotal for memory consolidation (Watson et al., 2016). Thus, a decrease in REM sleep would also affect the efficiency of hippocampal-cortical communication and ultimately, it could affect memory consolidation in A30P animals (Staresina et al., 2015). In fact, there is evidence that A30P have an age-dependent deficiency in memory consolidation (Freichel et al., 2007). However, in view our findings in Chapter 4 of a spindle dysfunction in A30P mice, this memory deficit could also be related to an altered spindle/SWR coupling (Cox et al., 2014).

Finally, CAP A-type modulations are essential for guarding sleep against perturbations that could induce awakenings (Parrino & Vaudano, 2018). However, a loss of CAP related modulations implies that this sleep protection mechanism, enforced by A-type CAP modulations, fails more easily resulting in sleep fragmentation as seen in patients with DLB (Cagnin et al., 2017). In our study, we found a decrease in ISM frequency that, as argued earlier, is consistent with reports of a decrease in the frequency A-type CAP modulations in patients with DLB and amnesic dementia (Carnicelli et al., 2019; Melpignano et al., 2019). Hence, during natural sleep, ISM/A-type CAP events may fail to prevent sleep disruption, resulting in sleep discontinuity, a further decrease in glymphatic clearance,  $\alpha$ -syn accumulation and consequently in more sleep fragmentation (Parrino & Vaudano, 2018).

## 6.5. Conclusion

A30P animals showed greater high frequency activity on the Up- and Down-states during the ISM in the CA1 region of the hippocampus, compared to WT animals. Although the high frequency oscillatory power content of the ISM in the mPFC is comparable between A30P and WT animals, the mPFC shows more disorganised firing during the ISM in relation to the SO, and a lower ISM frequency. Moreover, in A30P mice both the mPFC and CA1 regions showed an increase in SO frequency and a decrease in SO amplitude during the ISM, compared to WT animals. We believe that our findings indicate altered E/I dynamics due to the abnormal expression of mutant  $\alpha$ -syn in A30P mice. Furthermore, we believe that both the mPFC and hippocampus in A30P animals show evidence of network hyperexcitability and possible compensation mechanisms developed in response. However, the CA1 appears unable to contain the significant excitatory drive of the ISM, likely due to the fact that its inherently more epileptogenic compared to the mPFC. These changes in high frequency activity on the Up- and Down-states that occur during the ISM in the hippocampus of A30P mice are likely to affect the essential functions of SWS, such as memory consolidation and  $\alpha$ -syn clearance and production, exacerbating the  $\alpha$ -syn pathology. In a similar way, abnormal sleep cycle or sleep-like rhythms, could also exacerbate  $\alpha$ -syn pathology and affect cognitive performance in patients with DLB.

## **Chapter 7. Discussion**



## 7.1. Overview of the main findings

In this study we analysed EEG data from patients with DLB, PDD and AD and compared findings with healthy age matched control subjects. Our analysis of human EEG data confirmed the well-established slowing of EEG power and dominant frequency (DF) from the alpha to the theta frequency range in DLB and PDD groups, compared to healthy controls and AD patients. In contrast to previous reports (Walker et al., 2000; Bonanni et al., 2008), the DF variability (DFV) over time within the theta/alpha range was similar between DLB/PDD patients and healthy controls. However, we found a DLB specific correlation between the theta DFV and slow-theta DFP, with CFs measured by the CAF score. These findings suggest that a slower, and more temporally variable DF, specifically relates to the CFs seen in DLB. We also found a significantly higher theta/alpha DFV in AD patients compared to the DLB, PDD and control groups, which is another novel finding. Previous studies had shown that AD patients only had a slight increase in DFV compared to healthy controls, and lower DFV compared to the DLB/PDD groups (Bonanni et al., 2008). Exploratory analysis showed that qEEG measures of the EEG slowing seen in DLB patients, and the increased theta/alpha DFV seen in AD patients could identify the correct diagnosis with high accuracy, sensitivity and specificity.

We were also interested to characterise the electrophysiological nature of another DLB symptom, early sleep disturbances. However, EEG sleep studies are difficult to conduct in patients with dementia. Thus, we proceeded to investigate for changes in network oscillations under urethane anaesthesia in the mPFC and CA1 of the hippocampus of A30P mice at a young age, which represent an early stage of DLB. We found that A30P mice had aberrant neuronal firing in the SO cycle in the mPFC, characterised by a greater percentage of the total firing occurring on the normally neuronally “silent” Down-state, and a lower unit firing / SO coherence. A30P animals also had a higher SO frequency in the mPFC and CA1 regions, that can be attributed to shorter Down-states, and to a lesser extent shorter Up-states. Furthermore there was a reduction in the variability of these states’ lengths over time in the A30 mice suggesting a loss of longer states. A30P animals also had an altered distribution of power on the Up-state, specifically an increased latency to the peak power in the beta and gamma bands in the mPFC, and in the gamma band in the hippocampus. Importantly, A30P animals had altered spindle patterns, including a lower spindle

density, spindle-duration and fewer high-amplitude spindles. We found no changes in SO synchrony between the cortex and hippocampus, or changes in the SWR or in high frequency oscillatory power in the SO cycle between A30P and WT animals.

During our EEG recordings in urethane-anaesthetised mice, we also observed a rhythmic phenomenon characterised by a sudden burst of activity across frequency bands. Thus, we proceeded to characterise this rhythm we termed the infra-slow modulation (ISM), in WT animals. The ISM events had a periodicity of  $3.7 \pm 0.2$  min (0.0045 Hz) in the mPFC and  $3.89 \pm 0.35$  min (0.0043 Hz) in the CA1. Analysis of the high frequency power content of the SO during the ISM showed an increase in the average beta band power on the Up-state. Moreover, the peak power in the theta, beta and gamma frequency bands on the Up-state was decreased during the ISM compared to the non-ISM segment, suggesting that the timing of the high frequency oscillatory activity on the Up-state is altered during the ISM. Moreover, the ISM was characterised by increased theta, beta and gamma power on the Down-state, where such rhythms are not normally observed. The abovementioned findings were more apparent in the mPFC compared to the CA1 region of the hippocampus, where the high frequency oscillatory power on the Up- and Down-states was greater in the ISM compared to the pre-ISM and post-ISM segments, but not the non-ISM segment.

The ISM was also characterised by a higher SO frequency and amplitude, which shows that the SO is maintained during this period, in contrast to REM sleep that involves a transition to theta frequency activity. However, we did find a decrease in the SO/theta power ratio. We also found decreased spindle activity during the ISM. The pre-ISM and post-ISM segments were characterised by lower high frequency activity compared to the ISM, and an SO frequency similar to non-ISM segments. Finally, single neurons changed their firing in different ways in response to the ISM, with about 40% of neurons in the mPFC increasing their firing rate while the rest had unaltered or reduced firing.

Finally, we compared the ISM between WT and A30P animals. Our most important finding was that A30P mice had greater high frequency activity on the Up- and Down-state in the CA1 during the ISM, compared to WT animals. Although the mPFC was not affected in terms of high frequency oscillatory power in the SO cycle, neurons exhibited a more disorganised pattern of firing during the ISM compared to non-ISM segments. These findings suggest that the neuronal networks in A30P mice

are hyperexcitable in both the mPFC and hippocampus. Moreover, A30P mice showed a decrease in SO amplitude and Up-state length during the ISM, in the mPFC and CA1 regions, compared to WT animals. Lastly, we found a lower ISM frequency in the mPFC of A30P compared to WT animals.

## **7.2. Early DLB is characterised by an excitation/inhibition imbalance**

### **7.2.1. *EEG disturbances in DLB patients***

One of the main theories regarding CF generation is that they arise due to disturbances in large-scale networks that govern resting state and attention (O'Dowd et al., 2019). Normally, the brain can shift between attentional networks and resting state networks (RSNs) such as the default mode network (DMN) in response to an internal or an external drive (Raichle, 2015). For example, the fMRI BOLD signal and hence the activity in the main DMN hubs increases during attention lapses in healthy individuals, while before such lapses, activity in the regions related to control of attention decreases (Weissman et al., 2006). These findings reflect competition between resources for internally and externally focused modes of cognition, governed by networks functioning antagonistically to one another (Buckner et al., 2008).

In DLB patients, the activity of the DMN is comparable to healthy individuals during rest, but there is evidence of DMN hypoactivity during attentional tasks (Peraza et al., 2014; O'Dowd et al., 2019; Kenny et al., 2012; Firbank et al., 2018). Moreover, in DLB patients the transitions between RSNs and attention networks are more rigid (Schumacher et al., 2018; Peraza et al., 2014; Firbank et al., 2016), while the activity of attentional networks such as the dorsal and ventral attention networks (DAN; VAN) and their interaction with the DMN is also altered (Kobeleva et al., 2017). Thus, we postulated that although the DLB patients in our study might not have a significant DFV increase, the correlation between DFV and CFs could reflect altered interactions between the DMN and the attention networks.

The abovementioned changes in network dynamics have been proposed to reflect an  $\alpha$ -syn related alteration in the E/I balance (O'Dowd et al., 2019). The DLB/PDD patient cohorts used in this study had mild cognitive decline and, at this early stage of disease progression, the levels of neurodegeneration might be low but subtler synaptic changes have been extensively described (Calo et al., 2016; Colom-Cadena

et al., 2017; Peter et al., 2018). Early synaptic dysfunction can be largely attributed to small  $\alpha$ -syn inclusions located in the pre-synaptic terminal (see review Schulz-Schaeffer, 2010). A study showed that, the majority of the pre-synaptic  $\alpha$ -syn is in the aggregated, phosphorylated form in DLB patients (Colom-Cadena et al., 2017). These small inclusions of  $\alpha$ -syn are accompanied by lower levels of the normal synaptic proteins that are crucial for synaptic release. Furthermore, there were fewer dendritic spines observed post-synaptically, showing a clear synaptic deficit (Henstridge et al., 2016; Lim et al., 2011). *In vitro* and *in vivo* studies have shown that toxic oligomeric mutant  $\alpha$ -syn can also have detrimental effects, including the formation of membrane pores that change the cell's membrane potential (Ghiglieri et al., 2018), induce mitochondrial damage and cellular stress, and impede long-term potentiation (van Diggelen et al., 2019). Thus, it is highly possible that  $\alpha$ -syn mediated toxicity could influence the ability of different regions to engage synchronously in widespread RSNs and attention networks (O'Dowd et al., 2019).

### **7.2.2. Hyperexcitability in the A30P mouse model**

In Chapter 4, we proposed that our findings of changes in the SO cycle such as an increase in SO frequency, a decrease in Up-state and Down-state length, an altered distribution of high frequency activity on the Up-state and aberrant neuronal firing can be attributed to an  $\alpha$ -syn-induced hyperexcitability in the neuronal networks. Hyperexcitability is the result of the shift in the E/I balance and thus, can be attributed to changes in the function of excitatory and inhibitory neurons (Vossel et al., 2017). In fact, studies in LBD patients and animal models have shown that mutant  $\alpha$ -syn can enter both pyramidal cells and PV+ interneurons and polymerise (Tsigelny et al., 2012; Rockenstein et al., 2014; Flores-Cuadrado et al., 2016; Martin et al., 2013). Human mutant  $\alpha$ -syn localisation has also been reported in pyramidal cells and PV+ interneurons in A30P animals (unpublished observations) that could potentially influence the activity of these neurons and the properties of the SO. Since the mPFC and hippocampus are rich in pyramidal cells and PV+ interneurons and these cells are affected by mutant  $\alpha$ -syn, we would expect alterations in these cells' function to affect both regions (Ferguson & Gao, 2018; Sparta et al., 2014).

Hyperexcitability has been more extensively described in relation to AD (Introduction 1.6.3; Jin et al., 2018; Vossel et al., 2017) although there is increasing evidence of hyperexcitability in LBD patients and animal models of  $\alpha$ -

synucleinopathy. A recent study found that DLB patients had an 11.5% cumulative probability of developing seizures compared to 13.4% in AD and 5% in FTD, while DLB patients were by far the most likely to develop myoclonus with a probability of 58.1% (Beagle et al., 2017). A relationship between the incidence of myoclonus and DLB was also shown by a second study that also identified molecular changes indicative of hyperexcitability in the hippocampi of these patients (Morris et al., 2015). The same study also looked at a mouse model of  $\alpha$ -syn with evident epileptiform activity in the parietal cortex (Morris et al., 2015). In our lab, we have seen evidence of epileptiform discharges in the hippocampus of young A30P mice, *in vitro* (Tweedy et al., 2018). Therefore, it is not surprising that we found evidence of hyperexcitability in the A30P mouse model and it would be of immense interest to identify the mechanisms that underlie this shift in E/I balance.

As mentioned above, hyperexcitability is the result of an altered E/I balance that can be directly linked to altered synaptic function (Vossel et al., 2017). At 4 months of age, A30P animals represent an early stage of  $\alpha$ -synucleinopathy as they have no signs of major cognitive (Freichel et al., 2007) or motor impairments (Kahle et al., 2000). Cognitive and motor symptoms, as well as proteinase-K resistance  $\alpha$ -syn pathology in the brain stem, midbrain and spinal cord, appear at 12 months of age (Newman et al., 2012) and hyperphosphorylated  $\alpha$ -syn at 16 months of age (Schell et al., 2009). However, it is possible that the young (2.5 – 4 months) A30P animals used in this study have more subtle  $\alpha$ -syn-related changes. Consistent with this idea, there is evidence of very fine motor impairments in A30P mice at 2 months of age (Ekmark-Lewén et al., 2018), hyperlocomotion from 2 months of age that persisted up to 10 months, and altered electrophysiological activity at 2 – 4 months of age (Tweedy et al., 2018). Moreover, these animals express monomeric mutant  $\alpha$ -syn all over the brain (Kahle et al., 2001), that we know can impact neuronal function (Killinger et al., 2019). It is also expected that they express soluble oligomeric  $\alpha$ -syn, as *in vitro* incubation of A30P  $\alpha$ -syn forms oligomers extremely quickly (Li et al., 2019).  $\alpha$ -syn oligomers are known to impact neuronal function and to exert a neurotoxic effect (Chinta et al., 2010; Lashuel et al., 2002). Thus, although more studies need to be performed to characterise the immunohistochemical profile of  $\alpha$ -syn aggregation in A30P mice, mutant  $\alpha$ -syn very likely affects neuronal function early in these animals.

### **7.2.3. Possible mechanisms underlying hyperexcitability**

#### **7.2.3.1. Hyperexcitability and altered neuronal membrane dynamics**

An interesting recent study has shown that doubling the frequency of the SO (from 0.6 to 1.2 Hz) for a month in a mouse model of AD using optogenetic tools, resulted in excess APP cleavage and increased amyloidosis (Kastanenka et al., 2019). The authors proposed that the increase in SO frequency led to an increase in A $\beta$  production which elevated the intracellular Ca<sup>2+</sup> levels and thus the resting membrane potential, inducing hyperexcitability (Arbel-Ornath et al., 2017). In AD, Ca<sup>2+</sup> dysfunction is the result of a direct A $\beta$ -mediated exacerbation in NMDAR function, and/or of an A $\beta$ -mediated blockade of glutamate uptake (Texidó et al., 2011). Moreover, A $\beta$  has been shown to influence the intra-cellular capacity for Ca<sup>2+</sup> buffering (Demuro & Parker, 2013) as well as the function of astroglial cells, eliciting glutamate release (Kuchibhotla et al., 2009) and increasing neuronal excitability (Arbel-Ornath et al., 2017; Busche et al., 2008). The increase in SO frequency and the hyperexcitability we observed in A30P animals could involve a similar feedback loop that also implicates increased  $\alpha$ -syn release and elevated Ca<sup>2+</sup> levels.

In both its wild-type and mutant forms,  $\alpha$ -syn can alter neuronal network excitability through modulating ion channel function (Snead & Eliezer, 2014; Feng et al., 2010; Kaufmann et al., 2016). Voltage-gated Ca<sup>2+</sup> channels are pivotal for neuronal activity as they modulate the levels of Ca<sup>2+</sup> in the cell through the influx of Ca<sup>2+</sup> from the extra-cellular space or its release from intracellular Ca<sup>2+</sup> stores. In PD patients, dopaminergic neurons in the SNc become increasingly more dependent on type L voltage-gated Ca<sup>2+</sup> channels (Cav1) which elicit long-lasting currents and are normally only activated at high-depolarisation levels (Chan et al., 2007). Hence, abnormal expression of these Ca<sup>2+</sup> channels can lead to neuronal hyperexcitability. Similar changes were also observed in cortical neurons, as Cav1 channels are also widely expressed across cortical regions, in both projection neurons and in some interneurons (Hurley & Dexter, 2012). It is possible that intracellular Ca<sup>2+</sup> levels are elevated in A30P mice through a similar mechanism, in pyramidal cells and/or interneurons of the mPFC and CA1 regions, making them hyperexcitable. Moreover, the pharmacological properties of these channels impose a large bio-energetic cost and mitochondrial oxidative stress (Schapira, 2013; Ilijic et al., 2011), which is evident in A30P mice (Robson et al., 2018). Interestingly, Cav1 channel blockade eliminated neuronal hyperexcitability in the mPFC in a mouse model of HIV-1 associated hyperexcitability

(Khodr et al., 2016), suggesting that these channels could also be a potential target for drug development.

In Chapter 4, we argued that the increase in neuronal excitability seen in our study could be the result of changes in the  $K^+$  conductances that elicit long lasting after-hyperpolarisations (AHPs) in pyramidal cells and govern the duration of the Down-state.  $Ca^{2+}$ -dependent  $K^+$  channels ( $K_{Ca}$ ) are one of the main  $K^+$  channel subtypes that sustain the AHP (Lopantsev et al., 2003). Since  $K_{Ca}$  channels are modulated by the intracellular  $Ca^{2+}$  levels,  $\alpha$ -syn related increase in  $Ca^{2+}$  levels could make a neuron more depolarised, reducing the effectiveness of the  $K_{Ca}$  channel-induced AHPs.  $K^+$  conductances can also be affected by the overall expression of the  $K^+$  channels and their subunit composition (Lopantsev et al., 2003). For example, alterations in the subunit composition of  $K_{Ca}$  channels have been seen in aged rats, resulting in decreased repolarization time of CA3 pyramidal neurons and hyperexcitability (Moyer et al., 2000; Simkin et al., 2015).  $K^+$  channels can also be voltage-gated. In a mouse model of AD, Tau induced the depletion of voltage-gated  $K^+$  channels in the dendrites CA1 pyramidal cells, inducing aberrant activity (Hall et al., 2015). Thus, it is possible that the function of  $K^+$  channels is directly, or indirectly, influenced by  $\alpha$ -syn, impairing the AHPs and thus making neurons more hyperexcitable.

Extracellular adenosine or intracellular ATP, both of which are increased with the energy demanding spiking activity, can also influence the properties of  $K^+$  channels (Phillis et al., 1975; Cunningham et al., 2006). Monomeric  $\alpha$ -syn deficiency, that is associated with increased levels of misfolded protein, has been shown to reduce ATP synthase efficiency and ATP levels (Ludtmann et al., 2016), while mutant  $\alpha$ -syn can lower ATP production (Paillusson et al., 2017). As mentioned, previous work from our lab has shown mitochondrial dysfunction in A30P animals (Robson et al., 2018), adding to the growing literature of the deleterious effects of pathological  $\alpha$ -syn in mitochondrial function (Hsu et al., 2000; Martin et al., 2006; Chinta et al., 2010). Therefore, a mitochondrial dysfunction resulting in lower ATP and/or adenosine levels could affect the activation of  $K^+$  conductances in A30P animals, facilitating earlier depolarisation and hence, premature Up-states.

A-syn can also alter the E/I dynamics by influencing neurotransmitter release and receptor binding. The normal function of  $\alpha$ -syn is elusive but we know it is implicated in pre-synaptic neurotransmitter release (Ghosh et al., 2017). Hence, a loss

or gain of  $\alpha$ -syn function due to abnormal  $\alpha$ -syn oligomerisation could influence the synaptic output of neurons, causing an E/I imbalance (Chesselet et al., 2012). The expression of wild-type  $\alpha$ -syn in hippocampal glutamatergic cells in culture has been shown to impair neurotransmitter release by inhibiting synaptic vesicle re-clustering (Ghiglieri et al., 2018). Thus, impaired vesicle release due to  $\alpha$ -syn aggregation could result in excess neuronal firing. In addition,  $\alpha$ -syn can also impair post-synaptic function. As shown in cultured neurons,  $\alpha$ -syn with the A53T mutation causes a decrease in the amplitude of post-synaptic currents in pyramidal neurons and in the AMPAR to NMDAR ratio, reflecting a decrease in synaptic plasticity (Teravskis et al., 2018). Moreover, long exposure to  $\alpha$ -syn oligomers has been shown to increase basal synaptic transmission between the CA1-CA3 regions of the hippocampus by increasing NMDAR function (Diógenes et al., 2012). Similar mechanisms might be applicable to our work, as changes in the synaptic output and/or the expression of specific receptors could render the networks more excitable.

#### 7.2.3.2. *A compensation mechanism may control the hyperexcitability*

We have so far discussed the ways in which  $\alpha$ -syn can increase neuronal excitability, however, our findings show aberrant firing on the Down-state but not increased firing on the Up-state. Thus, we proposed that a compensation mechanism might be in place that controls the levels of hyperexcitability and prevents excessive neuronal firing. The compensation hypothesis is strengthened by our findings in Chapter 6 that in A30P mice, the CA1 region of the hippocampus responds to the ISM drive with an abnormal burst in high frequency oscillatory power, irrespective of Up- and Down-states. This finding could relate to a failure of the compensation mechanisms to control the local excitation upon additional excitatory drive in the CA1, but not in the mPFC region where the high frequency content of the ISM is comparable between A30P and WT animals. As argued in Chapter 6, an alternative explanation is that the hippocampus is more susceptible to  $\alpha$ -syn-induced changes and hyperexcitability compared to the mPFC (discussed in section 6.4.4).

The development of compensation mechanisms is a common phenomenon in models of hyperexcitability, as argued in Chapter 4 (section 4.4.5), including evidence of a PV+ interneuron compensation mechanism in the hippocampus of A30P mice (Tweedy et al., 2018). Specifically, the IPSPs recorded from the CA3 of the hippocampus of young A30P mice *in vitro* were of greater amplitude and frequency,

(Tweedy et al., 2018) while at the same time, the numbers of PV+ interneurons were reduced (unpublished data). There are numerous possible compensation mechanisms with a net effect of either decreasing excitatory function and/or increasing inhibitory activity (Palop et al., 2007). For example, in the study in which the SO frequency was optogenetically increased in a model of AD, there was a compensatory decrease in spine density in cortical dendrites to counteract the hyperexcitability induced by increased A $\beta$  production (Kastanenka et al., 2019). These compensation mechanisms develop in time, as acute, optogenetically-induced hyperexcitability in the hippocampus of A $\beta$  animals also resulted to increased A $\beta$  levels similarly to Kastanenka et al., (2019), but it also caused epileptic activity (Yamamoto et al., 2015), suggesting that there was no time for compensation mechanisms to develop that would control the hyperexcitability. In the figure below, we present the possible compensation mechanisms that may develop in A30P animals in response to the possible human mutant  $\alpha$ -syn-induced perturbations (Figure 7.1).

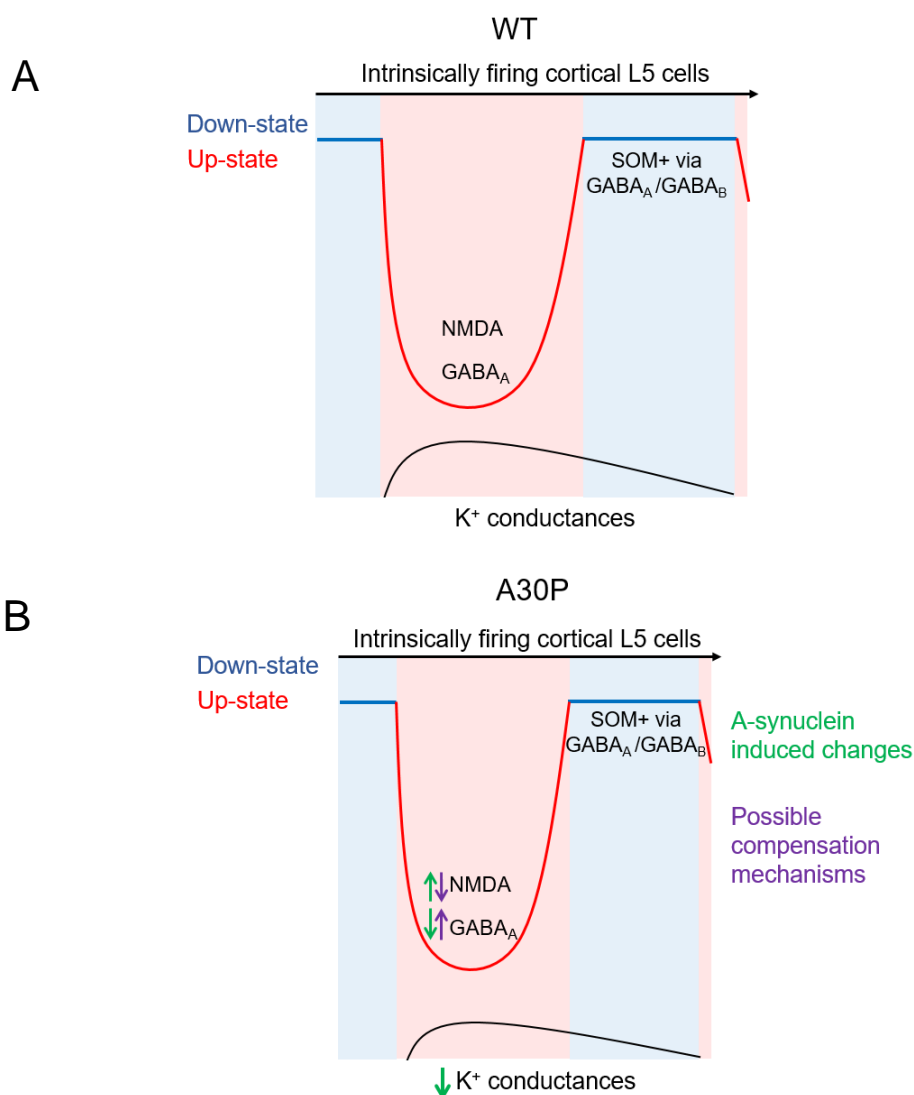


**Figure 7.1:** Alterations in the dynamics that govern the Up- and Down-states in local neuronal circuits, in A30P compared to WT mice. **A)** Up- and Down-state generation in WT animals. The Up-state is maintained by the firing of pyramidal neurons and PV+ interneurons that act on NMDARs and GABA<sub>A</sub>Rs respectively, in the form of a feedback loop. The high levels of neuronal activity lead to the activation of K<sup>+</sup> conductances and the AHP of the pyramidal neurons, terminating the Up-state. SOM+ interneurons influence both GABA<sub>A</sub>Rs and GABA<sub>B</sub>Rs on pyramidal neurons, contributing to the synchronous termination of the Up-state. The Down-state is sustained until the pyramidal neurons have recovered from the AHP, allowing for intrinsic-firing pyramidal neurons in cortical layer 5 to initiate a widespread wave of depolarisation across layers thus, starting the next Up-state. **B)** The mechanisms we proposed drive the altered SO in A30P animals. The K<sup>+</sup> conductances that govern the Down-state are altered in a manner that the resulting AHP levels are lower, allowing pyramidal cells to recover faster from the AHP and engage in a premature Up-state, resulting in a shorter Down-state. We also see a decrease in Up-state duration that can be attributed to the altered dynamics between excitation and inhibition and hence, between hyperexcitability and compensation mechanisms. We propose the PV+ interneurons decrease in number due to  $\alpha$ -syn pathology but at the same time, the remaining interneurons develop a compensation mechanism and increase their activity levels. Moreover, we propose that the hyperexcitable pyramidal neurons might also lower their firing to reduce the hyperexcitability, although the net effect could still be a shift of the network towards excitation. Finally, SOM+ interneurons are driven by pyramidal cells and thus, if the firing of the pyramidal cells is altered so will the function of these cells and consequently, the inhibition through GABA<sub>B</sub>Rs could induce a faster Up-state termination.

### **7.3. The ISM and the resting state are governed by ISOs**

As discussed earlier, we propose that the CFs seen in DLB/PDD patients are the product of altered large-scale network dynamics between the networks that govern rest and attention. The activity of RSNs, and specifically of the DMN, can be viewed as an ISO of the fMRI BOLD signal (Vanhatalo et al., 2004). This signal reflects ISO-mediated modulations of local, faster frequency oscillations (Van Someren et al., 2011), while a number of studies have reported that the connectivity within the DMN nodes and between the DMN and attention networks reflected by the BOLD signal is altered in DLB (Kobeleva et al., 2017; Franciotti et al., 2013; Schumacher et al., 2019). In a similar manner, the ISM is a widespread ISO that also modulates higher frequency activity and appears to be altered in relation to  $\alpha$ -syn pathology. Specifically, in A30P animals, the ISM has a lower amplitude and greater high frequency power content on the Up- and Down-states in the hippocampus. Moreover, it is possible that the

synchronicity of the ISM across regions is also altered, as we see different patterns of changes in the mPFC and CA1 regions in A30P animals, although we did not explicitly investigate for this hypothesis. We could therefore conclude that A30P animals and DLB patients show a deficiency in widespread ISO that reflects  $\alpha$ -syn-induced changes in the E/I balance in the brain.

Both the mPFC and hippocampus in which the ISM was characterised are also nodes of the resting state and attention networks. Human fMRI and PET scans have shown that the mPFC is one of the main DMN hubs, showing very high levels of baseline activity that decrease upon engaging in goal-oriented tasks (Raichle et al., 2001). This decrease in activity upon engaging in a task is particularly obvious in the dorsal mPFC, which is involved in emotional and affective processes and is thus, expected to participate in a state of self-reflection such as rest. On the other hand, the ventral DMN is associated with more complex cognitive processing (Raichle et al., 2001). The mPFC also shows functional connectivity with other nodes of the DMN and specifically the inferior parietal lobe and precuneus/posterior cingulate cortex (pC/PCC) (Fransson & Marrelec, 2008). In attention networks, the mPFC is strongly correlated with VAN during attention tasks (Kobeleva et al., 2017). There is also evidence that the hippocampus participates in RSNs including the DMN (De Luca et al., 2006), and has a strong interaction with the mPFC (Alves et al., 2019). Hence, we could extrapolate that  $\alpha$ -syn-induced changes in the local mPFC and hippocampal networks could affect the function of the DMN during quiet wakefulness, although this theory needs to be addressed experimentally in awake animals.

The dynamic function of RSNs and specifically of the DMN extends to sleep, with evidence of sleep ISOs engaging RSNs in rodents, monkeys and humans (Watson, 2018). The integrity of the DMN persists during sleep stages N1 and N2 but increasingly decays in SWS (Horovitz et al., 2009; Larson-Prior et al., 2009), although it is not completely abolished (Horovitz et al., 2009; Tagliazucchi et al., 2013). Interestingly, one study investigated correlations between the ISO (< 0.1 Hz) recorded by the EEG, and the DMN function imaged via fMRI, during SWS and found a positive functional correlation for sub-cortical nodes such as the hippocampus and parahippocampal gyri, and a negative correlation for para-median nodes including the mPFC and precuneus (Picchioni et al., 2011). The authors suggested that the ISOs organise the hippocampal and neocortical elements of the DMN in a manner that

promotes memory consolidation (Picchioni et al., 2011). Moreover, during the awake state, the DMN always engages after the hippocampus, while the opposite pattern is seen during SWS, suggesting a reversal of information flow to facilitate memory consolidation in the cortex (Mitra et al., 2016). Thus, a study regarding the integrity of the DMN in the A30P mouse model would be of particular interest, not only during the awake state but also during SWS.

#### **7.4. Cholinergic and thalamic implications**

DLB patients have a prominent cholinergic dysfunction that is thought to contribute to altered network dynamics and CFs. Early  $\alpha$ -syn pathology is evident in cholinergic neurons in the basal cholinergic system including the nucleus basalis of Meynert (NBM), which results in decreased cholinergic innervation in the cortex (Lippa et al., 1999). The NBM is pivotal in directing attention in a bottom-up manner and thus, if dysfunctional, it can induce abnormal shifts in attention and CFs (Liu et al., 2015; Newman et al., 2012). In support to this theory, cholinesterase inhibitors reduce CFs in DLB patients while MRI studies have shown a correlation between grey matter atrophy and CFs (Onofrj et al., 2003). Moreover, the basal cholinergic deficit has been associated with the slowing of the EEG seen in the both DLB and AD patients, as it can be reversed through acetylcholinesterase inhibitor administration (AChI; Bosboom et al., 2009; Briel et al., 1999).

The thalamus is also implicated in CFs as it has a central role in attention and awareness and can regulate the activity of numerous cortical networks in relation to goal-directed behaviour (Rikhye et al., 2018). In LBD, the thalamus shows high levels of  $\alpha$ -syn pathology (Kotagal et al., 2012), while in DLB patients, the levels of thalamic atrophy and decreased connectivity with prefrontal and parieto-occipital regions correlate with the severity of CFs (Delli Pizzi et al., 2015). Moreover, lower levels of nAChRs have been measured in all the thalamic nuclei (including the TRN) of DLB patients with CFs than those without CFs (Pimlott *et al.*, 2006). The TRN is also implicated in attention as part of a top-down selection process (Young & Wimmer, 2017). Hence, the pathology observed in the thalamus of DLB patients could also impact attention.

It has been suggested that there are two different types of CFs, one associated with attention (discussed above), and one associated with arousal, which is controlled

by the same pathways that control sleep (Delli Pizzi et al., 2015). The ascending reticular activating system (ARAS) regulates sleep-wake homeostasis and REM sleep and, although it involves a number of neurotransmitters, ACh has a pivotal function (Watson et al., 2012). The dorsal branch of the ARAS originating in the brainstem cholinergic system and specifically the PPT/LDT cholinergic nuclei, projects to the thalamus that in turn projects to the cortex. The PPT/LDT also project diffusely to the basal forebrain cholinergic system that constitutes the source of the ventral ARAS pathway and also projects to the cortex (Brown et al., 2012). Thus, the aforementioned disturbances in the cholinergic system in DLB patients could have sleep related implications in these patients, although there is no evidence that CFs correlate with polysomnography disturbances at the moment (Pao et al., 2013).

We have also suggested that cholinergic-related disturbances might be in place in the young A30P mice. One of our main observations in A30P mice was a decrease in relative spindle density (spindles number / Up-state number), as well as a decrease in spindle duration and in the number of large-amplitude spindles. Spindles require thalamocortical connections to be generated, while the TRN has a pivotal role in generating the bursts of inhibition that give rise to the spindle (Fernandez et al., 2018). Thus, although  $\alpha$ -syn related pathology in the TRN could affect sleep spindles, spindle generation has an important cortical component as well (Mak-McCully et al., 2017) and we have discerned that the local mPFC network function in A30P mice is indeed altered. Interestingly, there are no differences in the relative sleep spindle density during the ISM between A30P and WT mice, which indicates that the spindle reduction that occurs during the ISM is also successful in A30P mice. Thus, we cannot definitively conclude that changes in the TRN in A30P mice definitely contribute to our observed alterations in spindle patterns.

Moreover, in Chapter 5 (section 5.4.7) we hypothesised that the ISM is a thalamic and/or acetylcholine-mediated rhythm. According to this hypothesis, direct thalamic and/or cholinergic inputs to the cortex (Destexhe et al., 1998) and indirect inputs to the hippocampus (Vertes et al., 2007), drive higher frequency oscillations in the form of the ISM. Although we postulated that the increases in high frequency oscillatory power during the ISM in A30P animals can be related to hyperexcitability in the local hippocampal network, we also suggested that the ISM input itself may be altered in A30P animals. However, currently we have no evidence indicating the source

of the ISM, or showing a cholinergic deficit or  $\alpha$ -syn pathology in the thalamus or the TRN of the young A30P mice.

Finally, we do not believe that there is any relationship between the evidence of hyperexcitability in A30P mice and a cholinergic dysfunction. In support of this theory, Morris et al. (2015) investigated for a relationship between hyperexcitability in the CA1 and the EEG slowing seen in a mouse model of DLB, which can be attributed to a loss of cholinergic tone (Bosboom et al., 2009). However, the authors found that the pharmacological blockade of hyperexcitability did not affect the EEG slowing in their mouse model. Conversely, a mouse model of A $\beta$  that showed hyperexcitability did not have the EEG slowing, suggesting that the EEG slowing and hyperexcitability have different origins (Morris et al., 2015). In A30P animals, we have not looked for an EEG slowing as theta and alpha frequency rhythms are not evident during SWS (Castano-Prat et al., 2019; Gretenkord et al., 2017; Kuki et al., 2015), but it would be important to explore this in future experiments in awake behaving animals.

#### **7.5. SWS disturbances can have detrimental effects**

One of our main findings was a loss of sleep spindles in A30P mice, which can have numerous implications in any mammalian species (Rasch & Born, 2013). Firstly, cortical spindles and hippocampal SWRs are highly coordinated with each other during the SO, with SWRs clustering in the trough of spindles in humans (Staresina et al., 2015) and rodents (Wang & Ikemoto, 2016). This synchrony mediates the transfer of information from the hippocampus to the cortex facilitating memory consolidation (Colgin, 2011; Witton et al., 2016). Considering the synchrony between these events we would also expect SWRs to be altered in our analysis but we found not differences in SWRs between WT and A30P animals. However, due to the low number of concomitant CA1/mPFC recordings we did not look at the spindle/SWR coherence. Thus, a next step would be to carry out more simultaneous CA1/mPFC recordings and to investigate the synchrony between the spindles and SWRs occurring in each region respectively, and their synchrony with the SO.

In addition to the importance of sleep spindles in memory consolidation, spindles are also considered pivotal in “protecting” sleep from internal or external perturbations that can cause a sleep disruption (Terzano & Parrino, 2000; Parrino & Vaudano, 2018). According to the glymphatic hypothesis of dementia, the disruption in

SWS and the resulting awake-like brain activity can prevent the clearance of pathological forms of amyloid- $\beta$ , tau and possibly  $\alpha$ -syn, and even promote excess production of these peptides (Mander et al., 2016). Hence, impaired spindle generation could set off a cycle of increasing levels of  $\alpha$ -syn and SWS interruption (Bohnen & Hu, 2019). In fact, sleep fragmentation is one of the most common sleep-related symptoms in DLB patients, suggesting a relationship between awakenings and  $\alpha$ -syn pathology (Cagnin et al., 2017).

Our findings of changes in the SO in terms of frequency and high frequency power content in A30P mice can also contribute to  $\alpha$ -syn pathology. Similarly to the previously presented study in a mouse model of AD (Kastanenka et al., 2019), the increase in SO frequency seen in the young A30P mice could further exacerbate  $\alpha$ -syn aggregation and cytotoxicity that in turn, further increases the SO frequency, leading to a vicious loop that results in neurodegeneration. We also observed an abnormal increase in the power of high frequency activity in the CA1 region of the hippocampus during the ISM in A30P animals. This burst of activity would be expected to add to the already increased levels of  $\alpha$ -syn production and reduced levels of clearance, according to the aforementioned hypothesis of SWS disruption. Moreover, increased activity and lower levels of metabolic waste clearance can induce cytotoxicity in local circuits, especially in regions that have fast-spiking, high energy demanding neurons like the CA1 region of the hippocampus (Bohnen & Hu, 2019).

Lastly, in Chapter 5, we proposed that the ISM is an A3 subtype CAP modulation. If this is the case, our results of a decrease in ISM frequency in the mPFC also imply a decrease in REM sleep as A3 events immediately precede REM transitions during natural sleep (Terzano & Parrino, 2000), although this hypothesis needs to be investigated during natural sleep. REM sleep is essential for the dissociation of the cortex and the hippocampus during SWS, allowing for the rearrangement of local circuits (Watson et al., 2016; Staresina et al., 2015). Thus, a decrease in REM sleep could further impede efficient hippocampal-cortical communication in A30P mice.

## **7.6. The clinical significance of our findings in A30P mice**

Excess neuronal excitability in patients with epilepsy is treated with antiepileptic medications. Hence, it was considered possible that these drugs could be beneficial in

patients with AD, where neuronal network hyperexcitability and epilepsy are well described (review by Pandis and Scarmeas, 2012). However, some antiepileptics have detrimental cognitive defects in AD patients (phenobarbital), while others improve aspects of cognition like attention (levetiracetam), or mood (lamotrigine; review by Cumbo and Ligori, 2010). Thus, according to the clinical guidelines, antiepileptics are only prescribed for AD patients with electrophysiological signs of hyperexcitability (Giorgi et al., 2017). Similarly, in view of our findings of early network hyperexcitability in A30P mice, and the evidence of myoclonus in DLB (Beagle et al., 2017), antiepileptics could be beneficial in patients with DLB. The antiepileptic drug zonisamide is currently in a phase-2 clinical trial for DLB patients as it has been shown to improve the parkinsonism symptoms, although it does not improve or worsen cognition (Murata et al., 2018). Moreover, cortical myoclonus which is frequently reported in DLB patients and reflects aberrant neuronal activity (Beagle et al., 2017), can be treated with levetiracetam (Caviness, 2019; Frucht et al., 2001). This antiepileptic medication may also be beneficial for RBD in DLB patients (Batalini et al., 2016). Finally, the NMDAR antagonist memantine has been shown to improve cognitive function in DLB/PDD patients with mild to moderate dementia, including improving their performance in tests of attention and episodic memory (Wesnes et al., 2015).

Our study has also revealed a potential correlation between hyperexcitability and sleep abnormalities in young A30P animals, including an increase in SO frequency. The integrity of the SO rhythm is closely linked to the level of metabolic by-product clearance during SWS, as in animal models of AD the levels of A $\beta$  clearance through the glymphatic system correlate with SWA (Hablitz et al., 2019). Hence, sleep promoting agents may also be beneficial in clearing  $\alpha$ -syn, if is indeed cleared via the glymphatic system as hypothesised (Mander et al., 2015). A potential medication is gamma hydroxybutyrate, which promotes inhibition and has been shown to increase SWS in patients with narcolepsy and fatal familial insomnia (Reder et al., 1995). It would be particularly interesting to test whether acute or chronic administration of gamma hydroxybutyrate, antiepileptic drugs or memantine could restore the SO and reduce hyperexcitability in the young A30P mice.

## **7.7. Limitations and future work**

### **7.7.1. *Human EEG analysis***

A few issues relating to the studies in this thesis need to be considered. In relation to the human EEG analysis (Chapter 3), an important next step would be the confirmation of our findings in independent prospective cohorts, especially regarding the ROC analysis. Moreover, we excluded the delta frequencies in our study and hence, we might have missed changes occurring in the qEEG variables within that frequency range. In addition, the recordings were not always continuous as we focused on discarding as much of the noise as possible and preferred to occasionally reject epochs, across all channels. Furthermore, CFs were measured using the CAF score (Walker et al., 2000) which is considered a fairly reliable measure of CFs only if used by an experienced clinician (Van Dyk et al., 2016). However in this study, experienced old age psychiatrists calculated the CAF score and we do, therefore, consider the CAF score values used for our correlation analysis reliable.

Another limitation was that the patients did not undergo post-mortem immunohistological examination and thus we did not account for mixed AD-DLB pathology that has been shown to relate to greater cognitive impairment in DLB patients and can alter the qEEG profile (Gomperts et al., 2012). However, our clinical diagnostic approaches were robust enough to enhance the specificity of our group selections. Evidence for this include DaT scans that were available for 9 of the DLB patients and were all positive, and a multi-modal MRI/EEG analysis on data from all the patients that were recruited in the same cohort as the patients included in this study, where AD and DLB patients were classified with 90% accuracy (Colloby et al., 2016).

### **7.7.2. *Investigation of the SO and ISM in A30P and WT mice***

In order to better understand the nature of the ISM observed in the mouse recordings, it would be very important to investigate additional parameters such as the cardiac rhythm, respiration and temperature, which are influenced both by CAP modulations in humans and REM sleep/activated state in animals (Terzano & Parrino, 2000; Pagliardini et al., 2013). Moreover, we would like to investigate whether the ISM is followed by REM transitions in animals under lighter-urethane anaesthesia, as this would be the case if the ISM is indeed an A3 subtype CAP modulation. Moreover, it

would be extremely interesting to investigate the source of the ISM. We have proposed that the ISM could be a thalamic rhythm and hence, it would be valuable to obtain concomitant thalamic, mPFC and CA1 recordings. We also suggested that the ISM could be due to a direct cholinergic input to the mPFC. Thus, the application of cholinergic agonists and antagonists locally in the mPFC or the thalamus could start to delineate this hypothesis. We could also proceed with a direct electrical stimulation of specific thalamic nuclei, although the small size of the mouse brain may not allow a high level of spatial accuracy. In a more elaborate study we could use optogenetics to modulate the thalamus in relation to the ISM.

Regarding our investigation of changes in the SO patterns in A30P animals, one of the main limitations of our study is the lack of unit firing data from the CA1 of the hippocampus, as we were not able to record sufficient, high quality unit firing data from this region. Although we support our conclusions of hyperexcitability in that region with *in vitro* results from our lab (Tweedy et al., 2018), performing single neuron recordings in the hippocampus would be pivotal to confirming our hypothesis. Moreover, we would need to carry out more concomitant recordings from the mPFC and CA1 in order to investigate more thoroughly for changes in SO synchrony and spindle/SWR synchrony in the two regions, in A30P mice.

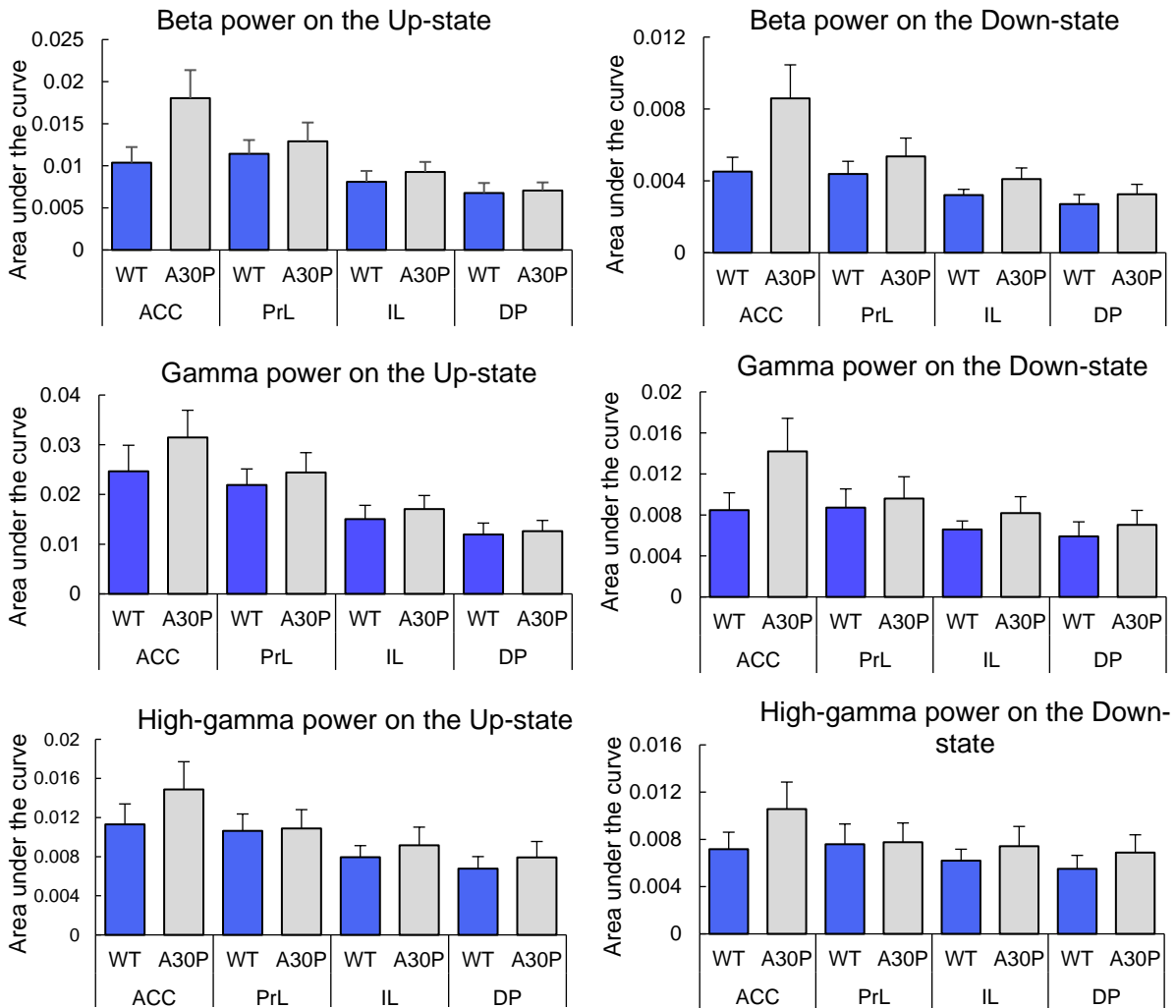
Although urethane is considered an excellent model of SWS, verifying our results during natural sleep would be an important next step. Up- and Down-states are comparable between anaesthetised and WT animals as are spindles, although the latter tend to be of lower amplitude under urethane anaesthesia (Barthó et al., 2014). *In vivo* recordings would also allow us to record electrophysiological data from these animals during quiet wakefulness (resting state) in order to compare with our data from the human EEG and specifically, look for an EEG spectral slowing. We would also be able to investigate changes in sleep architecture such as the time spent in NREM and REM sleep and the transition to deep sleep. Finally, *in vivo* recordings would allow us to record simultaneously from a larger number of cortical and sub-cortical regions including the thalamus (Varela & Wilson, 2019).

We can also investigate our hypothesis of hyperexcitability and the development of a compensation mechanism through pharmacological manipulations in A30P animals under urethane anaesthesia. Specifically, we could administer incremental doses of NMDAR agonists or GABA<sub>A</sub>R or GABA<sub>B</sub>R antagonists to see whether A30P mice

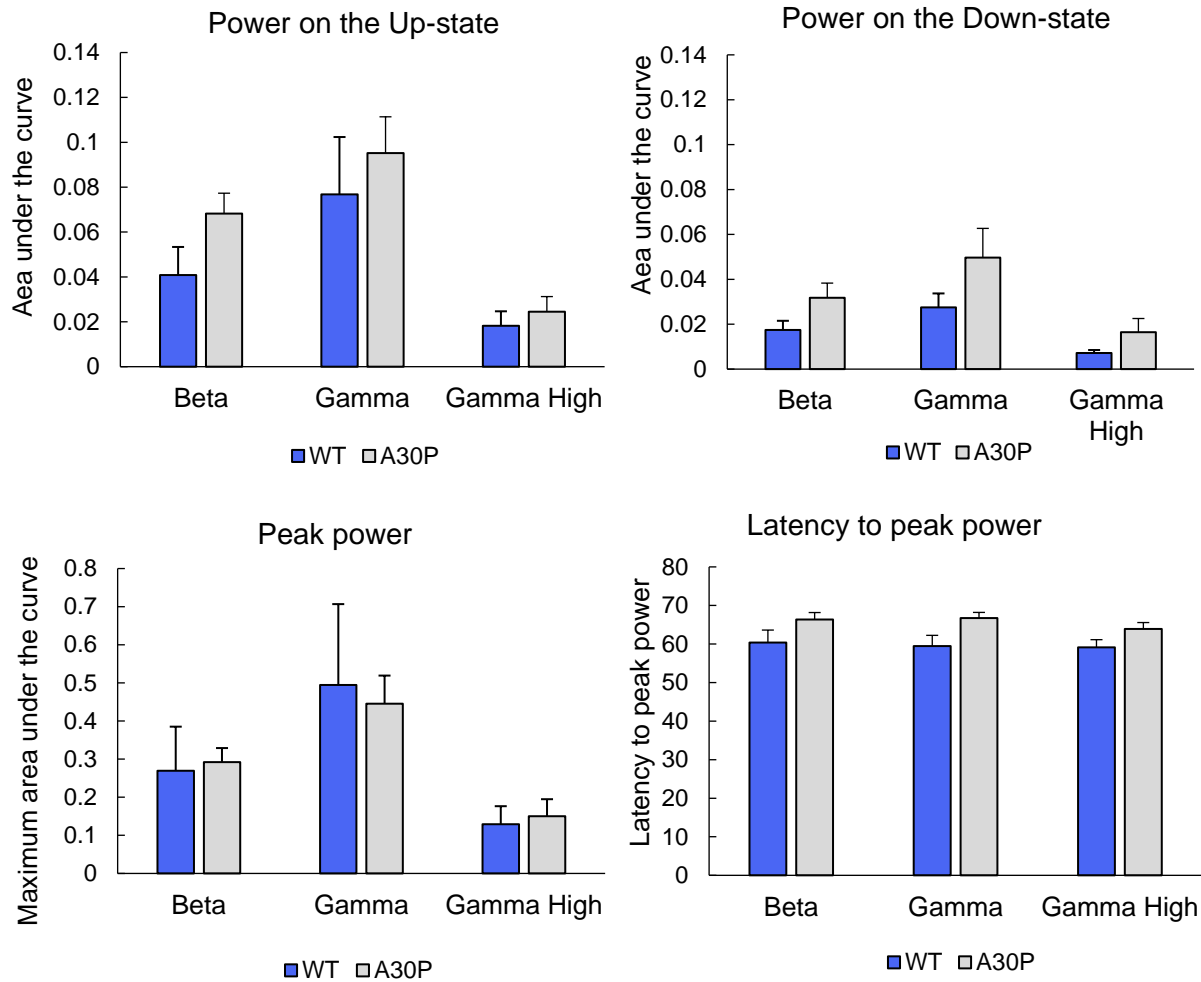
would exhibit hyperexcitability or even epileptiform activity, compared to WT animals. In contrast, we could also administer NMDAR antagonists and GABA<sub>A</sub> agonists to investigate whether the neuronal circuits would be less hyperexcitable and if the SO frequency would return to its normal levels. Ideally, we would like to perform these manipulations at the local level through intra-cortical injections instead of peritoneal or intravenous administration that influence the overall brain function. It would also be interesting to see whether these manipulations would influence the response of local networks to the ISM and whether they could restore the aberrant increases in power seen in the CA1 of these animals, or conversely, whether they would evolve to epileptiform activity. Moreover, the spindle impairment in A30P animals has its origin in the TRN and/or the cortex and thus, we could investigate whether stimulation and/or pharmacological manipulation in these regions has an impact on spindle density and amplitude. Finally, we could perform similar recordings in other mouse models of  $\alpha$ -synucleinopathy such as the A53T mouse model that also expresses a human mutant  $\alpha$ -syn form (Spira et al., 2001).



## Appendix



**Appendix A:** Changes in the levels of higher-frequency oscillation wavelet power in the normalised SO/Up-Down cycle (0 = start of Down-state, 50 = Down to Up-state transition, 100 = end of Up-state) in A30P (N = 13) and WTs (N = 8) animals, in the mPFC subregions (ACC, PrL, IL, DP). The frequency bands examined are the beta (15 – 30 Hz), gamma (30 – 80 Hz) and high-gamma (80 – 130 Hz). Error bars indicate the SEM.



**Appendix B:** Changes in the levels of higher-frequency oscillation wavelet power in the normalised SO/Up-Down cycle (0 = start of Down-state, 50 = Down to Up-state transition, 100 = end of Up-state) in A30P (N = 13) and WT (N = 8) animals, in the CA1 of the hippocampus. The frequency bands examined are the beta (15 – 29.9 Hz), gamma (30 – 79.9 Hz) and high-gamma (80 – 130 Hz). Error bars indicate the SEM.

**Appendix C:** High frequency oscillatory power in the SO cycle in the 4 mPFC subregions: ACC, PrL, IL and DP, in 4 frequency bands: Theta, Beta, and High-gamma, in the non-ISM, pre-ISM, ISM and post-ISM segments, in WT (N = 8) and A30P (N = 13) animals.

Theta frequency band									
		WT				A30P			
		Non-ISM	Pre-ISM	ISM	Post-ISM	Non-ISM	Pre-ISM	ISM	Post-ISM
Power on the Upstate (x10 <sup>3</sup> )	ACC	8.81 ± 1.72	8.44 ± 1.45	13.56 ± 2.9	7.9 ± 1.35	16.28 ± 3.5	15.09 ± 3.38	20.78 ± 4.22	16.07 ± 3.47
	PrL	9.63 ± 1.85	7.45 ± 0.66	10.94 ± 1.23	6.88 ± 0.71	10.85 ± 1.22	10.45 ± 1.39	14.1 ± 1.64	10.57 ± 1.33
	IL	9.72 ± 2.09	7.8 ± 1.24	10.6 ± 1.26	6.99 ± 0.86	9.45 ± 1.1	8.57 ± 1.24	12.02 ± 1.48	8.93 ± 1.39
	DP	10.23 ± 1.89	7.29 ± 0.86	10.48 ± 1.09	6.72 ± 0.7	9.14 ± 1.06	8.57 ± 1.12	12.4 ± 1.49	8.6 ± 1.18
Power on the Down-State (x10 <sup>3</sup> )	ACC	4.53 ± 0.96	4.67 ± 1.02	8.09 ± 1.42	4.95 ± 0.9	8.05 ± 2.02	7.77 ± 1.9	11.89 ± 1.99	8.94 ± 2.2
	PrL	3.8 ± 0.85	3.31 ± 0.85	5.77 ± 1.41	3.63 ± 0.93	4.49 ± 0.56	4.44 ± 0.55	9.25 ± 1.76	4.97 ± 0.63
	IL	3.33 ± 0.56	3.04 ± 0.67	5.9 ± 1.14	3.32 ± 0.71	3.8 ± 0.58	3.58 ± 0.52	7.54 ± 1.46	4.17 ± 0.82
	DP	3 ± 0.52	2.64 ± 0.64	5.31 ± 1.09	2.89 ± 0.7	3.77 ± 0.66	3.82 ± 0.69	9.14 ± 2.77	4.29 ± 0.78
Peak power (x10 <sup>3</sup> )	ACC	55.51 ± 1.77	55.48 ± 4.22	55.84 ± 3.36	58.04 ± 2.79	44.92 ± 10.15	14.11 ± 1.98	26.64 ± 9.8	13.63 ± 1.88
	PrL	59.15 ± 0.87	61.08 ± 5.46	60.04 ± 4.41	60.19 ± 1.84	25.84 ± 2.96	13.94 ± 2.26	21.33 ± 4.9	13.95 ± 2.05
	IL	59.22 ± 1.61	56.98 ± 4.97	58.35 ± 3.57	58 ± 2.48	21.94 ± 2.51	18.22 ± 3.03	28.81 ± 7.43	17.71 ± 2.41
	DP	60.85 ± 1	61.04 ± 4.5	63.96 ± 2.52	59.29 ± 2.89	21.74 ± 2.55	27.65 ± 6.53	36.5 ± 7.35	30.66 ± 7.82
Latency to peak power cycle	ACC	40.85 ± 7.84	17.37 ± 2.7	24.04 ± 4.92	16.94 ± 3.04	58.27 ± 1.09	62.66 ± 2.51	58.49 ± 2.63	61.5 ± 3.17
	PrL	43.5 ± 6.53	14.22 ± 1.36	17.8 ± 1.71	13.15 ± 1.29	60.04 ± 0.62	62.87 ± 1.11	59.89 ± 1.89	61.56 ± 2.5
	IL	31.51 ± 3.96	15.16 ± 2.18	17.18 ± 1.79	13.66 ± 1.46	61.57 ± 0.67	59.75 ± 1.62	58.49 ± 1.3	57.51 ± 3.55
	DP	27.45 ± 3.84	13.82 ± 1.52	15.58 ± 1.68	12.57 ± 1.25	62.18 ± 1.06	59.43 ± 1.7	55.72 ± 2.13	57.77 ± 3.05
Beta frequency band									
		WT				A30P			
		Non-ISM	Pre-ISM	Non-ISM	Pre-ISM	Non-ISM	Pre-ISM	Non-ISM	Pre-ISM

<b>Power on the Upstate (x10<sup>3</sup>)</b>	ACC	9.28 ± 1.7	8.02 ± 1.41	12.5 ± 2.01	7.88 ± 1.21	16.62 ± 3.51	15.23 ± 3.16	22.32 ± 4.8	15.75 ± 3.2
	PrL	10.34 ± 1.39	7.59 ± 0.71	12.34 ± 1.63	7.68 ± 0.68	12 ± 1.76	11.51 ± 1.78	16.91 ± 2.42	11.72 ± 1.72
	IL	7.64 ± 1.37	6.15 ± 1.31	9.59 ± 1.36	5.7 ± 0.7	8.5 ± 1.22	7.78 ± 1.18	12.03 ± 1.69	7.85 ± 1.37
	DP	6.77 ± 1.19	4.56 ± 0.49	7.84 ± 0.93	4.4 ± 0.45	6.98 ± 1.04	6.43 ± 0.94	10.44 ± 1.44	6.56 ± 1.15
<b>Power on the Down-State (x10<sup>3</sup>)</b>	ACC	4.41 ± 0.9	4.41 ± 0.91	7.22 ± 1.25	4.99 ± 0.94	7.46 ± 1.61	6.45 ± 1.29	11.6 ± 2.01	6.91 ± 1.45
	PrL	4.03 ± 0.7	3.37 ± 0.81	5.78 ± 1.43	3.83 ± 0.84	87.92 ± 23.37	15.48 ± 2.35	80.1 ± 60.31	14.02 ± 2
	IL	3.16 ± 0.36	2.88 ± 0.55	5.67 ± 1.02	3.27 ± 0.59	61.27 ± 11.04	19.72 ± 2.97	57.74 ± 33.32	17.64 ± 2.34
	DP	2.71 ± 0.53	2.21 ± 0.51	4.54 ± 0.97	2.42 ± 0.58	39.57 ± 4.6	32.01 ± 5.47	60.69 ± 22.63	31.2 ± 6.2
<b>Peak power (x10<sup>3</sup>)</b>	ACC	55.78 ± 9.55	25.93 ± 3.66	34.62 ± 5.33	24.43 ± 3.84	76.82 ± 18.93	14.15 ± 3.16	109.7 ± 95.89	13.98 ± 3.09
	PrL	64.75 ± 9.39	26.94 ± 3.94	35.96 ± 8.04	26.24 ± 3.53	58.24 ± 12.47	16.22 ± 4	56.57 ± 40.33	16.36 ± 4.1
	IL	47.21 ± 8.56	21.52 ± 5.25	26.43 ± 5.84	19.37 ± 3.76	49.16 ± 13.56	21.92 ± 4.25	39.79 ± 17.37	21.9 ± 4.39
	DP	38.28 ± 6.89	13.91 ± 2.13	18 ± 3.73	13.3 ± 1.83	42.38 ± 11.18	31.41 ± 7.39	52.21 ± 22.27	29.76 ± 6.89
<b>Latency to peak power cycle</b>	ACC	57.38 ± 2.43	57.71 ± 2.8	57.03 ± 3.47	57.01 ± 3.34	60.35 ± 1.28	66.28 ± 2.98	62.9 ± 3.49	60.75 ± 4.2
	PrL	58.53 ± 0.84	61.63 ± 3.81	60.5 ± 3.51	60.58 ± 3.69	61.48 ± 0.8	63.37 ± 2.12	61.25 ± 2.5	59.09 ± 3.8
	IL	58.77 ± 1.13	58.49 ± 3.1	57.97 ± 3.44	56.03 ± 2.73	63.22 ± 0.94	58.57 ± 2.5	56.06 ± 3.66	56.22 ± 3
	DP	60.72 ± 1.33	63.64 ± 3.28	59.54 ± 3.63	61.79 ± 2.94	64.28 ± 1.43	59.69 ± 1.79	55.8 ± 2.91	56.66 ± 2.8
<b>Gamma frequency band</b>									
		<b>WT</b>				<b>A30P</b>			
		<b>Non-ISM</b>	<b>Pre-ISM</b>	<b>Non-ISM</b>	<b>Pre-ISM</b>	<b>Non-ISM</b>	<b>Pre-ISM</b>	<b>Non-ISM</b>	<b>Pre-ISM</b>
<b>Power on the Upstate (x10<sup>3</sup>)</b>	ACC	21.50 ± 4.75	16.60 ± 3.7	21.31 ± 4.39	17.51 ± 3.9	29.93 ± 5.95	27.7 ± 5.68	35.7 ± 7.09	28.94 ± 6.15
	PrL	19.78 ± 2.72	14.39 ± 0.9	18.32 ± 1.92	14.70 ± 1.08	23.52 ± 3.49	22.49 ± 3.51	29.44 ± 4.33	22.76 ± 3.66
	IL	15.76 ± 3.27	10.98 ± 2.23	15.10 ± 2.47	10.94 ± 1.84	15.99 ± 3.09	14.66 ± 2.86	20.42 ± 3.74	14.69 ± 3.16

	DP	11.95 ± 2.29	7.89 ± 1.03	11.69 ± 1.68	7.82 ± 1.04	12.49 ± 2.33	11.49 ± 2.05	16.71 ± 2.78	11.46 ± 2.29
<b>Power on the Down-State (x10<sup>3</sup>)</b>	ACC	8.29 ± 1.9	8.46 ± 1.6	12.76 ± 2.3	9.51 ± 1.57	12.7 ± 2.55	12.21 ± 2.27	19.39 ± 3.16	13.57 ± 2.74
	PrL	8.01 ± 1.9	6.86 ± 1.62	10.66 ± 2.55	8.00 ± 1.84	8.56 ± 1.54	8.22 ± 1.33	15.7 ± 3.15	9.21 ± 1.7
	IL	6.41 ± 0.93	5.80 ± 1	9.89 ± 1.67	6.56 ± 1.07	7.37 ± 1.68	6.74 ± 1.32	14.27 ± 3.6	7.18 ± 1.68
	DP	5.91 ± 1.41	4.85 ± 1.07	8.57 ± 1.85	5.25 ± 1.16	7.02 ± 1.53	6.64 ± 1.24	16.59 ± 6.13	7.02 ± 1.52
<b>Peak power (x10<sup>3</sup>)</b>	ACC	93.12 ± 17.26	45.31 ± 10.87	39.82 ± 6.68	41.18 ± 8.33	135.1 2 ± 28.76	25.01 ± 4.51	149.4 9 ± 120.3 4	23 ± 3.74
	PrL	86.59 ± 11.89	35.56 ± 3.79	33.50 ± 2.95	33.13 ± 3.19	102.9 2 ± 14.8	32.34 ± 6.51	110.7 ± 73.3	30.41 ± 5.62
	IL	65.00 ± 12.8	26.80 ± 5.95	27.11 ± 5.94	25.08 ± 5.65	69.15 ± 11.42	50.97 ± 8.94	89.68 ± 30.58	49.9 ± 8.69
	DP	54.14 ± 9.29	17.87 ± 2.05	18.90 ± 2.26	16.36 ± 2.03	53.48 ± 8.68	65.71 ± 15.49	113.5 1 ± 42.42	66.46 ± 16.69
<b>Latency to peak power cycle</b>	ACC	67.17 ± 1.07	59.05 ± 3.31	61.03 ± 2.85	59.29 ± 3.24	62.49 ± 1.41	67.63 ± 3.15	62.44 ± 4.6	66.31 ± 2.6
	PrL	61.94 ± 1.02	62.73 ± 2.42	65.15 ± 2.28	61.5 ± 2.7	65.2 ± 0.92	66.01 ± 3.59	64.47 ± 2.87	66.92 ± 1.63
	IL	60.41 ± 1.83	59.98 ± 3.66	61.4 ± 2.99	58.43 ± 2.9	65.46 ± 0.68	66.97 ± 1.24	63.83 ± 1.94	64.4 ± 1.63
	DP	62.73 ± 0.86	66.4 ± 3.12	67.93 ± 2.1	63.76 ± 2.18	65.39 ± 1.02	63.99 ± 2.27	59.15 ± 2.21	60.39 ± 3.14
<b>High-gamma frequency band</b>									
		<b>WT</b>				<b>A30P</b>			
		<b>Non-ISM</b>	<b>Pre-ISM</b>	<b>Non-ISM</b>	<b>Pre-ISM</b>	<b>Non-ISM</b>	<b>Pre-ISM</b>	<b>Non-ISM</b>	<b>Pre-ISM</b>
<b>Power on the Upstate (x10<sup>3</sup>)</b>	ACC	10.11 ± 1.94	8.9 ± 1.47	9.77 ± 1.63	9.11 ± 1.51	15.06 ± 3.33	14.37 ± 3.16	15.29 ± 3.26	14.44 ± 3.17
	PrL	9.26 ± 1.17	7.38 ± 0.7	8.15 ± 0.81	7.51 ± 0.7	11.19 ± 2.13	10.85 ± 1.98	11.65 ± 2.05	10.97 ± 2.04
	IL	7.41 ± 1.2	6.33 ± 1	6.95 ± 1.07	6.35 ± 0.96	8.82 ± 2.2	8.16 ± 2.06	8.74 ± 2.07	8.17 ± 2.06
	DP	6.78 ± 1.24	5.08 ± 0.88	5.66 ± 1.01	5.11 ± 0.92	7.9 ± 1.76	7.38 ± 1.6	7.93 ± 1.62	7.41 ± 1.6
<b>Power on the Down-State (x10<sup>3</sup>)</b>	ACC	6.53 ± 1.46	6.44 ± 1.08	7.16 ± 1.24	6.64 ± 1.07	10.79 ± 2.62	10.44 ± 2.44	11.93 ± 2.5	10.75 ± 2.56
	PrL	6.29 ± 1.26	5.42 ± 1.04	5.85 ± 1.14	5.52 ± 1.01	8.1 ± 1.87	7.86 ± 1.67	9.06 ± 1.72	8.07 ± 1.81
	IL	5.71 ± 0.94	5.07 ± 0.81	5.68 ± 0.93	5.24 ± 0.83	7.25 ± 1.99	6.58 ± 1.78	8.39 ± 2.17	6.69 ± 1.83

	DP	5.51 ± 1.14	4.52 ± 0.93	5 ± 1.03	4.51 ± 0.91	6.92 ± 1.62	6.48 ± 1.45	10.35 ± 3.78	6.55 ± 1.49
<b>Peak power (x10<sup>3</sup>)</b>	ACC	58.5 ± 1.31	59.58 ± 3.07	59.27 ± 2.32	60.01 ± 3.23	76.82 ± 18.93	14.15 ± 3.16	109.77 ± 95.89	13.98 ± 3.09
	PrL	58.76 ± 0.93	59.57 ± 1.49	61.83 ± 1.52	58.55 ± 1.54	58.24 ± 12.47	16.22 ± 4	56.57 ± 40.33	16.36 ± 4.1
	IL	57.35 ± 1.08	60.52 ± 2.36	59.27 ± 1.36	59.51 ± 1.8	49.16 ± 13.56	21.92 ± 4.25	39.79 ± 17.37	21.9 ± 4.39
	DP	58.16 ± 0.98	58.13 ± 4.25	66.7 ± 2.24	61.54 ± 2.75	42.38 ± 11.18	31.41 ± 7.39	52.21 ± 22.27	29.76 ± 6.89
<b>Latency to peak power cycle</b>	ACC	51.63 ± 11.56	20.98 ± 3.52	19.98 ± 3.35	20.74 ± 3.61	58.25 ± 0.76	62.57 ± 3.26	61.5 ± 1.58	62.93 ± 1.54
	PrL	48.9 ± 8.66	16.42 ± 1.56	15.39 ± 1.19	17.18 ± 2.11	58.88 ± 0.94	60.36 ± 2.59	62.64 ± 1.75	61.25 ± 1.92
	IL	40.01 ± 8.6	13.15 ± 2.53	12.18 ± 2.22	12.96 ± 2.4	57.21 ± 0.99	63.87 ± 1.47	63.1 ± 1.87	61.97 ± 1.09
	DP	36.85 ± 8.42	10.28 ± 2.23	9.35 ± 1.84	10.12 ± 2.3	56.37 ± 1.16	62.29 ± 1.5	59.38 ± 2.27	61.41 ± 1.99

**Appendix D:** High frequency oscillatory power in the SO cycle in the CA1 region of the hippocampus, in 4 frequency bands: theta, beta, and high-gamma, in the non-ISM, pre-ISM, ISM and post-ISM segments, in WT (N = 7) animals and A30P (N = 8) animals.

<b>Mean power on the Up-state (x10<sup>3</sup>)</b>								
	<b>WT</b>				<b>A30P</b>			
Theta	20.39 ± 4.86	14.49 ± 2.05	21.33 ± 2.88	16.39 ± 2.48	30.52 ± 3.15	25.83 ± 3.19	46.9 ± 7.01	32.51 ± 5.34
Beta	40.86 ± 12.51	25.96 ± 5.07	49.04 ± 8.8	28.9 ± 6.52	68.21 ± 8.42	66.09 ± 12.25	189.73 ± 59.92	65.87 ± 10.54
Gamma	76.81 ± 25.56	47.43 ± 8.1	83.37 ± 14.43	46.82 ± 7.96	95.21 ± 14.95	93.17 ± 15.8	248.15 ± 78.06	91.19 ± 16.63
High-Gamma	18.26 ± 5.29	9.53 ± 2.06	14.21 ± 2.98	9.23 ± 2.94	24.49 ± 4.64	21.89 ± 4.62	33.64 ± 16.24	21.89 ± 4.66
<b>Mean power on the Down-state (x10<sup>3</sup>)</b>								
	<b>WT</b>				<b>A30P</b>			
Theta	8.18 ± 1.15	5.31 ± 0.59	11.61 ± 0.48	6.78 ± 0.84	12.49 ± 2.38	11.11 ± 2.22	28.76 ± 4.63	17.12 ± 3.7
Beta	17.46 ± 4.08	11.17 ± 3.05	33.02 ± 6.7	13.37 ± 2.95	31.8 ± 6.03	40.15 ± 12.16	155.89 ± 53.19	35.47 ± 5.86
Gamma	27.51 ± 6.22	18.64 ± 5.51	50.18 ± 10.59	22.18 ± 6.99	49.69 ± 12.03	61.83 ± 19.14	212 ± 74.93	55.57 ± 12.39
High-Gamma	7.21 ± 1.79	5.41 ± 0.9	9.46 ± 1.13	5.87 ± 0.95	16.47 ± 3.31	15.37 ± 3.3	28.29 ± 9.73	16.28 ± 3.34
<b>Peak in the normalised SO cycle (x10<sup>3</sup>)</b>								
	<b>WT</b>				<b>A30P</b>			
Theta	60.29 ± 1.13	65.53 ± 1.85	61.85 ± 1.42	58.91 ± 1.88	72.8 ± 9.14	37.57 ± 4.89	62.59 ± 9.83	48.62 ± 8.44
Beta	60.36 ± 3.26	62.89 ± 3.57	60.22 ± 2.8	62.13 ± 4.06	292.02 ± 34.24	274.77 ± 56.94	829.45 ± 275.38	276.24 ± 48.84
Gamma	59.48 ± 2.78	61.06 ± 2.9	61.06 ± 2.85	61.43 ± 3.09	445.33 ± 68.38	427.69 ± 80.43	1219.1 ± 395.58	423.86 ± 90.04
High-Gamma	59.12 ± 1.79	59.16 ± 5.61	60.01 ± 5.44	60.86 ± 4.94	150.1 ± 17.87	127.52 ± 8.34	211.39 ± 32.4	135.88 ± 10.61
<b>Peak latency in the normalised SO cycle (x10<sup>3</sup>)</b>								
	<b>WT</b>				<b>A30P</b>			

Theta	58.3 ± 14.89	26.64 ± 3.86	29.3 ± 4.07	27.15 ± 3.49	62.72 ± 1.09	69.79 ± 1.99	63.61 ± 1.09	58.61 ± 3.56
Beta	269.56 ± 115.57	127.01 ± 25.08	218.95 ± 36.6	127.2 ± 28.49	66.34 ± 1.68	70.17 ± 2.6	62.82 ± 1.47	60.18 ± 3.76
Gamma	494.7 ± 211.99	242.45 ± 47.28	385.21 ± 67.06	211.82 ± 33.02	66.71 ± 1.38	69.3 ± 0.6	63.94 ± 1.53	61.26 ± 2.61
High-Gamma	129.27 ± 31.43	65.74 ± 4.52	90.48 ± 4.38	57.97 ± 4.71	63.9 ± 1.52	63.15 ± 2.79	62.22 ± 8.14	59.9 ± 5.56

**Appendix E:** Characterisation of the SO cycle in the 4 mPFC subregions: ACC, PrL, IL and DP, in the non-ISM, pre-ISM, ISM and post-ISM segments, in WT (N = 8) and A30P (N = 13) animals.

SO Frequency $\pm$ SEM (Hz)								
	WT				A30P			
	Non-ISM	Pre-ISM	ISM	Post-ISM	Non-ISM	Pre-ISM	ISM	Post-ISM
ACC	0.27 $\pm$ 0.03	0.39 $\pm$ 0.04	0.47 $\pm$ 0.04	0.4 $\pm$ 0.04	0.36 $\pm$ 0.02	0.44 $\pm$ 0.02	0.48 $\pm$ 0.02	0.46 $\pm$ 0.02
PrL	0.29 $\pm$ 0.02	0.38 $\pm$ 0.04	0.47 $\pm$ 0.04	0.4 $\pm$ 0.04	0.37 $\pm$ 0.02	0.43 $\pm$ 0.02	0.48 $\pm$ 0.02	0.45 $\pm$ 0.02
IL	0.3 $\pm$ 0.02	0.38 $\pm$ 0.03	0.46 $\pm$ 0.03	0.39 $\pm$ 0.02	0.37 $\pm$ 0.02	0.41 $\pm$ 0.02	0.46 $\pm$ 0.02	0.43 $\pm$ 0.03
DP	0.3 $\pm$ 0.02	0.37 $\pm$ 0.03	0.46 $\pm$ 0.03	0.39 $\pm$ 0.03	0.37 $\pm$ 0.02	0.42 $\pm$ 0.02	0.46 $\pm$ 0.02	0.44 $\pm$ 0.02
Mean cycle length $\pm$ SEM (s)								
	WT				A30P			
	Non-ISM	Pre-ISM	Non-ISM	Pre-ISM	Non-ISM	Pre-ISM	Non-ISM	Pre-ISM
ACC	3.78 $\pm$ 0.32	2.76 $\pm$ 0.25	2.24 $\pm$ 0.24	2.6 $\pm$ 0.19	2.89 $\pm$ 0.14	2.26 $\pm$ 0.11	2.07 $\pm$ 0.08	2.16 $\pm$ 0.11
PrL	3.47 $\pm$ 0.21	2.75 $\pm$ 0.23	2.22 $\pm$ 0.21	2.6 $\pm$ 0.18	2.79 $\pm$ 0.13	2.34 $\pm$ 0.13	2.1 $\pm$ 0.08	2.21 $\pm$ 0.12
IL	3.29 $\pm$ 0.18	2.63 $\pm$ 0.15	2.2 $\pm$ 0.14	2.57 $\pm$ 0.11	2.77 $\pm$ 0.11	2.41 $\pm$ 0.14	2.2 $\pm$ 0.09	2.35 $\pm$ 0.15
DP	3.32 $\pm$ 0.15	2.67 $\pm$ 0.16	2.24 $\pm$ 0.15	2.61 $\pm$ 0.14	2.72 $\pm$ 0.11	2.38 $\pm$ 0.13	2.16 $\pm$ 0.08	2.26 $\pm$ 0.12
Mean Up-state length $\pm$ SEM (s)								
	WT				A30P			
	Non-ISM	Pre-ISM	Non-ISM	Pre-ISM	Non-ISM	Pre-ISM	Non-ISM	Pre-ISM
ACC	1.46 $\pm$ 0.17	1.17 $\pm$ 0.13	1 $\pm$ 0.14	1.13 $\pm$ 0.1	1.21 $\pm$ 0.04	0.93 $\pm$ 0.03	0.86 $\pm$ 0.02	0.89 $\pm$ 0.03
PrL	1.38 $\pm$ 0.12	1.14 $\pm$ 0.1	0.94 $\pm$ 0.11	1.09 $\pm$ 0.07	1.16 $\pm$ 0.03	0.91 $\pm$ 0.03	0.87 $\pm$ 0.02	0.86 $\pm$ 0.02
IL	1.36 $\pm$ 0.09	1.11 $\pm$ 0.09	0.95 $\pm$ 0.07	1.1 $\pm$ 0.06	1.2 $\pm$ 0.03	0.98 $\pm$ 0.04	0.93 $\pm$ 0.03	0.94 $\pm$ 0.04
DP	1.31 $\pm$ 0.09	1.07 $\pm$ 0.07	0.92 $\pm$ 0.06	1.06 $\pm$ 0.07	1.16 $\pm$ 0.03	0.94 $\pm$ 0.03	0.91 $\pm$ 0.02	0.9 $\pm$ 0.02
Mean Down-state length $\pm$ SEM (s)								
	WT				A30P			
	Non-ISM	Pre-ISM	Non-ISM	Pre-ISM	Non-ISM	Pre-ISM	Non-ISM	Pre-ISM
ACC	2.32 $\pm$ 0.17	1.59 $\pm$ 0.14	1.24 $\pm$ 0.11	1.47 $\pm$ 0.11	1.75 $\pm$ 0.1	1.34 $\pm$ 0.08	1.21 $\pm$ 0.06	1.27 $\pm$ 0.09

<b>PrL</b>	2.13 ± 0.14	1.62 ± 0.16	1.29 ± 0.13	1.52 ± 0.13	1.66 ± 0.09	1.42 ± 0.1	1.23 ± 0.07	1.34 ± 0.1
<b>IL</b>	1.95 ± 0.15	1.53 ± 0.13	1.25 ± 0.12	1.48 ± 0.11	1.65 ± 0.08	1.43 ± 0.1	1.27 ± 0.06	1.4 ± 0.11
<b>DP</b>	2.06 ± 0.12	1.62 ± 0.11	1.33 ± 0.11	1.55 ± 0.1	1.59 ± 0.09	1.44 ± 0.1	1.25 ± 0.07	1.36 ± 0.1
<b>Mean cycle length variability ± SEM (s)</b>								
	<b>WT</b>				<b>A30P</b>			
	<b>Non-ISM</b>	<b>Pre-ISM</b>	<b>Non-ISM</b>	<b>Pre-ISM</b>	<b>Non-ISM</b>	<b>Pre-ISM</b>	<b>Non-ISM</b>	<b>Pre-ISM</b>
<b>ACC</b>	2.43 ± 0.28	1.48 ± 0.17	1.13 ± 0.15	1.35 ± 0.16	1.45 ± 0.13	0.99 ± 0.08	1.01 ± 0.06	1.04 ± 0.1
<b>PrL</b>	2.23 ± 0.19	1.39 ± 0.16	1.08 ± 0.15	1.29 ± 0.14	1.37 ± 0.12	0.94 ± 0.09	0.96 ± 0.05	0.98 ± 0.1
<b>IL</b>	2.07 ± 0.22	1.28 ± 0.12	1.01 ± 0.1	1.19 ± 0.11	1.3 ± 0.11	0.97 ± 0.09	0.99 ± 0.07	1.04 ± 0.1
<b>DP</b>	2.15 ± 0.22	1.3 ± 0.11	1.07 ± 0.11	1.21 ± 0.1	1.25 ± 0.11	0.93 ± 0.09	0.93 ± 0.06	0.96 ± 0.09
<b>Mean Up-state length variability ± SEM (s)</b>								
	<b>WT</b>				<b>A30P</b>			
	<b>Non-ISM</b>	<b>Pre-ISM</b>	<b>Non-ISM</b>	<b>Pre-ISM</b>	<b>Non-ISM</b>	<b>Pre-ISM</b>	<b>Non-ISM</b>	<b>Pre-ISM</b>
<b>ACC</b>	0.7 ± 0.1	0.66 ± 0.1	0.55 ± 0.09	0.59 ± 0.08	0.52 ± 0.04	0.46 ± 0.05	0.44 ± 0.02	0.44 ± 0.05
<b>PrL</b>	0.66 ± 0.08	0.64 ± 0.08	0.51 ± 0.1	0.56 ± 0.06	0.46 ± 0.03	0.39 ± 0.03	0.41 ± 0.02	0.36 ± 0.01
<b>IL</b>	0.64 ± 0.08	0.57 ± 0.08	0.49 ± 0.07	0.53 ± 0.06	0.49 ± 0.03	0.44 ± 0.04	0.45 ± 0.04	0.41 ± 0.03
<b>DP</b>	0.6 ± 0.04	0.56 ± 0.07	0.48 ± 0.06	0.52 ± 0.05	0.45 ± 0.03	0.38 ± 0.03	0.42 ± 0.02	0.37 ± 0.02
<b>SO frequency ± SEM (Hz)</b>								
	<b>WT</b>				<b>A30P</b>			
	<b>Non-ISM</b>	<b>Pre-ISM</b>	<b>Non-ISM</b>	<b>Pre-ISM</b>	<b>Non-ISM</b>	<b>Pre-ISM</b>	<b>Non-ISM</b>	<b>Pre-ISM</b>
<b>ACC</b>	2.08 ± 0.28	1.17 ± 0.13	0.86 ± 0.1	1.07 ± 0.11	1.21 ± 0.13	0.81 ± 0.07	0.82 ± 0.06	0.86 ± 0.09
<b>PrL</b>	1.91 ± 0.18	1.13 ± 0.15	0.82 ± 0.12	1.03 ± 0.12	1.14 ± 0.12	0.8 ± 0.08	0.76 ± 0.06	0.85 ± 0.1
<b>IL</b>	1.73 ± 0.23	1.02 ± 0.12	0.75 ± 0.1	0.92 ± 0.1	1.05 ± 0.1	0.78 ± 0.08	0.78 ± 0.06	0.86 ± 0.1
<b>DP</b>	1.86 ± 0.22	1.1 ± 0.1	0.86 ± 0.09	0.99 ± 0.09	1.02 ± 0.11	0.79 ± 0.08	0.74 ± 0.06	0.81 ± 0.09
<b>SO amplitude ± SEM (mV)</b>								
	<b>WT</b>				<b>A30P</b>			
	<b>Non-ISM</b>	<b>Pre-ISM</b>	<b>Non-ISM</b>	<b>Pre-ISM</b>	<b>Non-ISM</b>	<b>Pre-ISM</b>	<b>Non-ISM</b>	<b>Pre-ISM</b>

<b>ACC</b>	0.43 ± 0.04	0.47 ± 0.04	0.48 ± 0.04	0.47 ± 0.04	0.34 ± 0.03	0.42 ± 0.03	0.42 ± 0.03	0.41 ± 0.03
<b>PrL</b>	0.49 ± 0.06	0.56 ± 0.05	0.58 ± 0.05	0.56 ± 0.05	0.42 ± 0.04	0.46 ± 0.03	0.47 ± 0.04	0.46 ± 0.03
<b>IL</b>	0.55 ± 0.05	0.59 ± 0.04	0.61 ± 0.04	0.59 ± 0.04	0.47 ± 0.03	0.53 ± 0.03	0.54 ± 0.03	0.53 ± 0.03
<b>DP</b>	0.52 ± 0.04	0.58 ± 0.03	0.62 ± 0.03	0.59 ± 0.03	0.47 ± 0.03	0.53 ± 0.03	0.54 ± 0.03	0.53 ± 0.03

**Appendix F:** Characterisation of the SO cycle in the CA1 region of the hippocampus in the non-ISM, pre-ISM, ISM and post-ISM segments, in WT (N = 7) animals and A30P (N = 8) animals.

Variable	WT				A30P			
	Non-ISM	Pre-ISM	Non-ISM	Pre-ISM	Non-ISM	Pre-ISM	Non-ISM	Pre-ISM
SO frequency (Hz)	0.29 ± 0.02	0.35 ± 0.02	0.41 ± 0.03	0.37 ± 0.03	0.37 ± 0.01	0.45 ± 0.03	0.49 ± 0.03	0.47 ± 0.04
Cycle length (s)	3.46 ± 0.2	2.81 ± 0.18	2.47 ± 0.21	2.61 ± 0.15	2.69 ± 0.1	2.15 ± 0.11	2.06 ± 0.13	2.08 ± 0.15
Up-state length (s)	2.13 ± 0.06	1.29 ± 0.04	1.21 ± 0.06	1.27 ± 0.04	1.17 ± 0.02	0.9 ± 0.03	0.87 ± 0.03	0.89 ± 0.05
Down-state length (s)	1.33 ± 0.19	1.08 ± 0.07	1 ± 0.1	1.08 ± 0.1	0.09 ± 0.09	0.09 ± 0.09	0.11 ± 0.11	0.12 ± 0.12
Cycle length variability (s)	2.01 ± 0.21	1.4 ± 0.09	1.12 ± 0.06	1.22 ± 0.09	1.12 ± 0.06	0.77 ± 0.05	0.88 ± 0.07	0.84 ± 0.06
Up-state length variability (s)	1.69 ± 0.08	1.18 ± 0.06	0.9 ± 0.04	1 ± 0.03	0.42 ± 0.03	0.39 ± 0.06	0.36 ± 0.05	0.41 ± 0.06
Down-state length variability (s)	0.49 ± 0.21	0.38 ± 0.1	0.44 ± 0.06	0.41 ± 0.08	0.92 ± 0.08	0.64 ± 0.05	0.7 ± 0.07	0.71 ± 0.07
Amplitude (mV)	0.32 ± 0.04	0.49 ± 0.07	0.45 ± 0.05	0.43 ± 0.05	0.25 ± 0.03	0.35 ± 0.04	0.31 ± 0.03	0.31 ± 0.03

## Appendix G

The significant effects of the between subjects variables (ISM segment, mPFC subregion) as indicated by rmANOVA analysis of the high frequency oscillatory power in the SO cycle in the mPFC region for WT and A30P animals. We did not pursue a further analysis as there was not effect of genotypic group, or a genotype/segment or genotype/region interaction unless otherwise specified.

### *i. Effect of ISM segment*

Theta band power on the Up-state was highly affected by segment ( $F(3, 57) = 20.14, p < 0.001$ ) with greater power during the ISM compared to all other segments (non-ISM:  $p < 0.05$ ; pre-ISM, post-ISM ( $p < 0.001$ )). Beta band power on the Up-state was also greatly affected by segment ( $F(3, 57) = 46.45, p < 0.001$ ), with greater power during the ISM compared to all other segments ( $p < 0.001$ ), and in the non-ISM compared to the pre-ISM and post-ISM segments ( $p < 0.05$ ). The power on the Up-state in the gamma ( $F(2.69, 51.04) = 20.35, p < 0.001$ ) and high-gamma ( $F(1.36, 25.76) = 10.26, p < 0.001$ ) frequency ranges was greater power in the ISM ( $p < 0.01$ ) and non-ISM segments ( $p < 0.05$ ) compared to the pre-ISM and post-ISM segments.

On the Down-state, theta and beta band power were affected by segment ( $F(3, 57) = 25.09, p < 0.001$ ;  $F(1.4, 26.65) = 17.61, p < 0.001$ ), with higher levels of power in these bands during the ISM compared to all other segments ( $p < 0.001$ ). In the gamma band, power on the Down-state was affected by segment ( $F(1.32, 25.01) = 11.92, p < 0.01$ ) as the gamma band power was greater during the ISM segment compared to all other segments (non-ISM, post-ISM:  $p < 0.05$ ; pre-ISM:  $p < 0.01$ ), and in the post-ISM compared to the non-ISM segment ( $p < 0.05$ ). Finally, high-gamma power was not influenced by segment.

The next variable of interest was the peak power. The theta band peak power was highly affected by segment ( $F(2.1, 39.83) = 20.46, p < 0.001$ ), with a greater peak identified in the non-ISM compared to the pre-ISM and post-ISM segments ( $p < 0.001$ ), and in the ISM segment compared to the post-ISM segment ( $p < 0.05$ ). The beta band peak power was also influenced by segment ( $F(1.25, 23.69) = 15.64, p < 0.001$ ) and so was the high-gamma band peak power ( $F(1.76, 33.39) = 33.45, p < 0.001$ ), as they were lower in the pre-ISM and post-ISM segments compared to the non-ISM segment

( $p < 0.001$ ). Finally, the gamma peak power was affected by segment ( $F(1.18, 22.46) = 15.1, p < 0.001$ ), as it was greater in the non-ISM segment compared to all other segments (non-ISM, post-ISM:  $p < 0.001$ ; pre-ISM:  $p < 0.05$ ). We did not find specific effects of segment in the peak power latency.

ii. *Effect of mPFC subregion*

The mPFC subregion also affected a number of our high frequency power-related variables. Gamma band power on the Up-state was significantly affected by subregion ( $F(1.95, 37.12) = 12.12, p < 0.001$ ), with the greatest gamma band power found in the IL and ACC subregions compared to the DP ( $p < 0.01$ ). Beta power on the Up-state was affected by region ( $F(1.86, 35.39) = 8.46, p < 0.01$ ), with greater power in the PrL ( $p < 0.01$ ) and ACC ( $p < 0.05$ ) subregions compared to the DP subregion, and in the PrL compared to the IL subregion ( $p < 0.05$ ). High-gamma power on the Up-state ( $F(3, 57) = 7.02, p < 0.01$ ) was also greater in the PrL and ACC subregions compared to the DP subregion ( $p < 0.05$ ). We did not find an effect of region in power on the Down-state in any frequency band.

The mPFC subregion also influenced the peak power in most frequency bands. In the beta band ( $F(2.13, 40.37) = 9.76, p < 0.001$ ), the peak power was lower in the DP compared to the ACC, IL ( $p < 0.05$ ) and PrL ( $p < 0.01$ ) subregions. The peak was also shorter in the PrL compared to the IL subregion ( $p < 0.05$ ). Similarly in the gamma ( $F(2.29, 43.44) = 15.1, p < 0.001$ ) and high-gamma bands ( $F(3, 57) = 10.07, p < 0.001$ ), the DP peak power was the shortest, as it was lower than the IL ( $p < 0.05$ ), PrL ( $p < 0.001$ ) and ACC ( $p < 0.01$ ) subregions. The second smallest peak was in the IL, as it was shorter than the PrL ( $p < 0.01$ ) and ACC ( $p < 0.05$ ) subregions. The theta peak power was not affected by region. We did not find specific effects of region in the latency to peak power.

## Appendix H

The significant effects of the between subjects variables (ISM segment, mPFC subregion) as indicated by rmANOVA analysis of the SO cycle characteristics, for WT and A30P animals. We did not pursue a further analysis as there was not effect of genotypic group, or a genotype/segment or genotype/region interaction unless otherwise specified.

### I. Medial prefrontal cortex (mPFC)

The SO amplitude was significantly affected by segment ( $F(1.17, 3.05) = 34.12$ ,  $p < 0.001$ ), with significantly greater amplitude in the ISM compared to all other segments, and in the pre-ISM and post-ISM segments compared to the non-ISM one ( $p < 0.001$ ). The SO frequency was also influenced by segment ( $F(3, 57) = 20.36$ ,  $p < 0.001$ ), as it was highest in the ISM compared to all other segments ( $p < 0.001$ ). As expected, the SO cycle length ( $F(1.17, 3.05) = 36.08$ ,  $p < 0.001$ ) was shorter in the ISM compared to all other segments ( $p < 0.001$ ), and in the post-ISM compared to the non-ISM segment ( $p < 0.01$ ). The Up-state length t ( $F(3, 57) = 71.59$ ,  $p < 0.001$ ) was significantly shorter during the ISM compared to the non-ISM ( $p < 0.001$ ), pre-ISM ( $p < 0.01$ ) and post-ISM ( $p < 0.05$ ) segments, and in the post-ISM and pre-ISM compared to the non-ISM segment ( $p < 0.001$ ). The Down-state ( $F(3, 57) = 18.27$ ,  $p < 0.001$ ) was shorter in the ISM compared to all other segments ( $p < 0.001$ ).

We next looked at measures of state length variability. The SO cycle length variability was affected by segment ( $F(3, 57) = 25.22$ ,  $p < 0.001$ ), with lower variability in the ISM compared to the other segments (non-ISM:  $p < 0.001$ ; pre-ISM, post-ISM:  $p < 0.01$ ), and in the post-ISM compared to the non-ISM segment ( $p < 0.01$ ). Up-state length variability ( $F(3, 57) = 19.36$ ,  $p < 0.001$ ) was greater in the non-ISM compared to all other segments ( $p < 0.001$ ). Down-state length variability ( $F(2.78, 52.57) = 14.64$ ,  $p < 0.001$ ) was lower in the non-ISM compared to all other segments (non-ISM:  $p < 0.001$ ; pre-ISM, post-ISM:  $p < 0.01$ ).

The SO amplitude was significantly affected by region ( $F(3, 57) = 17.65$ ,  $p < 0.001$ ), with lower amplitude in the ACC compared to the other regions ( $p < 0.01$ ). The effect of region in the SO frequency ( $F(1.94, 36.9) = 4.59$ ,  $p < 0.05$ ) was also due to a lower frequency in the ACC compared to the PrL region ( $p < 0.05$ ). The cycle length

was also affected by region ( $F(1.66, 31.61) = 5.51, p < 0.05$ ) although we could not identify where that difference occurred. No effect of region was seen in the Up-state while Down-state length ( $F(2.41, 45.73) = 7.18, p < 0.01$ ), was longer in the ACC compared to the DP and IL regions ( $p < 0.05$ ). Region also affected the SO state-length variability over time ( $F(2.31, 43.82) = 9.29, p < 0.01$ ), with more variability in the ACC compared to the DP ( $p < 0.01$ ) and IL ( $p < 0.05$ ) regions. This finding cannot be attributed to the Up-state as we did not find an effect of region in this variable. However, we found that the variability of the Down-state length ( $F(3, 57) = 8.05, p < 0.001$ ) was also greater in the ACC compared to the IL and DP regions ( $p < 0.05$ ). Generally, the ACC appears to differ a little to the other segments. However, this may be attributed to the shorter SO amplitude of this region that makes state-length detection harder. Hence, the differences in the ACC it might be the effect of less-accurate state detection rather than a physiological effect.

## II. CA1 region of the hippocampus

The SO amplitude was significantly affected by segment ( $F(1.67, 21.7) = 20.09, p < 0.001$ ), with significantly greater amplitude in the ISM compared to the non-ISM ( $p < 0.001$ ) and post-ISM segments ( $p < 0.01$ ) and in the pre-ISM and post-ISM segments compared to the non-ISM one ( $p < 0.01$ ). The SO frequency was also influenced by segment ( $F(3, 39) = 20.93, p < 0.001$ ), as it was lowest in the non-ISM compared to all other segments ( $p < 0.001$ ). As expected, the SO cycle length ( $F(3, 39) = 8.53, p < 0.01$ ) was longer in the non-ISM compared to the ISM ( $p < 0.001$ ) and post-ISM segment ( $p < 0.01$ ). Similarly, the Up-state length ( $F(3, 39) = 43.43, p < 0.001$ ) was significantly longer in non-ISM compared to all other segments ( $p < 0.001$ ). The Down-state ( $F(2.02, 26.21) = 4.66, p < 0.05$ ) was only longer in the non-ISM compared the ISM segment ( $p < 0.05$ ).

The SO cycle length variability was affected by segment ( $F(2.49, 32.34) = 5.11, p < 0.05$ ), with greater variability in the non-ISM compared to the ISM ( $p < 0.05$ ) and post-ISM segments ( $p < 0.01$ ). The Up-state length variability was not affected by segment, but the Down-state length variability ( $F(2.46, 32) = 4.4, p < 0.05$ ) was greater in the non-ISM compared to the post-ISM ( $p < 0.05$ ) and likely to the ISM segment ( $p = 0.052$ ).



## References

- Adamowicz, D.H., Roy, S., Salmon, D.P., Galasko, D.R., Hansen, L.A., Masliah, E. & Gage, F.H. (2017) Hippocampal  $\alpha$ -Synuclein in Dementia with Lewy Bodies Contributes to Memory Impairment and Is Consistent with Spread of Pathology. *Journal of Neuroscience*. 37 (7), 1675–1684.
- Adler, G., Brassens, S., Chwalek, K., Dieter, B. & Teufel, M. (2004) Prediction of treatment response to rivastigmine in Alzheimer's dementia. *Journal of neurology, neurosurgery, and psychiatry*. 75 (2), 292–4.
- Adragna, M.G. & Klein, E.F. (2003) 'Acid-base balance', in *Wylie and Churchill-Davidsons: A Practice of Anesthesia, Seventh Edition*. [Online]. CRC Press. pp. 321–332.
- Agosta, F., Pievani, M., Geroldi, C., Copetti, M., Frisoni, G.B. & Filippi, M. (2012) Resting state fMRI in Alzheimer's disease: beyond the default mode network. *Neurobiology of Aging*. 33 (8), 1564–1578.
- Aldridge, G.M., Birnschein, A., Denburg, N.L. & Narayanan, N.S. (2018) Parkinson's Disease Dementia and Dementia with Lewy Bodies Have Similar Neuropsychological Profiles. *Frontiers in Neurology*. 9 (123).
- Alhola, P. & Polo-Kantola, P. (2007) Sleep deprivation: Impact on cognitive performance. *Neuropsychiatric Disease and Treatment* 3 (5) p.553–567.
- Alves, P.N., Foulon, C., Karolis, V., Bzdok, D., Margulies, D.S., Volle, E. & Thiebaut de Schotten, M. (2019) An improved neuroanatomical model of the default-mode network reconciles previous neuroimaging and neuropathological findings. *Communications Biology*. 2 (1).
- Amzica, F. & da Silva, F.H.L. (2017) 'Cellular Substrates of Brain Rhythms', in D. L. Schomer & F. H. L. da Silva (eds.) *Niedermeyer's Electroencephalography: Basic Principles, Clinical Applications, and Related Fields - Oxford Medicine*. 7th edition [Online]. Oxford University Press.
- Andersson, M., Hansson, O., Minthon, L., Ros&eacut;n, I. & Londos, E. (2008) Electroencephalogram Variability in Dementia with Lewy Bodies, Alzheimer's

Disease and Controls. *Dementia and Geriatric Cognitive Disorders*. 26 (3), 284–290.

Andrillon, T., Nir, Y., Staba, R.J., Ferrarelli, F., Cirelli, C., Tononi, G. & Fried, I. (2011) Sleep spindles in humans: insights from intracranial EEG and unit recordings. *The Journal of neuroscience : the official journal of the Society for Neuroscience*. 31 (49), 17821–34.

Arbel-Ornath, M., Hudry, E., Boivin, J.R., Hashimoto, T., Takeda, S., Kuchibhotla, K. V., Hou, S., Lattarulo, C.R., Belcher, A.M., Shakerdge, N., Trujillo, P.B., Muzikansky, A., Betensky, R.A., Hyman, B.T. & Bacskai, B.J. (2017) Soluble oligomeric amyloid- $\beta$  induces calcium dyshomeostasis that precedes synapse loss in the living mouse brain. *Molecular Neurodegeneration*. 12 (1), 27.

Ashford, J.W. (2019) The Dichotomy of Alzheimer's Disease Pathology: Amyloid- $\beta$  and Tau. *Journal of Alzheimer's Disease* 68 (1) p.77–83.

Astori, S., Wimmer, R.D. & Lüthi, A. (2013) Manipulating sleep spindles - expanding views on sleep, memory, and disease. *Trends in Neurosciences* 36 (12) p.738–748.

Avery, M.C. & Krichmar, J.L. (2017) Neuromodulatory systems and their interactions: A review of models, theories, and experiments. *Frontiers in Neural Circuits* 11.

Babiloni, C., Binetti, G., Cassetta, E., Forno, G.D., Percio, C. Del, Ferreri, F., Ferri, R., Frisoni, G., Hirata, K., Lanuzza, B., Miniussi, C., Moretti, D. V., Nobili, F., Rodriguez, G., Romani, G.L., Salinari, S. & Rossini, P.M. (2006) Sources of cortical rhythms change as a function of cognitive impairment in pathological aging: a multicenter study. *Clinical Neurophysiology*. 117 (2), 252–268.

Babiloni, C., Del Percio, C., Bordet, R., Bourriez, J.-L., Bentivoglio, M., Payoux, P., Derambure, P., Dix, S., Infarinato, F., Lizio, R., Triggiani, A.I., Richardson, J.C. & Rossini, P.M. (2013) Effects of acetylcholinesterase inhibitors and memantine on resting-state electroencephalographic rhythms in Alzheimer's disease patients. *Clinical Neurophysiology*. 124 (5), 837–850.

Badiola, N., de Oliveira, R.M., Herrera, F., Guardia-Laguarta, C., Gonçalves, S.A., Pera, M., Suárez-Calvet, M., Clarimon, J., Outeiro, T.F. & Lleó, A. (2011) Tau

- Enhances  $\alpha$ -Synuclein Aggregation and Toxicity in Cellular Models of Synucleinopathy Koichi M. Iijima (ed.). *PLoS ONE*. 6 (10), e26609.
- Ballard, C.G., Aarsland, D., McKeith, I., O'Brien, J., Gray, A., Cormack, F., Burn, D., Cassidy, T., Starfeldt, R., Larsen, J.-P., Brown, R. & Tovee, M. (2002) Fluctuations in attention: PD dementia vs DLB with parkinsonism. *Neurology*. 59 (11), 1714–20.
- Ballinger, E.C., Ananth, M., Talmage, D.A. & Role, L.W. (2016) Basal Forebrain Cholinergic Circuits and Signaling in Cognition and Cognitive Decline. *Neuron* 91 (6) p.1199–1218.
- Barage, S.H. & Sonawane, K.D. (2015) Amyloid cascade hypothesis: Pathogenesis and therapeutic strategies in Alzheimer's disease. *Neuropeptides* 52 p.1–18.
- Barber, P.A., Varma, A.R., Lloyd, J.J., Haworth, B., Snowden, J.S. & Neary, D. (2000) The electroencephalogram in dementia with Lewy bodies. *Acta neurologica Scandinavica*. 101 (1), 53–6.
- Barraud, Q., Lambrecq, V., Forni, C., McGuire, S., Hill, M., Bioulac, B., Balzamo, E., Bezard, E., Tison, F. & Ghorayeb, I. (2009) Sleep disorders in Parkinson's disease: The contribution of the MPTP non-human primate model. *Experimental Neurology*. 219 (2), 574–582.
- Barthó, P., Slézia, A., Mátyás, F., Faradzs-Zade, L., Ulbert, I., Harris, K.D. & Acsády, L. (2014) Ongoing network state controls the length of sleep spindles via inhibitory activity. *Neuron*. 82 (6), 1367–79.
- Bartlett, M.S. (1950) Periodogram Analysis and Continuous Spectra. *Biometrika*. 37 (1/2), 1.
- Bartos, M., Vida, I. & Jonas, P. (2007) Synaptic mechanisms of synchronized gamma oscillations in inhibitory interneuron networks. *Nature Reviews Neuroscience*. 8 (1), 45–56.
- Batalini, F., Avidan, A., Moseley, B.D. & Ringman, J.M. (2016) Improvement of Dream Enactment Behavior Associated with Levetiracetam Treatment in Dementia with Lewy Bodies. *Alzheimer Disease and Associated Disorders*. 30 (2), 175–177.

- Bazanov, O.M. & Vernon, D. (2014) Interpreting EEG alpha activity. *Neuroscience & Biobehavioral Reviews*. 4494–110.
- Beach, T.G., Adler, C.H., Sue, L.I., Vedders, L., Lue, L., White Iii, C.L., Akiyama, H., Caviness, J.N., Shill, H.A., Sabbagh, M.N., Walker, D.G. & Arizona Parkinson's Disease Consortium, D.G. (2010) Multi-organ distribution of phosphorylated alpha-synuclein histopathology in subjects with Lewy body disorders. *Acta neuropathologica*. 119 (6), 689–702.
- Beagle, A.J., Darwish, S.M., Ranasinghe, K.G., La, A.L., Karageorgiou, E. & Vossel, K.A. (2017) Relative Incidence of Seizures and Myoclonus in Alzheimer's Disease, Dementia with Lewy Bodies, and Frontotemporal Dementia. *Journal of Alzheimer's disease : JAD*. 60 (1), 211–223.
- Beckstead, R.M. (1979) An autoradiographic examination of corticocortical and subcortical projections of the mediodorsal-projection (prefrontal) cortex in the rat. *The Journal of Comparative Neurology*. 184 (1), 43–62.
- Beenhakker, M.P. & Huguenard, J.R. (2009) Neurons that fire together also conspire together: is normal sleep circuitry hijacked to generate epilepsy? *Neuron*. 62 (5), 612–32.
- Bell, A.J. & Sejnowski, T.J. (1995) An information-maximization approach to blind separation and blind deconvolution. *Neural computation*. 7 (6), 1129–59.
- Belluscio, M.A., Mizuseki, K., Schmidt, R., Kempter, R. & Buzsáki, G. (2012) Cross-frequency phase-phase coupling between  $\theta$  and  $\gamma$  oscillations in the hippocampus. *The Journal of neuroscience : the official journal of the Society for Neuroscience*. 32 (2), 423–35.
- Bergmann, B.M., Winter, J.B., Rosenberg, R.S. & Rechtschaffen, A. (1987) NREM Sleep with Low-Voltage EEG in the Rat. *Sleep*. 10 (1), 1–11.
- Berke, J.D., Hetrick, V., Breck, J. & Greene, R.W. (2008) Transient 23-30 Hz oscillations in mouse hippocampus during exploration of novel environments. *Hippocampus*. 18 (5), 519–529.
- Bernardi, G., Siclari, F., Handjaras, G., Riedner, B.A. & Tononi, G. (2018) Local and

Widespread Slow Waves in Stable NREM Sleep: Evidence for Distinct Regulation Mechanisms. *Frontiers in Human Neuroscience*. 12248.

Bertram, E.H. & Zhang, D.X. (1999) Thalamic excitation of hippocampal CA1 neurons: A comparison with the effects of CA3 stimulation. *Neuroscience*. 92 (1), 15–26.

Binnewijzend, M.A.A., Schoonheim, M.M., Sanz-Arigita, E., Wink, A.M., van der Flier, W.M., Tolboom, N., Adriaanse, S.M., Damoiseaux, J.S., Scheltens, P., van Berckel, B.N.M. & Barkhof, F. (2012) Resting-state fMRI changes in Alzheimer's disease and mild cognitive impairment. *Neurobiology of aging*. 33 (9), 2018–28.

Bird, C.M. & Burgess, N. (2008) The hippocampus and memory: insights from spatial processing. *Nature Reviews Neuroscience*. 9 (3), 182–194.

Bliwise, D.L., Trotti, L.M., Wilson, A.G., Greer, S.A., Wood-Siverio, C., Juncos, J.J., Factor, S.A., Freeman, A. & Rye, D.B. (2012) Daytime alertness in Parkinson's disease: potentially dose-dependent, divergent effects by drug class. *Movement disorders : official journal of the Movement Disorder Society*. 27 (9), 1118–24.

Blumenfeld, H. (2005) Cellular and Network Mechanisms of Spike-Wave Seizures. *Epilepsia*. 46 (s9), 21–33.

Bódizs, R., Kántor, S., Szabó, G., Szûcs, A., Eröss, L. & Halász, P. (2001) Rhythmic hippocampal slow oscillation characterizes REM sleep in humans. *Hippocampus*. 11 (6), 747–753.

Boeve, B.F., Silber, M.H., Ferman, T.J., Lin, S.C., Benarroch, E.E., Schmeichel, A.M., Ahlskog, J.E., Caselli, R.J., Jacobson, S., Sabbagh, M., Adler, C., Woodruff, B., Beach, T.G., Iranzo, A., Gelpi, E., Santamaria, J., Tolosa, E., Singer, C., Mash, D.C., et al. (2013) Clinicopathologic correlations in 172 cases of rapid eye movement sleep behavior disorder with or without a coexisting neurologic disorder. *Sleep Medicine*. 14 (8), 754–762.

Boeve, B.F., Silber, M.H., Parisi, J.E., Dickson, D.W., Ferman, T.J., Benarroch, E.E., Schmeichel, A.M., Smith, G.E., Petersen, R.C., Ahlskog, J.E., Matsumoto, J.Y., Knopman, D.S., Schenck, C.H. & Mahowald, M.W. (2003) Synucleinopathy pathology and REM sleep behavior disorder plus dementia or parkinsonism. *Neurology*. 61 (1), 40–5.

- Bohnen, N.I. & Albin, R.L. (2011) The cholinergic system and Parkinson disease. *Behavioural brain research*. 221 (2), 564–73.
- Bohnen, N.I. & Hu, M.T.M.M. (2019) Sleep Disturbance as Potential Risk and Progression Factor for Parkinson's Disease. *Journal of Parkinson's disease*. 9 (3), 603–614.
- Bonanni, L., Franciotti, R., Nobili, F., Kramberger, M.G., Taylor, J.-P., Garcia-Ptacek, S., Falasca, N.W., Famá, F., Cromarty, R., Onofrj, M., Aarsland, D. & E-DLB study group (2016) EEG Markers of Dementia with Lewy Bodies: A Multicenter Cohort Study. *Journal of Alzheimer's Disease*. 54 (4), 1649–1657.
- Bonanni, L., Franciotti, R., Onofrj, V., Anzellotti, F., Mancino, E., Monaco, D., Gambi, F., Manzoli, L., Thomas, A. & Onofrj, M. (2010) Revisiting P300 cognitive studies for dementia diagnosis: Early dementia with Lewy bodies (DLB) and Alzheimer disease (AD). *Neurophysiologie Clinique/Clinical Neurophysiology*. 40 (5), 255–265.
- Bonanni, L., Perfetti, B., Bifulchetti, S., Taylor, J.-P., Franciotti, R., Parnetti, L., Thomas, A. & Onofrj, M. (2015) Quantitative electroencephalogram utility in predicting conversion of mild cognitive impairment to dementia with Lewy bodies. *Neurobiology of aging*. 36 (1), 434–45.
- Bonanni, L., Thomas, A., Tiraboschi, P., Perfetti, B., Varanese, S. & Onofrj, M. (2008) EEG comparisons in early Alzheimer's disease, dementia with Lewy bodies and Parkinson's disease with dementia patients with a 2-year follow-up. *Brain: a journal of neurology*. 131 (Pt 3), 690–705.
- Bonini, N.M. & Giasson, B.I. (2005) Snaring the Function of  $\alpha$ -Synuclein. *Cell*. 123 (3), 359–361.
- Bonjean, M., Baker, T., Lemieux, M., Timofeev, I., Sejnowski, T. & Bazhenov, M. (2011) Corticothalamic feedback controls sleep spindle duration in vivo. *Journal of Neuroscience*. 31 (25), 9124–9134.
- Booth, V. & Poe, G.R. (2006) Input source and strength influences overall firing phase of model hippocampal CA1 pyramidal cells during theta: relevance to REM sleep reactivation and memory consolidation. *Hippocampus*. 16 (2), 161–73.

- Bosboom, J.L.W., Stoffers, D., Stam, C.J., Berendse, H.W. & Wolters, E.C. (2009) Cholinergic modulation of MEG resting-state oscillatory activity in Parkinson's disease related dementia. *Clinical Neurophysiology*. 120 (5), 910–915.
- Bradshaw, J., Saling, M., Hopwood, M., Anderson, V. & Brodtmann, A. (2004) Fluctuating cognition in dementia with Lewy bodies and Alzheimer's disease is qualitatively distinct. *Journal of neurology, neurosurgery, and psychiatry*. 75 (3), 382–7.
- Brassen, S. & Adler, G. (2003) Short-term Effects of Acetylcholinesterase Inhibitor Treatment on EEG and Memory Performance in Alzheimer Patients: An Open, Controlled Trial. *Pharmacopsychiatry*. 36 (6), 304–308.
- Briel, R.C., McKeith, I.G., Barker, W.A., Hewitt, Y., Perry, R.H., Ince, P.G. & Fairbairn, A.F. (1999) EEG findings in dementia with Lewy bodies and Alzheimer's disease. *Journal of neurology, neurosurgery, and psychiatry*. 66 (3), 401–3.
- Brown, R.E., Basheer, R., McKenna, J.T., Strecker, R.E. & McCarley, R.W. (2012) Control of sleep and wakefulness. *Physiological Reviews*. 92 (3), 1087–1187.
- Buckner, R.L., Andrews-Hanna, J.R. & Schacter, D.L. (2008) The brain's default network: anatomy, function, and relevance to disease. *Annals of the New York Academy of Sciences*. 11241–38.
- Busche, M.A., Chen, X., Henning, H.A., Reichwald, J., Staufenbiel, M., Sakmann, B. & Konnerth, A. (2012) Critical role of soluble amyloid- $\beta$  for early hippocampal hyperactivity in a mouse model of Alzheimer's disease. *PNAS*. 109 (22), 8740–8745.
- Busche, M.A., Eichhoff, G., Adelsberger, H., Abramowski, D., Wiederhold, K.H., Haass, C., Staufenbiel, M., Konnerth, A. & Garaschuk, O. (2008) Clusters of hyperactive neurons near amyloid plaques in a mouse model of Alzheimer's disease. *Science*. 321 (5896), 1686–1689.
- Busche, M.A., Kekuš, M., Adelsberger, H., Noda, T., Förstl, H., Nelken, I. & Konnerth, A. (2015) Rescue of long-range circuit dysfunction in Alzheimer's disease models. *Nature Neuroscience*. 18 (11), 1623–1630.

- Butler, J.L., Mendonça, P.R.F., Robinson, H.P.C. & Paulsen, O. (2016) Systems/Circuits Intrinsic Cornu Ammonis Area 1 Theta-Nested Gamma Oscillations Induced by Optogenetic Theta Frequency Stimulation. *Journal of Neuroscience*. 36 (15), 4155–4169.
- Buzsáki, G. (2015) Hippocampal sharp wave-ripple: A cognitive biomarker for episodic memory and planning. *Hippocampus*. 25 (10), 1073–188.
- Buzsáki, G. & Draguhn, A. (2004) Neuronal Oscillations in Cortical Networks. *Science*. 304 (5679), 1926–1929.
- Buzsáki, G., Lai-Wo S., L. & Vanderwolf, C.H. (1983) Cellular bases of hippocampal EEG in the behaving rat. *Brain Research Reviews* 6 (2) p.139–171.
- Buzsáki, G. & Silva, F.L. da (2012) High frequency oscillations in the intact brain. *Progress in Neurobiology* 98 (3) p.241–249.
- Cagnin, A., Fragiaco, F., Camporese, G., Turco, M., Bussè, C., Ermani, M. & Montagnese, S. (2017) Sleep-Wake Profile in Dementia with Lewy Bodies, Alzheimer's Disease, and Normal Aging. *Journal of Alzheimer's Disease*. 55 (4), 1529–1536.
- Calderon, J., Perry, R.J., Erzinclioglu, S.W., Berrios, G.E., Dening, T.R. & Hodges, J.R. (2001) Perception, attention, and working memory are disproportionately impaired in dementia with Lewy bodies compared with Alzheimer's disease. *Journal of Neurology Neurosurgery and Psychiatry*. 70 (2), 157–164.
- Calo, L., Wegrzynowicz, M., Santivañez-Perez, J. & Grazia Spillantini, M. (2016) Synaptic failure and  $\alpha$ -synuclein. *Movement Disorders*. 31 (2), 169–177.
- Cantero, J.L., Atienza, M., Stickgold, R., Kahana, M.J., Madsen, J.R., Kocsis, B., Sotnikova, T.D., Gainetdinov, R.R., Caron, M.G. & Nicolelis, M.A.L. (2003) Sleep-Dependent theta Oscillations in the Human Hippocampus and Neocortex. *Journal of Neuroscience*. 23 (34), 10897–10903.
- Cape, E.G. & Jones, B.E. (1998) Differential modulation of high-frequency  $\gamma$ -electroencephalogram activity and sleep-wake state by noradrenaline and serotonin microinjections into the region of cholinergic basal ganglia neurons. *Journal of*

*Neuroscience*. 18 (7), 2653–2666.

- Carnicelli, L., Maestri, M., Di Coscio, E., Tognoni, G., Fabbrini, M., Schirru, A., Giorgi, F.S., Siciliano, G., Bonuccelli, U. & Bonanni, E. (2019) A longitudinal study of polysomnographic variables in patients with mild cognitive impairment converting to Alzheimer's disease. *Journal of Sleep Research*. 28 (5), 1–9.
- Carr, G.J. & Chi, E.M. (1992) Analysis of variance for repeated measures data: A generalized estimating equations approach. *Statistics in Medicine*. 11 (8), 1033–1040.
- Carrier, J., Viens, I., Poirier, G., Robillard, R., Lafortune, M., Vandewalle, G., Martin, N., Barakat, M., Paquet, J. & Filipini, D. (2011) Sleep slow wave changes during the middle years of life. *European Journal of Neuroscience*. 33 (4), 758–766.
- Carskadon, M.A. & Dement, W.C. (1980) Distribution of REM Sleep on a 90 Minute Sleep-Wake Schedule. *Sleep* 2 (3).
- Cartelli, D., Aliverti, A., Barbiroli, A., Santambrogio, C., Ragg, E.M., Casagrande, F.V.M., Cantele, F., Beltramone, S., Marangon, J., De Gregorio, C., Pandini, V., Emanuele, M., Chieregatti, E., Pieraccini, S., Holmqvist, S., Bubacco, L., Roybon, L., Pezzoli, G., Grandori, R., et al. (2016)  $\alpha$ -Synuclein is a Novel Microtubule Dynamase. *Scientific Reports*. 6.
- Castano-Prat, P., Perez-Mendez, L., Perez-Zabalza, M., Sanfeliu, C., Giménez-Llort, L. & Sanchez-Vives, M. V. (2019) Altered slow (<1 Hz) and fast (beta and gamma) neocortical oscillations in the 3xTg-AD mouse model of Alzheimer's disease under anesthesia. *Neurobiology of Aging*. 79142–151.
- Cavanagh, J.F. & Frank, M.J. (2014) Frontal theta as a mechanism for cognitive control. *Trends in cognitive sciences*. 18 (8), 414–21.
- Caviness, J.N. (2019) 'Treatment of myoclonus in degenerative disorders', in *Current Clinical Neurology*. [Online]. Humana Press Inc. pp. 277–280.
- Cedernaes, J., Osorio, R.S., Varga, A.W., Kam, K., Schiöth, H.B. & Benedict, C. (2017) Candidate mechanisms underlying the association between sleep-wake disruptions and Alzheimer's disease. *Sleep Medicine Reviews*. 31102–111.

- Chabran, E., Roquet, D., Gounot, D., Sourty, M., Armspach, J.-P. & Blanc, F. (2018) Functional Disconnectivity during Inter-Task Resting State in Dementia with Lewy Bodies. *Dementia and Geriatric Cognitive Disorders*. 45 (1–2), 105–120.
- Chai, C. & Lim, K.-L. (2014) Genetic Insights into Sporadic Parkinson's Disease Pathogenesis. *Current Genomics*. 14 (8), 486–501.
- Chan, C.S., Guzman, J.N., Ilijic, E., Mercer, J.N., Rick, C., Tkatch, T., Meredith, G.E. & Surmeier, D.J. (2007) 'Rejuvenation' protects neurons in mouse models of Parkinson's disease. *Nature*. 447 (7148), 1081–1086.
- Changeux, J.P., Bertrand, D., Corringier, P.J., Dehaene, S., Edelstein, S., Léna, C., Le Novère, N., Marubio, L., Picciotto, M. & Zoli, M. (1998) 'Brain nicotinic receptors: Structure and regulation, role in learning and reinforcement', in *Brain Research Reviews*. [Online]. May 1998 pp. 198–216.
- Chenkov, N.A., Kunst, S., Grimm, B., Gutachter, D.-I., Kempter, R., Sprekeler, H. & Both, M. (2017) *Network mechanisms underlying sharp-wave ripples and memory replay GABAergic modulation of sharp-wave ripples incidence Dissertation*. [Online]. Humboldt-Universität zu Berlin von.
- Chesselet, M.F., Richter, F., Zhu, C., Magen, I., Watson, M.B. & Subramaniam, S.R. (2012) A Progressive Mouse Model of Parkinson's Disease: The Thy1-aSyn ('Line 61') Mice. *Neurotherapeutics* 9 (2) p.297–314.
- Chinta, S.J., Mallajosyula, J.K., Rane, A. & Andersen, J.K. (2010) Mitochondrial alpha-synuclein accumulation impairs complex I function in dopaminergic neurons and results in increased mitophagy in vivo. *Neuroscience Letters*. 486 (3), 235–239.
- Christensen, J.A.E., Kempfner, J., Zoetmulder, M., Leonthin, H.L., Arvastson, L., Christensen, S.R., Sorensen, H.B.D. & Jennum, P. (2014) Decreased sleep spindle density in patients with idiopathic REM sleep behavior disorder and patients with Parkinson's disease. *Clinical Neurophysiology*. 125 (3), 512–519.
- Chwyszczuk, L., Breitve, M., Hynninen, M., Gjerstad, M.D., Aarsland, D. & Rongve, A. (2016) Higher Frequency and Complexity of Sleep Disturbances in Dementia with Lewy Bodies as Compared to Alzheimer's Disease. *Neurodegenerative Diseases*. 16 (3–4), 152–160.

- Clark, R.E., Broadbent, N.J. & Squire, L.R. (2005) Impaired remote spatial memory after hippocampal lesions despite extensive training beginning early in life. *Hippocampus*. 15 (3), 340–346.
- Clemens, Z., Mölle, M., Erőss, L., Jakus, R., Rásonyi, G., Halász, P. & Born, J. (2011) Fine-tuned coupling between human parahippocampal ripples and sleep spindles. *European Journal of Neuroscience*. 33 (3), 511–520.
- Clement, E.A., Richard, A., Thwaites, M., Ailon, J., Peters, S. & Dickson, C.T. (2008) Cyclic and Sleep-Like Spontaneous Alternations of Brain State Under Urethane Anaesthesia Ernest Greene (ed.). *PLoS ONE*. 3 (4), e2004.
- Clinton, L.K., Blurton-Jones, M., Myczek, K., Trojanowski, J.Q. & LaFerla, F.M. (2010) Synergistic interactions between A $\beta$ , tau, and  $\alpha$ -synuclein: Acceleration of neuropathology and cognitive decline. *Journal of Neuroscience*. 30 (21), 7281–7289.
- Colby-Milley, J., Cavanagh, C., Jegu, S., Breitner, J.C.S., Quirion, R. & Adamantidis, A. (2015) Sleep-Wake Cycle Dysfunction in the TgCRND8 Mouse Model of Alzheimer's Disease: From Early to Advanced Pathological Stages Vladyslav Vyazovskiy (ed.). *PLOS ONE*. 10 (6), e0130177.
- Colgin, L.L. (2013) Mechanisms and Functions of Theta Rhythms. *Annual Review of Neuroscience*. 36 (1), 295–312.
- Colgin, L.L. (2011) Oscillations and hippocampal–prefrontal synchrony. *Current Opinion in Neurobiology*. 21 (3), 467–474.
- Colgin, L.L., Denninger, T., Fyhn, M., Hafting, T., Bonnevie, T., Jensen, O., Moser, M.-B. & Moser, E.I. (2009) Frequency of gamma oscillations routes flow of information in the hippocampus. *Nature*. 462 (7271), 353–357.
- Colgin, L.L. & Moser, E.I. (2010) Gamma Oscillations in the Hippocampus. *Physiology*. 25 (5), 319–329.
- Colloby, S.J., Cromarty, R.A., Peraza, L.R., Johnsen, K., Jóhannesson, G., Bonanni, L., Onofrj, M., Barber, R., O'Brien, J.T. & Taylor, J.-P. (2016) Multimodal EEG-MRI in the differential diagnosis of Alzheimer's disease and dementia with Lewy

bodies. *Journal of psychiatric research*. 7848–55.

Colom-Cadena, M., Pegueroles, J., Herrmann, A.G., Henstridge, C.M., Muñoz, L., Querol-Vilaseca, M., Martín-Paniello, C.S., Luque-Cabecerans, J., Clarimon, J., Belbin, O., Núñez-Llaves, R., Blesa, R., Smith, C., McKenzie, C.A., Frosch, M.P., Roe, A., Fortea, J., Andilla, J., Loza-Alvarez, P., et al. (2017) Synaptic phosphorylated  $\alpha$ -synuclein in dementia with Lewy bodies. *Brain*. 140 (12), 3204–3214.

Combi, R., Ferini-Strambi, L. & Tenchini, M.L. (2009) CHRNA2 mutations are rare in the NFLE population: evaluation of a large cohort of Italian patients. *Sleep medicine*. 10 (1), 139–42.

Contestabile, A. (2011) The history of the cholinergic hypothesis. *Behavioural brain research*. 221 (2), 334–40.

Coulon, P., Budde, T. & Pape, H.C. (2012) The sleep relay-the role of the thalamus in central and decentral sleep regulation. *Pflugers Archiv European Journal of Physiology* 463 (1) p.53–71.

Cox, R., van Driel, J., de Boer, M. & Talamini, L.M. (2014) Slow oscillations during sleep coordinate interregional communication in cortical networks. *The Journal of neuroscience : the official journal of the Society for Neuroscience*. 34 (50), 16890–901.

Cox, R., Hofman, W.F. & Talamini, L.M. (2012) Involvement of spindles in memory consolidation is slow wave sleep-specific. *Learning & memory (Cold Spring Harbor, N.Y.)*. 19 (7), 264–7.

Cox, R., Schapiro, A.C., Manoach, D.S. & Stickgold, R. (2017) Individual Differences in Frequency and Topography of Slow and Fast Sleep Spindles. *Frontiers in Human Neuroscience*. 11433.

Craig, M.T. & McBain, C.J. (2015) Fast gamma oscillations are generated intrinsically in CA1 without the involvement of fast-spiking basket cells. *Journal of Neuroscience*. 35 (8), 3616–3624.

Cromarty, R.A., Elder, G.J., Graziadio, S., Baker, M., Bonanni, L., Onofrj, M., O'Brien,

- J.T. & Taylor, J.-P. (2016) Neurophysiological biomarkers for Lewy body dementias. *Clinical neurophysiology: official journal of the International Federation of Clinical Neurophysiology*. 127 (1), 349–59.
- Cruikshank, S.J., Ahmed, O.J., Stevens, T.R., Patrick, S.L., Gonzalez, A.N., Elmaleh, M. & Connors, B.W. (2012) Thalamic control of layer 1 circuits in prefrontal cortex. *Journal of Neuroscience*. 32 (49), 17813–17823.
- Crunelli, V. & Hughes, S.W. (2010) The slow (1 Hz) rhythm of non-REM sleep: A dialogue between three cardinal oscillators. *Nature Neuroscience* 13 (1) p.9–17.
- Cumbo, E. & Ligorì, L.D. (2010) Levetiracetam, lamotrigine, and phenobarbital in patients with epileptic seizures and Alzheimer's disease. *Epilepsy and Behavior*. 17 (4), 461–466.
- Cunningham, M.O., Pervouchine, D.D., Racca, C., Kopell, N.J., Davies, C.H., Jones, R.S.G., Traub, R.D. & Whittington, M.A. (2006) Neuronal metabolism governs cortical network response state. *Proceedings of the National Academy of Sciences of the United States of America*. 103 (14), 5597–5601.
- Dal Prà, I., Chiarini, A., Gui, L., Chakravarthy, B., Pacchiana, R., Gardenal, E., Whitfield, J.F. & Armato, U. (2015) Do Astrocytes Collaborate with Neurons in Spreading the “Infectious” A $\beta$  and Tau Drivers of Alzheimer's Disease? *The Neuroscientist*. 21 (1), 9–29.
- Damoiseaux, J.S., Prater, K.E., Miller, B.L. & Greicius, M.D. (2012) Functional connectivity tracks clinical deterioration in Alzheimer's disease. *Neurobiology of Aging*. 33 (4), 828.e19-828.e30.
- Dang-Vu, T.T., Schabus, M., Desseilles, M., Albouy, G., Boly, M., Darsaud, A., Gais, S., Rauchs, G., Sterpenich, V., Vandewalle, G., Carrier, J., Moonen, G., Balteau, E., Degueldre, C., Luxen, A., Phillips, C. & Maquet, P. (2008) Spontaneous neural activity during human slow wave sleep. *Proceedings of the National Academy of Sciences of the United States of America*. 105 (39), 15160–5.
- David, F., Schmiedt, J.T., Taylor, H.L., Orban, G., Di Giovanni, G., Uebele, V.N., Renger, J.J., Lambert, R.C., Leresche, N. & Crunelli, V. (2013) Essential thalamic contribution to slow waves of natural sleep. *Journal of Neuroscience*. 33 (50),

19599–19610.

- Davis, K.E., Fox, S. & Gigg, J. (2014) Increased Hippocampal Excitability in the 3xTgAD Mouse Model for Alzheimer's Disease In Vivo Christian Holscher (ed.). *PLoS ONE*. 9 (3), e91203.
- Delli Pizzi, S., Franciotti, R., Taylor, J.-P., Thomas, A., Tartaro, A., Onofrij, M. & Bonanni, L. (2015) Thalamic Involvement in Fluctuating Cognition in Dementia with Lewy Bodies: Magnetic Resonance Evidences. *Cerebral cortex (New York, N.Y. : 1991)*. 25 (10), 3682–9.
- Delorme, A. & Makeig, S. (2004) EEGLAB: an open source toolbox for analysis of single-trial EEG dynamics including independent component analysis. *Journal of Neuroscience Methods*. 134 (1), 9–21.
- Demuro, A. & Parker, I. (2013) Cytotoxicity of intracellular A $\beta$ 42 amyloid oligomers involves Ca<sup>2+</sup> release from the endoplasmic reticulum by stimulated production of inositol trisphosphate. *Journal of Neuroscience*. 33 (9), 3824–3833.
- Destexhe, A., Contreras, D. & Steriade, M. (1998) Mechanisms underlying the synchronizing action of corticothalamic feedback through inhibition of thalamic relay cells. *Journal of neurophysiology*. 79 (2), 999–1016.
- Destexhe, A., Hughes, S.W., Rudolph, M. & Crunelli, V. (2007) Are corticothalamic UP states fragments of wakefulness? *Trends in neurosciences*. 30 (7), 334.
- Détári, L., Rasmusson, D.D. & Semba, K. (1997) Phasic relationship between the activity of basal forebrain neurons and cortical EEG in urethane-anesthetized rat. *Brain research*. 759 (1), 112–21.
- DeVos, S.L., Corjuc, B.T., Oakley, D.H., Nobuhara, C.K., Bannon, R.N., Chase, A., Commins, C., Gonzalez, J.A., Dooley, P.M., Frosch, M.P. & Hyman, B.T. (2018) Synaptic Tau Seeding Precedes Tau Pathology in Human Alzheimer's Disease Brain. *Frontiers in Neuroscience*. 12 (261), 1–15.
- van Diggelen, F., Hrle, D., Apetri, M., Christiansen, G., Rammes, G., Tepper, A. & Otzen, D.E. (2019) Two conformationally distinct  $\alpha$ -synuclein oligomers share common epitopes and the ability to impair long-term potentiation. *PLoS ONE*. 14

(3), 1–22.

Diógenes, M.J., Dias, R.B., Rombo, D.M., Miranda, H.V., Maiolino, F., Guerreiro, P., Näsström, T., Franquelim, H.G., Oliveira, L.M.A., Castanho, M.A.R.B., Lannfelt, L., Bergström, J., Ingelsson, M., Quintas, A., Sebastião, A.M., Lopes, L. V & Outeiro, T.F. (2012) *Cellular/Molecular Extracellular Alpha-Synuclein Oligomers Modulate Synaptic Transmission and Impair LTP Via NMDA-Receptor Activation*.

Donaghy, P., Thomas, A.J. & O'Brien, J.T. (2015) Amyloid PET Imaging in Lewy Body Disorders. *The American Journal of Geriatric Psychiatry*. 23 (1), 23–37.

Donaghy, P.C. & McKeith, I.G. (2014) The clinical characteristics of dementia with Lewy bodies and a consideration of prodromal diagnosis. *Alzheimer's research & therapy*. 6 (4), 46.

Donahue, C.J., Glasser, M.F., Preuss, T.M., Rilling, J.K. & Van Essen, D.C. (2018) Quantitative assessment of prefrontal cortex in humans relative to nonhuman primates. *Proceedings of the National Academy of Sciences of the United States of America*. 115 (22), E5183–E5192.

Drexel, M., Kirchmair, E., Wieselthaler-Hölzl, A., Preidt, A.P. & Sperk, G. (2012) Somatostatin and neuropeptide Y neurons undergo different plasticity in parahippocampal regions in kainic acid-induced epilepsy. *Journal of Neuropathology and Experimental Neurology*. 71 (4), 312–329.

Drummond, E. & Wisniewski, T. (2017) Alzheimer's disease: experimental models and reality. *Acta Neuropathologica* 133 (2) p.155–175.

Durán, E., Oyanedel, C.N., Niethard, N., Inostroza, M. & Born, J. (2018) Sleep stage dynamics in neocortex and hippocampus. *Sleep*. 41 (6).

Van Dyk, K., Towns, S., Tatarina, O., Yeung, P., Dorrejo, J., Zahodne, L.B. & Stern, Y. (2016) Assessing Fluctuating Cognition in Dementia Diagnosis: Interrater Reliability of the Clinician Assessment of Fluctuation. *American journal of Alzheimer's disease and other dementias*. 31 (2), 137–43.

Ekmark-Lewén, S., Lindström, V., Gumucio, A., Ihse, E., Behere, A., Kahle, P.J., Nordström, E., Eriksson, M., Erlandsson, A., Bergström, J. & Ingelsson, M. (2018)

Early fine motor impairment and behavioral dysfunction in (Thy-1)-h[A30P] alpha-synuclein mice. *Brain and Behavior*. 8 (3), e00915.

Elder, G.J., Colloby, S.J., Firbank, M.J., McKeith, I.G. & Taylor, J.-P. (2019) Consecutive sessions of transcranial direct current stimulation do not remediate visual hallucinations in Lewy body dementia: a randomised controlled trial. *Alzheimer's Research & Therapy*. 11 (1), 9.

Emmer, K.L., Waxman, E.A., Covy, J.P. & Giasson, B.I. (2011) E46K human  $\alpha$ -synuclein transgenic mice develop lewy-like and tau pathology associated with age-dependent, detrimental motor impairment. *Journal of Biological Chemistry*. 286 (40), 35104–35118.

Emre, M., Aarsland, D., Brown, R., Burn, D.J., Duyckaerts, C., Mizuno, Y., Broe, G.A., Cummings, J., Dickson, D.W., Gauthier, S., Goldman, J., Goetz, C., Korszyn, A., Lees, A., Levy, R., Litvan, I., McKeith, I., Olanow, W., Poewe, W., et al. (2007) Clinical diagnostic criteria for dementia associated with Parkinson's disease. *Movement Disorders*. 22 (12), 1689–1707.

Engedal, K., Snaedal, J., Hoegh, P., Jelic, V., Bo Andersen, B., Naik, M., Wahlund, L.-O. & Oeksengaard, A.-R. (2015) Quantitative EEG Applying the Statistical Recognition Pattern Method: A Useful Tool in Dementia Diagnostic Workup. *Dementia and geriatric cognitive disorders*. 40 (1–2), 1–12.

Engel, A.K. & Fries, P. (2010) Beta-band oscillations — signalling the status quo? *Current Opinion in Neurobiology*. 20 (2), 156–165.

English, D.F., Peyrache, A., Stark, E., Roux, L., Vallentin, D., Long, M.A. & Buzsáki, G. (2014) Excitation and inhibition compete to control spiking during hippocampal ripples: intracellular study in behaving mice. *The Journal of neuroscience : the official journal of the Society for Neuroscience*. 34 (49), 16509–17.

Erskine, D., Thomas, A.J., Taylor, J.-P., Savage, M.A., Attems, J., McKeith, I.G., Morris, C.M. & Khundakar, A.A. (2017) Neuronal Loss and A-Synuclein Pathology in the Superior Colliculus and Its Relationship to Visual Hallucinations in Dementia with Lewy Bodies. *The American Journal of Geriatric Psychiatry*. 25 (6), 595–604.

Van Erum, J., Van Dam, D., Sheorajpanday, R. & De Deyn, P.P. (2019) Sleep

- architecture changes in the APP23 mouse model manifest at onset of cognitive deficits. *Behavioural Brain Research*. 373.
- Eschenko, O., Ramadan, W., Mölle, M., Born, J. & Sara, S.J. (2008) Sustained increase in hippocampal sharp-wave ripple activity during slow-wave sleep after learning. *Learning & memory (Cold Spring Harbor, N.Y.)*. 15 (4), 222–8.
- Euston, D.R., Gruber, A.J. & McNaughton, B.L. (2012) The Role of Medial Prefrontal Cortex in Memory and Decision Making. *Neuron*. 76 (6), 1057.
- Feng, L.R., Federoff, H.J., Vicini, S. & Maguire-Zeiss, K.A. (2010)  $\alpha$ -Synuclein mediates alterations in membrane conductance: A potential role for  $\alpha$ -synuclein oligomers in cell vulnerability. *European Journal of Neuroscience*. 32 (1), 10–17.
- Ferguson, B.R. & Gao, W.J. (2018) Pv interneurons: critical regulators of E/I balance for prefrontal cortex-dependent behavior and psychiatric disorders. *Frontiers in Neural Circuits*. 12 (37), 1–13.
- Ferguson, C.J. (2009) *An Effect Size Primer: A Guide for Clinicians and Researchers*.
- Ferman, T.J. & Boeve, B.F. (2007) Dementia with Lewy bodies. *Neurologic clinics*. 25 (3), 741–60, vii.
- Ferman, T.J., Boeve, B.F., Smith, G.E., Lin, S.C., Silber, M.H., Pedraza, O., Wszolek, Z., Graff-Radford, N.R., Uitti, R., Van Gerpen, J., Pao, W., Knopman, D., Pankratz, V.S., Kantarci, K., Boot, B., Parisi, J.E., Dugger, B.N., Fujishiro, H., Petersen, R.C., et al. (2011) Inclusion of RBD improves the diagnostic classification of dementia with Lewy bodies. *Neurology*. 77 (9), 875–882.
- Fernández-Arcos, A., Morenas-Rodríguez, E., Santamaria, J., Sánchez-Valle, R., Lladó, A., Gaig, C., Lleó, A. & Iranzo, A. (2019) Clinical and video-polysomnographic analysis of rapid eye movement sleep behavior disorder and other sleep disturbances in dementia with Lewy bodies. *Sleep*. 42 (7), 1–18.
- Fernandez, L.M., Vantomme, G., Osorio-Forero, A., Cardis, R., Béard, E. & Lüthi, A. (2018) Thalamic reticular control of local sleep in mouse sensory cortex. *eLife*. 7 (e39111), 1–25.
- Ferrara, M., Moroni, F., De Gennaro, L. & Nobili, L. (2012) Hippocampal Sleep

Features: Relations to Human Memory Function. *Frontiers in Neurology*. 357.

Ferree, T.C. (2006) Spherical Splines and Average Referencing in Scalp Electroencephalography. *Brain Topography*. 19 (1–2), 43–52.

Ferri, R., Huber, R., Aricò, D., Drago, V., Rundo, F., Ghilardi, M.F., Massimini, M. & Tononi, G. (2008) The slow-wave components of the cyclic alternating pattern (CAP) have a role in sleep-related learning processes. *Neuroscience Letters*. 432 (3), 228–231.

Ferron, J.-F., Kroeger, D., Chever, O. & Amzica, F. (2009) *Behavioral/Systems/Cognitive Cortical Inhibition during Burst Suppression Induced with Isoflurane Anesthesia*.

Fifel, K., Piggins, H. & Deboer, T. (2016) Modeling sleep alterations in Parkinson's disease: How close are we to valid translational animal models? *Sleep Medicine Reviews*. 2595–111.

Filippov, I. V., Williams, W.C., Krebs, A.A. & Pugachev, K.S. (2008) Dynamics of infraslow potentials in the primary auditory cortex: Component analysis and contribution of specific thalamic-cortical and non-specific brainstem-cortical influences. *Brain Research*. 121966–77.

Firbank, M., Kobeleva, X., Cherry, G., Killen, A., Gallagher, P., Burn, D.J., Thomas, A.J., O'Brien, J.T. & Taylor, J.P. (2016) Neural correlates of attention-executive dysfunction in lewy body dementia and Alzheimer's disease. *Human Brain Mapping*. 37 (3), 1254–1270.

Firbank, M.J., O'Brien, J.T. & Taylor, J.P. (2018) Long reaction times are associated with delayed brain activity in lewy body dementia. *Human brain mapping*. 39 (2), 633–643.

Flores-Cuadrado, A., Ubeda-Bañon, I., Saiz-Sanchez, D., de la Rosa-Prieto, C. & Martinez-Marcos, A. (2016) Hippocampal  $\alpha$ -synuclein and interneurons in Parkinson's disease: Data from human and mouse models. *Movement Disorders*. 31 (7), 979–988.

Fortin, D.L., Nemani, V.M., Voglmaier, S.M., Anthony, M.D., Ryan, T.A. & Edwards,

- R.H. (2005) Neural activity controls the synaptic accumulation of  $\alpha$ -synuclein. *Journal of Neuroscience*. 25 (47), 10913–10921.
- Franciotti, R., Falasca, N.W., Bonanni, L., Anzellotti, F., Maruotti, V., Comani, S., Thomas, A., Tartaro, A., Taylor, J.P. & Onofrj, M. (2013) Default network is not hypoactive in dementia with fluctuating cognition: An Alzheimer disease/dementia with Lewy bodies comparison. *Neurobiology of Aging*. 34 (4), 1148–1158.
- Fransson, P. & Marrelec, G. (2008) The precuneus/posterior cingulate cortex plays a pivotal role in the default mode network: Evidence from a partial correlation network analysis. *NeuroImage*. 42 (3), 1178–1184.
- Frauscher, B., von Ellenrieder, N., Ferrari-Marinho, T., Avoli, M., Dubeau, F. & Gotman, J. (2015) Facilitation of epileptic activity during sleep is mediated by high amplitude slow waves. *Brain*. 138 (6), 1629–1641.
- Freichel, C., Neumann, M., Ballard, T., Müller, V., Woolley, M., Ozmen, L., Borroni, E., Kretschmar, H.A., Haass, C., Spooren, W. & Kahle, P.J. (2007) Age-dependent cognitive decline and amygdala pathology in  $\alpha$ -synuclein transgenic mice. *Neurobiology of Aging*. 28 (9), 1421–1435.
- Freund, T.F. & Buzsáki, G. (1998) Interneurons of the hippocampus. *Hippocampus*. 6 (4), 347–470.
- Friedman, D., Honig, L.S. & Scarmeas, N. (2012) Seizures and epilepsy in Alzheimer's disease. *CNS neuroscience & therapeutics*. 18 (4), 285–94.
- Frucht, S.J., Louis, E.D., Chuang, C. & Fahn, S. (2001) A pilot tolerability and efficacy study of levetiracetam in patients with chronic myoclonus. *Neurology*. 57 (6), 1112–4.
- Fuentealba, P., Timofeev, I. & Steriade, M. (2004) Prolonged hyperpolarizing potentials precede spindle oscillations in the thalamic reticular nucleus. *Proceedings of the National Academy of Sciences of the United States of America*. 101 (26), 9816–9821.
- Funk, C.M., Peelman, K., Bellesi, M., Marshall, W., Cirelli, C. & Tononi, G. (2017) Role of Somatostatin-Positive Cortical Interneurons in the Generation of Sleep Slow

Waves. *The Journal of Neuroscience*. 37 (38), 9132.

Fuster, J.M. (2001) The Prefrontal Cortex—An Update: Time Is of the Essence. *Neuron* 30.

Fymat, A. (2018) Dementia: A Review. *J Clin Psychiatr Neurosci*. 1 (3), 27–34.

Garn, H., Coronel, C., Waser, M., Caravias, G. & Ransmayr, G. (2017) Differential diagnosis between patients with probable Alzheimer's disease, Parkinson's disease dementia, or dementia with Lewy bodies and frontotemporal dementia, behavioral variant, using quantitative electroencephalographic features. *Journal of Neural Transmission*. 1–13.

Gehrman, P., Marler, M., Martin, J.L., Shochat, T., Corey-Bloom, J. & Ancoli-Israel, S. (2005) The relationship between dementia severity and rest/activity circadian rhythms. *Neuropsychiatric Disease and Treatment*. 1 (2), 155–163.

Gerrard, L.B., Tantirigama, M.L.S. & Bekkers, J.M. (2018) Pre- and Postsynaptic Activation of GABAB Receptors Modulates Principal Cell Excitation in the Piriform Cortex. *Frontiers in Cellular Neuroscience*. 12 (28), 1–11.

Ghiglieri, V., Calabrese, V. & Calabresi, P. (2018) Alpha-synuclein: From early synaptic dysfunction to neurodegeneration. *Frontiers in Neurology* 9 (295) p.1–14.

Ghosh, D., Mehra, S., Sahay, S., Singh, P.K. & Maji, S.K. (2017)  $\alpha$ -synuclein aggregation and its modulation. *International Journal of Biological Macromolecules*. 10037–54.

Giasson, B.I., Duda, J.E., Quinn, S.M., Zhang, B., Trojanowski, J.Q. & Lee, V.M.Y. (2002) Neuronal  $\alpha$ -synucleinopathy with severe movement disorder in mice expressing A53T human  $\alpha$ -synuclein. *Neuron*. 34 (4), 521–533.

Giorgi, F.S., Guida, M., Vergallo, A., Bonuccelli, U. & Zaccara, G. (2017) Treatment of epilepsy in patients with Alzheimer's disease. *Expert Review of Neurotherapeutics* 17 (3) p.309–318.

Gomperts, S.N., Locascio, J.J., Marquie, M., Santarlaschi, A.L., Rentz, D.M., Maye, J., Johnson, K.A. & Growdon, J.H. (2012) Brain amyloid and cognition in Lewy body diseases. *Movement disorders : official journal of the Movement Disorder Society*.

27 (8), 965–73.

- Gottesmann, C. (1992) Detection of seven sleep-waking stages in the rat. *Neuroscience & Biobehavioral Reviews*. 16 (1), 31–38.
- Goudsmit, E., Hofman, M.A., Fliers, E. & Swaab, F. (1990) The supraoptic and paraventricular nuclei of the human hypothalamus in relation to sex, age and Alzheimer's disease. *Neurobiology of Aging*. 11 (5), 529–536.
- Gretenkord, S. (2015) *Slow wave activity in the medial prefrontal cortex of the anaesthetised rat: sub-regional characterisation and dopaminergic modulation*. [Online]. Newcastle University.
- Gretenkord, S., Rees, A., Whittington, M.A., Gartside, S.E. & LeBeau, F.E.N. (2017) Dorsal vs. ventral differences in fast Up-state-associated oscillations in the medial prefrontal cortex of the urethane-anesthetized rat. *Journal of Neurophysiology*. 117 (3), 1126–1142.
- Guarnieri, B. & Sorbi, S. (2015) Sleep and Cognitive Decline: A Strong Bidirectional Relationship. It Is Time for Specific Recommendations on Routine Assessment and the Management of Sleep Disorders in Patients with Mild Cognitive Impairment and Dementia. *European Neurology*. 74 (1–2), 43–48.
- Guerreiro, R., Escott-Price, V., Hernandez, D.G., Kun-Rodrigues, C., Ross, O.A., Orme, T., Neto, J.L., Carmona, S., Dehghani, N., Eicher, J.D., Shepherd, C., Parkkinen, L., Darwent, L., Heckman, M.G., Scholz, S.W., Troncoso, J.C., Pletnikova, O., Dawson, T., Rosenthal, L., et al. (2019) Heritability and genetic variance of dementia with Lewy bodies. *Neurobiology of Disease*. 127492–501.
- Guerreiro, R., Ross, O.A., Kun-Rodrigues, C., Hernandez, D.G., Orme, T., Eicher, J.D., Shepherd, C.E., Parkkinen, L., Darwent, L., Heckman, M.G., Scholz, S.W., Troncoso, J.C., Pletnikova, O., Ansorge, O., Clarimon, J., Lleo, A., Morenas-Rodriguez, E., Clark, L., Honig, L.S., et al. (2018) Investigating the genetic architecture of dementia with Lewy bodies: a two-stage genome-wide association study. *The Lancet Neurology*. 17 (1), 64–74.
- Guerrini, R. & Takahashi, T. (2013) 'Myoclonus and epilepsy', in *Handbook of Clinical Neurology*. [Online]. Elsevier B.V. pp. 667–679.

- Hablitz, L.M., Vinitzky, H.S., Sun, Q., Stæger, F.F., Sigurdsson, B., Mortensen, K.N., Lilius, T.O. & Nedergaard, M. (2019) Increased glymphatic influx is correlated with high EEG delta power and low heart rate in mice under anesthesia. *Science Advances*. 5 (2), eaav5447.
- Hahn, T.T.G., Sakmann, B. & Mehta, M.R. (2007) Differential responses of hippocampal subfields to cortical up-down states. *Proceedings of the National Academy of Sciences of the United States of America*. 104 (12), 5169–74.
- Haider, B., Duque, A., Hasenstaub, A.R. & McCormick, D.A. (2006) Neocortical network activity in vivo is generated through a dynamic balance of excitation and inhibition. *Journal of Neuroscience*. 26 (17), 4535–4545.
- Halász, P. (2004) Chapter 55 The microstructure of sleep. *Supplements to Clinical Neurophysiology*. 57 (C), 521–533.
- Hall, A.M., Throesch, B.T., Buckingham, S.C., Markwardt, S.J., Peng, Y., Wang, Q., Hoffman, D.A. & Roberson, E.D. (2015) Tau-dependent Kv4.2 depletion and dendritic hyperexcitability in a mouse model of Alzheimer's disease. *Journal of Neuroscience*. 35 (15), 6221–6230.
- Hansen, L.A., Masliah, E., Terry, R.D. & Mirra, S.S. (1989) A neuropathological subset of Alzheimer's disease with concomitant Lewy body disease and spongiform change. *Acta neuropathologica*. 78 (2), 194–201.
- Hara, K. & Harris, R.A. (2002) The Anesthetic Mechanism of Urethane: The Effects on Neurotransmitter-Gated Ion Channels. *Anesthesia & Analgesia*. 94 (2), 313–318.
- Hardy, J.A. & Higgins, G.A. (1992) Alzheimer's disease: The amyloid cascade hypothesis. *Science* 256 (5054) p.184–185.
- Hatami, A. & Chesselet, M.F. (2014) Transgenic rodent models to study alpha-synuclein pathogenesis, with a focus on cognitive deficits. *Current Topics in Behavioral Neurosciences*. 22303–330.
- Hazra, A., Gu, F., Aulakh, A., Berridge, C., Eriksen, J.L. & Žiburkus, J. (2013) Inhibitory Neuron and Hippocampal Circuit Dysfunction in an Aged Mouse Model of Alzheimer's Disease Chad A. Dickey (ed.). *PLoS ONE*. 8 (5), e64318.

- Henry, J.C. (2006) *Electroencephalography: Basic Principles, Clinical Applications, and Related Fields, Fifth Edition*. 5th edition. E. Niedermeyer & F. L. da Silva (eds.). Vol. 67. Ovid Technologies (Wolters Kluwer Health).
- Henstridge, C.M., Pickett, E. & Spires-Jones, T.L. (2016) Synaptic pathology: A shared mechanism in neurological disease. *Ageing Research Reviews* 28 p.72–84.
- Hentschke, H., Perkins, M.G., Pearce, R.A. & Banks, M.I. (2007) Muscarinic blockade weakens interaction of gamma with theta rhythms in mouse hippocampus. *European Journal of Neuroscience*. 26 (6), 1642–1656.
- Hepp, D.H., Vergoossen, D.L.E., Huisman, E., Lemstra, A.W., Berendse, H.W., Rozemuller, A.J., Foncke, E.M.J. & van de Berg, W.D.J. (2016) Distribution and Load of Amyloid- $\beta$  Pathology in Parkinson Disease and Dementia with Lewy Bodies. *Journal of Neuropathology & Experimental Neurology*. 75 (10), 936–945.
- Herrera, C.G., Cadavieco, M.C., Jego, S., Ponomarenko, A., Korotkova, T. & Adamantidis, A. (2016) Hypothalamic feedforward inhibition of thalamocortical network controls arousal and consciousness. *Nature Neuroscience*. 19 (2), 290–298.
- Hita-Yañez, E., Atienza, M. & Cantero, J.L. (2013) Polysomnographic and Subjective Sleep Markers of Mild Cognitive Impairment. *Sleep*. 36 (9), 1327–1334.
- Hooper, S.L. & Schmidt, J. (2017) 'Electrophysiological Recording Techniques', in *Neurobiology of Motor Control*. [Online]. Hoboken, NJ, USA: John Wiley & Sons, Inc. pp. 7–53.
- Horovitz, S.G., Braun, A.R., Carr, W.S., Picchioni, D., Balkin, T.J., Fukunaga, M. & Duyn, J.H. (2009) Speech and Language Branch, National Institute on Deafness and Other Communication Disorders. *National Institutes of Health*. 106 (27), .
- Horváth, A., Szcs, A., Barcs, G. & Kamondi, A. (2017) Sleep EEG Detects Epileptiform Activity in Alzheimer's Disease with High Sensitivity. *Journal of Alzheimer's Disease*. 56 (3), 1175–1183.
- Hsiao, F.-J., Wang, Y.-J., Yan, S.-H., Chen, W.-T. & Lin, Y.-Y. (2013) Altered Oscillation and Synchronization of Default-Mode Network Activity in Mild

Alzheimer's Disease Compared to Mild Cognitive Impairment: An Electrophysiological Study Ching-Po Lin (ed.). *PLoS ONE*. 8 (7), e68792.

Hsu, L.J., Sagara, Y., Arroyo, A., Rockenstein, E., Sisk, A., Mallory, M., Wong, J., Takenouchi, T., Hashimoto, M. & Masliah, E. (2000)  $\alpha$ -synuclein promotes mitochondrial deficit and oxidative stress. *American Journal of Pathology*. 157 (2), 401–410.

Huang, Y., Halliday, G., Okazaki, H., Lipkin, L., Aronson, S., Kosaka, K., Yoshimura, M., Ikeda, K., Budka, H., Dickson, D., Davies, P., Mayeux, R., Crystal, H., Horoupian, D., Thompson, A., Goldman, J., McKeith, I., Galasko, D., Kosaka, K., et al. (2013) Can we clinically diagnose dementia with Lewy bodies yet? *Translational Neurodegeneration*. 2 (4), 1–9.

Hughes, S.W., Lorincz, M.L., Parri, H.R. & Crunelli, V. (2011) Infralow (<0.1 Hz) oscillations in thalamic relay nuclei basic mechanisms and significance to health and disease states. *Progress in brain research*. 193:145–62.

Hurley, M.J. & Dexter, D.T. (2012) Voltage-gated calcium channels and Parkinson's disease. *Pharmacology and Therapeutics* 133 (3) p.324–333.

Iizuka, T. & Kameyama, M. (2016) Cingulate island sign on FDG-PET is associated with medial temporal lobe atrophy in dementia with Lewy bodies. *Annals of Nuclear Medicine*. 30 (6), 421–429.

Ilijic, E., Guzman, J.N. & Surmeier, D.J. (2011) The L-type channel antagonist isradipine is neuroprotective in a mouse model of Parkinson's disease. *Neurobiology of Disease*. 43 (2), 364–371.

Isomura, Y., Sirota, A., Özen, S., Montgomery, S., Mizuseki, K., Henze, D.A. & Buzsáki, G. (2006) Integration and Segregation of Activity in Entorhinal-Hippocampal Subregions by Neocortical Slow Oscillations. *Neuron*. 52 (5), 871–882.

Jackson, C.E., Snyder, P.J., Khachaturian, Z.S., Brookmeyer, R., Johnson, E., Ziegler-Graham, K., Arrighi, H.M., Ankri, J., Poupard, M., Braak, H., Rub, U., Schultz, C., Tredici, K. Del, Terry, A., Buccafusco, J., Braak, H., Braak, E., Ghebremedhin, E., Schultz, C., et al. (2008) Electroencephalography and event-related potentials as

- biomarkers of mild cognitive impairment and mild Alzheimer's disease. *Alzheimer's & dementia : the journal of the Alzheimer's Association*. 4 (1 Suppl 1), S137-43.
- Jarosiewicz, B., McNaughton, B.L. & Skaggs, W.E. (2002) Hippocampal population activity during the small-amplitude irregular activity state in the rat. *Journal of Neuroscience*. 22 (4), 1373–1384.
- Jellinger, K.A. & Attems, J. (2011) Prevalence and pathology of dementia with lewy bodies in the oldest old: A comparison with other dementing disorders. *Dementia and Geriatric Cognitive Disorders*. 31 (4), 309–316.
- Jellinger, K.A. & Korczyn, A.D. (2018) Are dementia with Lewy bodies and Parkinson's disease dementia the same disease? *BMC Medicine*. 16 (1).
- Jellinger, K.A. & Lantos, P.L. (2010) Papp-Lantos inclusions and the pathogenesis of multiple system atrophy: An update. *Acta Neuropathologica* 119 (6) p.657–667.
- Jessen, N.A., Munk, A.S.F., Lundgaard, I. & Nedergaard, M. (2015) The Glymphatic System: A Beginner's Guide. *Neurochemical Research*. 40 (12), 2583–2599.
- Jia, X. & Kohn, A. (2011) Gamma rhythms in the brain. *PLoS biology*. 9 (4), e1001045.
- Jin, N., Lipponen, A., Koivisto, H., Gurevicius, K. & Tanila, H. (2018) Increased cortical beta power and spike-wave discharges in middle-aged APP/PS1 mice. *Neurobiology of Aging*. 71127–141.
- Jing, W., Wang, Y., Fang, G., Chen, M., Xue, M., Guo, D., Yao, D. & Xia, Y. (2016) EEG Bands of Wakeful Rest, Slow-Wave and Rapid-Eye-Movement Sleep at Different Brain Areas in Rats. *Frontiers in computational neuroscience*. 10 (79), 1–13.
- Jobert, M., Poiseau, E., Jähnig, P., Schulz, H. & Kubicki, S. (1992) Topographical Analysis of Sleep Spindle Activity. *Neuropsychobiology*. 26 (4), 210–217.
- Ju, Y.-E.S., Ooms, S.J., Sutphen, C., Macauley, S.L., Zangrilli, M.A., Jerome, G., Fagan, A.M., Mignot, E., Zempel, J.M., Claassen, J.A.H.R. & Holtzman, D.M. (2017) Slow wave sleep disruption increases cerebrospinal fluid amyloid- $\beta$  levels. *Brain*. 140 (8), 2104–2111.

- Jung, T.P., Makeig, S., Humphries, C., Lee, T.W., McKeown, M.J., Iragui, V. & Sejnowski, T.J. (2000) Removing electroencephalographic artifacts by blind source separation. *Psychophysiology*. 37 (2), 163–78.
- Kahle, P.J., Neumann, M., Ozmen, L., Müller, V., Jacobsen, H., Schindzielorz, A., Okochi, M., Leimer, U., van der Putten, H., Probst, A., Kremmer, E., Kretschmar, H.A. & Haass, C. (2000) Subcellular Localization of Wild-Type and Parkinson's Disease-Associated Mutant  $\alpha$ -Synuclein in Human and Transgenic Mouse Brain. *Journal of Neuroscience*. 20 (17), 6365–6373.
- Kahle, P.J., Neumann, M., Ozmen, L., Müller, V., Odoy, S., Okamoto, N., Jacobsen, H., Iwatsubo, T., Trojanowski, J.Q., Takahashi, H., Wakabayashi, K., Bogdanovic, N., Riederer, P., Kretschmar, H.A. & Haass, C. (2001) Selective Insolubility of  $\alpha$ -Synuclein in Human Lewy Body Diseases Is Recapitulated in a Transgenic Mouse Model. *The American Journal of Pathology*. 159 (6), 2215–2225.
- Kane, J.P.M., Surendranathan, A., Bentley, A., Barker, S.A.H., Taylor, J.-P., Thomas, A.J., Allan, L.M., McNally, R.J., James, P.W., McKeith, I.G., Burn, D.J. & O'Brien, J.T. (2018) Clinical prevalence of Lewy body dementia. *Alzheimer's Research & Therapy*. 10 (1), 19.
- Kastanenka, K. V., Calvo-Rodriguez, M., Hou, S.S., Zhou, H., Takeda, S., Arbel-Ornath, M., Lariviere, A., Lee, Y.F., Kim, A., Hawkes, J.M., Logan, R., Feng, D., Chen, X., Gomperts, S.N. & Bacskai, B.J. (2019) Frequency-dependent exacerbation of Alzheimer's disease neuropathophysiology. *Scientific Reports*. 9 (8964), 1–13.
- Katsageorgiou, V.-M., Sona, D., Zannotto, M., Lassi, G., Garcia-Garcia, C., Tucci, V. & Murino, V. (2018) A novel unsupervised analysis of electrophysiological signals reveals new sleep substages in mice Karunesh Ganguly (ed.). *PLOS Biology*. 16 (5), e2003663.
- Kaufmann, T.J., Harrison, P.M., Richardson, M.J.E., Pinheiro, T.J.T. & Wall, M.J. (2016) Intracellular soluble  $\alpha$ -synuclein oligomers reduce pyramidal cell excitability. *The Journal of Physiology*. 594 (10), 2751–2772.
- Kazim, S.F., Chuang, S.C., Zhao, W., Wong, R.K.S., Bianchi, R. & Iqbal, K. (2017)

- Early-onset network hyperexcitability in presymptomatic Alzheimer's disease transgenic mice is suppressed by passive immunization with anti-human APP/A $\beta$  antibody and by mGluR5 blockade. *Frontiers in Aging Neuroscience*. 9 (71), 1–17.
- Kemshead, J.T., Ritter, M.A., Cotmore, S.F. & Greaves, M.F. (1982) Human Thy-1: Expression on the cell surface of neuronal and glial cells. *Brain Research*. 236 (2), 451–461.
- Kenny, E.R., Blamire, A.M., Firbank, M.J. & O'Brien, J.T. (2012) Functional connectivity in cortical regions in dementia with Lewy bodies and Alzheimer's disease. *Brain*. 135 (2), 569–581.
- Kent, B.A., Strittmatter, S.M. & Nygaard, H.B. (2018) Sleep and EEG Power Spectral Analysis in Three Transgenic Mouse Models of Alzheimer's Disease: APP/PS1, 3xTgAD, and Tg2576. *Journal of Alzheimer's disease : JAD*. 64 (4), 1325–1336.
- Khodr, C.E., Chen, L., Dave, S., Al-Harathi, L. & Hu, X.T. (2016) Combined chronic blockade of hyper-active L-type calcium channels and NMDA receptors ameliorates HIV-1 associated hyper-excitability of mPFC pyramidal neurons. *Neurobiology of Disease*. 9485–94.
- Killinger, B.A., Melki, R., Brundin, P. & Kordower, J.H. (2019) Endogenous alpha-synuclein monomers, oligomers and resulting pathology: let's talk about the lipids in the room. *npj Parkinson's Disease*. 5 (23), 1–8.
- Kilpeläinen, T., Julku, U.H., Svarebaks, R. & Myöhänen, T.T. (2019) Behavioural and dopaminergic changes in double mutated human A30P\*A53T alpha-synuclein transgenic mouse model of Parkinson's disease. *Scientific Reports*. 9 (1), 17382.
- Kim, D., Hwang, E., Lee, M., Sung, H. & Choi, J.H. (2015) Characterization of Topographically Specific Sleep Spindles in Mice. *Sleep*. 38 (1), 85–96.
- Kim, W.S., Kågedal, K., Halliday, G.M., Kaufmann, H., Singer, W., Biaggioni, I., Freeman, R., Perlman, S., Hauser, R., Cheshire, W., Lessig, S., Vernino, S., Mandrekar, J., Dupont, W., Chelimsky, T., Galpern, W., Anderson, J., Jobling, M., Buell, A., et al. (2014) Alpha-synuclein biology in Lewy body diseases. *Alzheimer's Research & Therapy*. 6 (5–8), 73.

- Kirik, D., Rosenblad, C., Burger, C., Lundberg, C., Johansen, T.E., Muzyczka, N., Mandel, R.J. & Björklund, A. (2002) Parkinson-Like Neurodegeneration Induced by Targeted Overexpression of  $\alpha$ -Synuclein in the Nigrostriatal System. *Journal of Neuroscience*. 22 (7), 2780–2791.
- Kiss, T., Feng, J., Hoffmann, W.E., Shaffer, C.L. & Hajós, M. (2013) Rhythmic theta and delta activity of cortical and hippocampal neuronal networks in genetically or pharmacologically induced N-methyl-d-aspartate receptor hypofunction under urethane anesthesia. *Neuroscience*. 237255–267.
- Klausberger, T. & Somogyi, P. (2008) Neuronal diversity and temporal dynamics: The unity of hippocampal circuit operations. *Science* 321 (5885) p.53–57.
- Klein, R.L., King, M.A., Hamby, M.E. & Meyer, E.M. (2002) Dopaminergic cell loss induced by human A30P  $\alpha$ -synuclein gene transfer to the rat substantia nigra. *Human Gene Therapy*. 13 (5), 605–612.
- Klimesch, W., Sauseng, P. & Hanslmayr, S. (2007) EEG alpha oscillations: The inhibition–timing hypothesis. *Brain Research Reviews*. 53 (1), 63–88.
- Knyazev, G.G., Slobodskoj-Plusnin, J.Y., Bocharov, A. V. & Pylkova, L. V. (2011) The default mode network and EEG alpha oscillations: An independent component analysis. *Brain Research*. 140267–79.
- Ko, A.L., Darvas, F., Poliakov, A., Ojemann, J. & Sorensen, L.B. (2011) Quasi-periodic fluctuations in default mode network electrophysiology. *Journal of Neuroscience*. 31 (32), 11728–11732.
- Kobeleva, X., Firbank, M., Peraza, L., Gallagher, P., Thomas, A., Burn, D.J., O'Brien, J. & Taylor, J.P. (2017) Divergent functional connectivity during attentional processing in Lewy body dementia and Alzheimer's disease. *Cortex*. 928–18.
- Kopell, N., Ermentrout, G.B., Whittington, M.A. & Traub, R.D. (2000) Gamma rhythms and beta rhythms have different synchronization properties. *Proceedings of the National Academy of Sciences of the United States of America*. 97 (4), 1867–72.
- Koprach, J.B., Kalia, L. V. & Brotchie, J.M. (2017) Animal models of  $\alpha$ -synucleinopathy for Parkinson disease drug development. *Nature Reviews Neuroscience*. 18 (9),

515–529.

- Kotagal, V., Müller, M.L.T.M., Kaufer, D.I., Koeppe, R.A. & Bohnen, N.I. (2012) Thalamic cholinergic innervation is spared in Alzheimer disease compared to parkinsonian disorders. *Neuroscience letters*. 514 (2), 169–72.
- Kropotov, J.D. & Kropotov, J.D. (2009a) 'Chapter 14 – Memory Systems', in *Quantitative EEG, Event-Related Potentials and Neurotherapy*. [Online]. pp. 310–324.
- Kropotov, J.D. & Kropotov, J.D. (2009b) 'Chapter 3 – Beta Rhythms', in *Quantitative EEG, Event-Related Potentials and Neurotherapy*. [Online]. pp. 59–76.
- Kropotov, J.D. & Kropotov, J.D. (2009c) 'Chapter 8 – Methods of Analysis of Background EEG', in *Quantitative EEG, Event-Related Potentials and Neurotherapy*. [Online]. pp. 116–160.
- Kropotov, J.D. & Kropotov, J.D. (2009d) 'Introduction', in *Quantitative EEG, Event-Related Potentials and Neurotherapy*. [Online]. pp. 385–392.
- Kuchibhotla, K. V., Lattarulo, C.R., Hyman, B.T. & Bacskai, B.J. (2009) Synchronous hyperactivity and intercellular calcium waves in astrocytes in Alzheimer mice. *Science*. 323 (5918), 1211–1215.
- Kuki, T., Fujihara, K., Miwa, H., Tamamaki, N., Yanagawa, Y. & Mushiake, H. (2015) Contribution of parvalbumin and somatostatin-expressing GABAergic neurons to slow oscillations and the balance in beta-gamma oscillations across cortical layers. *Frontiers in neural circuits*. 9 (6), 1–12.
- Kumar, A., Singh, A. & Ekavali (2015) A review on Alzheimer's disease pathophysiology and its management: an update. *Pharmacological Reports*. 67 (2), 195–203.
- Kvitsiani, D., Ranade, S., Hangya, B., Taniguchi, H., Huang, J. & Kepecs, A. (2013) Distinct behavioural and network correlates of two interneuron types in prefrontal cortex. *Nature*. 498 (7454), 363.
- Lacroix, M.M., De Lavilléon, G., Lefort, J., Kanbi, K. El, Bagur, S., Laventure, S., Dauvilliers, Y., Peyron, C. & Benchenane, K. (2018) Improved sleep scoring in

mice reveals human-like stages. *bioRxiv*.

- Lam, A.D., Deck, G., Goldman, A., Eskandar, E.N., Noebels, J. & Cole, A.J. (2017) Silent hippocampal seizures and spikes identified by foramen ovale electrodes in Alzheimer's disease. *Nature Medicine*. 23 (6), 678–680.
- Larson-Prior, L.J., Zempel, J.M., Nolan, T.S., Prior, F.W., Snyder, A. & Raichle, M.E. (2009) Cortical network functional connectivity in the descent to sleep. *Proceedings of the National Academy of Sciences of the United States of America*. 106 (11), 4489–4494.
- Lashuel, H.A., Petre, B.M., Wall, J., Simon, M., Nowak, R.J., Walz, T. & Lansbury, P.T. (2002) Alpha-synuclein, especially the Parkinson's disease-associated mutants, forms pore-like annular and tubular protofibrils. *Journal of molecular biology*. 322 (5), 1089–102.
- Latreille, V., Carrier, J., Lafortune, M., Postuma, R.B., Bertrand, J.-A., Panisset, M., Chouinard, S. & Gagnon, J.-F. (2015) Sleep spindles in Parkinson's disease may predict the development of dementia. *Neurobiology of Aging*. 36 (2), 1083–1090.
- Lázár, Z.I., Dijk, D.-J. & Lázár, A.S. (2019) Infralow oscillations in human sleep spindle activity. *Journal of Neuroscience Methods*. 31622–34.
- Lecci, S., Fernandez, L.M.J., Weber, F.D., Cardis, R., Chatton, J.-Y., Born, J. & Lüthi, A. (2017) Coordinated infralow neural and cardiac oscillations mark fragility and offline periods in mammalian sleep. *Science Advances*. 3 (2), e1602026.
- Lee, C. & Jones, T.A. (2018) Effects of ketamine compared with urethane anesthesia on vestibular sensory evoked potentials and systemic physiology in mice. *Journal of the American Association for Laboratory Animal Science*. 57 (3), 268–277.
- Lee, D.R., Taylor, J.-P. & Thomas, A.J. (2012) Assessment of cognitive fluctuation in dementia: a systematic review of the literature. *International journal of geriatric psychiatry*. 27 (10), 989–98.
- Lelan, F., Lescaudron, L., Boyer, C., Thinard, R., Rémy, S., Usal, C., Tesson, L., Anegon, I., Neveu, I., Damier, P. & Naveilhan, P. (2011) Effects of human alpha-synuclein A53T-A30P mutations on SVZ and local olfactory bulb cell proliferation

- in a transgenic rat model of Parkinson disease. *Parkinson's Disease*. 2011.
- Lemieux, M., Chauvette, S. & Timofeev, I. (2015) Neocortical inhibitory activities and long-range afferents contribute to the synchronous onset of silent states of the neocortical slow oscillation. *Journal of Neurophysiology*. 113 (3), 768–779.
- Lemieux, M., Chen, J.-Y., Lonjers, P., Bazhenov, M. & Timofeev, I. (2014) The impact of cortical deafferentation on the neocortical slow oscillation. *The Journal of neuroscience : the official journal of the Society for Neuroscience*. 34 (16), 5689–703.
- Lemstra, A.W., de Beer, M.H., Teunissen, C.E., Schreuder, C., Scheltens, P., van der Flier, W.M. & Sikkes, S.A.M. (2017) Concomitant AD pathology affects clinical manifestation and survival in dementia with Lewy bodies. *Journal of neurology, neurosurgery, and psychiatry*. 88 (2), 113–118.
- Leopold, D.A., Murayama, Y. & Logothetis, N.K. (2003) Very slow activity fluctuations in monkey visual cortex: Implications for functional brain imaging. *Cerebral Cortex*. 13 (4), 422–433.
- Leung, L.S. (1992) Fast (beta) rhythms in the hippocampus: A review. *Hippocampus*. 2 (2), 93–98.
- Lewis, L.D., Voigts, J., Flores, F.J., Ian Schmitt, L., Wilson, M.A., Halassa, M.M. & Brown, E.N. (2015) Thalamic reticular nucleus induces fast and local modulation of arousal state. *eLife*. 4.
- Li, W., Ma, L., Yang, G. & Gan, W.B. (2017) REM sleep selectively prunes and maintains new synapses in development and learning. *Nature Neuroscience*. 20 (3), 427–437.
- Li, X., Morita, K., Robinson, H.P.C. & Small, M. (2013) Control of layer 5 pyramidal cell spiking by oscillatory inhibition in the distal apical dendrites: a computational modeling study. *Journal of Neurophysiology*. 109 (11), 2739–2756.
- Li, X., Tong, X., Lu, W., Yu, D., Diao, J. & Zhao, Q. (2019) Label-free detection of early oligomerization of  $\alpha$ -synuclein and its mutants A30P/E46K through solid-state nanopores. *Nanoscale*. 11 (13), 6480–6488.

- Lim, J. & Dinges, D.F. (2008) 'Sleep deprivation and vigilant attention', in *Annals of the New York Academy of Sciences*. [Online]. 2008 Blackwell Publishing Inc. pp. 305–322.
- Lim, M.M., Gerstner, J.R. & Holtzman, D.M. (2014) The sleep-wake cycle and Alzheimer's disease: what do we know? *Neurodegenerative disease management*. 4 (5), 351–62.
- Lim, Y., Kehm, V.M., Lee, E.B., Soper, J.H., Li, C., Trojanowski, J.Q. & Lee, V.M.Y. (2011)  $\alpha$ -syn suppression reverses synaptic and memory defects in a mouse model of dementia with lewy bodies. *Journal of Neuroscience*. 31 (27), 10076–10087.
- Lin, X., Parisiadou, L., Sgobio, C., Liu, G., Yu, J., Sun, L., Shim, H., Gu, X.L., Luo, J., Long, C.X., Ding, J., Mateo, Y., Sullivan, P.H., Wu, L.G., Goldstein, D.S., Lovinger, D. & Cai, H. (2012) Conditional expression of Parkinson's disease-related mutant  $\alpha$ -synuclein in the midbrain dopaminergic neurons causes progressive neurodegeneration and degradation of transcription factor nuclear receptor related 1. *Journal of Neuroscience*. 32 (27), 9248–9264.
- Lippa, C.F., Duda, J.E., Grossman, M., Hurtig, H.I., Aarsland, D., Boeve, B.F., Brooks, D.J., Dickson, D.W., Dubois, B., Emre, M., Fahn, S., Farmer, J.M., Galasko, D., Galvin, J.E., Goetz, C.G., Growdon, J.H., Gwinn-Hardy, K.A., Hardy, J., Heutink, P., et al. (2007) DLB and PDD boundary issues: Diagnosis, treatment, molecular pathology, and biomarkers. *Neurology*. 68 (11), 812–819.
- Lippa, C.F., Smith, T.W. & Perry, E. (1999) Dementia with Lewy bodies: choline acetyltransferase parallels nucleus basalis pathology. *Journal of Neural Transmission*. 106 (5–6), 525–535.
- Liu, A.K.L., Chang, R.C.-C., Pearce, R.K.B. & Gentleman, S.M. (2015) Nucleus basalis of Meynert revisited: anatomy, history and differential involvement in Alzheimer's and Parkinson's disease. *Acta neuropathologica*. 129 (4), 527–40.
- Liu, Y., Yang, X.J., Xia, H., Tang, C.M. & Yang, K. (2019) GABA releases from parvalbumin-expressing and unspecific GABAergic neurons onto CA1 pyramidal cells are differentially modulated by presynaptic GABAB receptors in mouse

- hippocampus. *Biochemical and Biophysical Research Communications*. 520 (2), 449–452.
- Lockmann, A.L. V, Laplagne, D.A., Leão, R.N. & Tort, A.B.L. (2016) A Respiration-Coupled Rhythm in the Rat Hippocampus Independent of Theta and Slow Oscillations. *The Journal of neuroscience : the official journal of the Society for Neuroscience*. 36 (19), 5338–52.
- Lopantsev, V., Tempel, B.L. & Schwartzkroin, P.A. (2003) Hyperexcitability of CA3 Pyramidal Cells in Mice Lacking the Potassium Channel Subunit Kv1.1. *Epilepsia*. 44 (12), 1506–1512.
- Lorincz, M.L., Geall, F., Bao, Y., Crunelli, V. & Hughes, S.W. (2009) ATP-dependent infra-slow (<0.1 Hz) oscillations in thalamic networks. *PLoS ONE*. 4 (2), e4447.
- Lórinicz, M.L., Gunner, D., Bao, Y., Connelly, W.M., Isaac, J.T.R., Hughes, S.W. & Crunelli, V. (2015) A distinct class of slow (~0.2–2 Hz) intrinsically bursting layer 5 pyramidal neurons determines UP/DOWN state dynamics in the neocortex. *Journal of Neuroscience*. 35 (14), 5442–5458.
- De Luca, M., Beckmann, C.F., De Stefano, N., Matthews, P.M. & Smith, S.M. (2006) fMRI resting state networks define distinct modes of long-distance interactions in the human brain. *NeuroImage*. 29 (4), 1359–1367.
- Lucey, B.P., Hicks, T.J., McLeland, J.S., Toedebusch, C.D., Boyd, J., Elbert, D.L., Patterson, B.W., Baty, J., Morris, J.C., Ovod, V., Mawuenyega, K.G. & Bateman, R.J. (2018) Effect of sleep on overnight cerebrospinal fluid amyloid  $\beta$  kinetics. *Annals of Neurology*. 83 (1), 197–204.
- Lucey, B.P. & Holtzman, D.M. (2015) How amyloid, sleep and memory connect. *Nature Neuroscience*. 18 (7), 933–934.
- Lucey, B.P., McCullough, A., Landsness, E.C., Toedebusch, C.D., McLeland, J.S., Zaza, A.M., Fagan, A.M., McCue, L., Xiong, C., Morris, J.C., Benzinger, T.L.S. & Holtzman, D.M. (2019) Reduced non-rapid eye movement sleep is associated with tau pathology in early Alzheimer's disease. *Science translational medicine*. 11 (474), 1–13.

- Luczak, A. & Barthó, P. (2012) Consistent sequential activity across diverse forms of UP states under ketamine anesthesia. *European Journal of Neuroscience*. 36 (6), 2830–2838.
- Luczak, A., Barthó, P., Marguet, S.L., Buzsáki, G. & Harris, K.D. (2007) Sequential structure of neocortical spontaneous activity in vivo. *Proceedings of the National Academy of Sciences of the United States of America*. 104 (1), 347–352.
- Ludtmann, M.H.R., Angelova, P.R., Ninkina, N.N., Gandhi, S., Buchman, V.L. & Abramov, A.Y. (2016) Monomeric alpha-synuclein exerts a physiological role on brain ATP synthase. *Journal of Neuroscience*. 36 (41), 10510–10521.
- Lundqvist, M., Herman, P., Palva, M., Palva, S., Silverstein, D. & Lansner, A. (2013) Stimulus detection rate and latency, firing rates and 1–40 Hz oscillatory power are modulated by infra-slow fluctuations in a bistable attractor network model. *NeuroImage*. 83458–471.
- MacLin, J.M.A., Wang, T. & Xiao, S. (2019) Biomarkers for the diagnosis of Alzheimer’s disease, dementia Lewy body, frontotemporal dementia and vascular dementia. *General Psychiatry* 32 (1) p.5–13.
- Maji, S.K., Anoop, A., Singh, P.K. & Jacob, R.S. (2010) CSF biomarkers for Alzheimer’s disease diagnosis. *International Journal of Alzheimer’s Disease*
- Major, G., Larkum, M.E. & Schiller, J. (2013) Active Properties of Neocortical Pyramidal Neuron Dendrites. *Annual Review of Neuroscience*. 36 (1), 1–24.
- Mak-Mccully, R.A., Rolland, M., Sargsyan, A., Gonzalez, C., Magnin, M., Chauvel, P., Rey, M., Bastuji, H. & Halgren, E. (2017) Coordination of cortical and thalamic activity during non-REM sleep in humans. *Nature Communications*. 8 (15499), 1–11.
- Mak, E., Su, L., Williams, G.B. & O’Brien, J.T. (2014) Neuroimaging characteristics of dementia with Lewy bodies. *Alzheimer’s Research and Therapy* 6 (2).
- Manconi, M., Silvani, A. & Ferri, R. (2017) Commentary: Coordinated infraslow neural and cardiac oscillations mark fragility and offline periods in mammalian sleep. *Frontiers in Physiology*. 8847.

- Mander, B.A., Marks, S.M., Vogel, J.W., Rao, V., Lu, B., Saletin, J.M., Ancoli-Israel, S., Jagust, W.J. & Walker, M.P. (2015)  $\beta$ -amyloid disrupts human NREM slow waves and related hippocampus-dependent memory consolidation. *Nature Neuroscience*. 18 (7), 1051–1057.
- Mander, B.A., Winer, J.R., Jagust, W.J. & Walker, M.P. (2016) Sleep: A Novel Mechanistic Pathway, Biomarker, and Treatment Target in the Pathology of Alzheimer's Disease? *Trends in neurosciences*. 39 (8), 552–566.
- Mann, E.O., Kohl, M.M. & Paulsen, O. (2009) Distinct Roles of GABAA and GABAB Receptors in Balancing and Terminating Persistent Cortical Activity. *Journal of Neuroscience*. 29 (23), 7513–7518.
- Manoach, D.S. & Stickgold, R. (2019) Abnormal Sleep Spindles, Memory Consolidation, and Schizophrenia. *Annual Review of Clinical Psychology*. 15 (1), 451–479.
- Mantini, D., Perrucci, M.G., Del Gratta, C., Romani, G.L. & Corbetta, M. (2007) Electrophysiological signatures of resting state networks in the human brain. *Proceedings of the National Academy of Sciences of the United States of America*. 104 (32), 13170–5.
- Marshall, L., Helgadóttir, H., Mölle, M. & Born, J. (2006) Boosting slow oscillations during sleep potentiates memory. *Nature*. 444 (7119), 610–613.
- Martin, L.J., Pan, Y., Price, A.C., Sterling, W., Copeland, N.G., Jenkins, N.A., Price, D.L. & Lee, M.K. (2006) Parkinson's Disease  $\alpha$ -Synuclein Transgenic Mice Develop Neuronal Mitochondrial Degeneration and Cell Death. *J. Neurosci*. 22 (7), 2780–2791.
- Martin, L.J., Semenkow, S., Hanaford, A. & Wong, M. (2014) The mitochondrial permeability transition pore regulates Parkinson's disease development in mutant  $\alpha$ -synuclein transgenic mice. *Neurobiology of Aging*. 35 (5), 1132–1152.
- Martin, N., Lafortune, M., Godbout, J., Barakat, M., Robillard, R., Poirier, G., Bastien, C. & Carrier, J. (2013) Topography of age-related changes in sleep spindles. *Neurobiology of Aging*. 34 (2), 468–476.

- Massi, L., Lagler, M., Hartwich, K., Borhegyi, Z., Somogyi, P. & Klausberger, T. (2012) Temporal dynamics of parvalbumin-expressing axo-axonic and basket cells in the rat medial prefrontal cortex in vivo. *Journal of Neuroscience*. 32 (46), 16496–16502.
- Mathangi, D.C., Shyamala, R. & Subhashini, A.S. (2012) Effect of REM sleep deprivation on the antioxidant status in the brain of Wistar rats. *Annals of Neurosciences*. 19 (4), 161–164.
- McCormick, D.A. (1989) Cholinergic and noradrenergic modulation of thalamocortical processing. *Trends in Neurosciences*. 12 (6), 215–221.
- McDowell, K.A., Shin, D., Roos, K.P. & Chesselet, M.-F. (2014) Sleep dysfunction and EEG alterations in mice overexpressing alpha-synuclein. *Journal of Parkinson's disease*. 4 (3), 531–539.
- McKeith, I., Fairbairn, A., Perry, R., Thompson, P. & Perry, E. (1992) Neuroleptic sensitivity in patients with senile dementia of Lewy body type. *BMJ*. 305 (6855), .
- McKeith, I., Mintzer, J., Aarsland, D., Burn, D., Chiu, H., Cohen-Mansfield, J., Dickson, D., Dubois, B., Duda, J.E., Feldman, H., Gauthier, S., Halliday, G., Lawlor, B., Lippa, C., Lopez, O.L., Machado, J.C., O'Brien, J. & Playfer, J. (2004) Dementia with Lewy bodies. *The Lancet Neurology*. 3 (1), 19–28.
- McKeith, I.G., Boeve, B.F., Dickson, D.W., Halliday, G., Taylor, J.P., Weintraub, D., Aarsland, D., Galvin, J., Attems, J., Ballard, C.G., Bayston, A., Beach, T.G., Blanc, F., Bohnen, N., Bonanni, L., Bras, J., Brundin, P., Burn, D., Chen-Plotkin, A., et al. (2017) Diagnosis and management of dementia with Lewy bodies: Fourth consensus report of the DLB Consortium. *Neurology*. 89 (1), 88–100.
- McKeith, I.G., Dickson, D.W., Lowe, J., Emre, M., O'Brien, J.T., Feldman, H., Cummings, J., Duda, J.E., Lippa, C., Perry, E.K., Aarsland, D., Arai, H., Ballard, C.G., Boeve, B., Burn, D.J., Costa, D., Del Ser, T., Dubois, B., Galasko, D., et al. (2005) Diagnosis and management of dementia with Lewy bodies: Third report of the DLB consortium. *Neurology*. 65 (12), 1863–1872.
- McKeith, I.G., Galasko, D., Kosaka, K., Perry, E.K., Dickson, D.W., Hansen, L.A., Salmon, D.P., Lowe, J., Mirra, S.S., Byrne, E.J., Lennox, G., Quinn, N.P.,

- Edwardson, J.A., Ince, P.G., Bergeron, C., Burns, A., Miller, B.L., Lovestone, S., Collerton, D., et al. (1996) Consensus guidelines for the clinical and pathologic diagnosis of dementia with Lewy bodies (DLB): report of the consortium on DLB international workshop. *Neurology*. 47 (5), 1113–24.
- McKhann, G.M., Knopman, D.S., Chertkow, H., Hyman, B.T., Jack, C.R., Kawas, C.H., Klunk, W.E., Koroshetz, W.J., Manly, J.J., Mayeux, R., Mohs, R.C., Morris, J.C., Rossor, M.N., Scheltens, P., Carrillo, M.C., Thies, B., Weintraub, S., Phelps, C.H. & Phelps, C.H. (2011) The diagnosis of dementia due to Alzheimer's disease: recommendations from the National Institute on Aging-Alzheimer's Association workgroups on diagnostic guidelines for Alzheimer's disease. *Alzheimer's & dementia : the journal of the Alzheimer's Association*. 7 (3), 263–9.
- McShane, B.B., Galante, R.J., Biber, M., Jensen, S.T., Wyner, A.J. & Pack, A.I. (2012) Assessing REM Sleep in Mice Using Video Data. *Sleep*. 35 (3), 433–442.
- Meldrum, B.S. (2000) Glutamate as a Neurotransmitter in the Brain: Review of Physiology and Pathology. *The Journal of Nutrition*. 130 (4), 1007S-1015S.
- Melpignano, A., Parrino, L., Santamaria, J., Gaig, C., Trippi, I., Serradell, M., Mutti, C., Riccò, M. & Iranzo, A. (2019) Isolated rapid eye movement sleep behavior disorder and cyclic alternating pattern: is sleep microstructure a predictive parameter of neurodegeneration? *Sleep*. 42 (10), 1–7.
- Meltzer, J.A., Negishi, M., Mayes, L.C. & Constable, R.T. (2007) Individual differences in EEG theta and alpha dynamics during working memory correlate with fMRI responses across subjects. *Clinical neurophysiology: official journal of the International Federation of Clinical Neurophysiology*. 118 (11), 2419–36.
- Mendez, M.O., Chouvarda, I., Alba, A., Bianchi, A.M., Grassi, A., Arce-Santana, E., Milioli, G., Terzano, M.G. & Parrino, L. (2016) Analysis of A-phase transitions during the cyclic alternating pattern under normal sleep. *Medical and Biological Engineering and Computing*. 54 (1), 133–148.
- Menkes-Caspi, N., Yamin, H.G., Kellner, V., Spires-Jones, T.L., Cohen, D. & Stern, E.A. (2015) Pathological tau disrupts ongoing network activity. *Neuron*. 85 (5), 959–966.

- Mesulam, M. (2004) The Cholinergic Lesion of Alzheimer's Disease: Pivotal Factor or Side Show? *Learning & Memory*. 11 (1), 43–49.
- Metzler-Baddeley, C. (2007) A Review of Cognitive Impairments in Dementia with Lewy Bodies Relative to Alzheimer's Disease and Parkinson's Disease with Dementia. *Cortex*. 43 (5), 583–600.
- Micanovic, C. & Pal, S. (2014) The diagnostic utility of EEG in early-onset dementia: A systematic review of the literature with narrative analysis. *Journal of Neural Transmission* 121 (1) p.59–69.
- Mitchell, D.J., McNaughton, N., Flanagan, D. & Kirk, I.J. (2008) Frontal-midline theta from the perspective of hippocampal "theta". *Progress in Neurobiology*. 86 (3), 156–185.
- Mitra, A., Snyder, A.Z., Hacker, C.D., Pahwa, M., Tagliazucchi, E., Laufs, H., Leuthardt, E.C. & Raichle, M.E. (2016) Human cortical-hippocampal dialogue in wake and slow-wave sleep. *Proceedings of the National Academy of Sciences of the United States of America*. 113 (44), E6868–E6876.
- Miyawaki, H., Billeh, Y.N. & Diba, K. (2017) Low Activity Microstates During Sleep. *Sleep*. 40 (6), 1–13.
- Mölle, M. & Born, J. (2009) Hippocampus Whispering in Deep Sleep to Prefrontal Cortex-For Good Memories? *Neuron* 61 (4) p.496–498.
- Mölle, M., Yeshenko, O., Marshall, L., Sara, S.J. & Born, J. (2006) Hippocampal Sharp Wave-Ripples Linked to Slow Oscillations in Rat Slow-Wave Sleep. *Journal of Neurophysiology*. 96 (1), 62–70.
- Molter, C., O'Neill, J., Yamaguchi, Y., Hirase, H. & Leinekugel, X. (2012) Rhythmic Modulation of Theta Oscillations Supports Encoding of Spatial and Behavioral Information in the Rat Hippocampus. *Neuron*. 75 (5), 889–903.
- Moretti, D. V (2015) Theta and alpha EEG frequency interplay in subjects with mild cognitive impairment: evidence from EEG, MRI, and SPECT brain modifications. *Frontiers in aging neuroscience*. 7 (31), 1–14.
- Morris, M., Sanchez, P.E., Verret, L., Beagle, A.J., Guo, W., Dubal, D., Ranasinghe,

- K.G., Koyama, A., Ho, K., Yu, G.-Q., Vossel, K.A. & Mucke, L. (2015) Network dysfunction in  $\alpha$ -synuclein transgenic mice and human Lewy body dementia. *Annals of clinical and translational neurology*. 2 (11), 1012–28.
- Moulard, B., Picard, F., le Hellard, S., Agulhon, C., Weiland, S., Favre, I., Bertrand, S., Malafosse, A. & Bertrand, D. (2001) Ion channel variation causes epilepsies. *Brain Research Reviews*. 36 (2–3), 275–284.
- Moyer, J.R., Power, J.M., Thompson, L.T. & Disterhoft, J.F. (2000) Increased excitability of aged rabbit CA1 neurons after trace eyeblink conditioning. *Journal of Neuroscience*. 20 (14), 5476–5482.
- Murata, M., Odawara, T., Hasegawa, K., Iiyama, S., Nakamura, M., Tagawa, M. & Kosaka, K. (2018) Adjunct zonisamide to levodopa for DLB parkinsonism: A randomized double-blind phase 2 study. *Neurology*. 90 (8), e664–e672.
- Murphy, M., Riedner, B.A., Huber, R., Massimini, M., Ferrarelli, F. & Tononi, G. (2009) Source modeling sleep slow waves. *Proceedings of the National Academy of Sciences of the United States of America*. 106 (5), 1608–13.
- Murray, M.E., Dugger, B.N. & Dickson, D.W. (2010) Mixed Alzheimer's and Lewy Body Disease Pathology Patterns. *Alzheimer's & Dementia*. 6 (4).
- Naghavi, H.R. & Nyberg, L. (2005) Common fronto-parietal activity in attention, memory, and consciousness: Shared demands on integration? *Consciousness and Cognition*. 14 (2), 390–425.
- Naidoo, N., Ferber, M., Master, M., Zhu, Y. & Pack, A.I. (2008) Aging impairs the unfolded protein response to sleep deprivation and leads to proapoptotic signaling. *Journal of Neuroscience*. 28 (26), 6539–6548.
- Nair, J., Klaassen, A.-L., Arato, J., Vyssotski, A.L., Harvey, M. & Rainer, G. (2018) Basal forebrain contributes to default mode network regulation. *PNAS*. 115 (6), 1352–1357.
- Narayanan, N.S., Horst, N.K. & Laubach, M. (2006) Reversible inactivations of rat medial prefrontal cortex impair the ability to wait for a stimulus. *Neuroscience*. 139 (3), 865–876.

- Nazer, F. & Dickson, C.T. (2009) Slow Oscillation State Facilitates Epileptiform Events in the Hippocampus. *Journal of Neurophysiology*. 102 (3), 1880–1889.
- Neske, G.T. (2015) The Slow Oscillation in Cortical and Thalamic Networks: Mechanisms and Functions. *Frontiers in neural circuits*. 9 (88), 1–25.
- Neske, G.T. & Connors, B.W. (2016) Synchronized gamma-frequency inhibition in neocortex depends on excitatory-inhibitory interactions but not electrical synapses. *Journal of Neurophysiology*. 116 (2), 351–368.
- Neufeld, M.Y., Blumen, S., Aitkin, I., Parmet, Y. & Korczyn, A.D. (1994) EEG frequency analysis in demented and nondemented parkinsonian patients. *Dementia and Geriatric Cognitive Disorders*. 5 (1), 23–28.
- Neumann, M., Kahle, P.J., Giasson, B.I., Ozmen, L., Borroni, E., Spooen, W., Müller, V., Odoy, S., Fujiwara, H., Hasegawa, M., Iwatsubo, T., Trojanowski, J.Q., Kretschmar, H.A. & Haass, C. (2002) Misfolded proteinase K-resistant hyperphosphorylated  $\alpha$ -synuclein in aged transgenic mice with locomotor deterioration and in human  $\alpha$ -synucleinopathies. *Journal of Clinical Investigation*. 110 (10), 1429–1439.
- Neuner, I., Arrubla, J., Werner, C.J., Hitz, K., Boers, F., Kawohl, W. & Shah, N.J. (2014) The default mode network and EEG regional spectral power: a simultaneous fMRI-EEG study. *PloS one*. 9 (2), e88214.
- Newman, E.L., Gupta, K., Climer, J.R., Monaghan, C.K. & Hasselmo, M.E. (2012) Cholinergic modulation of cognitive processing: Insights drawn from computational models. *Frontiers in Behavioral Neuroscience* (6) p.1–19.
- Niedermeyer, E. & Lopes da Silva, F.H. (2004) *Electroencephalography: basic principles, clinical applications, and related fields* Ernst Niedermeyer (ed.). *Neurology*. 67 (11), 1332.
- Niethard, N., Ngo, H.-V.V. V., Ehrlich, I., Born, J. & Hertie, D. (2018) Cortical circuit activity underlying sleep slow oscillations and spindles. *Proceedings of the National Academy of Sciences of the United States of America*. 115 (39), E9220–E9229.

- Nigro, M.J., Hashikawa-Yamasaki, Y. & Rudy, B. (2018) Diversity and connectivity of layer 5 somatostatin-expressing interneurons in the mouse barrel cortex. *Journal of Neuroscience*. 38 (7), 1622–1633.
- Nikolaus, S., Antke, C. & Müller, H.-W. (2009) In vivo imaging of synaptic function in the central nervous system: I. Movement disorders and dementia. *Behavioural brain research*. 204 (1), 1–31.
- Nir, Y., Staba, R.J., Andrillon, T., Vyazovskiy, V. V., Cirelli, C., Fried, I. & Tononi, G. (2011) Regional Slow Waves and Spindles in Human Sleep. *Neuron*. 70 (1), 153–169.
- Noebels, J. (2011) A perfect storm: Converging paths of epilepsy and Alzheimer's dementia intersect in the hippocampal formation. *Epilepsia*. 5239–46.
- Nuber, S., Petrasch-Parwez, E., Winner, B., Winkler, J., Von Hörsten, S., Schmidt, T., Boy, J., Kuhn, M., Nguyen, H.P., Teismann, P., Schulz, J.B., Neumann, M., Pichler, B.J., Reischl, G., Holzmann, C., Schmitt, I., Bornemann, A., Kuhn, W., Zimmermann, F., et al. (2008) Neurodegeneration and motor dysfunction in a conditional model of Parkinson's disease. *Journal of Neuroscience*. 28 (10), 2471–2484.
- O'Dowd, S., Schumacher, J., Burn, D.J., Bonanni, L., Onofrj, M., Thomas, A. & Taylor, J.-P. (2019) Fluctuating cognition in the Lewy body dementias. *Brain*. 2019 (0), 1–13.
- O'Keefe, J., Burgess, N., Donnett, J.G., Jeffery, K.J. & Maguire, E.A. (1998) Place cells, navigational accuracy, and the human hippocampus. *Philosophical Transactions of the Royal Society B: Biological Sciences*. 353 (1373), 1333–1340.
- O'Leary, D.D.M., Chou, S.J. & Sahara, S. (2007) Area patterning of the mammalian cortex. *Neuron* 56 (2) p.252–269.
- Olichney, J.M., Galasko, D., Salmon, D.P., Hofstetter, C.R., Hansen, L.A., Katzman, R. & Thal, L.J. (1998) Cognitive decline is faster in Lewy body variant than in Alzheimer's disease. *Neurology*. 51 (2), 351–7.
- Onofrj, M., Thomas, A., Iacono, D., Luciano, A.L. & Di Iorio, A. (2003) The effects of a

cholinesterase inhibitor are prominent in patients with fluctuating cognition: a part 3 study of the main mechanism of cholinesterase inhibitors in dementia. *Clinical neuropharmacology*. 26 (5), 239–51.

Oostenveld, R. & Praamstra, P. (2001) The five percent electrode system for high-resolution EEG and ERP measurements. *Clinical Neurophysiology*. 112 (4), 713–719.

Outeiro, T.F., Koss, D.J., Erskine, D., Walker, L., Kurzawa-Akanbi, M., Burn, D., Donaghy, P., Morris, C., Taylor, J.-P., Thomas, A., Attems, J. & McKeith, I. (2019) Dementia with Lewy bodies: an update and outlook. *Molecular Neurodegeneration*. 14 (1), 5.

Ozaki, A., Nishida, M., Koyama, K., Ishikawa, K. & Nishikawa, T. (2012) Donepezil-induced sleep spindle in a patient with dementia with Lewy bodies: a case report. *Psychogeriatrics*. 12 (4), 255–258.

Pagliardini, S., Gosgnach, S. & Dickson, C.T. (2013) Spontaneous Sleep-Like Brain State Alternations and Breathing Characteristics in Urethane Anesthetized Mice Guglielmo Foffani (ed.). *PLoS ONE*. 8 (7), e70411.

Paillusson, S., Gomez-Suaga, P., Stoica, R., Little, D., Gissen, P., Devine, M.J., Noble, W., Hanger, D.P. & Miller, C.C.J. (2017)  $\alpha$ -Synuclein binds to the ER–mitochondria tethering protein VAPB to disrupt  $\text{Ca}^{2+}$  homeostasis and mitochondrial ATP production. *Acta Neuropathologica*. 134 (1), 129–149.

Pal, D. & Mallick, B.N. (2007) Neural mechanism of rapid eye movement sleep generation with reference to REM-OFF neurons in locus coeruleus. *Indian Journal of Medical Research* 125 (6) p.721–739.

Palop, J.J., Chin, J., Roberson, E.D., Wang, J., Thwin, M.T., Bien-Ly, N., Yoo, J., Ho, K.O., Yu, G.Q., Kreitzer, A., Finkbeiner, S., Noebels, J.L. & Mucke, L. (2007) Aberrant Excitatory Neuronal Activity and Compensatory Remodeling of Inhibitory Hippocampal Circuits in Mouse Models of Alzheimer's Disease. *Neuron*. 55 (5), 697–711.

Palop, J.J. & Mucke, L. (2009) Epilepsy and cognitive impairments in Alzheimer disease. *Archives of neurology*. 66 (4), 435–40.

- Palop, J.J., Mucke, L. & Roberson, E.D. (2011) Quantifying biomarkers of cognitive dysfunction and neuronal network hyperexcitability in mouse models of Alzheimer's disease: Depletion of calcium-dependent proteins and inhibitory hippocampal remodeling. *Methods in Molecular Biology*. 670245–262.
- Palva, J.M. & Palva, S. (2012) Infra-slow fluctuations in electrophysiological recordings, blood-oxygenation-level-dependent signals, and psychophysical time series. *NeuroImage*. 62 (4), 2201–2211.
- Palva, S. & Palva, J.M. (2012) Discovering oscillatory interaction networks with M/EEG: challenges and breakthroughs. *Trends in Cognitive Sciences*. 16 (4), 219–230.
- Pan, W.-J., Thompson, G.J., Magnuson, M.E., Jaeger, D. & Keilholz, S. (2013) Infraslow LFP correlates to resting-state fMRI BOLD signals. *NeuroImage*. 74288–97.
- Pandis, D. & Scarmeas, N. (2012) Seizures in alzheimer disease: Clinical and epidemiological data. *Epilepsy Currents*. 12 (5), 184–187.
- Pao, W.C., Boeve, B.F., Ferman, T.J., Lin, S.-C., Smith, G.E., Knopman, D.S., Graff-Radford, N.R., Petersen, R.C., Parisi, J.E., Dickson, D.W. & Silber, M.H. (2013) Polysomnographic Findings in Dementia With Lewy Bodies. *The Neurologist*. 19 (1), 1–6.
- Park, I.S., Yoo, S.W., Lee, K.-S. & Kim, J.-S. (2014) Epileptic seizure presenting as dementia with Lewy bodies. *General Hospital Psychiatry*. 36 (2), 230.e3-230.e5.
- Parri, H.R. & Crunelli, V. (2001) Pacemaker calcium oscillations in thalamic astrocytes in sit... : NeuroReport. *NeuroReport*. 12 (18), 3897–3900.
- Parrino, L., Ferri, R., Bruni, O. & Terzano, M.G. (2012) Cyclic alternating pattern (CAP): The marker of sleep instability. *Sleep Medicine Reviews*. 16 (1), 27–45.
- Parrino, L., Halasz, P., Tassinari, C.A. & Terzano, M.G. (2006) CAP, epilepsy and motor events during sleep: the unifying role of arousal. *Sleep Medicine Reviews*. 10 (4), 267–285.
- Parrino, L. & Vaudano, A.E. (2018) The resilient brain and the guardians of sleep: New

perspectives on old assumptions. *Sleep Medicine Reviews*. 3998–107.

Paxinos, G. & Watson, C. (1998) *The Rat Brain in Stereotaxic Coordinates*. San Diego: CA: Academic.

Peever, J. & Fuller, P.M. (2017) The Biology of REM Sleep. *Current Biology*. 27 (22), R1237–R1248.

Penttonen, M., Nurminen, N., Miettinen, R., Sirviö, J., Henze, D., Csicsvári, J. & Buzsáki, G. (1999) Ultra-slow oscillation (0.025 Hz) triggers hippocampal afterdischarges in Wistar rats. *Neuroscience*. 94 (3), 735–743.

Peraza, L.R., Cromarty, R., Kobeleva, X., Firbank, M.J., Killen, A., Graziadio, S., Thomas, A.J., O'Brien, J.T. & Taylor, J.-P. (2018) Electroencephalographic derived network differences in Lewy body dementia compared to Alzheimer's disease patients. *Scientific Reports*. 8 (4637), 1–13.

Peraza, L.R., Kaiser, M., Firbank, M., Graziadio, S., Bonanni, L., Onofrj, M., Colloby, S.J., Blamire, A., O'Brien, J. & Taylor, J.-P. (2014) fMRI resting state networks and their association with cognitive fluctuations in dementia with Lewy bodies. *NeuroImage. Clinical*. 4558–65.

Peraza, L.R., Taylor, J.-P. & Kaiser, M. (2015) Divergent brain functional network alterations in dementia with Lewy bodies and Alzheimer's disease. *Neurobiology of aging*. 36 (9), 2458–67.

Perl, D.P. (2010) Neuropathology of Alzheimer's disease. *Mount Sinai Journal of Medicine* 77 (1) p.32–42.

Phillis, J.W., Kostopoulos, G.K. & Limacher, J.J. (1975) A potent depressant action of adenine derivatives on cerebral cortical neurones. *European Journal of Pharmacology*. 30 (1), 125–129.

Picchioni, D., Horovitz, S.G., Fukunaga, M., Carr, W.S., Meltzer, J.A., Balkin, T.J., Duyn, J.H. & Braun, A.R. (2011) Infraslow EEG oscillations organize large-scale cortical-subcortical interactions during sleep: A combined EEG/fMRI study. *Brain Research*. 137463–72.

Picciotto, M.R., Higley, M.J. & Mineur, Y.S. (2012) Acetylcholine as a Neuromodulator:

Cholinergic Signaling Shapes Nervous System Function and Behavior. *Neuron* 76 (1) p.116–129.

Pievani, M., de Haan, W., Wu, T., Seeley, W.W. & Frisoni, G.B. (2011) Functional network disruption in the degenerative dementias. *The Lancet Neurology*. 10 (9), 829–843.

Piggott, M.A., Ballard, C.G., Dickinson, H.O., McKeith, I.G., Perry, R.H. & Perry, E.K. (2007) Thalamic D2 receptors in dementia with Lewy bodies, Parkinson's disease, and Parkinson's disease dementia. *The international journal of neuropsychopharmacology / official scientific journal of the Collegium Internationale Neuropsychopharmacologicum (CINP)*. 10 (2), 231–44.

Pimlott, S.L., Piggott, M., Ballard, C., McKeith, I., Perry, R., Kometa, S., Owens, J., Wyper, D. & Perry, E. (2006) Thalamic nicotinic receptors implicated in disturbed consciousness in dementia with Lewy bodies. *Neurobiology of Disease*. 21 (1), 50–56.

Platt, B., Drever, B., Koss, D., Stoppelkamp, S., Jyoti, A., Plano, A., Utan, A., Merrick, G., Ryan, D., Melis, V., Wan, H., Mingarelli, M., Porcu, E., Scrocchi, L., Welch, A. & Riedel, G. (2011) Abnormal Cognition, Sleep, EEG and Brain Metabolism in a Novel Knock-In Alzheimer Mouse, PLB1 Huaibin Cai (ed.). *PLoS ONE*. 6 (11), e27068.

Polymeropoulos, M.H., Lavedan, C., Leroy, E., Ide, S.E., Dehejia, A., Dutra, A., Pike, B., Root, H., Rubenstein, J., Boyer, R., Stenroos, E.S., Chandrasekharappa, S., Athanassiadou, A., Papapetropoulos, T., Johnson, W.G., Lazzarini, A.M., Duvoisin, R.C., Di Iorio, G., Golbe, L.I., et al. (1997) Mutation in the  $\alpha$ -synuclein gene identified in families with Parkinson's disease. *Science*. 276 (5321), 2045–2047.

Ponjoan, A., Garre-Olmo, J., Blanch, J., Fages, E., Alves-Cabrato, L., Martí-Lluch, R., Comas-Cufí, M., Parramon, D., Garcia-Gil, M. & Ramos, R. (2019) Epidemiology of dementia: Prevalence and incidence estimates using validated electronic health records from primary care. *Clinical Epidemiology*. 2019 (11), 217–228.

- Porter, V.R., Buxton, W.G. & Avidan, A.Y. (2015) Sleep, Cognition and Dementia. *Current Psychiatry Reports*. 17 (97).
- Puig, M.V., Ushimaru, M. & Kawaguchi, Y. (2008) Two distinct activity patterns of fast-spiking interneurons during neocortical UP states. *Proceedings of the National Academy of Sciences of the United States of America*. 105 (24), 8428–8433.
- Raichle, M.E. (2015) The Brain's Default Mode Network. *Annual Review of Neuroscience*. 38 (1), 433–447.
- Raichle, M.E., MacLeod, A.M., Snyder, A.Z., Powers, W.J., Gusnard, D.A. & Shulman, G.L. (2001) A default mode of brain function. *Proceedings of the National Academy of Sciences of the United States of America*. 98 (2), 676–82.
- Rasch, B. & Born, J. (2013) About sleep's role in memory. *Physiological Reviews*. 93 (2), 681–766.
- Rebollo, B., Perez-Zabalza, M., Ruiz-Mejias, M., Perez-Mendez, L. & Sanchez-Vives, M. V. (2018) Beta and Gamma Oscillations in Prefrontal Cortex During NMDA Hypofunction: An In Vitro Model of Schizophrenia Features. *Neuroscience*. 383138–149.
- Reder, A.T., Mednick, A.S., Brown, P., Spire, J.P., Van Cauter, E., Wollmann, R.L., Cervenàková, L., Goldfarb, L.G., Garay, A. & Ovsiew, F. (1995) Clinical and genetic studies of fatal familial insomnia. *Neurology*. 45 (6), 1068–75.
- Reichinnek, S., Künsting, T., Draguhn, A. & Both, M. (2010) Field potential signature of distinct multicellular activity patterns in the mouse hippocampus. *Journal of Neuroscience*. 30 (46), 15441–15449.
- Remondes, M. & Wilson, M.A. (2013) Cingulate-hippocampus coherence and trajectory coding in a sequential choice task. *Neuron*. 80 (5), 1277–89.
- Reynolds, C.F., Kupfer, D.J., Houck, P.R., Hoch, C.C., Stack, J.A., Berman, S.R. & Zimmer, B. (1988) Reliable Discrimination of Elderly Depressed and Demented Patients by Electroencephalographic Sleep Data. *Archives of General Psychiatry*. 45 (3), 258–264.
- Riedner, B.A., Hulse, B.K., Murphy, M.J., Ferrarelli, F. & Tononi, G. (2011) Temporal

dynamics of cortical sources underlying spontaneous and peripherally evoked slow waves. *Progress in brain research*. 193201–18.

Riga, D., Matos, M.R., Glas, A., Smit, A.B., Spijker, S. & Van den Oever, M.C. (2014) Optogenetic dissection of medial prefrontal cortex circuitry. *Frontiers in Systems Neuroscience* 8 (230) p.1–19.

Rikhye, R. V, Wimmer, R.D. & Halassa, M.M. (2018) Toward an Integrative Theory of Thalamic Function. *Annu. Rev. Neurosci.* 41163–183.

Rizzo, G., Arcuti, S., Copetti, M., Alessandria, M., Savica, R., Fontana, A., Liguori, R. & Logroscino, G. (2018) Accuracy of clinical diagnosis of dementia with Lewy bodies: a systematic review and meta-analysis. *Journal of neurology, neurosurgery, and psychiatry*. 89 (4), 358–366.

Robson, E., Tweedy, C., Manzanza, N., Taylor, J.-P., Atkinson, P., Randall, F., Reeve, A., Clowry, G.J. & LeBeau, F.E.N. (2018) Impaired Fast Network Oscillations and Mitochondrial Dysfunction in a Mouse Model of Alpha-synucleinopathy (A30P). *Neuroscience*. 377161–173.

Rockenstein, E., Nuber, S., Overk, C.R., Ubhi, K., Mante, M., Patrick, C., Adame, A., Trejo-Morales, M., Gerez, J., Picotti, P., Jensen, P.H., Campioni, S., Riek, R., Winkler, J., Gage, F.H., Winner, B. & Masliah, E. (2014) Accumulation of oligomer-prone  $\alpha$ -synuclein exacerbates synaptic and neuronal degeneration in vivo. *Brain*. 137 (5), 1496–1513.

Rodriguez, G., Copello, F., Vitali, P., Perego, G. & Nobili, F. (1999) EEG spectral profile to stage Alzheimer's disease. *Clinical neurophysiology: official journal of the International Federation of Clinical Neurophysiology*. 110 (10), 1831–7.

Roks, G., Korf, E.S.C., van der Flier, W.M., Scheltens, P. & Stam, C.J. (2008) The use of EEG in the diagnosis of dementia with Lewy bodies. *Journal of neurology, neurosurgery, and psychiatry*. 79 (4), 377–80.

Roopun, A.K., Middleton, S.J., Cunningham, M.O., LeBeau, F.E.H., Bibbig, A., Whittington, M.A. & Traub, R.D. (2006) A beta2-frequency (20-30 Hz) oscillation in nonsynaptic networks of somatosensory cortex. *Proceedings of the National Academy of Sciences of the United States of America*. 103 (42), 15646–15650.

- Rothman, S.M. & Mattson, M.P. (2012) Sleep Disturbances in Alzheimer's and Parkinson's Diseases. *NeuroMolecular Medicine*. 14 (3), 194–204.
- Ruiz-Mejias, M., Ciria-Suarez, L., Mattia, M. & Sanchez-Vives, M. V. (2011) Slow and fast rhythms generated in the cerebral cortex of the anesthetized mouse. *Journal of Neurophysiology*. 106 (6), 2910–2921.
- Sadiq, D., Whitfield, T., Lee, L., Stevens, T., Costafreda, S. & Walker, Z. (2017) Prodromal Dementia with Lewy Bodies and Prodromal Alzheimer's Disease: A Comparison of the Cognitive and Clinical Profiles. *Journal of Alzheimer's Disease*. 58 (2), 463–470.
- Sakono, M. & Zako, T. (2010) Amyloid oligomers: Formation and toxicity of A $\beta$  oligomers. *FEBS Journal* 277 (6) p.1348–1358.
- Salib, M., Joshi, A., Katona, L., Howarth, M., Micklem, B.R., Somogyi, P. & Viney, T.J. (2019) GABAergic medial septal neurons with low-rhythmic firing innervating the dentate gyrus and hippocampal area CA3. *Journal of Neuroscience*. 39 (23), 4527–4549.
- Sanchez-Vives, M. V., Mattia, M., Compte, A., Perez-Zabalza, M., Winograd, M., Descalzo, V.F. & Reig, R. (2010) Inhibitory Modulation of Cortical Up States. *Journal of Neurophysiology*. 104 (3), 1314–1324.
- Sanchez-Vives, M. V. & McCormick, D.A. (2000) Cellular and network mechanisms of rhythmic recurrent activity in neocortex. *Nature Neuroscience*. 3 (10), 1027–1034.
- Sánchez, M.P., García-Cabrero, A.M., Sánchez-Elexpuru, G., Burgos, D.F. & Serratos, J.M. (2018) Tau-Induced Pathology in Epilepsy and Dementia: Notions from Patients and Animal Models. *International journal of molecular sciences*. 19 (1092), 1–20.
- Sarkis, R.A., Dickerson, B.C., Cole, A.J. & Chemali, Z.N. (2016) Clinical and Neurophysiologic Characteristics of Unprovoked Seizures in Patients Diagnosed With Dementia. *The Journal of Neuropsychiatry and Clinical Neurosciences*. 28 (1), 56–61.
- Savage, L.M., Buzzetti, R.A. & Ramirez, D.R. (2004) The effects of hippocampal

- lesions on learning, memory, and reward expectancies. *Neurobiology of Learning and Memory*. 82 (2), 109–119.
- Savica, R., Grossardt, B.R., Bower, J.H., Boeve, B.F., Ahlskog, J.E. & Rocca, W.A. (2013) Incidence of dementia with Lewy bodies and Parkinson disease dementia. *JAMA Neurology*. 70 (11), 1396–1402.
- Schapira, A.H.V. (2013) *Calcium dysregulation in Parkinson's disease*. 2015–2016.
- Scheeringa, R., Bastiaansen, M.C.M., Petersson, K.M., Oostenveld, R., Norris, D.G. & Hagoort, P. (2008) Frontal theta EEG activity correlates negatively with the default mode network in resting state. *International Journal of Psychophysiology*. 67 (3), 242–251.
- Schell, H., Hasegawa, T., Neumann, M. & Kahle, P.J. (2009) Nuclear and neuritic distribution of serine-129 phosphorylated  $\alpha$ -synuclein in transgenic mice. *Neuroscience*. 160 (4), 796–804.
- Schindelin, J., Arganda-Carreras, I., Frise, E., Kaynig, V., Longair, M., Pietzsch, T., Preibisch, S., Rueden, C., Saalfeld, S., Schmid, B., Tinevez, J.Y., White, D.J., Hartenstein, V., Eliceiri, K., Tomancak, P. & Cardona, A. (2012) Fiji: An open-source platform for biological-image analysis. *Nature Methods* 9 (7) p.676–682.
- Schmeichel, A.M., Buchhalter, L.C., Low, P.A., Parisi, J.E., Boeve, B.W., Sandroni, P. & Benarroch, E.E. (2008) Mesopontine cholinergic neuron involvement in Lewy body dementia and multiple system atrophy. *Neurology*. 70 (5), 368–373.
- Schneider, C.A., Rasband, W.S. & Eliceiri, K.W. (2012) NIH Image to ImageJ: 25 years of image analysis. *Nature Methods* 9 (7) p.671–675.
- Schulz-Schaeffer, W.J. (2010) The synaptic pathology of alpha-synuclein aggregation in dementia with Lewy bodies, Parkinson's disease and Parkinson's disease dementia. *Acta neuropathologica*. 120 (2), 131–43.
- Schumacher, J., Peraza, L., Firbank, M., Thomas, A., Kaiser, M., Gallagher, P., O'Brien, J., Blamire, A. & Taylor, J.-P. (2018) Dynamic functional connectivity changes in dementia with Lewy bodies and Alzheimer's disease. *bioRxiv*. 374538.
- Schumacher, J., Peraza, L.R., Firbank, M., Thomas, A.J., Kaiser, M., Gallagher, P.,

- O'Brien, J.T., Blamire, A.M. & Taylor, J.-P. (2019) Dysfunctional brain dynamics and their origin in Lewy body dementia. *Brain*. 142 (6), 1767–1782.
- Selkoe, D.J. (2002) Alzheimer's Disease Is a Synaptic Failure. *Science*. 298 (5594), 789–791.
- Sengupta, U., Nilson, A.N. & Kaye, R. (2016) The Role of Amyloid- $\beta$  Oligomers in Toxicity, Propagation, and Immunotherapy. *EBioMedicine* 6 p.42–49.
- Serrano-Pozo, A., Frosch, M.P., Masliah, E. & Hyman, B.T. (2011) Neuropathological alterations in Alzheimer disease. *Cold Spring Harbor perspectives in medicine*. 2011 (1), 1–23.
- Sesack, S.R., Deutch, A.Y., Roth, R.H. & Bunney, B.S. (1989) Topographical organization of the efferent projections of the medial prefrontal cortex in the rat: An anterograde tract-tracing study with *Phaseolus vulgaris* leucoagglutinin. *The Journal of Comparative Neurology*. 290 (2), 213–242.
- Sethi, M., Joshi, S.S., Webb, R.L., Beckett, T.L., Donohue, K.D., Murphy, M.P., O'Hara, B.F. & Duncan, M.J. (2015) Increased fragmentation of sleep-wake cycles in the 5XFAD mouse model of Alzheimer's disease. *Neuroscience*. 29080–89.
- Sharma, A. V., Wolansky, T. & Dickson, C.T. (2010) A comparison of sleep-like slow oscillations in the hippocampus under ketamine and urethane anesthesia. *Journal of Neurophysiology*. 104 (2), 932–939.
- Shu, Y., Hasenstaub, A. & McCormick, D.A. (2003) Turning on and off recurrent balanced cortical activity. *Nature*. 423 (6937), 288–293.
- Siapas, A.G. & Wilson, M.A. (1998) Coordinated interactions between hippocampal ripples and cortical spindles during slow-wave sleep. *Neuron*. 21 (5), 1123–1128.
- Siddiqui, I.J., Pervaiz, N. & Abbasi, A.A. (2016) The Parkinson Disease gene SNCA: Evolutionary and structural insights with pathological implication. *Scientific Reports*. 6 (24475), 1–11.
- Silberberg, G. & Markram, H. (2007) Disynaptic Inhibition between Neocortical Pyramidal Cells Mediated by Martinotti Cells. *Neuron*. 53 (5), 735–746.

- da Silva, F.L. (2009) 'EEG: Origin and Measurement', in *EEG - fMRI*. [Online]. Berlin, Heidelberg: Springer Berlin Heidelberg. pp. 19–38.
- Silva, L.R., Amitai, Y. & Connors, B.W. (1991) Intrinsic oscillations of neocortex generated by layer 5 pyramidal neurons. *Science*. 251 (4992), 432–435.
- Silva, R.H., Abílio, V.C., Takatsu, A.L., Kameda, S.R., Grassl, C., Chehin, A.B., Medrano, W.A., Calzavara, M.B., Registro, S., Andersen, M.L., Machado, R.B., Carvalho, R.C., Ribeiro, R.D.A., Tufik, S. & Frussa-Filho, R. (2004) Role of hippocampal oxidative stress in memory deficits induced by sleep deprivation in mice. *Neuropharmacology*. 46 (6), 895–903.
- Simkin, D., Hattori, S., Ybarra, N., Musia, T.F., Buss, E.W., Richter, H., Matthew Oh, M., Nicholson, D.A. & Disterhoft, J.F. (2015) Aging-related hyperexcitability in CA3 pyramidal neurons is mediated by enhanced A-type K<sup>+</sup> channel function and expression. *Journal of Neuroscience*. 35 (38), 13206–13218.
- Sirota, A., Csicsvari, J., Buhl, D. & Buzsáki, G. (2003) Communication between neocortex and hippocampus during sleep in rodents. *Proceedings of the National Academy of Sciences of the United States of America*. 100 (4), 2065–9.
- Sloviter, R.S., Ali-Akbarian, L., Elliott, R.C., Bowery, B.J. & Bowery, N.G. (1999) Localization of GABA(B) (R1) receptors in the rat hippocampus by immunocytochemistry and high resolution autoradiography, with specific reference to its localization in identified hippocampal interneuron subpopulations. *Neuropharmacology*. 38 (11), 1707–21.
- Snaedal, J., Johannesson, G.H., Gudmundsson, T.E., Blin, N.P., Emilsdottir, A.L., Einarsson, B. & Johnsen, K. (2012) Diagnostic Accuracy of Statistical Pattern Recognition of Electroencephalogram Registration in Evaluation of Cognitive Impairment and Dementia. *Dementia and Geriatric Cognitive Disorders*. 34 (1), 51–60.
- Snead, D. & Eliezer, D. (2014) Alpha-Synuclein Function and Dysfunction on Cellular Membranes. *Experimental Neurobiology*. 23 (4), 292–313.
- Snyder, S.H. (2017) A Life of Neurotransmitters. *Annual Review of Pharmacology and Toxicology*. 57 (1), 1–11.

- Sohal, V.S., Zhang, F., Yizhar, O. & Deisseroth, K. (2009) Parvalbumin neurons and gamma rhythms enhance cortical circuit performance. *Nature*. 459 (7247), 698–702.
- Van Someren, E.J.W., Van Der Werf, Y.D., Roelfsema, P.R., Mansvelder, H.D. & Lopes da Silva, F.H. (2011) Slow brain oscillations of sleep, resting state, and vigilance. *Progress in Brain Research*. 1933–15.
- Somogyi, P., Shepherd, G. & Grillner, S. (2010) *Handbook of brain microcircuits*. 2nd edition. Oxford University Press.
- Sparta, D.R., Hovelsø, N., Mason, A.O., Kantak, P.A., Ung, R.L., Decot, H.K. & Stuber, G.D. (2014) Activation of prefrontal cortical parvalbumin interneurons facilitates extinction of reward-seeking behavior. *Journal of Neuroscience*. 34 (10), 3699–3705.
- Spillantini, M.G., Crowther, R.A., Jakes, R., Hasegawa, M. & Goedert, M. (1998)  $\alpha$ -Synuclein in filamentous inclusions of Lewy bodies from Parkinson's disease and dementia with Lewy bodies. *Proceedings of the National Academy of Sciences of the United States of America*. 95 (11), 6469–6473.
- Spira, P.J., Sharpe, D.M., Halliday, G., Cavanagh, J. & Nicholson, G.A. (2001) Clinical and pathological features of a Parkinsonian syndrome in a family with an Ala53Thr alpha-synuclein mutation. *Annals of neurology*. 49 (3), 313–9.
- Spruston, N. (2008) Pyramidal neurons: Dendritic structure and synaptic integration. *Nature Reviews Neuroscience* 9 (3) p.206–221.
- Stafstrom, C.E. & Carmant, L. (2015) Seizures and epilepsy: An overview for neuroscientists. *Cold Spring Harbor Perspectives in Biology*. 7 (5), 1–19.
- Staresina, B.P., Bergmann, T.O., Bonnefond, M., Van Der Meij, R., Jensen, O., Deuker, L., Elger, C.E., Axmacher, N. & Fell, J. (2015) Hierarchical nesting of slow oscillations, spindles and ripples in the human hippocampus during sleep. *Nature Neuroscience*. 18 (11), 1679–1686.
- van Steenoven, I., van der Flier, W.M., Scheltens, P., Teunissen, C.E. & Lemstra, A.W. (2019) Amyloid- $\beta$  peptides in cerebrospinal fluid of patients with dementia with

- Lewy bodies. *Alzheimer's Research & Therapy*. 11 (1), 83.
- Steriade, M., Amzica, F. & Contreras, D. (1996) Synchronization of fast (30-40 Hz) spontaneous cortical rhythms during brain activation. *Journal of Neuroscience*. 16 (1), 392–417.
- Steriade, M., Domich, L., Oakson, G. & Deschenes, M. (1987) The deafferented reticular thalamic nucleus generates spindle rhythmicity. *Journal of Neurophysiology*. 57 (1), 260–273.
- Steriade, M., Nunez, A. & Amzica, F. (1993a) A novel slow (< 1 Hz) oscillation of neocortical neurons in vivo: Depolarizing and hyperpolarizing components. *Journal of Neuroscience*. 13 (8), 3252–3265.
- Steriade, M., Nunez, A. & Amzica, F. (1993b) Intracellular analysis of relations between the slow (<1 Hz) neocortical oscillation and other sleep rhythms of the electroencephalogram. *Journal of Neuroscience*. 13 (8), 3266–3283.
- Steriade, M. & Timofeev, I. (2003) Neuronal plasticity in thalamocortical networks during sleep and waking oscillations. *Neuron* 37 (4) p.563–576.
- Stewart, M. & Fox, S.E. (1989) Firing relations of medial septal neurons to the hippocampal theta rhythm in urethane anesthetized rats. *Experimental Brain Research*. 77 (3), 507–516.
- Strimbu, K. & Tavel, J.A. (2010) What are biomarkers? *Current Opinion in HIV and AIDS* 5 (6) p.463–466.
- Stylianou, M., Murphy, N., Peraza, L.R., Graziadio, S., Cromarty, R., Killen, A., O'Brien, J.T., Thomas, A.J., LeBeau, F.E.N. & Taylor, J.-P. (2018) Quantitative electroencephalography as a marker of cognitive fluctuations in dementia with Lewy bodies and an aid to differential diagnosis. *Clinical Neurophysiology*. 129 (6), 1209–1220.
- Sullivan, D., Csicsvari, J., Mizuseki, K., Montgomery, S., Diba, K. & Buzsáki, G. (2011) Relationships between Hippocampal Sharp Waves, Ripples, and Fast Gamma Oscillation: Influence of Dentate and Entorhinal Cortical Activity. *Journal of Neuroscience*. 31 (23), 8605–8616.

- Suzuki, S.S. & Smith, G.K. (1988) Spontaneous EEG spikes in the normal hippocampus. V. Effects of ether, urethane, pentobarbital, atropine, diazepam and bicuculline. *Electroencephalography and Clinical Neurophysiology*. 70 (1), 84–95.
- Swindle, M.M., Vogler, G.A., Fulton, L.K., Marini, R.P. & Popilskis, S. (2002) 'Preanesthesia, Anesthesia, Analgesia, and Euthanasia', in J. G. Fox, F. M. Loew, L. C. Anderson, & F. W. Quimby (eds.) *Laboratory Animal Medicine*. 2nd edition [Online]. Academic Press. pp. 955–1003.
- Tabuchi, M., Lone, S.R., Liu, S., Liu, Q., Zhang, J., Spira, A.P. & Wu, M.N. (2015) Sleep Interacts with A $\beta$  to Modulate Intrinsic Neuronal Excitability. *Current Biology*. 25 (6), 702–712.
- Tagliazucchi, E., Von Wegner, F., Morzelewski, A., Brodbeck, V., Jahnke, K. & Laufs, H. (2013) Breakdown of long-range temporal dependence in default mode and attention networks during deep sleep. *Proceedings of the National Academy of Sciences of the United States of America*. 110 (38), 15419–15424.
- Tanaka, M., Kim, Y.M., Lee, G., Junn, E., Iwatsubo, T. & Mouradian, M.M. (2004) Aggresomes Formed by  $\alpha$ -Synuclein and Synphilin-1 Are Cytoprotective. *Journal of Biological Chemistry*. 279 (6), 4625–4631.
- Taylor, J.-P., Collerton, D., LeBeau, F. & Perry, E. (2017) 'Cholinergic Pathology in Dementia with Lewy Bodies', in *Dementia with Lewy Bodies*. [Online]. Tokyo: Springer Japan. pp. 23–39.
- Taylor, J.-P., Firbank, M., Barnett, N., Pearce, S., Livingstone, A., Mosimann, U., Eyre, J., McKeith, I.G. & O'Brien, J.T. (2011) Visual hallucinations in dementia with Lewy bodies: transcranial magnetic stimulation study. *British Journal of Psychiatry*. 199 (6), 492–500.
- Teravskis, P.J., Covelo, A., Miller, E.C., Singh, B., Martell-Martínez, H.A., Benneyworth, M.A., Gallardo, C., Oxnard, B.R., Araque, A., Lee, M.K. & Liao, D. (2018) A53t mutant alpha-synuclein induces tau-dependent postsynaptic impairment independently of neurodegenerative changes. *Journal of Neuroscience*. 38 (45), 9754–9767.
- Terzaghi, M., Arnaldi, D., Rizzetti, M.C., Minafra, B., Cremascoli, R., Rustioni, V.,

- Zangaglia, R., Pasotti, C., Sinforiani, E., Pacchetti, C. & Manni, R. (2013) Analysis of video-polysomnographic sleep findings in dementia with Lewy bodies. *Movement Disorders*. 28 (10), 1416–1423.
- Terzano, M.G., Mancina, D., Salati, M.R., Costani, G., Decembrino, A. & Parrino, L. (1985) The Cyclic Alternating Pattern as a Physiologic Component of Normal NREM Sleep. *Sleep*. 8 (2), 137–145.
- Terzano, M.G. & Parrino, L. (1993) Clinical applications of cyclic alternating pattern. *Physiology & Behavior*. 54 (4), 807–813.
- Terzano, M.G. & Parrino, L. (2000) Origin and Significance of the Cyclic Alternating Pattern (CAP). *Sleep Medicine Reviews*. 4 (1), 101–123.
- Texidó, L., Martín-Satué, M., Alberdi, E., Solsona, C. & Matute, C. (2011) Amyloid  $\beta$  peptide oligomers directly activate NMDA receptors. *Cell Calcium*. 49 (3), 184–190.
- Timofeev, I. (2000) Origin of Slow Cortical Oscillations in Deafferented Cortical Slabs. *Cerebral Cortex*. 10 (12), 1185–1199.
- Timofeev, I., Bazhenov, M., Sejnowski, T.J. & Steriade, M. (2001) Contribution of intrinsic and synaptic factors in the desynchronization of thalamic oscillatory activity. *Thalamus & Related Systems* 1.
- Timofeev, I., Grenier, F. & Steriade, M. (2001) Disfacilitation and active inhibition in the neocortex during the natural sleep-wake cycle: An intracellular study. *Proceedings of the National Academy of Sciences*. 98 (4), 1924–1929.
- Tiraboschi, P., Hansen, L.A., Alford, M., Merdes, A., Masliah, E., Thal, L.J. & Corey-Bloom, J. (2002) Early and widespread cholinergic losses differentiate dementia with Lewy bodies from Alzheimer disease. *Archives of general psychiatry*. 59 (10), 946–51.
- Tofaris, G.K., Reitböck, P.G., Humby, T., Lambourne, S.L., O’Connell, M., Ghetti, B., Gossage, H., Emson, P.C., Wilkinson, L.S., Goedert, M. & Spillantini, M.G. (2006) Pathological changes in dopaminergic nerve cells of the substantia nigra and olfactory bulb in mice transgenic for truncated human  $\alpha$ -synuclein(1- 120):

Implications for lewy body disorders. *Journal of Neuroscience*. 26 (15), 3942–3950.

Toledo, J.B., Gopal, P., Raible, K., Irwin, D.J., Brettschneider, J., Sedor, S., Waits, K., Boluda, S., Grossman, M., Van Deerlin, V.M., Lee, E.B., Arnold, S.E., Duda, J.E., Hurtig, H., Lee, V.M.Y., Adler, C.H., Beach, T.G. & Trojanowski, J.Q. (2016) Pathological  $\alpha$ -synuclein distribution in subjects with coincident Alzheimer's and Lewy body pathology. *Acta Neuropathologica*. 131 (3), 393–409.

Tononi, G. & Cirelli, C. (2006) Sleep function and synaptic homeostasis. *Sleep Medicine Reviews*. 10 (1), 49–62.

Trachsel, L., Tobler, I., Achermann, P. & Borbély, A.A. (1991) Sleep continuity and the REM-nonREM cycle in the rat under baseline conditions and after sleep deprivation. *Physiology and Behavior*. 49 (3), 575–580.

Del Tredici, K. & Braak, H. (2016) Review: Sporadic Parkinson's disease: development and distribution of  $\alpha$ -synuclein pathology. *Neuropathology and Applied Neurobiology*. 42 (1), 33–50.

Tsigelny, I.F., Sharikov, Y., Wrasidlo, W., Gonzalez, T., Desplats, P.A., Crews, L., Spencer, B. & Masliah, E. (2012) Role of  $\alpha$ -synuclein penetration into the membrane in the mechanisms of oligomer pore formation. *FEBS Journal*. 279 (6), 1000–1013.

Tukker, J.J., Fuentealba, P., Hartwich, K., Somogyi, P. & Klausberger, T. (2007) Cell type-specific tuning of hippocampal interneuron firing during gamma oscillations in vivo. *Journal of Neuroscience*. 27 (31), 8184–8189.

Tweedy, C., Lebeau, F., Clowry, G., Reeve, A., Taylor, J.-P., Randall, F. & Atkinson, P. (2018) *Age-dependent hippocampal network dysfunction in a mouse model of alpha-synucleinopathy*. [Online]. Newcastle University.

Ukai, K., Fujishiro, H., Watanabe, M., Kosaka, K. & Ozaki, N. (2017) Similarity of symptoms between transient epileptic amnesia and Lewy body disease. *Psychogeriatrics*. 17 (2), 120–125.

Uusisaari, M. (2003) *GABAergic mechanisms of excitation and hypersynchrony in*

*adult rat hippocampus Academic dissertation.* 12 (11).

- Uylings, H.B.M., Groenewegen, H.J. & Kolb, B. (2003) Do rats have a prefrontal cortex? *Behavioural Brain Research* 146 (1–2) p.3–17.
- Valderrama, M., Crépon, B., Botella-Soler, V., Martinerie, J., Hasboun, D., Alvarado-Rojas, C., Baulac, M., Adam, C., Navarro, V. & Le Van Quyen, M. (2012) Human Gamma Oscillations during Slow Wave Sleep Olaf Sporns (ed.). *PLoS ONE*. 7 (4), e33477.
- Valdinocci, D., Radford, R.A.W., Siow, S.M., Chung, R.S. & Pountney, D.L. (2017) Potential modes of intercellular  $\alpha$ -synuclein transmission. *International Journal of Molecular Sciences* 18 (2).
- Valencia, M., Artieda, J., Bolam, J.P. & Mena-Segovia, J. (2013) Dynamic Interaction of Spindles and Gamma Activity during Cortical Slow Oscillations and Its Modulation by Subcortical Afferents. *PLoS ONE*. 8 (7), e67540.
- Valero, M., Averkin, R.G., Fernandez-Lamo, I., Aguilar, J., Lopez-Pigozzi, D., Brotons-Mas, J.R., Cid, E., Tamas, G. & Menendez de la Prida, L. (2017) Mechanisms for Selective Single-Cell Reactivation during Offline Sharp-Wave Ripples and Their Distortion by Fast Ripples. *Neuron*. 94 (6), 1234-1247.e7.
- Le Van Quyen, M., Staba, R., Bragin, A., Dickson, C., Valderrama, M., Fried, I. & Engel, J. (2010) Large-scale microelectrode recordings of high-frequency gamma oscillations in human cortex during sleep. *The Journal of neuroscience : the official journal of the Society for Neuroscience*. 30 (23), 7770–82.
- Vanhatalo, S., Palva, J.M., Holmes, M.D., Miller, J.W., Voipio, J. & Kaila, K. (2004) Infralow oscillations modulate excitability and interictal epileptic activity in the human cortex during sleep. *Proceedings of the National Academy of Sciences of the United States of America*. 101 (14), 5053–7.
- Vann Jones, S.A. & O'Brien, J.T. (2014) The prevalence and incidence of dementia with Lewy bodies: A systematic review of population and clinical studies. *Psychological Medicine* 44 (4) p.673–683.
- Vantomme, G., Osorio-Forero, A., Lüthi, A. & Fernandez, L.M.J. (2019) Regulation of

local sleep by the thalamic reticular nucleus. *Frontiers in Neuroscience* 13 (JUN) p.576.

Varanese, S., Perfetti, B., Monaco, D., Thomas, A., Bonanni, L., Tiraboschi, P. & Onofri, M. (2010) Fluctuating cognition and different cognitive and behavioural profiles in Parkinson's disease with dementia: comparison of dementia with Lewy bodies and Alzheimer's disease. *Journal of Neurology*. 257 (6), 1004–1011.

Varela, C. & Wilson, M. (2019) mPFC Spindle Cycles Organize Sparse Thalamic Activation and Recently Active CA1 cells During non-REM Sleep. *bioRxiv*.

Vaz Fragoso, C.A., Van Ness, P.H., Araujo, K.L.B., Iannone, L.P. & Klar Yaggi, H. (2015) Age-related differences in sleep-wake symptoms of adults undergoing polysomnography. *Journal of the American Geriatrics Society*. 63 (9), 1845–1851.

Vertes, R.P., Hoover, W.B., Szigeti-Buck, K. & Leranth, C. (2007) Nucleus reuniens of the midline thalamus: Link between the medial prefrontal cortex and the hippocampus. *Brain Research Bulletin*. 71 (6), 601–609.

Videnovic, A. & Golombek, D. (2013) Circadian and sleep disorders in Parkinson's disease. *Experimental neurology*. 24345–56.

Volgushev, M., Chauvette, S., Mukovski, M. & Timofeev, I. (2006) Precise long-range synchronization of activity and silence in neocortical neurons during slow-wave sleep. *Journal of Neuroscience*. 26 (21), 5665–5672.

Vossel, K.A., Tartaglia, M.C., Nygaard, H.B., Zeman, A.Z. & Miller, B.L. (2017) Epileptic activity in Alzheimer's disease: causes and clinical relevance. *The Lancet Neurology*. 16 (4), 311–322.

Vossel, S., Geng, J.J. & Fink, G.R. (2014) Dorsal and ventral attention systems: distinct neural circuits but collaborative roles. *The Neuroscientist: a review journal bringing neurobiology, neurology and psychiatry*. 20 (2), 150–159.

Vucic, S., Nicholson, G.A. & Kiernan, M.C. (2008) Cortical hyperexcitability may precede the onset of familial amyotrophic lateral sclerosis. *Brain*. 131 (6), 1540–1550.

Vyazovskiy, V. V., Faraguna, U., Cirelli, C. & Tononi, G. (2009) Triggering slow waves

- during NREM sleep in the rat by intracortical electrical stimulation: Effects of sleep/wake history and background activity. *Journal of Neurophysiology*. 101 (4), 1921–1931.
- Vyazovskiy, V. V & Harris, K.D. (2013) Sleep and the single neuron: the role of global slow oscillations in individual cell rest. *Nature reviews. Neuroscience*. 14 (6), 443–51.
- Vyazovskiy, V. V, Olcese, U., Lazimy, Y.M., Faraguna, U., Esser, S.K., Williams, J.C., Cirelli, C. & Tononi, G. (2009) Cortical firing and sleep homeostasis. *Neuron*. 63 (6), 865–78.
- Walker, M.P. (2009) The role of slow wave sleep in memory processing. *Journal of Clinical Sleep Medicine*. 5 (2), S20–S26.
- Walker, M.P., Ayre, G.A., Cummings, J.L., Wesnes, K., McKeith, I.G., O'Brien, J.T. & Ballard, C.G. (2000) Quantifying fluctuation in dementia with Lewy bodies, Alzheimer's disease, and vascular dementia. *Neurology*. 54 (8), 1616–25.
- Walker, Z., Possin, K.L., Boeve, B.F. & Aarsland, D. (2015) Lewy body dementias. *The Lancet*. 386 (10004), 1683–1697.
- Wang, D. V & Ikemoto, S. (2016) Coordinated Interaction between Hippocampal Sharp-Wave Ripples and Anterior Cingulate Unit Activity. *The Journal of neuroscience : the official journal of the Society for Neuroscience*. 36 (41), 10663–10672.
- Wang, X.-J. (2010) Neurophysiological and computational principles of cortical rhythms in cognition. *Physiological reviews*. 90 (3), 1195–268.
- Watson, B.O. (2018) Cognitive and Physiologic Impacts of the Infralow Oscillation. *Frontiers in systems neuroscience*. 12 (44), 1–13.
- Watson, B.O., Levenstein, D., Greene, J.P., Gelinas, J.N. & Buzsáki, G. (2016) Network Homeostasis and State Dynamics of Neocortical Sleep. *Neuron*. 90 (4), 839–852.
- Watson, R., Blamire, A.M., Colloby, S.J., Wood, J.S., Barber, R., He, J. & O'Brien, J.T. (2012) Characterizing dementia with Lewy bodies by means of diffusion tensor

imaging. *Neurology*. 79 (9), 906–14.

Weisman, D., Cho, M., Taylor, C., Adame, A., Thal, L.J. & Hansen, L.A. (2007) In dementia with Lewy bodies, Braak stage determines phenotype, not Lewy body distribution. *Neurology*. 69 (4), 356–359.

Weissman, D.H., Roberts, K.C., Visscher, K.M. & Woldorff, M.G. (2006) The neural bases of momentary lapses in attention. *Nature neuroscience*. 9 (7), 971–8.

Van De Werd, H.J.J.M., Rajkowska, G., Evers, P. & Uylings, H.B.M. (2010) Cytoarchitectonic and chemoarchitectonic characterization of the prefrontal cortical areas in the mouse. *Brain Structure and Function*. 214 (4), 339–353.

Wesnes, K.A., Aarsland, D., Ballard, C. & Londos, E. (2015) Memantine improves attention and episodic memory in Parkinson's disease dementia and dementia with Lewy bodies. *International Journal of Geriatric Psychiatry*. 30 (1), 46–54.

Wester, J.C. & Contreras, D. (2013) Differential modulation of spontaneous and evoked thalamocortical network activity by acetylcholine level in vitro. *Journal of Neuroscience*. 33 (45), 17951–17966.

Westerberg, C.E., Mander, B.A., Florczak, S.M., Weintraub, S., Mesulam, M.-M., Zee, P.C. & Paller, K.A. (2012) Concurrent Impairments in Sleep and Memory in Amnesic Mild Cognitive Impairment. *Journal of the International Neuropsychological Society*. 18 (03), 490–500.

Whitham, E.M., Pope, K.J., Fitzgibbon, S.P., Lewis, T., Clark, C.R., Loveless, S., Broberg, M., Wallace, A., DeLosAngeles, D., Lillie, P., Hardy, A., Fronsco, R., Pulbrook, A. & Willoughby, J.O. (2007) Scalp electrical recording during paralysis: Quantitative evidence that EEG frequencies above 20Hz are contaminated by EMG. *Clinical Neurophysiology*. 118 (8), 1877–1888.

Whittington, M.A. & Traub, R.D. (2003) Interneuron Diversity series: Inhibitory interneurons and network oscillations in vitro. *Trends in Neurosciences* 26 (12) p.676–682.

Whittington, M.A., Traub, R.D., Kopell, N., Ermentrout, B. & Buhl, E.H. (2000) 'Inhibition-based rhythms: Experimental and mathematical observations on

- network dynamics', in *International Journal of Psychophysiology*. [Online]. 2000 pp. 315–336.
- Wierzynski, C.M., Lubenov, E. V., Gu, M. & Siapas, A.G. (2009) State-Dependent Spike-Timing Relationships between Hippocampal and Prefrontal Circuits during Sleep. *Neuron*. 61 (4), 587–596.
- Wisor, J.P., Edgar, D.M., Yesavage, J., Ryan, H.S., McCormick, C.M., Lapustea, N. & Murphy, G.M. (2005) Sleep and circadian abnormalities in a transgenic mouse model of Alzheimer's disease: A role for cholinergic transmission. *Neuroscience*. 131 (2), 375–385.
- Witton, J., Staniaszek, L.E., Bartsch, U., Randall, A.D., Jones, M.W. & Brown, J.T. (2016) Disrupted hippocampal sharp-wave ripple-associated spike dynamics in a transgenic mouse model of dementia. *The Journal of physiology*. 594 (16), 4615–30.
- Wolansky, T., Clement, E.A., Peters, S.R., Palczak, M.A. & Dickson, C.T. (2006) Hippocampal slow oscillation: a novel EEG state and its coordination with ongoing neocortical activity. *The Journal of neuroscience : the official journal of the Society for Neuroscience*. 26 (23), 6213–6229.
- Wolpert, E.A. (1969) A Manual of Standardized Terminology, Techniques and Scoring System for Sleep Stages of Human Subjects. *Archives of General Psychiatry*. 20 (2), 246.
- Wood, J.N. & Grafman, J. (2003) Human prefrontal cortex: Processing and representational perspectives. *Nature Reviews Neuroscience*. 4 (2), 139–147.
- Wulff, P., Ponomarenko, A.A., Bartos, M., Korotkova, T.M., Fuchs, E.C., Böhner, F., Both, M., Tort, A.B.L., Kopell, N.J., Wisden, W. & Monyer, H. (2009) Hippocampal theta rhythm and its coupling with gamma oscillations require fast inhibition onto parvalbumin-positive interneurons. *Proceedings of the National Academy of Sciences of the United States of America*. 106 (9), 3561–3566.
- Xie, L., Kang, H., Xu, Q., Chen, M.J., Liao, Y., Thiyagarajan, M., O'Donnell, J., Christensen, D.J., Nicholson, C., Iliff, J.J., Takano, T., Deane, R. & Nedergaard, M. (2013) Sleep drives metabolite clearance from the adult brain. *Science (New*

York, N.Y.). 342 (6156), 1–11.

Yamamoto, K., Tanei, Z. ichi, Hashimoto, T., Wakabayashi, T., Okuno, H., Naka, Y., Yizhar, O., Fenno, L.E., Fukayama, M., Bito, H., Cirrito, J.R., Holtzman, D.M., Deisseroth, K. & Iwatsubo, T. (2015) Chronic Optogenetic Activation Augments A $\beta$  Pathology in a Mouse Model of Alzheimer Disease. *Cell Reports*. 11 (6), 859–865.

Yanovsky, Y., Ciatipis, M., Draguhn, A., Tort, A.B.L. & Brankačk, J. (2014) Slow oscillations in the mouse hippocampus entrained by nasal respiration. *The Journal of neuroscience : the official journal of the Society for Neuroscience*. 34 (17), 5949–64.

Yasenkov, R. & Deboer, T. (2012) 'Circadian modulation of sleep in rodents', in *Progress in Brain Research*. [Online]. Elsevier B.V. pp. 203–218.

Ylinen, A., Bragin, A., Nádasdy, Z., Jandó, G., Szabó, I., Sik, A. & Buzsáki, G. (1995) Sharp wave-associated high-frequency oscillation (200 Hz) in the intact hippocampus: network and intracellular mechanisms. *The Journal of neuroscience : the official journal of the Society for Neuroscience*. 15 (1), 30–46.

Yoder, R.M. & Pang, K.C.H. (2005) Involvement of GABAergic and cholinergic medial septal neurons in hippocampal theta rhythm. *Hippocampus*. 15 (3), 381–392.

Yoo, S.S., Hu, P.T., Gujar, N., Jolesz, F.A. & Walker, M.P. (2007) A deficit in the ability to form new human memories without sleep. *Nature Neuroscience*. 10 (3), 385–392.

Young, A. & Wimmer, R.D. (2017) Implications for the thalamic reticular nucleus in impaired attention and sleep in schizophrenia. *Schizophrenia Research* 180 p.44–47.

Zarow, C., Lyness, S.A., Mortimer, J.A. & Chui, H.C. (2003) Neuronal loss is greater in the locus coeruleus than nucleus basalis and substantia nigra in Alzheimer and Parkinson diseases. *Archives of Neurology*. 60 (3), 337–341.

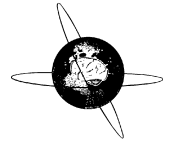
Zavalko, I., Ukraintseva, Y., Manolov, A., Dolgikh, V., Dorokhov, V. & Kovalzon, V. (2013) Activity and sleep in a mouse model of Parkinson disease. *Sleep Medicine*.

14e40–e41.

- Zhang, B., Veasey, S.C., Wood, M.A., Leng, L.Z., Kaminski, C., Leight, S., Abel, T., Lee, V.M.Y. & Trojanowski, J.Q. (2005) Impaired rapid eye movement sleep in the Tg2576 APP murine model of Alzheimer's disease with injury to pedunculopontine cholinergic neurons. *American Journal of Pathology*. 167 (5), 1361–1369.
- Zhang, F., Zhong, R., Li, S., Fu, Z., Wang, R., Wang, T., Huang, Z. & Le, W. (2019) Alteration in sleep architecture and electroencephalogram as an early sign of Alzheimer's disease preceding the disease pathology and cognitive decline. *Alzheimer's & Dementia*. 15 (4), 590–597.
- Zhang, J., Zhu, Y., Zhan, G., Fenik, P., Panossian, L., Wang, M.M., Reid, S., Lai, D., Davis, J.G., Baur, J.A. & Veasey, S. (2014) Extended wakefulness: Compromised metabolics in and degeneration of locus ceruleus neurons. *Journal of Neuroscience*. 34 (12), 4418–4431.
- Zhang, W., Zhang, L., Liang, B., Schroeder, D., Zhang, Z.W., Cox, G.A., Li, Y. & Lin, D.T. (2016) Hyperactive somatostatin interneurons contribute to excitotoxicity in neurodegenerative disorders. *Nature Neuroscience*. 19 (4), 557–559.
- Zhurakovskaya, E., Leikas, J., Pirttimäki, T., Casas Mon, F., Gynther, M., Aliev, R., Rantamäki, T., Tanila, H., Forsberg, M.M., Gröhn, O., Paasonen, J. & Jalkanen, A.J. (2019) Sleep-State Dependent Alterations in Brain Functional Connectivity under Urethane Anesthesia in a Rat Model of Early-Stage Parkinson's Disease. *eNeuro*. 6 (1), 1–12.
- Zhurakovskaya, E., Paasonen, J., Shatillo, A., Lipponen, A., Salo, R., Aliev, R., Tanila, H. & Gröhn, O. (2016) Global Functional Connectivity Differences between Sleep-Like States in Urethane Anesthetized Rats Measured by fMRI. *PloS one*. 11 (5), e0155343.
- Zou, W., Pu, T., Feng, W., Lu, M., Zheng, Y., Du, R., Xiao, M. & Hu, G. (2019) Blocking meningeal lymphatic drainage aggravates Parkinson's disease-like pathology in mice overexpressing mutated  $\alpha$ -synuclein. *Translational Neurodegeneration*. 8 (7), 1–17.
- Zucca, S., D'Urso, G., Pasquale, V., Vecchia, D., Pica, G., Bovetti, S., Moretti, C.,

Varani, S., Molano-Mazón, M., Chiappalone, M., Panzeri, S. & Fellin, T. (2017) An inhibitory gate for state transition in cortex. *eLife*. 6.

Zupancic, M., Mahajan, A. & Handa, K. (2011) Dementia with lewy bodies: diagnosis and management for primary care providers. *The primary care companion for CNS disorders*. 13 (5).



## Quantitative electroencephalography as a marker of cognitive fluctuations in dementia with Lewy bodies and an aid to differential diagnosis



Myrto Stylianou<sup>a,\*</sup>, Nicholas Murphy<sup>a,1</sup>, Luis R. Peraza<sup>a</sup>, Sara Graziadio<sup>b</sup>, Ruth Cromarty<sup>a</sup>, Alison Killen<sup>a</sup>, John T. O' Brien<sup>c</sup>, Alan J. Thomas<sup>a</sup>, Fiona E.N. LeBeau<sup>a,2</sup>, John-Paul Taylor<sup>a,2</sup>

<sup>a</sup> Institute of Neuroscience, Newcastle University Medical School, Newcastle University, Newcastle upon Tyne, UK

<sup>b</sup> NIHR Newcastle In Vitro Diagnostics Co-operative, Newcastle Upon Tyne Hospitals Foundation Trust, Newcastle upon Tyne, UK

<sup>c</sup> Department of Psychiatry, University of Cambridge, Cambridgeshire and Peterborough NHS Foundation Trust, Cambridge, UK

### ARTICLE INFO

#### Article history:

Accepted 10 March 2018

Available online 3 April 2018

#### Keywords:

Dementia with Lewy bodies  
Alzheimer's disease  
Parkinson's disease dementia  
Cognitive fluctuations  
Quantitative electroencephalography

### HIGHLIGHTS

- EEG slowing was evident in dementia with Lewy bodies (DLB) and Parkinson's disease dementia (PDD) and less in Alzheimer's disease (AD) patients compared to controls.
- Dominant rhythm variability was larger in AD but only correlated with cognitive fluctuations in DLB.
- QEEG variables classified DLB and AD patients with high sensitivity and specificity.

### ABSTRACT

**Objective:** We investigated for quantitative EEG (QEEG) differences between Alzheimer's disease (AD), dementia with Lewy bodies (DLB) and Parkinson's disease dementia (PDD) patients and healthy controls, and for QEEG signatures of cognitive fluctuations (CFs) in DLB.

**Methods:** We analysed eyes-closed, resting state EEGs from 18 AD, 17 DLB and 17 PDD patients with mild dementia, and 21 age-matched controls. Measures included spectral power, dominant frequency (DF), frequency prevalence (FP), and temporal DF variability (DFV), within defined EEG frequency bands and cortical regions.

**Results:** DLB and PDD patients showed a leftward shift in the power spectrum and DF. AD patients showed greater DFV compared to the other groups. In DLB patients only, greater DFV and EEG slowing were correlated with CFs, measured by the clinician assessment of fluctuations (CAF) scale. The diagnostic accuracy of the QEEG measures was 94% (90.4–97.9%), with 92.26% (80.4–100%) sensitivity and 83.3% (73.6–93%) specificity.

**Conclusion:** Although greater DFV was only shown in the AD group, within the DLB group a positive DFV – CF correlation was found. QEEG measures could classify DLB and AD patients with high sensitivity and specificity.

**Significance:** The findings add to an expanding literature suggesting that EEG is a viable diagnostic and symptom biomarker in dementia, particularly DLB.

© 2018 Published by Elsevier B.V. on behalf of International Federation of Clinical Neurophysiology.

\* Corresponding author at: Institute of Neuroscience, Newcastle University Medical School, Framlington Place, Newcastle upon Tyne NE2 4HH, UK.

E-mail addresses: [M.Stylianou2@ncl.ac.uk](mailto:M.Stylianou2@ncl.ac.uk) (M. Stylianou), [Nicholas.Murphy@bcm.edu](mailto:Nicholas.Murphy@bcm.edu) (N. Murphy), [luis.peraza-rodriguez@ncl.ac.uk](mailto:luis.peraza-rodriguez@ncl.ac.uk) (L.R. Peraza), [sara.graziadio@ncl.ac.uk](mailto:sara.graziadio@ncl.ac.uk) (S. Graziadio), [Ruth.Cromarty@ncl.ac.uk](mailto:Ruth.Cromarty@ncl.ac.uk) (R. Cromarty), [alison.killen@ncl.ac.uk](mailto:alison.killen@ncl.ac.uk) (A. Killen), [john.obrien@medschl.cam.ac.uk](mailto:john.obrien@medschl.cam.ac.uk) (J.T. O' Brien), [alan.thomas@ncl.ac.uk](mailto:alan.thomas@ncl.ac.uk) (A.J. Thomas), [fiona.lebeau@ncl.ac.uk](mailto:fiona.lebeau@ncl.ac.uk) (F.E.N. LeBeau), [john-paul.taylor@ncl.ac.uk](mailto:john-paul.taylor@ncl.ac.uk) (J.-P. Taylor).

<sup>1</sup> Current address: Baylor College of Medicine, Department of Neuropsychiatry, Houston, TX 77030, USA.

<sup>2</sup> These authors are joint senior authors.

### 1. Introduction

Dementia with Lewy bodies (DLB) is a common type of dementia after Alzheimer's disease, accounting for approximately 10–15% of cases at autopsy (McKeith et al., 2004). DLB is associated with quality of life and significant carer burden. It is frequently under-diagnosed and often misdiagnosed as AD, especially at early stages where both diseases manifest with similar cognitive deficits (Metzler-Baddeley, 2007). Estimates of sensitivity and specificity

for DLB diagnosis using established clinical criteria (McKeith et al., 2017) have been quite variable but have a common tendency for relatively high specificity but lower sensitivity (Huang et al., 2013). The fact that DLB patients are sensitive to neuroleptics (McKeith et al., 1992), and demonstrate a faster disease progression compared to other dementias (Ballard et al., 2001), underpin the necessity to improve diagnostic accuracy for this group of patients.

Cognitive fluctuations (CFs) are one of the core symptoms of DLB and refer to spontaneous alterations in cognition, attention and arousal (McKeith et al., 2017). CFs are of clinical importance as they have been correlated with visual hallucinations (Varanese et al., 2010), impairment in daily activities and care burden. Moreover, CFs are an important diagnostic feature for DLB as their prevalence reaches 90% of cases, compared to just 20% of AD and 29% of Parkinson's disease dementia (PDD; Ballard et al., 2002). CFs are also qualitatively different between DLB and AD as in the former case they relate more to executive and perceptual performance, while in the later they are primarily linked to memory impairment (Zupancic et al., 2011). The Clinician Assessment of Fluctuation (CAF) is a clinical scale devised for the psychometric assessment of CFs (Walker et al., 2000). Although CAF is regarded as a fairly reliable measure of CFs if used by an experienced clinician (Van Dyk et al., 2016), the high variability in fluctuation severity and duration of confusional episodes, along with difficulties for informants in separating out what are true intrinsic fluctuations from what are simply responses to external stressors, impose a considerable limitation in CF identification (Bradshaw et al., 2004).

Electroencephalography is an emerging modality for differential diagnosis between dementia subtypes as it is simple, cost-effective, easily accessible and non-invasive compared to imaging approaches. The most prominent QEEG finding in DLB and PDD is a shift of power and dominant frequency (DF) from the alpha frequency range towards high-theta, described as "EEG slowing". This EEG slowing is most prevalent posteriorly (Briel et al., 1999) and although it is also observed in AD patients (Jackson et al., 2008), it is not as prominent as in the Lewy body diseases – DLB and PDD. In studies quantifying differences between DLB or DLB/PDD, or AD and controls, QEEG variables such as coherence (Snaedal et al., 2012), temporal dominant frequency variability (DFV) (Andersson et al., 2008), power ratio between bands and statistical measures such as Granger causality (Garn et al., 2017), have all achieved high diagnostic sensitivity and specificity, reaching 100% in the latter study.

Previous investigations have found electrophysiological correlations of CFs in DLB patients. Early work using quantitative electroencephalography (QEEG) has shown a correlation between epoch-by-epoch DFV and CFs in DLB patients compared with healthy controls (Walker et al., 2000). Later work also showed that DLB patients with CFs had greater DFV compared to AD patients in posterior brain regions, and used the DFV together with other QEEG measures to classify AD, PDD-CFs, PDD-without CFs and DLB patients and controls (Bonanni et al., 2008). More recently, a multi-centre cohort analysis has verified these results (Bonanni et al., 2016).

The aforementioned findings of QEEG signatures in DLB in addition to the fact that the QEEG measures were shown to be correlated with the clinical phenotype of DLB and specifically with CFs, suggest that the QEEG could be utilised to investigate for a neurophysiological divergence between DLB and other dementias. The QEEG investigations performed so far have not yet managed to identify differences (Engedal et al., 2015; Garn et al., 2017) between DLB and PDD. Generally, these Lewy body dementia (LBD) subtypes demonstrate great similarities in neuropathological processes, symptom manifestation and treatment. However, DLB is

typically characterised by greater executive dysfunction, more psychiatric symptoms, poorer response to levodopa (L-DOPA) and greater amyloid burden compared to PDD (Edison et al., 2008). Moreover, the onset of motor symptoms precedes that of dementia in PDD while in DLB, dementia appears concurrently or before motor symptoms (McKeith et al., 1992). These discrepancies may indicate differences in the spatio-temporal sequence of pathology, with a predominant brain-stem start and rostral progression in PDD and a cortical inception in DLB (Beyer et al., 2007). Potential QEEG differences between PDD and DLB are of research interest, as they could provide insight for better understanding these LBD subtypes.

Earlier QEEG studies focused on investigating the capacity of such measures in aiding DLB differential diagnosis in clinical settings. Hence, they utilized methods such as assessment by visual observation (Bonanni et al., 2008), or attempted to develop an online method that performs analysis during and right-after EEG acquisition (Garn et al., 2017). Here we took a less clinically-orientated approach, as our primary goal was to characterise and compare the resting EEG rhythm in AD, DLB and PDD patients and in relation to healthy controls, and to investigate for DLB specific signatures of CFs. Thus, we performed extensive pre-processing analysis of the EEG signal and a thorough analysis for differences in QEEG measures within different frequency ranges and brain regions, between diagnostic groups. Based on the literature, we hypothesized that dementia patients will exhibit a differential pattern in the distribution of QEEG measures of power and DF within different frequency ranges compared to healthy controls, and that these QEEG measures in addition to DF variability in time (DFV) will also differ between the dementia groups. We also hypothesized that greater DFV will only characterise LBDs and possibly only DLB, and that greater DFV will correlate with more CFs within these groups. Finally, to assess the possible utility of these measures in the development of biomarkers, the QEEG measures that were found to be significantly different between groups were used to predict dementia diagnosis.

## 2. Material and methods

### 2.1. Diagnostic groups

Initially we pre-processed EEG data from 21 healthy controls, 19 AD, 20 DLB and 20 PDD participants (Table 1 for the demographic data of the final groups). Patients were individuals who were referred to local old age psychiatry and neurology services and diagnosis was determined by two independent experienced clinicians (Alan J. Thomas and John-Paul Taylor). Controls were age-matched volunteers. Patients with DLB fulfilled the 2005 and 2017 revised criteria for probable DLB (McKeith et al., 2005, 2017) and patients with PDD fulfilled the criteria for probable PDD (Emre et al., 2007). Individuals with AD met the revised criteria of the National Institute of Neurological and Communicative Diseases and Stroke/AD and Related Disorders Association for probable AD (McKhann et al., 2011). The CAF score was assessed by the clinicians and CFs were defined on the basis that they were typical of those seen in DLB and internally driven rather than a response to external environmental factors. Healthy participants demonstrated no evidence of dementia as determined by the Cambridge Cognitive Examination (CAMCOG) score (>80) and from clinical history. Exclusion criteria for all participants included significant history of neurological or psychiatric conditions. Prescriptions of acetylcholinesterase inhibitors (AChEIs), memantine and dopaminergic medications were allowed. Ethical approval was provided by the Northumberland Tyne and Wear NHS Trust and Newcastle University ethics committee.

**Table 1**

Demographics table for the healthy control (N = 21), Alzheimer's disease (AD; N = 18), dementia with Lewy bodies (DLB; N = 17) and Parkinson's disease dementia (PDD; N = 17) groups that were used for our analysis. L-DOPA = levo-dopa, LED = L-DOPA equivalent dose, AChEIs = acetylcholinesterase inhibitors, MMSE = Mini mental state examination, CAF = Clinician's assessment of fluctuations scale, UPDRS = Unified Parkinson's disease rating scale, NPI = Neuropsychiatric inventory total score. Although it is not shown in the table, 1 PDD patient (5.9%) was on memantine.

	Controls (N = 21)	AD (N = 18)	DLB (N = 17)	PDD (N = 17)
Age in yrs ± SD	76.19 ± 5.32	76.06 ± 7.81	75.71 ± 5.34	75.44 ± 4.66
Males (%)	66.7%	88.9%	88.2%	100%
L-DOPA	–	0%	52.9%	100%
LED	–	0%	348.94	423.42
AChEIs	–	94.4%	88.2%	76.5%
Age at diagnosis (yrs ± SD)	–	74.64 ± 7.63	73 ± 5.11	74.07 ± 6.29
Diagnosis duration (yrs ± SD)	–	1.5 ± 0.9	1.08 ± 0.70	0.94 ± 0.73
MMSE	29.19 ± 0.87	23.67 ± 1.68	25 ± 2.89	23.94 ± 2.59
CAF	–	0.47 ± 0.87	2.76 ± 3.78	6.59 ± 4.29
NPI total	–	7.29 ± 7.61	8 ± 5.27	20.35 ± 12.9
UPDRS	1.14 ± 1.42	1.67 ± 1.61	13.82 ± 5.32	27.06 ± 11.44

## 2.2. EEG recordings

High-density, eyes-closed resting-state EEG recordings were obtained using 128 channel ANT Waveguard caps (ANT Neuro, Netherlands) with an Ag/AgCl electrode montage set according to the 10-5 placement system (Oostenveld and Praamstra, 2001). Electrode impedance with kept below 5 kΩ. A reference electrode (Fz) was used, no filters were applied during acquisition and the sampling frequency was set at 1024 Hz. The patients that received medication had normally taken AChEIs at least 4 h before while the time of the last Levodopa dose was 1–3 h prior to the EEG session.

## 2.3. Pre-processing

Pre-processing of the EEG recordings was performed off-line after acquisition on the MATLAB environment (MATLAB 8.5, The MathWorks Inc., Natick, MA, 2015), using the EEGLAB toolbox version 13 (Delorme and Makeig, 2004). The EEG signal was filtered with a 4 Hz high-pass and a 46 Hz low-pass filter. Lower frequencies were filtered out as they imposed noise on the higher frequencies that were of more interest, and because the EEG generally has a limited accuracy in estimating very low and very high frequencies (Niedermeyer and Lopes da Silva, 2004). A notch filter was applied at 50 Hz. Recordings from all electrodes were visually inspected in the power-time domain and rejected if they had a kurtosis value over 3, or if they contained clear and consistent artifacts such as electrooculogram (EOG) and electromyogram (EMG) artifacts. The number of channels removed was kept to the minimum possible (mean = 17.7 ± 6.7, min. = 0, max. = 33).

Independent component analysis (ICA) was used to accurately estimate and remove the presence of additional ocular, muscular, and other neuronal activity (Kropotov and Kropotov, 2009). Individual recordings were reduced to 30 principal components and then decomposed using the extended RUNICA algorithm (Bell and Sejnowski, 1995; Delorme and Makeig, 2004). Components representing existing templates for muscular, ocular, and electrical (50 Hz line noise) artefacts (Jung et al., 2000) were rejected (mean = 5.2 ± 1.6, min. = 0, max. = 9) and the remaining ICs remixed. The recordings were then segmented into 2-s long epochs and were inspected for any remaining artefacts. Epochs containing large artefacts were removed across channels, in a conservative manner. Finally, the removed channels were replaced using spherical spline interpolation (Ferree, 2006). As a final step, the EEG montage was changed to average reference.

## 2.4. Variable extraction

The power spectral density (PSD) for each 2-s epoch was estimated using Bartlett's method (Bartlett, 1950) with a 0.25 Hz

frequency resolution using a 4-s FFT (fast Fourier transform) size and a Hamming window, for each electrode. To compensate for the between subject variability in factors such as brain neurophysiology, anatomy and physical tissue properties, the data were transformed to relative power spectral density (rPSD; Eq. (1); Rodriguez et al., 1999). The rPSD was extracted for each time point of each epoch (sampling frequency = 1024 Hz), and for each electrode. Then, for each epoch of a recording, the power was averaged across electrodes for each of four regions: frontal, central, posterior and lateral (Fig. 1). Seven subjects were rejected from further analysis due to an insufficient number of clean data (<47 epochs). For the remaining 73 subjects (21 healthy controls, 18 AD, 17 DLB and 17 PDD; Table 1), only the first 47 epochs of extracted power per region were utilised (total length of 94 s).

$$\bar{g}(f) = \frac{g(f)}{\sum_f g(f)} \quad (1)$$

Equation (1): Calculation of the relative PSD/power ( $\bar{g}$ ) across the power spectrum (4–46 Hz). At each point in the frequency spectrum the amplitude ( $g(f)$ ) is divided by the sum of all amplitudes across the frequency spectrum ( $\sum_f g(f)$ ) (Kropotov and Kropotov, 2009).

The mean power distributed in each of three frequency bands: theta (4–7.75 Hz), alpha (8–13.75 Hz), beta (14–20.75 Hz), was extracted as a percentage of the total power in that range, across epochs per region (Table 2; Fig. 2). Higher frequencies were excluded as they are prone to contamination by electromyogram rhythms (Whitham et al., 2007). The DF – the frequency with the highest power between 4 Hz and 20.75 Hz – was extracted for each epoch to calculate the mean DF and DF variability (DFV; SD from the mean DF) across epochs, for the slow-theta (4–5.5 Hz), fast-theta (5.5–7.75 Hz; defined by others as pre-alpha; Bonanni et al., 2008), theta, alpha and theta/alpha (4–13.75 Hz) frequency ranges (Table 3; Fig. 2). Since the DF was limited within the theta-alpha range, beta band activity was excluded. The theta-alpha DF was used to calculate the Frequency Prevalence (FP) distribution, which is the percentage of epochs having a DF falling within the slow-theta, fast-theta and alpha frequency ranges (Table 3; Fig. 2). These measures were calculated for each patient, for each diagnostic group and for each band and region combination.

## 2.5. Statistical analysis

The mean power, theta-alpha DF and theta, alpha and theta-alpha DFV were statistically compared using repeated measures ANOVA, for region as the within-subjects factor and diagnosis as the between-subjects factor. When a significant interaction was found we followed up by univariate ANOVA and post hoc analysis with a Bonferonni correction. The DFV (for all frequency ranges)

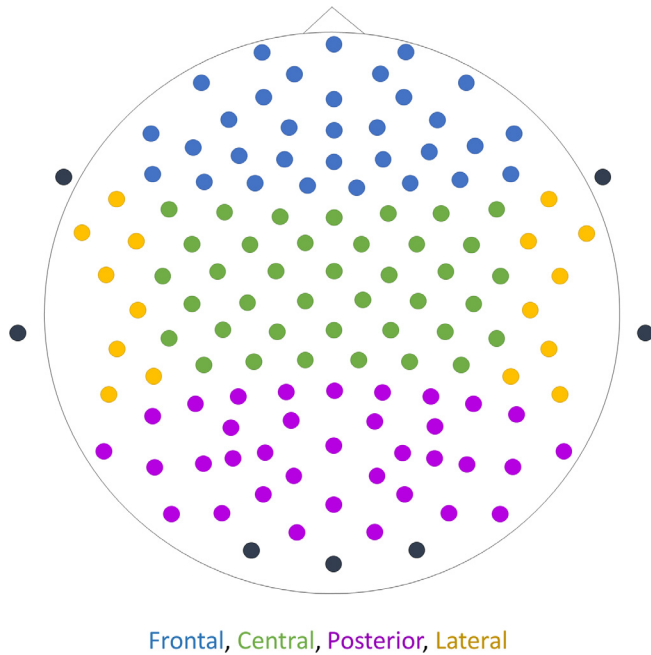


**Fig. 1.** Placement of the 128 electrodes according to the 10-5 placement system. The signal recorded from the electrodes indicated with black colour was selected out as it was deemed too noisy. The colours indicate the grouping of the electrodes into four regions: blue = frontal, green = central, purple = posterior, yellow = lateral. (For interpretation of the references to colour in this figure legend, the reader is referred to the web version of this article.)

and the theta-alpha DF values were logarithmically transformed to achieve homogeneity of variance/homoscedasticity. Heteroscedasticity could not be solved for the theta and alpha DF and hence we performed Welch's ANOVA followed by the Games-Howell test. To statistically compare the distribution of the FP in the slow-theta, fast-theta and alpha frequency ranges we performed Kruskal-Wallis H test followed by post hoc analysis. Pearson's product-moment correlation and Spearman's rank correlation were used to investigate for correlations between these variables and the CAF score, the MMSE score and the levodopa equivalent dose (LED), for each diagnostic group. Manual correction for multiple comparisons by appropriating the level of  $\alpha$  significance ( $\alpha/N$ ) was performed for the non-parametric statistical analyses and for the correlation analyses, where Bonferonni correction was not available with the statistical software.

In order to assess the capacity of the QEEG variables that were significantly different between the AD and DLB, and the DLB and PDD groups to predict diagnosis, the generalised estimating equations (GEE) procedure were used. This method allows the analysis

of repeated measurements without the assumption for normal distribution (Carr and Chi, 1992). The QEEG variables that introduce multicollinearity to the model (variance inflation factor >5) were excluded from this analysis. Region was defined as the within-subjects variable, diagnosis as the between-subjects variable and the QEEG variables and the CAF score as the co-factors. The variables that significantly predicted diagnosis were then used to calculate the receiver operating characteristic (ROC) curve, and obtain the area under the curve (AUC), sensitivity and specificity with asymptotic confidence intervals. The sensitivity/specificity cut-off was determined using Youden's index.

### 3. Results

#### 3.1. Data and demographics

Data from a total of 73 individuals (21 healthy controls, 18 AD, 17 DLB, 17 PDD; Table 1) were further analysed after data extraction. Participants were well matched for age at diagnosis and age at the time of the recording ( $p > 0.05$ ), as well as MMSE score ( $p > 0.05$ ). The PDD and DLB groups had significantly higher CAF scores than AD patients ( $p < 0.01$ ;  $p < 0.05$  respectively), with the PDD group also having a higher CAF score than the DLB group ( $p < 0.01$ ). Lastly, the neuropsychiatric inventory (NPI) total and Unified Parkinson's disease rating scale (UPDRS) scores were higher in the DLB/PDD subjects compared to the other groups, and in the PDD compared to the DLB group ( $p < 0.01$ ).

#### 3.2. EEG slowing

We found a significant effect of diagnosis on the mean power in the theta:  $F(3, 69) = 39.48, p < 0.01$ , alpha:  $F(3, 69) = 14.49, p < 0.01$  and beta:  $F(3, 69) = 12.825, p < 0.01$  ranges (Table 2; Fig. 3). In all regions, PDD and DLB groups had higher theta power than AD patients and healthy controls ( $p < 0.01$ ). In the alpha and beta ranges the opposite pattern was observed. Specifically, in the alpha band, controls had significantly higher power than PDD patients in all regions ( $p < 0.01$ ), and compared to DLB patients frontally, posteriorly and laterally ( $p < 0.01$ ). Moreover, AD patients had greater alpha power than PDD patients posteriorly and laterally ( $p < 0.01$ ), and also to DLB patients frontally ( $p < 0.05$ ), posteriorly and laterally ( $p < 0.01$ ). In the beta range, DLB patients had lower power than AD patients and controls in all regions ( $p < 0.01$ ). PDD patients had lower power than healthy controls frontally and centrally ( $p < 0.01$ ) and posteriorly and laterally ( $p < 0.05$ ), and from AD patients frontally, posteriorly ( $p < 0.05$ ) and centrally ( $p < 0.01$ ).

We also found a significant effect of diagnosis in the second measure of interest, the mean theta-alpha DF ( $F(3, 69) = 36.78, p < 0.01$ ), which was significantly higher in all cortical regions in

**Table 2**  
The mean percentage of the total power distributed in each of three frequency bands: theta (4–7.75 Hz), alpha (8–13.5 Hz), beta (14–30.75 Hz), in each region: frontal, central, posterior, lateral, for each group: healthy controls (N = 21), Alzheimer's disease (AD; N = 18), dementia with Lewy bodies (DLB; N = 17) and Parkinson's disease dementia (PDD; N = 17) patients.

	Regions	Controls	AD	DLB	PDD
Theta	Frontal	20.19 ± 5.22	24.57 ± 6.26	37.63 ± 6.36	35.89 ± 7.46
	Central	19.18 ± 4.96	23.02 ± 6.13	36.90 ± 7.05	35.33 ± 6.37
	Posterior	19.79 ± 5.77	23.51 ± 6.63	39.62 ± 7.53	39.10 ± 7.63
	Lateral	19.32 ± 5.29	24.39 ± 6.53	36.96 ± 6.07	35.35 ± 7.30
Alpha	Frontal	35.12 ± 5.66	32.11 ± 4.31	28.96 ± 5.10	27.42 ± 2.57
	Central	34.74 ± 5.11	32.61 ± 4.47	29.84 ± 4.91	29.04 ± 2.28
	Posterior	38.91 ± 6.04	35.49 ± 5.81	29.26 ± 5.75	23.91 ± 2.50
	Lateral	35.41 ± 5.10	33.43 ± 4.00	28.57 ± 4.98	26.75 ± 2.34
Beta	Frontal	44.69 ± 7.09	43.32 ± 7.03	33.40 ± 3.74	36.69 ± 7.52
	Central	46.07 ± 6.75	44.37 ± 6.71	33.26 ± 3.85	35.65 ± 6.20
	Posterior	41.30 ± 7.09	40.99 ± 8.38	31.11 ± 5.36	31.72 ± 7.67
	Lateral	45.27 ± 7.71	42.17 ± 6.59	34.47 ± 5.52	37.90 ± 7.80

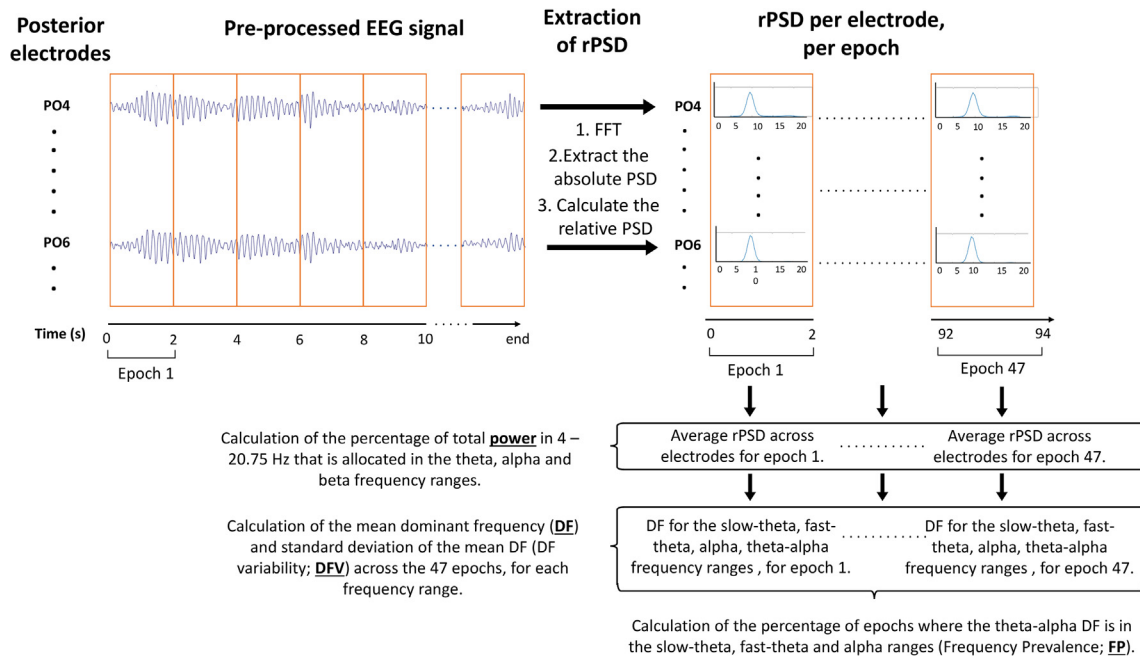


**Fig. 2.** Schematic diagram illustrating the process of extracting each of the four main quantitative EEG variables used in this study, for one participant in the posterior region. The filtered, pre-processed EEG signal on each of the electrodes in posterior derivations ( $N = 35$ ) is windowed in 2 s long epochs. The signal undergoes fast-Fourier transform (FFT) and using Bartlett's method the absolute power spectral density (PSD) is calculated for each epoch, for each electrode. The relative PSD (rPSD) is then calculated to normalize the signal. The mean rPSD is obtained across posterior electrodes, for each epoch (up to 47 epochs) of the recording, and the percentage of the total power in the 3–20.75 Hz range allocated to the theta (4–7.75 Hz), alpha (8–13.75 Hz) and beta (14–20.75 Hz) frequency ranges is calculated. The frequency with the highest power within the slow-theta (4–5.5 Hz), fast-theta (5.5–7.75 Hz), alpha and theta-alpha (4–13.75 Hz) frequency ranges was identified within each epoch, and that value corresponded to the dominant frequency (DF). The mean DF and the standard deviation of the mean DF (DF variability; DFV) across epochs were then calculated. Finally, the DF within each epoch was assessed and was characterised to be in the slow-theta, fast-theta or alpha range. The epochs that were characterised by a DF within each of these ranges are shown as a percentage of the total number of epochs. These percentages were the slow-theta, fast-theta and alpha frequency prevalence (FP). The same procedure was followed for the other three cortical regions.

controls and AD patients compared to the other patient groups (Table 3, Fig. 4). The mean theta DF was significantly higher in controls compared to the PDD group frontally, to the AD, DLB and PDD groups centrally and posteriorly, and to the DLB and PDD groups laterally. Significant differences were also found between groups in the alpha DF, in all regions. Specifically, the DLB group had significantly lower alpha DF than the control and AD group in all regions. The PPD group had higher alpha DF than the DLB group frontally, the AD group centrally and posteriorly and the control group laterally (Fig. 4). A trend for a greater alpha DF in the AD compared to the control group was observed, but was not verified by the statistical analysis.

For measures of frequency prevalence (FP; the percentage distribution of the theta-alpha DF in time in the slow-theta, fast-theta and alpha frequency ranges; Fig. 5, Table 3), the mean alpha FP was significantly higher in controls compared to all disease groups ( $p < 0.01$ ), and in AD patients compared to DLB and PDD patients ( $p < 0.01$ ), in all regions. In the fast-theta range the opposite pattern was observed, with controls exhibiting lower FP compared to AD patients frontally ( $p < 0.01$ ), and to DLB and PDD patients in all regions ( $p < 0.01$ ). Finally, in the slow-theta range controls had significantly lower FP than AD patients frontally ( $p < 0.01$ ), centrally and posteriorly ( $p < 0.05$ ), and to DLB and PDD patients in all regions ( $p < 0.01$ ). AD patients also have significantly lower slow-theta FP than PDD patients frontally and centrally ( $p < 0.05$ ).

### 3.3. Dominant frequency variability

Comparisons of the DFV between groups for different frequency band and region combinations revealed a significant effect of diagnosis in the theta/alpha ( $F(3, 69) = 2.77, p < 0.05$  and alpha ( $F(3, 69) = 6.29, p < 0.01$ ) ranges (Fig. 6), but not in the theta range. In the

theta-alpha band, the AD group had a significantly higher DFV compared to the control, DLB and PDD groups in the frontal, central and posterior regions, and only to the DLB group laterally. In the alpha band, AD patients had significantly higher DFV compared to the DLB group centrally, and to DLB and controls posteriorly. To further validate this finding we have included a short analysis on the effect of each electrode on the DFV in AD and DLB patients (Supplementary Material 1).

### 3.4. Correlations

We assessed correlations between CFs as measured by CAF and DFV measures similarly to previous studies (Walker et al., 2000), and with QEEG measures of slowing for all the different diagnostic groups and each band and region. This analysis revealed that within the DLB group only, there was a strong correlation between the CAF score and the theta DFV in the central ( $r = 0.789, p < 0.000$ ), posterior ( $r = 0.652, p < 0.005$ ) and lateral regions ( $r = 0.805, p < 0.000$ ). A positive, DLB specific correlation with CAF was also found with slow-theta FP in the frontal ( $r = 0.679, p = 0.003$ ), central ( $r = 0.747, p = 0.001$ ), posterior ( $r = 0.792, p < 0.001$ ) and lateral ( $r = 0.794, p = 0.001$ ) regions. A correlation between the CAF and MMSE score was only found in the PDD group ( $r = -0.671, p < 0.05$ ), while no significant correlation was found for any variable and the LED, for any group and region.

### 3.5. Exploratory GEE and ROC curve analysis

GEE analysis was performed for the variables that were significantly different between the AD and DLB diagnostic groups (theta power, alpha power, theta-alpha DFV, alpha DFV, alpha DF and fast-theta FP). The alpha-theta DF and alpha FP were rejected from

**Table 3**  
The mean dominant frequency (DF)  $\pm$  DFV (mean SD of the DF), DFV  $\pm$  SD and frequency prevalence (FP)  $\pm$  SD for the theta (4–7.75 Hz), slow-theta (4–5.5 Hz), fast-theta (5.75–7 Hz), alpha (8–13.75 Hz) and theta-alpha (4–13.75 Hz) frequency ranges in each region: frontal, central, posterior, lateral, for each group: healthy controls (N = 21), Alzheimer's disease (AD; N = 18), dementia with Lewy bodies (DLB; N = 17) and Parkinson's disease dementia (PDD; N = 17) patients.

	Regions	Variables	Controls	AD	DLB	PDD
Theta	Frontal	DF $\pm$ SD	6.93 $\pm$ 0.4	6.57 $\pm$ 0.54	6.49 $\pm$ 0.60	6.26 $\pm$ 0.31
		DFV $\pm$ SD	0.93 $\pm$ 0.25	0.98 $\pm$ 0.24	0.73 $\pm$ 0.24	0.80 $\pm$ 0.19
		FP $\pm$ SD	19.55 $\pm$ 22.14	44.92 $\pm$ 24.54	82.48 $\pm$ 21.00	91.36 $\pm$ 8.29
	Central	DF $\pm$ SD	7.11 $\pm$ 0.33	6.67 $\pm$ 0.59	6.65 $\pm$ 0.52	6.51 $\pm$ 0.35
		DFV $\pm$ SD	0.81 $\pm$ 0.28	0.86 $\pm$ 0.29	0.63 $\pm$ 0.22	0.67 $\pm$ 0.16
		FP $\pm$ SD	18.84 $\pm$ 24.96	41.02 $\pm$ 26.07	80.60 $\pm$ 21.02	90.49 $\pm$ 9.22
	Posterior	DF $\pm$ SD	7.17 $\pm$ 0.35	6.71 $\pm$ 0.60	6.57 $\pm$ 0.66	6.31 $\pm$ 0.29
		DFV $\pm$ SD	0.78 $\pm$ 0.33	0.86 $\pm$ 0.31	0.60 $\pm$ 0.21	0.72 $\pm$ 0.18
		FP $\pm$ SD	16.72 $\pm$ 23.49	34.99 $\pm$ 24.45	83.35 $\pm$ 23.68	94.99 $\pm$ 6.25
	Lateral	DF $\pm$ SD	7.18 $\pm$ 0.31	6.80 $\pm$ 0.54	6.65 $\pm$ 0.53	6.51 $\pm$ 0.36
		DFV $\pm$ SD	0.80 $\pm$ 0.30	0.83 $\pm$ 0.33	0.64 $\pm$ 0.26	0.72 $\pm$ 0.18
		FP $\pm$ SD	17.53 $\pm$ 22.06	39.24 $\pm$ 26.68	83.35 $\pm$ 18.76	89.36 $\pm$ 15.10
Slow-theta	Frontal	DF $\pm$ SD	4.88 $\pm$ 0.15	4.93 $\pm$ 0.17	5.01 $\pm$ 0.15	5.02 $\pm$ 0.14
		DFV $\pm$ SD	0.55 $\pm$ 0.06	0.52 $\pm$ 0.07	0.49 $\pm$ 0.08	0.50 $\pm$ 0.08
		FP $\pm$ SD	2.23 $\pm$ 4.28	10.52 $\pm$ 13.29	16.27 $\pm$ 21.06	18.77 $\pm$ 11.56
	Central	DF $\pm$ SD	4.95 $\pm$ 0.17	4.98 $\pm$ 0.18	5.16 $\pm$ 0.14	5.14 $\pm$ 0.13
		DFV $\pm$ SD	0.52 $\pm$ 0.06	0.49 $\pm$ 0.06	0.42 $\pm$ 0.10	0.43 $\pm$ 0.10
		FP $\pm$ SD	1.21 $\pm$ 3.05	9.46 $\pm$ 12.37	9.51 $\pm$ 14	11.14 $\pm$ 12.28
	Posterior	DF $\pm$ SD	4.91 $\pm$ 0.14	4.94 $\pm$ 0.18	5.11 $\pm$ 0.13	5.11 $\pm$ 0.15
		DFV $\pm$ SD	0.54 $\pm$ 0.06	0.51 $\pm$ 0.06	0.45 $\pm$ 0.07	0.45 $\pm$ 0.10
		FP $\pm$ SD	1.11 $\pm$ 3.34	6.97 $\pm$ 9.25	13.77 $\pm$ 23.03	16.15 $\pm$ 11.75
	Lateral	DF $\pm$ SD	4.86 $\pm$ 0.18	4.94 $\pm$ 0.16	5.09 $\pm$ 0.15	5.09 $\pm$ 0.16
		DFV $\pm$ SD	0.56 $\pm$ 0.05	0.51 $\pm$ 0.08	0.44 $\pm$ 0.11	0.46 $\pm$ 0.09
		FP $\pm$ SD	0.51 $\pm$ 1.15	5.44 $\pm$ 6.74	10.76 $\pm$ 17.41	11.76 $\pm$ 11.99
Fast Theta	Frontal	DF $\pm$ SD	7.20 $\pm$ 0.27	6.98 $\pm$ 0.32	6.74 $\pm$ 0.41	6.55 $\pm$ 0.22
		DFV $\pm$ SD	0.59 $\pm$ 0.14	0.62 $\pm$ 0.11	0.53 $\pm$ 0.12	0.55 $\pm$ 0.09
		FP $\pm$ SD	17.32 $\pm$ 21.02	34.4 $\pm$ 17.95	66.21 $\pm$ 20.86	72.59 $\pm$ 10.45
	Central	DF $\pm$ SD	7.31 $\pm$ 0.22	7.02 $\pm$ 0.31	6.79 $\pm$ 0.43	6.69 $\pm$ 0.24
		DFV $\pm$ SD	0.53 $\pm$ 0.16	0.60 $\pm$ 0.14	0.50 $\pm$ 0.11	0.52 $\pm$ 0.07
		FP $\pm$ SD	17.62 $\pm$ 24.30	31.56 $\pm$ 20.68	71.09 $\pm$ 20.34	79.35 $\pm$ 11.86
	Posterior	DF $\pm$ SD	7.35 $\pm$ 0.21	7.06 $\pm$ 0.36	6.76 $\pm$ 0.47	6.54 $\pm$ 0.20
		DFV $\pm$ SD	0.52 $\pm$ 0.17	0.58 $\pm$ 0.16	0.48 $\pm$ 0.11	0.52 $\pm$ 0.09
		FP $\pm$ SD	15.60 $\pm$ 22.51	28.01 $\pm$ 19.35	69.59 $\pm$ 27.37	78.85 $\pm$ 11.86
	Lateral	DF $\pm$ SD	7.36 $\pm$ 0.19	7.09 $\pm$ 0.30	6.81 $\pm$ 0.41	6.70 $\pm$ 0.24
		DFV $\pm$ SD	0.50 $\pm$ 0.15	0.58 $\pm$ 0.18	0.49 $\pm$ 0.13	0.52 $\pm$ 0.08
		FP $\pm$ SD	17.02 $\pm$ 21.95	33.81 $\pm$ 24.26	72.59 $\pm$ 21.64	77.60 $\pm$ 15.63
Alpha	Frontal	DF $\pm$ SD	9.13 $\pm$ 0.57	9.40 $\pm$ 0.88	8.64 $\pm$ 0.21	9.01 $\pm$ 0.44
		DFV $\pm$ SD	0.88 $\pm$ 0.40	1.07 $\pm$ 0.43	0.85 $\pm$ 0.32	1.19 $\pm$ 0.27
		FP $\pm$ SD	80.45 $\pm$ 22.14	55.08 $\pm$ 24.54	17.52 $\pm$ 21	8.64 $\pm$ 8.29
	Central	DF $\pm$ SD	9.13 $\pm$ 0.65	9.42 $\pm$ 0.90	8.48 $\pm$ 0.17	8.70 $\pm$ 0.39
		DFV $\pm$ SD	0.82 $\pm$ 0.41	1.04 $\pm$ 0.40	0.60 $\pm$ 0.17	0.87 $\pm$ 0.37
		FP $\pm$ SD	81.16 $\pm$ 24.96	58.98 $\pm$ 26.07	19.40 $\pm$ 21.02	9.51 $\pm$ 9.22
	Posterior	DF $\pm$ SD	9.03 $\pm$ 0.63	1.06 $\pm$ 0.96	8.49 $\pm$ 0.18	8.72 $\pm$ 0.33
		DFV $\pm$ SD	0.64 $\pm$ 0.35	0.86 $\pm$ 0.45	0.62 $\pm$ 0.25	0.93 $\pm$ 0.37
		FP $\pm$ SD	83.28 $\pm$ 23.49	65.01 $\pm$ 24.45	16.65 $\pm$ 23.68	5.01 $\pm$ 6.25
	Lateral	DF $\pm$ SD	9.12 $\pm$ 0.71	0.92 $\pm$ 0.82	8.48 $\pm$ 0.18	8.61 $\pm$ 0.41
		DFV $\pm$ SD	0.82 $\pm$ 0.37	0.82 $\pm$ 0.40	0.65 $\pm$ 0.24	0.84 $\pm$ 0.35
		FP $\pm$ SD	82.47 $\pm$ 22.06	60.76 $\pm$ 26.68	16.65 $\pm$ 18.76	10.64 $\pm$ 15.10
Theta-alpha	Frontal	DF $\pm$ SD	8.79 $\pm$ 0.75	8.24 $\pm$ 1.29	6.75 $\pm$ 0.80	6.45 $\pm$ 0.63
		DFV $\pm$ SD	1.07 $\pm$ 0.46	1.29 $\pm$ 0.59	0.91 $\pm$ 0.27	0.98 $\pm$ 0.33
	Central	DF $\pm$ SD	8.81 $\pm$ 0.82	8.36 $\pm$ 1.30	6.93 $\pm$ 0.71	6.68 $\pm$ 0.76
		DFV $\pm$ SD	0.92 $\pm$ 0.47	1.30 $\pm$ 0.60	0.80 $\pm$ 0.25	0.82 $\pm$ 0.25
	Posterior	DF $\pm$ SD	8.82 $\pm$ 0.79	8.65 $\pm$ 1.21	6.78 $\pm$ 0.86	6.41 $\pm$ 0.58
		DFV $\pm$ SD	0.78 $\pm$ 0.38	1.21 $\pm$ 0.75	0.73 $\pm$ 0.23	0.84 $\pm$ 0.27
	Lateral	DF $\pm$ SD	8.88 $\pm$ 0.81	8.42 $\pm$ 1.13	6.90 $\pm$ 0.71	6.74 $\pm$ 0.81
		DFV $\pm$ SD	0.93 $\pm$ 0.41	1.13 $\pm$ 0.51	0.79 $\pm$ 0.31	0.88 $\pm$ 0.35

this analysis as they introduced marked multicollinearity. The QEEG variables that best predicted diagnosis were the theta power (%) (Wald chi-square = 15.74,  $df = 1$ ,  $p < 0.01$ ), the fast-theta FP (Wald chi-square = 8.1,  $df = 1$ ,  $p < 0.01$ ) and the theta-alpha SD (Wald chi-square = 7.549,  $df = 1$ ,  $p < 0.01$ ). ROC analysis (Fig. 7) yielded AUC = 94% (90.4–97.9%), sensitivity = 92.26% (CI = 80.4–100%) and specificity = 83.3% (CI = 73.6–93%). Since no significant differences were found between the PDD and DLB groups for any of the QEEG variables in the variance analyses, all the QEEG variables were included in the GEE analysis. This analysis deviated from the analysis protocol and is therefore included in the [supple-](#)

[mentary material \(Supplementary Material 2\)](#), without drawing further conclusions.

#### 4. Discussion

Our analysis has revealed several novel findings, including greater theta-alpha DFV in AD patients compared to controls, DLB and PDD patients. Moreover, we did not identify any differences in the DFV between the DLB group compared to controls, as was previously reported (Bonanni et al., 2016, 2008; Walker et al., 2000). However, we found a significant, DLB specific positive

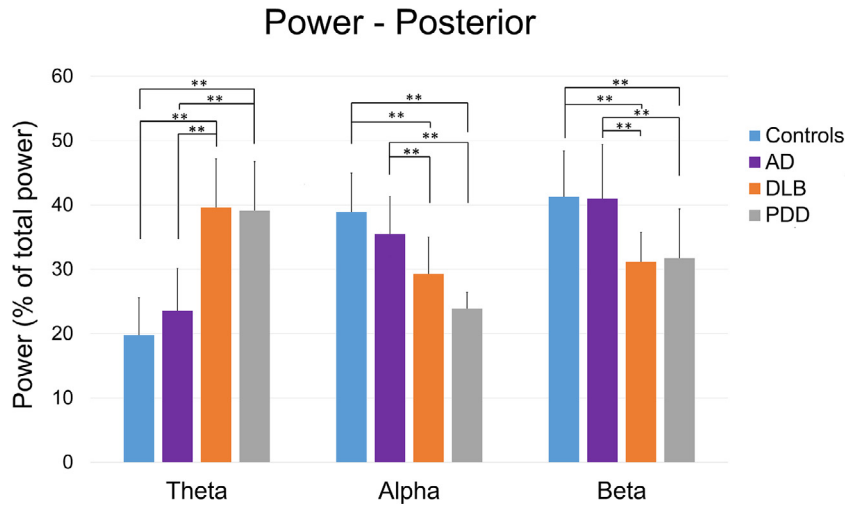


**Fig. 3.** The mean percentage distribution of the total relative power in three frequency bands (Hz): theta (4–7.75), alpha (8–13.5) and beta (20.75), for each of four diagnostic groups: healthy controls (N = 21), Alzheimer’s disease (AD; N = 18), dementia with Lewy bodies (DLB; N = 17) and Parkinson’s disease dementia (PDD; N = 17) patients, for the posterior region. Similar observations were made in the frontal, central and lateral regions but are not shown. Error bars indicate the standard deviation.

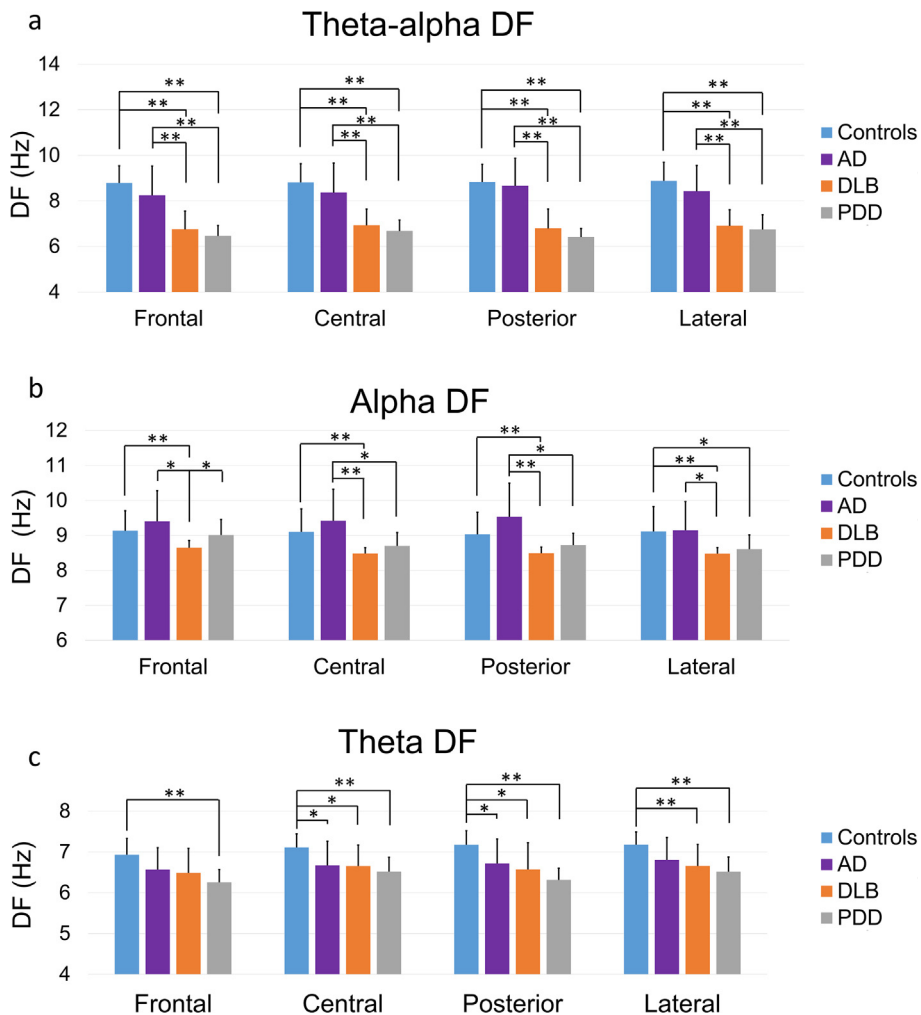


**Fig. 4.** The mean dominant frequency (DF) in the theta-alpha (4–13.75 Hz), alpha (8–13.75 Hz) and theta (4–7.75 Hz) frequency ranges, for each of four diagnostic groups: healthy controls (N = 21), Alzheimer’s disease (AD; N = 18), dementia with Lewy bodies (DLB; N = 17) and Parkinson’s disease dementia (PDD; N = 17) patients, in the frontal, central, posterior and lateral regions. Error bars indicate the standard deviation (SD), \*p < 0.05, \*\*p < 0.01.

correlation between the CAF score and the theta DFV, and the CAF score and slow-theta FP. Our findings confirm the widely reported shift of EEG power and dominant rhythm – from the alpha towards

the theta frequency range in the DLB and PDD groups compared to healthy controls and AD patients (Briel et al., 1999; Barber et al., 2000; Bonanni et al., 2008). A subtler slowing of the EEG was also

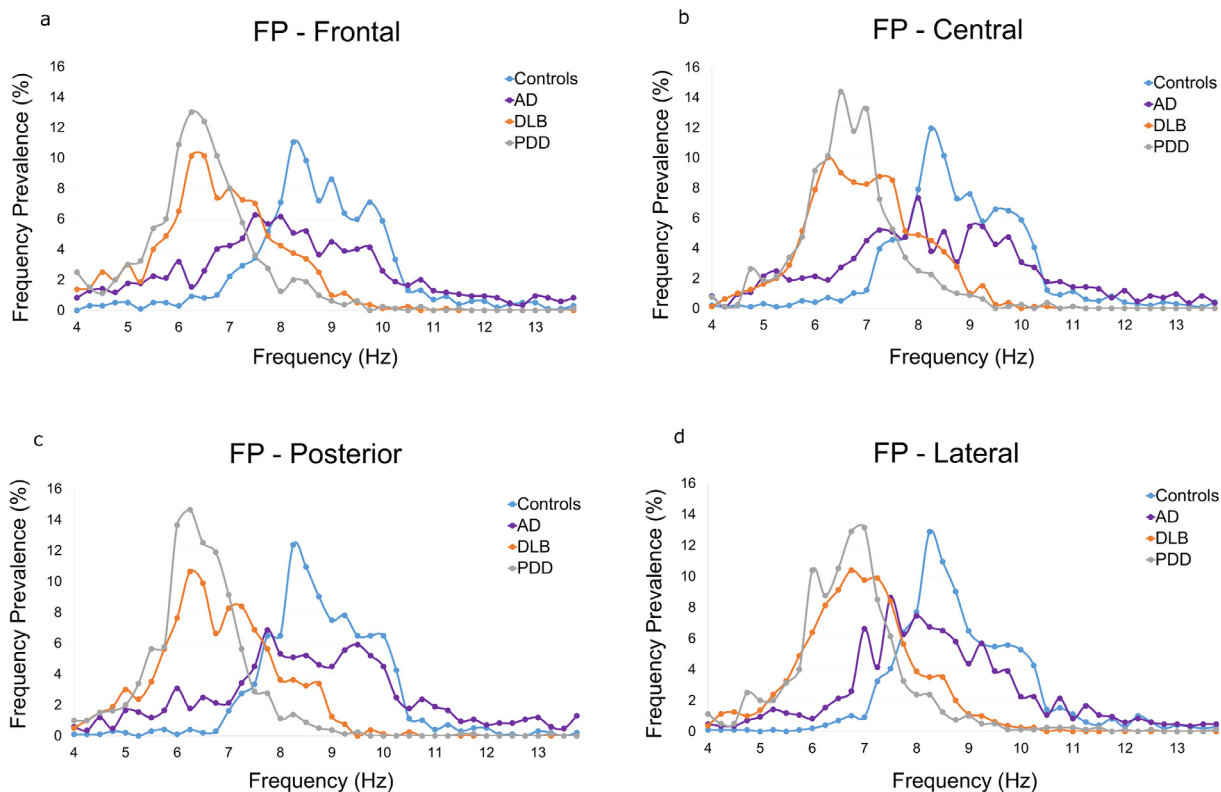


**Fig. 5.** The mean frequency prevalence (FP; percentage distribution of the mean dominant frequency (DF) in each frequency point in the theta-alpha frequency range with 0.25 Hz resolution) for each of four diagnostic groups: healthy controls (N = 21), Alzheimer's disease (AD; N = 18), dementia with Lewy bodies (DLB; N = 17) and Parkinson's disease dementia (PDD; N = 17) patients, in the (a) frontal, (b) central, (c) posterior and (d) lateral regions.

observed in AD patients compared to controls. Finally, a preliminary analysis investigating the possible diagnostic value of QEEG variables showed that the three QEEG variables describing the extent of EEG slowing and DFV (theta power, fast-theta FP and theta-alpha DFV) could predict a DLB versus an AD diagnosis with high sensitivity and specificity.

A more marked EEG slowing in DLB/PDD groups compared to healthy controls and AD patients has been extensively reported in the literature, mostly in posterior derivations (Briel et al., 1999; Barber et al., 2000; Roks et al., 2008). In our analysis we looked within four different cortical regions compared to three regions previously reported (Bonanni et al., 2016, 2008), and analysed three measures of EEG spectral distribution, the FP, DF and power, all of which indicated a greater EEG slowing in DLB/PDD patients compared to AD patients and controls.

In AD patients, EEG slowing of a lesser extent was observed, that was evident by a shift of FP from the alpha to the fast-theta and slow-theta ranges compared to healthy controls. This finding indicates that a higher percentage of measurements of the theta-alpha DF in time fell in the theta-band rather than in the alpha-band in AD patients compared to controls. This altered DF distribution towards lower frequencies in AD was "masked" with the calculation of the mean theta-alpha DF, as this measure does not account for variability. The DF in the AD group is highly variable and can take values towards the higher edge of the alpha band thus influencing the mean DF. This is evident by the significantly greater theta-alpha DFV and the trends for greater alpha DFV and alpha DF in the AD group.

A cholinergic deficit may partly account for the EEG slowing in LBDs and AD, as the administration of AChEIs can reverse the EEG slowing in both diseases (Adler et al., 2004; Babiloni et al., 2013; Bosboom et al., 2009). However, the loss of cholinergic neurons

projecting to the cortex is greater and has a faster progression in DLB and PDD compared to AD (Lippa et al., 1999) where the cholinergic deficit is not yet severe at mild stages of the disease (Bohnen and Albin, 2011). Pathological protein-related synaptic dysfunction that occurs before neuronal degeneration has also been associated with cognitive decline in AD and is thought to be even greater in DLB (Schulz-Schaeffer, 2010; Selkoe, 2002). Thus, a more advanced cholinergic deficit and synaptic dysfunction in the LBD groups could account for the greater extent of EEG slowing observed compared to the AD group, particularly given the relatively early disease stage/cognitive impairment that our participants exhibited.

Our analysis also revealed novel findings regarding temporal variability in the dominant rhythm as measured by DFV. Previous studies have shown a significant DFV increase in DLB patients compared to healthy controls, that correlated with CFs measured by CAF (Bonanni et al., 2008; Walker et al., 2000). Although we did not find an increase in the DFV of DLB patients compared to controls, we did find a positive correlation between theta DFV and the CAF score within the DLB group (Bonanni et al., 2015). This correlation was only significant in the theta frequency range, likely due to the shift of the DF towards these frequencies. A positive correlation was also found between slow-theta FP and the CAF score in DLB patients. Both these correlations were only seen in the DLB group and not in the PDD or AD groups.

Given the neuropathological similarities between PDD and DLB and the absence of other QEEG differences between these groups, the lack of a correlation between CAF and our QEEG measures in PDD was unexpected. Previous studies have reported that PDD patients with high CF scores show an EEG-slowing (Bonanni et al., 2008) and have more DLB-like symptoms such as visual hallucinations, while patients with lower CF scores resemble PD (Varanese et al., 2010). This PDD heterogeneity may have affected

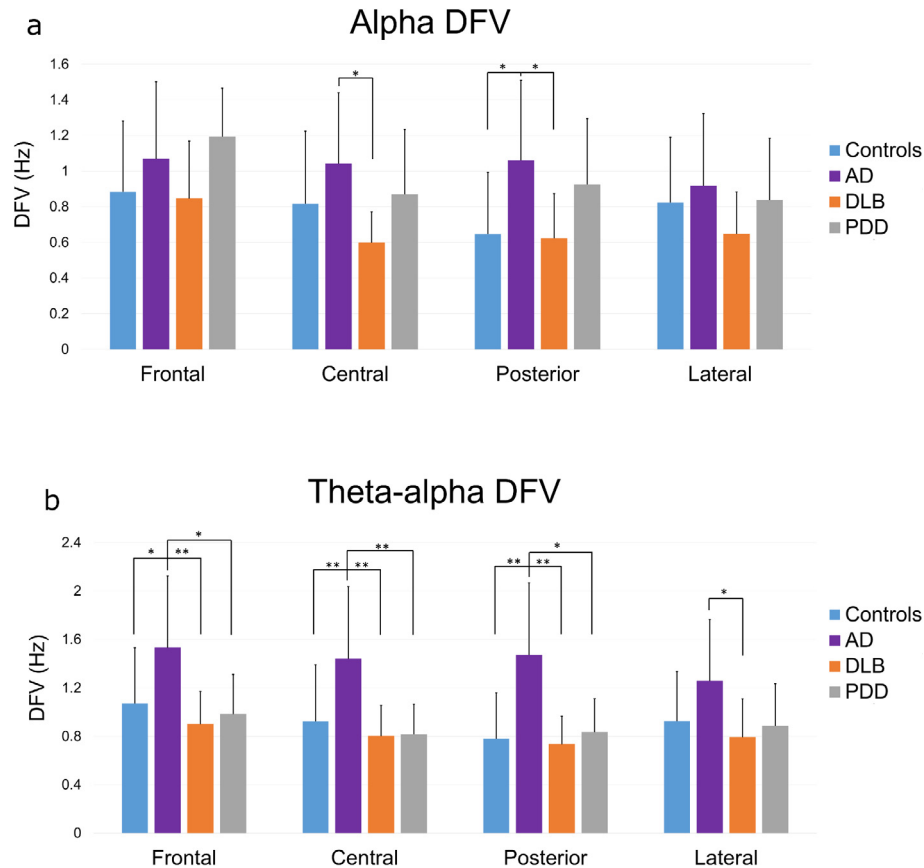


**Fig. 6.** The mean dominant frequency variability (DFV) in the (a) alpha (8–13.5 Hz) and (b) theta-alpha (4–13.75 Hz) frequency ranges, for each of four diagnostic groups: healthy controls (N = 21), Alzheimer's disease (AD; N = 18), dementia with Lewy bodies (DLB; N = 17) and Parkinson's disease dementia (PDD; N = 17) patients, in the frontal, central, posterior and lateral regions. Error bars indicate the standard deviation (SD), \*p < 0.05, \*\*p < 0.01.

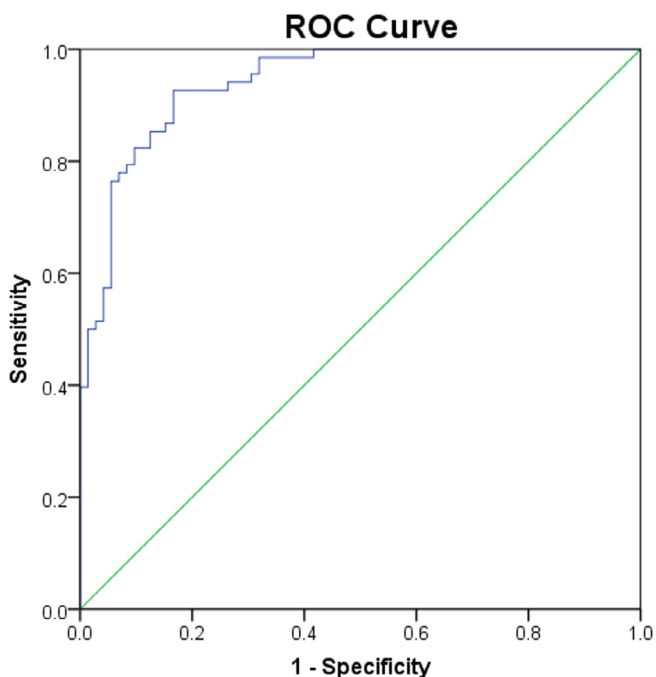


**Fig. 7.** Receiver operating curves (ROC) for a model composed of fast-theta frequency prevalence (FP), theta power and theta-alpha dominant frequency variability (DFV), for differentiating between Alzheimer's disease (AD; N = 18) and dementia with Lewy bodies (DLB; N = 17) with mild dementia.

our capacity to identify a correlation between the EEG measures and CAF score in this group. Moreover, DLB patients with parkinsonism have more impaired reaction times and vigilance measures that relate to CFs, compared to patients without motor symptoms, implying a connection between CFs and dopaminergic impairment (Ballard et al., 2002). Since PDD is characterised by greater dopaminergic impairment than DLB, this additional pathology could have a more dominant aetiological role in the CFs seen in PDD as compared to DLB and thus be less contingent on factors (e.g. cholinergic tone) which might drive a QEEG change that associates with CFs. Furthermore, fluctuations are likely to have at least two dimensions (arousal and attention; Bliwise et al., 2012) which are not discriminated by the CAF scale but which may be differentially expressed in our DLB and PDD groups given arousal/sleepiness is strongly influenced by dopaminergic medications. Another factor may be the amyloid burden as this is significantly greater in DLB compared to PDD (Donaghy et al., 2015) and the cortical amyloid- $\beta$  deposition relates more to dementia severity, visual hallucinations and delusion in DLB than PDD (McKeith et al., 2004). DLB is also characterised by a greater amyloid load in the putamen (Hepp et al., 2016), which is involved in attentional networks and in DLB has altered functional connectivity that correlates with CAF (Peraza et al., 2014). Improved quantification scales of fluctuations may help unpick these challenges.

Previous studies have also shown that DLB patients had a significantly higher DFV compared to AD patients, which did not differ significantly from controls, and that a higher DFV was an accurate indicator of DLB versus AD diagnosis (Bonanni et al., 2008). A QEEG analysis on the same patient cohorts as in this study, but with less spatial detail, also suggested a greater theta-alpha DFV in AD

patients compared to the DLB/PDD groups, posteriorly (Peraza et al., 2018). Here, we found that AD patients had a significantly higher theta-alpha DFV compared to the other groups in most regions while DLB patients were not significantly different than PPD patients or controls. In the current study looking within smaller frequency bands in the theta-alpha range we also identified a greater alpha DFV in AD patients compared to controls and DLB patients posteriorly, and to DLB patients alone centrally. These findings could be part of the pathology or alternatively, the result of a compensation mechanism that may occur at early stages of AD. At rest, early stage AD patients may have increased activity and functional connectivity in resting state networks which correlate with a lower MMSE score (Peraza et al., 2016). However, at more advanced stages activity and connectivity decrease to levels lower than those seen in controls (Agosta et al., 2012). Therefore, increases in DFV may be associated with a compensation mechanism in early stage AD.

A number of other factors may account for the discrepancies between our findings and those of previous studies. The lack of a greater DFV in DLB patients compared to controls may be attributed to the fact that the majority of our DLB patients were on AChEIs, although we would argue that this adds to the clinical relevance of our findings, particularly from a diagnostic perspective; it is likely that any use of the EEG will be when patients are beginning or have already been initiated on treatment. In DLB patients, CFs have been shown to correlate with cholinergic imbalances in networks involved in the resting state (Delli Pizzi et al., 2015). AChEIs restore this imbalance and improve both the cognitive symptoms of DLB and the electrophysiological markers, including the EEG spectrum and connectivity (Onofrij et al., 2003). That said, it is important to acknowledge that more AD (94.4%) than DLB (88.2%) patients were on AChEIs in our study groups and the former group showed greater DFV. However, as outlined above, cholinergic deficits are greater and occur earlier in DLB compared to AD (Tiraboschi et al., 2002), while the brainstem cholinergic innervations of the thalamus are relatively spared in AD (Mesulam, 2004) but not in DLB (Taylor et al., 2017). Hence, at the stage of mild dementia AChEIs could have a differential effect in DLB and AD. Although AChEIs may have normalized the DFV in DLB patients in relation to healthy individuals, the CAF/DFV correlation was still maintained within the DLB group. In previous studies, none (Walker et al., 2000), or only a small proportion (Bonanni et al., 2008) of the patients were on AChEIs. Differences in the participant cohorts, as well as methodological differences in the analysis of the recordings must also be considered. Specifically, we used a different pre-processing and spatial analysis approach, as well as a different way to estimate DFV; here DFV was defined as the standard deviation from the mean DF across epochs, in an epoch-by-epoch basis, while in Bonanni et al. (2008, 2016), DFV was defined using a visual rating of DF range on sequential EEG segments.

Finally, we proceeded with a preliminary analysis to investigate the capacity of the QEEG variables to correctly differentiate between AD and DLB patients with mild dementia. The theta power, fast-theta FP and theta-alpha DFV yielded accuracy of 94% (CI = 90.4–97.9%), sensitivity of 92.26% (CI = 80.4–100%) and specificity of 83.3% (73.6–93%). The high predictive accuracy of this model is in-line with previous classifications using QEEG variables, although different EEG pre-processing and analysis methods were used (Andersson et al., 2008; Garn et al., 2017).

A few issues relating to this study need to be considered and an important next step would be the confirmation of our findings in independent prospective cohorts, especially regarding the ROC analysis. We excluded the delta frequencies and hence, we might have missed changes in the QEEG variables within that range. In addition, the recordings were not always continuous as we focused

on discarding as much of the noise as possible and preferred to occasionally reject epochs, across all channels. Moreover, the patients did not undergo post-mortem immunohistological examination and thus we did not account for mixed AD-DLB pathology that has been shown to relate to greater cognitive impairment in DLB patients (Gomperts et al., 2012) and which may alter the QEEG pattern. However, our clinical diagnostic approaches were robust enough to enhance the specificity of our group selections. Evidence for this include DaT scans that were available for 9 of the DLB patients and were all positive, and a multi-modal MRI/EEG analysis on data from all the patients that were recruited in the same cohort as the patients included in this study, where AD and DLB patients were classified with 90% accuracy (Colloby et al., 2016).

## 5. Conclusions

Our findings confirm the well-established slowing of the EEG in the Lewy body dementia groups compared to healthy controls and AD patients. Although we did not find higher DFV in DLB patients compared to controls as expected, theta DFV and slow-theta FP were positively correlated with CFs as measured by CAF. This DLB specific correlation suggests that a slower and more temporally variable DF specifically relates to the CFs seen in DLB, and could reveal differential mechanisms underlying CFs in dementia subtypes. Another novel finding was a significantly higher DFV in AD patients compared to the other groups. Exploratory analysis showed that QEEG measures could predict a DLB versus an AD diagnosis with high accuracy, sensitivity and specificity. In conclusion, this study supports the hypothesis that QEEG analysis can be a valuable tool for identifying CFs in DLB and for differential diagnosis between dementia subtypes, once replicated with low density EEG currently used in standard clinical practice after the feasibility and cost-effectiveness of these methodologies has been investigated.

## Acknowledgements

We thank the Alzheimer's Society for funding this research as part of the Alzheimer's Society Doctoral Training center at Newcastle University. This research was supported by the NIHR Newcastle Biomedical Research Centre awarded to the Newcastle upon Tyne Hospitals NHS Foundation Trust and Newcastle University, the Newcastle Hospitals NHS Charity, the Northumberland, Tyne and Wear NHS Foundation Trust, the Wellcome Trust (grant numbers: BH120812, BH120878) and by the Alzheimer's Research UK. S.G. was supported by the NIHR MedTech In Vitro Diagnostic Co-operatives scheme (ref MIC-2016-014).

## Conflict of interest

None.

## Appendix A. Supplementary material

Supplementary data associated with this article can be found, in the online version, at <https://doi.org/10.1016/j.clinph.2018.03.013>.

## References

- Adler G, Brassens S, Chwalek K, Dieter B, Teufel M. Prediction of treatment response to rivastigmine in Alzheimer's dementia. *J Neurol Neurosurg Psychiatry* 2004;75:292–4.
- Agosta F, Pievani M, Geroldi C, Copetti M, Frisoni GB, Filippi M. Resting state fMRI in Alzheimer's disease: beyond the default mode network. *Neurobiol Aging* 2012;33:1564–78. <https://doi.org/10.1016/j.neurobiolaging.2011.06.007>
- Andersson M, Hansson O, Minthon L, Rosén I, Lönnerdal E. Electroencephalogram variability in dementia with Lewy bodies, Alzheimer's disease and controls.

- Dement Geriatr Cogn Disord 2008;26:284–90. <https://doi.org/10.1159/000160962>.
- Babiloni C, Del Percio C, Bordet R, Bourriez J-L, Bentivoglio M, Payoux P, et al. Effects of acetylcholinesterase inhibitors and memantine on resting-state electroencephalographic rhythms in Alzheimer's disease patients. *Clin Neurophysiol* 2013;124:837–50. <https://doi.org/10.1016/j.clinph.2012.09.017>.
- Ballard C, O'Brien J, Morris CM, Barber R, Swann A, Neill D, et al. The progression of cognitive impairment in dementia with Lewy bodies, vascular dementia and Alzheimer's disease. *Int J Geriatr Psychiatry* 2001;16:499–503. <https://doi.org/10.1002/gps.381>.
- Ballard CG, Aarsland D, McKeith I, O'Brien J, Gray A, Cormack F, et al. Fluctuations in attention: PD dementia vs DLB with Parkinsonism. *Neurology* 2002;59:1714–20.
- Barber PA, Varma AR, Lloyd JJ, Haworth B, Snowden JS, Neary D. The electroencephalogram in dementia with Lewy bodies. *Acta Neurol Scand* 2000;101:53–6.
- Bartlett MS. Periodogram analysis and continuous spectra. *Biometrika* 1950;37:1. <https://doi.org/10.2307/2332141>.
- Bell AJ, Sejnowski TJ. An information-maximization approach to blind separation and blind deconvolution. *Neural Comput* 1995;7:1129–59.
- Beyer MK, Larsen JP, Aarsland D. Gray matter atrophy in Parkinson disease with dementia and dementia with Lewy bodies. *Neurology* 2007;69:747–54. <https://doi.org/10.1212/01.wnl.0000266966.62598.1c>.
- Blivise DL, Trotti LM, Wilson AG, Greer SA, Wood-Siverio C, Juncos JJ, et al. Daytime alertness in Parkinson's disease: potentially dose-dependent, divergent effects by drug class. *Mov Disord* 2012;27:1118–24. <https://doi.org/10.1002/mds.25082>.
- Bohnen NI, Albin RL. The cholinergic system and Parkinson disease. *Behav Brain Res* 2011;221:564–73. <https://doi.org/10.1016/j.bbr.2009.12.048>.
- Bonanni L, Franciotti R, Nobili F, Kramberger MG, Taylor J-P, Garcia-Platac S, et al. EEG markers of dementia with Lewy bodies: a multicenter Cohort study. *J Alzheimer's Dis* 2016;54:1649–57. <https://doi.org/10.3233/JAD-160435>.
- Bonanni L, Perfetti B, Bifulchetti S, Taylor J-P, Franciotti R, Parnetti L, et al. Quantitative electroencephalogram utility in predicting conversion of mild cognitive impairment to dementia with Lewy bodies. *Neurobiol Aging* 2015;36:434–45. <https://doi.org/10.1016/j.neurobiolaging.2014.07.009>.
- Bonanni L, Thomas A, Tiraboschi P, Perfetti B, Varanese S, Onofrij M. EEG comparisons in early Alzheimer's disease, dementia with Lewy bodies and Parkinson's disease with dementia patients with a 2-year follow-up. *Brain* 2008;131:690–705. <https://doi.org/10.1093/brain/awn322>.
- Bosboom JLW, Stoffers D, Stam CJ, Berendse HW, Wolters EC. Cholinergic modulation of MEG resting-state oscillatory activity in Parkinson's disease related dementia. *Clin Neurophysiol* 2009;120:910–5. <https://doi.org/10.1016/j.clinph.2009.03.004>.
- Bradshaw J, Saling M, Hopwood M, Anderson V, Brodtmann A. Fluctuating cognition in dementia with Lewy bodies and Alzheimer's disease is qualitatively distinct. *J Neurol Neurosurg Psychiatry* 2004;75:382–7.
- Briel RC, McKeith IG, Barker WA, Hewitt Y, Perry RH, Ince PG, et al. EEG findings in dementia with Lewy bodies and Alzheimer's disease. *J Neurol Neurosurg Psychiatry* 1999;66:401–3. <https://doi.org/10.1136/INNP.66.3.401>.
- Carr GJ, Chi EM. Analysis of variance for repeated measures data: a generalized estimating equations approach. *Stat Med* 1992;11:1033–40. <https://doi.org/10.1002/sim.4780110805>.
- Colloby SJ, Cromarty RA, Peraza LR, Johnsen K, Jóhannesson G, Bonanni L, et al. Multimodal EEG-MRI in the differential diagnosis of Alzheimer's disease and dementia with Lewy bodies. *J Psychiatr Res* 2016;78:48–55. <https://doi.org/10.1016/j.ipsychires.2016.03.010>.
- Delli Pizzi S, Franciotti R, Taylor J-P, Thomas A, Tartaro A, Onofrij M, et al. Thalamic involvement in fluctuating cognition in dementia with Lewy bodies: magnetic resonance evidences. *Cereb Cortex* 2015;25:3682–9. <https://doi.org/10.1093/cercor/bhu220>.
- Delorme A, Makeig S. EEGLAB: an open source toolbox for analysis of single-trial EEG dynamics including independent component analysis. *J Neurosci Methods* 2004;134:9–21. <https://doi.org/10.1016/j.jneumeth.2003.10.009>.
- Donaghy P, Thomas AJ, O'Brien JT. Amyloid PET imaging in Lewy body disorders. *Am J Geriatr Psychiatry* 2015;23:23–37. <https://doi.org/10.1016/j.jagp.2013.03.001>.
- Van Dyk K, Towns S, Tatarina O, Yeung P, Dorrejo J, Zahodne LB, et al. Assessing fluctuating cognition in dementia diagnosis: interrater reliability of the clinician assessment of fluctuation. *Am J Alzheimer's Dis Other Demen* 2016;31:137–43. <https://doi.org/10.1177/1533317515603359>.
- Edison P, Rowe CC, Rinne JO, Ng S, Ahmed I, Kemppainen N, et al. Amyloid load in Parkinson's disease dementia and Lewy body dementia measured with [11C]PIB positron emission tomography. *J Neurol Neurosurg Psychiatry* 2008;79:1331–8. <https://doi.org/10.1136/jnnp.2007.127878>.
- Emre M, Aarsland D, Brown R, Burn DJ, Duyckaerts C, Mizuno Y, et al. Clinical diagnostic criteria for dementia associated with Parkinson's disease. *Mov Disord* 2007;22:1689–707. <https://doi.org/10.1002/mds.21507>.
- Egedal K, Snaedal J, Hoegh P, Jelic V, Bo Andersen B, Naik M, et al. Quantitative EEG applying the statistical recognition pattern method: a useful tool in dementia diagnostic workup. *Dement Geriatr Cogn Disord* 2015;40:1–12. <https://doi.org/10.1159/000381016>.
- Ferree TC. Spherical splines and average referencing in scalp electroencephalography. *Brain Topogr* 2006;19:43–52. <https://doi.org/10.1007/s10548-006-0011-0>.
- Garn H, Coronel C, Waser M, Caravias G, Ransmayr G. Differential diagnosis between patients with probable Alzheimer's disease, Parkinson's disease dementia, or dementia with Lewy bodies and frontotemporal dementia, behavioral variant, using quantitative electroencephalographic features. *J Neural Transm* 2017;1–13. <https://doi.org/10.1007/s00702-017-1699-6>.
- Gomperts SN, Locascio JJ, Marquie M, Santarlasci AL, Rentz DM, Maye J, et al. Brain amyloid and cognition in Lewy body diseases. *Mov Disord* 2012;27:965–73. <https://doi.org/10.1002/mds.25048>.
- Hepp DH, Vergoossen DLE, Huisman E, Lemstra AW, Berendse HW, Rozemuller AJ, et al. Distribution and load of amyloid- $\beta$  pathology in Parkinson disease and dementia with Lewy bodies. *J Neuropathol Exp Neurol* 2016;75:936–45. <https://doi.org/10.1093/jnen/nlw070>.
- Huang Y, Halliday G, Okazaki H, Lipkin L, Aronson S, Kosaka K, et al. Can we clinically diagnose dementia with Lewy bodies yet? *Transl Neurodegener* 2013;2:4. <https://doi.org/10.1186/2047-9158-2-4>.
- Jackson CE, Snyder PJ, Khachaturian ZS, Brookmeyer R, Johnson E, Ziegler-Graham K, et al. Electroencephalography and event-related potentials as biomarkers of mild cognitive impairment and mild Alzheimer's disease. *Alzheimers Dement* 2008;4:S137–43. <https://doi.org/10.1016/j.jalz.2007.10.008>.
- Jung TP, Makeig S, Humphries C, Lee TW, McKeown MJ, Iragui V, et al. Removing electroencephalographic artifacts by blind source separation. *Psychophysiology* 2000;37:163–78.
- Kropotov JD, Kropotov JD. Methods of analysis of background EEG. *Quant. EEG, event-related potentials neurother.*; 2009. p. 116–60. <http://doi.org/10.1016/B978-0-12-374512-5.00008-6> [chapter 8].
- Lippa CF, Smith TW, Perry E. Dementia with Lewy bodies: choline acetyltransferase parallels nucleus basalis pathology. *J Neural Transm* 1999;106:525–35. <https://doi.org/10.1007/s007020050176>.
- McKeith I, Fairbairn A, Perry R, Thompson P, Perry E. Neuroleptic sensitivity in patients with senile dementia of Lewy body type. *BMJ* 1992;305:673–8.
- McKeith I, Mintzer J, Aarsland D, Burn D, Chiu H, Cohen-Mansfield J, et al. Dementia with Lewy bodies. *Lancet Neurol* 2004;3:19–28. [https://doi.org/10.1016/S1474-4422\(03\)00619-7](https://doi.org/10.1016/S1474-4422(03)00619-7).
- McKeith IG, Dickson DW, Lowe J, Emre M, O'Brien JT, Feldman H, et al. Diagnosis and management of dementia with Lewy bodies: third report of the DLB consortium. *Neurology* 2005;65:1863–72. <https://doi.org/10.1212/01.wnl.0000187889.17253.b1>.
- McKeith IG, Boeve BF, Dickson DW, Halliday G, Taylor J-P, Weintraub D, et al. Diagnosis and management of dementia with Lewy bodies: fourth consensus report of the DLB Consortium. *Neurology* 2017;89:88–100. <https://doi.org/10.1212/WNL.0000000000004058>.
- McKhann GM, Knopman DS, Chertkow H, Hyman BT, Jack CR, Kawas CH, et al. The diagnosis of dementia due to Alzheimer's disease: recommendations from the National Institute on Aging-Alzheimer's Association workgroups on diagnostic guidelines for Alzheimer's disease. *Alzheimers Dement* 2011;7:263–9. <https://doi.org/10.1016/j.jalz.2011.03.005>.
- Mesulam M. The cholinergic lesion of Alzheimer's disease: pivotal factor or side show? *Learn Mem* 2004;11:43–9. <https://doi.org/10.1101/jm.69204>.
- Metzler-Baddeley C. A review of cognitive impairments in dementia with Lewy bodies relative to Alzheimer's disease and Parkinson's disease with dementia. *Cortex* 2007;43:583–600. [https://doi.org/10.1016/S0010-9452\(08\)70489-1](https://doi.org/10.1016/S0010-9452(08)70489-1).
- Niedermeyer E, Lopes da Silva FH. In: Niedermeyer E, Lopes Da Silva FH, editors. *Electroencephalography: basic principles, clinical applications, and related fields*. 5th ed. Lippincott Williams & Wilkins; 2004.
- Onofrij M, Thomas A, Iacono D, Luciano AL, Di Iorio A. The effects of a cholinesterase inhibitor are prominent in patients with fluctuating cognition: a part 3 study of the main mechanism of cholinesterase inhibitors in dementia. *Clin Neuropharmacol* 2003;26:239–51.
- Oostenveld R, Praamstra P. The five percent electrode system for high-resolution EEG and ERP measurements. *Clin Neurophysiol* 2001;112:713–9. [https://doi.org/10.1016/S1388-2457\(00\)00527-7](https://doi.org/10.1016/S1388-2457(00)00527-7).
- Peraza LR, Kaiser M, Firbank M, Graziadio S, Bonanni L, Onofrij M, et al. FMRI resting state networks and their association with cognitive fluctuations in dementia with Lewy bodies. *NeuroImage Clin* 2014;4:558–65. <https://doi.org/10.1016/j.nicl.2014.03.013>.
- Peraza LR, Colloby SJ, Deboys L, O'Brien JT, Kaiser M, Taylor J-P. Regional functional synchronizations in dementia with Lewy bodies and Alzheimer's disease. *Int Psychogeriatr*. 2016;28(7):1143–51.
- Peraza L, Cromarty R, Kobeleva X, Firbank MJ, Killen A, Graziadio S, Thomas AJ, O'Brien JT, Taylor J-P. Electroencephalographic derived network differences in Lewy body dementia compared to Alzheimer's disease. *Sci Rep*. 2018;8:4637. <https://doi.org/10.1038/s41598-018-22984-5>.
- Rodriguez G, Copello F, Vitali P, Perego G, Nobili F. EEG spectral profile to stage Alzheimer's disease. *Clin Neurophysiol* 1999;110:1831–7.
- Roks G, Korf ESC, van der Flier WM, Scheltens P, Stam CJ. The use of EEG in the diagnosis of dementia with Lewy bodies. *J Neurol Neurosurg Psychiatry* 2008;79:377–80. <https://doi.org/10.1136/jnnp.2007.125385>.
- Schulz-Schaeffer WJ. The synaptic pathology of alpha-synuclein aggregation in dementia with Lewy bodies, Parkinson's disease and Parkinson's disease dementia. *Acta Neuropathol* 2010;120:131–43. <https://doi.org/10.1007/s00401-010-0711-0>.
- Selkoe DJ. Alzheimer's disease is a synaptic failure. *Science* 2002;298:789–91. <https://doi.org/10.1126/science.1074069>.
- Snaedal J, Jóhannesson GH, Gudmundsson TE, Blin NP, Emilsdottir AL, Einarsson B, et al. Diagnostic accuracy of statistical pattern recognition of electroencephalogram registration in evaluation of cognitive impairment and dementia. *Dement Geriatr Cogn Disord* 2012;34:51–60. <https://doi.org/10.1159/000339996>.

- Taylor J-P, Collerton D, LeBeau F, Perry E. Cholinergic pathology in dementia with Lewy bodies. *Dement. with Lewy bodies*. Tokyo: Springer Japan; 2017. p. 23–39. [http://doi.org/10.1007/978-4-431-55948-1\\_3](http://doi.org/10.1007/978-4-431-55948-1_3).
- Tiraboschi P, Hansen LA, Alford M, Merdes A, Masliah E, Thal LJ, et al. Early and widespread cholinergic losses differentiate dementia with Lewy bodies from Alzheimer disease. *Arch Gen Psychiatry* 2002;59:946–51.
- Varanese S, Perfetti B, Monaco D, Thomas A, Bonanni L, Tiraboschi P, et al. Fluctuating cognition and different cognitive and behavioural profiles in Parkinson's disease with dementia: comparison of dementia with Lewy bodies and Alzheimer's disease. *J Neurol* 2010;257:1004–11. <https://doi.org/10.1007/s00415-010-5453-3>.
- Walker MP, Ayre GA, Cummings JL, Wesnes K, McKeith IG, O'Brien JT, et al. Quantifying fluctuation in dementia with Lewy bodies, Alzheimer's disease, and vascular dementia. *Neurology* 2000;54:1616–25.
- Whitham EM, Pope KJ, Fitzgibbon SP, Lewis T, Clark CR, Loveless S, et al. Scalp electrical recording during paralysis: quantitative evidence that EEG frequencies above 20 Hz are contaminated by EMG. *Clin Neurophysiol* 2007;118:1877–88. <https://doi.org/10.1016/j.clinph.2007.04.027>.
- Zupancic M, Mahajan A, Handa K. Dementia with Lewy bodies: diagnosis and management for primary care providers. *Prim Care Companion CNS Disord* 2011;13. <http://doi.org/10.4088/PCC.11r01190>.